

AEDC-TR- 76-1
AFATL-TR-76-25

cy.2

JUL 0 1976

MAR 25 1992



INFLUENCES OF STING SUPPORT ON AERODYNAMIC LOADS ACTING ON CAPTIVE STORE MODELS

**PROPULSION WIND TUNNEL FACILITY
ARNOLD ENGINEERING DEVELOPMENT CENTER
AIR FORCE SYSTEMS COMMAND
ARNOLD AIR FORCE STATION, TENNESSEE 37389**

March 1976

Final Report for Period April 1973 — June 1975

Approved for public release; distribution unlimited.

Prepared for

**AIR FORCE ARMAMENT LABORATORY (DLJC)
EGLIN AFB, FLORIDA 32542**

NOTICES

When U. S. Government drawings specifications, or other data are used for any purpose other than a definitely related Government procurement operation, the Government thereby incurs no responsibility nor any obligation whatsoever, and the fact that the Government may have formulated, furnished, or in any way supplied the said drawings, specifications, or other data, is not to be regarded by implication or otherwise, or in any manner licensing the holder or any other person or corporation, or conveying any rights or permission to manufacture, use, or sell any patented invention that may in any way be related thereto.

Qualified users may obtain copies of this report from the Defense Documentation Center.

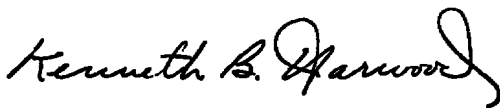
References to named commercial products in this report are not to be considered in any sense as an endorsement of the product by the United States Air Force or the Government.

This report has been reviewed by the Information Office (OI) and is releasable to the National Technical Information Service (NTIS). At NTIS, it will be available to the general public, including foreign nations.

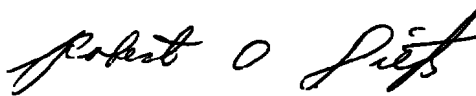
APPROVAL STATEMENT

This technical report has been reviewed and is approved for publication.

FOR THE COMMANDER



KENNETH B. HARWOOD
Major, CF
Research & Development
Division
Directorate of Technology



ROBERT O. DIETZ
Director of Technology

UNCLASSIFIED

REPORT DOCUMENTATION PAGE		READ INSTRUCTIONS BEFORE COMPLETING FORM
1 REPORT NUMBER AEDC-TR-76-1 AFATL-TR-76-25	2 GOVT ACCESSION NO.	3 RECIPIENT'S CATALOG NUMBER
4 TITLE (and Subtitle) INFLUENCES OF STING SUPPORT ON AERODYNAMIC LOADS ACTING ON CAPTIVE STORE MODELS		5 TYPE OF REPORT & PERIOD COVERED Final Report- April 1973 - June 1975
7 AUTHOR(s) R. E. Dix, ARO, Inc.		6 PERFORMING ORG. REPORT NUMBER
9 PERFORMING ORGANIZATION NAME AND ADDRESS Arnold Engineering Development Center(DY) Arnold Air Force Station, Tennessee 37389		8 CONTRACT OR GRANT NUMBER(s)
11. CONTROLLING OFFICE NAME AND ADDRESS Arnold Engineering Development Center (DYFS) Arnold Air Force Station, Tennessee 37389		10 PROGRAM ELEMENT, PROJECT, TASK AREA & WORK UNIT NUMBERS Program Element 62602F Project 2567 Task 0217
14 MONITORING AGENCY NAME & ADDRESS (if different from Controlling Office)		12. REPORT DATE March 1976
		13 NUMBER OF PAGES 329
		15 SECURITY CLASS. (of this report) UNCLASSIFIED
		15a. DECLASSIFICATION/DOWNGRADING SCHEDULE N/A
16 DISTRIBUTION STATEMENT (of this Report) Approved for public release; distribution unlimited.		
17 DISTRIBUTION STATEMENT (of the abstract entered in Block 20, if different from Report)		
18 SUPPLEMENTARY NOTES Available in DDC		
19 KEY WORDS (Continue on reverse side if necessary and identify by block number) <div style="display: flex; justify-content: space-between;"> <div> wind tunnel model tests influences support (sting) </div> <div> aerodynamic loads store (captive) F-4C </div> <div> aircraft (parent) </div> </div>		
20 ABSTRACT (Continue on reverse side if necessary and identify by block number) <p>In a series of wind tunnel tests, measurements were made of the aerodynamic loads acting on eight different store configurations mounted in the external captive position on a one-twentieth-scale model of the F-4C aircraft. Store models included blunt and contoured afterbody shapes, stable and unstable designs, and large (one per pylon) and small (rack-mounted) configurations. The tests were conducted in an effort to evaluate sting effects on captive</p>		

UNCLASSIFIED

UNCLASSIFIED

20. ABSTRACT (Continued)

store loads. Sting effects were considered to consist of two contributions: the effect of altering the afterbody of a store to allow insertion of a sting, and the effect of the presence of the sting. Altering the afterbody of an unstable store influenced captive loads less than altering a stable configuration. It was also determined that the presence of a sting affected most the pitching and yawing moments. It is believed that both altering the afterbody and the presence of a sting influence the loads acting on the store by changing the pressure distribution over the afterbody. All effects were dependent on position of the store in the flow field of the aircraft. Throughout variations in Mach number, angle of attack, and position in the flow field rolling moment was essentially insensitive to either alterations of the afterbody or the presence of a sting.

PREFACE

The work reported herein was conducted by the Arnold Engineering Development Center (AEDC), Air Force Systems Command (AFSC), at the request of the Air Force Armament Laboratory (AFATL), under Program Element 62602F, Project 2567. The monitor of the project was Capt. Visi Arajs, AFATL (DLJC). The results were obtained by ARO, Inc. (a subsidiary of Sverdrup & Parcel and Associates, Inc.), contract operator of AEDC, (AFSC), Arnold Air Force Station, Tennessee. The work was done under ARO Project Numbers PF219, PF419, and P32A-35A. The author of this report was R. E. Dix, ARO, Inc. Analysis of the data was completed in June 1975, and the manuscript (ARO Control No. ARO-PWT-TR-75-95) was submitted for publication on June 26, 1975.

CONTENTS

	<u>Page</u>
1.0 INTRODUCTION	9
2.0 EXPERIMENTAL APPARATUS	
2.1 Test Facility	10
2.2 Models	10
2.3 Instrumentation	13
3.0 DESCRIPTION OF TESTS	
3.1 Flow Conditions and Test Procedures	13
3.2 Corrections	13
3.3 Precision of Measurements	14
4.0 DISCUSSION OF RESULTS	14
4.1 Presence of a Sting	15
4.2 Alteration of the Afterbody	21
5.0 CONCLUSIONS	25
REFERENCES	26

ILLUSTRATIONS

Figure

1. Two Methods of Supporting a Store in the Captive Position in Wind Tunnel Tests	29
2. Schematic Illustration of the Captive Trajectory System	30
3. Schematic Illustration of a Typical Model Installation in Tunnel 4T	31
4. Five-Percent Scale Model of the F-4C Aircraft	32
5. Details of the Models of the Multiple and Triple Ejector Racks	33
6. Nomenclature of Ejector Rack Stations	34
7. Details of the Models of the F-4C Pylons	35
8. Dimensions of Pylon-Mounted Store Models	36
9. Dimensions of Rack-Mounted Store Models	39
10. Typical Installation of an Internal Balance-Supporting Bracket	42
11. Details of the Dummy Stings	43
12. Sketch of the Dummy Sting Support System	44
13. Comparison of Dummy Sting and Active Sting Installations	45

<u>Figure</u>	<u>Page</u>
14. Sting-Induced Aerodynamic Load Increments as a Function of Angle of Attack, Unstable Pylon-Mounted Store, C-L Pylon	46
15. Sting-Induced Aerodynamic Load Increments as a Function of Angle of Attack, Unstable Pylon-Mounted Stores, LIB Pylon	52
16. Sting-Induced Aerodynamic Load Increments as a Function of Angle of Attack, Unstable Pylon-Mounted Store, LOB Pylon	58
17. Sting-Induced Aerodynamic Load Increments as a Function of Angle of Attack, Stable Pylon-Mounted Store, C-L Pylon	64
18. Sting-Induced Aerodynamic Load Increments as a Function of Angle of Attack, Stable Pylon-Mounted Stores, LIB Pylon	70
19. Sting-Induced Aerodynamic Load Increments as a Function of Angle of Attack, Stable Pylon-Mounted Store, LOB Pylon	76
20. Sting-Induced Aerodynamic Load Increments at Zero Angle of Attack as a Function of Pylon Position, Unstable Stores	82
21. Sting-Induced Aerodynamic Load Increments at Zero Angle of Attack as a Function of Pylon Position, Stable Pylon-Mounted Stores	88
22. Sting-Induced Aerodynamic Load Increments at Zero Angle of Attack as a Function of Mach Number, Unstable Pylon-Mounted Stores	94
23. Sting-Induced Aerodynamic Load Increments at Zero Angle of Attack as a Function of Mach Number, Stable Pylon-Mounted Stores	100
24. Sting-Induced Aerodynamic Load Increments as a Function of Angle of Attack, Unstable Rack-Mounted Store, MER Station 1, C-L Pylon	106
25. Sting-Induced Aerodynamic Load Increments as a Function of Angle of Attack, Unstable Rack-Mounted Store, MER Station 2, C-L Pylon	112
26. Sting-Induced Aerodynamic Load Increments as a Function of Angle of Attack, Unstable Rack-Mounted Store, MER Station 3, C-L Pylon	118

<u>Figure</u>	<u>Page</u>
27. Sting-Induced Aerodynamic Load Increments as a Function of Angle of Attack, Unstable Rack-Mounted Store, MER Station 4, C-L Pylon	124
28. Sting-Induced Aerodynamic Load Increments as a Function of Angle of Attack, Unstable Rack-Mounted Store, MER Station 1, LOB Pylon	130
29. Sting-Induced Aerodynamic Load Increments as a Function of Angle of Attack, Unstable Rack-Mounted Store, MER Station 2, LOB Pylon	136
30. Sting-Induced Aerodynamic Load Increments as a Function of Angle of Attack, Unstable Rack-Mounted Store, MER Station 3, LOB Pylon	142
31. Sting-Induced Aerodynamic Load Increments as a Function of Angle of Attack, Unstable Rack-Mounted Store, MER Station 4, LOB Pylon	148
32. Sting-Induced Aerodynamic Load Increments as a Function of Angle of Attack, Unstable Rack-Mounted Store, TER Stations 2 and 3, LIB Pylon	154
33. Sting-Induced Aerodynamic Load Increments as a Function of Angle of Attack, Stable Rack-Mounted Store, MER Station 1, C-L Pylon	160
34. Sting-Induced Aerodynamic Load Increments as a Function of Angle of Attack, Stable Rack-Mounted Store, MER Station 2, C-L Pylon	166
35. Sting-Induced Aerodynamic Load Increments as a Function of Angle of Attack, Stable Rack-Mounted Store, MER Station 3, C-L Pylon	172
36. Sting-Induced Aerodynamic Load Increments as a Function of Angle of Attack, Stable Rack-Mounted Store, MER Station 4, C-L Pylon	178
37. Sting-Induced Aerodynamic Load Increments as a Function of Angle of Attack, Stable Rack-Mounted Store, MER Station 1, LOB Pylon	184
38. Sting-Induced Aerodynamic Load Increments as a Function of Angle of Attack, Stable Rack-Mounted Store, MER Station 2, LOB Pylon	190
39. Sting-Induced Aerodynamic Load Increments as a Function of Angle of Attack, Stable Rack-Mounted Store, MER Station 3, LOB Pylon	196

<u>Figure</u>	<u>Page</u>
40. Sting-Induced Aerodynamic Load Increments as a Function of Angle of Attack, Stable Rack-Mounted Store, MER Station 4, LOB Pylon	202
41. Sting-Induced Aerodynamic Load Increments as a Function of Angle of Attack, Stable Rack-Mounted Store, TER Station 3, LIB Pylon	208
42. Sting-Induced Aerodynamic Load Increments as a Function of Mach Number, Unstable Rack-Mounted Store, C-L and LOB Pylon	214
43. Sting-Induced Aerodynamic Load Increments as a Function of Mach Number, Unstable Rack-Mounted Store, LIB Pylon	220
44. Sting-Induced Aerodynamic Load Increments as a Function of Mach Number, Stable Rack-Mounted Store, LIB Pylon	226
45. Sting-Induced Aerodynamic Load Increments as a Function of Mach Number, Stable Rack-Mounted Store, C-L and LOB Pylon	227
46. Aerodynamic Load Increments Attributable to Truncation of the Afterbody of an Unstable Pylon-Mounted Store, BLU-1 Store with AB2, LIB Pylon	233
47. Aerodynamic Load Increments Attributable to Truncation of the Afterbody of Unstable Pylon-Mounted Store, BLU-1 Store with AB3, LIB Pylon	239
48. Aerodynamic Load Increments Attributable to Truncation of the Afterbody of Unstable Pylon-Mounted Store, BLU-1 Store with AB4, LIB Pylon	245
49. Aerodynamic Load Increments Attributable to Reshaping the Afterbody of an Unstable Pylon-Mounted Store, BLU-1 Store with AB5, LIB Pylon	251
50. Aerodynamic Load Increments Attributable to Cylindrical Distortion of the Afterbody of a Stable Pylon-Mounted Store, M-118 Store with AB2, LIB Pylon	257
51. Aerodynamic Load Increments Attributable to Cylindrical Distortion of the Afterbody of a Stable Pylon-Mounted Store, M-118 Store with AB3, LIB Pylon	263
52. Aerodynamic Load Increments Attributable to Cylindrical Distortion of the Afterbody of a Stable Pylon-Mounted Store, M-118 Store with AB4, LIB Pylon	269

<u>Figure</u>	<u>Page</u>
53. Aerodynamic Load Increments Attributable to Truncation of the Afterbody of an Unstable Rack-Mounted Store, CBU-46 with AB2, TER Station 2, LIB Pylon	275
54. Aerodynamic Load Increments Attributable to Truncation of the Afterbody of an Unstable Rack-Mounted Store, CBU-46 with AB3, TER Station 2, LIB Pylon	281
55. Aerodynamic Load Increments Attributable to Truncation of the Afterbody of an Unstable Rack-Mounted Store, CBU-46 with AB4, TER Station 2, LIB Pylon	287
56. Aerodynamic Load Increments Attributable to Truncation of the Afterbody of an Unstable Rack-Mounted Store, CBU-46 with AB2, TER Station 3, LIB Pylon	293
57. Aerodynamic Load Increments Attributable to Truncation of the Afterbody of an Unstable Rack-Mounted Store, CBU-46 with AB4, TER Station 3, LIB Pylon	299
58. Aerodynamic Load Increments Attributable to Cylindrical Distortion of the Afterbody of a Stable Rack-Mounted Store, MK-83 with AB2, TER Station 3, LIB Pylon	305
59. Aerodynamic Load Increments Attributable to Cylindrical Distortion of the Afterbody of a Stable Rack-Mounted Store, MK-83 with AB3, TER Station 3, LIB Pylon	311

TABLES

1. Miscellaneous Dimensions of Store Models	317
2. Uncertainty Intervals in Force and Moment Coefficients for Store Models	319

APPENDIX

A. Effects of Dummy Sting Misalignment	321
NOMENCLATURE	328

1.0 INTRODUCTION

A large and varied assortment of engines, fuel tanks, mission assistance pods, and weapons can be stored aboard contemporary aircraft. In many cases, these stores are attached to the exterior of the carrier, or parent aircraft. Therefore, prior to routine flight operations, it is necessary to evaluate the aerodynamic and functional compatibility of a specified aircraft-store configuration. Two questions of compatibility that must be answered are: (1) can the aircraft be flown safely with the captive store, and (2) can the store be separated safely from the aircraft during flight? Answers to these questions are customarily based on data acquired during tests of appropriate models in wind tunnels. As part of the answer to the first question, aerodynamic loads acting on the store in the captive position must be measured over an appropriate range of parameters describing both the physical configuration and the flight regime. In the majority of wind tunnel tests, captive loads are measured using conventional "force" test techniques. The reactions of a strain-gage balance mounted within the store to the actions of the store under the influence of the flow field are monitored as a measure of the aerodynamic forces acting on the store. Several "techniques" of supporting a store in the captive position have been used, but all of these techniques may be classified as applications of one of two "methods," either the internal balance support method, or the dual support method, as illustrated in Fig. 1, and discussed in Ref. 1.

To aid in answering the second question, the captive trajectory system (CTS), a dual-support technique, has been developed. Using the CTS, a store can be moved in six degrees of freedom with respect to the aircraft. Electrical signals commanding movements of the store result from calculations performed by a digital computer. Input information for the computer consists of measurements of parameters describing the flow and the output signals from the strain-gage balance mounted within the store. A diagram of the CTS is provided in Fig. 2. A more detailed discussion of the CTS is available in Ref. 2.

An interest in identifying and evaluating the effects of using either of the above methods to support the store in the captive position led to the study described herein. It was recognized that when a store was supported in the captive position using the internal-support method, the resulting configuration would be firmly held at the correct distance from the aircraft, and with no alteration of the afterbody. The sole distortion of the correct configuration would be the bracket protruding through the upper surface of the store body. It was also clear that, when using the dual-support method, alteration of the afterbody of many stores was required to accommodate the sting, and an unrealistic gap was maintained between the two sting-supported bodies to prevent physical contact during testing.

A series of wind tunnel tests has been conducted in an effort to evaluate all of the above effects for eight stores carried by a typical contemporary fighter aircraft. Only the effects of the presence of a sting and of altering the shape of the afterbody are presented herein.

2.0 EXPERIMENTAL APPARATUS

2.1 TEST FACILITY

Tests were conducted in the Aerodynamic Wind Tunnel (4T) of the Propulsion Wind Tunnel Facility, a closed-circuit design in which continuous flow can be maintained at various density settings. Mach number in the free stream can be set at any value from 0.2 to 1.3. Nozzle blocks can be installed to provide discrete Mach numbers of 1.6 and 2.0. Stagnation pressure can be established at values from 300 to 3,700 psfa. The test section is 4 ft square, 12.5 ft long, and is equipped with perforated walls that can be adjusted by remote control to provide a porosity in the nominal range of from zero to ten-percent open area. A desired fraction of the flow through the test section can be evacuated through the porous walls into a plenum chamber in which the test section is completely enclosed.

Models are supported in the test section with a conventional strut-sting system. A model can be pitched from approximately -12 to 28 deg with respect to the centerline of the tunnel. A capability of rolling a model from -180 to 180 deg about the centerline of the sting is also available. An illustration of a typical model installed for testing using the CTS is presented in Fig. 3.

2.2 MODELS

2.2.1 Aircraft

Data were obtained for realistic aircraft and store configurations rather than for highly simplified and idealized wing-body shapes. The F-4C was selected as parent aircraft (Fig. 4). A primary reason for the selection was the capability of the F-4C to carry both pylon-mounted and rack-mounted stores. ("Pylon-mounted" stores include rather large stores. In flight, only one of these stores is normally mounted on a pylon. "Rack-mounted" stores include rather small stores, several of which can be carried on a pylon through the use of either a triple ejector rack (TER), or a multiple ejector rack (MER), (Fig. 5)). Several other specific factors also influenced the selection: (1) the F-4C is a low-wing configuration and, as such, the flow field in the vicinity of the stores is uncomplicated by sidewash from the fuselage; (2) an extensive collection of data was available from

previous flow-field and store separation tests using the F-4C; and (3) a model of suitable scale was available.

For the tests involving pylon-mounted stores, the right-wing pylons were omitted, but the centerline (C-L), left inboard (LIB), and left outboard (LOB) pylons were always installed. During the tests involving rack-mounted stores, the right inboard and right outboard pylons were also installed. Pylon-mounted store models were tested on only one pylon at a time, with other pylons empty. Rack-mounted store models were tested on only one specified rack, mounted on only one specified pylon at a time, with other pylons empty. On the rack, however, the store model with the internal balance was moved from station to station in a realistic release sequence. All other appropriate rack stations were fitted with dummy (empty) models of the store configuration. An example of MER loading would be as follows: with the balance-supported store model on MER station 4 (see Fig. 6 for rack station numbers), stations 1, 2, and 3 would be empty, and dummy models would be mounted on stations 5 and 6. When testing models on the TER, only stations 2 and 3 were used; station 1 was always empty. A dummy model was always installed on the TER station opposite the station on which the balance-supported model was installed.

Additional details of the pylons are presented in Fig. 7. Throughout all tests, the tail surfaces of the F-4C model were omitted. Airflow was allowed through the simulated engine ducts with cruise-configuration exhaust ports installed.

2.2.2 Stores

During the process of selecting store configurations for the investigation, stores were classified first as either pylon-mounted or rack-mounted, as defined in Section 2.2.1. Within these two categories, stores were further classified as either stable or unstable. Further, two stores were selected from each of these four subcategories, one with a blunted-base design that would accommodate a sting without alteration of the afterbody, and one with an afterbody shape that would require significant alteration to allow insertion of a sting. Hence, eight stores were tested during the investigation.

Pylon-mounted stores included the unstable Black Crow gun pod, the stable Hard Structure Munition (HSM), the unstable BLU-1 bomb, and the stable M-118 bomb, all depicted in Fig. 8. Rack-mounted stores included the unstable All-Altitude Spin-Projected dispenser (ASP), the stable CBU-24 bomb, the unstable CBU-46 (SUU-7) launcher pod, and the stable MK-83 bomb, all depicted in Fig. 9. Dimensions of the store models are presented in Table 1.

2.2.3 Internal Balance Support (IBS) Brackets

Store models on which aerodynamic loads were being measured were securely fastened to one end of a six-component strain-gage balance. The other end of the balance was firmly supported through use of a rigid bracket protruding through the upper surface of the store model and tightly attached to the appropriate pylon or rack. To allow unrestricted reaction of the store model (hence the balance) to aerodynamic loading, the opening in the upper surface of the store model through which the bracket protruded was made large enough to ensure a clearance of at least 0.050 in. around the bracket. A drawing of a typical installation is presented in Fig. 10. The base of each bracket-mounted store model was either fabricated as solid, or later filled in with a plug to prevent flow through the interior of the store model and past the balance.

2.2.4 Stings

Two sets of dummy stings were used, one set for each of the fundamental categories of stores identified, i.e., pylon-mounted and rack-mounted. For the larger, pylon-mounted stores, three stings were used: one of 0.4-in. diam, one of 0.5-in. diam, and one of 0.6-in. diam. For the smaller, rack-mounted stores, three stings were also used, but only of 0.25-, 0.325-, and 0.40-in. diam, respectively. These stings represented typical sizes used with the selected (or similar) store models. No attempt was intended to repeat, in detail, other investigations of sting effects, e.g., Refs. 3 and 4. Instead, to determine the effects of just the presence of a sting, the above limited but practical range of values of sting diameter was adopted. As a result, the constant diameter of any sting was, in all cases, 0.31 to 0.67 of the maximum diameter of any store model with which it was tested (or, correspondingly, 0.31 to 0.92 of the base diameter, see Table 1).

Location of the conical "flare" of the sting was likewise not a basic parameter of the study. Following the recommendations made in Ref. 4, the flare was located at least five base diameters downstream of the base of any store (actually 5.1 to 12.3 base diameters). Dimensions of the stings are presented in Fig. 11.

A structural support for the dummy stings was mounted on the sting supporting the parent aircraft as depicted in Fig. 12. Adjustment of both the position and the attitude of a dummy sting was possible for six degrees of freedom: streamwise, lateral, and vertical translations, and pitch, yaw, and roll angular deflections, even though roll was superfluous. To assure isolation of the effect of the presence of the sting, the supporting structure remained in position throughout the tests, with just the dummy sting removed for the "no-sting" configurations. A considerable amount of test time was saved by having the dummy sting support attached to the parent-aircraft sting, since changes in attitude of

the dummy sting duplicated (and were simultaneous with) changes in attitude of the parent aircraft. A comparison of an actual sting-mounted configuration with the corresponding dummy sting installation is presented in Fig. 13.

2.3 INSTRUMENTATION

Conventional strain-gage balances were used to sense the aerodynamic forces acting on the store models. Six components of forces and moments were resolved, as described in Section 3.3.

The gravimetric angle of attack of the F-4C aircraft model was sensed with an oil-damped pendulum fitted with strain gages and mounted in the aircraft model. Using the internal sensor for setting and recording the angle of attack of the aircraft model rather than the purely mechanical indication associated with the standard tunnel pitch sector, it was unnecessary to separately account for deflections of the aircraft model-sting combination.

3.0 DESCRIPTION OF TESTS

3.1 FLOW CONDITIONS AND TEST PROCEDURES

Aerodynamic forces and moments acting on the captive, bracket-mounted store models were measured at nominal free-stream Mach numbers of 0.6, 0.8, 0.9, 1.1, and 1.2 for pylon-mounted stores and 0.6, 0.9, 1.1, and 1.2 for rack-mounted stores. Reynolds number was maintained at approximately 3.5×10^6 per foot throughout the tests. Porosity of the test section walls was varied in a manner determined through previous calibration studies in the tunnel to minimize wall interference and buoyancy effects (Refs. 5 and 6).

During a typical run, after establishing test conditions, data were recorded while the angle of attack of the aircraft model was varied from -4 to 12 deg in discrete 1- or 2-deg increments. After all aircraft attitudes had been set, a new value of Mach number was established, and the sequence of angles of attack was repeated.

3.2 CORRECTIONS

As stated in Section 2.3, the attitude of the aircraft model was set using a gravity-sensing device mounted in the model. Therefore, no correction was necessary for deflections of the aircraft model with respect to the sting, or deflections of the sting with respect to the pitching sector. For the balances used inside the store models, calibrations of the deflections of the mounting point of the store as a function of impressed

load were used to identify contributions of balance flexibility to the attitude of the store model. The calibration data were used in the data reduction equations to derive the correct gravimetric attitude of the store model. (It is prudent to recall here that all store models were installed with a 1-deg nose-down attitude with respect to the waterline of the aircraft model, see Fig. 7.) No corrections were made in either aircraft or store model attitude to account for flow angularity in the free stream.

3.3 PRECISION OF MEASUREMENTS

Uncertainty intervals (including 95 percent of the calibration data) for the basic flow parameters, i.e., $p_{t_{\infty}}$ and M_{∞} , were estimated from both repeat calibrations of the instrumentation and the repeatability and uniformity of the free-stream flow in the test section during tunnel calibration. Uncertainty intervals for the instrumentation systems were estimated from repeated calibrations of the systems using secondary standards with accuracies traceable to the National Bureau of Standards. Uncertainty intervals for values of forces and moments derived from the output of the balance gages were determined from a root-mean-square analysis of the calibration data for the balance. Values of the above uncertainties were combined using the Taylor series method of error propagation to determine the precision of the force and moment coefficients. Values of the uncertainty intervals for the force and moment coefficients for all models tested are presented in Table 2.

For all flow conditions, the uncertainty interval for gravimetric angle of attack was ± 0.1 deg. However, two uncertainty intervals must be cited for Mach number. First, the uncertainty in setting Mach number was ± 0.002 , reflecting instrumentation capabilities. Second, there was the uncertainty in Mach number in the free stream, attributable to non-uniform flow. Values of the resultant uncertainty interval for Mach number are presented below:

<u>Nominal M_{∞}</u>	<u>Uncertainty Interval for M_{∞}</u>
0.6	± 0.005
0.8	± 0.005
0.9	± 0.003
1.1	± 0.006
1.2	± 0.010

4.0 DISCUSSION OF RESULTS

Even though the size, shape, and salient design features of both aircraft and store models were correctly scaled, the store models were mounted on the aircraft model in positions that may not correspond to accepted flight practice. For instance, pylon and

rack installations were certainly not realistic, since the aircraft model was loaded asymmetrically. Further, during tests of pylon-mounted store models, an excessive gap was maintained between store models and pylons (2.5 in. full scale), while throughout the tests of rack-mounted store models the gap was varied slightly from store to store. Equivalent full-scale gaps were 0.8 in. for the ASP and CBU-24 stores, 1.0 in. for the CBU-46 (SUU-7) store, and 1.8 in. for the MK-83 bomb. These gaps were maintained throughout the tests. To assure valid intercomparisons of test results, the dummy sting supporting structure (Section 2.2.4) remained in place for all tests; for no-sting configurations, only the dummy sting was removed.

The test data are presented in an increment format, i.e., the effects on loads attributable to an isolated change in configuration are presented as differences between the altered configuration and the unaltered configuration.

4.1 PRESENCE OF A STING

4.1.1 Pylon-Mounted Store Configurations

The isolated effects of simply the presence of a sting were investigated by testing store configurations with afterbodies that require no alteration for mounting on a sting. By testing such a configuration both with and without a dummy sting, the increment in aerodynamic loading of the store model attributable to the presence of the sting was determined. Although the study included only two pylon-mounted store configurations with afterbodies requiring no alteration for mounting on a sting, viz., the unstable Black Crow and the stable HSM, data definitive of the presence of a sting were also gleaned from tests of the two pylon-mounted store configurations that do require alteration of the afterbody for sting mounting, i.e., the BLU-1 and the M-118. These two configurations were considered to be simply "other" store configurations but were tested on only the left inboard pylon. The Black Crow and HSM configurations were tested on the centerline, left inboard, and left outboard pylons.

4.1.1.1 Influence of Angle of Attack

For the unstable stores, increments in the force and moment coefficients attributable to the presence of a sting are presented as functions of angle of attack of the store model in Figs. 14 through 16. In the case of the blunted-base Black Crow, the sting effect is virtually insensitive to angle of attack, except for pitching and yawing moments when mounted on the left inboard pylon, Figs. 15e and 15f, respectively. Since the normal- and side-force effects are not sensitive to angle of attack, the observed dependency for the moment effects must be attributable to a change in the pressure distribution over the store model. Furthermore, since the moment increments appear to be sensitive to

angle of attack only for subsonic Mach numbers, it is likely that the presence of the sting causes changes in the flow pattern in the base region that are transmitted forward through the boundary layer, thereby causing adjustments in the pressure distribution over the store model. Similar, but less severe, influences were observed when the store model was mounted on the left outboard pylon, Figs. 16e and 16f, but not at all on the centerline pylon. It is possible that in the compound vertical-sidewash flow field surrounding the inboard and outboard pylons, the dummy sting deflected out of alignment with the axis of the store model as a function of angle of attack, thereby causing more disturbance of the flow at the base of the store than would result with a perfectly aligned (and nondeflecting) sting. Deflections of the dummy sting were observed in several cases, prompting an ancillary investigation of one such configuration (see Appendix A).

Sting effect increments for the stable store configurations are presented in Figs. 17 through 19. For the blunted-base HSM, the sting effect on normal, side, and axial forces is not a function of angle of attack (Figs. 17a, b, and c; 18a, b, and c; and 19a, b, and c). Both pitching- and yawing-moment increments, however, vary with angle of attack at all pylon stations, primarily at the supersonic Mach numbers (Figs. 17e and f; 18e and f; and 19e and f). In these cases, shock systems associated with adjacent pylons could be impinging on the store model. By comparing Figs. 14a, 15a, and 16a with 17a, 18a and 19a, respectively, it is noted that, in general, the sting effect on normal force is less a function of angle of attack for the stable store configurations than for the unstable store configurations. Conversely, the sting effect on pitching and yawing moments is more a function of angle of attack for the stable store configurations than for the unstable store configurations (cf. Figs. 14e and f, 15e and f, and 16e and f with Figs. 17e and f, 18e and f, and 19e and f, respectively). These observations indicate a dominant influence on the aerodynamic loading of a store of the presence of stabilizing surfaces in the afterbody region despite the presence of a sting.

In general, data acquired using a small sting ($D_s < 0.5 D_B$) include effects not only smaller in magnitude, but also less sensitive to angle of attack than data acquired using a large sting. Further, from Figs. 14d, 15d, 16d, 17d, 18d, and 19d it is clear that rolling moment is insensitive to the presence of sting.

4.1.1.2 Influence of Position in the Flow Field

In Figs. 20 and 21, the increments in captive loads attributable to the presence of a sting are presented as a function of pylon position in the flow field. Only data for zero angle of attack of the store model are presented. It should be noted that changing pylon position involves both a spanwise and a chordwise shift in position of the store as indicated in Fig. 4.

For the unstable store models (Fig. 20), the effect of the presence of a sting on normal force, pitching moment, and yawing moment varied substantially with position in the flow field. The effects generally become more severe as the store model is moved from the centerline position (where a laterally symmetrical flow field exists) to the inboard and outboard positions (where there is substantial sidewash in addition to the up or downwash, Ref. 7). Since the pitching- and yawing-moment increments vary substantially with position in the flow field, but the force increments remain essentially constant, it is again deduced that the primary influence of the presence of the sting is to alter the pressure distribution over the store.

Far less effect of position is evident for the stable stores, Fig. 21. As in the case of the unstable stores, pitching- and yawing-moment increments are the most dependent on position; however, it is also important to note that the increments are, in nearly all cases, within the precision of the measurement. Nevertheless, the sting effect is clearly very significant at the outboard pylon position, where both magnitude and sign of the normal-force, pitching-moment, side-force, and yawing-moment increments depend on the diameter of the sting. The critical dependency is probably attributable to the presence of severe upwash in the vicinity of the plane of the base of the store model, just at the location of the face of the dummy sting (Ref. 7). A strong upwash at the face of the sting could cause a deflection of the sting toward the aircraft, creating an increase in pressure over the extreme after portion of the upper surface of the store model. An increase in positive pitching moment would follow, explaining the increase in pitching-moment increment noted in Fig. 21e. Since the flow field in which a store is carried is clearly determined by the configuration of both the parent aircraft and the store, it is not possible to predict that similar trends in sting effects will occur for other stores and/or other aircraft.

4.1.1.3 Effect of Mach Number

Variation of the sting effect increments with Mach number is shown in Figs. 22 and 23. Only data for zero angle of attack of the store model are presented. For both unstable and stable store configurations, it is apparent that the sting effect generally decreases with Mach number for all load components on the centerline and outboard pylons. On the inboard pylon, however, while there is no strong effect of Mach number, the absolute value of the sting increment tends to decrease with increasing Mach number for all load components except pitching and yawing moments. During the test series, there were adjacent, empty pylons installed on only one side of either the centerline or outboard pylons but on both sides of the inboard pylon. Bow shocks forming at the leading edge of the empty pylons would intersect a store model on the inboard pylon from both sides, but store models mounted on either of the other two pylons could receive interference

from shocks on only one side (Fig. 4). It is even conceivable that a shock from the leading edge of the outboard pylon could intersect only the dummy sting downstream of the inboard store model, causing a misalignment of the sting, with concomitant distortion of the pressure distribution on the captive store model. The variations in pitching- and yawing-moment increments at supersonic Mach numbers might be explained in this manner.

At subsonic conditions, the stronger effects of the presence of a sting are probably attributable to transmittal throughout the flow field of the changes in the wake region. Throughout the range of Mach number for the tests, however, it is clear that the sting effect is only slightly a function of Mach number, generally decreasing with increasing Mach number.

4.1.2 Rack-Mounted Store Configurations

As in the case of pylon-mounted store configurations, the study included two configurations with bases large enough to allow unaltered mounting on a sting, viz., the unstable ASP, and the stable CBU-24. However, data were acquired for two other stores with altered afterbody shapes, the unstable CBU-46 and the stable MK-83, by simply considering the altered configurations to be other store configurations. The ASP and CBU-24 models were tested on stations 2 through 4 of the MER-10A ejector rack and on both the centerline and left outboard pylons. The CBU-46 and MK-83 models were tested on stations 2 and 3 of the TER-9A ejector rack, left inboard pylon.

4.1.2.1 Influence of Angle of Attack

Increments in the force and moment coefficients attributable to the presence of a sting are presented in Figs. 24 through 41 as functions of the angle of attack of the store model. Sting effect increments for the blunted-base ASP are essentially independent of angle of attack on all MER stations, on both the centerline and outboard pylons (Figs. 24 through 31). In only a few unrelated cases the axial-force increment and the pitching- and yawing-moment increments indicate a substantial sensitivity to angle of attack (Figs. 24c, 25e, 26f, 27e, 28c, 28e, 29f, and 31f). In these instances, it is possible that the dummy sting deflected in a manner similar to that discussed in Section 4.1.1.1. Just as for the pylon-mounted stores, relatively small changes in normal and side forces coincide with disproportionately large changes in pitching and yawing moments, indicating that the presence of a sting affects primarily the pressure distribution over the aft portion of the store model. For a given pylon, the sting effect increments for rack-mounted unstable store configurations at subsonic Mach number are different from those of pylon-mounted unstable store configurations (cf. Figs. 25 and 29 with Figs. 14 and 16). This is a credible result in view of the completely different physical environment associated with a cluster of bodies as opposed to a single large body. Clearly, the detailed characteristics of the

sting effect depend intimately upon the characteristics of the local flow field. In supersonic flow, however, sting effects for both pylon-mounted and rack-mounted store configurations are virtually independent of angle of attack.

Supplementary data are available from tests of the CBU-46 configuration on TER stations 2 and 3 on the left inboard pylon (Fig. 32). It is apparent that the effect of the presence of a sting is almost completely independent of angle of attack. In fact, there is almost no effect at all of the presence of a sting. Similar results were obtained for the pylon-mounted unstable store configurations on the left inboard pylon (cf. Fig. 32 with Fig. 15).

Sting effect increments for the two stable rack-mounted store's, i.e., the CBU-24 and the MK-83, are presented in Figs. 33 through 41. These data reflect somewhat greater sensitivity of the sting effect to angle of attack than corresponding data for the unstable configurations. Since the afterbody of the CBU-24 store is tapered as well as finned, and since even the smallest sting diameter is such a large fraction of the base diameter, any misalignment of the dummy sting would exert a strong influence on the flow in the afterbody region. By comparing normal- and side-force increments with corresponding pitching- and yawing-moment increments (the (a) and (b) portions with the (e) and (f) portions, respectively, of Figs. 32 through 40), it again appears that the primary effect of the presence of the sting is on the pressure distribution over the afterbody of the store model. For example, in Figs. 35 and 36 a deflection or misalignment of the large-diameter dummy sting in the negative lateral direction could explain both the large positive increment in side force and the corresponding large negative increment in yawing moment on MER stations 3 and 4 on the centerline pylon. It is clear from the results of the tests using even the small-diameter sting that the sting effect is substantially more sensitive to angle of attack than for the unstable rack-mounted store configurations. This observation is in agreement with a result reported by Hill in Ref. 9 for the M-117, a store with similar physical features.

Sting-induced increments for the MK-83 mounted on TER station 3 on the left inboard pylon are presented in Fig. 41. Far less effect of angle of attack is apparent than for the CBU-24 on either the centerline or outboard pylons (cf. Fig. 41 with Figs. 33 through 40). Domination of the total loading by flow conditions over the afterbody is again demonstrated by the disproportionate changes in pitching and yawing moments that correspond to minor changes in normal and side forces (Figs. 41e and f and a and b, respectively).

Two general comments may be made with respect to the data for the rack-mounted store configurations. First, just as in the case of the pylon-mounted store configurations,

the effects of the presence of a sting are not only of smaller magnitude but also less sensitive to angle of attack when $D_S < 0.5 D_B$. Second, from the (d) portion of Figs. 24 through 41, it is clear that rolling moment is insensitive to the presence of a sting.

4.1.2.2 Influence of Position in the Flow Field

Data were obtained for the ASP and CBU-24 configurations at identical MER stations on both the centerline and left outboard pylons, Figs. 24 through 40. Comparing Figs. 24 through 27 with Figs. 28 through 31, respectively, reveals little difference in the sting effect for the unstable ASP store on either the centerline or left outboard pylons except for the pitching and yawing moments. At the subsonic condition ($M_\infty = 0.6$) the pitching- and yawing-moment increments for the store model mounted on MER station 4 vary substantially from the centerline to the left outboard pylon. For this case, however, the data for the basic configuration (without dummy sting) vary also; hence, deflection of the dummy sting is not indicated. The differences are considered to be attributable to the different flow field to which the store model is exposed on the outboard pylon as compared to the centerline pylon.

Comparing Figs. 33 through 36 with Figs. 37 through 40 for the stable CBU-24 reveals significantly different results at the same MER station on the different pylons, a result also described in Ref. 9. The sting effects for all components except axial force and rolling moment change significantly in magnitude and/or sign. Recalling corresponding data for the pylon-mounted store configuration (the HSM), Figs. 17 and 19, it is clear that the effects of the presence of a sting on the relatively large pylon-mounted store model are not as dependent on position in the flow field as for the smaller, rack-mounted store model (the CBU-24). Hence, few generalizations can be made concerning the character of sting effects on both pylon-mounted and rack-mounted store configurations. Two general observations may be made, however: (1) throughout the flow field, the sting effect on axial force is negative and largely insensitive to angle of attack and (2) rolling moment is unaffected by the presence of a sting.

4.1.2.3 Influence of Mach Number

Sting effect increments as a function of Mach number are presented in Figs. 42 through 45. Only data for zero angle of attack of the store model are presented. The normal-force increment tends to decrease with increasing Mach number for all configurations except the CBU-24 (Fig. 45a). The flow over the tapered and finned afterbody of the CBU-24 is significantly disturbed by the presence of a sting. The largest and most erratic Mach number effects occur with the largest sting. It is possible that local shock wave systems cause deflection of the sting out of alignment with the base of the store model. With the exception of the CBU-24 again, the sting effect on side force is not a significant

function of Mach number (Figs. 42b, 43b, 44b, and 45b). Sting effect increments in the pitching and yawing moments generally decrease with increasing Mach number for the unstable stores (Figs. 42e and f, and 43e and f) but are quite erratic for the stable stores at transonic Mach numbers (Figs. 44e and f and 45e and f). Deflections of the dummy sting are suspected in these cases.

The sting effect on axial force generally decreases with Mach number for all of the rack-mounted stores (Figs. 42c, 43c, 44c, and 45c), regardless of location. Rolling moment is uniformly insensitive to the presence of a sting at all Mach numbers (Figs. 42d, 43d, 44d, and 45d).

4.2 ALTERATION OF THE AFTERBODY

In addition to the direct effect of the presence of a sting, data accumulated during tests of sting-mounted models may include an indirect effect, the effect of altering the afterbody of the model to accommodate the presence of the sting. Alterations may be made in many ways, but only two methods were evaluated in this study: simple truncation, and cylindrical shape distortion. Simple truncation of the afterbody to create a base diameter large enough to accommodate a sting is primarily adaptable to unstable store configurations. Stable configurations are generally altered by creating, beginning at the base and extending forward, a circular-cylindrical section through which the sting is installed. A cylindrical distortion generally eclipses some of the exposed fin area.

In selecting store configurations for testing, one example of each type of alteration was included within the pylon-mounted and rack-mounted categories. In the pylon-mounted class, the BLU-1 was selected as an example of a store that would normally be altered by simple truncation. Truncations were included for 0.4-, 0.5-, and 0.6-in.-diam stings. In addition, an altered "equivalent" afterbody (both length and shape were altered in such a manner as to maintain the location of the center of pressure) was included for the sake of comparison (Fig. 8c). As an example of cylindrical distortion, the M-118 was selected (Fig. 8d). Decreases in fin area of approximately 16, 25, and 35 percent result for afterbody alterations 2, 3, and 4, respectively. In the rack-mounted category of store configurations, the CBU-46 configuration was selected for truncation (Fig. 9c) and the MK-83 for cylindrical distortion (Fig. 9d). Only two alterations of the MK-83 were tested, corresponding to approximately 33- and 56-percent decreases in fin area (afterbodies 2 and 3, respectively).

In each case, data are presented in an incremental format. Typically, one curve represents the difference in loads between an altered configuration and the corresponding unaltered, or basic, configuration. A second (and occasionally third) curve represents the difference between loads acting on the altered model with a dummy sting in place and

loads acting on the basic, unaltered model without a sting. Measurements of captive loads were made with the models mounted on only the left inboard pylon.

4.2.1 Pylon-Mounted Store Configurations

4.2.1.1 Unstable Configuration-Truncation

Aerodynamic captive load increments attributable to alterations of the unstable BLU-1 store configuration are presented in Figs. 46 through 49. For all configurations and Mach numbers, normal force is distorted by the truncated shape but with little influence of angle of attack in the range of -2 to 5 deg. A notable exception is the "equivalent" afterbody (AB5), Fig. 49a. Not only does the value of the effect of alteration vary with angle of attack, but the sign of the effect changes. The effect of truncation is apparently to decrease the normal force relatively uniformly, while the effect of "tailoring" the afterbody alteration to simulate the unaltered pressure distribution is to increase normal force at negative angles of attack and to decrease normal force at positive angles of attack. Interestingly, a fortuitous result occurs when a dummy sting is added to the truncated afterbody configuration: the presence of the sting tends to compensate for the truncation at subsonic conditions (Figs. 46a, 47a, and 48a). It has been pointed out by Cahn (Ref. 3) that the presence of a sting is accompanied by an increase in base pressure. The data presented in Figs. 46c, 47c, 48c, and 49c are consistent with Cahn's explanation. It is also observed by Cahn that with a sting in place, less turning of the flow at the base is required than for a truncated base without a sting. Hence, with a sting in place at subsonic conditions, it is plausible that little turning of the flow at the base is required, and separation of the flow from the afterbody is delayed. Further, from the pitching-moment increments (Figs. 46e, 47e, 48e, and 49e), a pressure distribution more nearly like the unaltered shape is apparently established. Consistently, at supersonic conditions, the presence of a sting has less compensating effect than at subsonic conditions. A decrease in pitching-moment increment with angle of attack for all truncations is evident but not for the AB5 alteration. This observation suggests caution in altering the shape of a boattail afterbody for use over a wide range of angle of attack. Pressure distribution is perhaps matched better at low angles of attack using an equivalent shape, but with the compensating effect of a sting, simple truncation may be more attractive for use over a wide range of angle of attack.

Side force is negligibly affected by truncation except for the largest alteration at the higher angles of attack (Fig. 48b). Yawing moment is clearly affected at all Mach numbers, with the sting compensating to a large extent except for the largest alteration (Figs. 46f, 47f, 48f, and 49f). Therefore, pressure distribution is clearly affected by the absence of afterbody surface area. It is plausible that severe truncations remove too much surface area to expect reasonable simulation of unaltered shapes. In the presence of a

sting, less severe truncations may adequately simulate the aerodynamic characteristics of unaltered shapes. Finally, from Figs. 46d, 47d, 48d, and 49d, rolling moment is insensitive to truncation.

4.2.1.2 Stable Configurations-Cylindrical Distortion

The effects of cylindrical distortion of a stable, pylon-mounted store configuration are presented in Figs. 50 through 52. Considering the reduction in fin area, a decrease in normal force is understandable (Figs. 50a, 51a, and 52a). In the case of afterbody 2, the same compensating effect of the sting is observed as for the BLU-1 (cf. Figs. 50a and 46a). For afterbodies 3 and 4, however, no compensation is evident, even with the largest sting (Figs. 51a and 52a). The overall effect of cylindrical distortion is virtually identical for the three alterations considered. Side force is affected only at the higher angles of attack for all three distortions (Figs. 50b, 51b, and 52b), an effect probably attributable to the character of the flow field under the wing of the parent aircraft. Deflections of the dummy sting are not the cause, since data for the altered afterbodies without dummy stings and data for the same afterbodies with dummy stings agree so well. Axial force is increased as a result of alteration, with little compensation (reduction) when a dummy sting is installed (Figs. 50c, 51c, and 52c). Rolling moment is slightly affected by alteration, but no separate effect of the presence of a dummy sting is visible (Figs. 50d, 51d, and 52d). Effects on rolling moment for sting-supported stable store models are therefore clearly attributable to the alteration of the afterbody required to allow mounting the store on the sting, rather than to the presence of the sting. Pitching- and yawing-moment increments indicate the substantial sensitivity of the pressure distribution over the store model to the configuration of the afterbody (Figs. 50e and f, 51e and f, and 52e and f). At supersonic conditions, the rather discontinuous character of the moment increments is probably attributable to shock systems in the flow field of the aircraft, especially when the repeatability of the curve shapes is considered (separate curves represent data acquired on tests punctuated by stops and starts of the flow to allow changes of the stings).

4.2.2 Rack-Mounted Store Configuration

4.2.2.1 Unstable Configuration-Truncation

In Figs. 53 through 57, increments in captive loads are presented for the truncated CBU-46 installed on first station 2, then station 3 of the TER mounted on the left inboard pylon. Within the resolution of the tests, there is virtually no effect of truncation on normal force at either of the TER stations (Figs. 53a, 54a, 55a, 56a, and 57a). Side force is not affected as a function of angle of attack except at TER station 2 for transonic conditions (cf. Figs. 53b and 55b with Figs. 56b and 57b). Since the presence of a sting

does not alter the shape of the curve, the effect is clearly an interaction of truncated shape with the flow field and cannot be identified as a general effect for other store configurations. Axial force is affected little (Figs. 53c, 54c, 55c, 56c, and 57c), with the presence of the sting again causing a compensation for the truncation as discussed in Section 4.2.1.1. Rolling moment (Figs. 53d, 54d, 55d, 56d, and 57d) is, for this unstable configuration, unaffected by truncation. The characteristics of pitching-moment increments for the same truncated shape vary from TER station 2 to TER station 3 (cf. Figs. 53e and 56e with 55e and 57e), even though minor. This observation again demonstrates the futility of drawing generalized conclusions from tests of a limited number of configurations. Yawing moment is affected most dramatically by truncation, but again, the effects vary from TER station 2 to TER station 3 (Figs. 53f and 55f with 56f and 57f). Little compensation results from the use of the sting. It can be seen from study of the force and corresponding moment curves that the truncations result in measurable changes in forces but apparently little in pressure distribution. This observation is slightly different from that for the BLU-1, perhaps because of the contoured design of the afterbody of the BLU-1.

4.2.2.2 Stable Configuration-Cylindrical Distortion

The effects of cylindrical distortion on a stable, rack-mounted store are presented in Figs. 58 and 59. In this case, two different afterbody alterations were tested on only TER station 3 on the left inboard pylon. The normal-force effects (Figs. 58a and 59a) vary substantially with angle of attack, with almost no compensation resulting from the use of a sting; hence, the effects are clearly associated with alteration of the afterbody. The decreasing effect at high angles of attack indicate separation, since little difference is evident between different degrees of alteration. Side force (Figs. 58b and 59b) is affected little at subsonic conditions, but the effect changes strongly with angle of attack in the low-to-medium range at transonic conditions. Axial force (Figs. 58c and 59c) is affected far more for AB3 than for AB2, indicating again the unique character of the loading of specific shapes in specific flow fields. Rolling moment (Figs. 58d and 59d) is affected, as in the case of the pylon-mounted M-118 (Section 4.2.1.2), but not as a function of the presence of a sting; hence, the effect is a function of distortion of the fin area, especially since the fins are canted 2 deg in pitch (Fig. 9d). The effects on pitching moment are virtually identical for the two alterations (Figs. 58e and 59e). A change in pressure distribution is definitely indicated by the large changes that result from relatively small changes in normal force at corresponding angles of attack. Yawing moment is affected in a completely different manner for the two alterations (Figs. 58f and 59f). Again, no generalizations can be made. The characteristics of a given afterbody alteration apparently determine both the value and sign of the affected yawing moment. Throughout, excellent repeatability of the data curves from run to run, after sting changes, indicates both credibility and lack of generality.

5.0 CONCLUSIONS

The influences of sting support techniques on aerodynamic loads acting on eight captive stores in the flow field of the F-4C aircraft were investigated in a wind tunnel test covering an angle of attack range of -4 to 12 deg and a Mach number range of 0.6 to 1.2. Specific conclusions that have been drawn from an analysis of the data are:

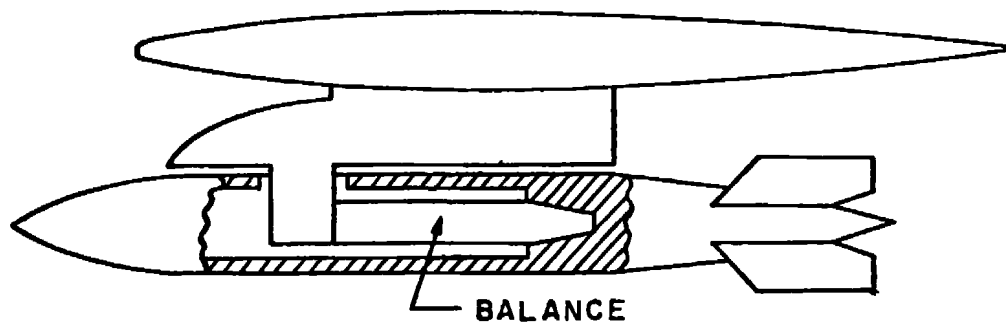
1. The presence of a sting influences pitching and yawing moments acting on the store model more than the other load components, both as a function of angle of attack and position in the flow field.
2. The effects of the presence of a sting generally decrease with increasing Mach number. (A notable exception was the CBU-24 model mounted on MER stations 1, 2, or 3 on the outboard pylon. Sting effects for these cases varied erratically with both angle of attack and Mach number.)
3. In both subsonic and transonic flow fields, the presence of a sting apparently affects the pressure distribution over the after portion of a store in such a manner that disproportionately large changes in aerodynamic moments occur with small changes in aerodynamic forces. In subsonic flow, the presence of a sting is probably communicated through adjustments in the flow in the base region. At transonic conditions, communication is likely through shock boundary-layer interaction.
4. The presence of a sting generally affects captive store loads acting on stable store models more than corresponding loads acting on unstable store models.
5. For both stable and unstable pylon-mounted and rack-mounted store configurations, rolling moment is essentially insensitive to the presence of a sting.
6. Altering the shape of a contoured afterbody on an unstable store can result in a configuration that has aerodynamic characteristics virtually identical to the unaltered configuration over a given range of angle of attack. However, it is also possible to gain acceptable aerodynamic characteristics over a wide range of angle of attack through simple truncation of the afterbody and installation of a sting.

7. Cylindrical distortion of the afterbody of a stable store configuration affects normal and side forces as well as pitching and yawing moments through the resulting decrease in exposed fin area. In addition, rolling moment is affected, an effect that is totally negligible when simply adding a sting to an unaltered stable store configuration.
8. Rolling moment acting on an unstable store configuration is unaffected by simple truncation of the afterbody, either with or without the presence of a sting.

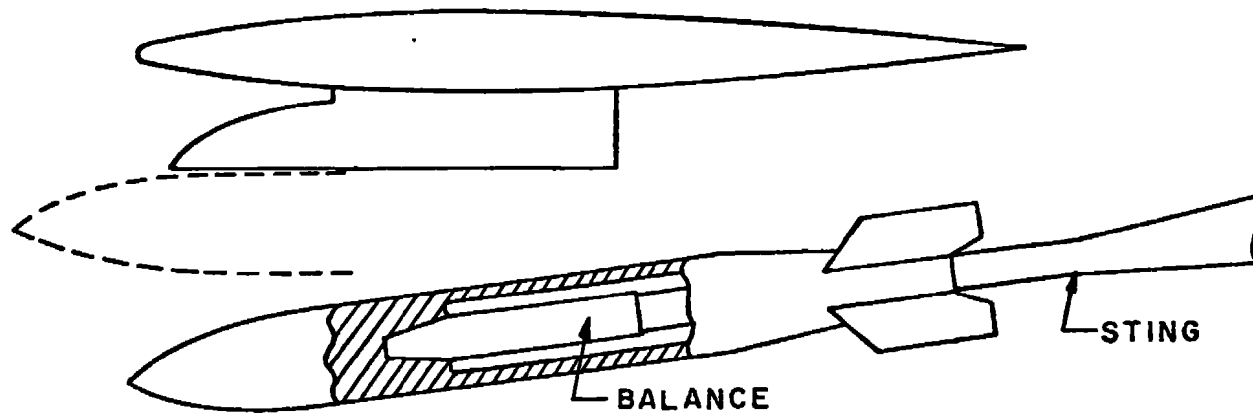
REFERENCES

1. Dix, R. E. "A Review of Methods of Measuring Aerodynamic Forces and Moments Acting on Captive Stores in Wind Tunnel Tests." AEDC-TR-72-108 (AD902816L), August 1972.
2. Christopher, J. P. and Carleton, W. E. "Captive-Trajectory Store-Separation System of the AEDC-PWT 4-Foot Transonic Tunnel." AEDC-TR-68-200 (AD839743), September 1968.
3. Cahn, Maurice S. "An Experimental Investigation of Sting-Support Effects on Drag and a Comparison with Jet Effects at Transonic Speeds." NACA Report 1353, 1958.
4. Tunnell, Phillips J. "An Investigation of Sting-Support Interference on Base Pressure and Forebody Chord Force at Mach Numbers from 0.60 to 1.30." NACA RMA54K16a, January 1955.
5. Jacocks, J. L. and Hartley, M. S. "Calibration of the AEDC-PWT 4-Foot Transonic Tunnel with Modified Walls." AEDC-TR-69-134 (AD853841), June 1969.
6. Gunn, J. A. "Calibration of the AEDC-PWT Aerodynamic Wind Tunnel (4T) Using Diffuser Flap Plenum Suction." AEDC-TR-70-74 (AD867975), April 1970.
7. Hill, David W., Jr. "Investigation of the Flow Field Beneath the Wing of the F-4C Aircraft with Various External Stores at Mach Number 0.85." AEDC-TR-72-92, AFATL-TR-72-113 (AD900393L), June 1972.

8. Marsden, P. and Haines, A. B. "Aerodynamic Loads on External Stores: A Review of Experimental Data and Method of Prediction." R & M No. 3503, November 1962.
9. Hill, David W., Jr. "Investigation of Factors Affecting the Wind Tunnel Measurements of Carriage-Position Airloads on External Store Models at Transonic Mach Numbers." AEDC-TR-75-12, AFATL-TR-75-22 (ADB002165L), February 1975.



INTERNAL BALANCE



DUAL - SUPPORT

Figure 1. Two methods of supporting a store in the captive position in wind tunnel tests.

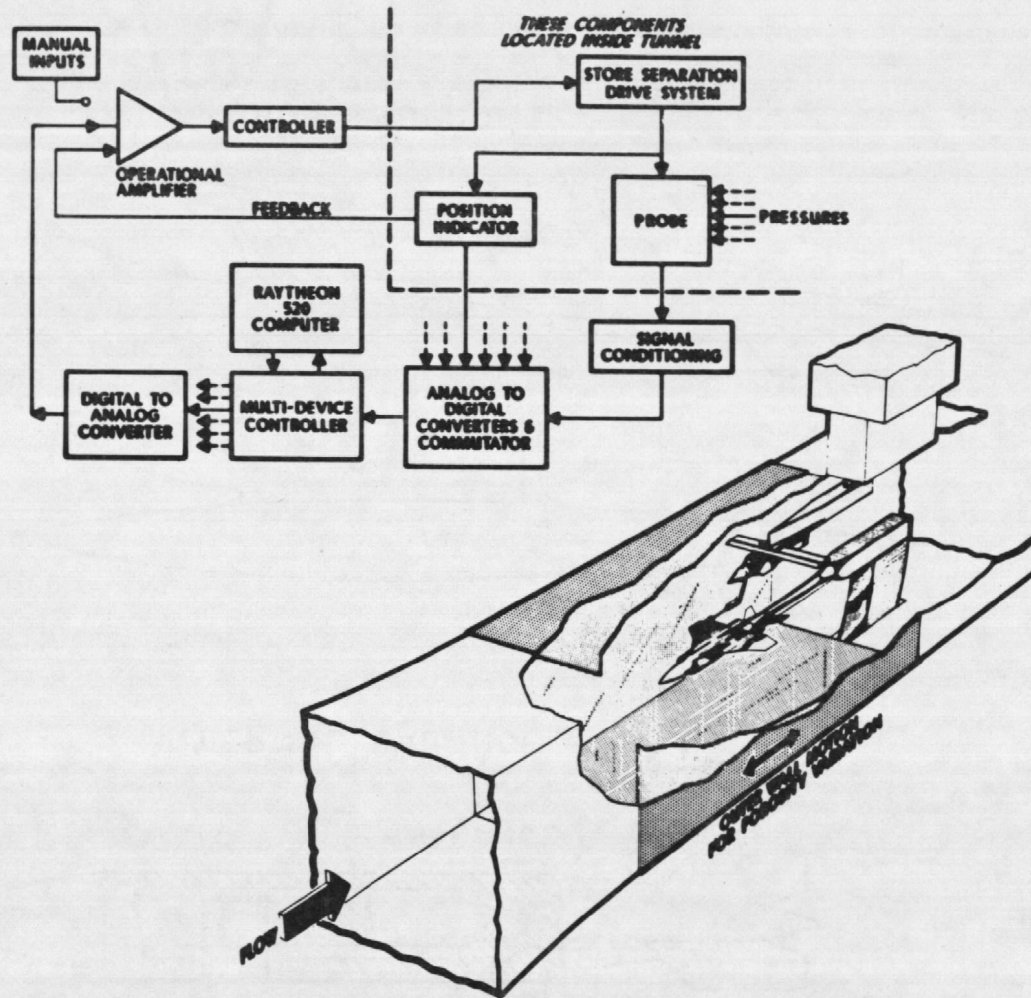
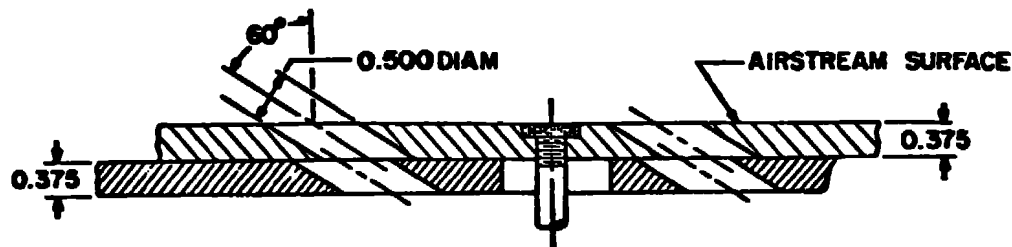


Figure 2. Schematic illustration of the captive trajectory system.



TYPICAL PERFORATED WALL CROSS SECTION

TUNNEL STATIONS AND DIMENSIONS
ARE IN INCHES

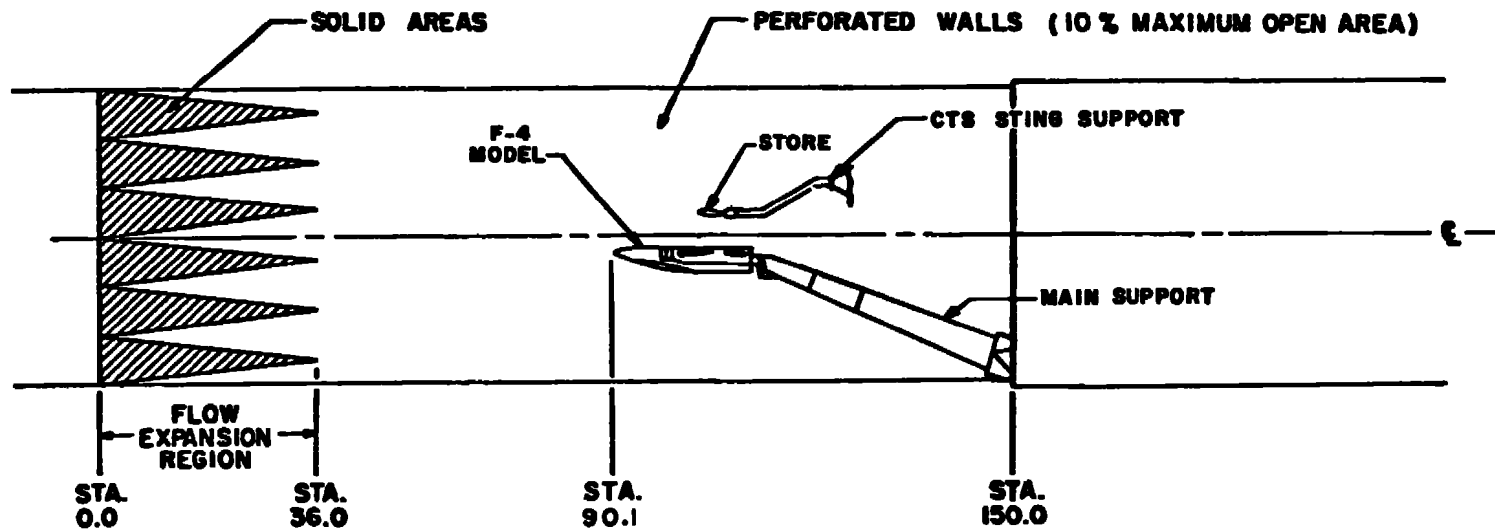


Figure 3. Schematic illustration of a typical model installation in Tunnel 4T.

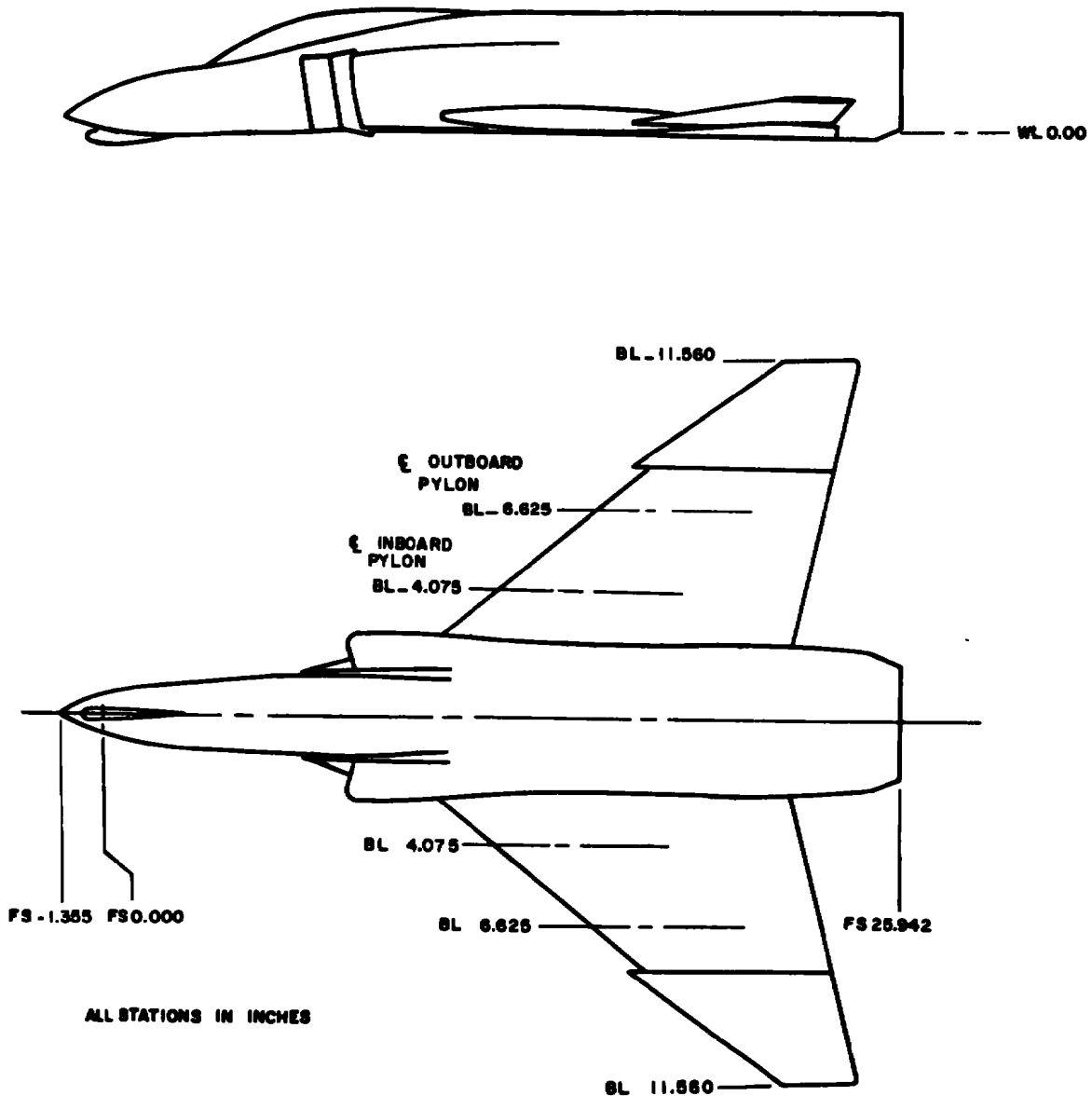
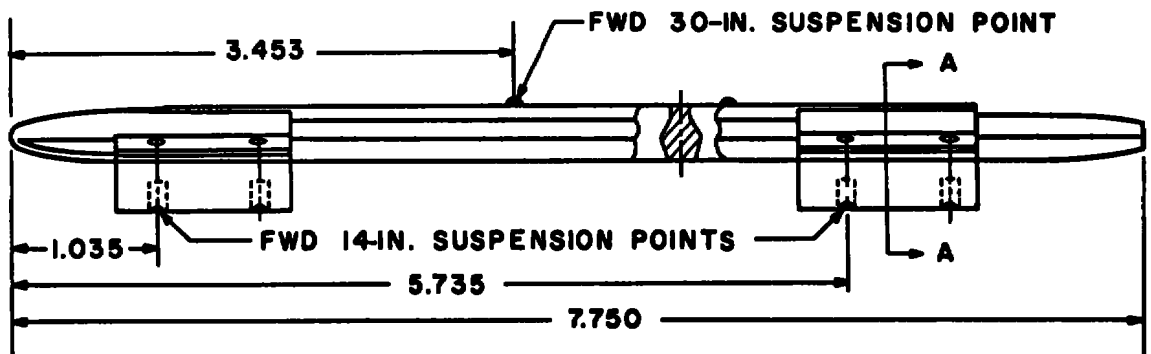
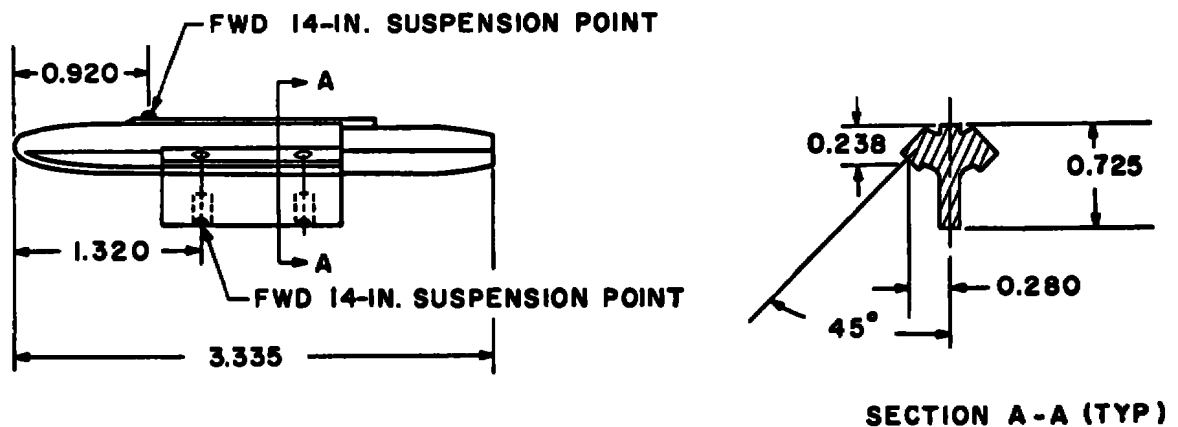


Figure 4. Five-percent scale model of the F-4C aircraft.



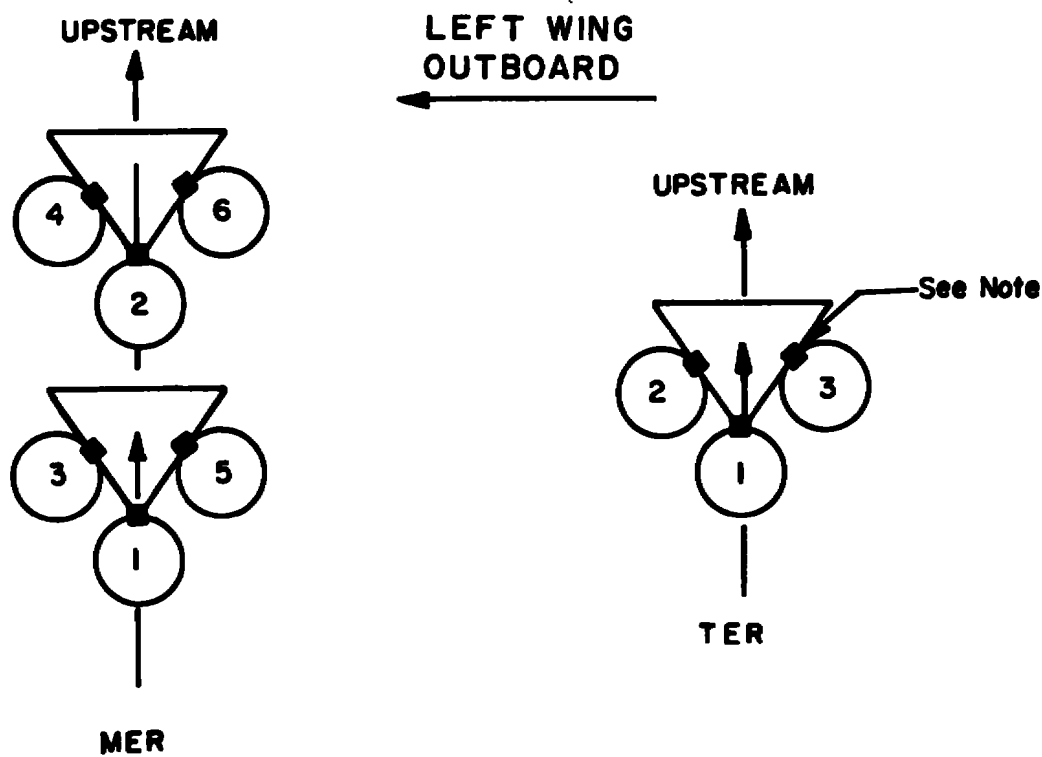
a. Multiple ejection rack, model MER-10A



ALL DIMENSIONS IN INCHES

b. Triple ejection rack, model TER-9A

Figure 5. Details of the models of the multiple and triple ejector racks.



NOTE: The square indicates the orientation of the suspension lugs

TYPE RACK	STATION	ROLL ORIENTATION,deg
MER	1	0
	2	0
	3	45
	4	45
	5	-45
	6	-45
TER	1	0
	2	45
	3	-45

Figure 6. Nomenclature of ejector rack stations.

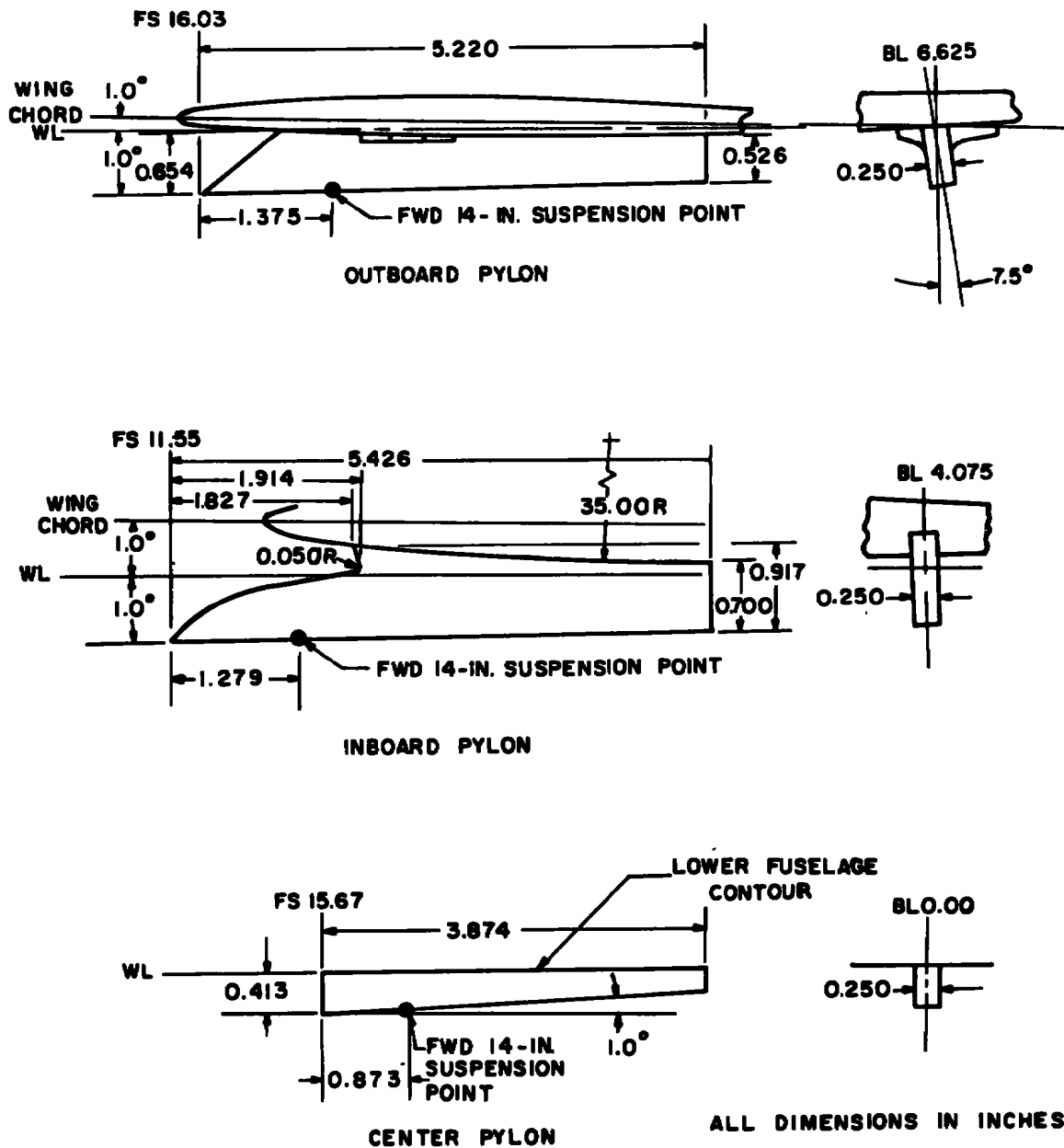
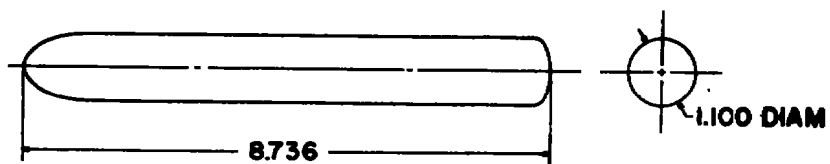
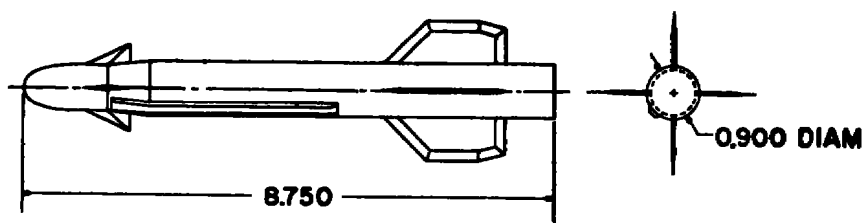


Figure 7. Details of the models of the F-4C pylons.



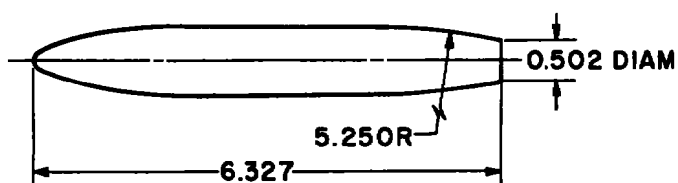
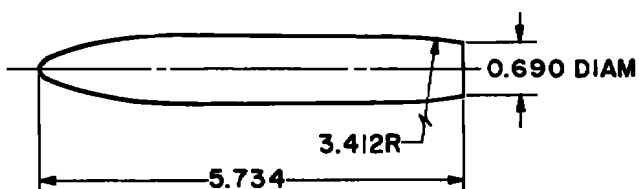
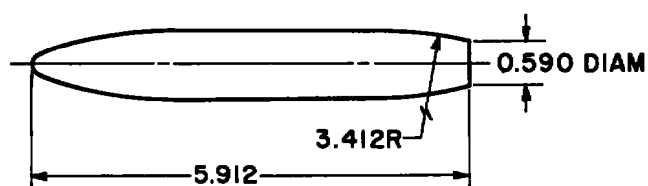
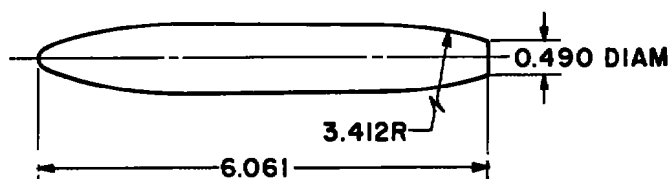
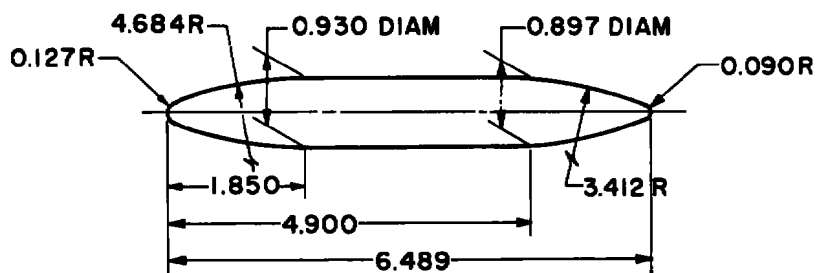
a. Black Crow (modified SUU-16/23)



ALL DIMENSIONS IN INCHES

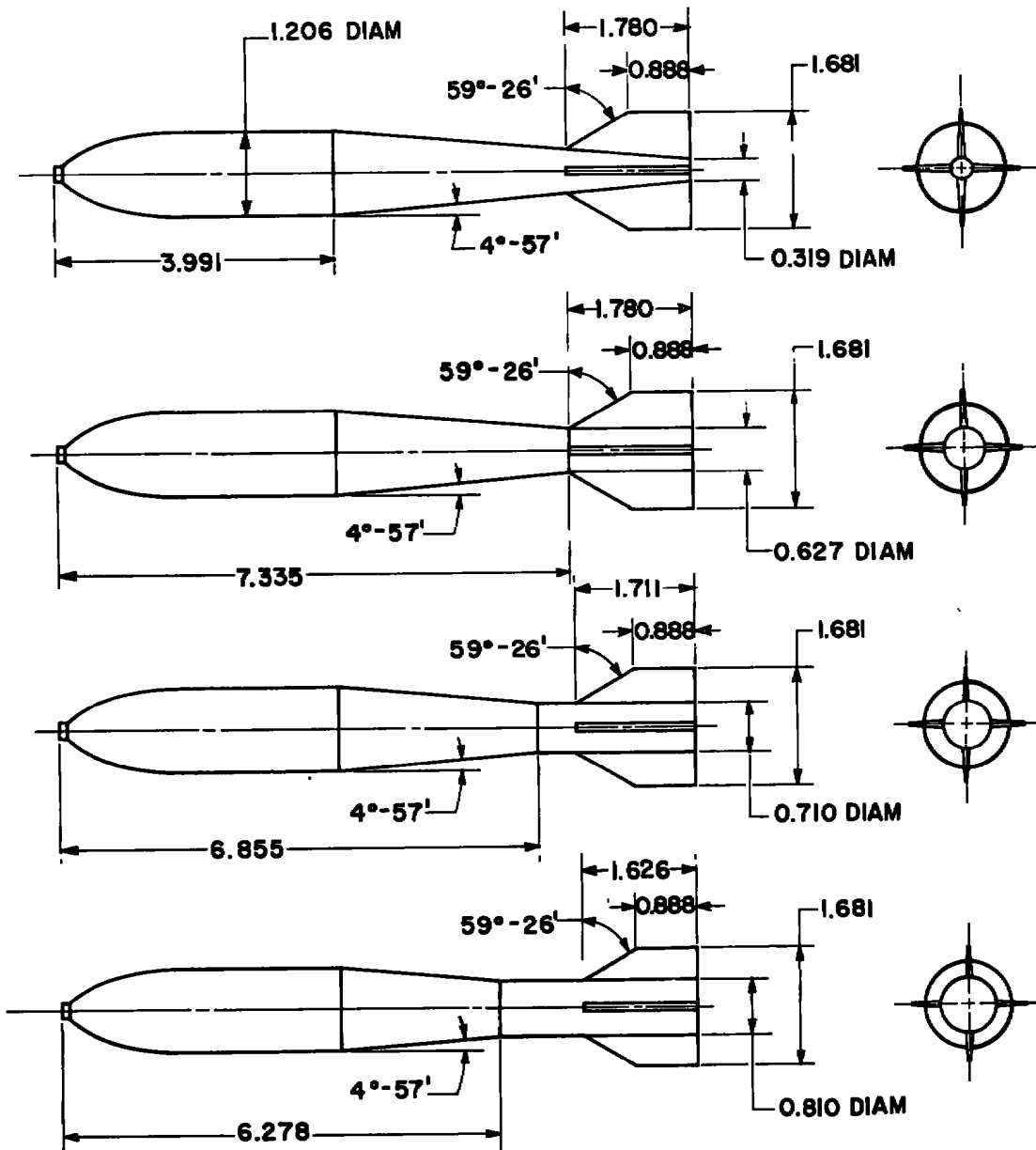
b. Hard Structure Munition

Figure 8. Dimensions of pylon-mounted store models.



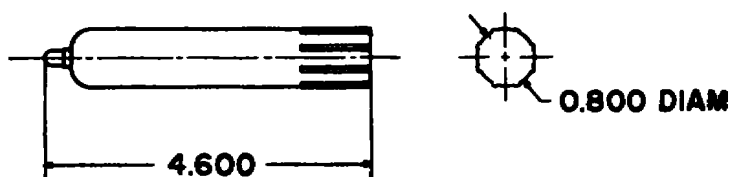
ALL DIMENSIONS IN INCHES

c. BLU-1 bomb
Figure 8. Continued.

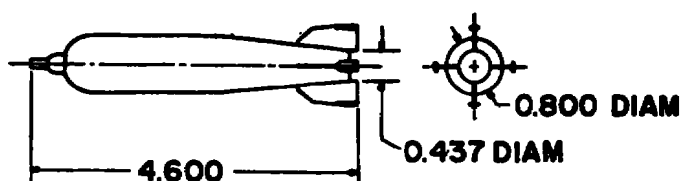


ALL DIMENSIONS IN INCHES

d. M-118 bomb
Figure 8. Concluded.



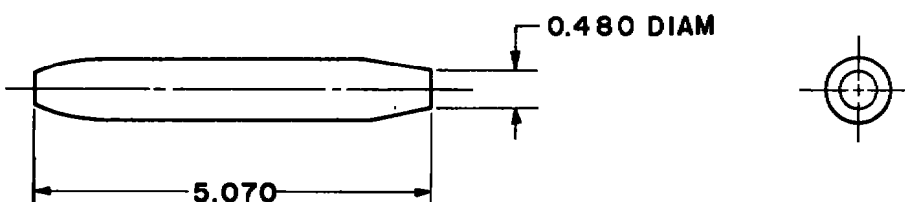
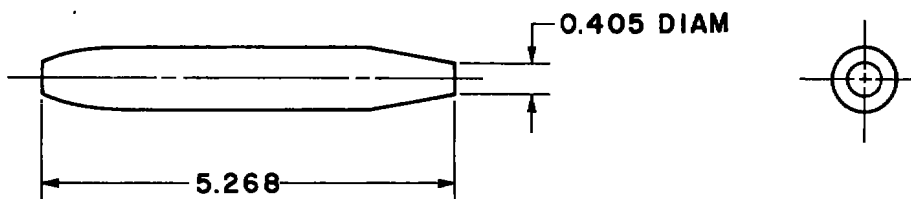
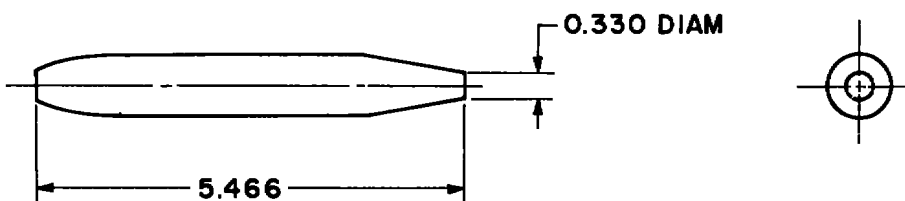
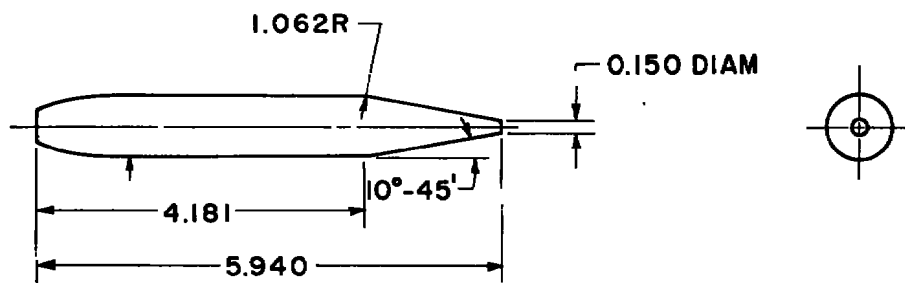
a. ASP



ALL DIMENSIONS IN INCHES

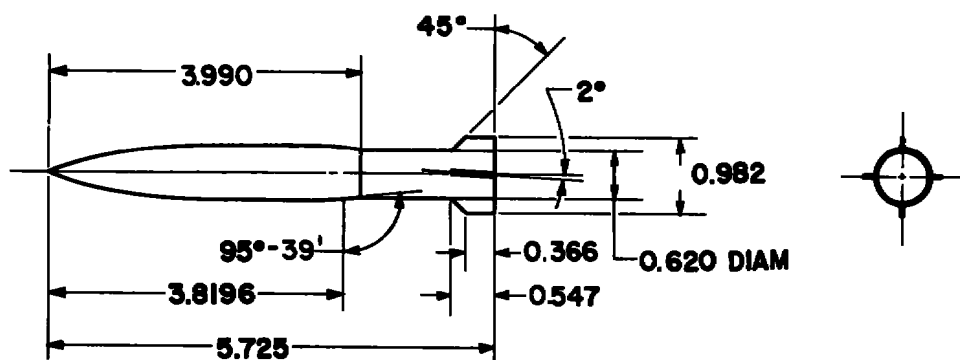
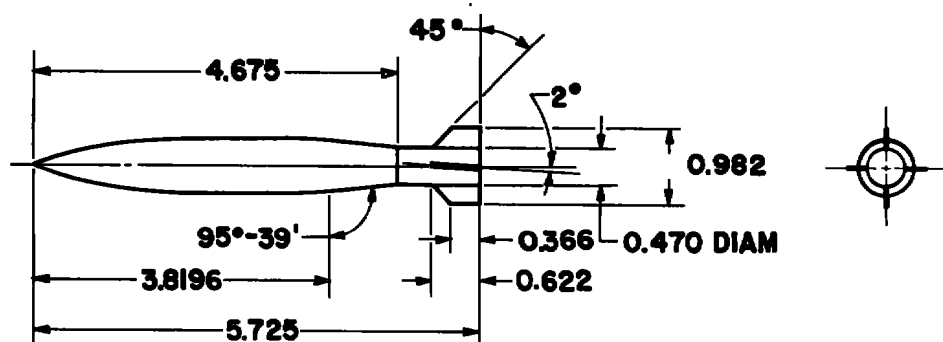
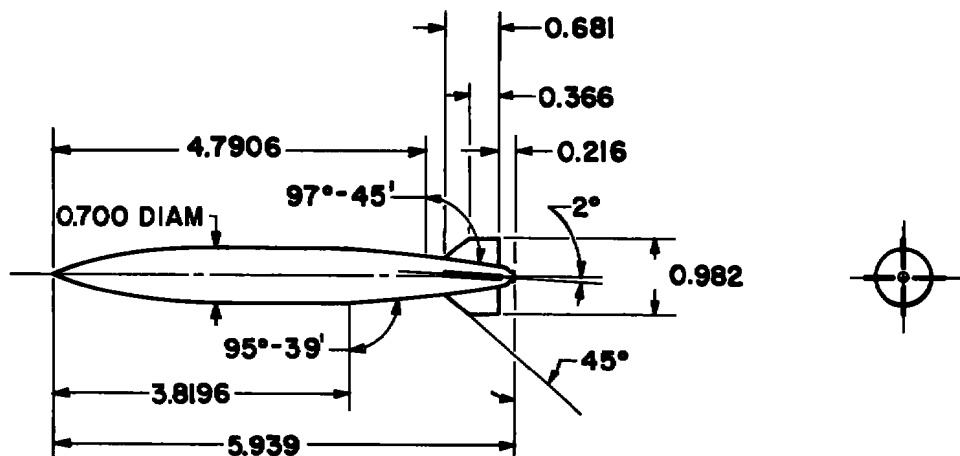
b. SUU-30B/B (CBU-24)

Figure 9. Dimensions of rack-mounted store models.



ALL DIMENSIONS IN INCHES

c. CBU-46 (SUU-7) launcher pod
Figure 9. Continued.



ALL DIMENSIONS IN INCHES

d. MK-83 bomb
Figure 9. Concluded.

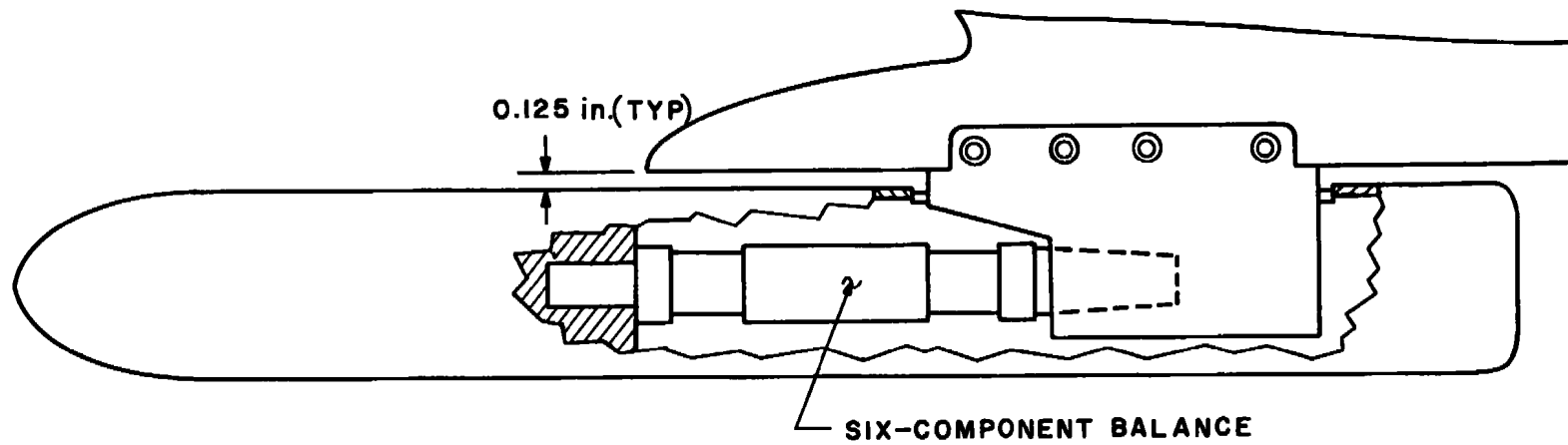
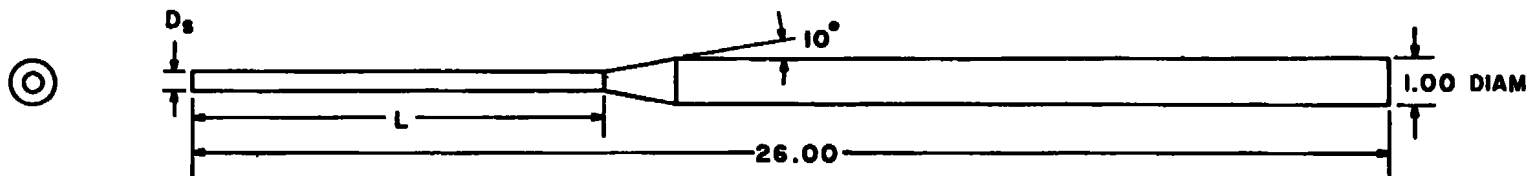
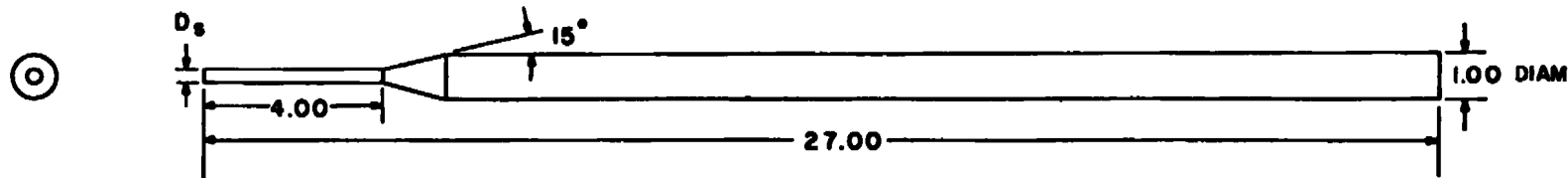


Figure 10. Typical installation of an internal balance-supporting bracket.



STING	D_s	L
1	0.40	8.93
2	0.50	9.22
3	0.60	9.50

a. For pylon-mounted stores



STING	D_s
4	0.250
5	0.325
6	0.400

ALL DIMENSIONS IN INCHES

b. For rack-mounted stores

Figure 11. Details of the dummy stings.

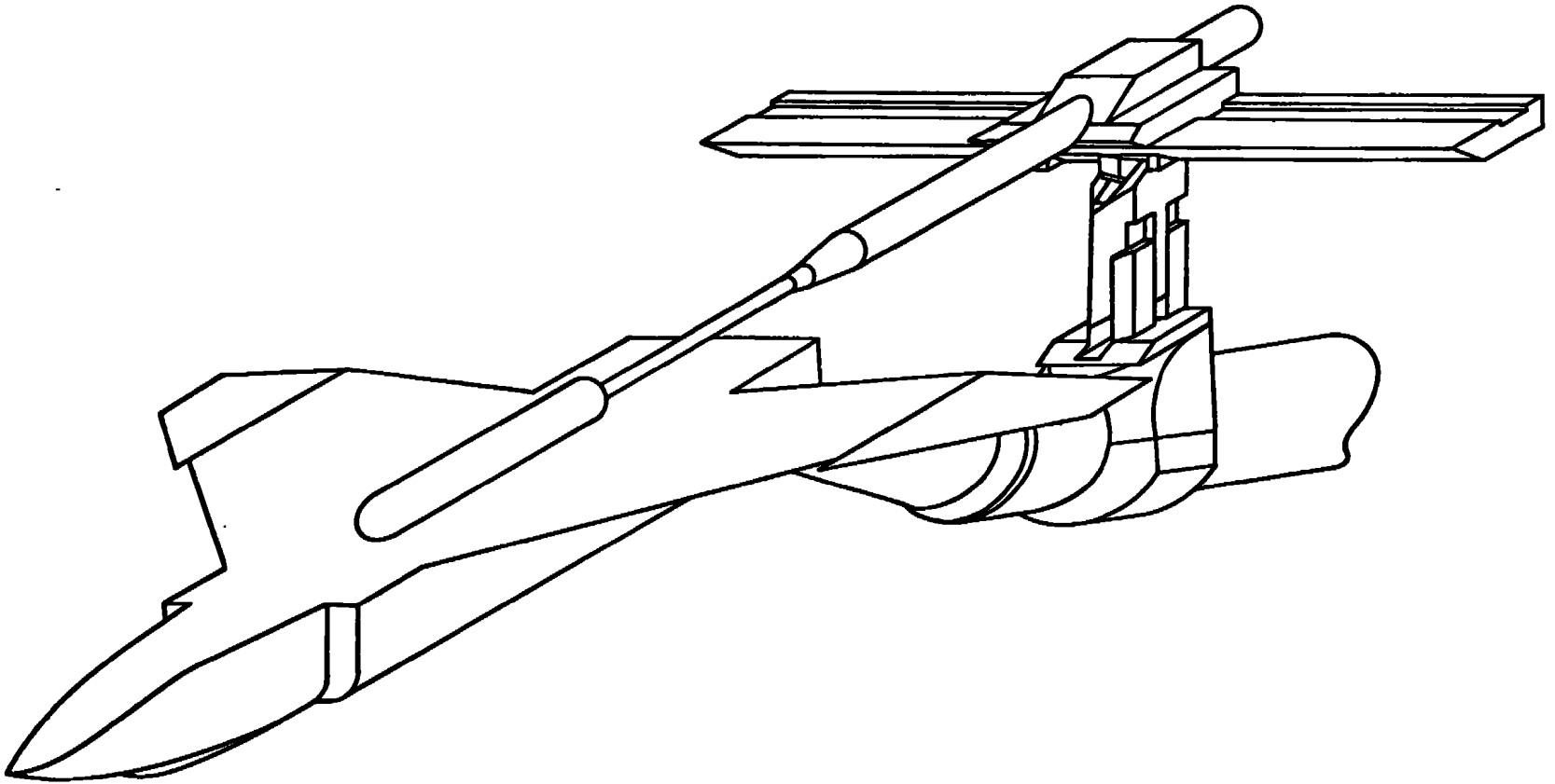
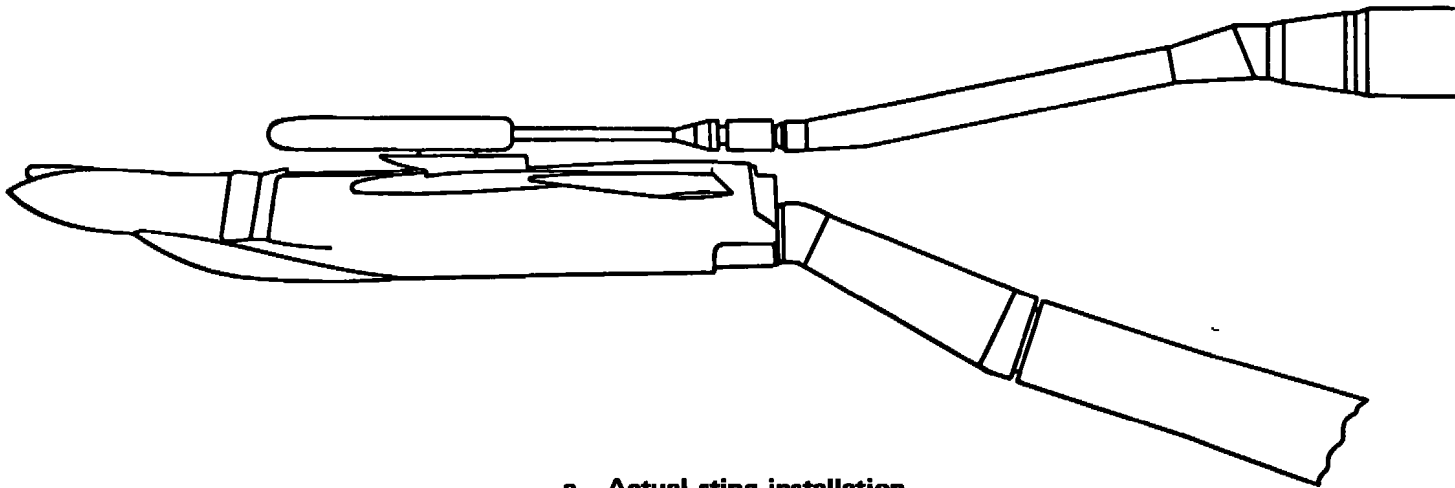
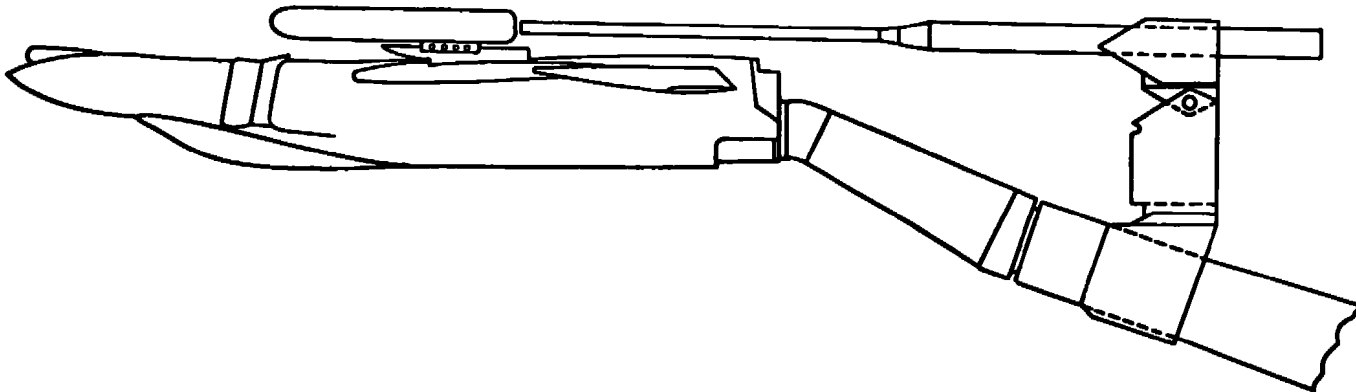


Figure 12. Sketch of the dummy sting support system.

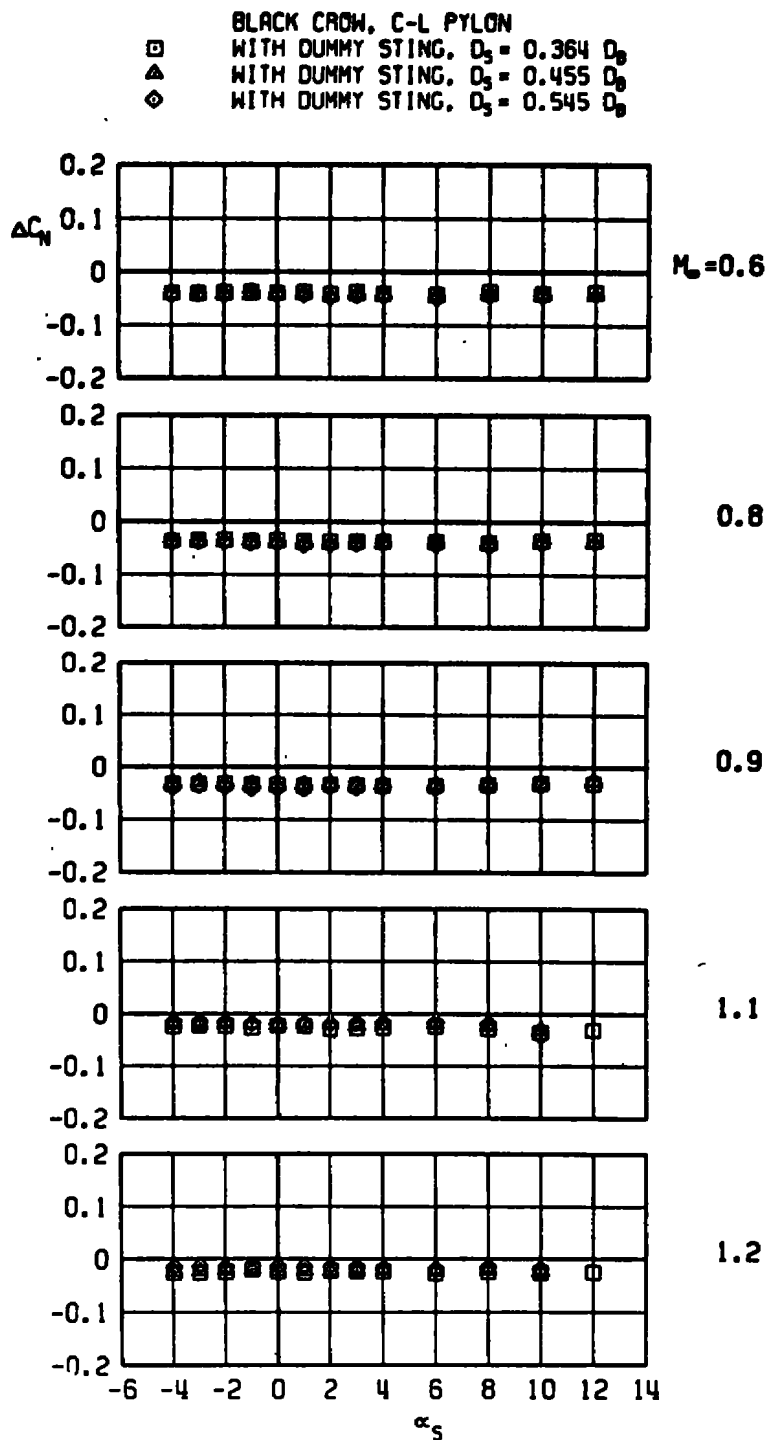


a. Actual sting installation



b. Dummy sting installation

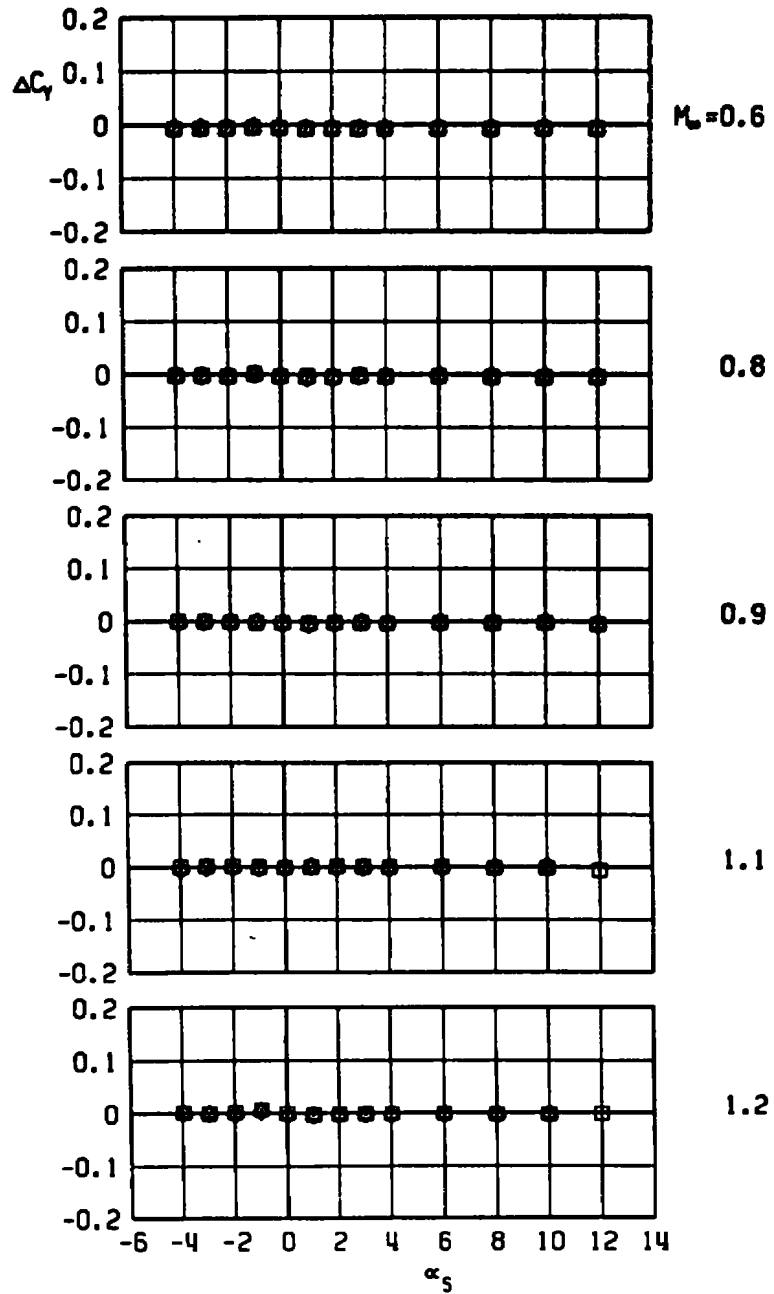
Figure 13. Comparison of dummy sting and active sting installations.



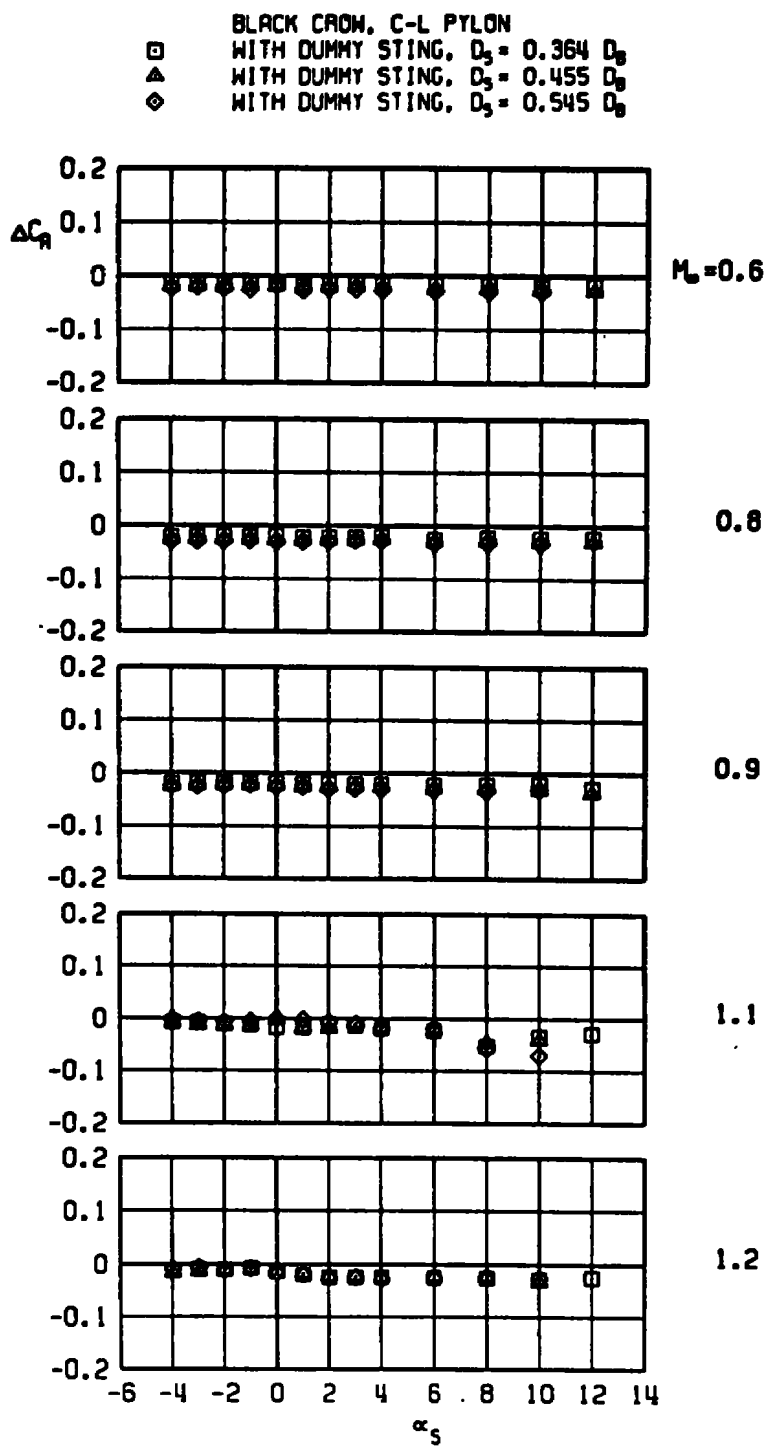
a. Normal-force increment

Figure 14. Sting-induced aerodynamic load increments as a function of angle of attack, unstable pylon-mounted store, C-L pylon.

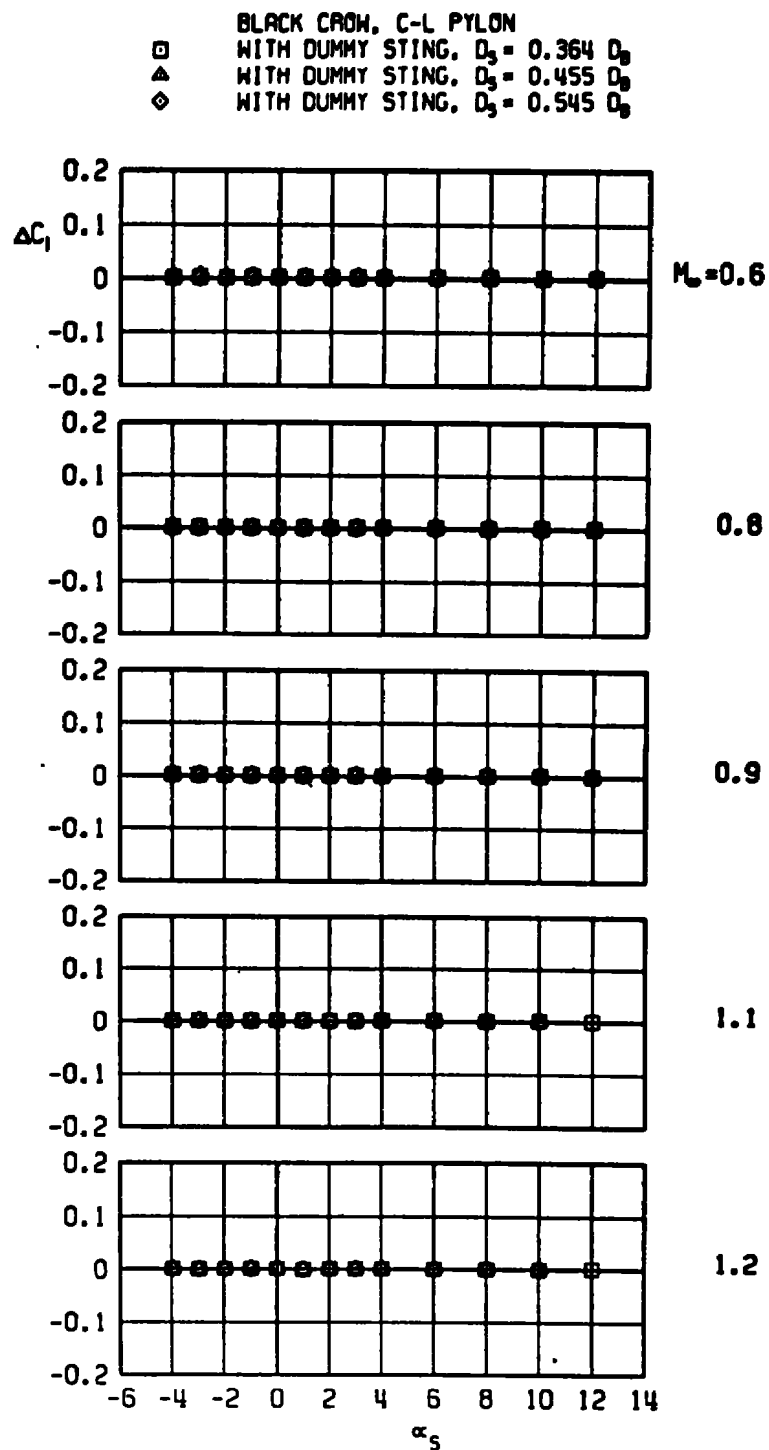
BLACK CROW, C-L PYLON
 □ WITH DUMMY STING, $D_3 = 0.364 D_0$
 △ WITH DUMMY STING, $D_3 = 0.455 D_0$
 ◇ WITH DUMMY STING, $D_3 = 0.545 D_0$



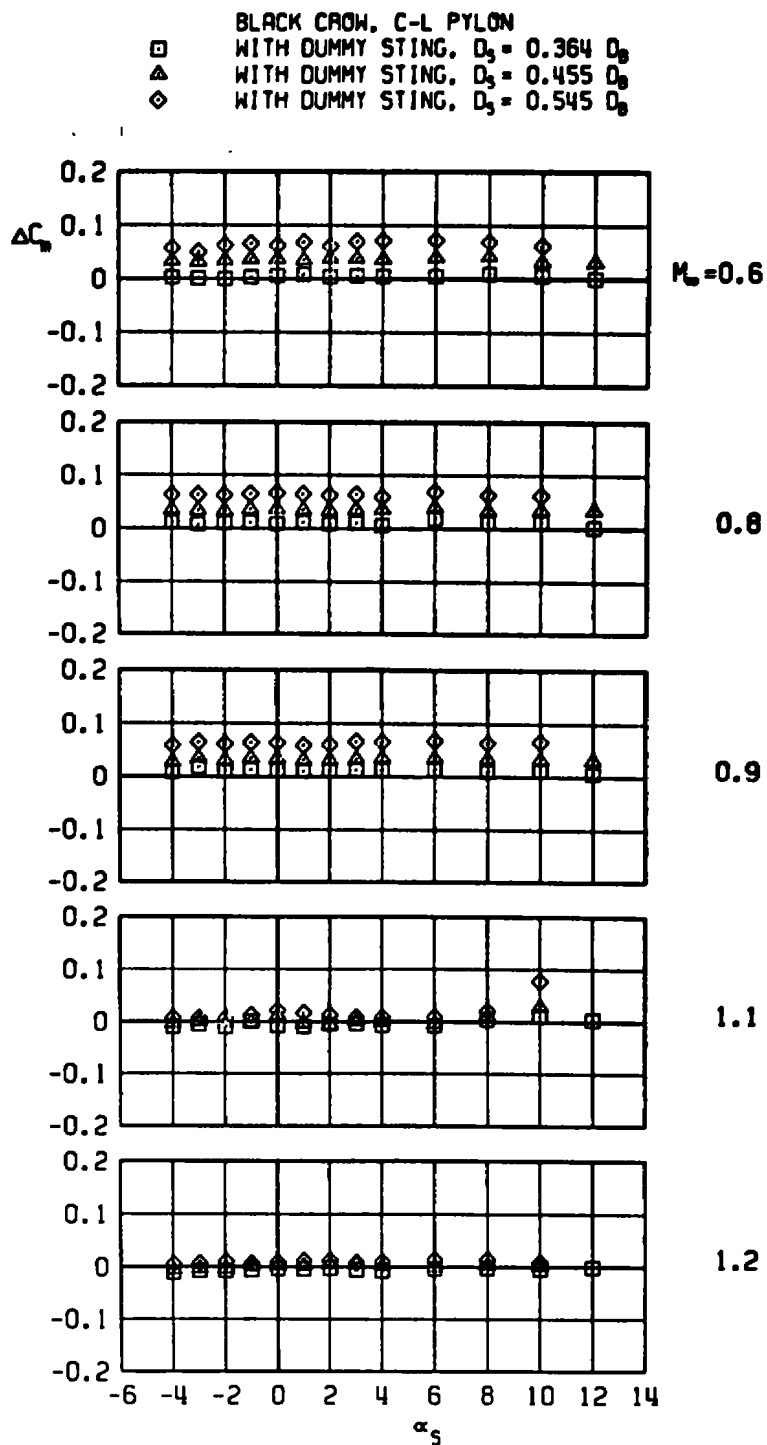
b. Side-force increment
 Figure 14. Continued.



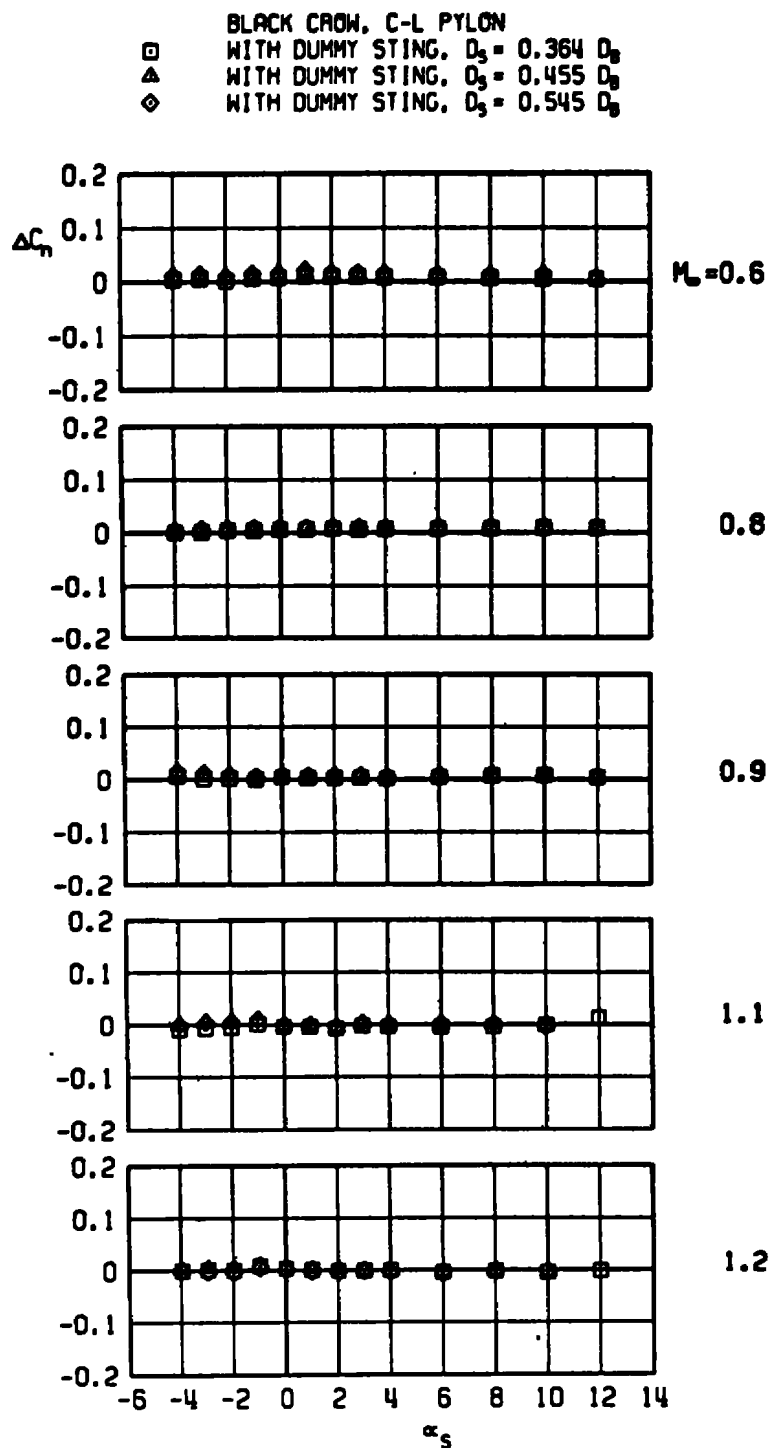
c. Axial-force increment
 Figure 14. Continued.



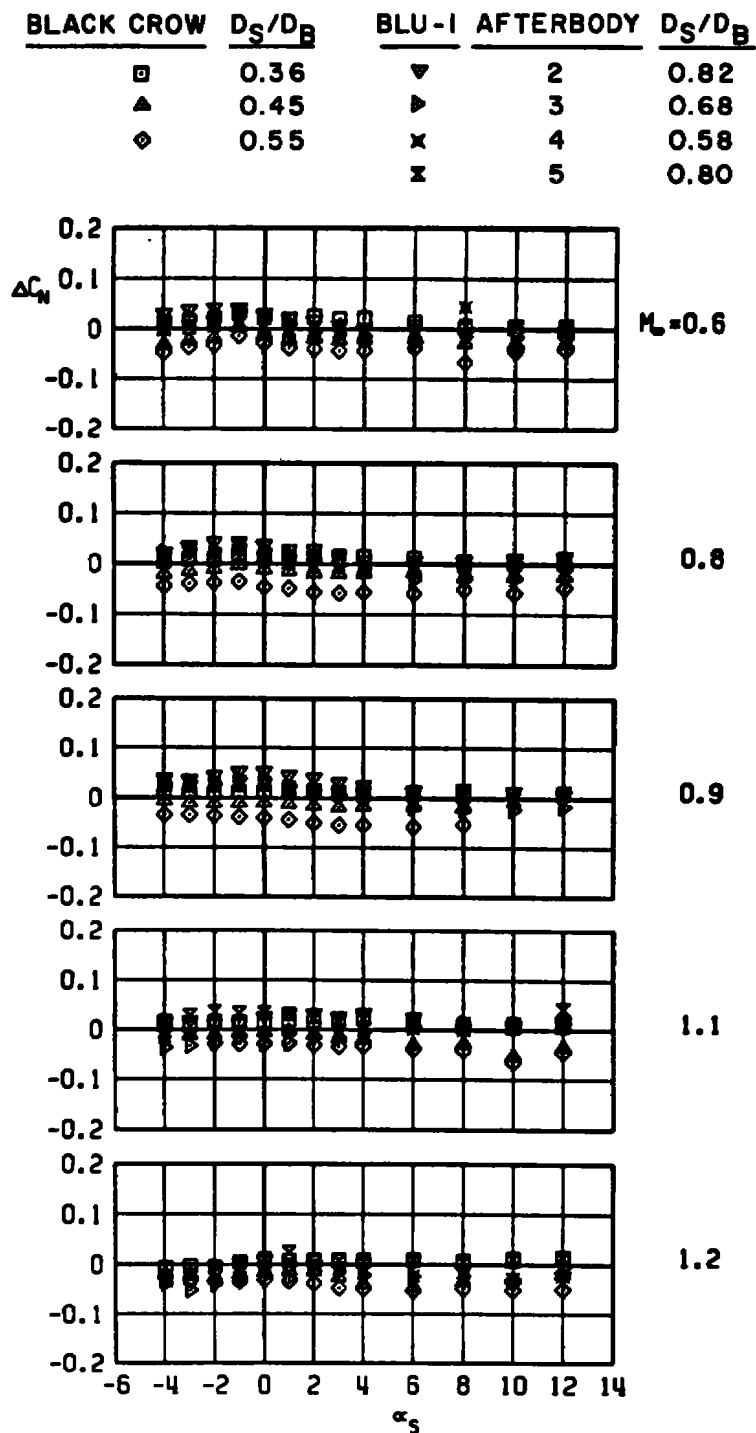
d. Rolling-moment increment
 Figure 14. Continued.



e. Pitching-moment increment
Figure 14. Continued.



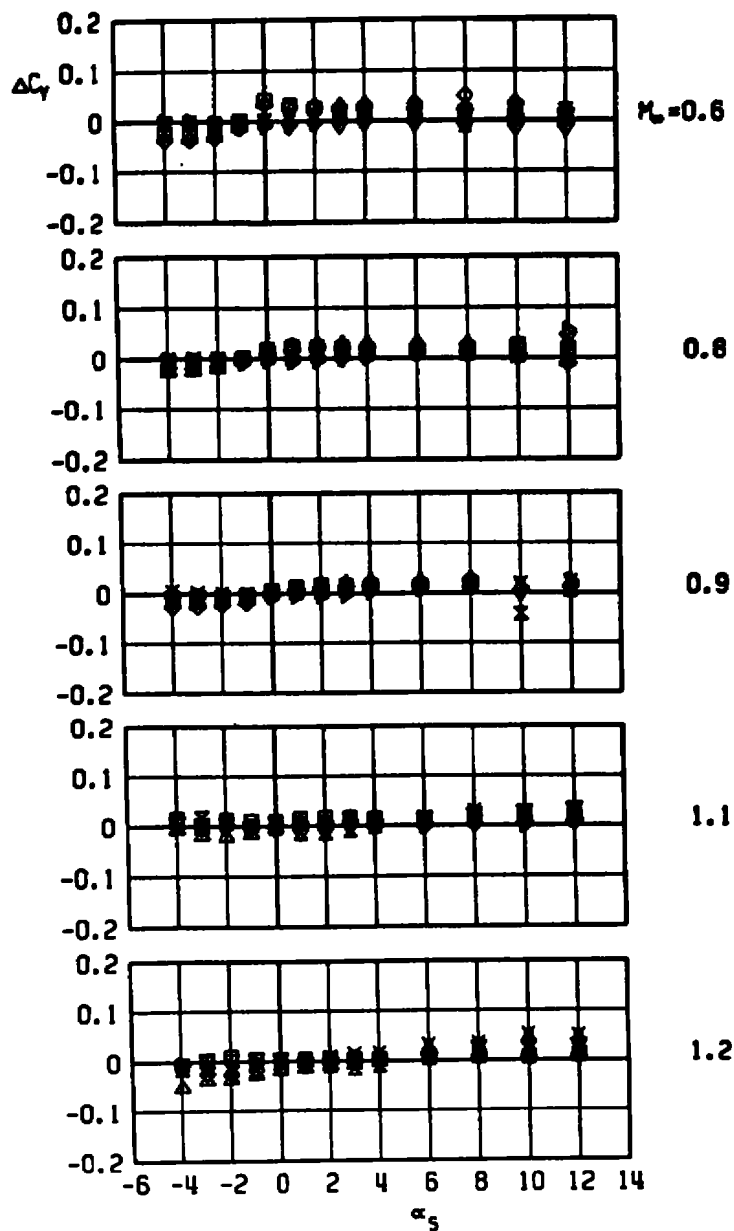
f. Yawing-moment increment
Figure 14. Concluded.



a. Normal-force increment

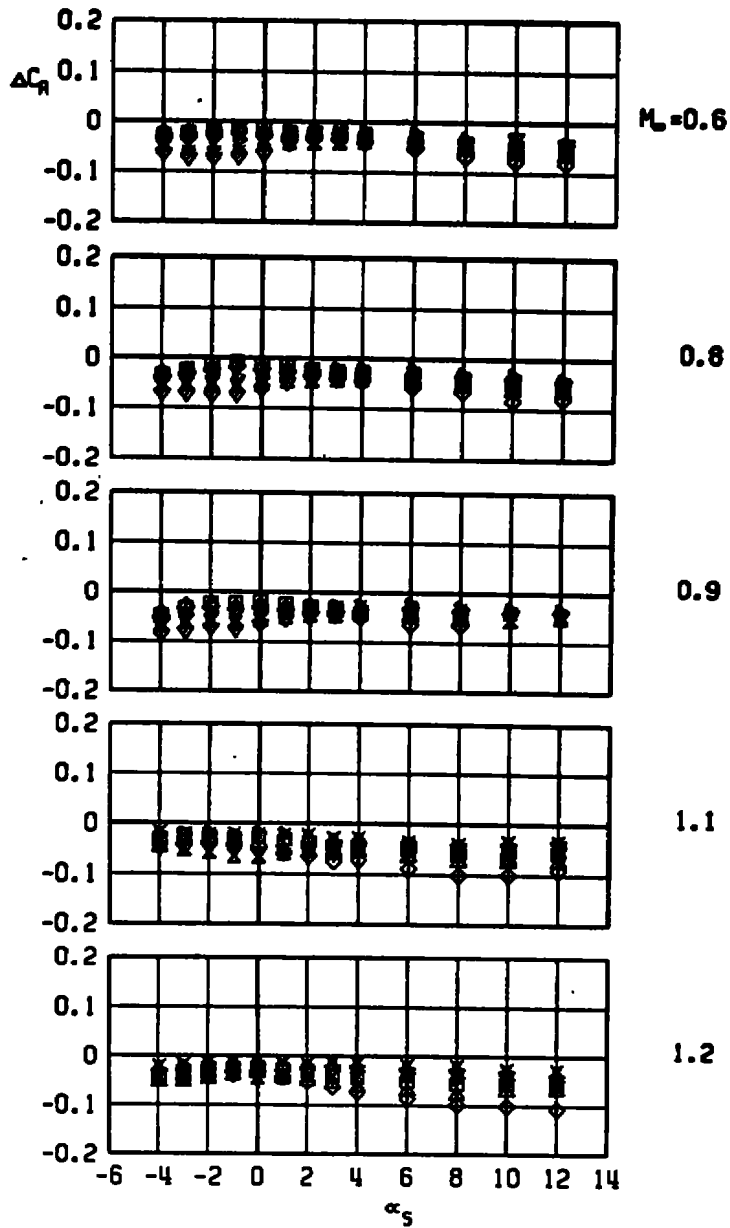
Figure 15. Sting-induced aerodynamic load increments as a function of angle of attack, unstable pylon-mounted stores, LIB pylon.

BLACK CROW	D_S/D_B	BLU-1	AFTERBODY	D_S/D_B
□	0.36	▼	2	0.82
▲	0.45	▷	3	0.68
◇	0.55	x	4	0.58
		Σ	5	0.80



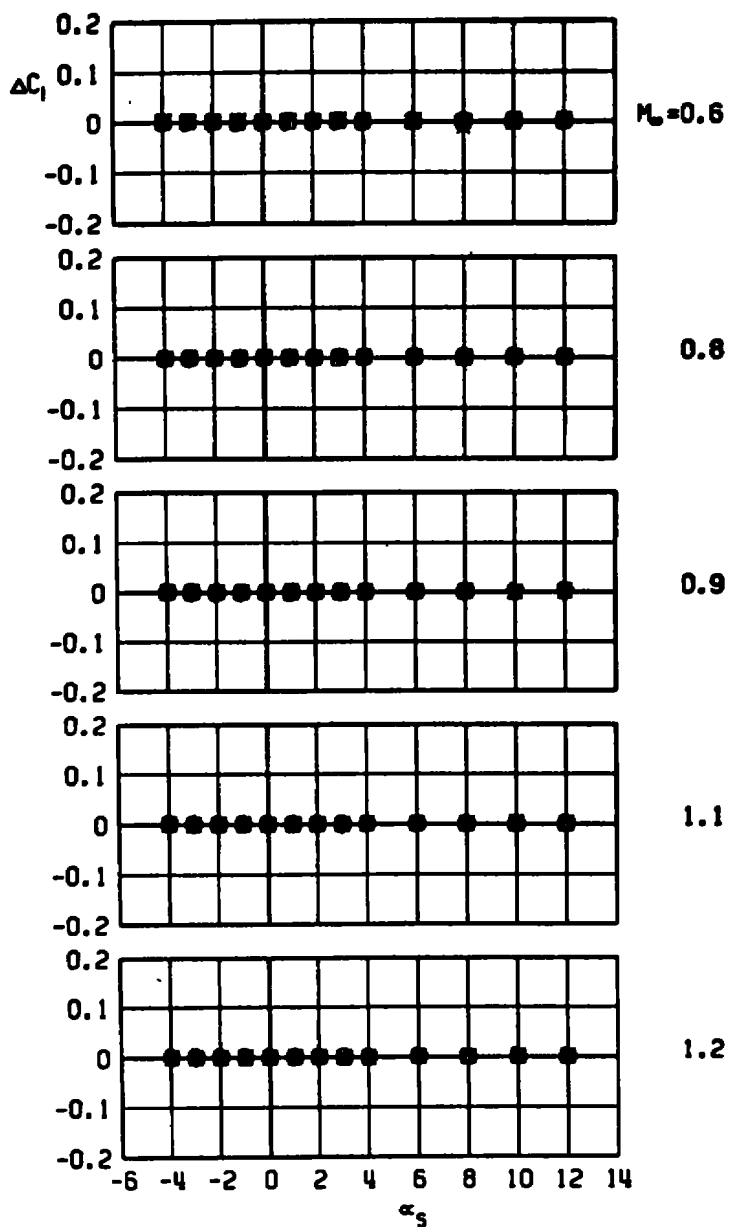
b. Side-force increment
Figure 15. Continued.

BLACK CROW	D_S/D_B	BLU-1	AFTERBODY	D_S/D_B
◻	0.36	▼	2	0.82
▲	0.45	►	3	0.68
◊	0.55	×	4	0.58
		⊗	5	0.80



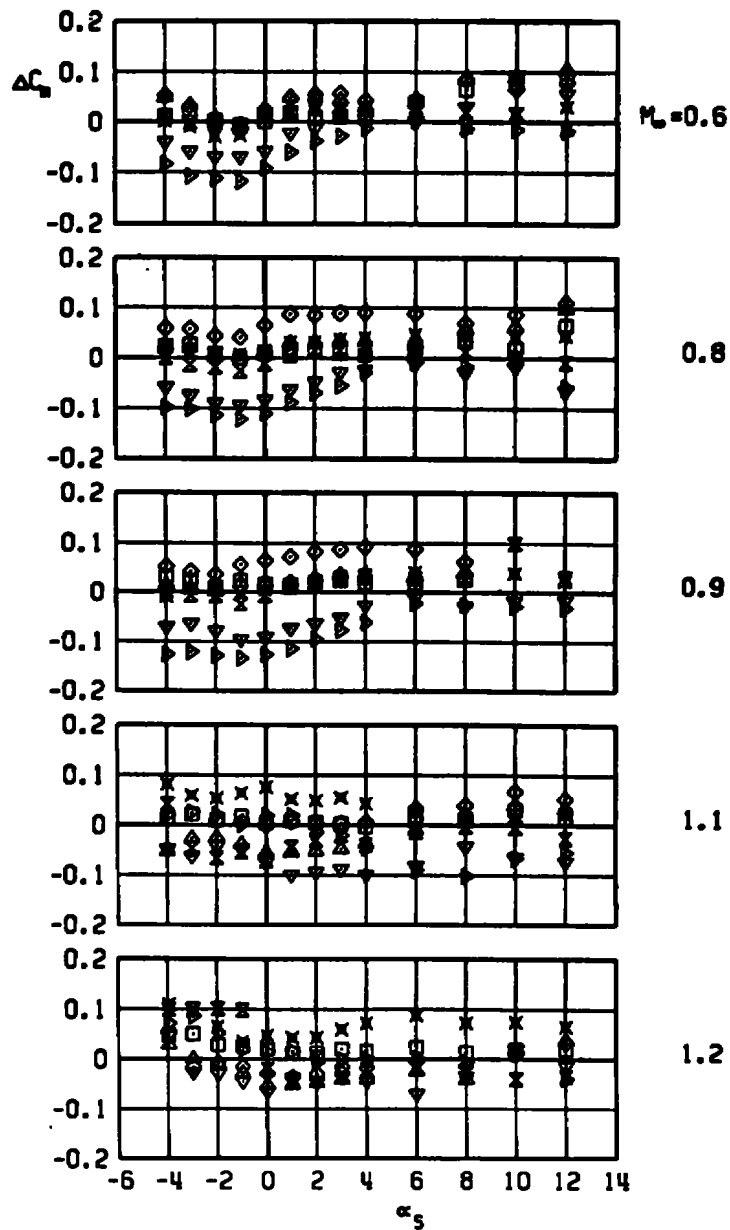
c. Axial-force increment
Figure 15. Continued.

BLACK CROW	D_S/D_B	BLU-1	AFTERBODY	D_S/D_B
▲	0.36	▼	2	0.82
▣	0.45	▷	3	0.68
◇	0.55	×	4	0.58
		⌘	5	0.80



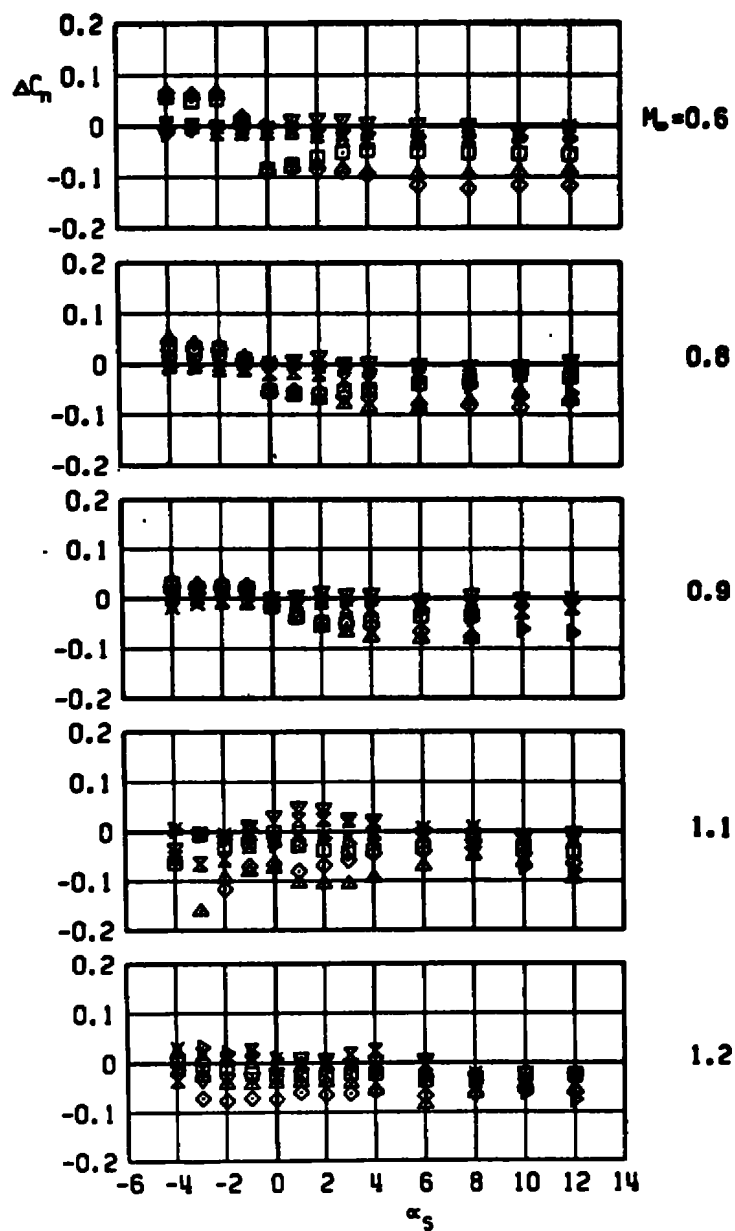
d. Rolling-moment increment
Figure 15. Continued.

BLACK CROW	D_S/D_B	BLU-1	AFTERBODY	D_S/D_B
□	0.36	▼	2	0.82
▲	0.45	▷	3	0.68
◇	0.55	×	4	0.58
		⊗	5	0.80

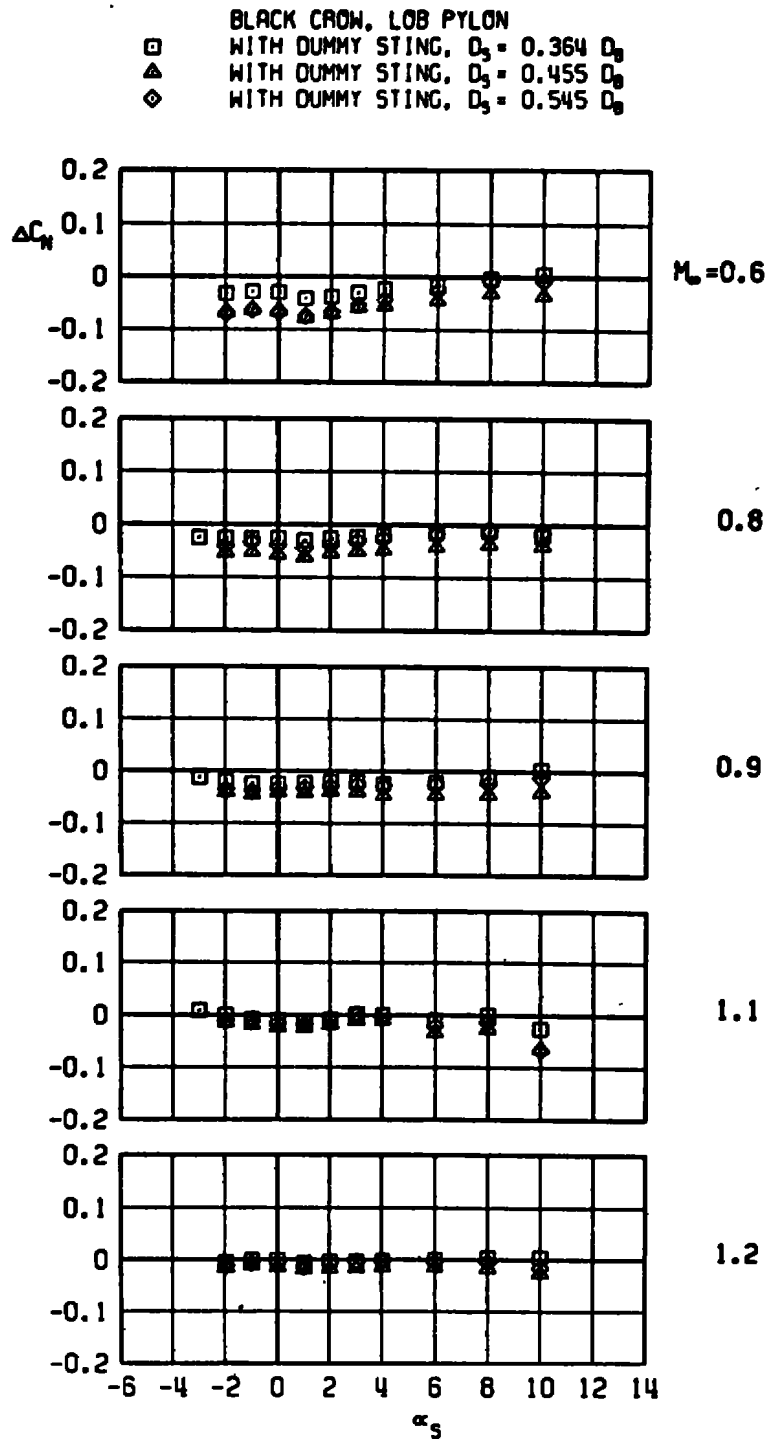


e. Pitching-moment increment
Figure 15. Continued.

BLACK CROW	D_S/D_B	BLU-1	AFTERBODY	D_S/D_B
□	0.36	▼	2	0.82
▲	0.45	►	3	0.68
◇	0.55	x	4	0.58
		⌘	5	0.80

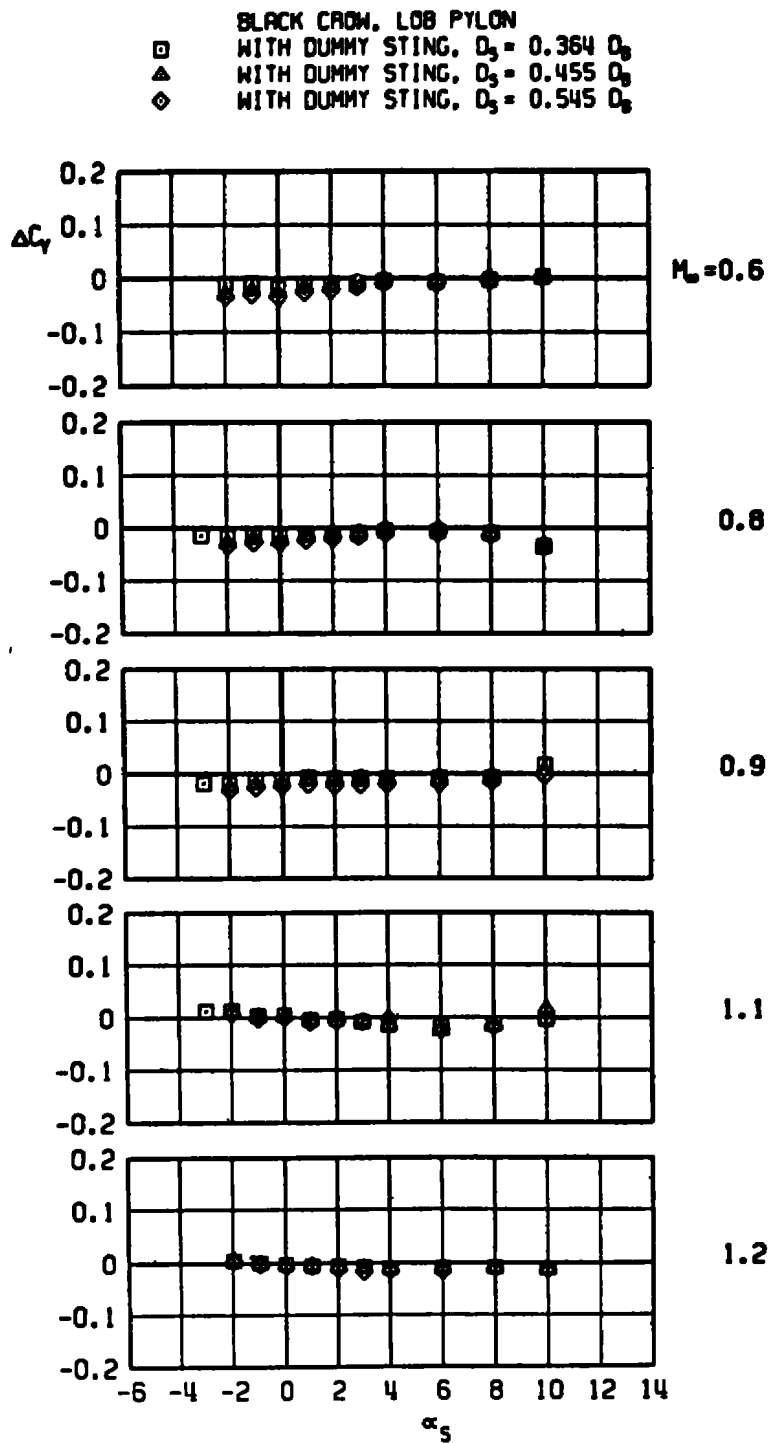


f. Yawing-moment increment
Figure 15. Concluded.

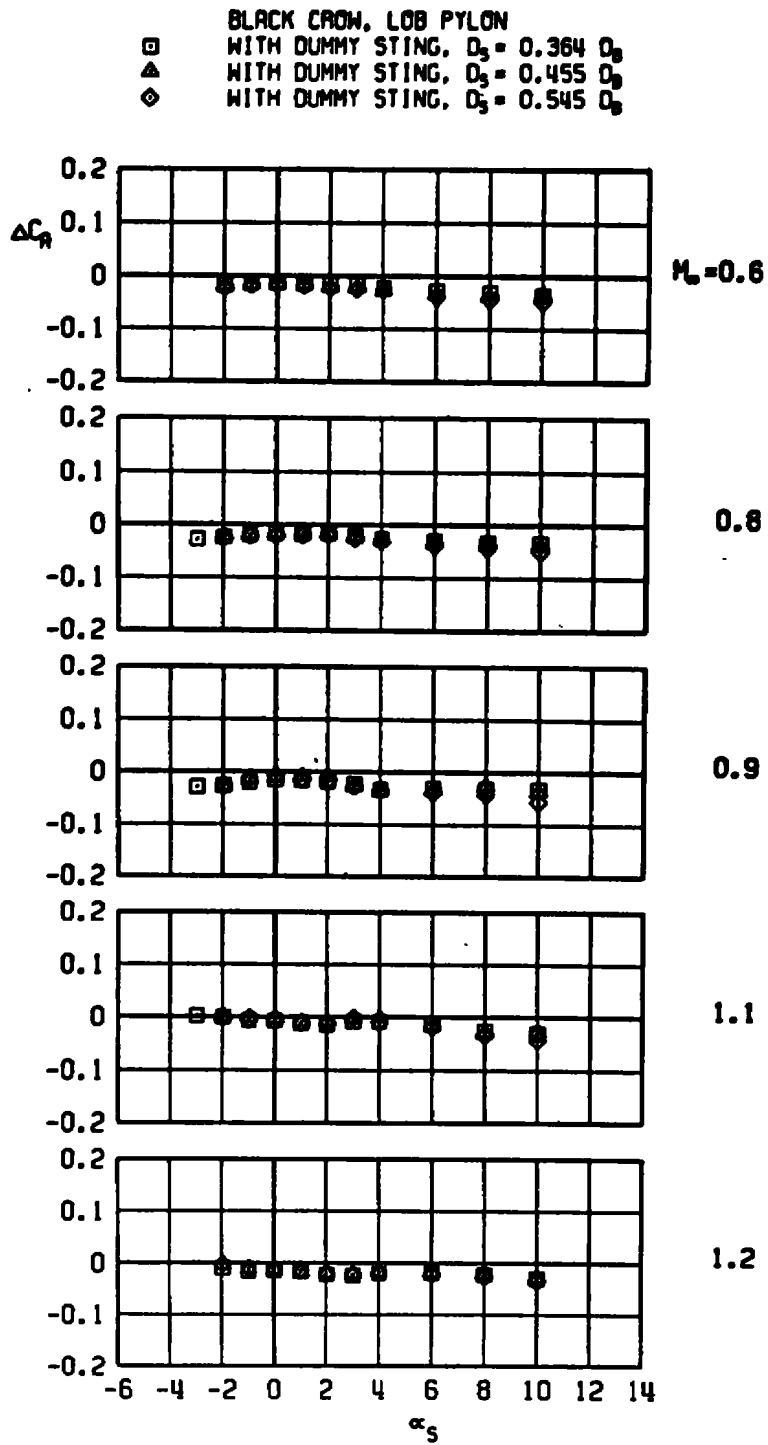


a. Normal-force increment

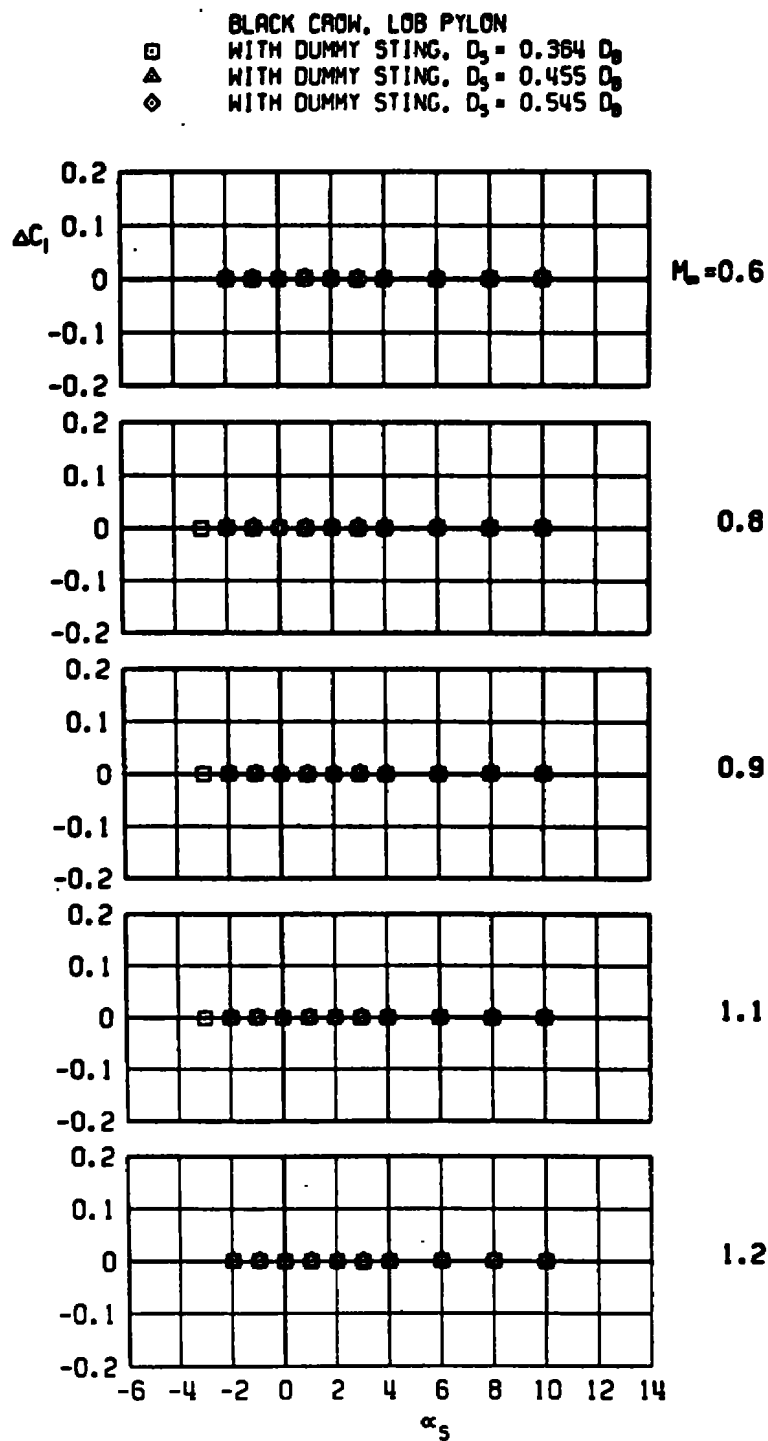
Figure 16. Sting-induced aerodynamic load increments as a function of angle of attack, unstable pylon-mounted store, LOB pylon.



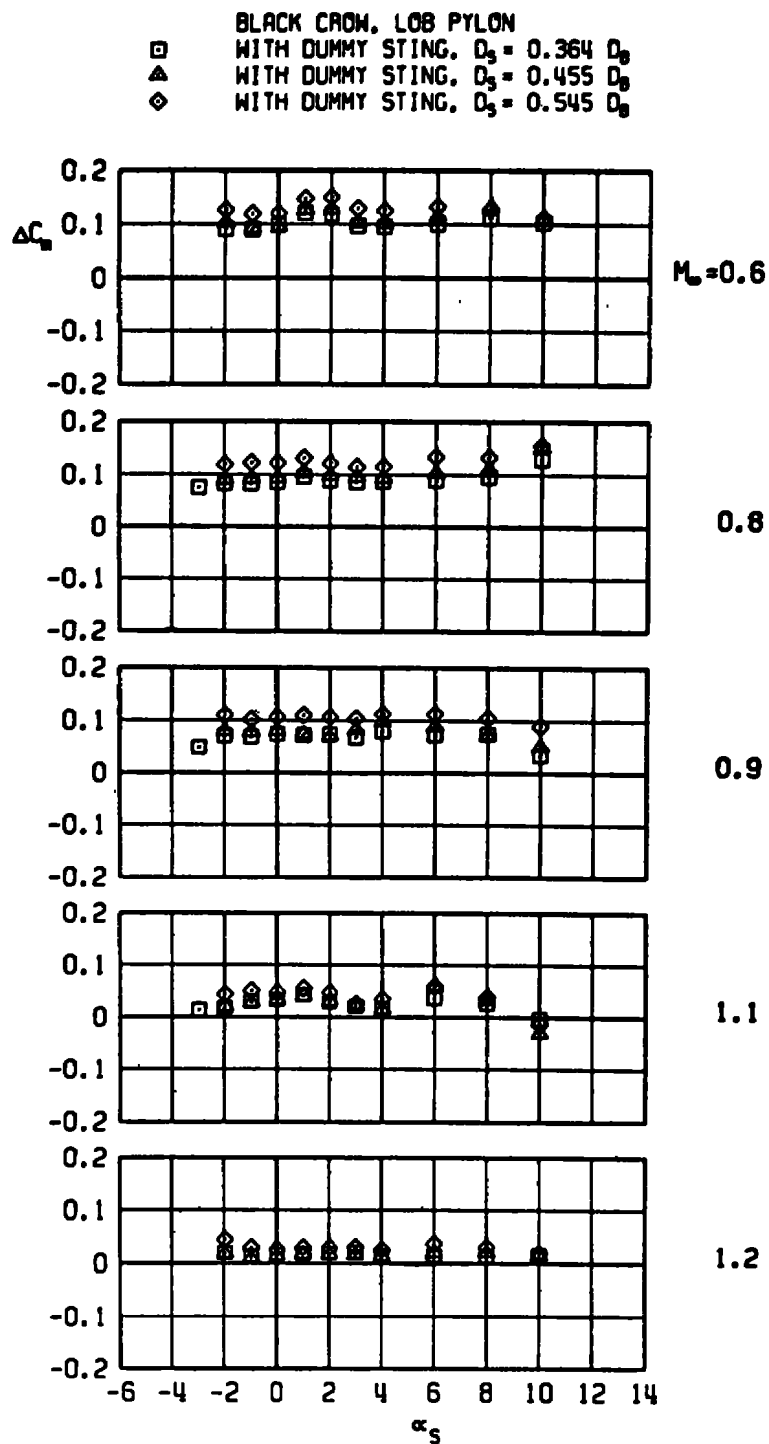
b. Side-force increment
Figure 16. Continued.



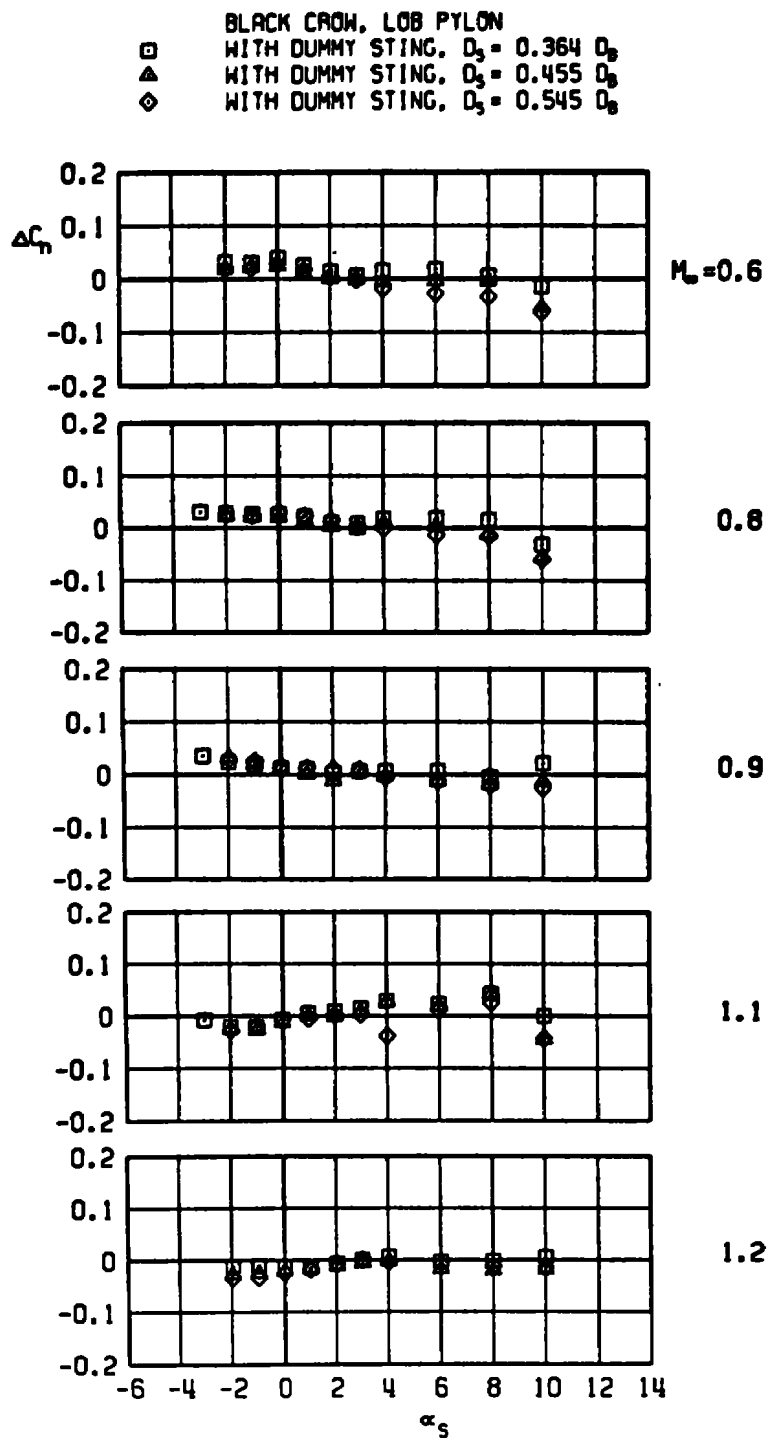
c. Axial-force increment
Figure 16. Continued.



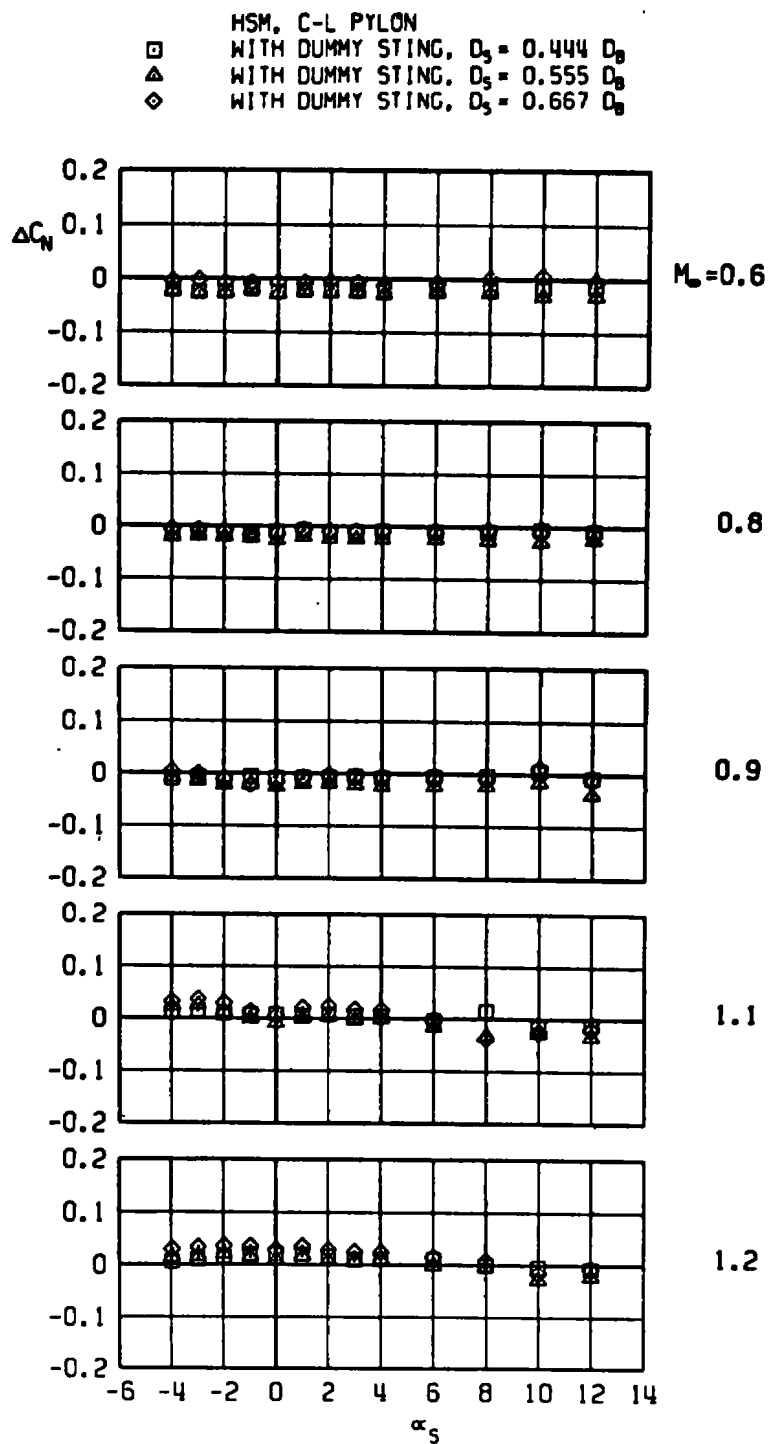
d. Rolling-moment increment
 Figure 16. Continued.



e. Pitching-moment increment
Figure 16. Continued.

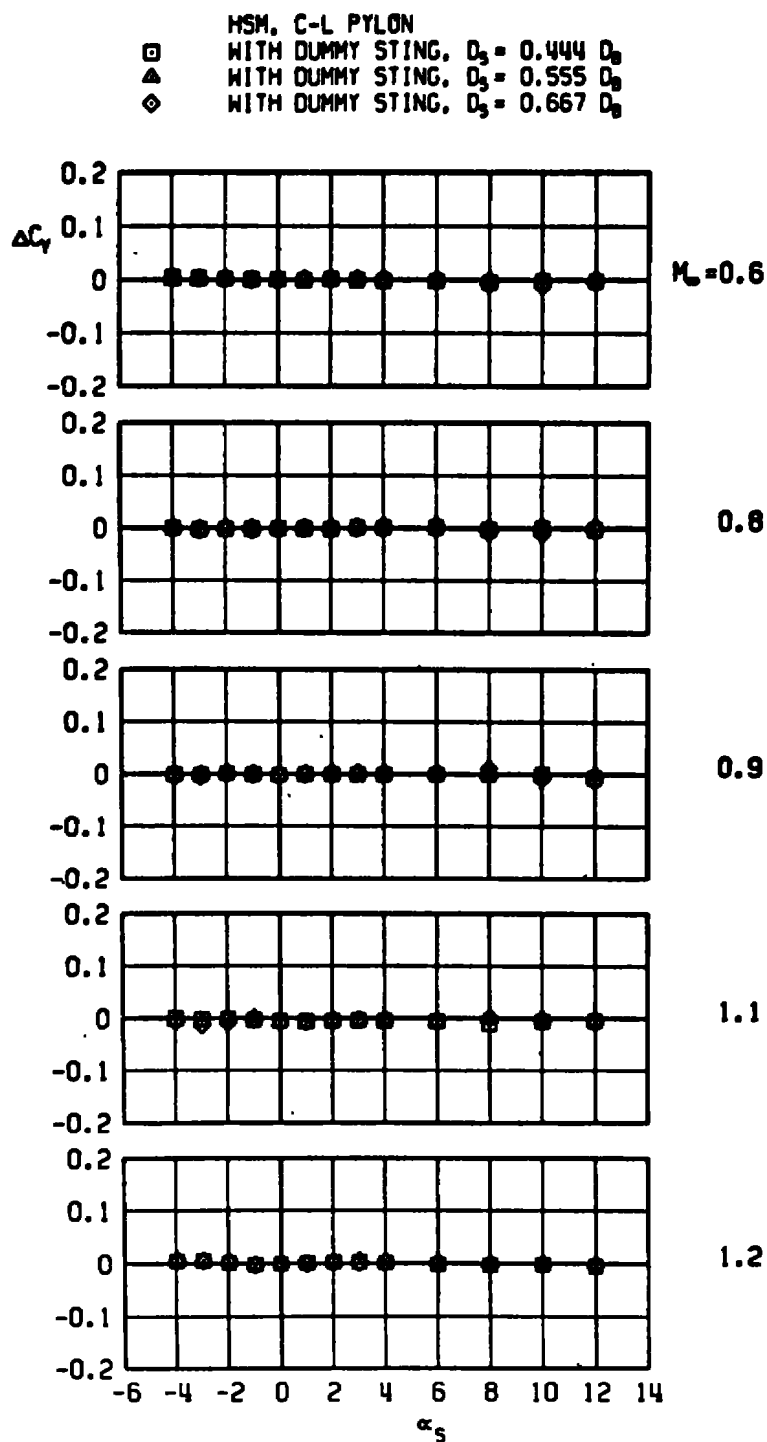


f. Yawing-moment increment
Figure 16. Concluded.

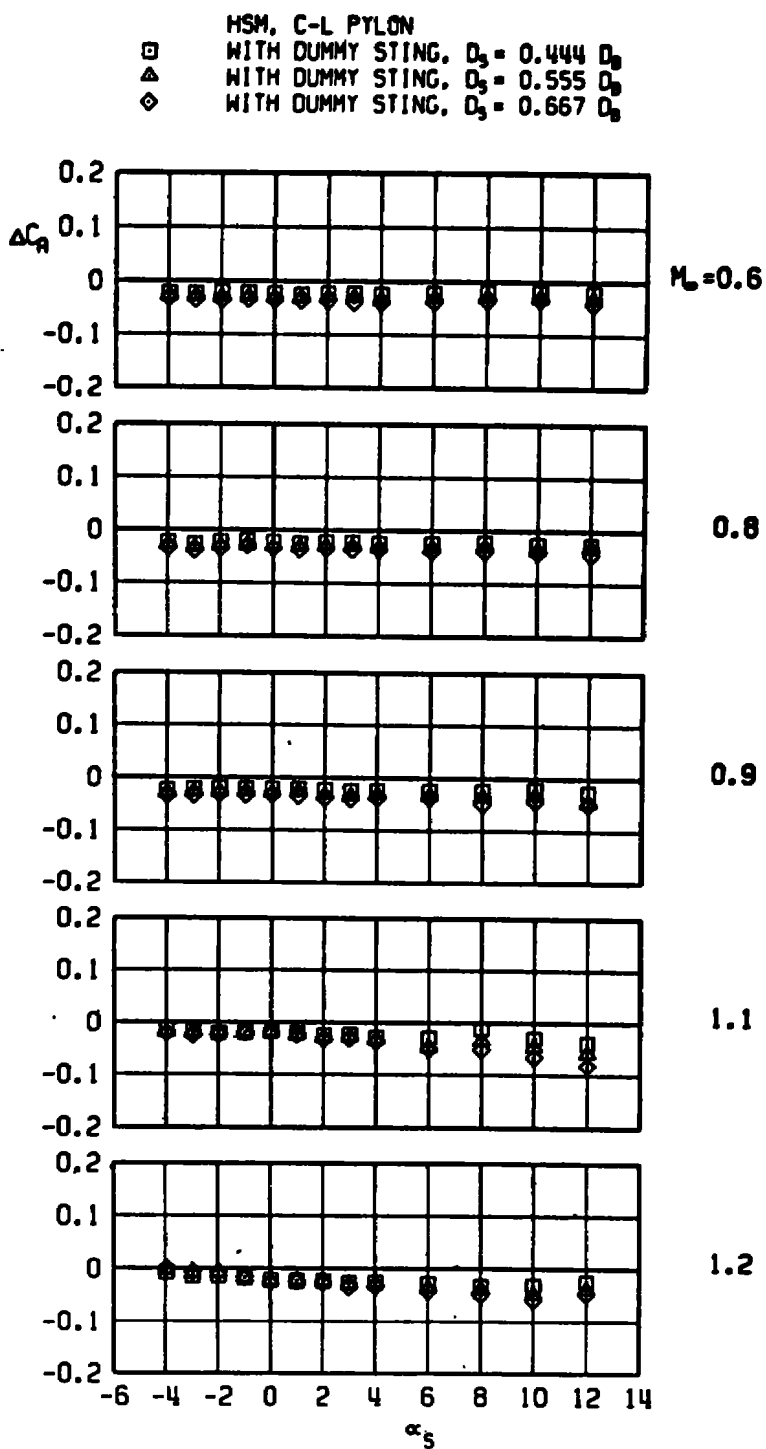


a. Normal-force increment

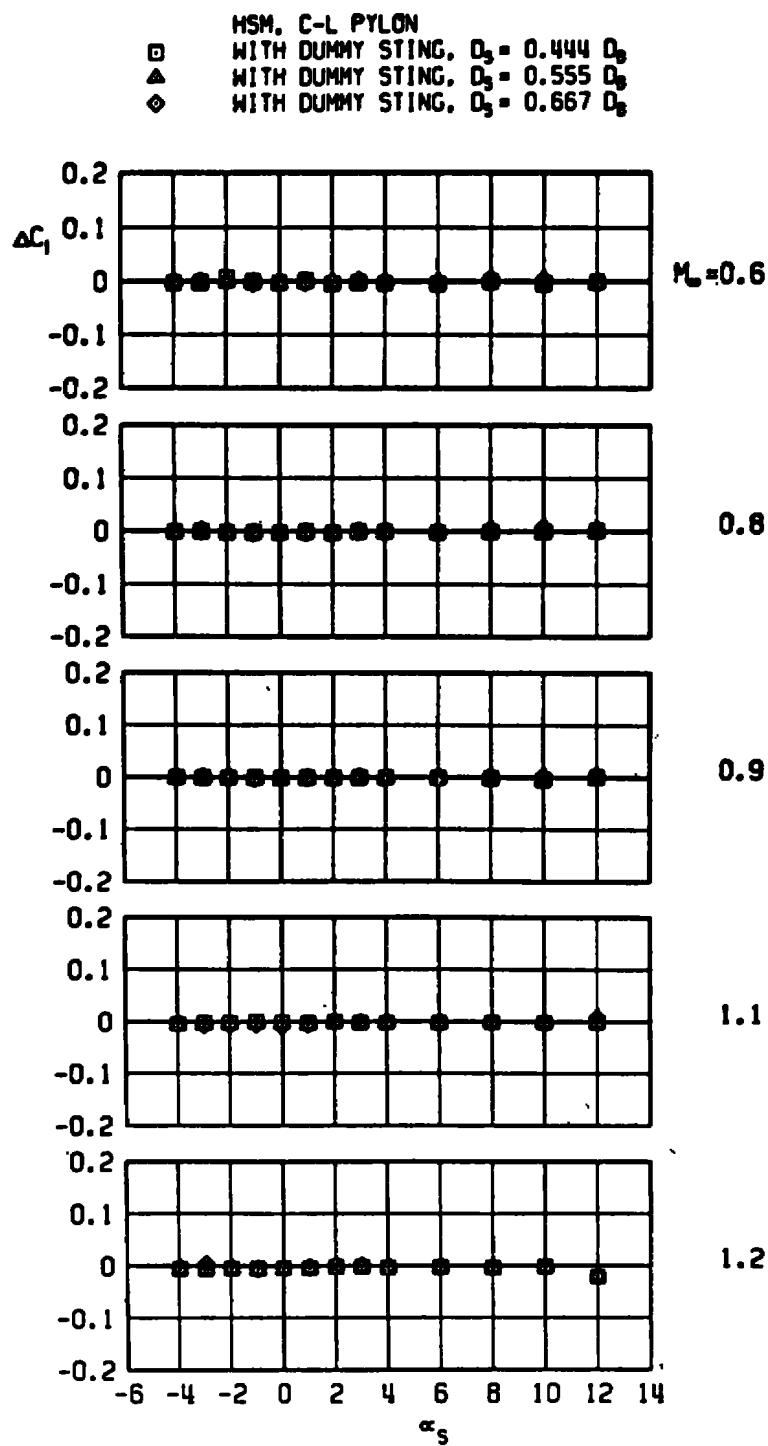
Figure 17. Sting-induced aerodynamic load increments as a function of angle of attack, stable pylon-mounted store, C-L pylon.



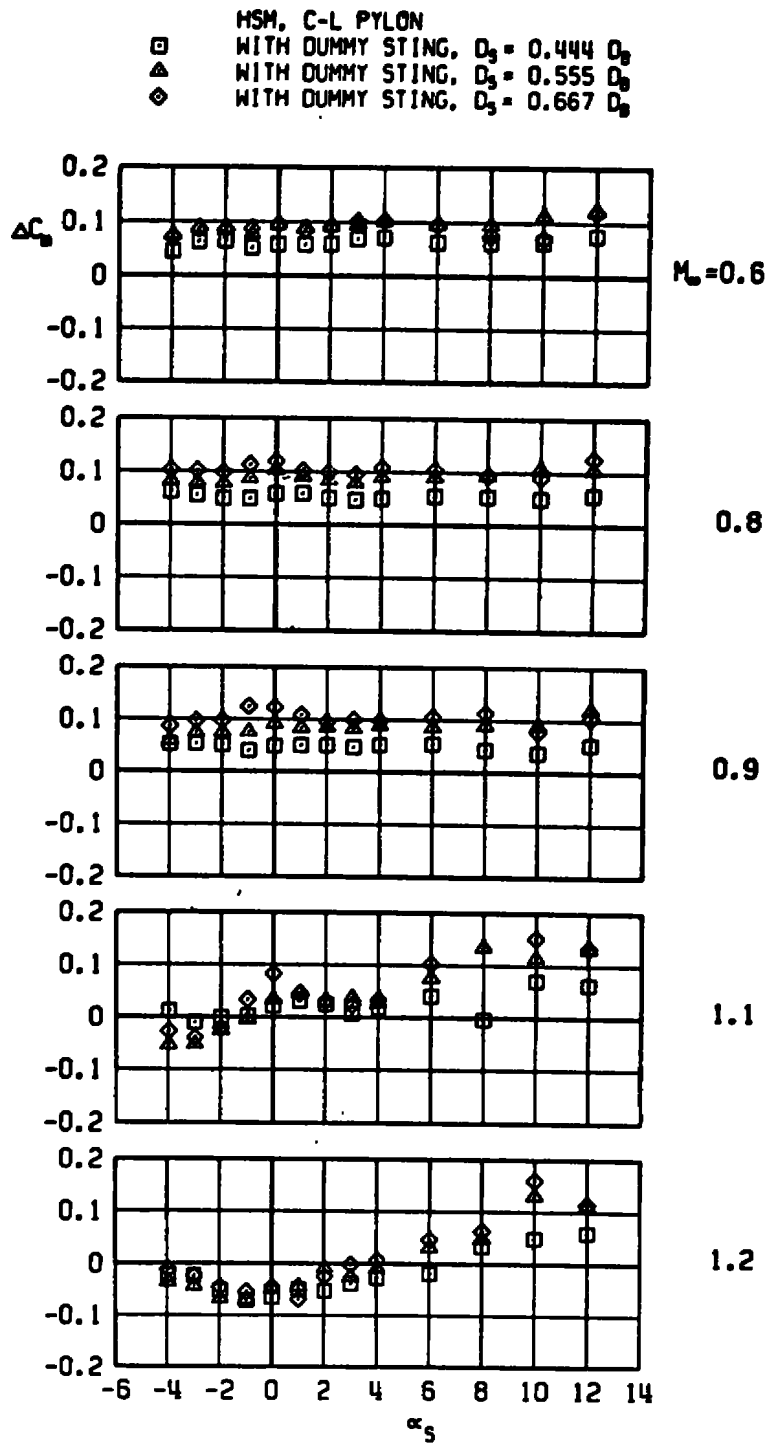
b. Side-force increment
 Figure 17. Continued.



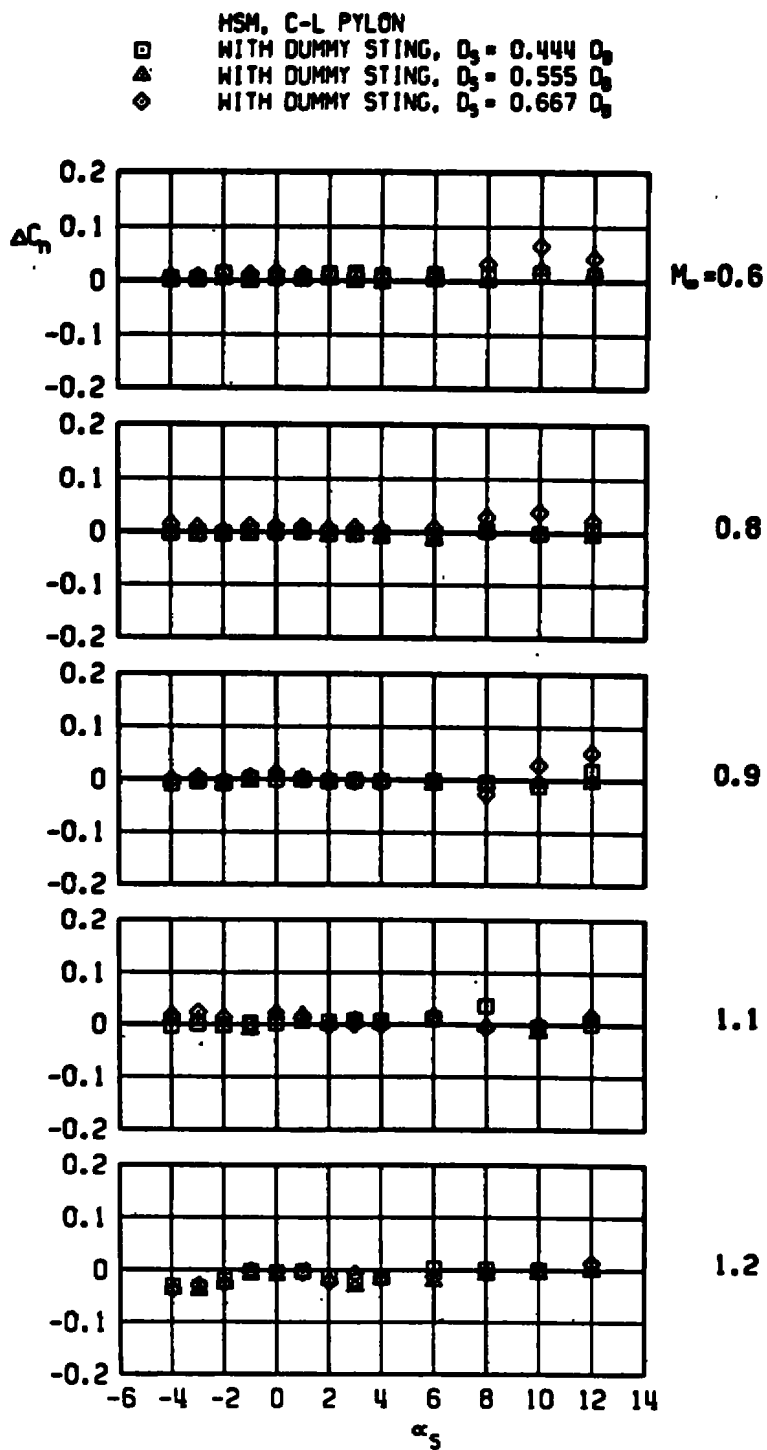
c. Axial-force increment
 Figure 17. Continued.



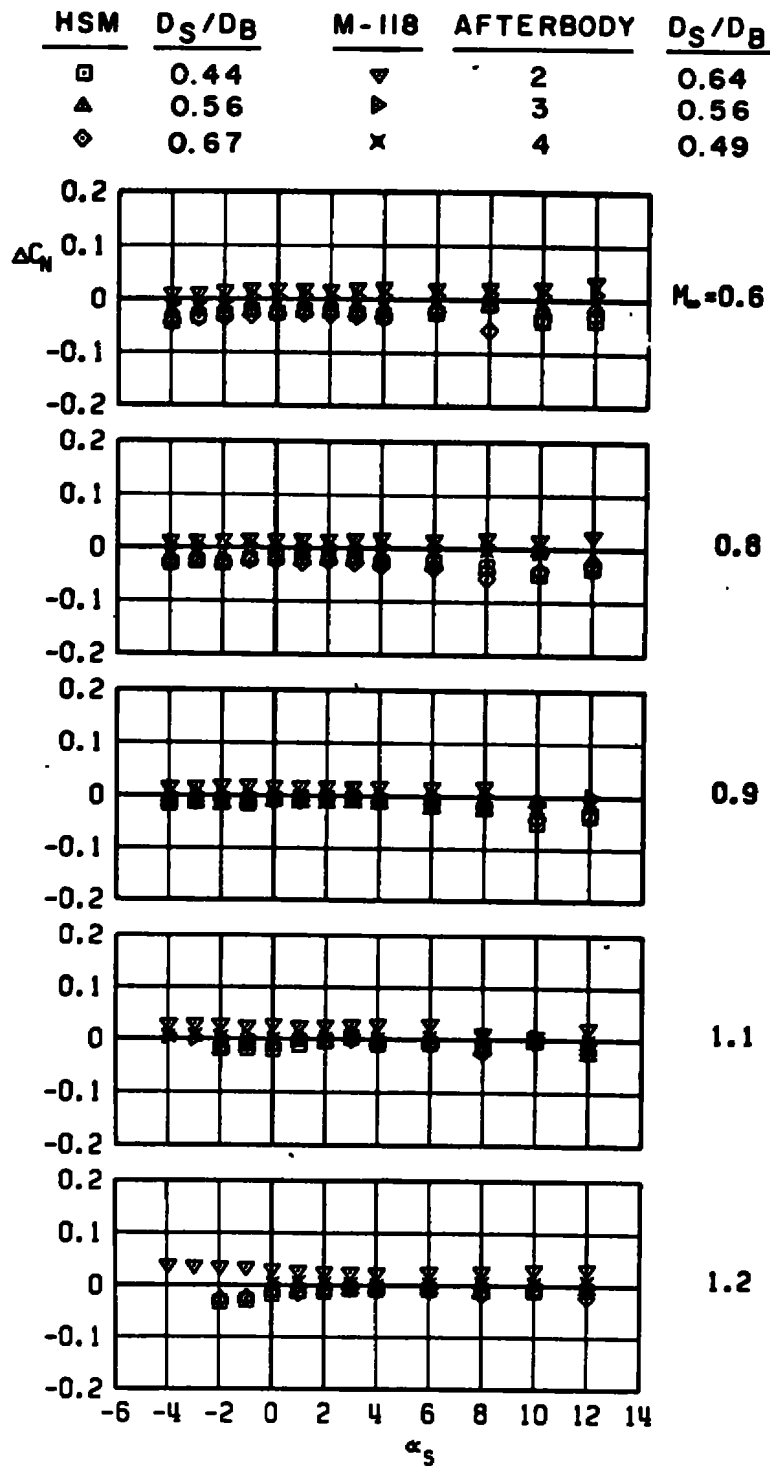
d. Rolling-moment increment
Figure 17. Continued.



e. Pitching-moment increment
 Figure 17. Continued.



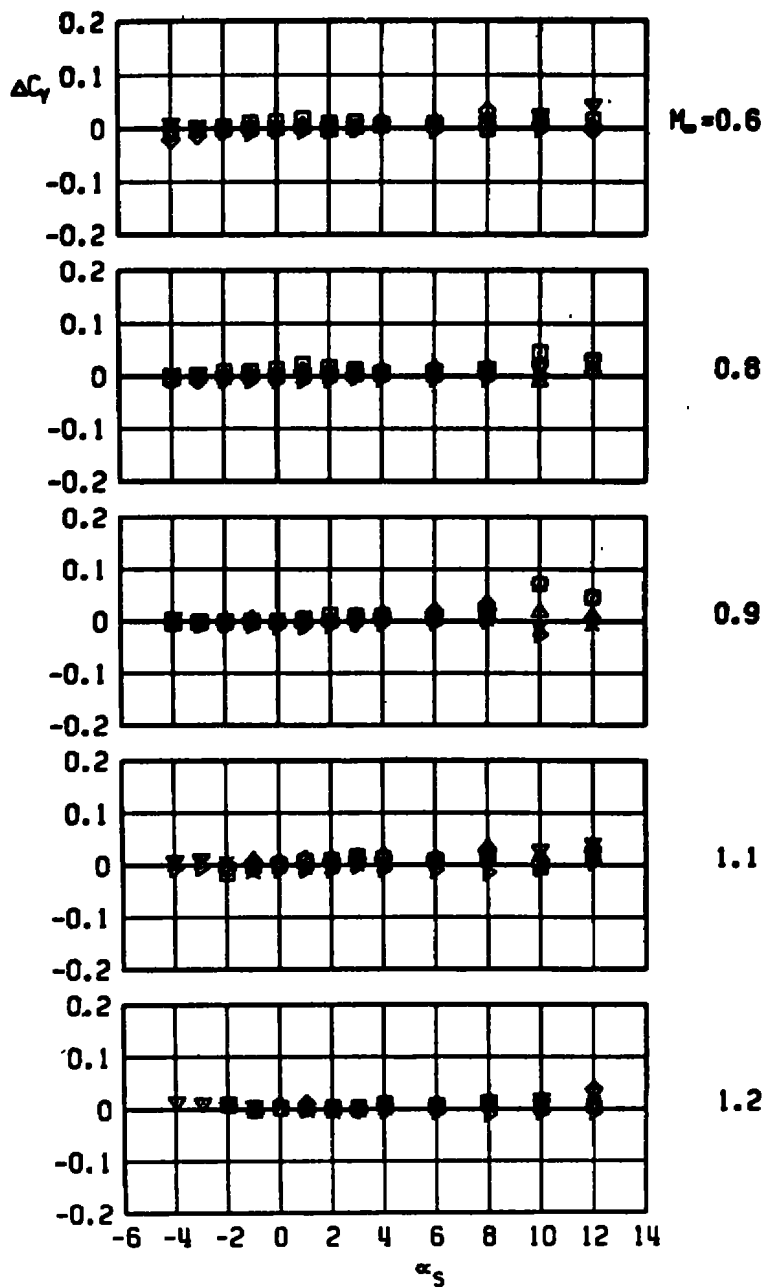
f. Yawing-moment increment
Figure 17. Concluded.



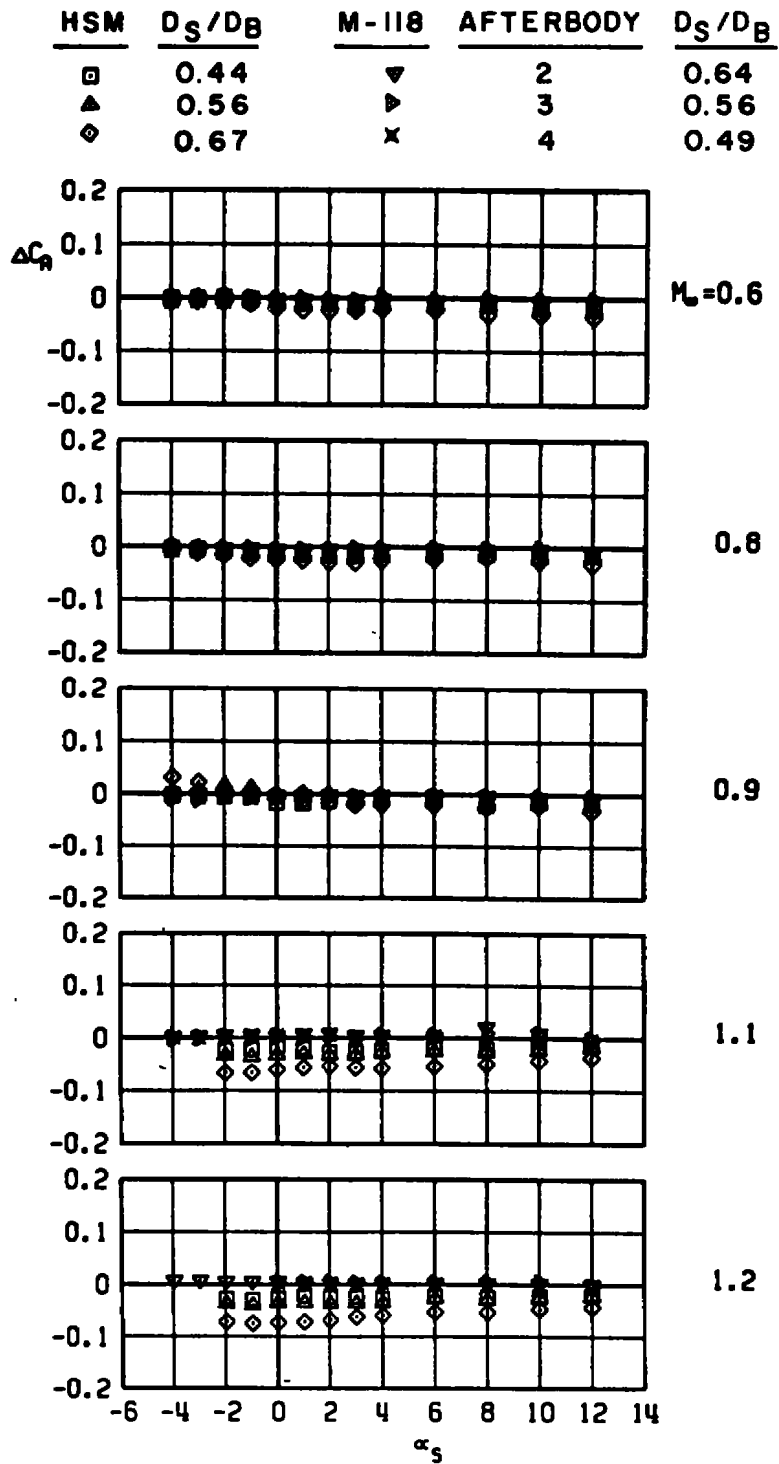
a. Normal-force increment

Figure 18. Sting-induced aerodynamic load increments as a function of angle of attack, stable pylon-mounted stores, LIB pylon.

HSM	D_S/D_B	M-118	AFTERBODY	D_S/D_B
□	0.44	▽	2	0.64
▲	0.56	▷	3	0.56
◇	0.67	×	4	0.49

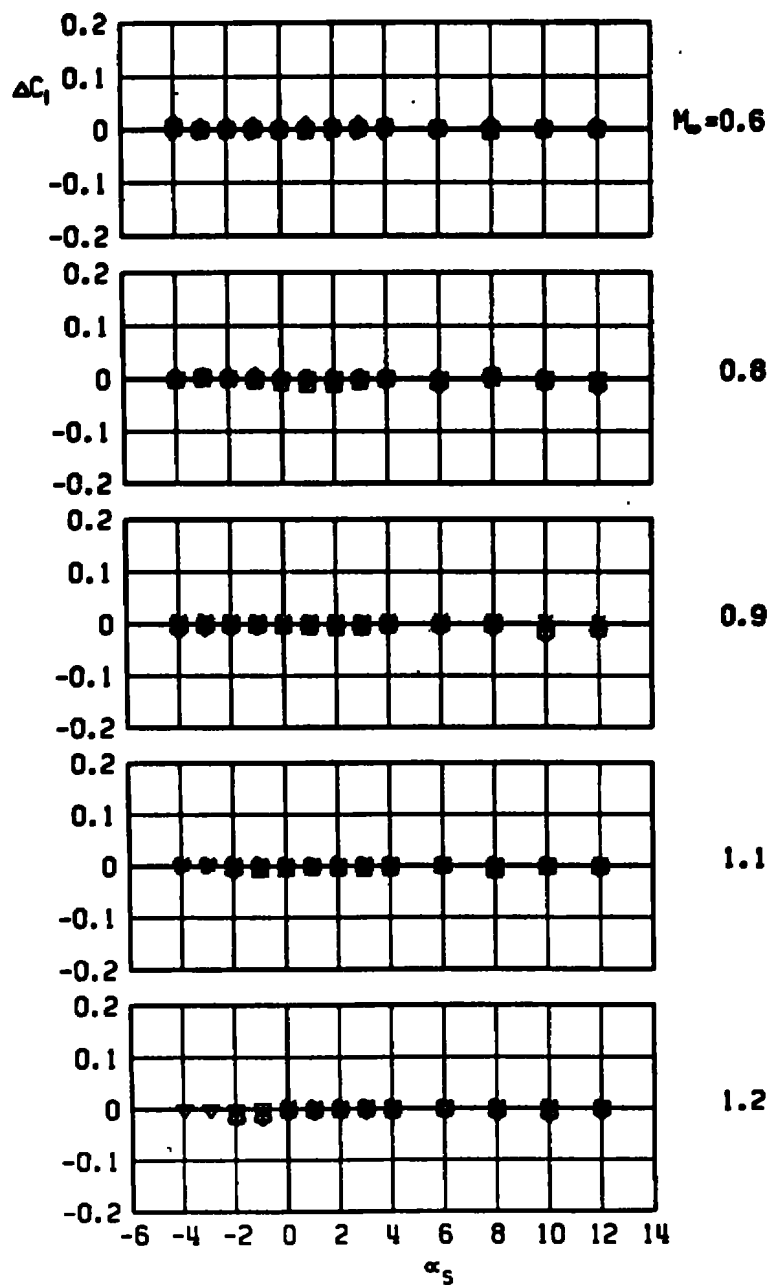


b. Side-force increment
Figure 18. Continued.

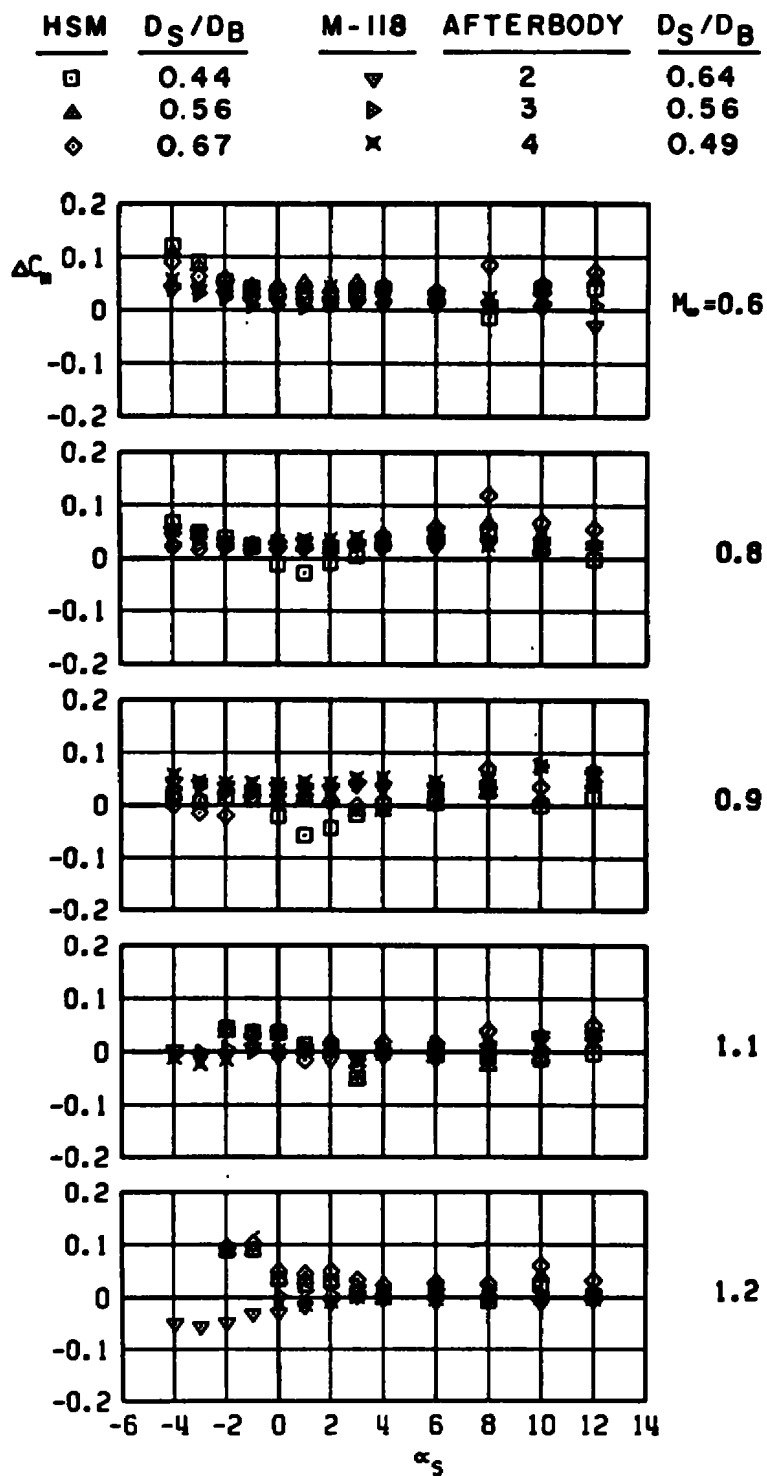


c. Axial-force increment
Figure 18. Continued.

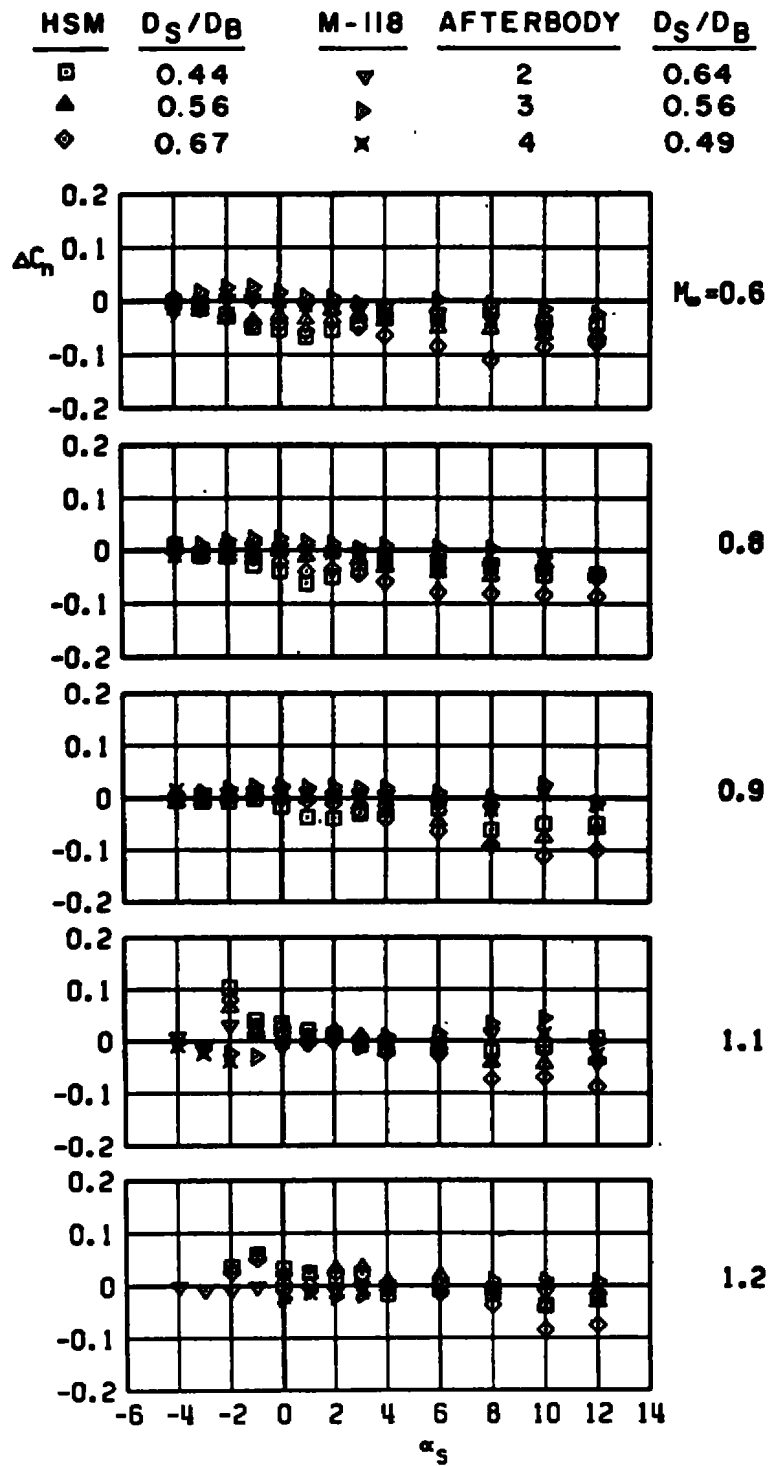
HSM	D_S/D_B	M-118	AFTERBODY	D_S/D_B
□	0.44	▽	2	0.64
▲	0.56	▷	3	0.56
◇	0.67	×	4	0.49



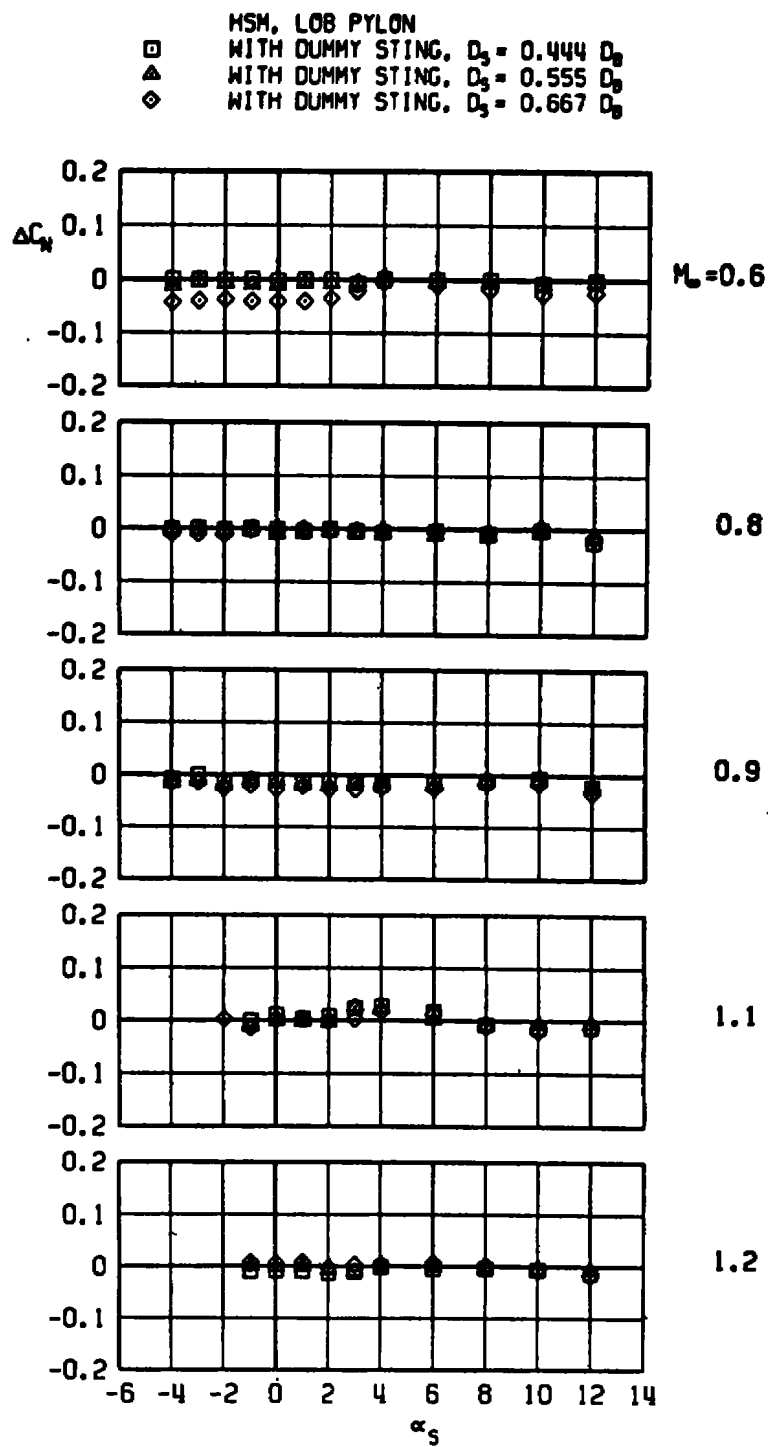
d. Rolling-moment increment
Figure 18. Continued.



e. Pitching-moment increment
Figure 18. Continued.

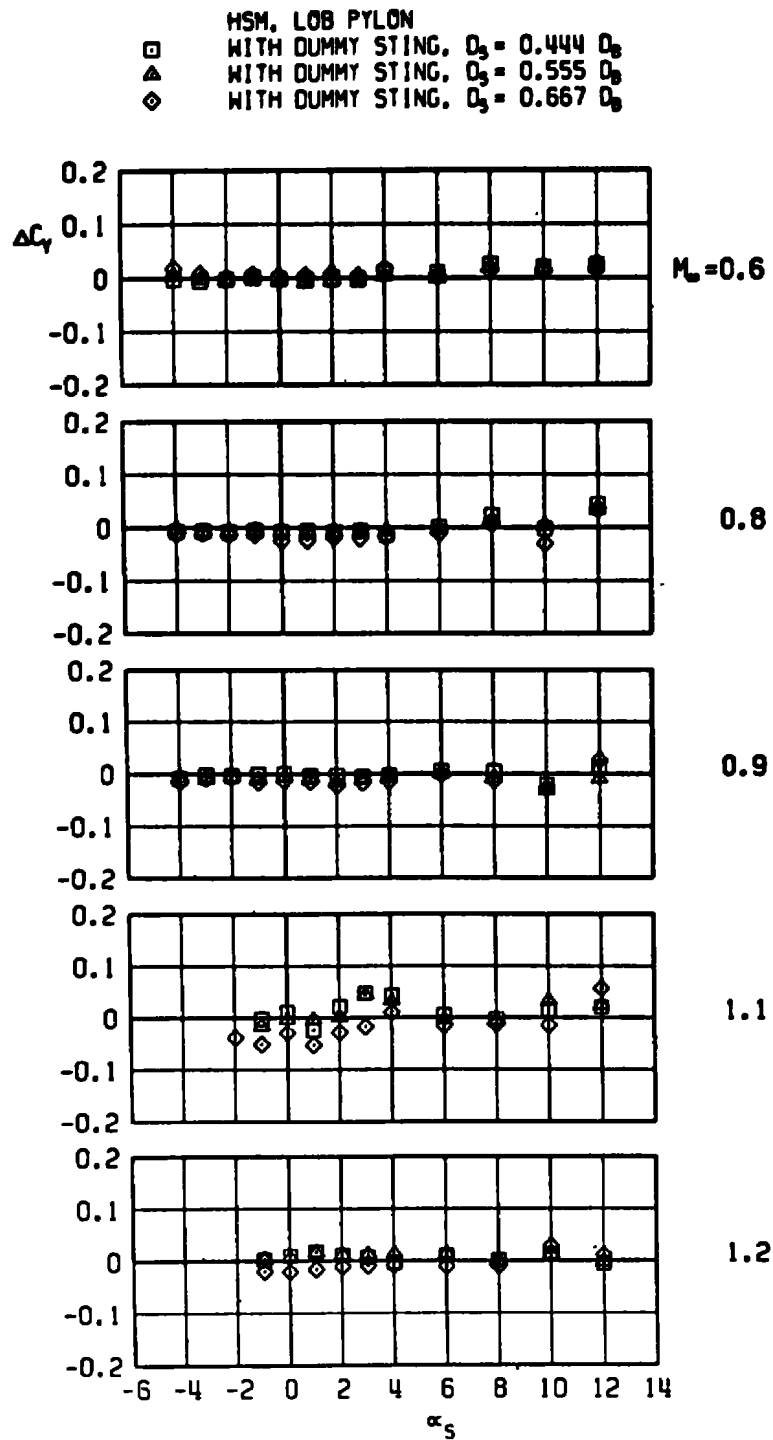


f. Yawing-moment increment
Figure 18. Concluded.

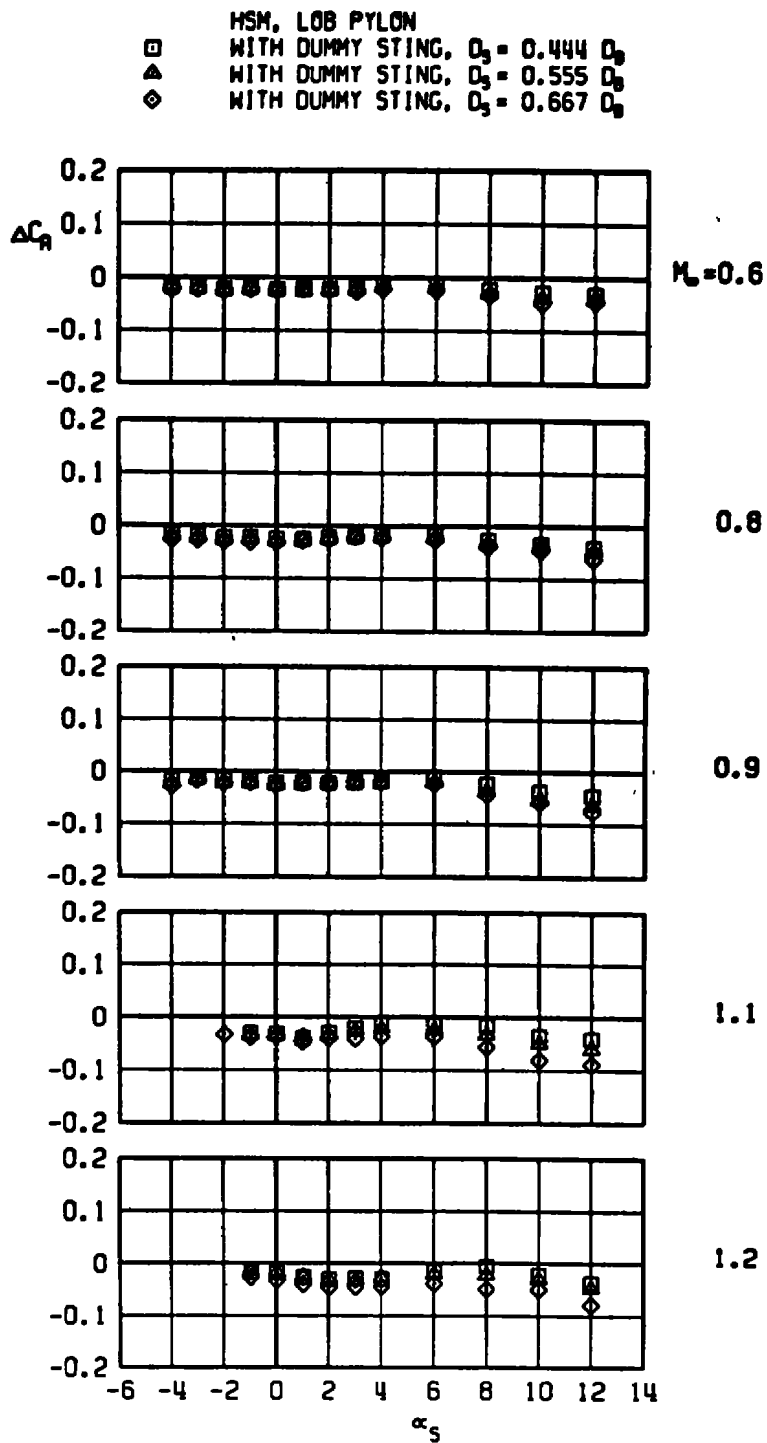


a. Normal-force increment

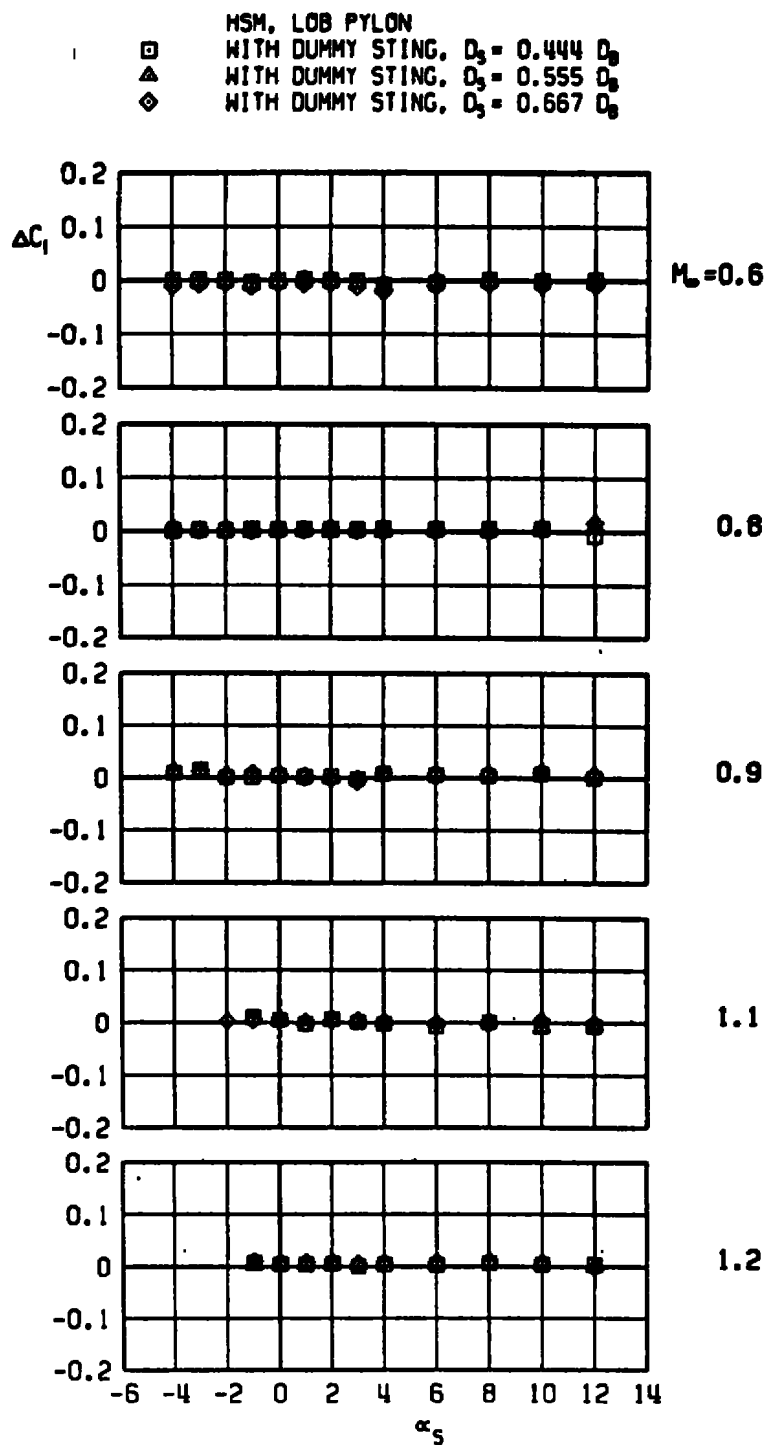
Figure 19. Sting-induced aerodynamic load increments as a function of angle of attack, stable pylon-mounted store, LOB pylon.



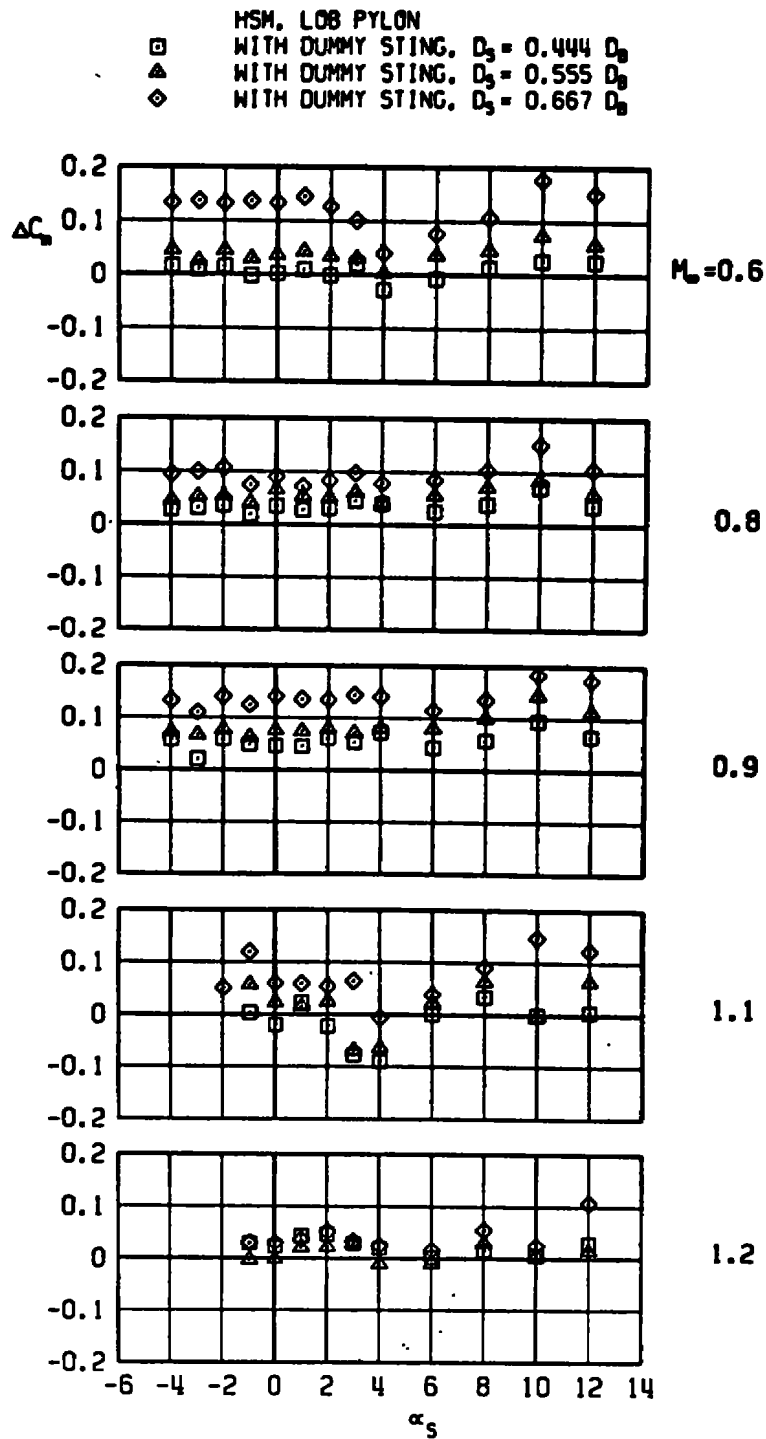
b. Side-force increment
 Figure 19. Continued.



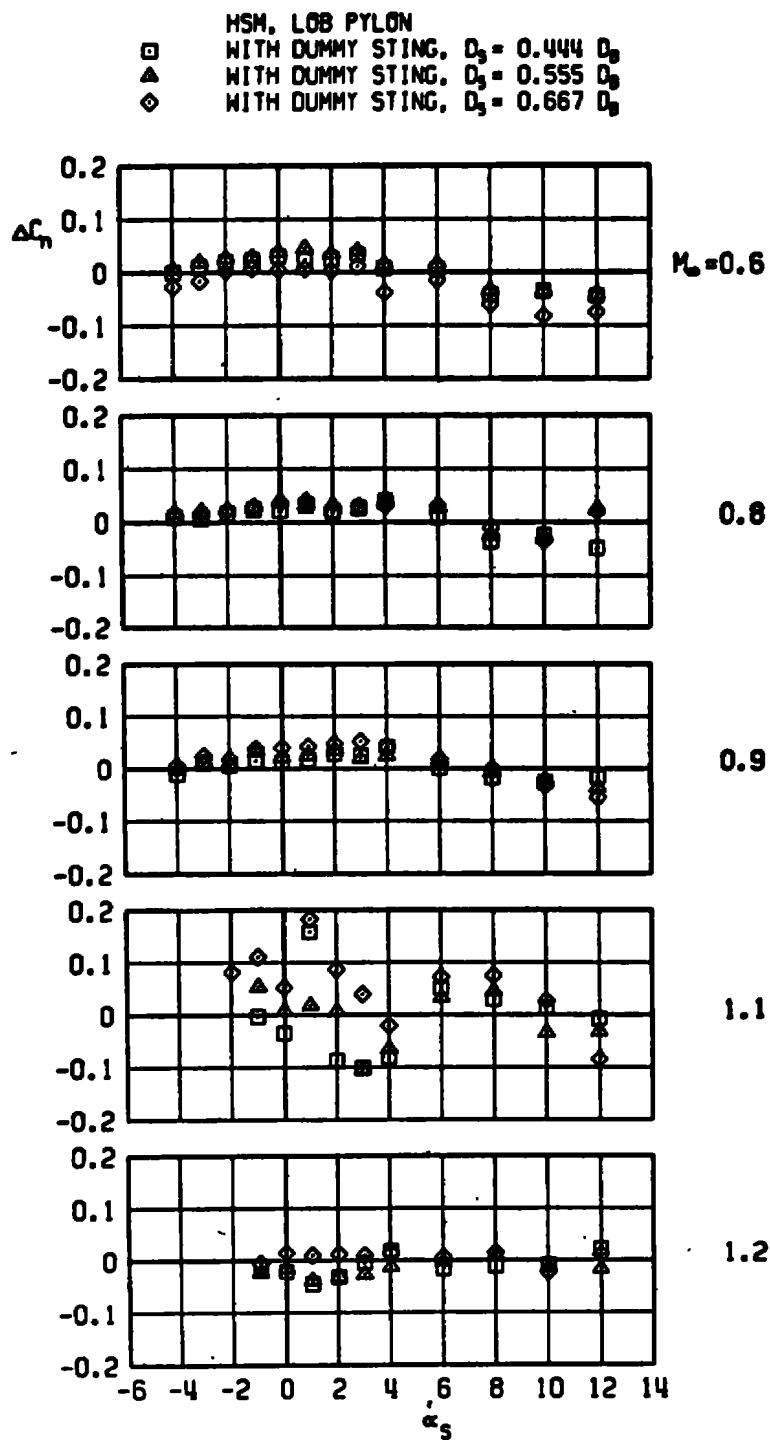
c. Axial-force increment
Figure 19. Continued.



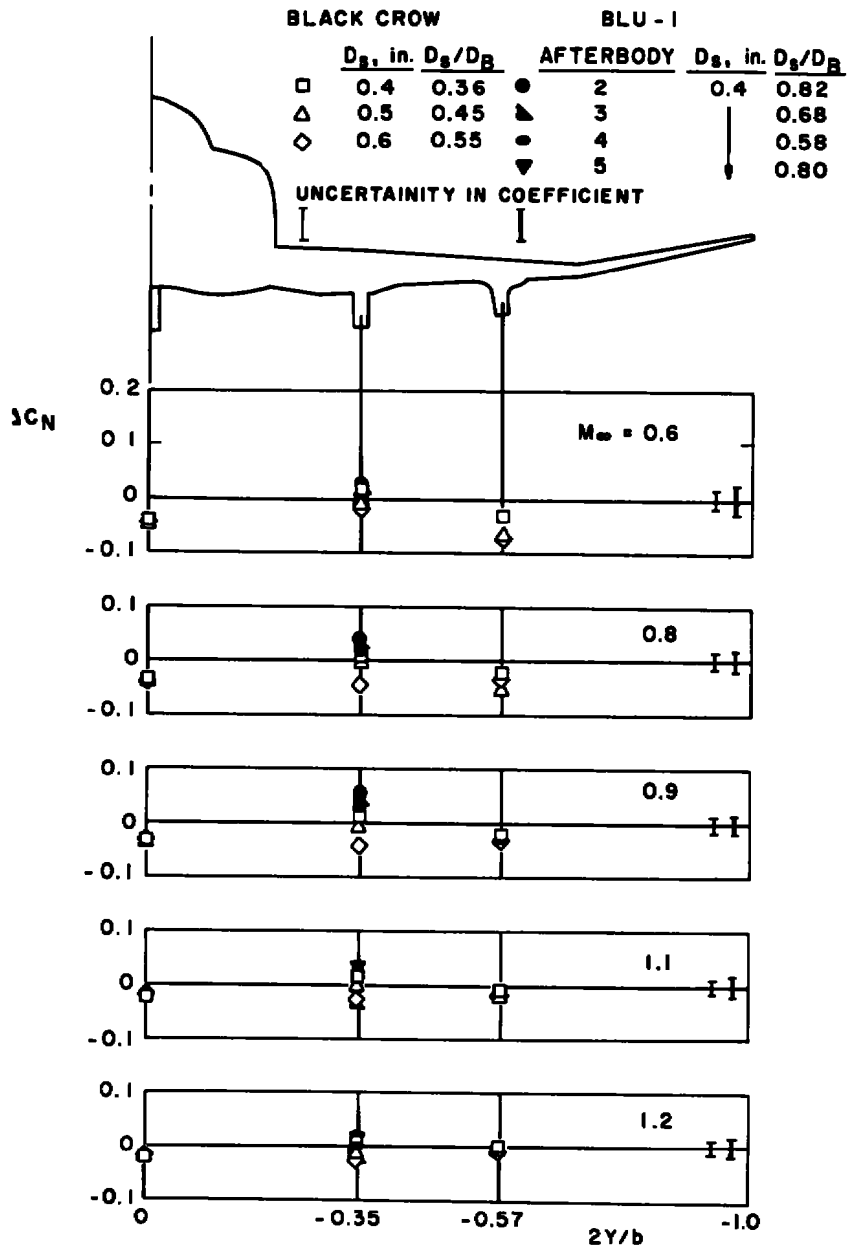
d. Rolling-moment increment
 Figure 19. Continued.



e. Pitching-moment increment
Figure 19. Continued.

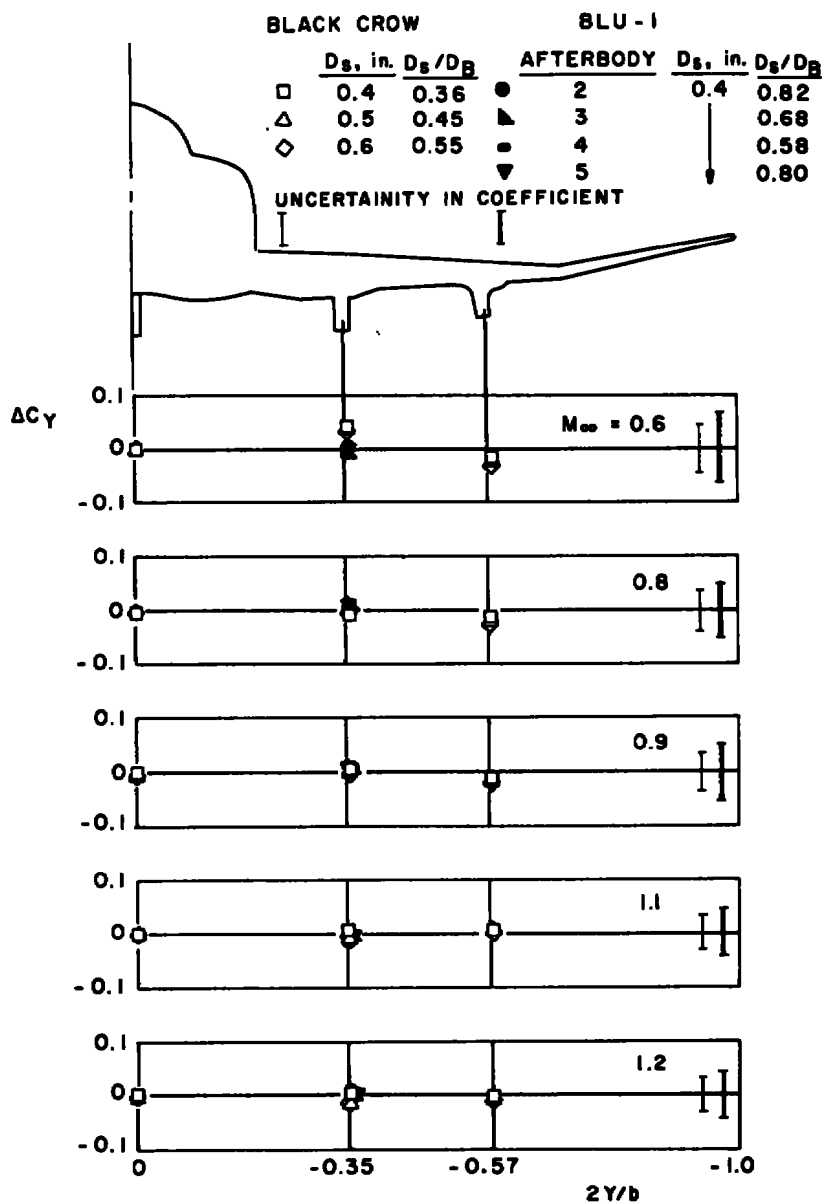


f. Yawing-moment increment
 Figure 19. Concluded.

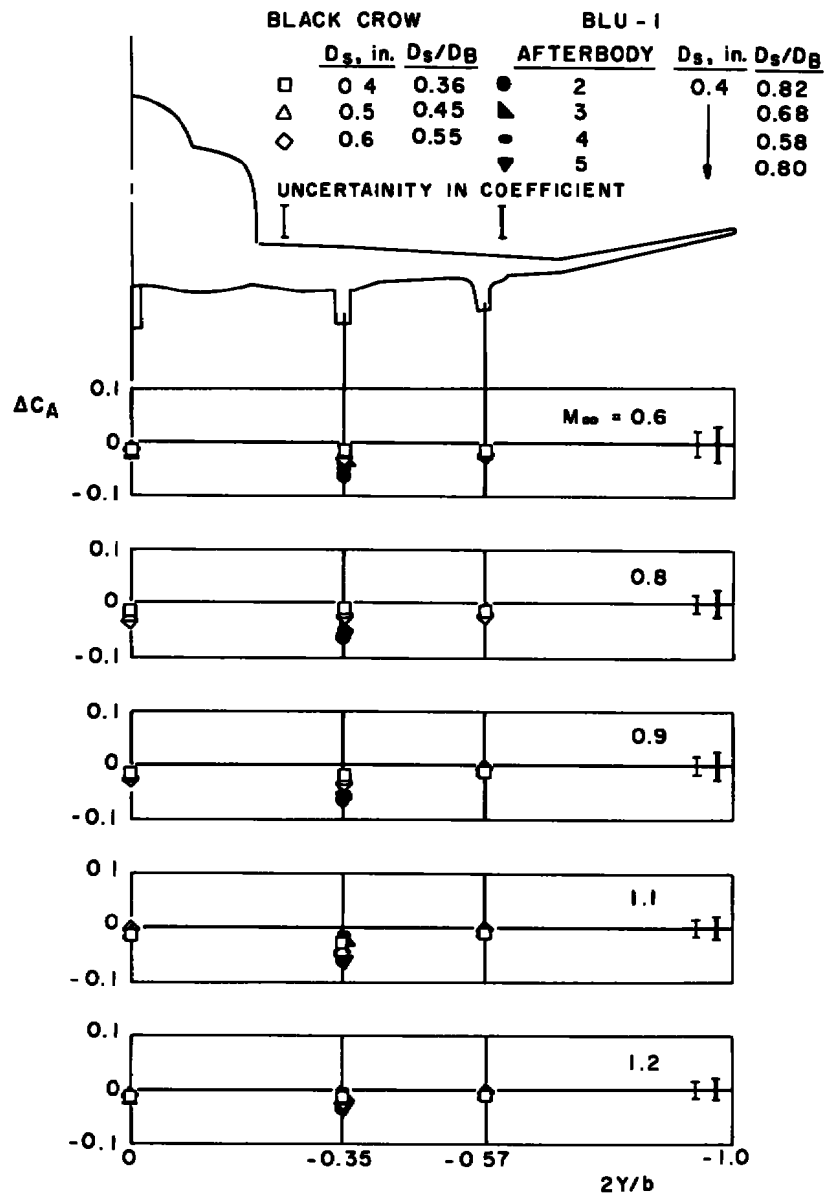


a. Normal-force increment

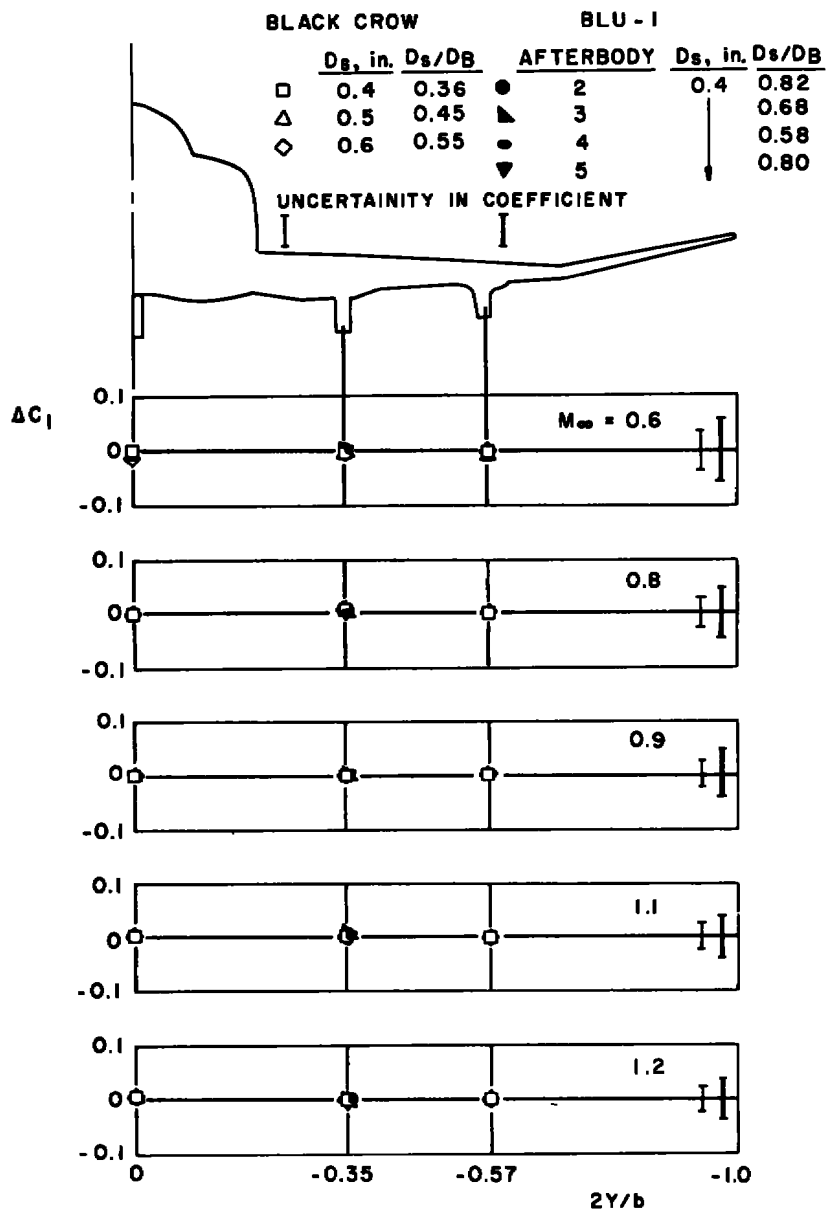
Figure 20. Sting-induced aerodynamic load increments at zero angle of attack as a function of pylon position, unstable stores.



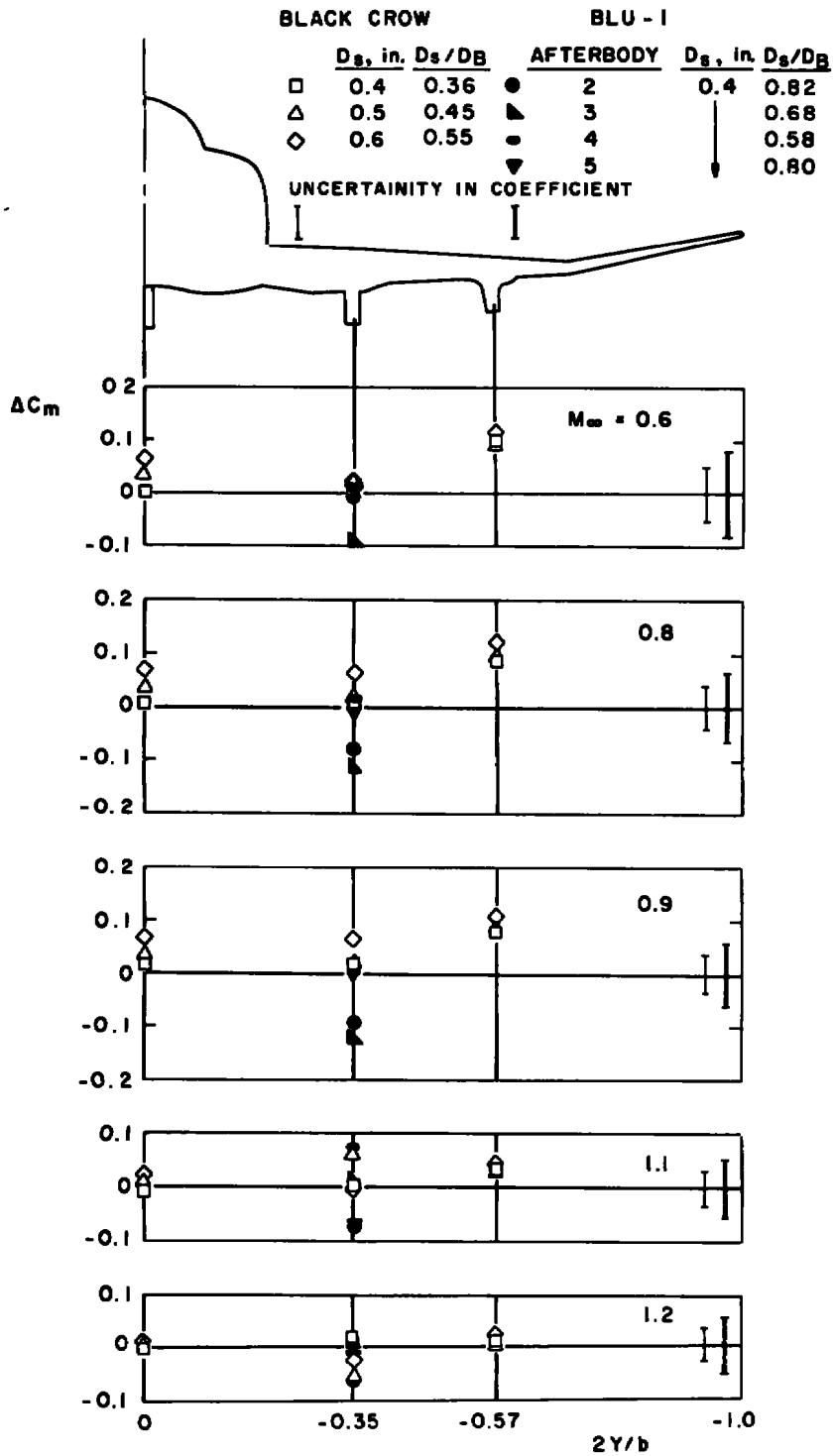
b. Side-force increment
Figure 20. Continued.



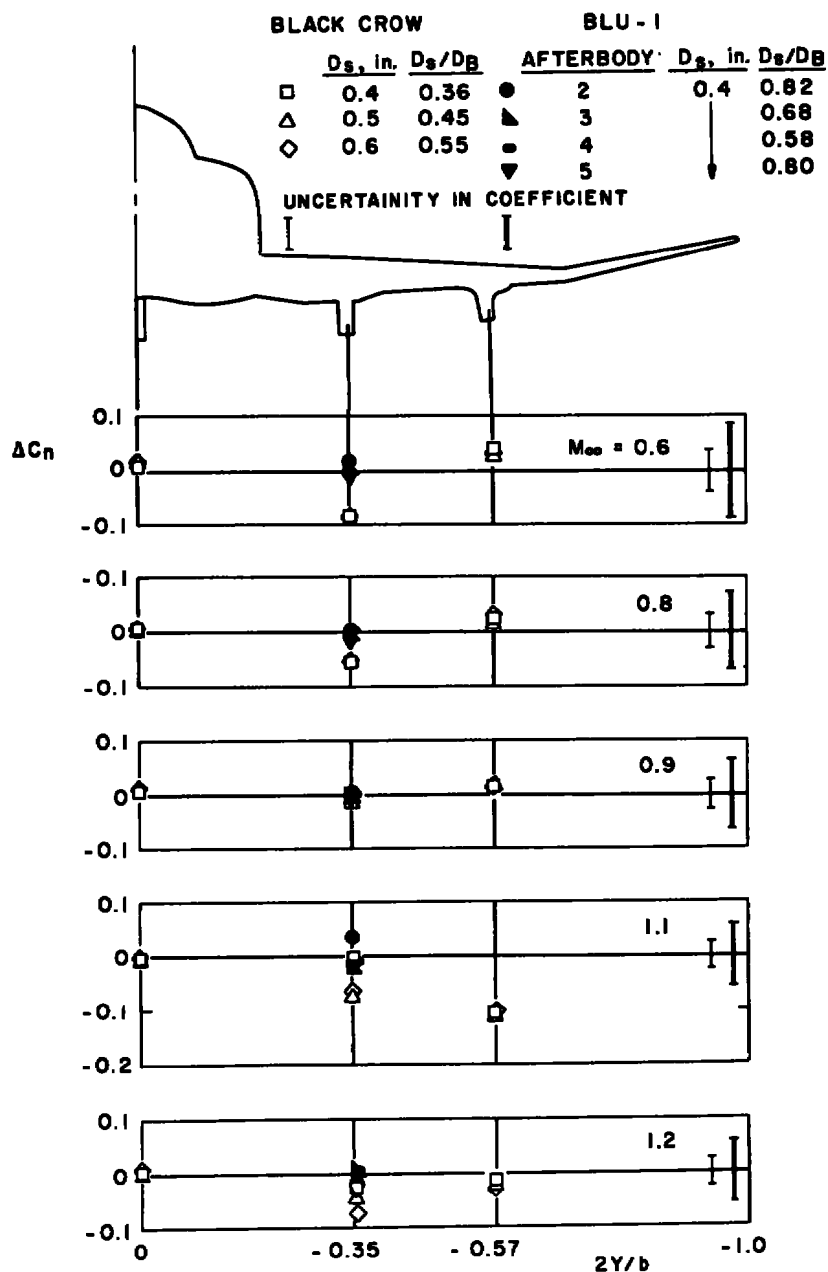
c. Axial-force increment
Figure 20. Continued.



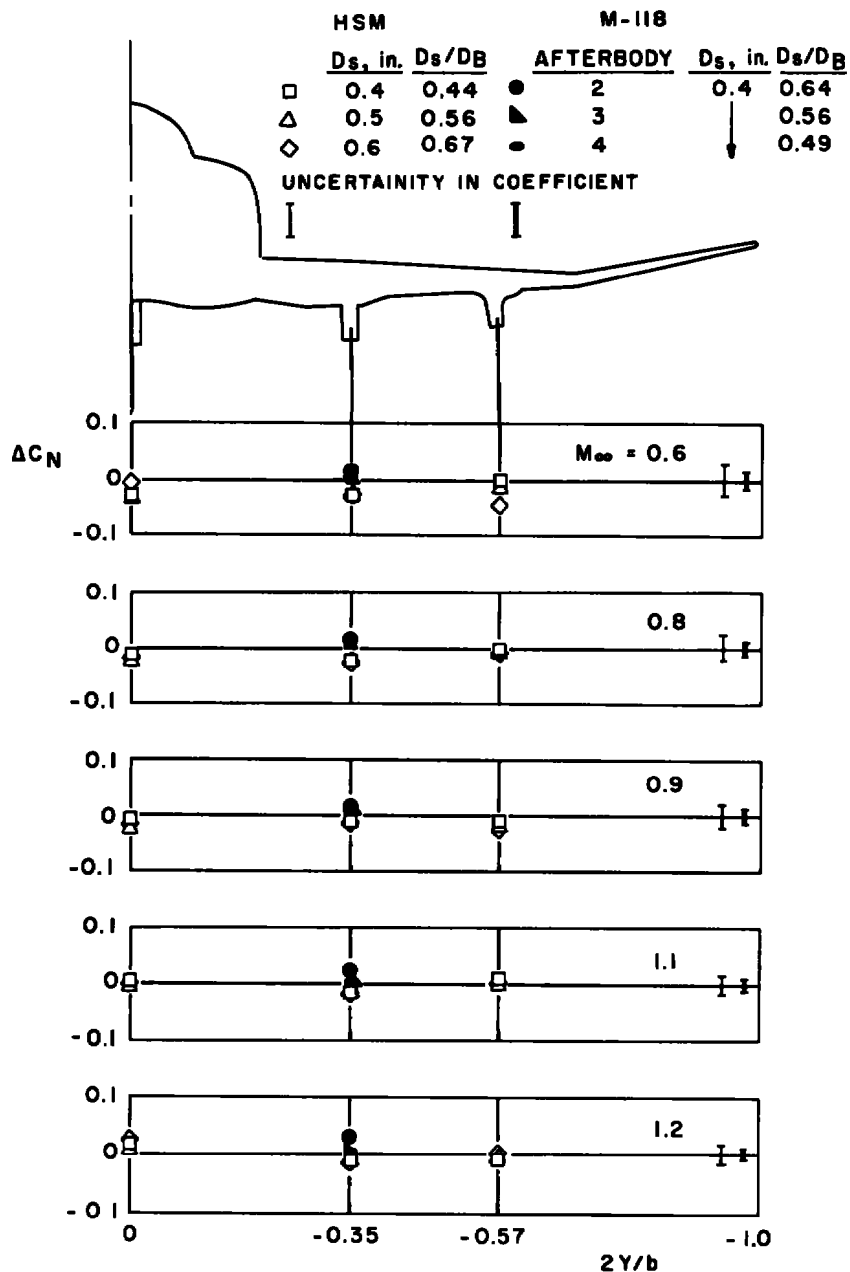
d. Rolling-moment increment
Figure 20. Continued.



e. Pitching-moment increment
Figure 20. Continued.

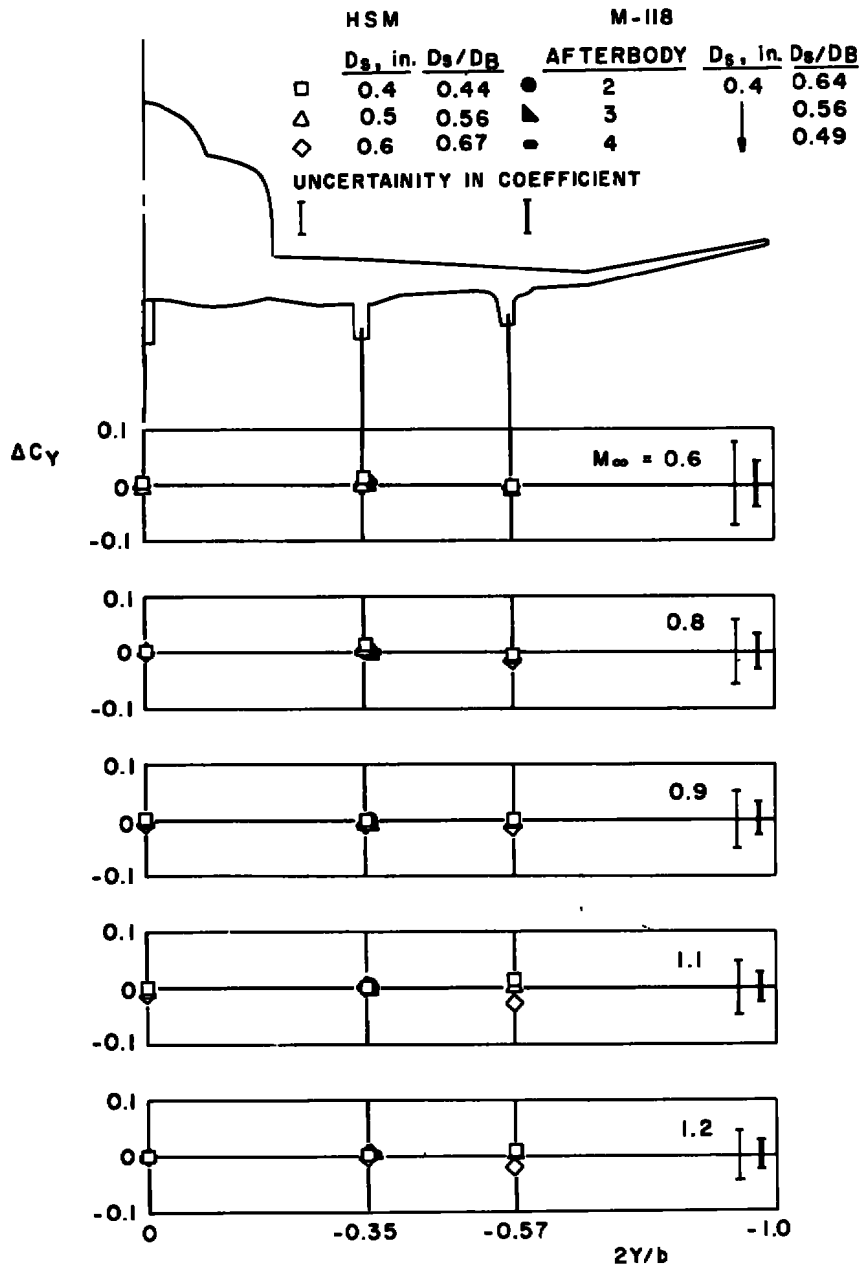


f. Yawing-moment increment
Figure 20. Concluded.

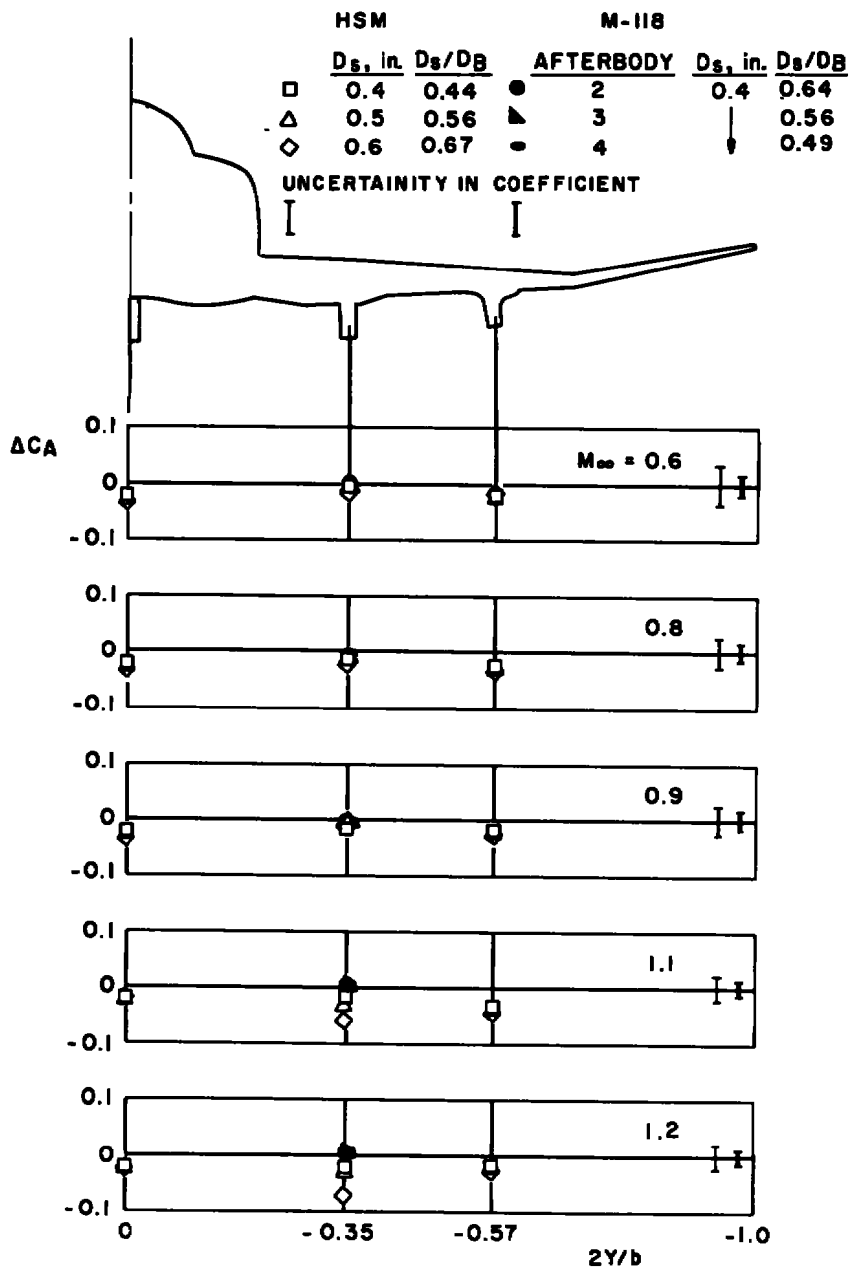


a. Normal-force increment

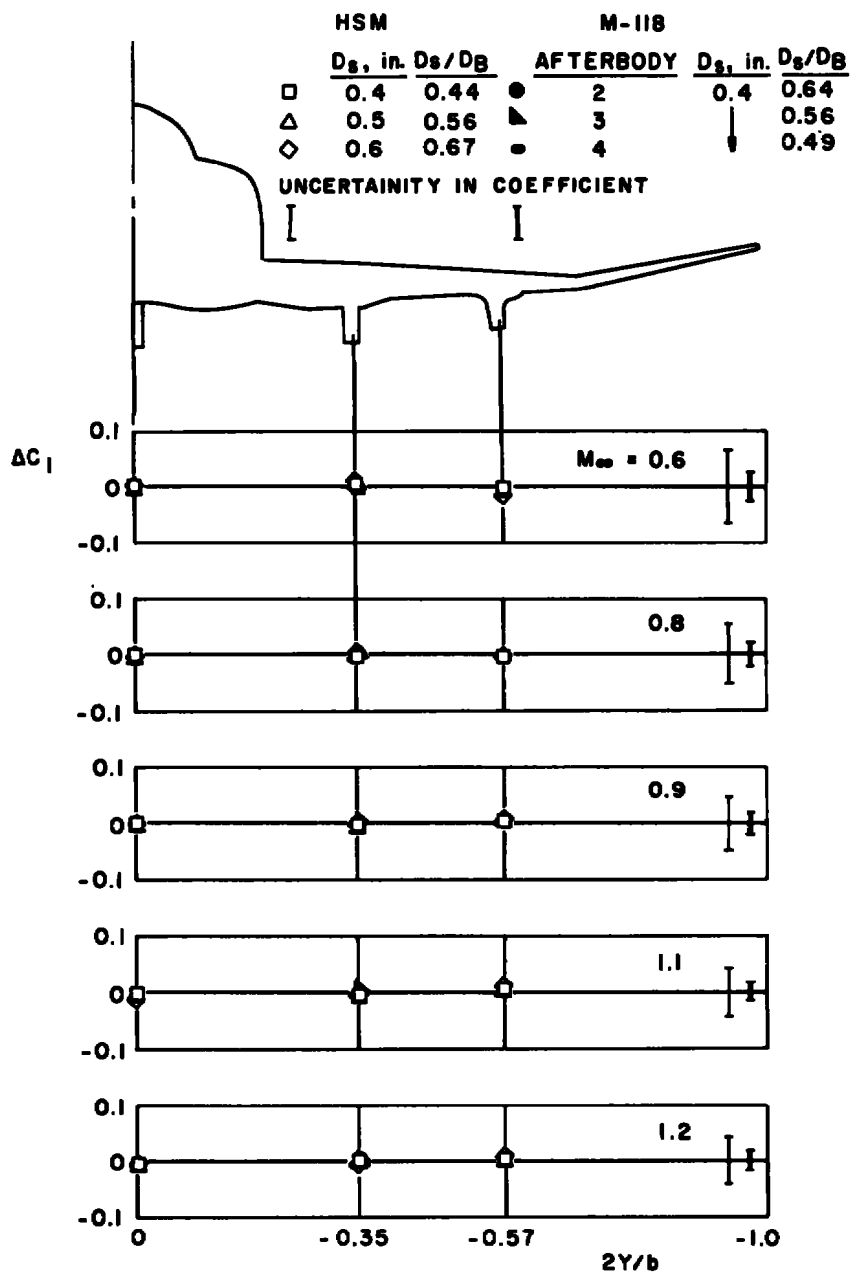
Figure 21. Sting-induced aerodynamic load increments at zero angle of attack as a function of pylon position, stable pylon-mounted stores.



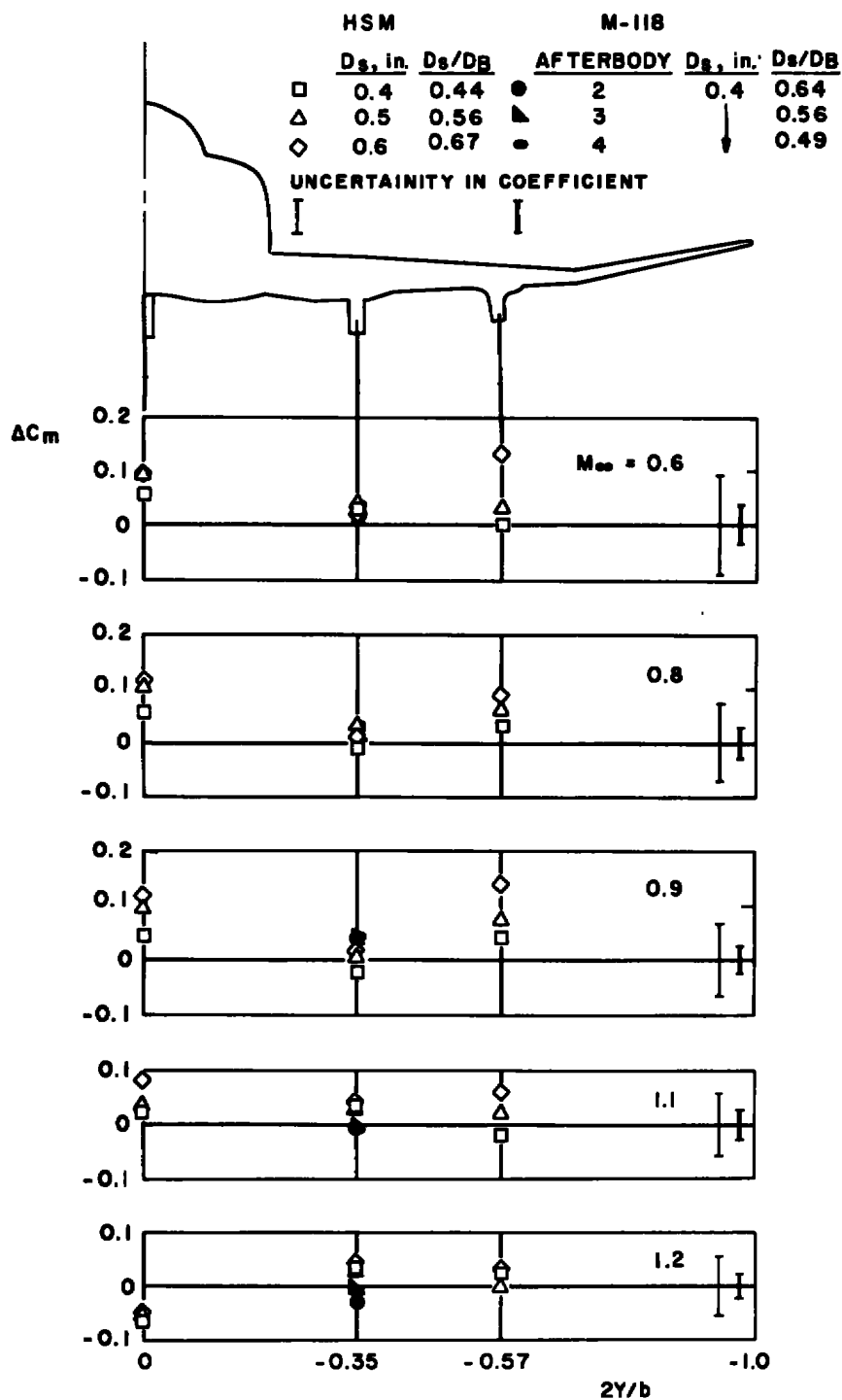
b. Side-force increment
Figure 21. Continued.



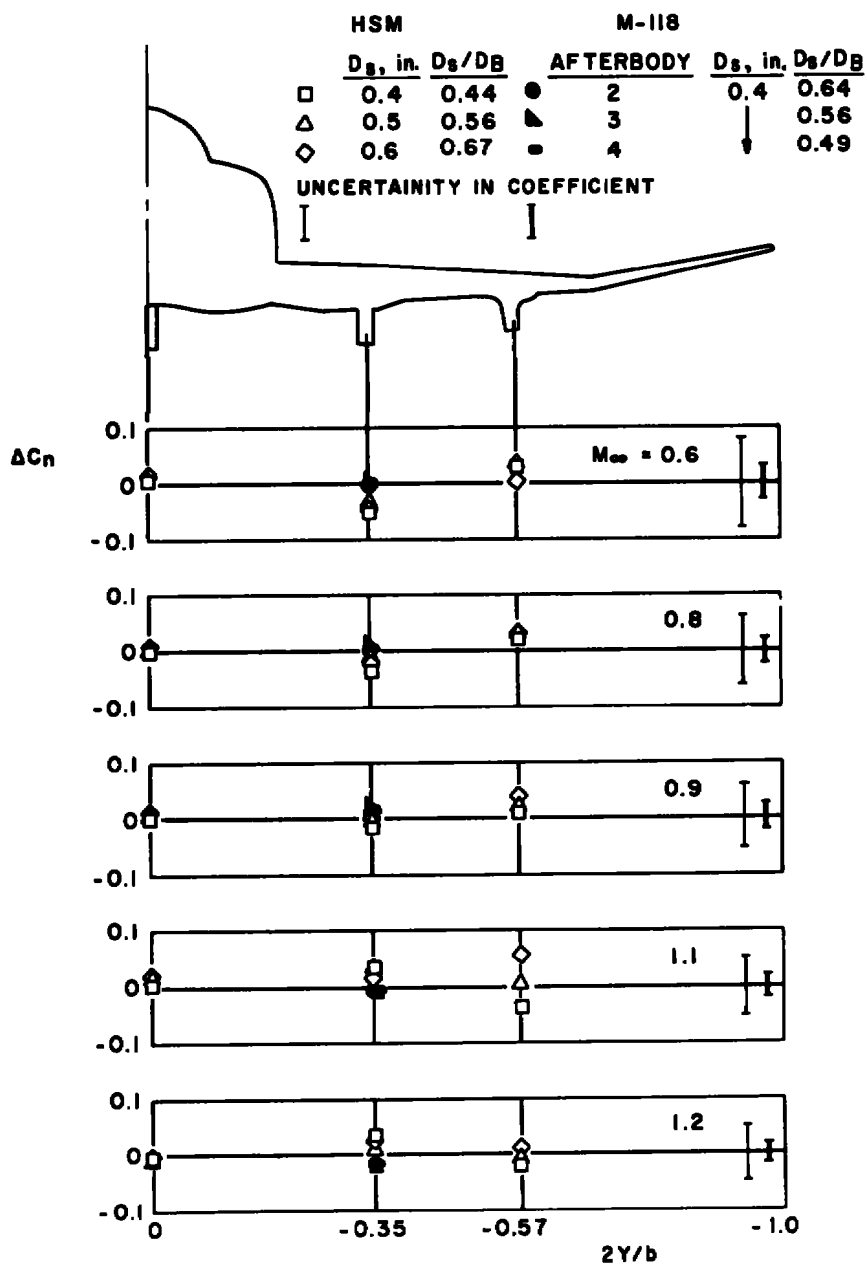
c. Axial-force increment
Figure 21. Continued.



d. Rolling-moment increment
Figure 21. Continued.



e. Pitching-moment increment
Figure 21. Continued.



f. Yawing-moment increment
Figure 21. Concluded.

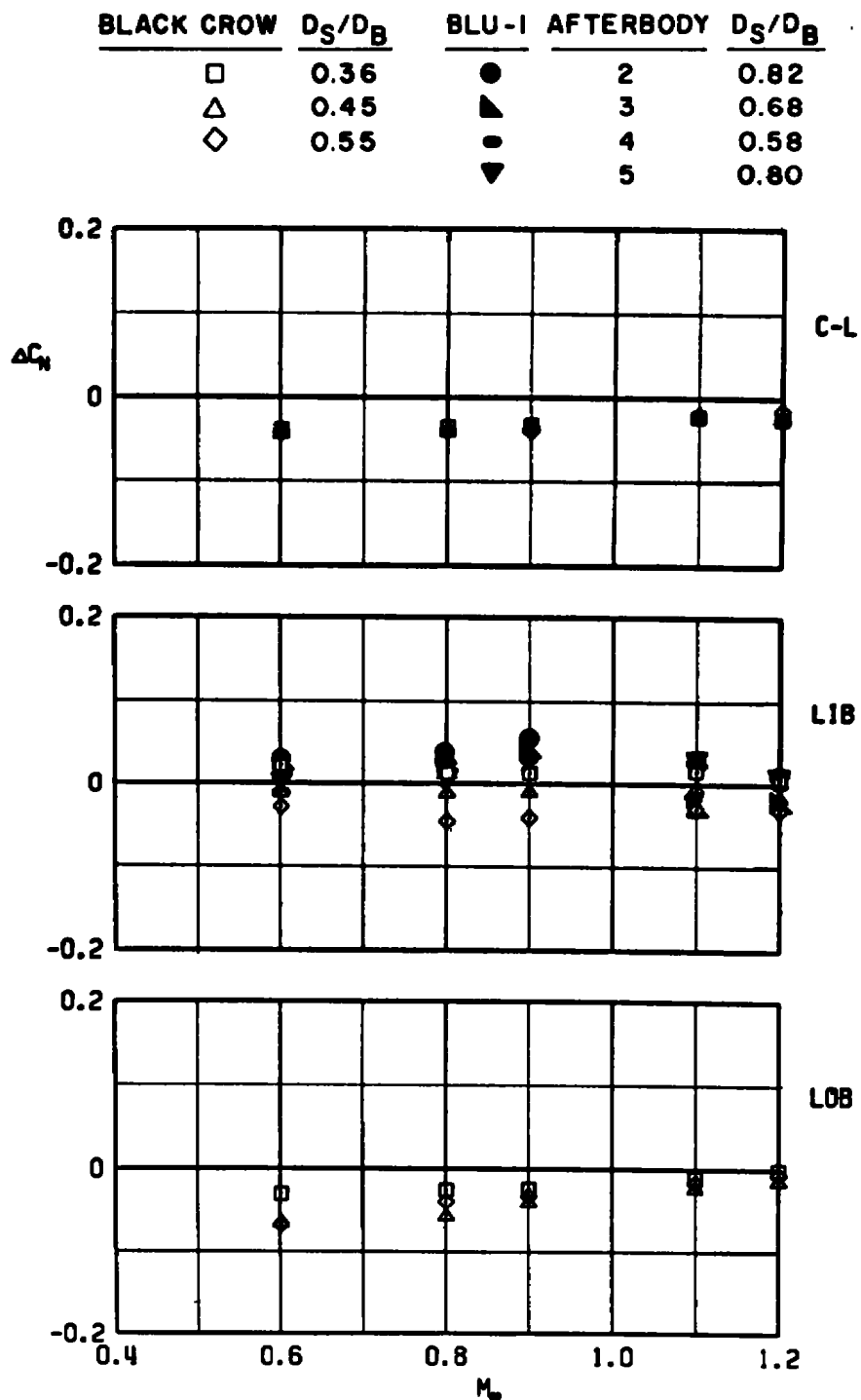
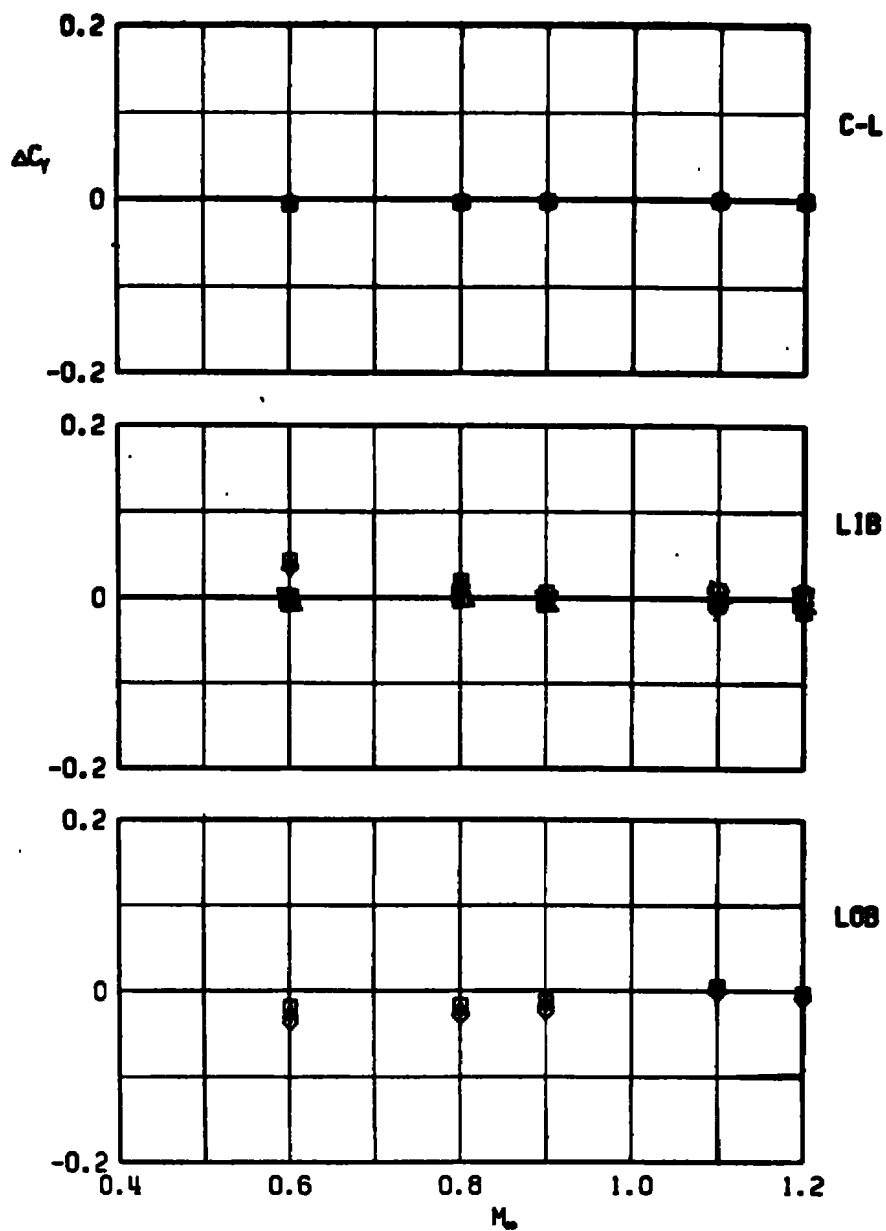
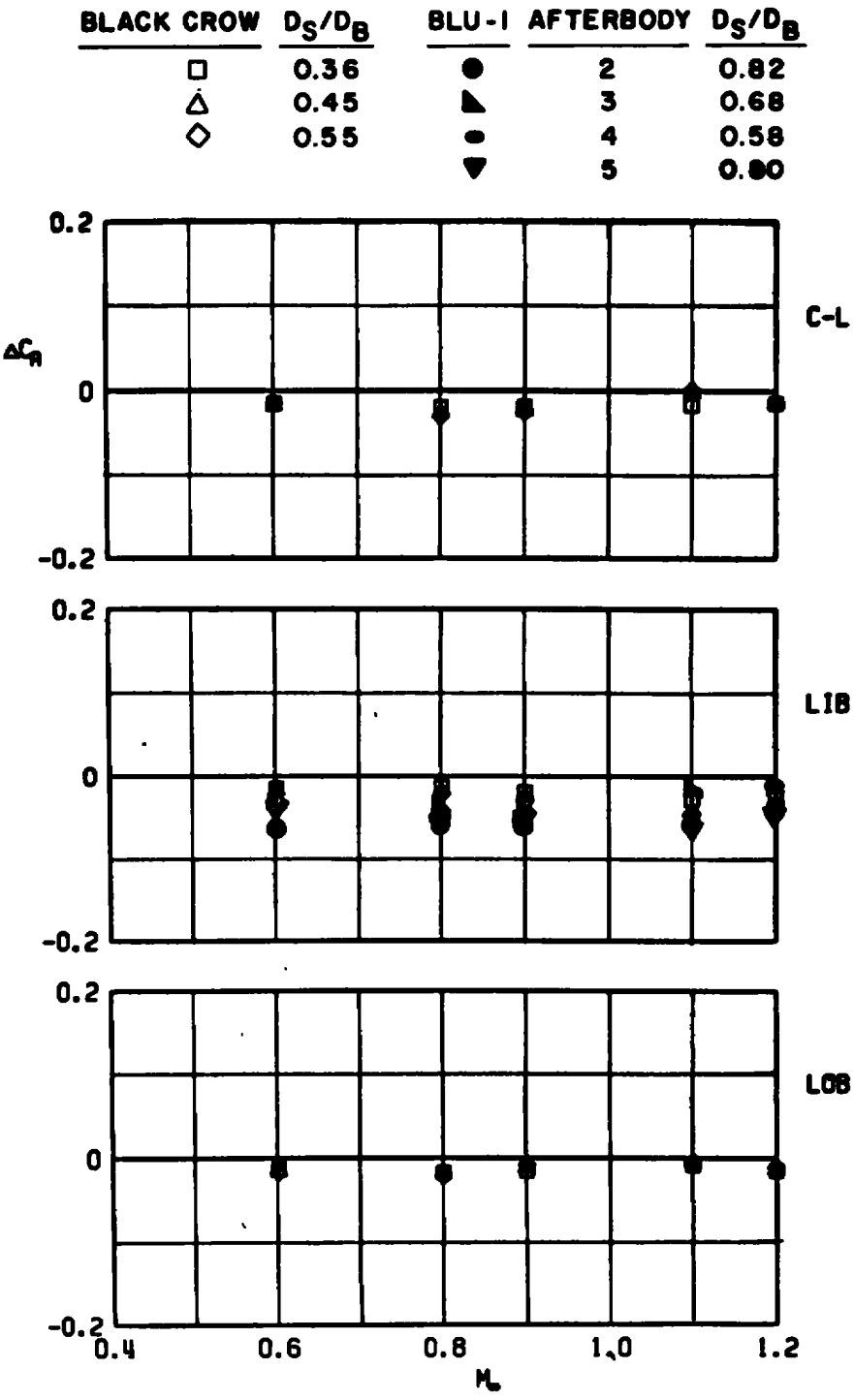


Figure 22. Sting-induced aerodynamic load increments at zero angle of attack as a function of Mach number, unstable pylon-mounted stores.

BLACK CROW	D_S/D_B	BLU-1	AFTERBODY	D_S/D_B
□	0.36	●	2	0.82
△	0.45	▲	3	0.68
◇	0.55	●	4	0.58
		▼	5	0.80

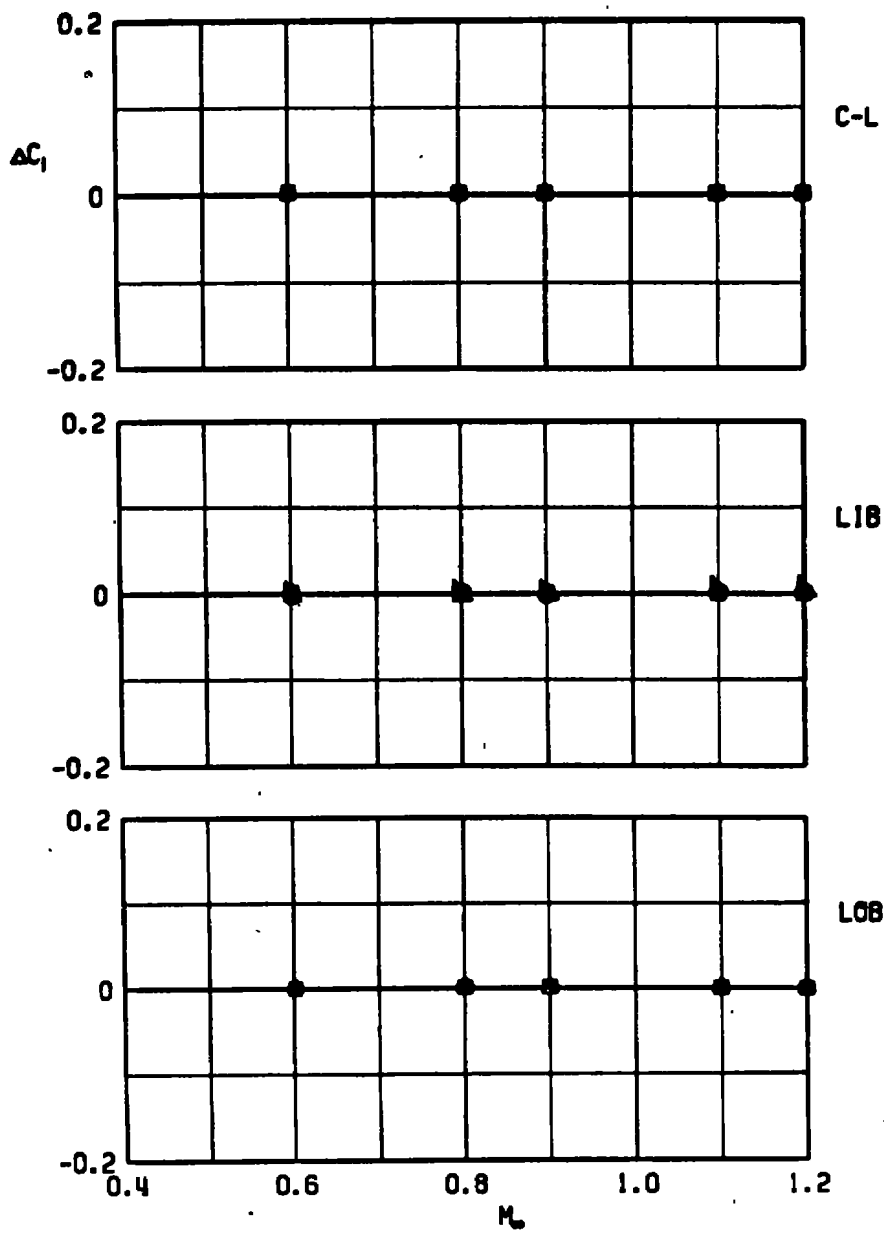


b. Side-force increment
Figure 22. Continued.

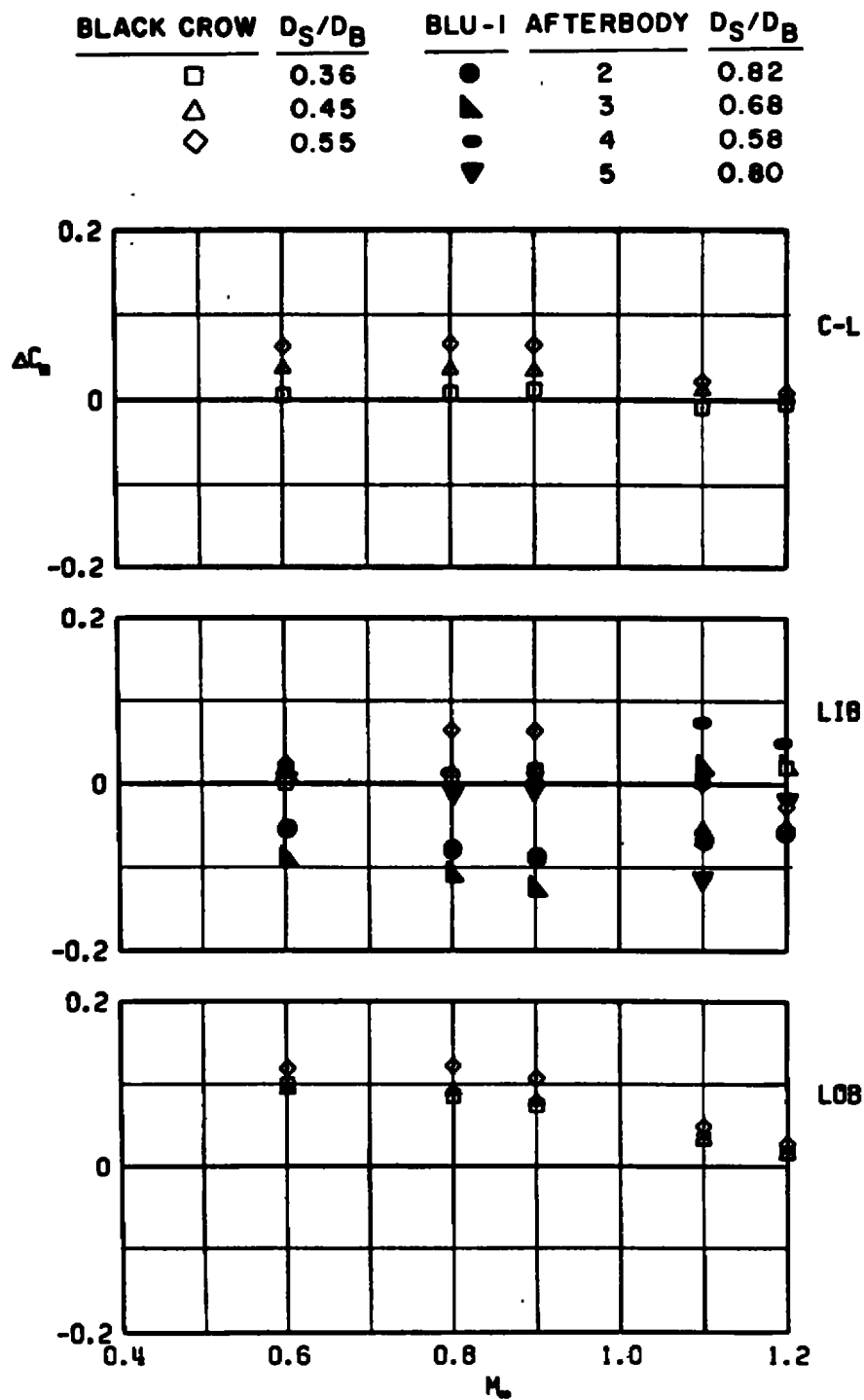


c. Axial-force increment
Figure 22. Continued.

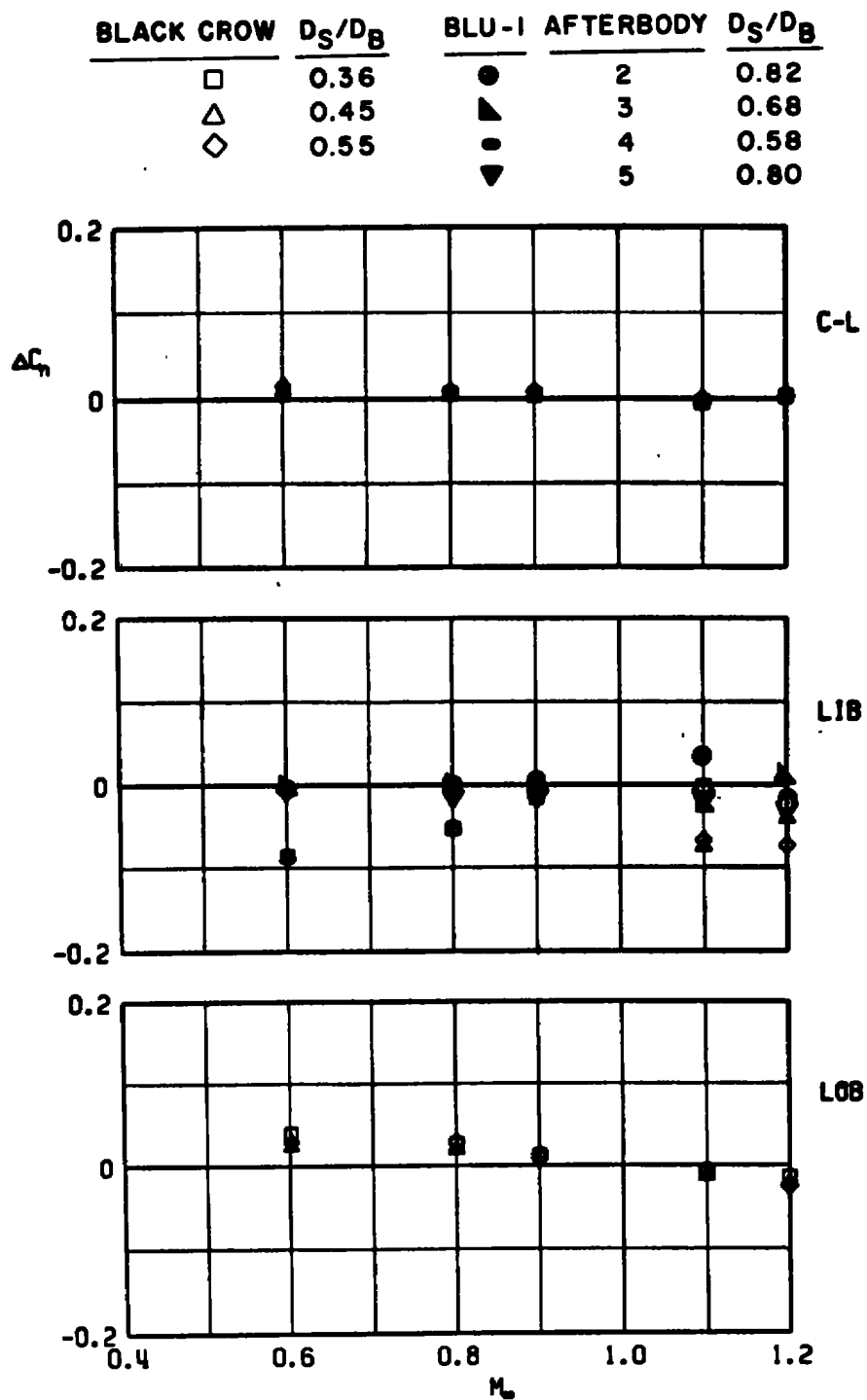
BLACK CROW	D_S/D_B	BLU-1	AFTERBODY	D_S/D_B
□	0.36	●	2	0.82
△	0.45	▲	3	0.68
◇	0.55	●	4	0.58
		▼	5	0.80



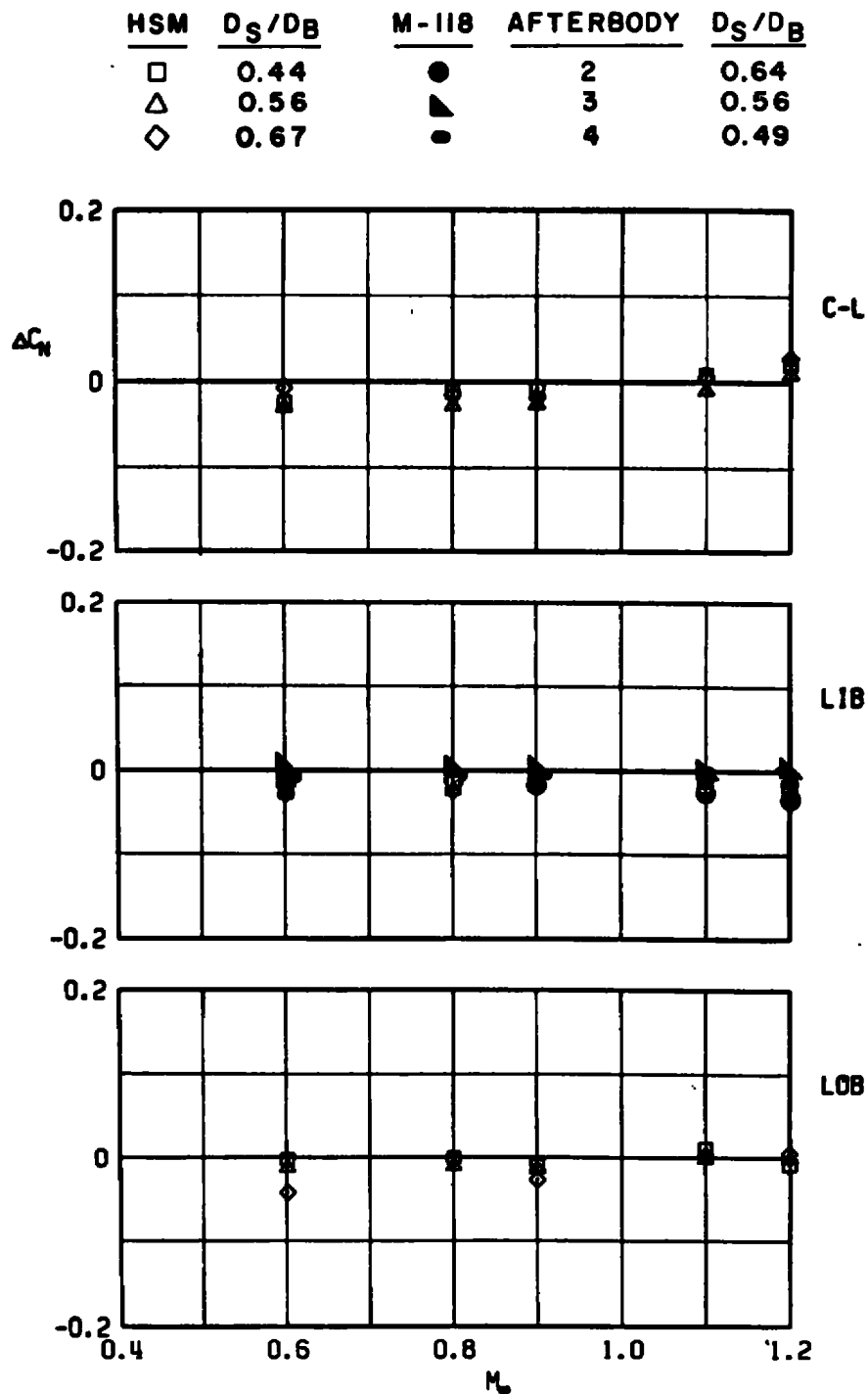
d. Rolling-moment increment
Figure 22. Continued.



e. Pitching-moment increment
Figure 22. Continued.



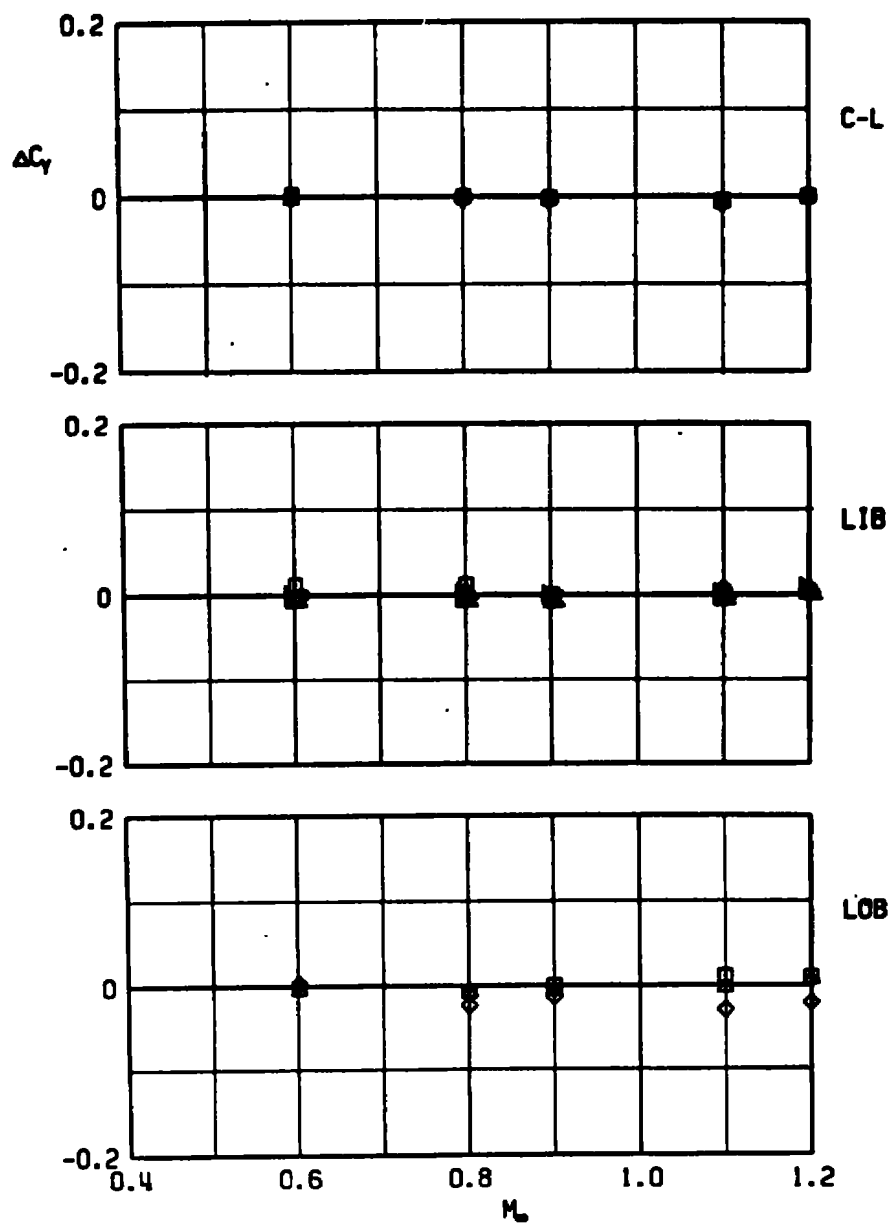
f. Yawing-moment increment
Figure 22. Concluded.



a. Normal-force increment

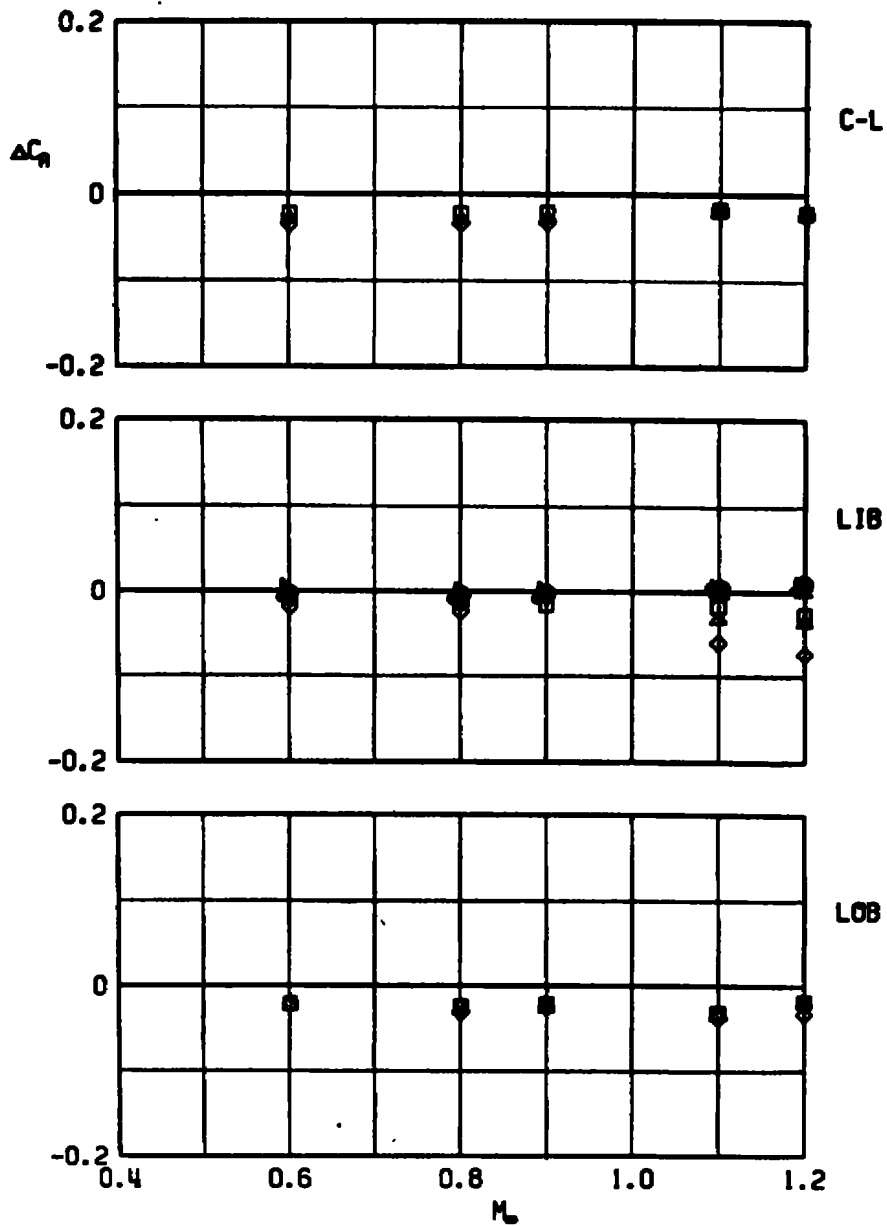
Figure 23. Sting-induced aerodynamic load increments at zero angle of attack as a function of Mach number, stable pylon-mounted stores.

HSM	D_S/D_B	M-118	AFTERBODY	D_S/D_B
□	0.44	●	2	0.64
△	0.56	▲	3	0.56
◇	0.67	●	4	0.49



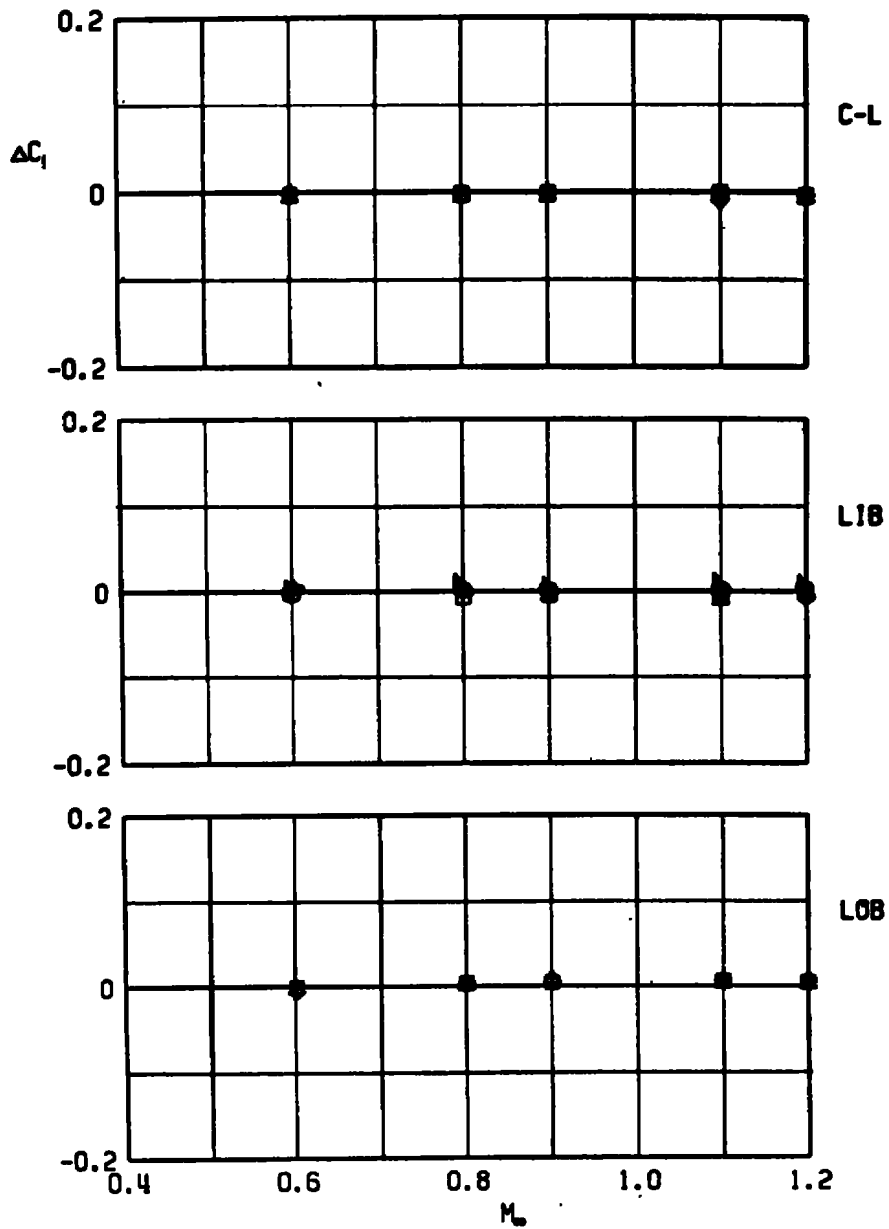
b. Side-force increment
Figure 23. Continued.

HSM	D_S/D_B	M-118	AFTERBODY	D_S/D_B
□	0.44	●	2	0.64
△	0.56	▲	3	0.56
◇	0.67	●	4	0.49

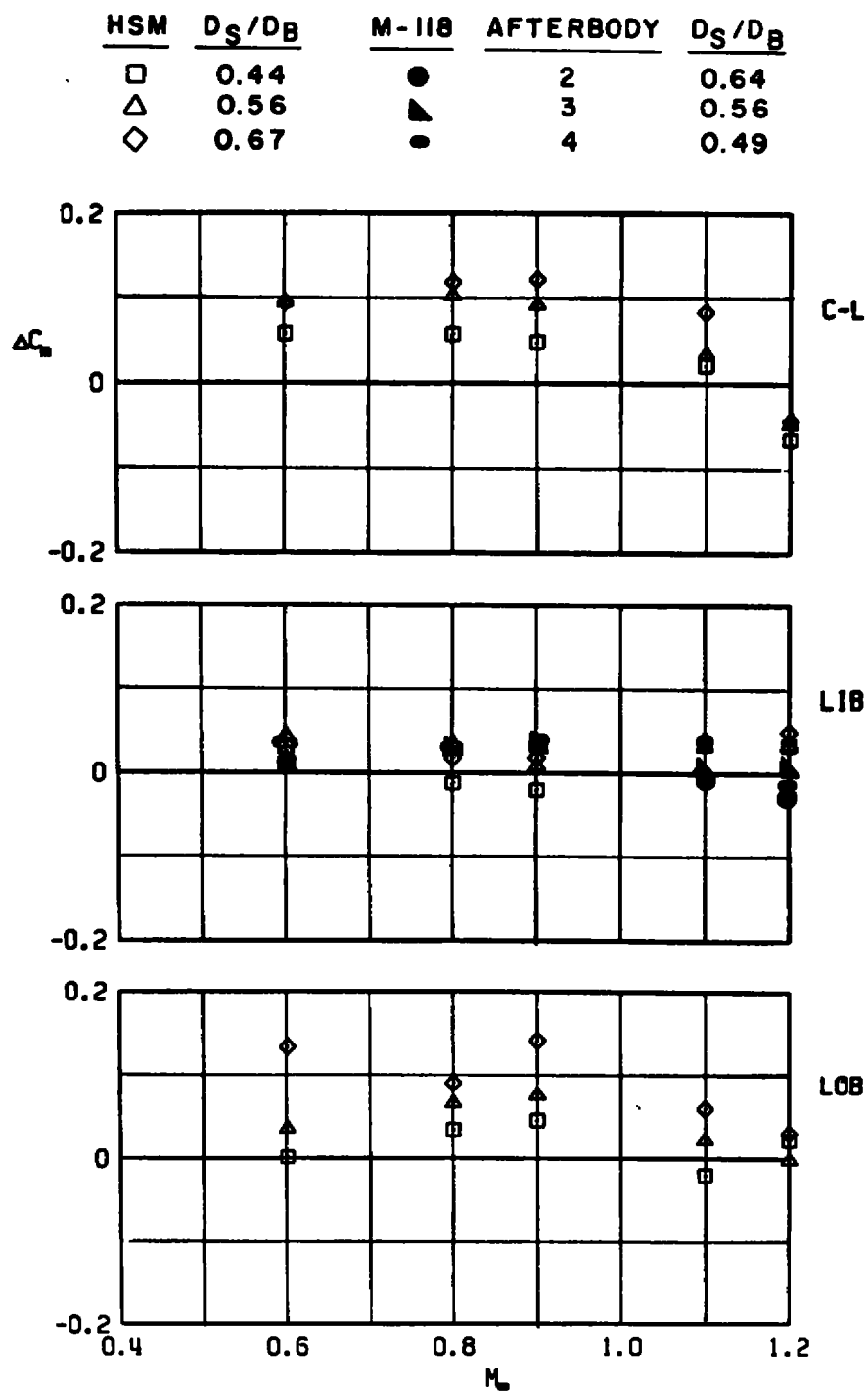


c. Axial-force increment
Figure 23. Continued.

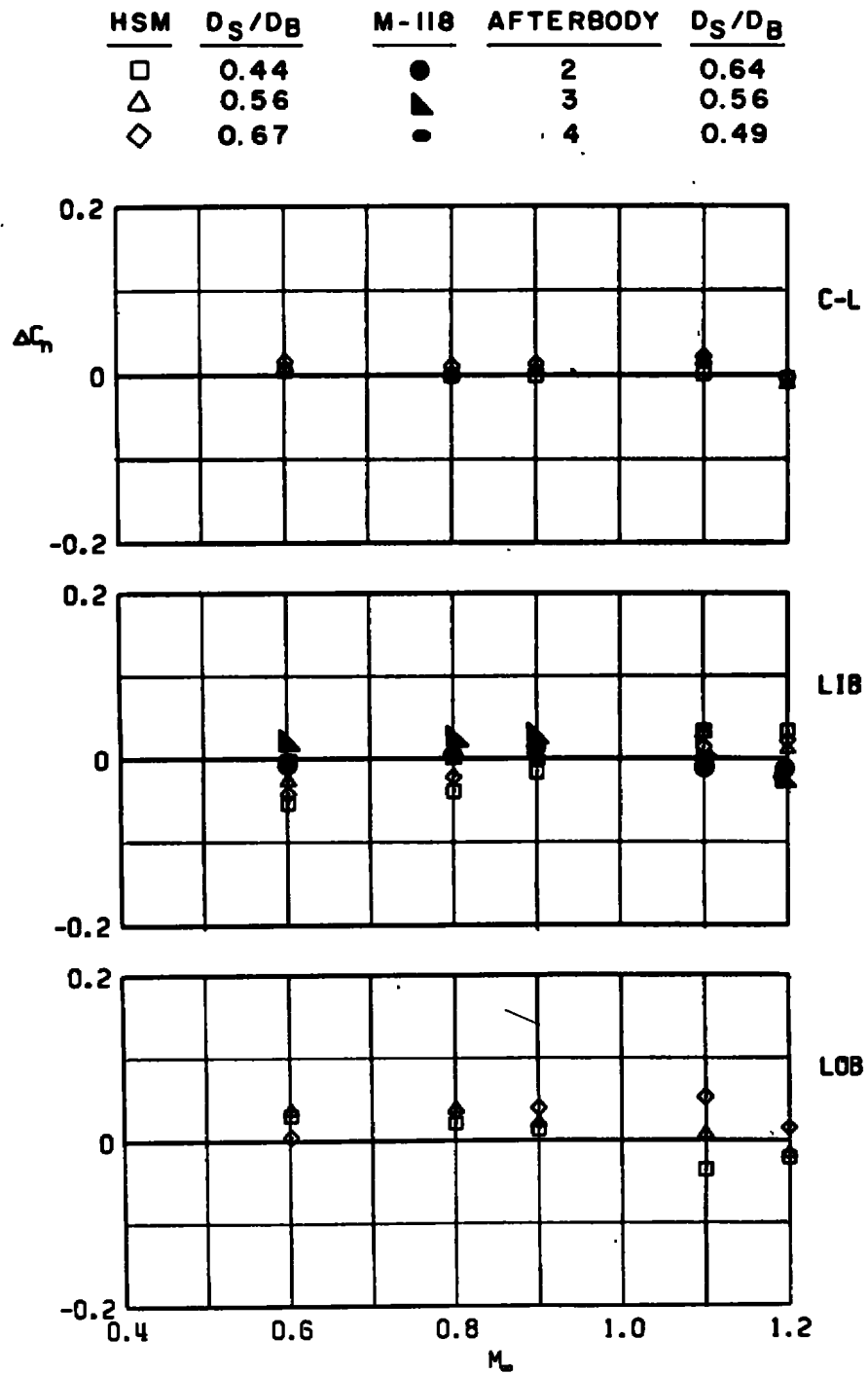
HSM	D_S/D_B	M-118	AFTERBODY	D_S/D_B
□	0.44	●	2	0.64
△	0.56	▲	3	0.56
◇	0.67	●	4	0.49



d. Rolling-moment increment
Figure 23. Continued.

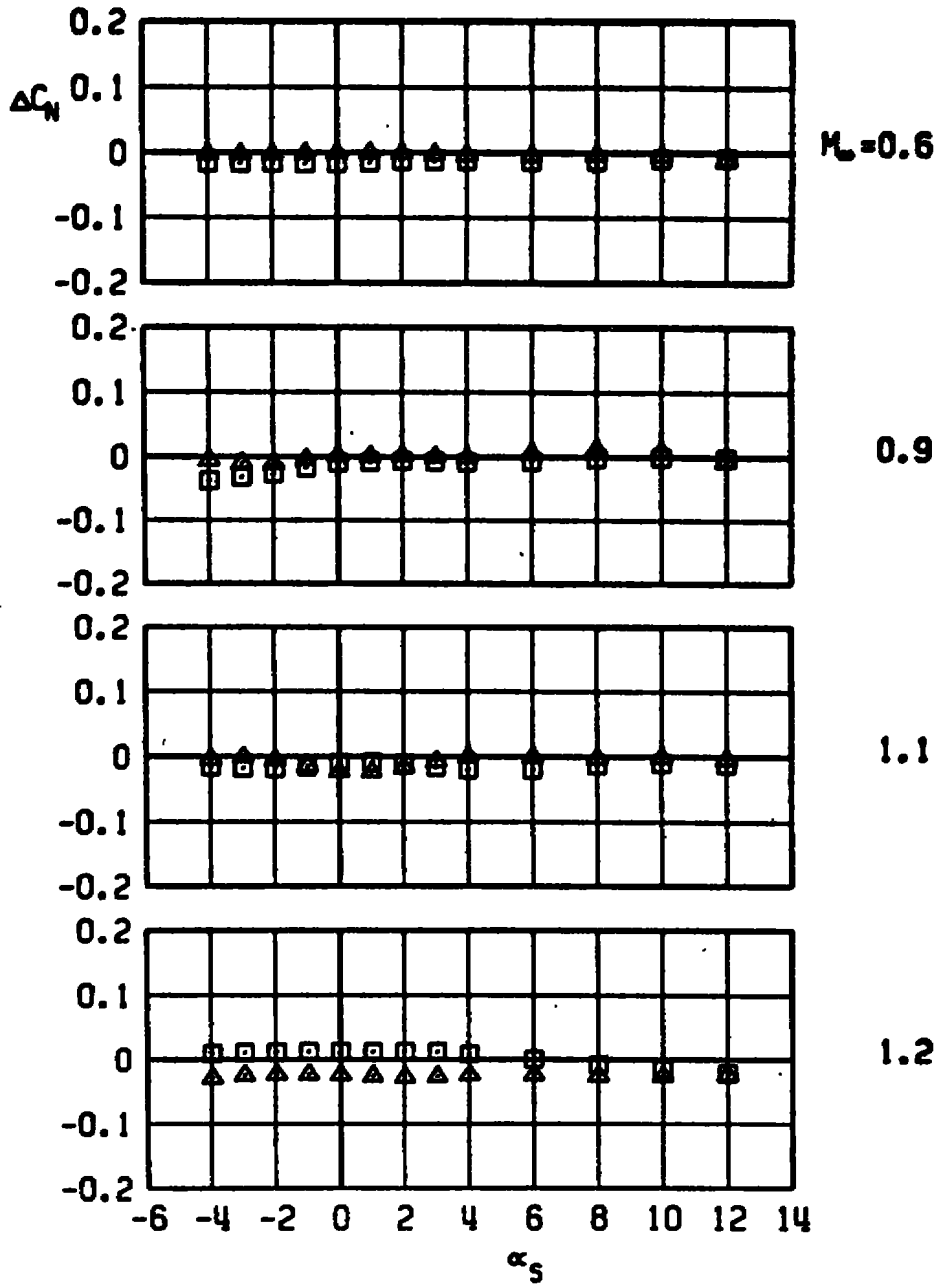


e. Pitching-moment increment
Figure 23. Continued.



f. Yawing-moment increment
Figure 23. Concluded.

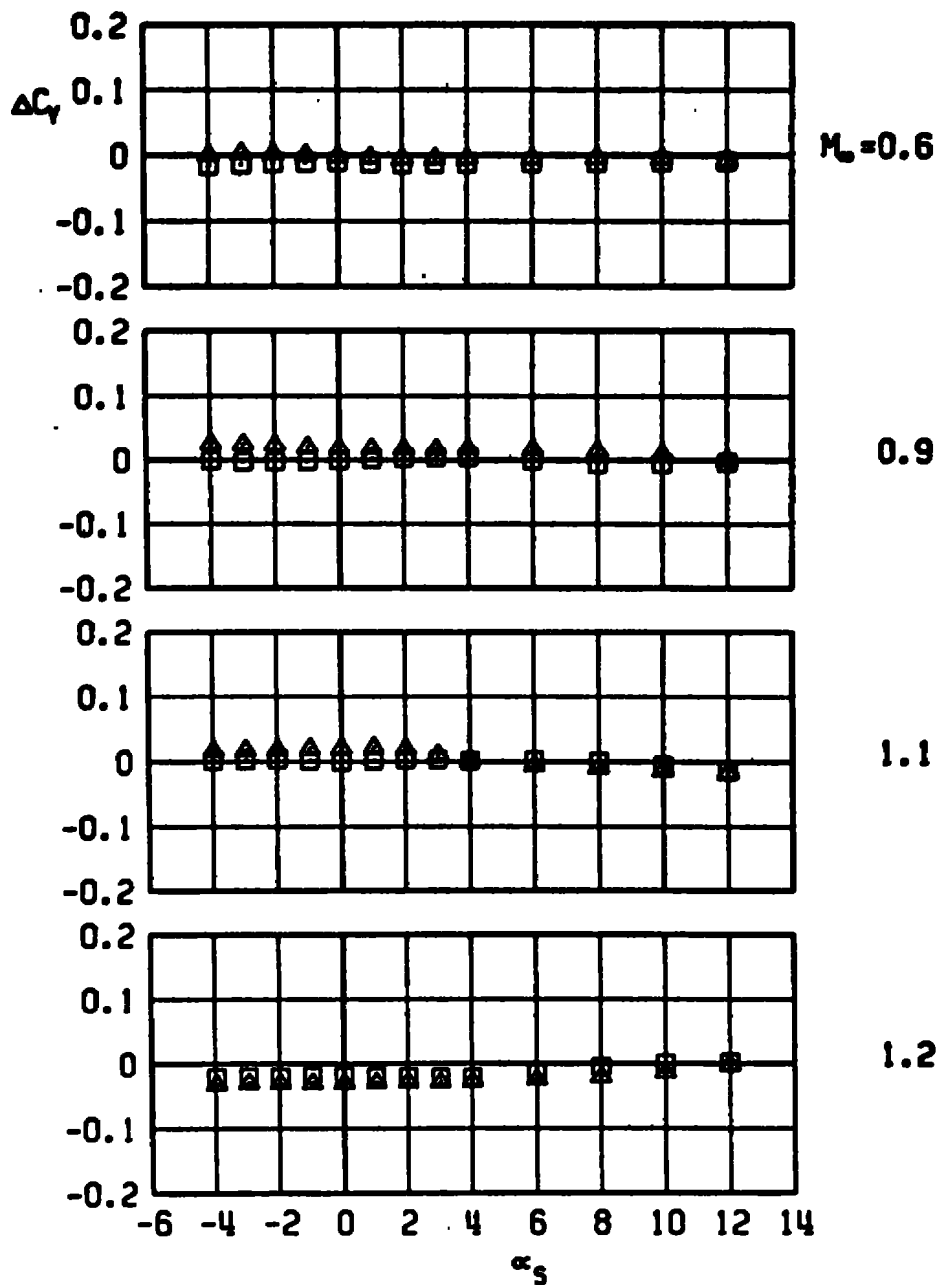
□ ASP, C-L PYLON, MER-1
 WITH DUMMY STING, $D_3 = 0.31 D_0$
 ▲ WITH DUMMY STING, $D_3 = 0.50 D_0$



a. Normal-force increment

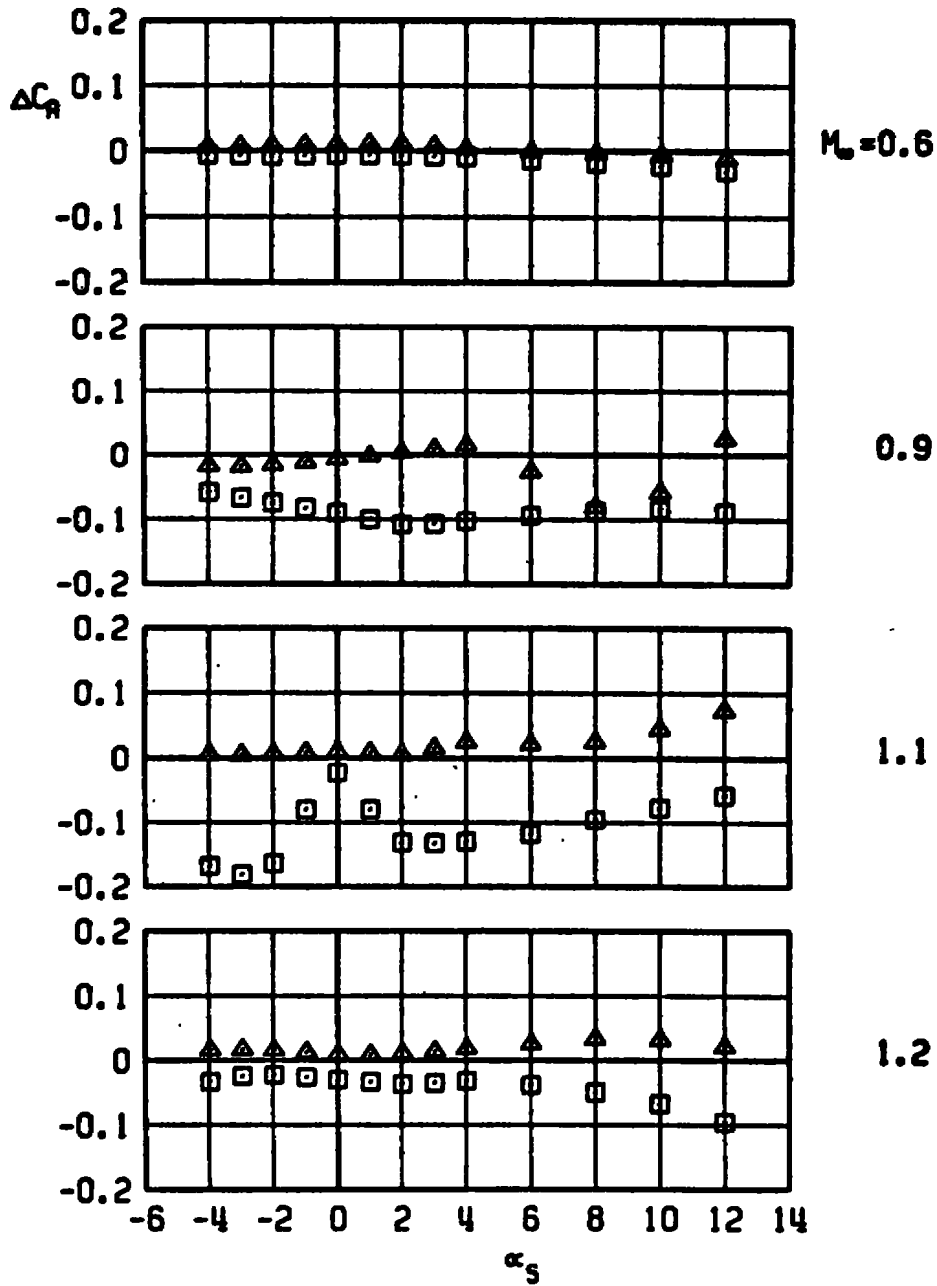
Figure 24. Sting-induced aerodynamic load increments as a function of angle of attack, unstable rack-mounted store, MER station 1, C-L pylon.

ASP, C-L PYLON, MER-1
 □ WITH DUMMY STING, $D_3 = 0.31 D_0$
 ▲ WITH DUMMY STING, $D_3 = 0.50 D_0$



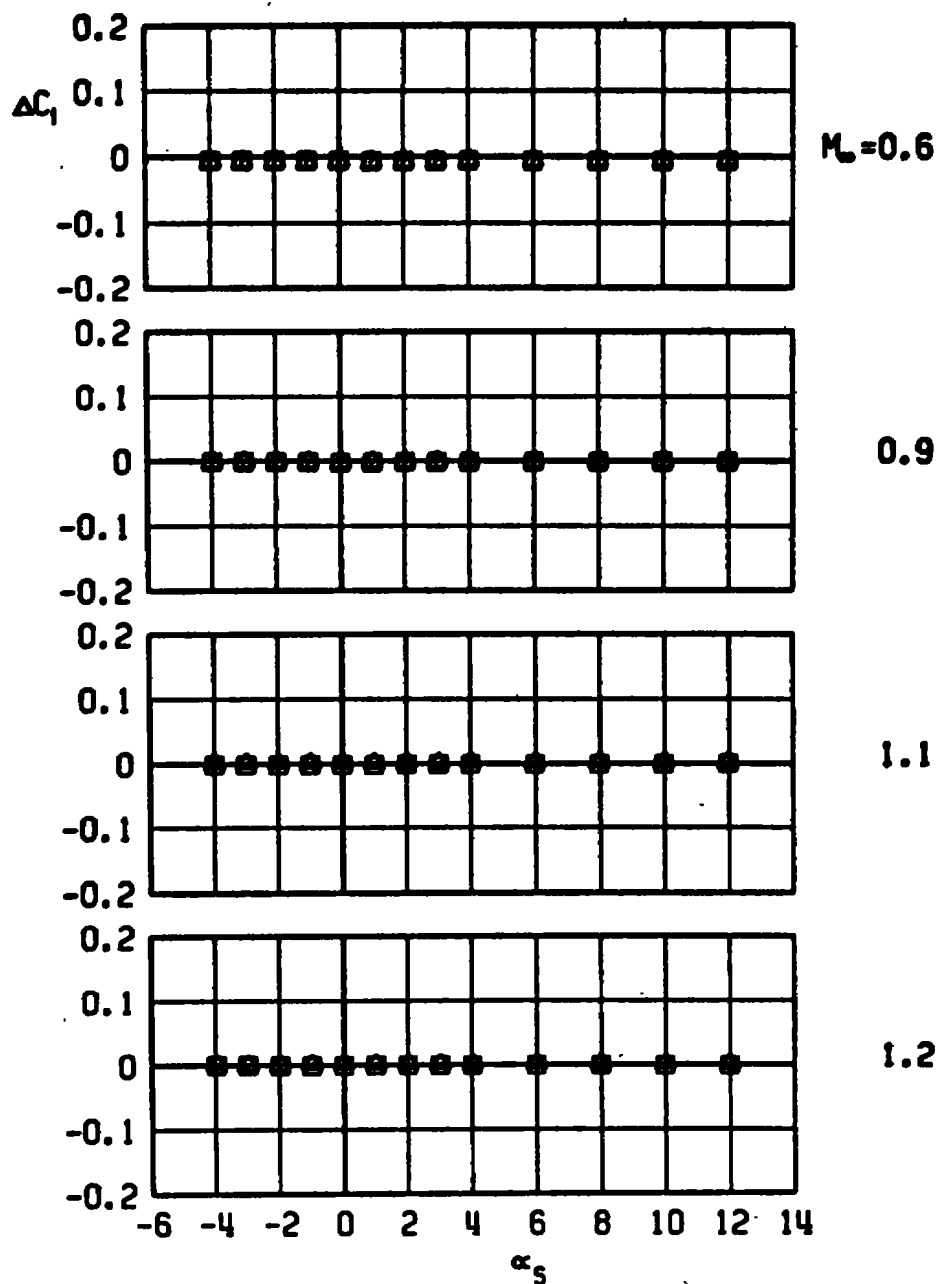
b. Side-force increment.
 Figure 24. Continued.

□ ASP, C-L PYLON, MER-1
 WITH DUMMY STING, $D_3 = 0.31 D_0$
 ▲ WITH DUMMY STING, $D_3 = 0.50 D_0$



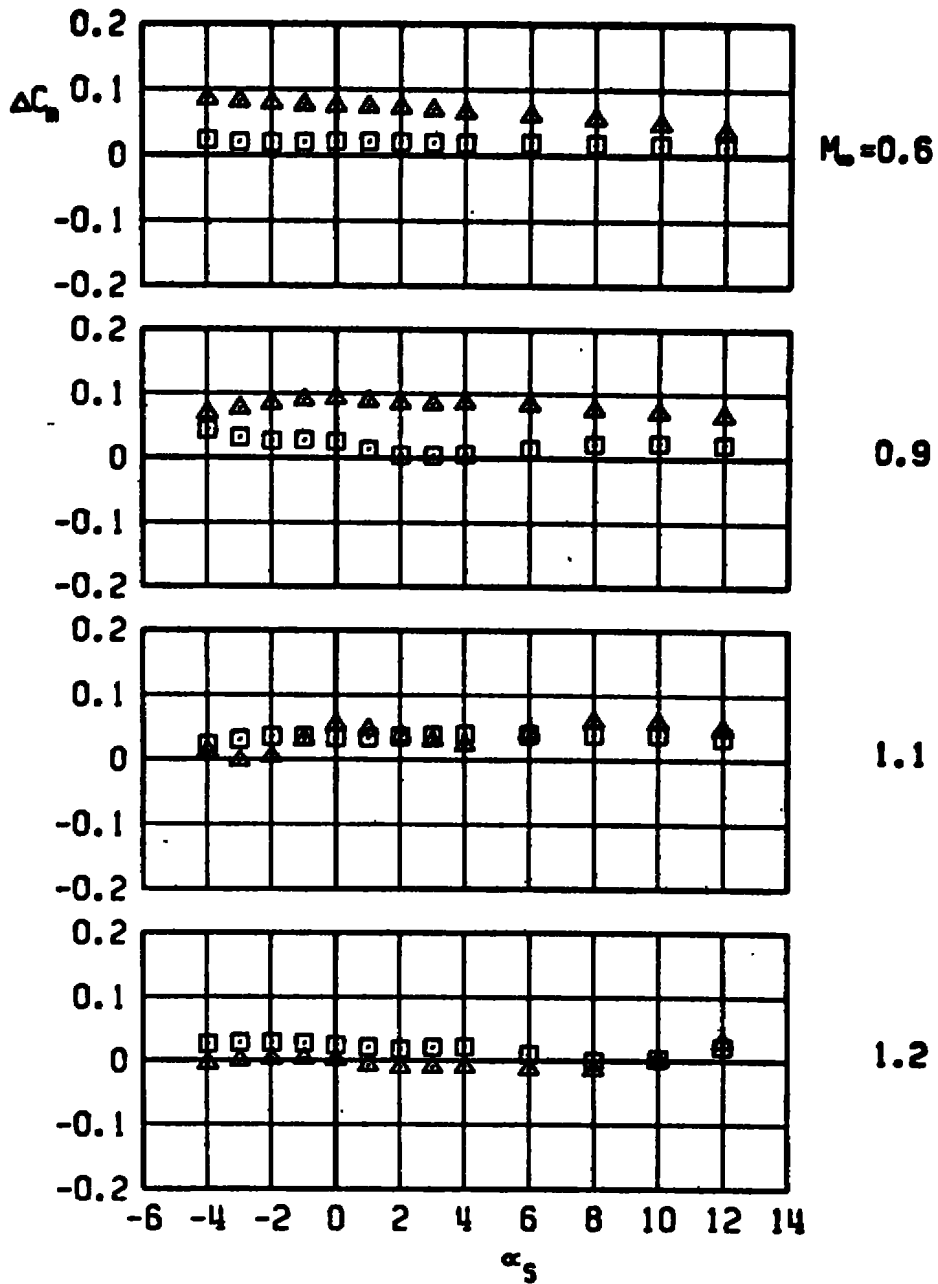
c. Axial-force increment
Figure 24. Continued.

□ ASP, C-L PYLON, MER-1
 WITH DUMMY STING, $D_3 = 0.31 D_9$
 ▲ WITH DUMMY STING, $D_3 = 0.50 D_9$



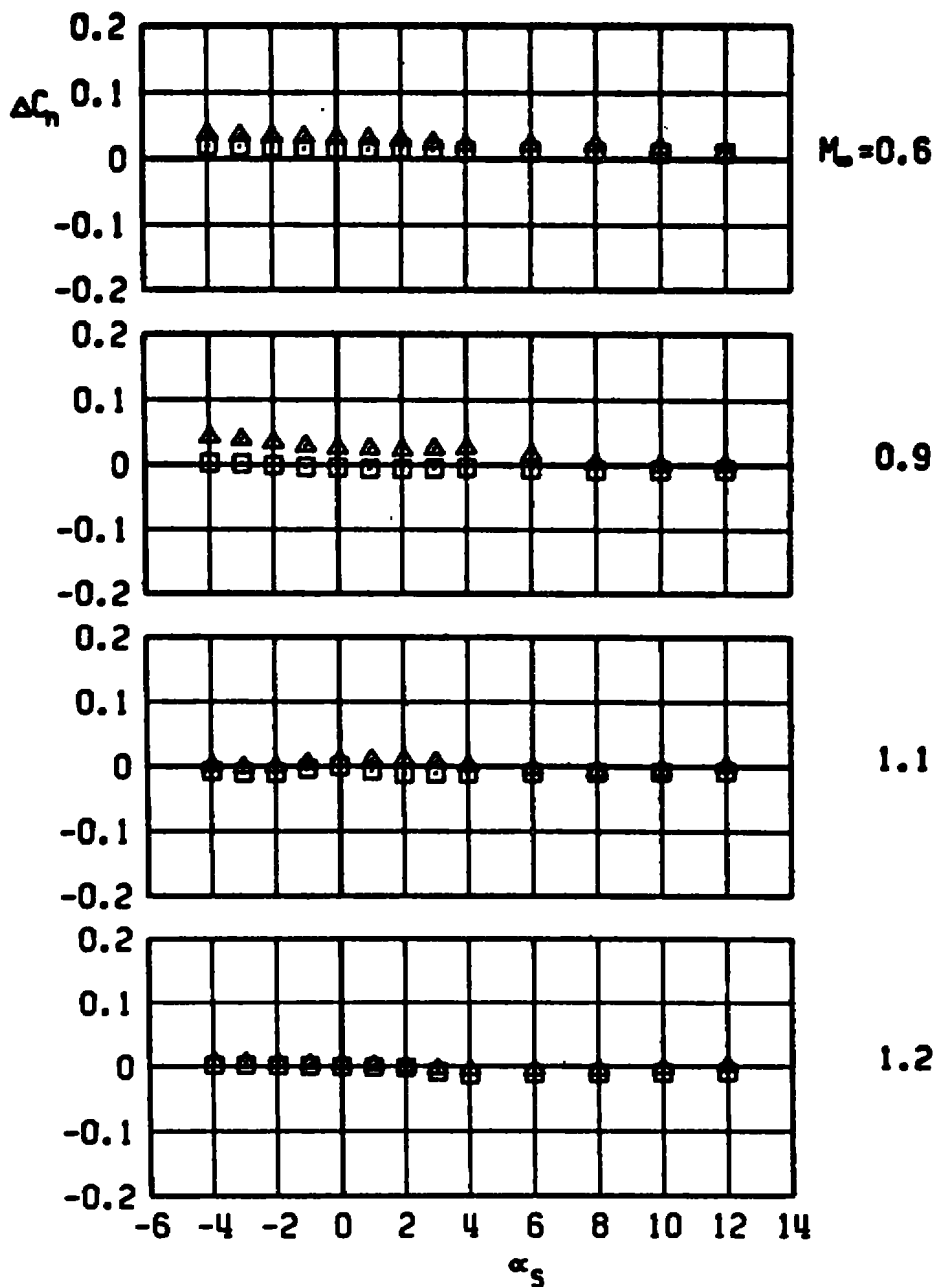
d. Rolling-moment increment
 Figure 24. Continued.

□ ASP, C-L PYLON, MER-1
 WITH DUMMY STING, $D_3 = 0.31 D_0$
 ▲ WITH DUMMY STING, $D_3 = 0.50 D_0$



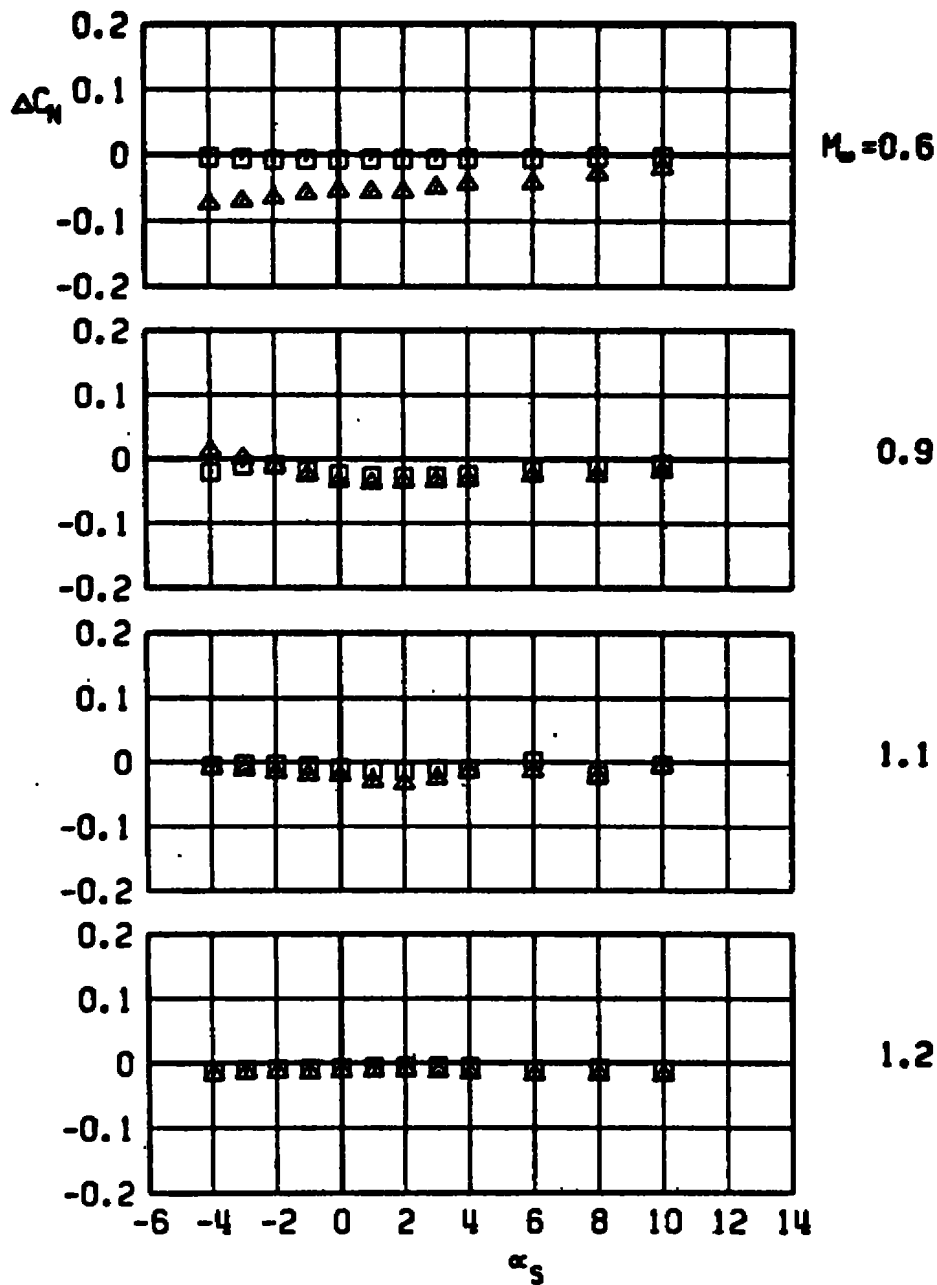
e. Pitching-moment increment
 Figure 24. Continued.

ASP, C-L PYLON, MEA-1
 □ WITH DUMMY STING, $D_3 = 0.31 D_0$
 ▲ WITH DUMMY STING, $D_3 = 0.50 D_0$



f. Yawing-moment increment
 Figure 24. Concluded.

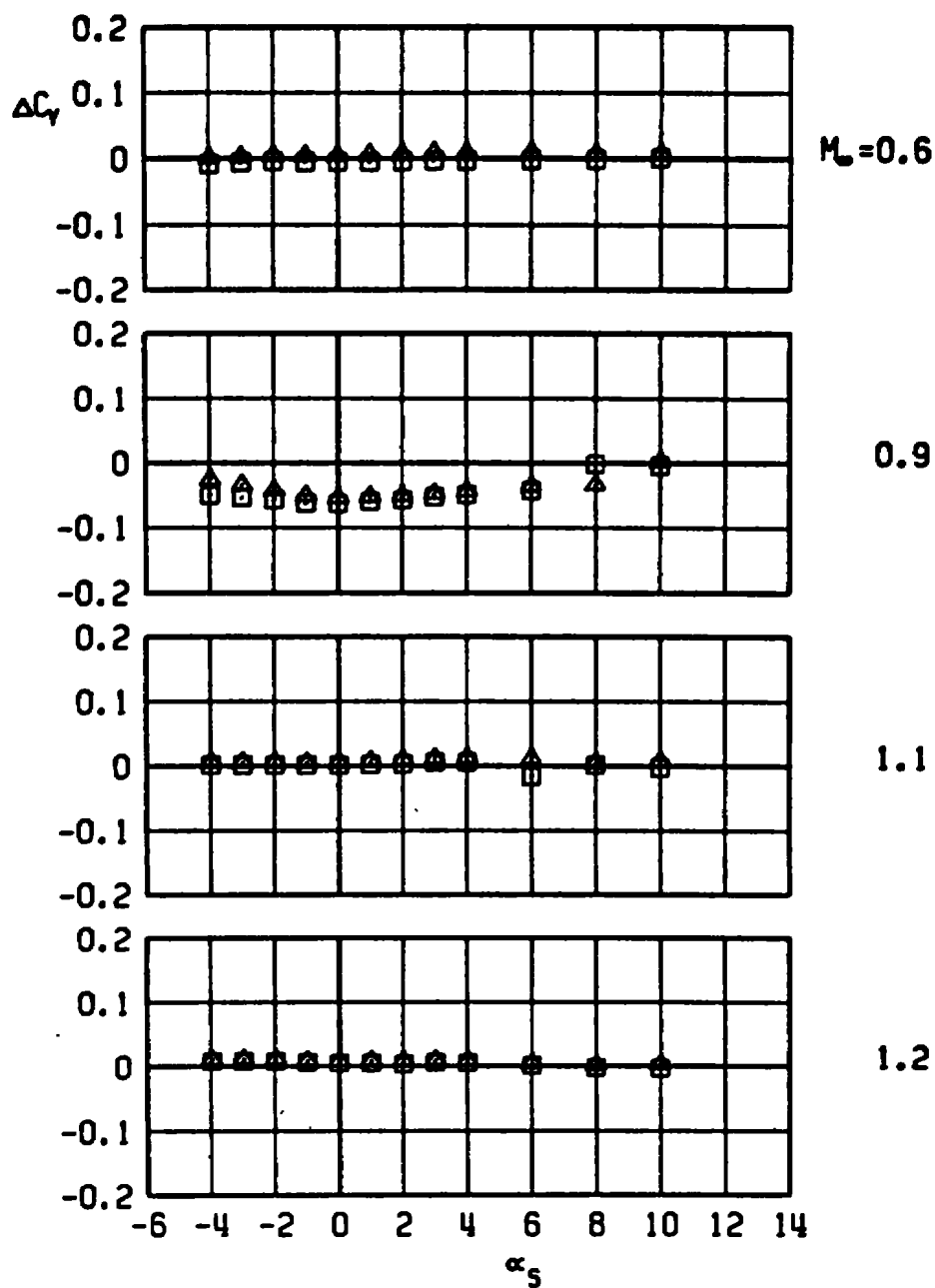
□ ASP, C-L PYLON, MER-2
 WITH DUMMY STING, $D_3 = 0.31 D_0$
 ▲ WITH DUMMY STING, $D_3 = 0.50 D_0$



a. Normal-force increment

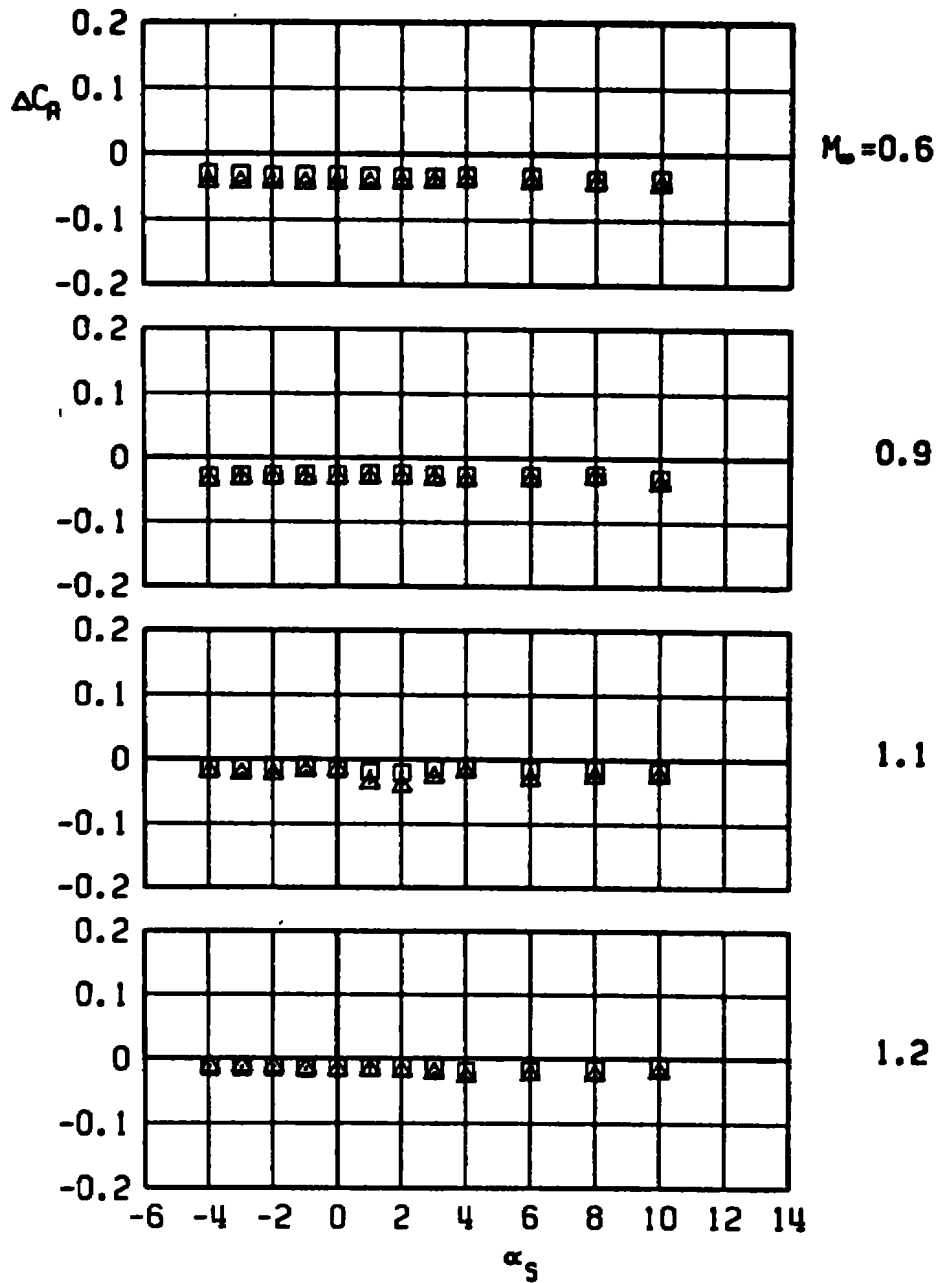
Figure 25. Sting-induced aerodynamic load increments as a function of angle of attack, unstable rack-mounted store, MER station 2, C-L pylon.

ASP, C-L PYLON, MER-2
 □ WITH DUMMY STING, $D_3 = 0.31 D_0$
 △ WITH DUMMY STING, $D_3 = 0.50 D_0$



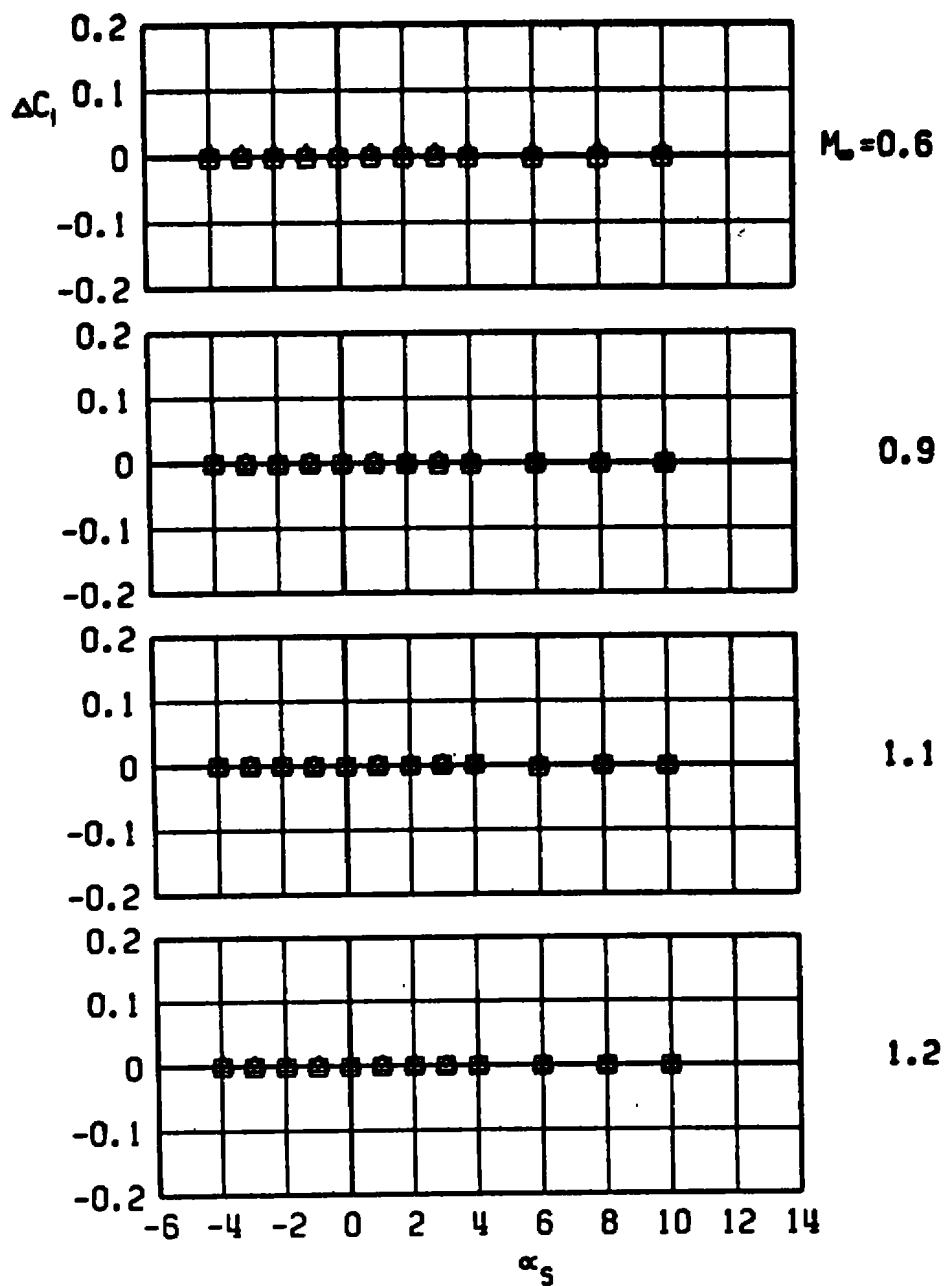
b. Side-force increment
 Figure 25. Continued.

□ ASP, C-L PYLON, MER-2
 WITH DUMMY STING, $D_3 = 0.31 D_9$
 ▲ WITH DUMMY STING, $D_3 = 0.50 D_9$



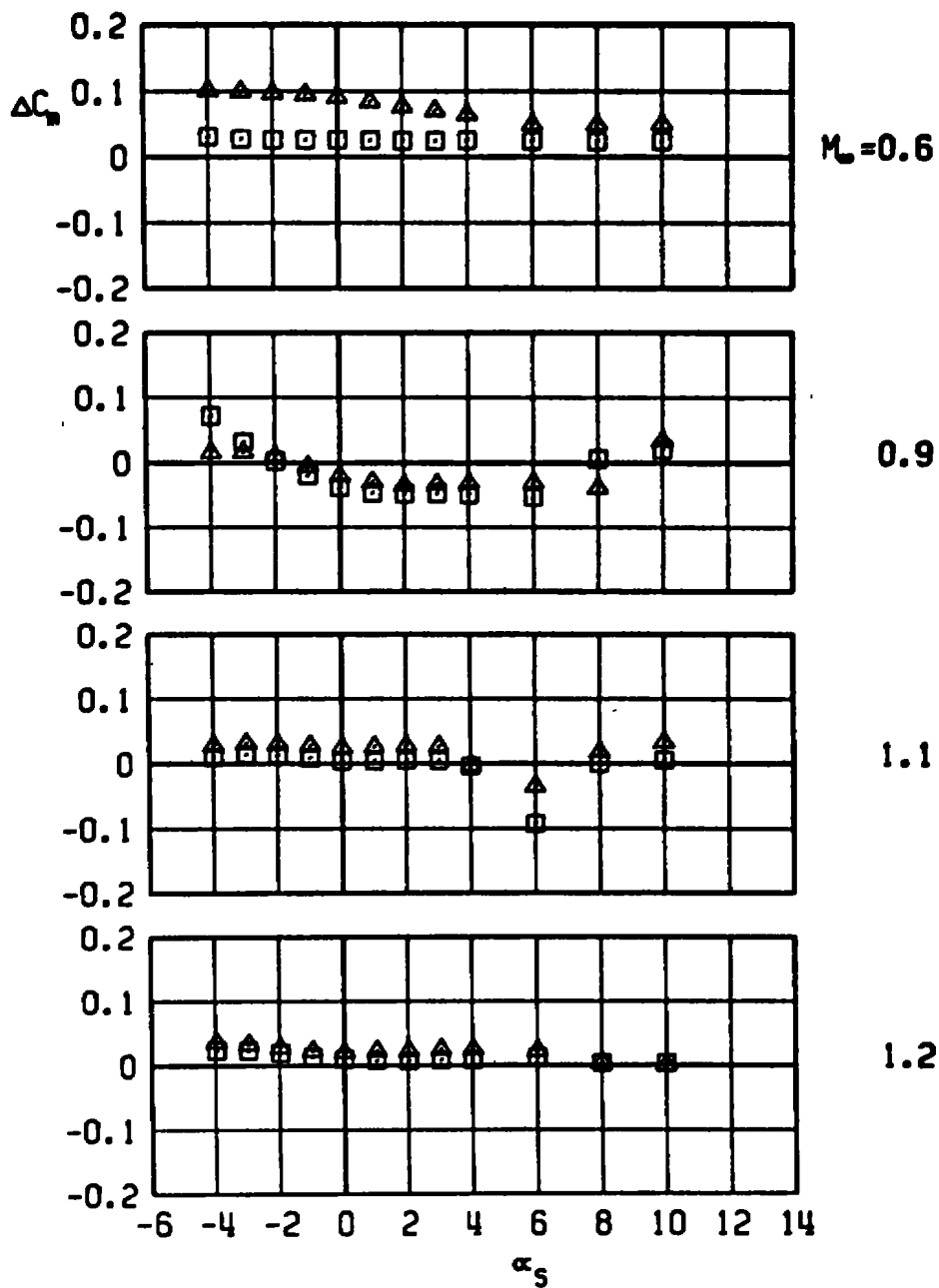
c. Axial-force increment
 Figure 25. Continued.

□ ASP, C-L PYLON, MER-2
 WITH DUMMY STING, $D_3 = 0.31 D_0$
 ▲ WITH DUMMY STING, $D_3 = 0.50 D_0$



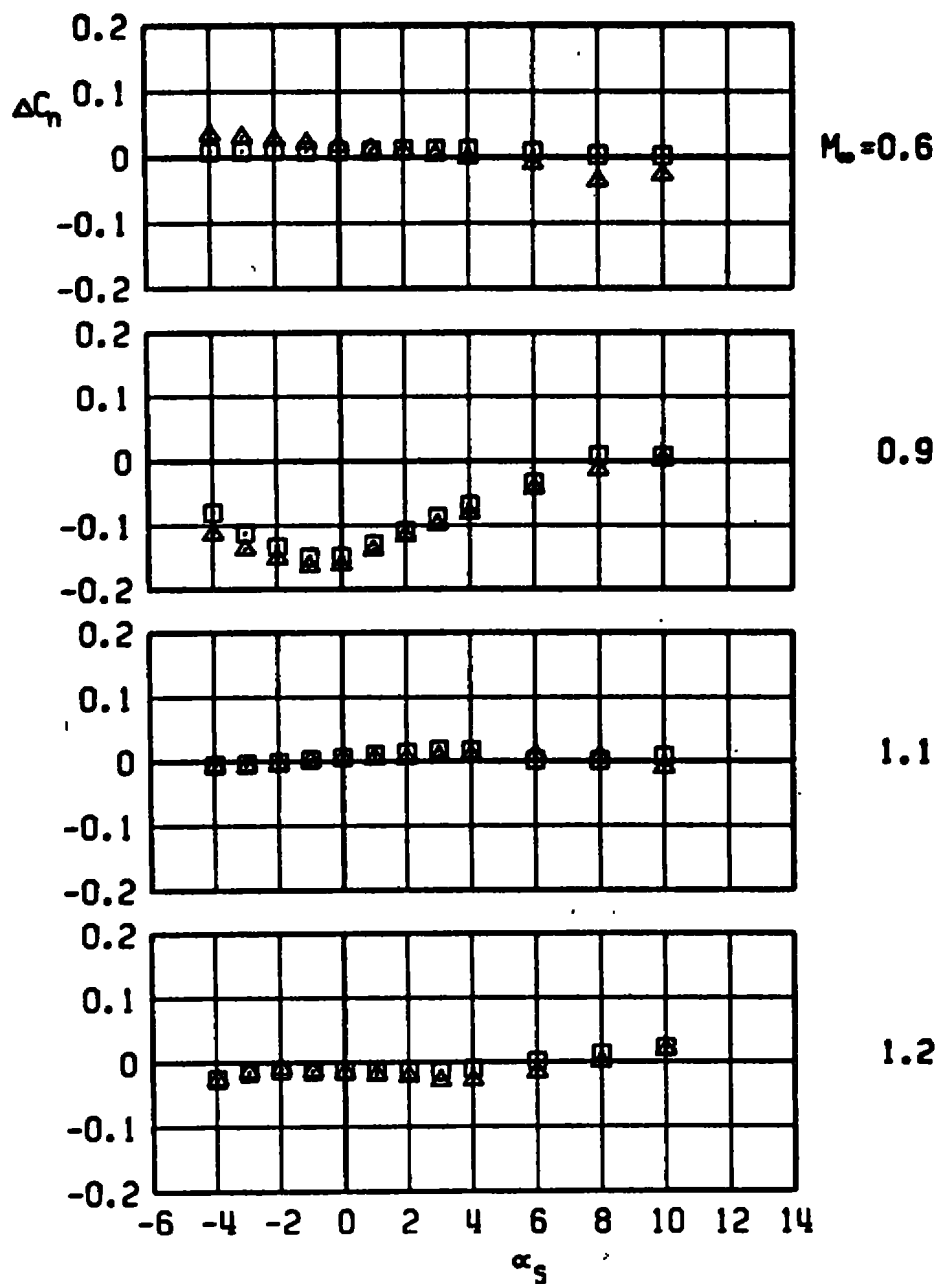
d. Rolling-moment increment
 Figure 25. Continued.

ASP, C-L PYLON, MER-2
 □ WITH DUMMY STING, $D_3 = 0.31 D_0$
 △ WITH DUMMY STING, $D_3 = 0.50 D_0$



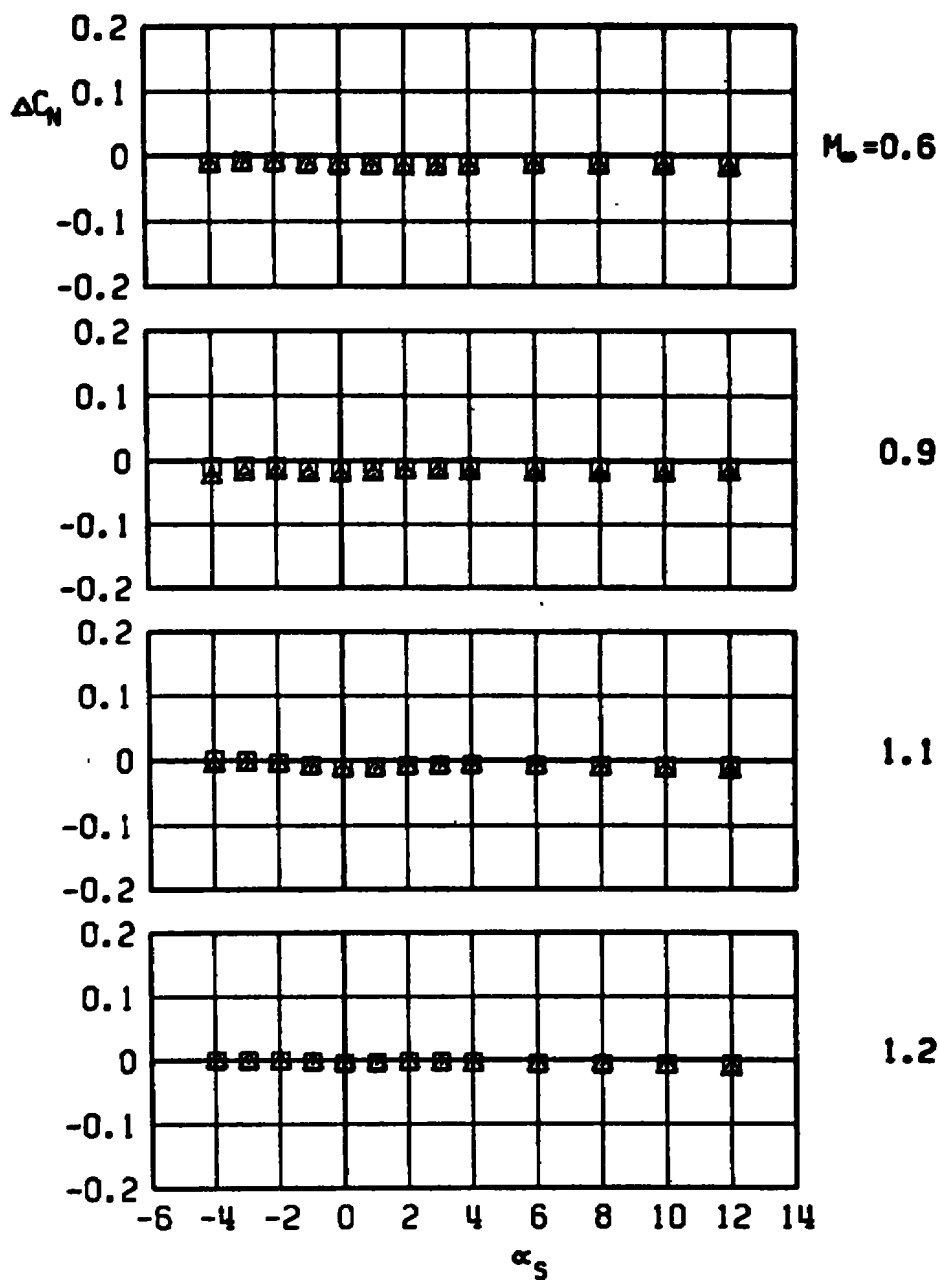
e. Pitching-moment increment
 Figure 25. Continued.

ASP, C-L PYLON, MER-2
 WITH DUMMY STING, $D_3 = 0.31 D_0$
 WITH DUMMY STING, $D_3 = 0.50 D_0$



f. Yawing-moment increment
 Figure 25. Concluded.

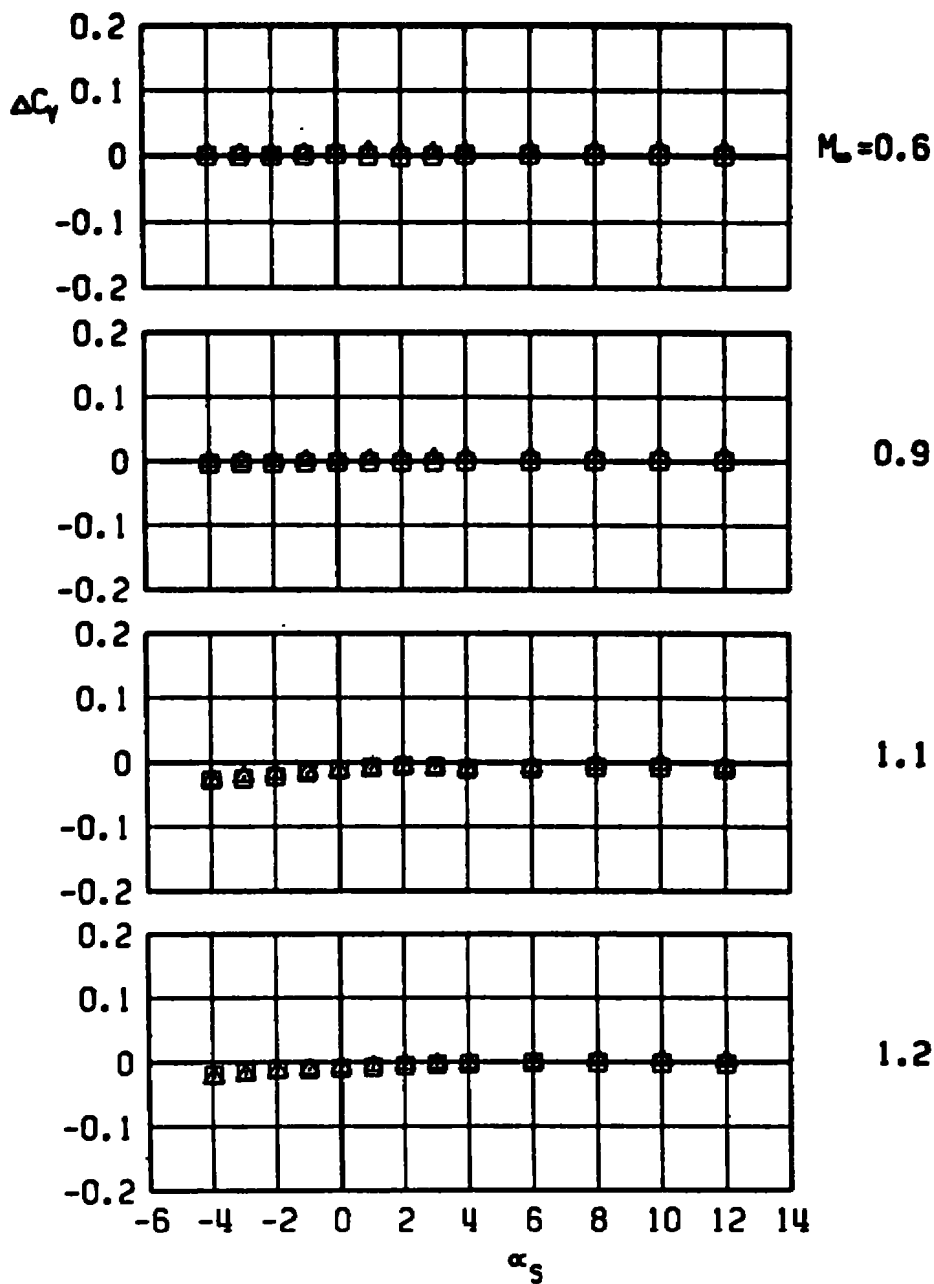
ASP, C-L PYLON, MER-3
 □ WITH DUMMY STING, $D_3 = 0.31 D_0$
 ▲ WITH DUMMY STING, $D_3 = 0.50 D_0$



a. Normal-force increment

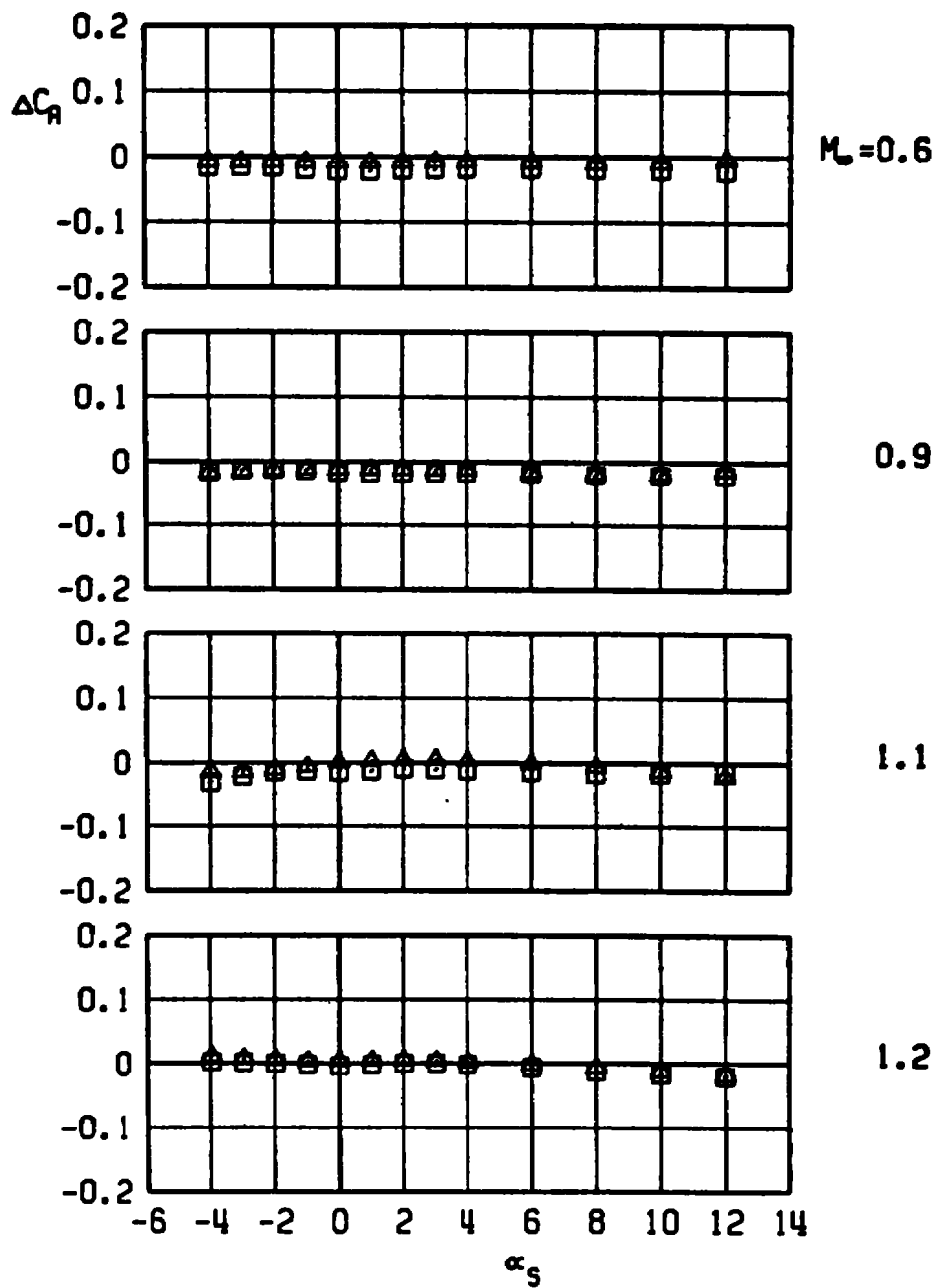
Figure 26. Sting-induced aerodynamic load increments as a function of angle of attack, unstable rack-mounted store, MER station 3, C-L pylon.

ASP, C-L PYLON, MER-3
 □ WITH DUMMY STING, $D_3 = 0.31 D_6$
 ▲ WITH DUMMY STING, $D_3 = 0.50 D_6$



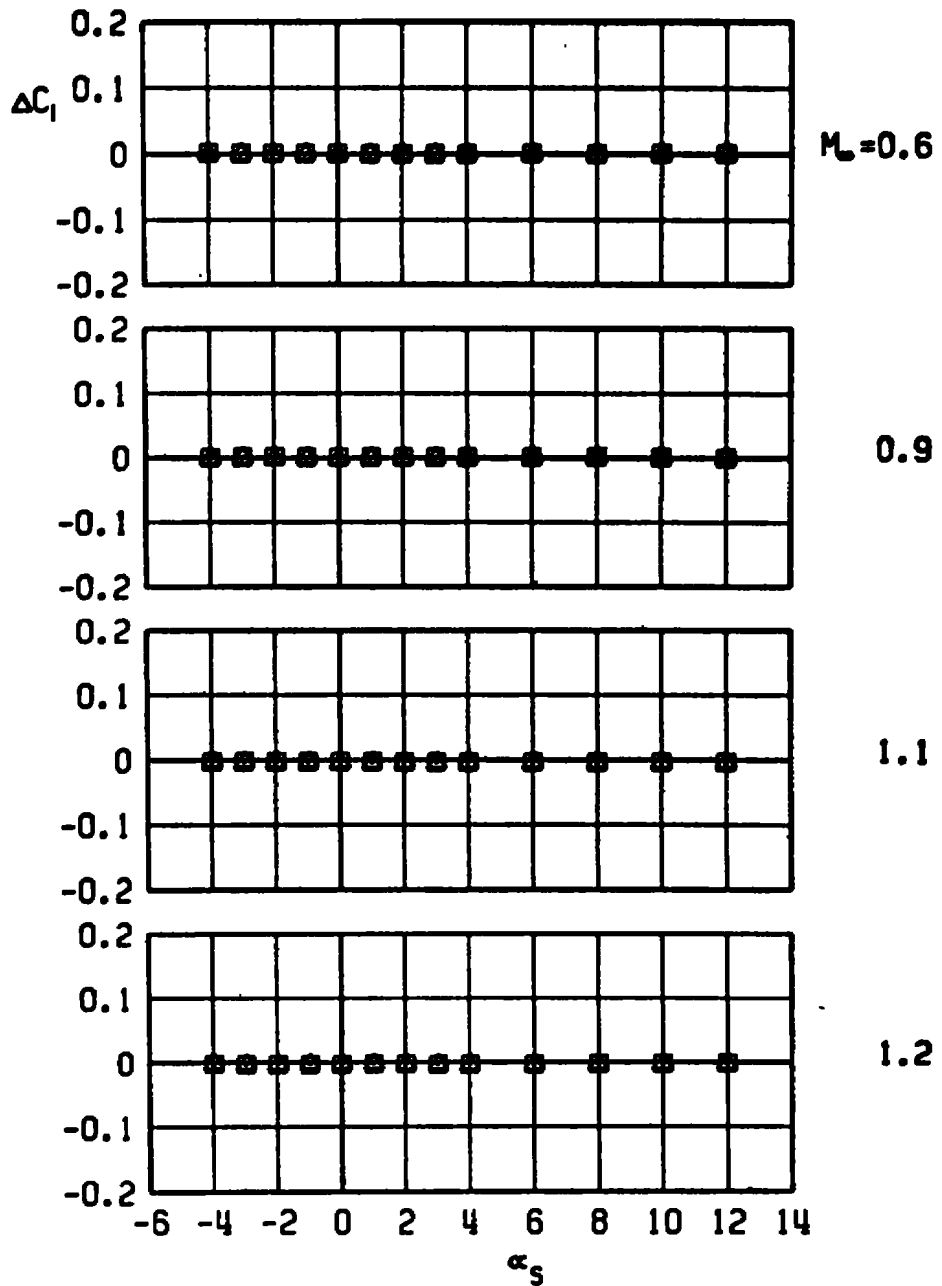
b. Side-force increment
 Figure 26. Continued.

ASP, C-L PYLON, MER-3
 □ WITH DUMMY STING, $D_3 = 0.31 D_0$
 ▲ WITH DUMMY STING, $D_3 = 0.50 D_0$



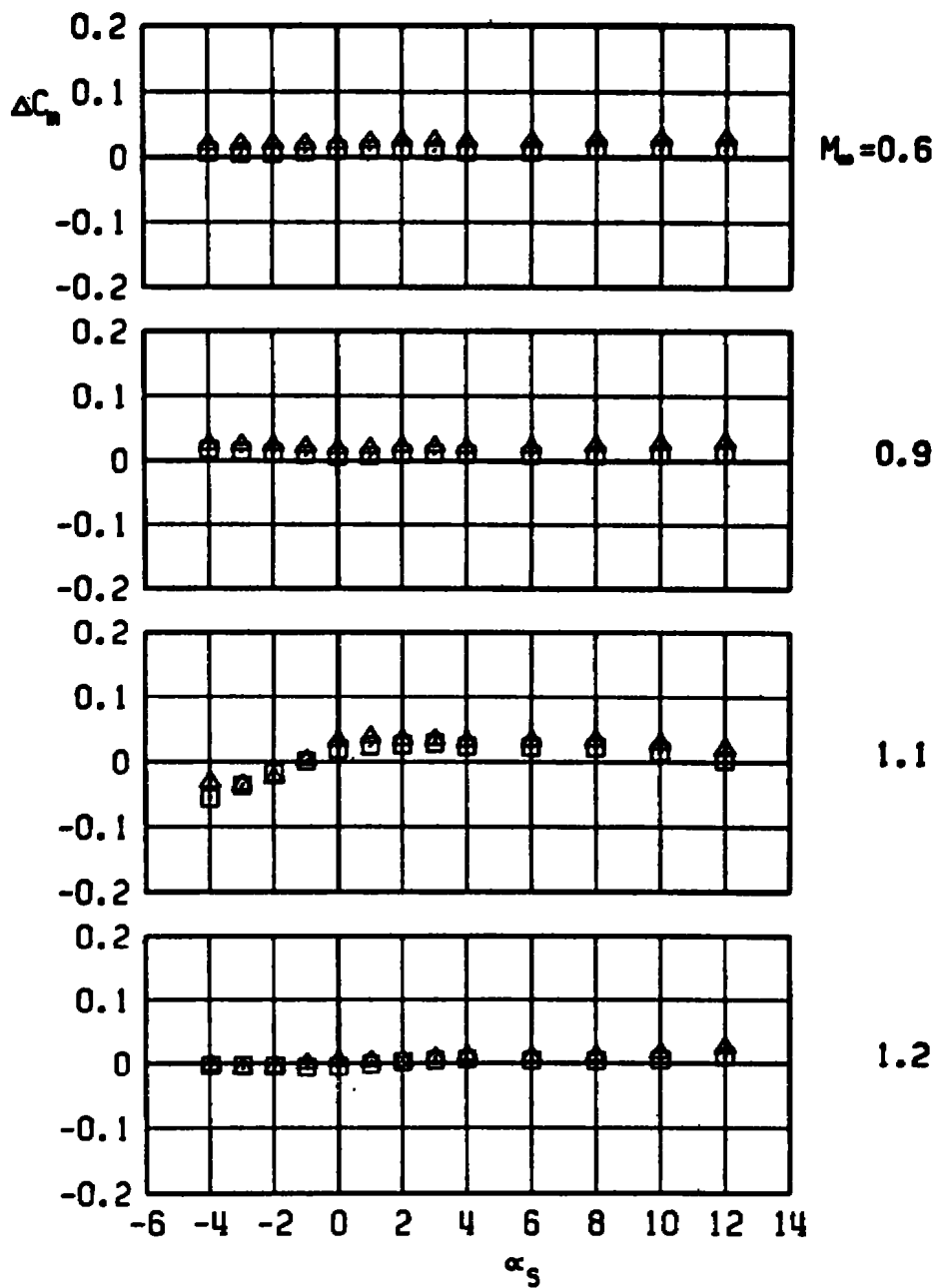
c. Axial-force increment
 Figure 26. Continued.

ASP, C-L PYLON, MER-3
 WITH DUMMY STING, $D_3 = 0.31 D_0$
 WITH DUMMY STING, $D_3 = 0.50 D_0$



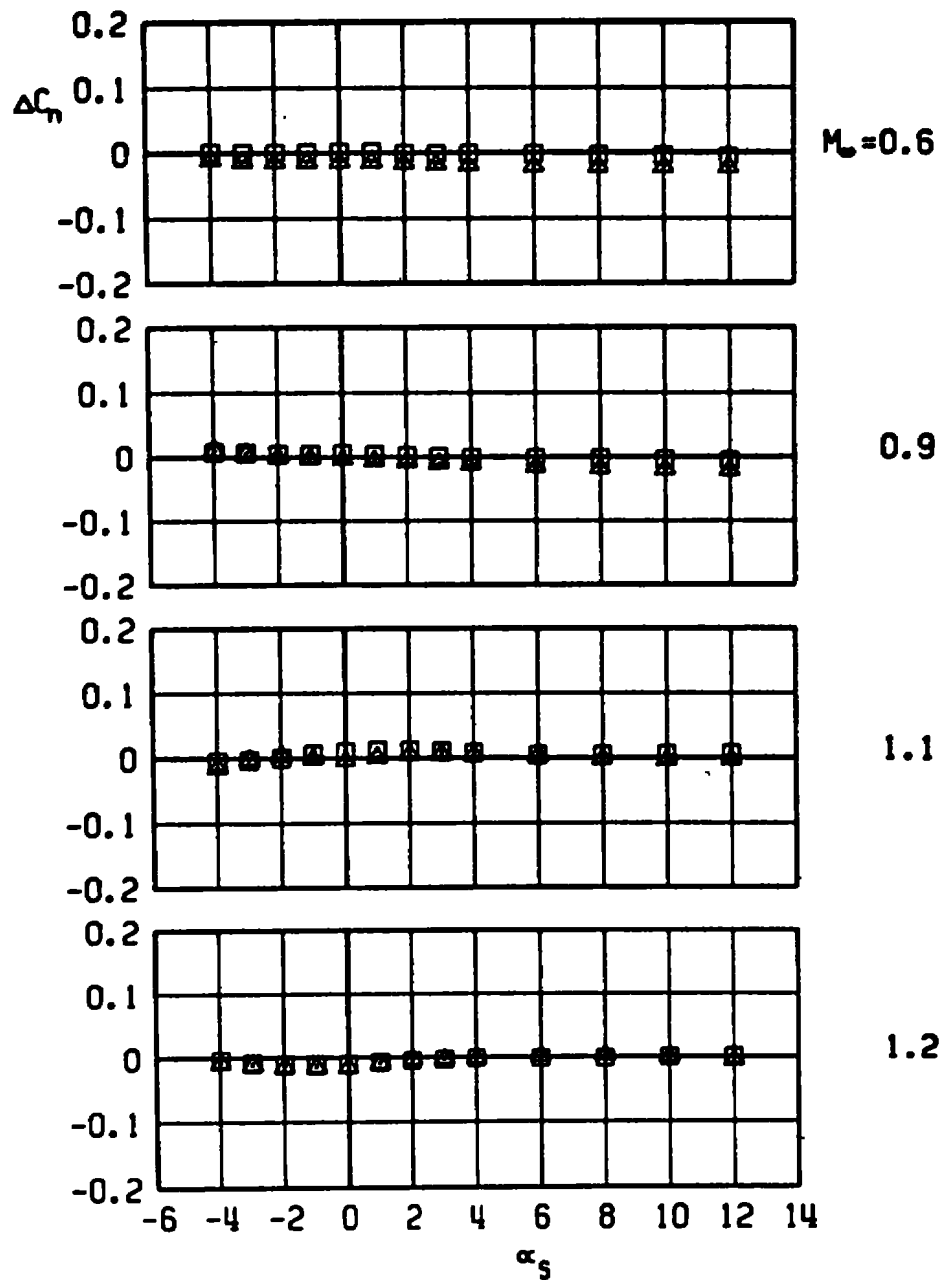
d. Rolling-moment increment
 Figure 26. Continued.

ASP, C-L PYLON, MER-3
 WITH DUMMY STING, $D_3 = 0.31 D_8$
 WITH DUMMY STING, $D_3 = 0.50 D_8$

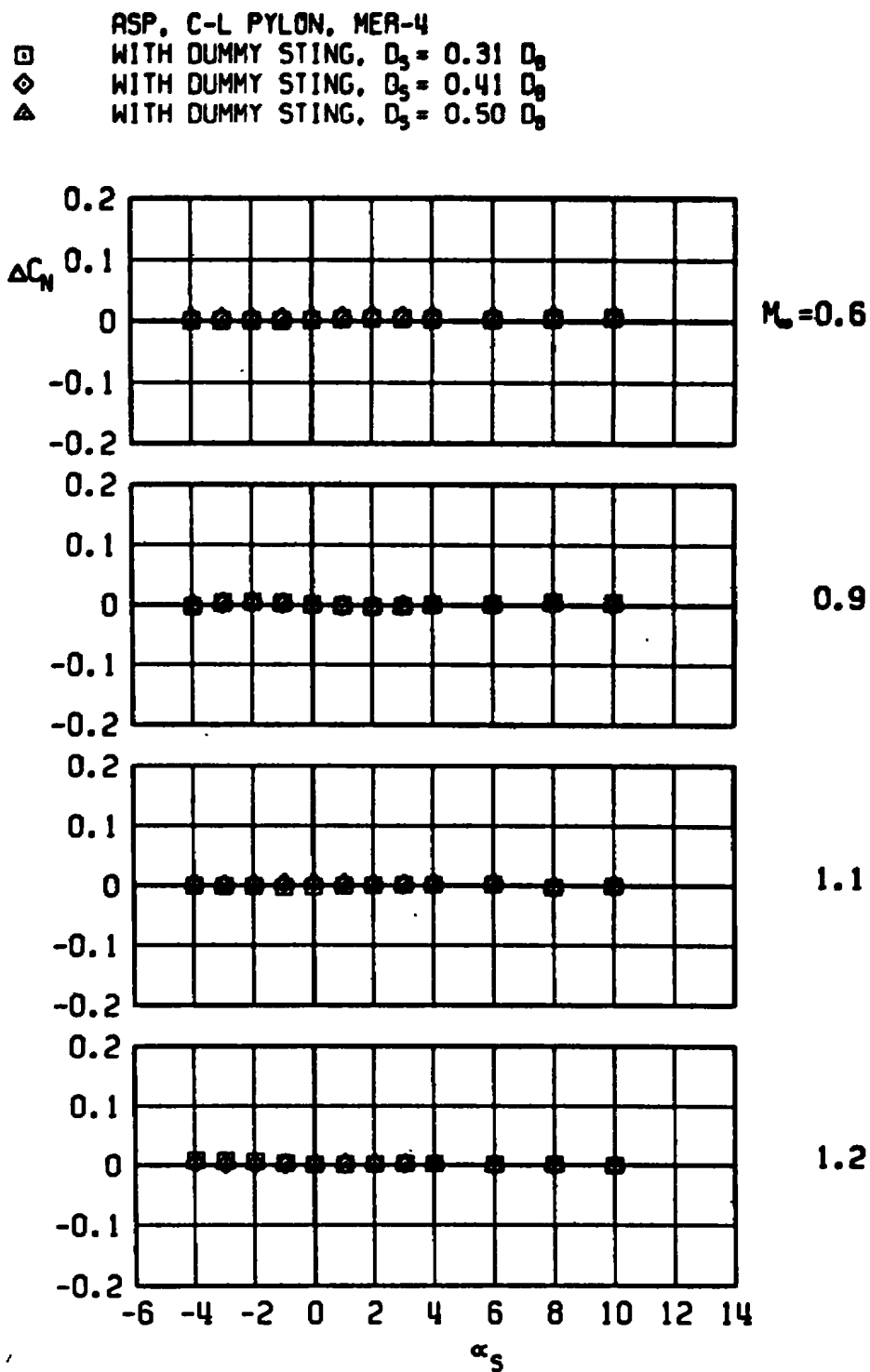


e. Pitching-moment increment
 Figure 26. Continued.

ASP, C-L PYLON, MER-3
 WITH DUMMY STING, $D_3 = 0.31 D_9$
 WITH DUMMY STING, $D_3 = 0.50 D_9$



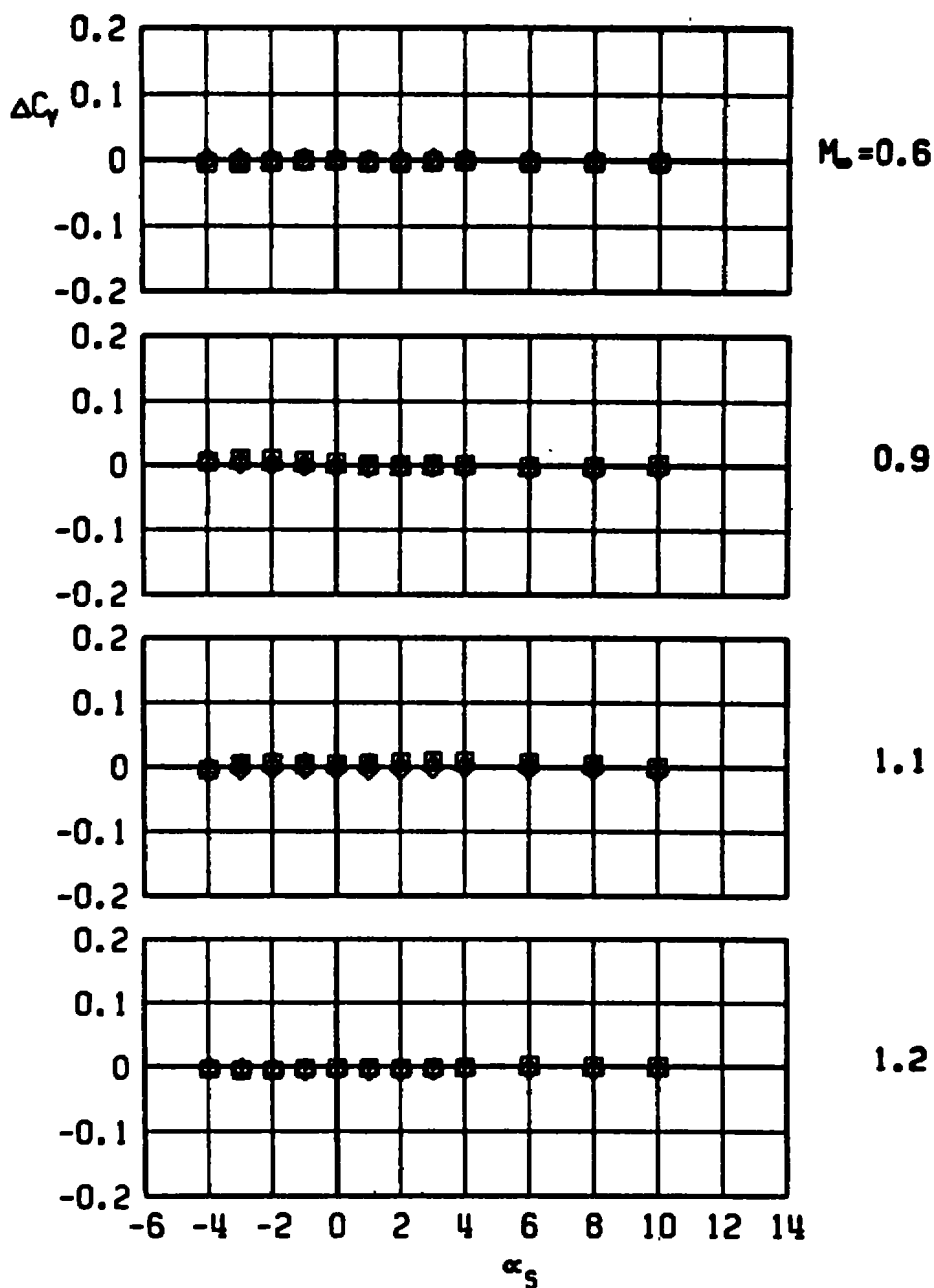
f. Yawing-moment increment
 Figure 26. Concluded.



a. Normal-force increment

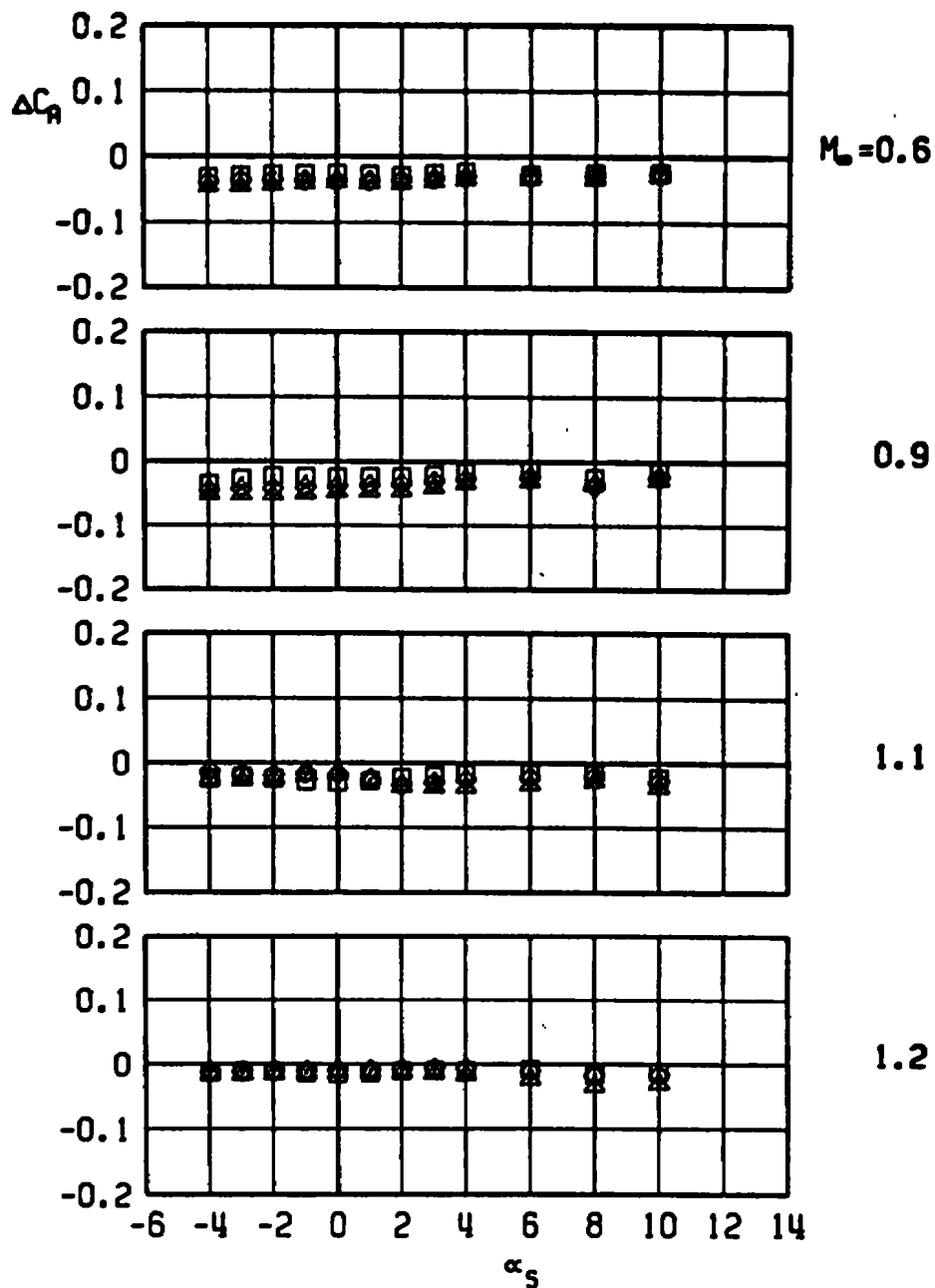
Figure 27. Sting-induced aerodynamic load increments as a function of angle of attack, unstable rack-mounted store, MER station 4, C-L pylon.

ASP, C-L PYLON, MER-4
 □ WITH DUMMY STING, $D_3 = 0.31 D_0$
 ◇ WITH DUMMY STING, $D_3 = 0.41 D_0$
 △ WITH DUMMY STING, $D_3 = 0.50 D_0$



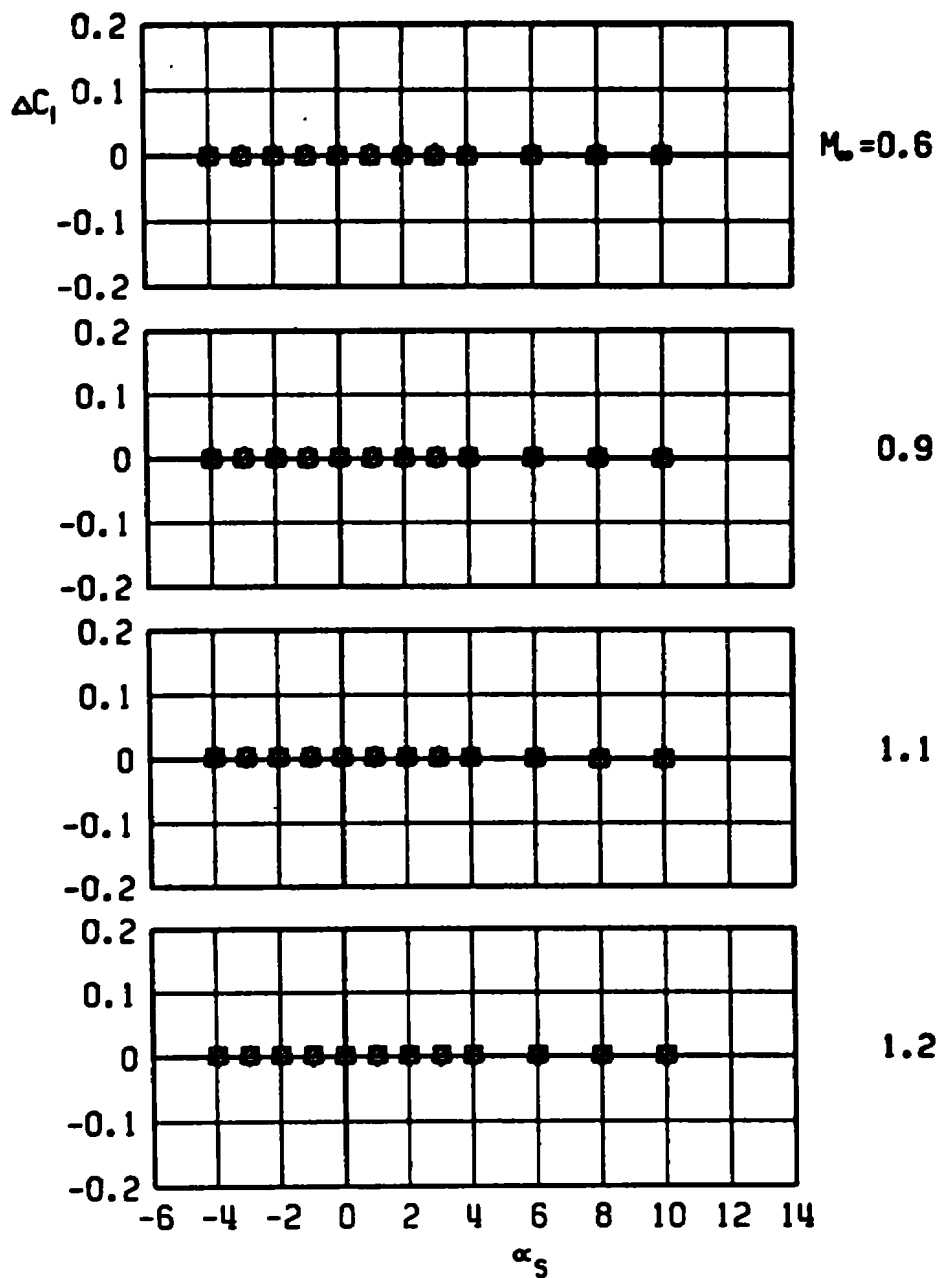
b. Side-force increment
 Figure 27. Continued.

ASP, C-L PYLON, MER-4
 □ WITH DUMMY STING, $D_3 = 0.31 D_0$
 ◇ WITH DUMMY STING, $D_3 = 0.41 D_0$
 △ WITH DUMMY STING, $D_3 = 0.50 D_0$



c. Axial-force increment
 Figure 27. Continued.

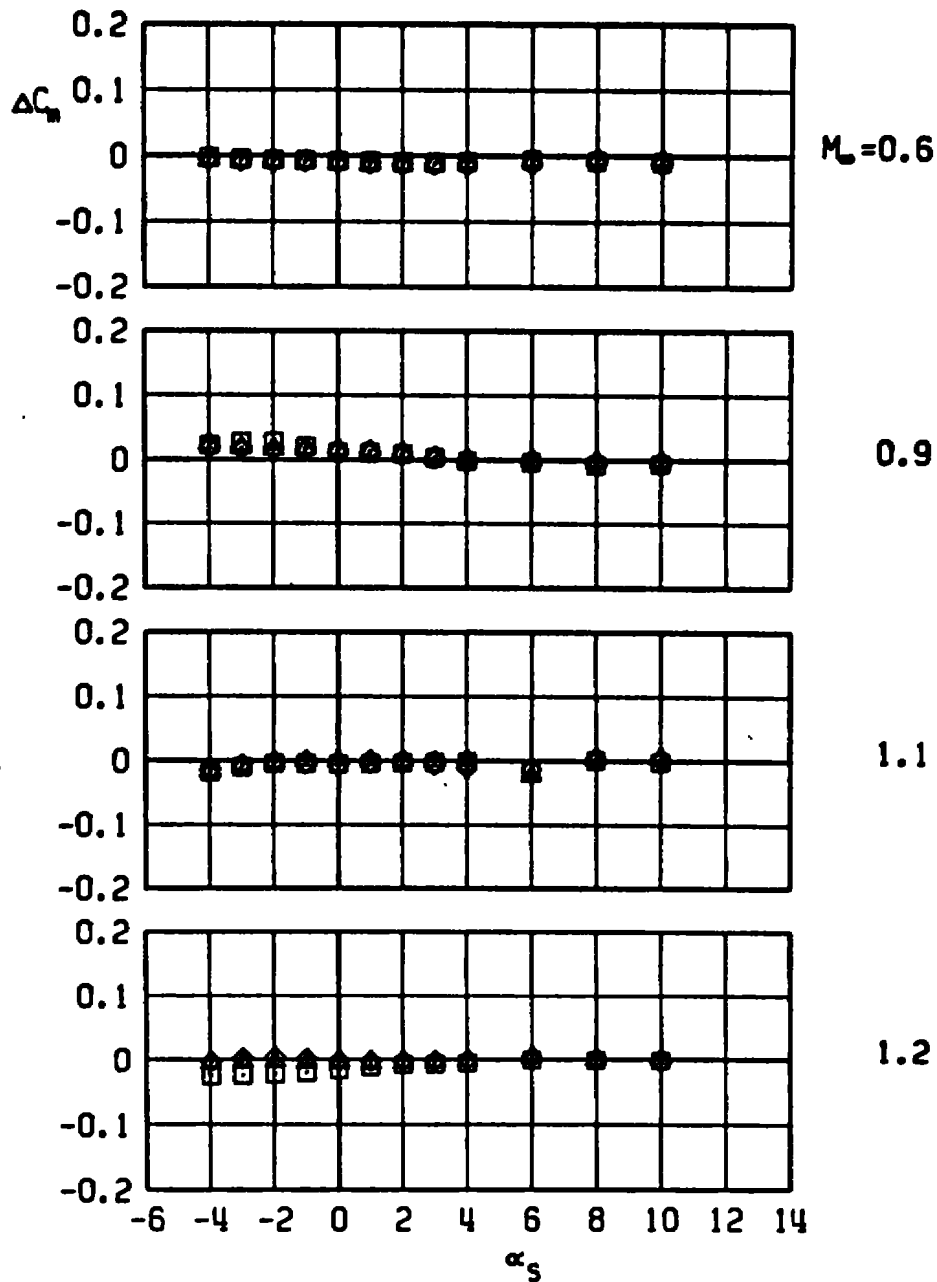
ASP, C-L PYLON, MER-4
 □ WITH DUMMY STING, $D_3 = 0.31 D_0$
 ◇ WITH DUMMY STING, $D_3 = 0.41 D_0$
 ▲ WITH DUMMY STING, $D_3 = 0.50 D_0$



d. Rolling-moment increment
 Figure 27. Continued.

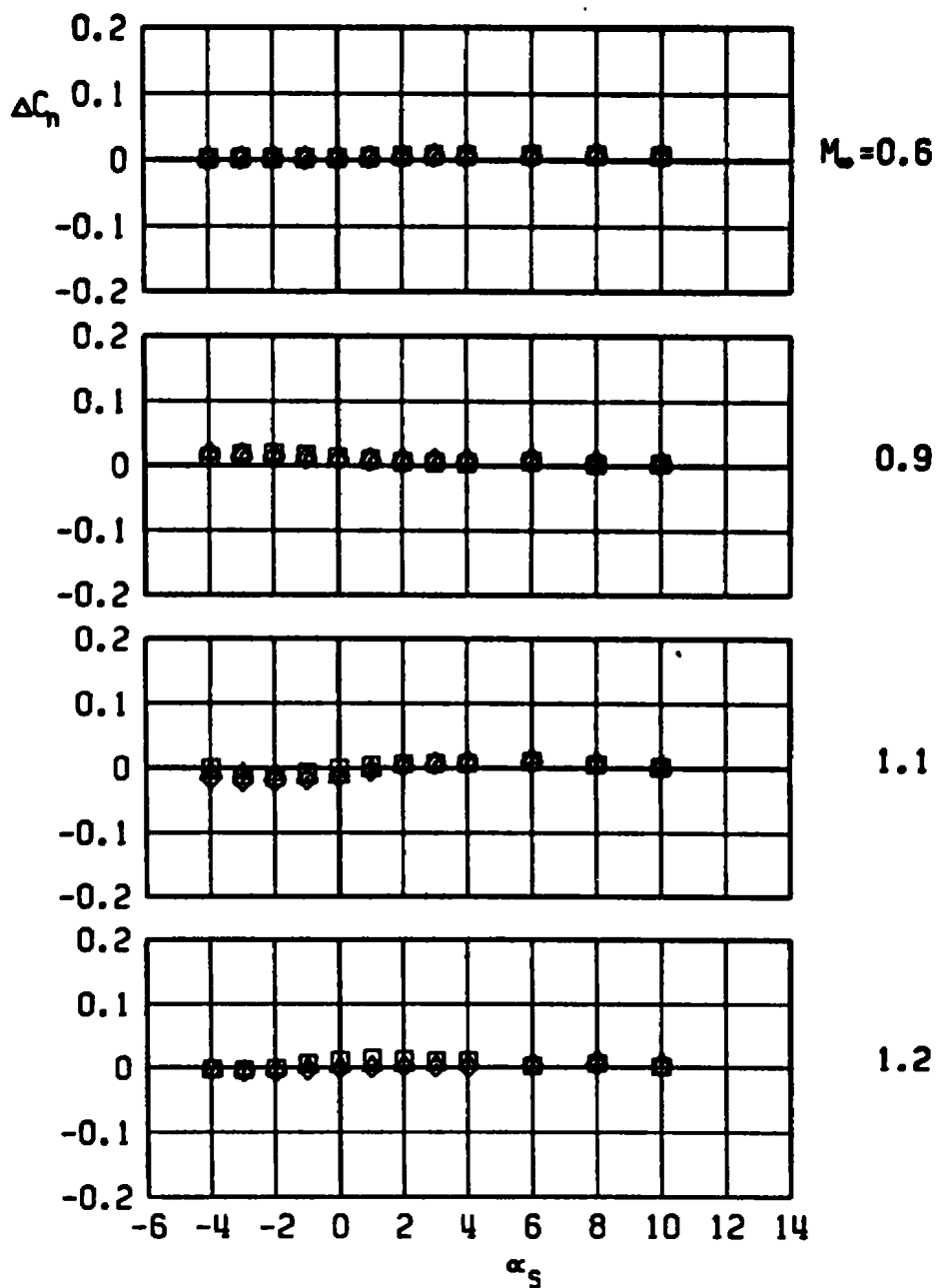
ASP, C-L PYLON, MER-4

- \square WITH DUMMY STING, $D_3 = 0.31 D_0$
 \diamond WITH DUMMY STING, $D_3 = 0.41 D_0$
 \triangle WITH DUMMY STING, $D_3 = 0.50 D_0$



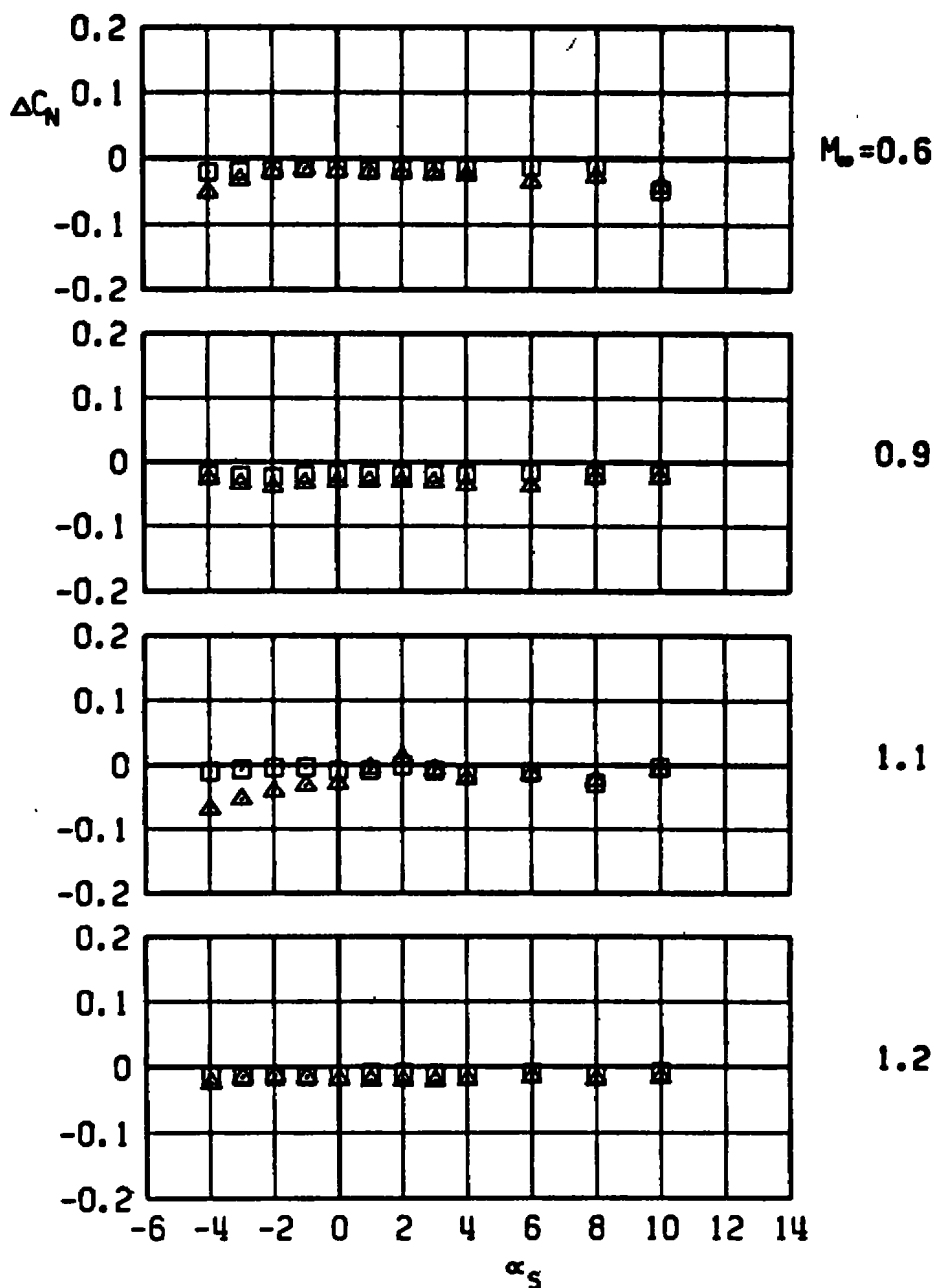
g. Pitching-moment increment
Figure 27. Continued.

ASP, C-L PYLON, MER-4
 WITH DUMMY STING, $D_3 = 0.31 D_0$
 WITH DUMMY STING, $D_3 = 0.41 D_0$
 WITH DUMMY STING, $D_3 = 0.50 D_0$



f. Yawing-moment increment
 Figure 27. Concluded.

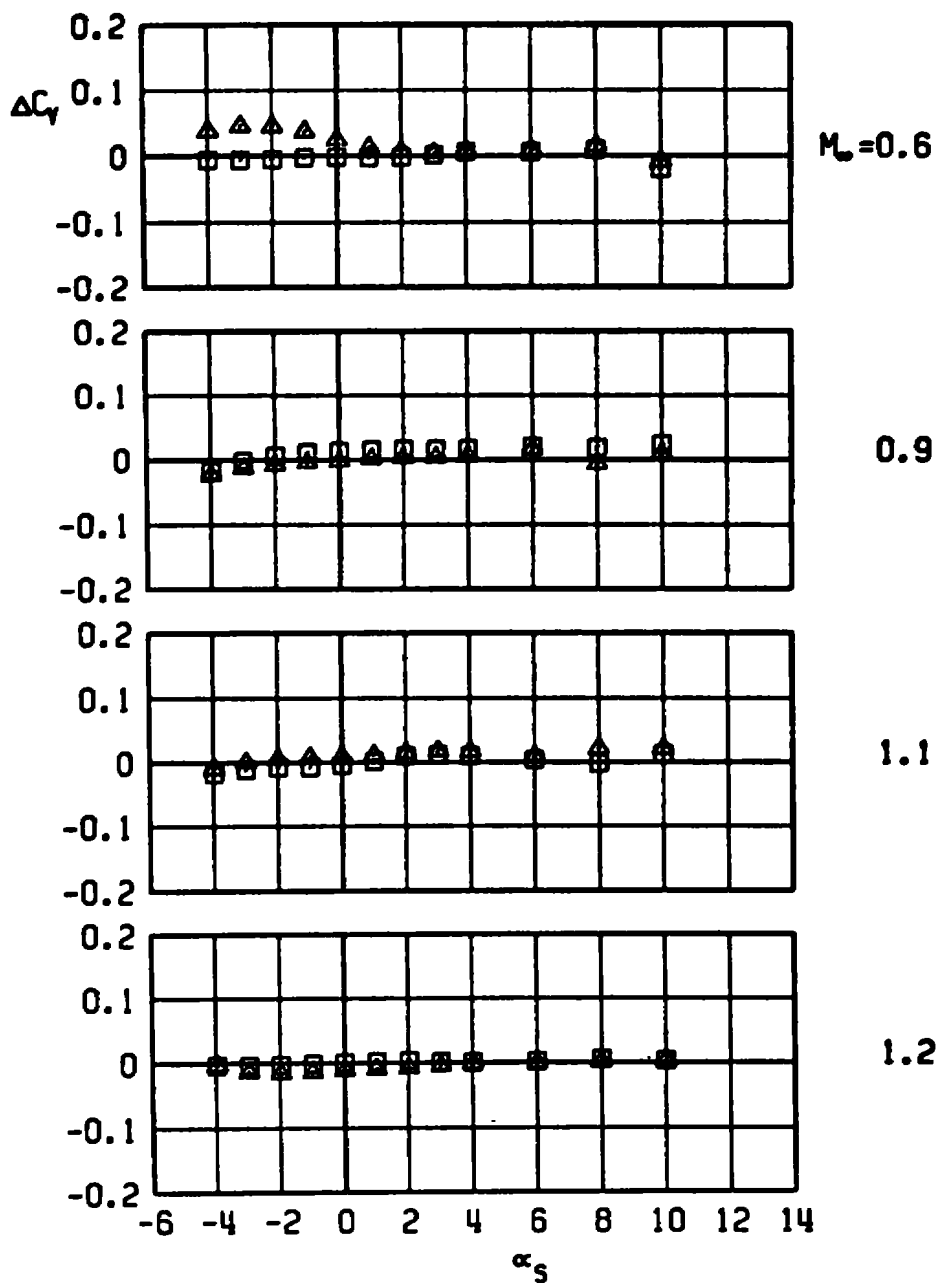
□ ASP, LOB PYLON, MER-1
 WITH DUMMY STING, $D_3 = 0.31 D_0$
 ▲ WITH DUMMY STING, $D_3 = 0.50 D_0$



a. Normal-force increment

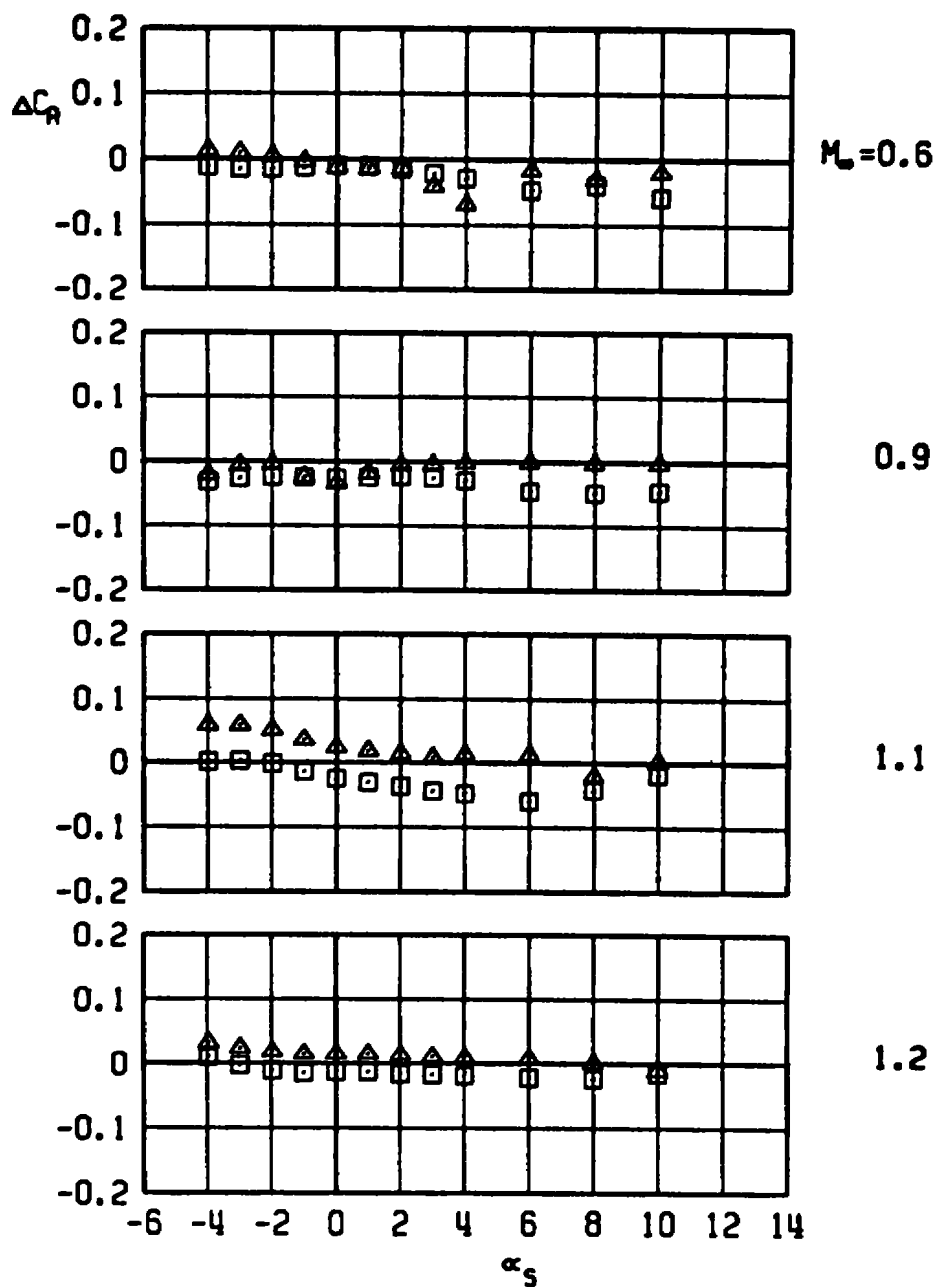
Figure 28. Sting-induced aerodynamic load increments as a function of angle of attack, unstable rack-mounted store, MER station 1, LOB pylon.

ASP, LOB PYLON, MER-1
 □ WITH DUMMY STING, $D_3 = 0.31 D_0$
 ▲ WITH DUMMY STING, $D_3 = 0.50 D_0$



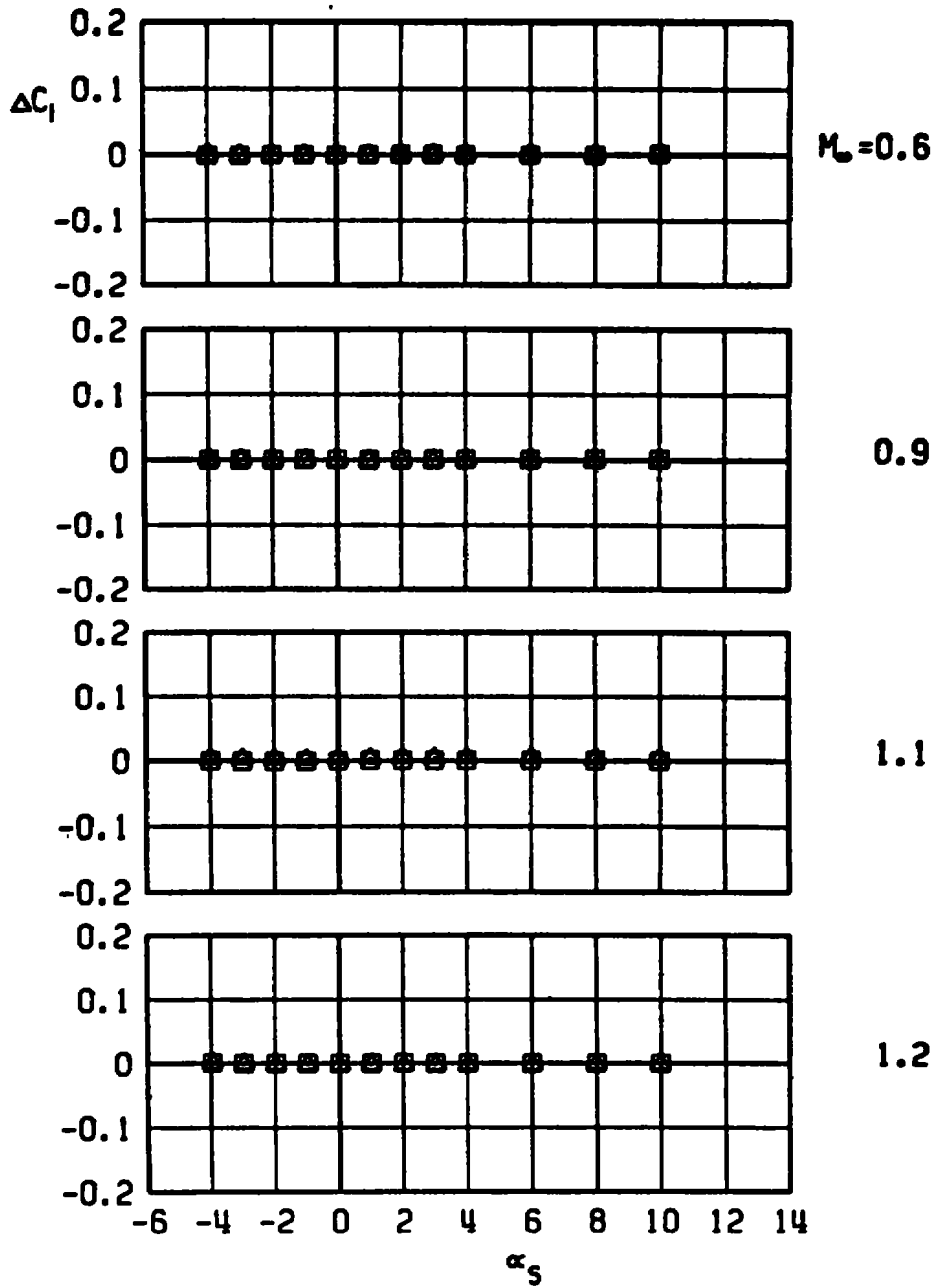
b. Side-force increment
 Figure 28. Continued.

ASP, LOB PYLON, MER-1
 □ WITH DUMMY STING, $D_3 = 0.31 D_0$
 ▲ WITH DUMMY STING, $D_3 = 0.50 D_0$



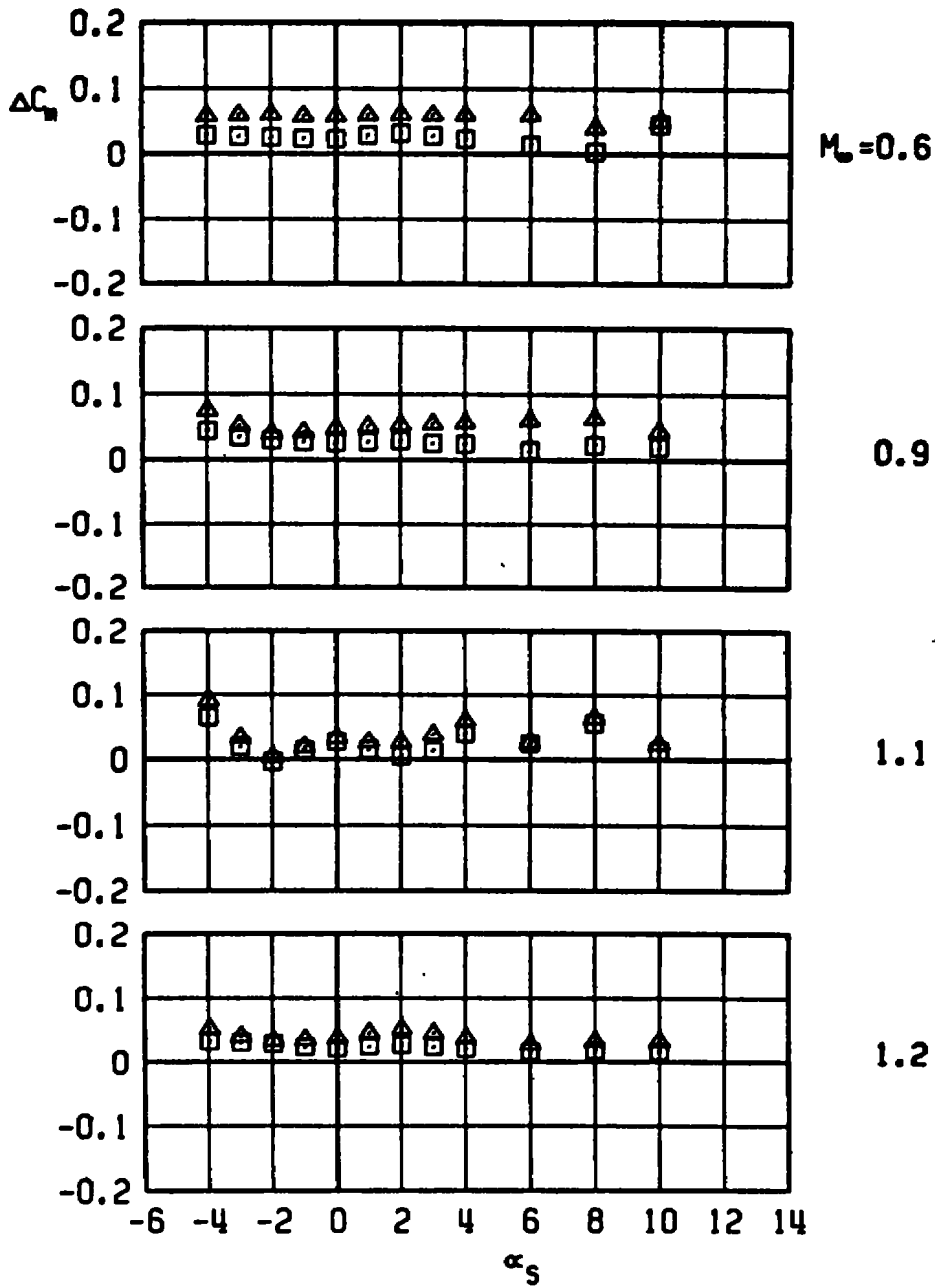
c. Axial-force increment
 Figure 28. Continued.

ASP, LOB PYLON, MER-1
 WITH DUMMY STING, $D_3 = 0.31 D_0$
 WITH DUMMY STING, $D_3 = 0.50 D_0$



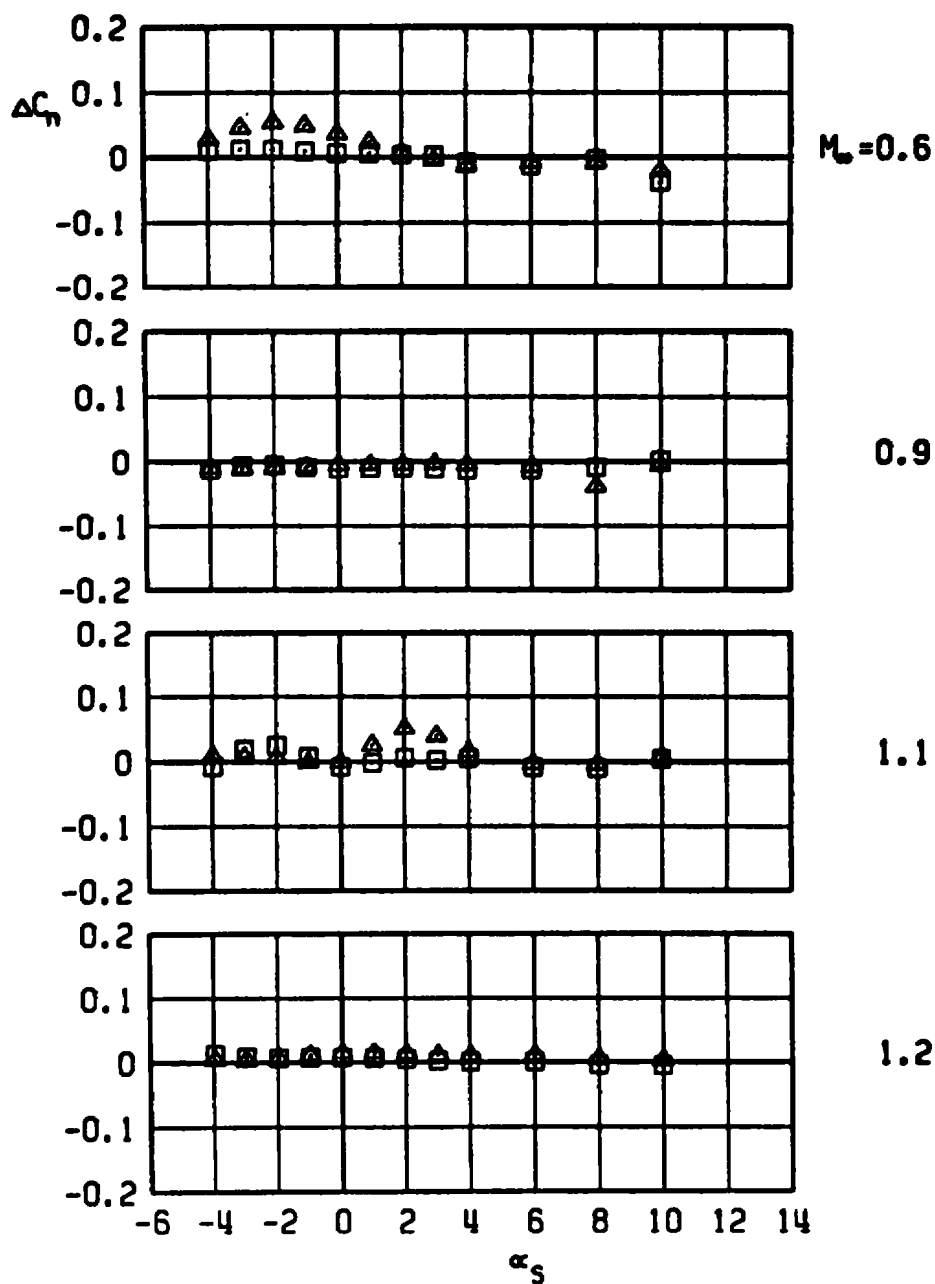
d. Rolling-moment increment
 Figure 28. Continued.

ASP, LOB PYLON, MER-1
 □ WITH DUMMY STING, $D_3 = 0.31 D_0$
 ▲ WITH DUMMY STING, $D_3 = 0.50 D_0$



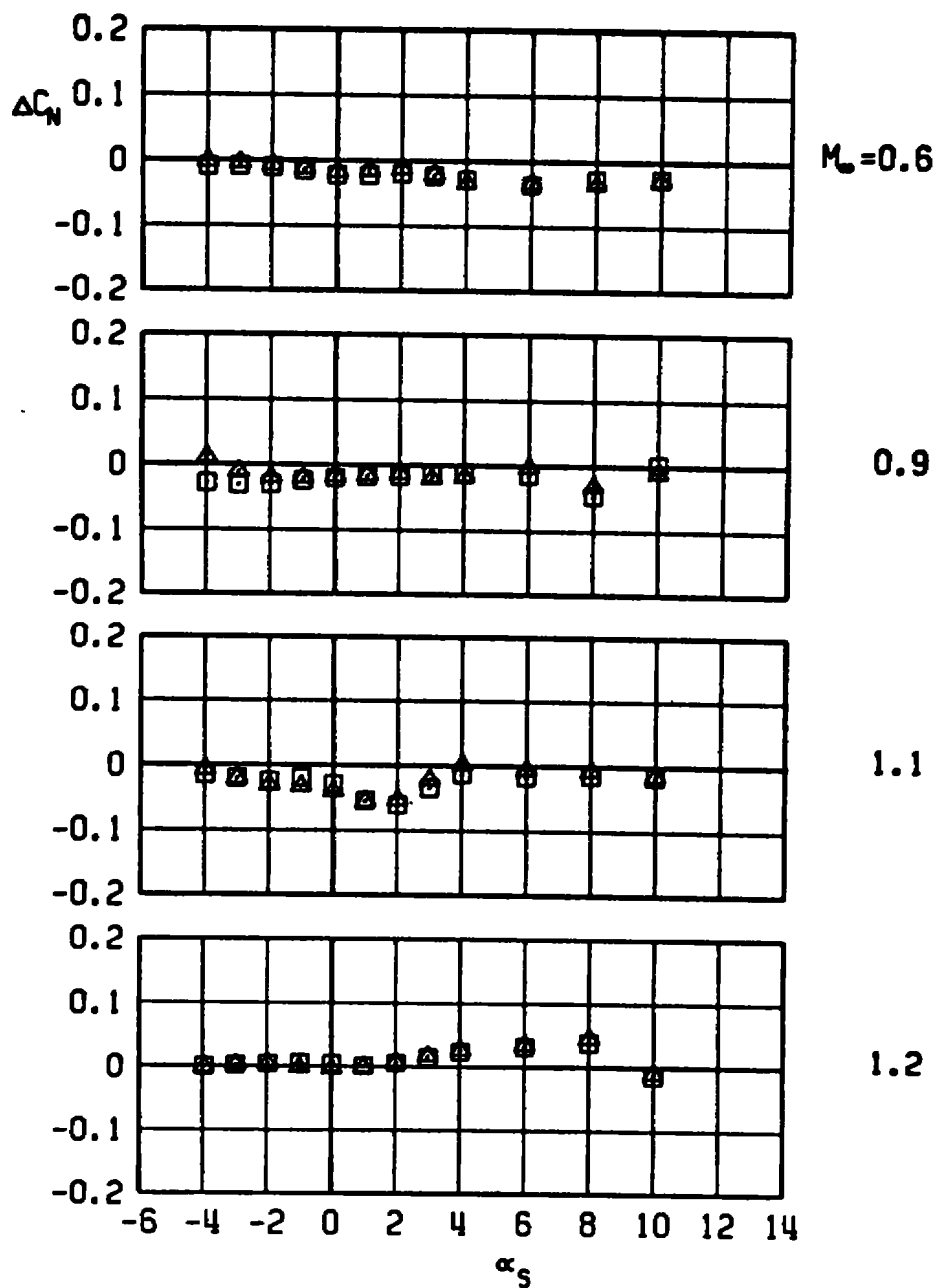
e. Pitching-moment increment
 Figure 28. Continued.

ASP, LOB PYLON, MER-1
 □ WITH DUMMY STING, $D_5 = 0.31 D_9$
 ▲ WITH DUMMY STING, $D_5 = 0.50 D_9$



f. Yawing-moment increment
 Figure 28. Concluded.

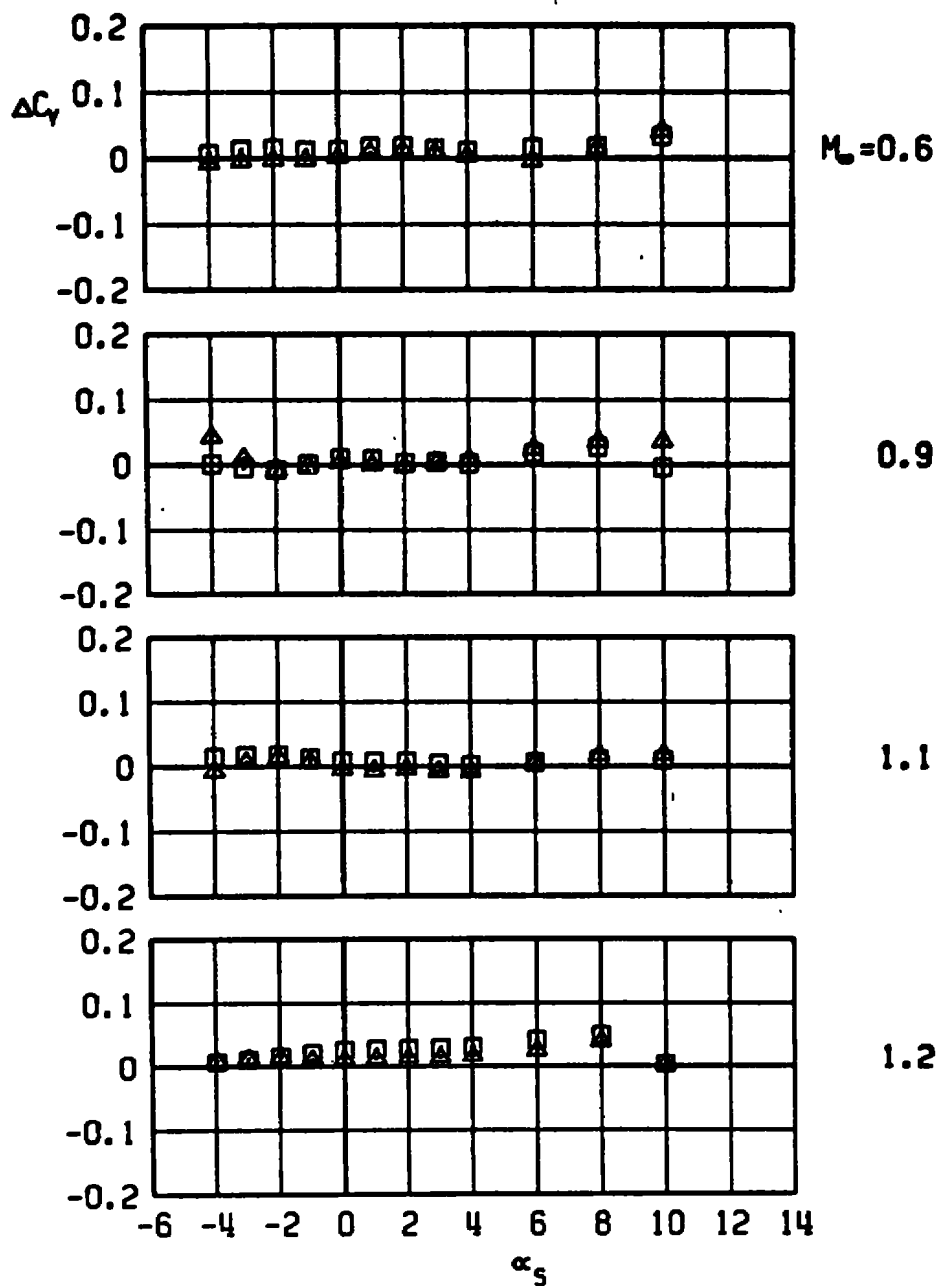
ASP, LOB PYLON, MER-2
 □ WITH DUMMY STING, $D_3 = 0.31 D_8$
 ▲ WITH DUMMY STING, $D_3 = 0.50 D_8$



a. Normal-force increment

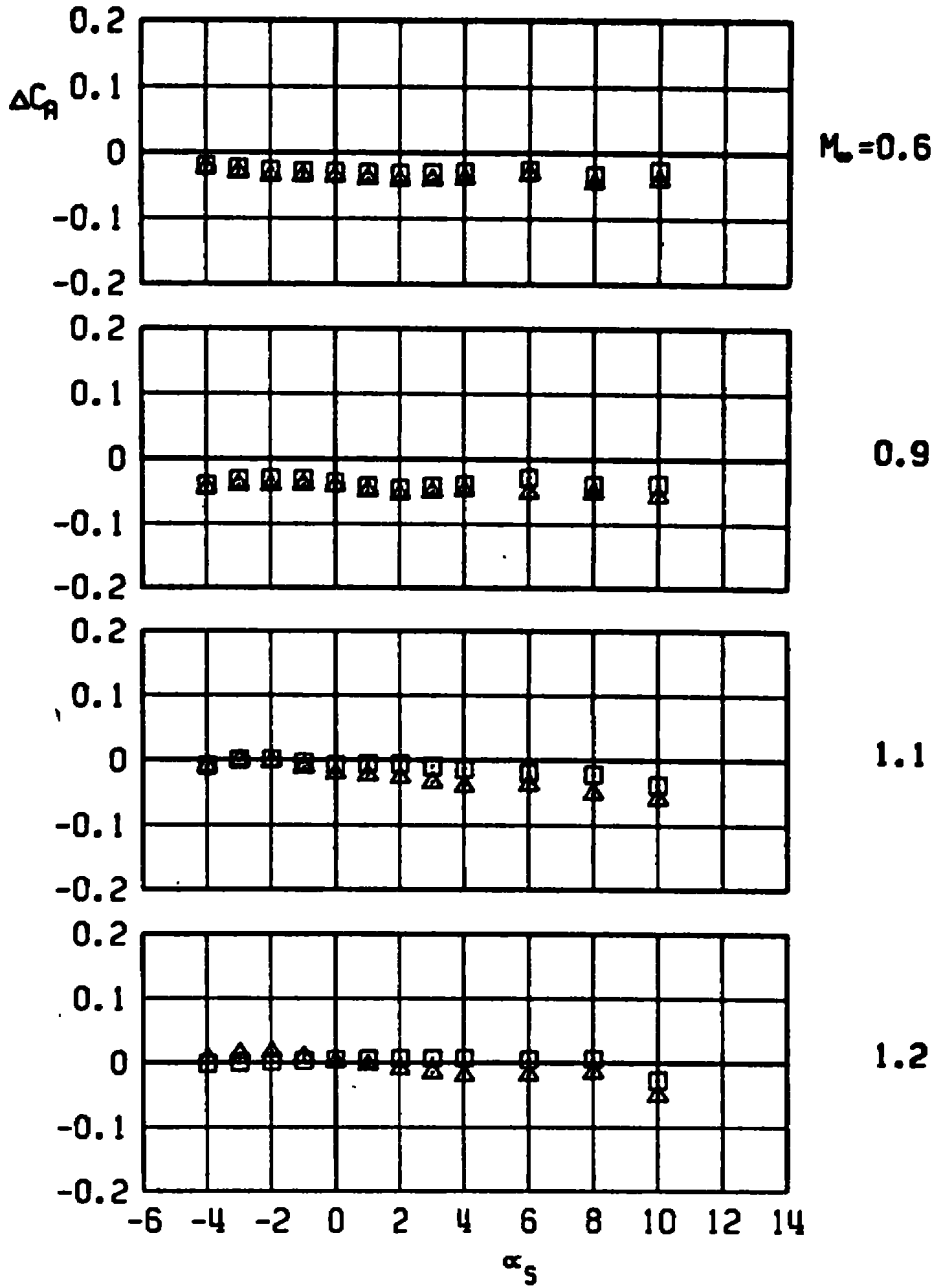
Figure 29. Sting-induced aerodynamic load increments as a function of angle of attack, unstable rack-mounted store, MER station 2, LOB pylon.

ASP, LOB PYLON, MER-2
 □ WITH DUMMY STING, $D_5 = 0.31 D_0$
 ▲ WITH DUMMY STING, $D_5 = 0.50 D_0$



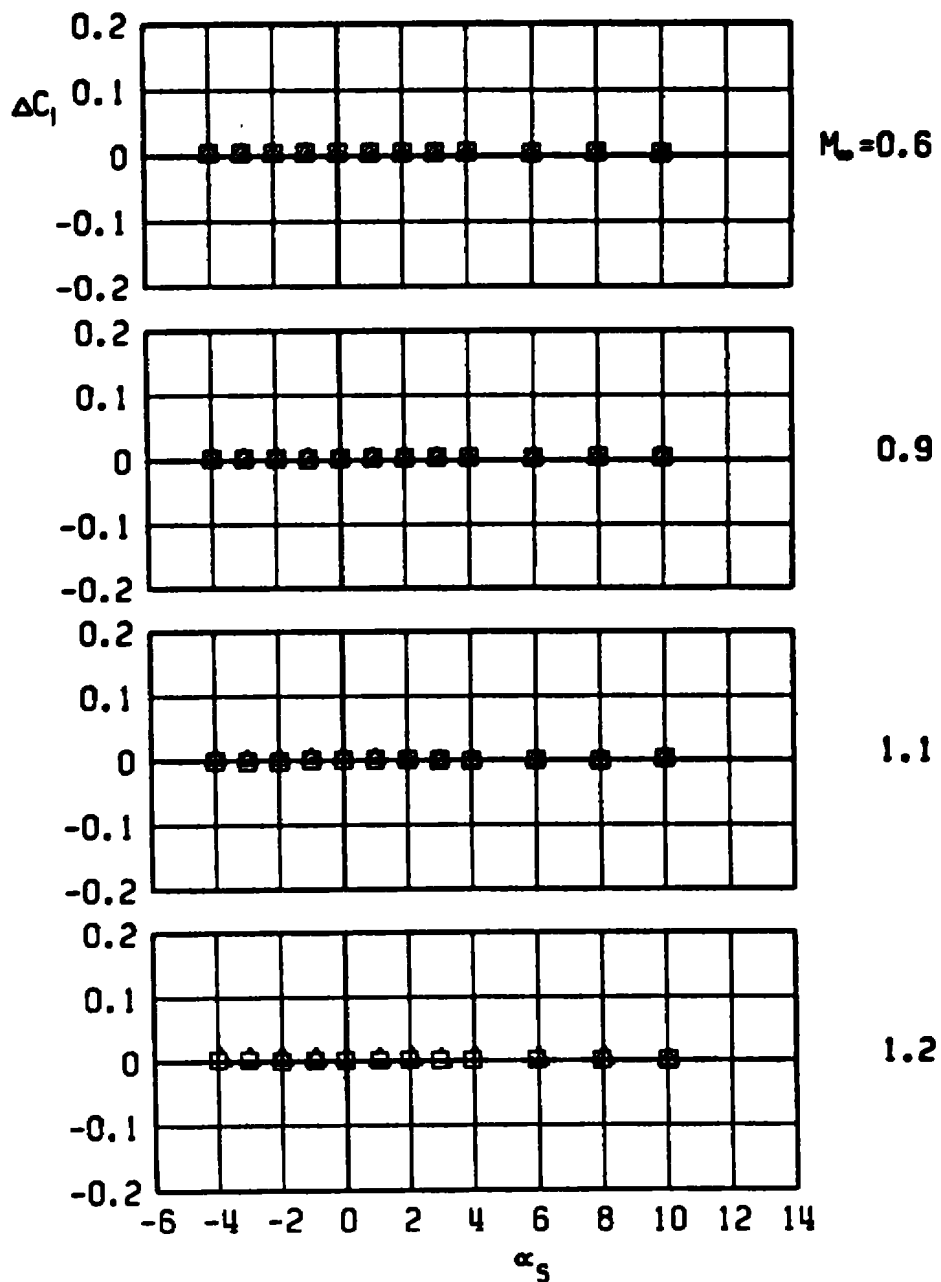
b. Side-force increment
 Figure 29. Continued.

ASP, LOB PYLON, MER-2
 WITH DUMMY STING, $D_3 = 0.31 D_0$
 WITH DUMMY STING, $D_3 = 0.50 D_0$



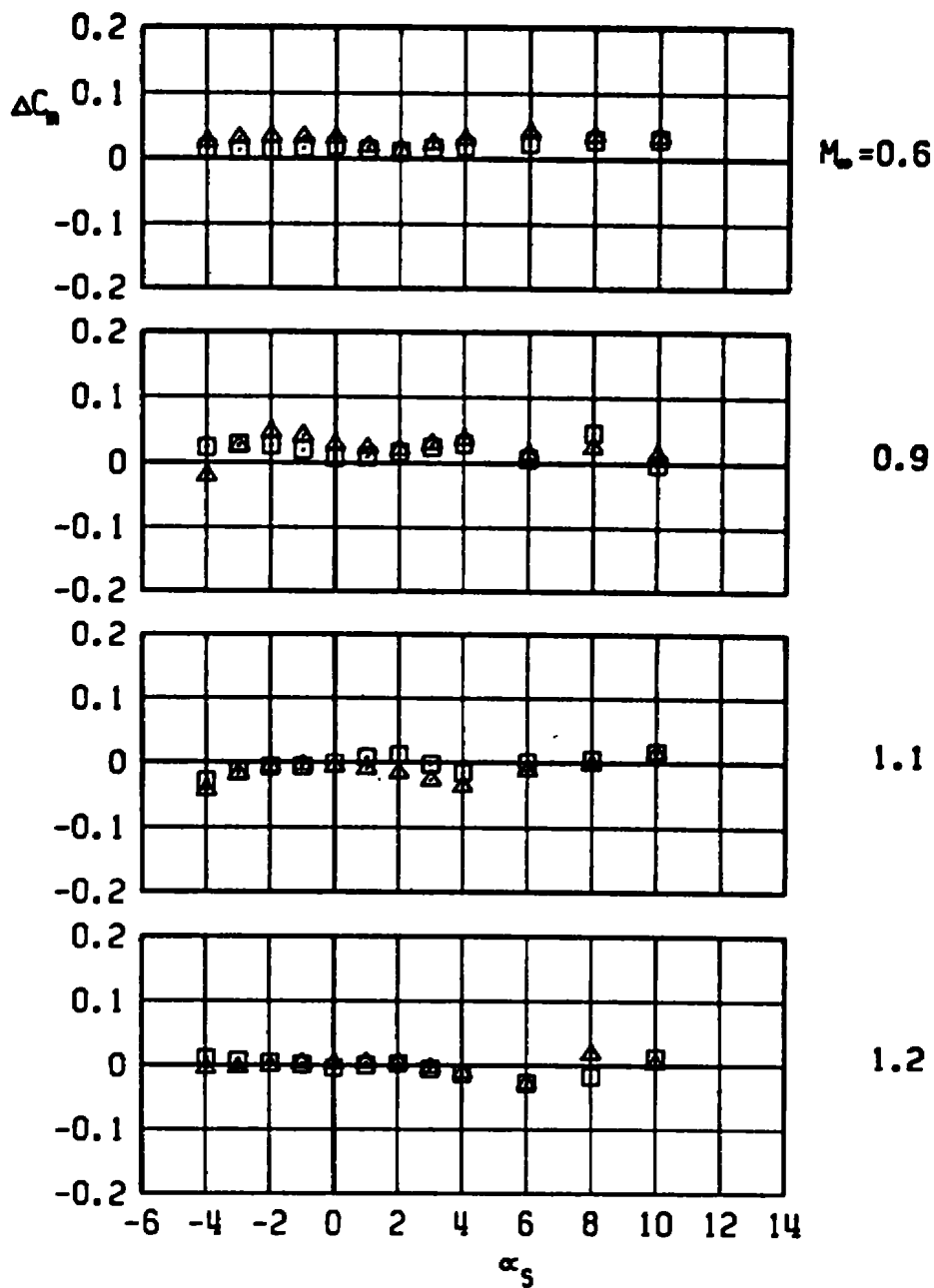
c. Axial-force increment
 Figure 29. Continued.

□ ASP, LOB PYLON, MER-2
 WITH DUMMY STING, $D_3 = 0.31 D_9$
 △ WITH DUMMY STING, $D_3 = 0.50 D_9$



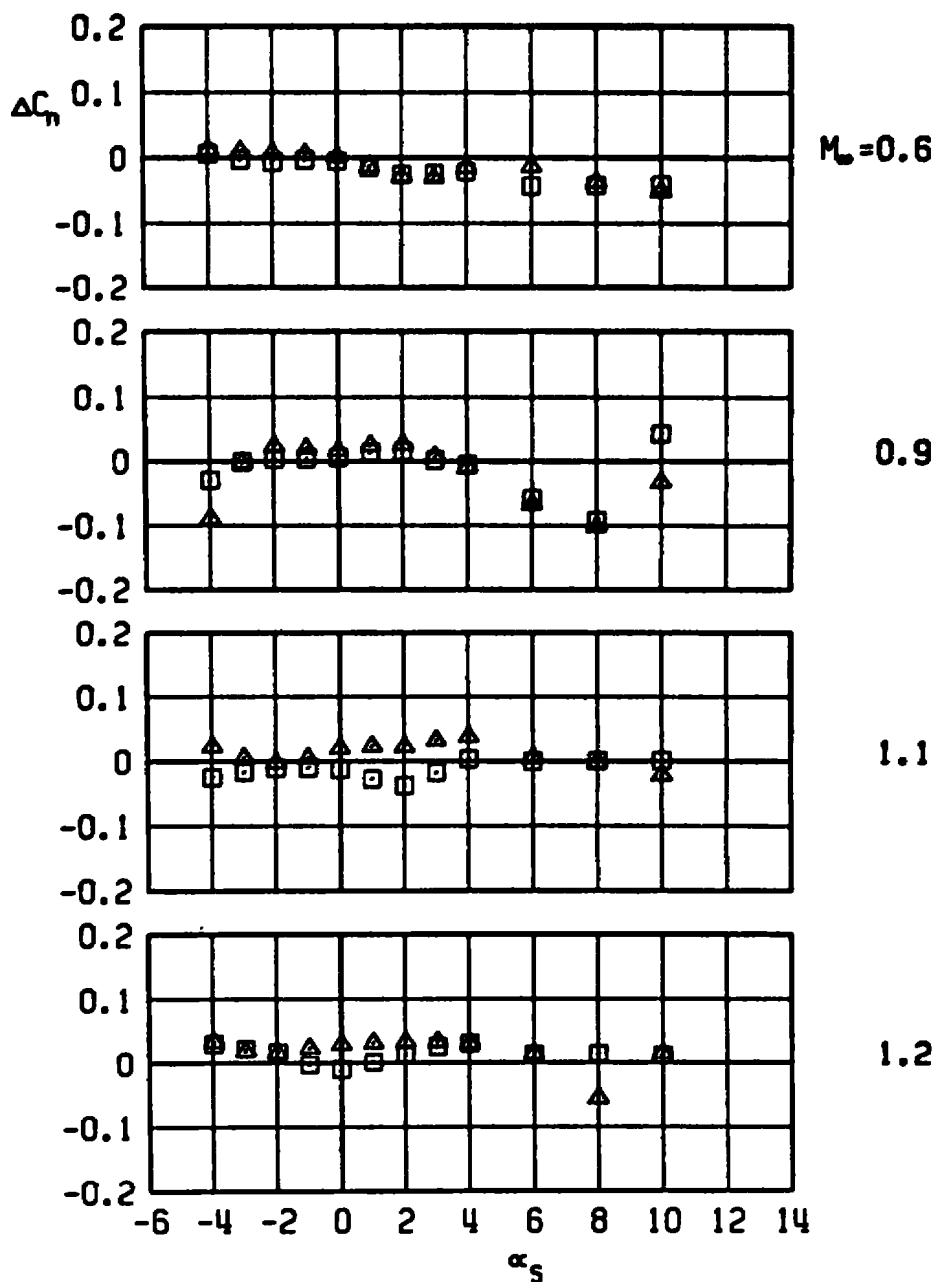
d. Rolling-moment increment
 Figure 29. Continued.

ASP, LOB PYLON, MER-2
 WITH DUMMY STING, $D_3 = 0.31 D_9$
 WITH DUMMY STING, $D_3 = 0.50 D_9$



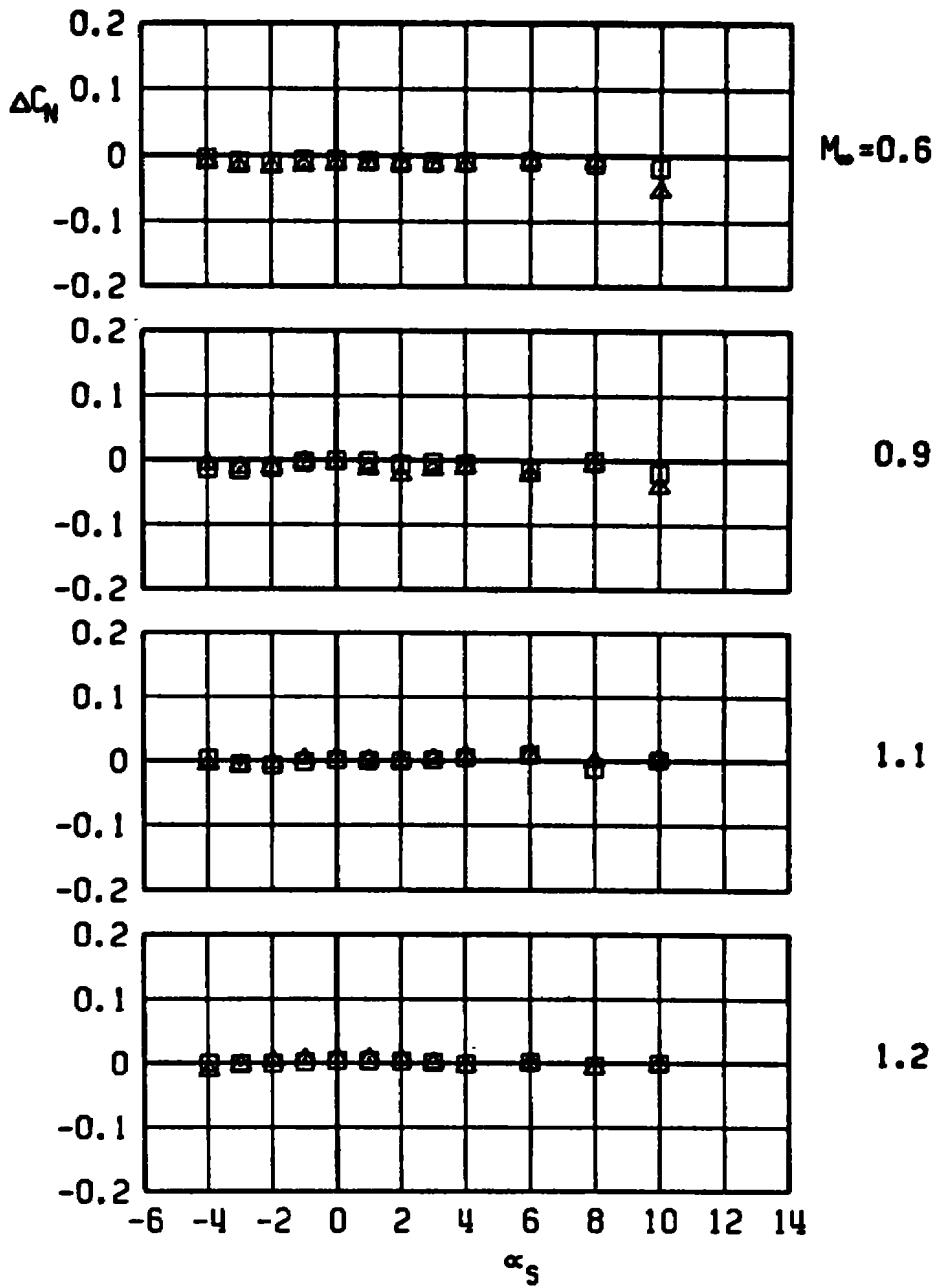
e. Pitching-moment increment
 Figure 29. Continued.

ASP, LOB PYLON, MER-2
 WITH DUMMY STING, $D_3 = 0.31 D_0$
 WITH DUMMY STING, $D_3 = 0.50 D_0$



f. Yawing-moment increment
 Figure 29. Concluded.

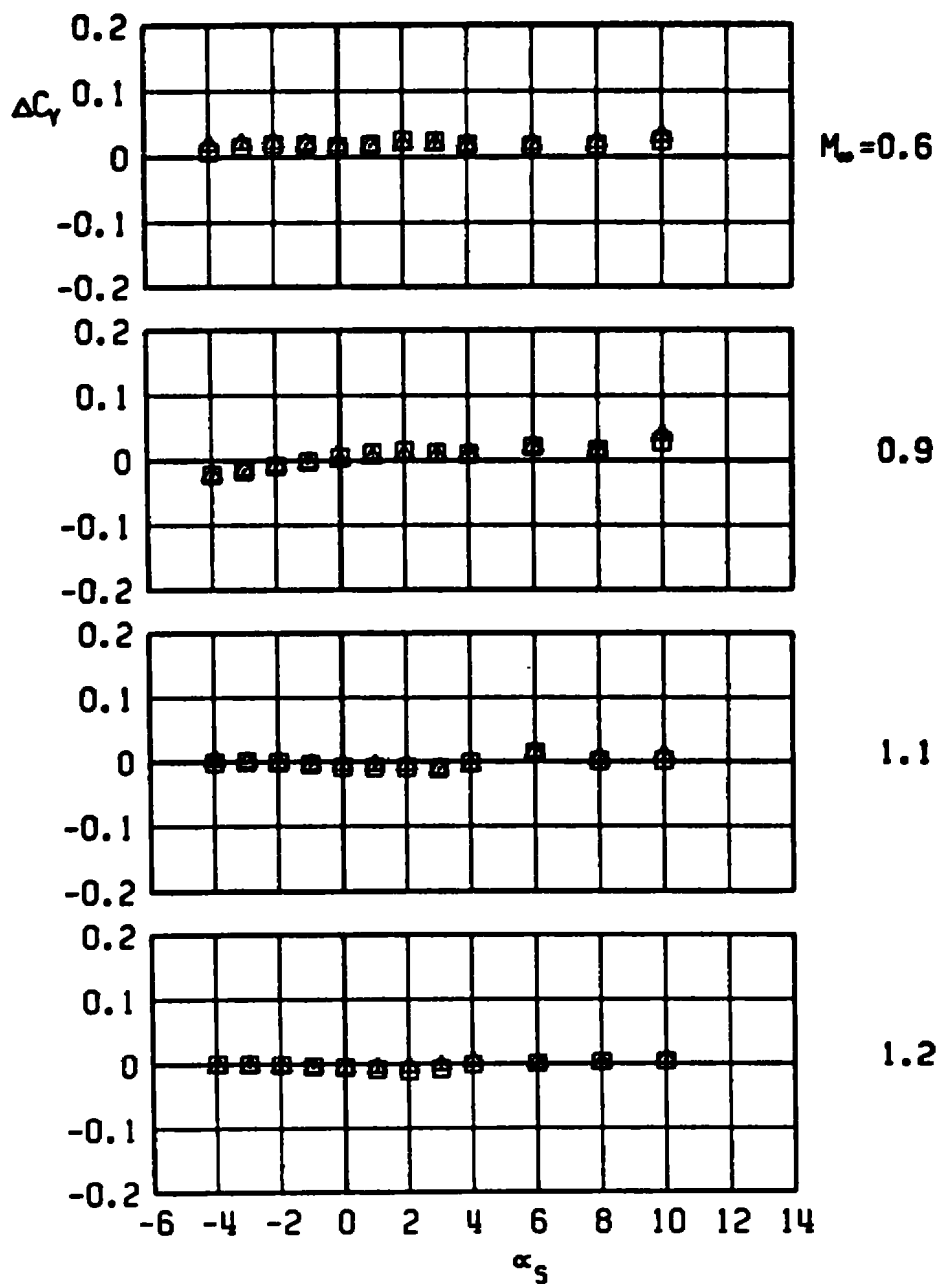
ASP, LOB PYLON, MER-3
 WITH DUMMY STING, $D_3 = 0.31 D_0$
 WITH DUMMY STING, $D_3 = 0.50 D_0$



a. Normal-force increment

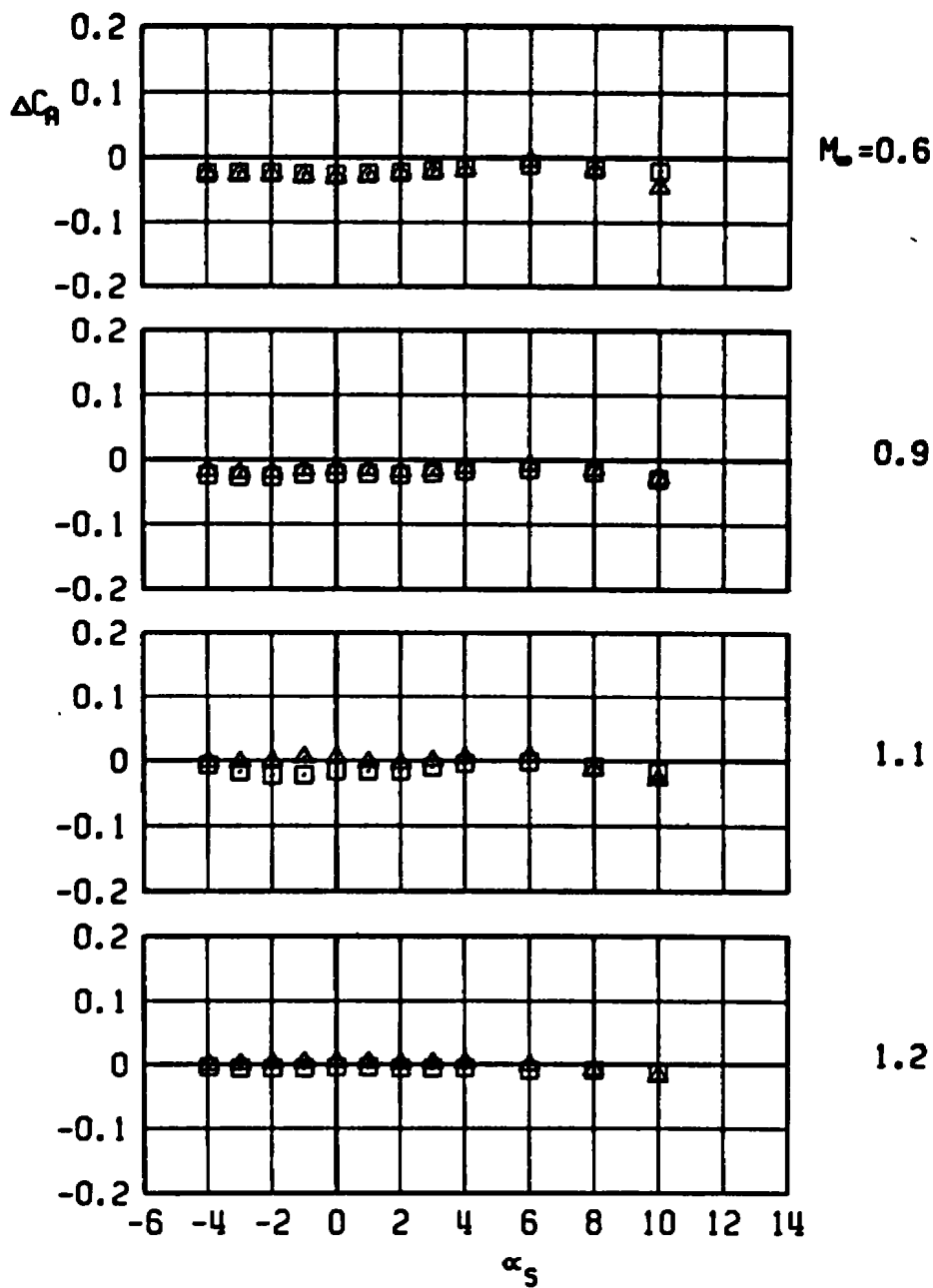
Figure 30. Sting-induced aerodynamic load increments as a function of angle of attack, unstable rack-mounted store, MER station 3, LOB pylon.

ASP, LOB PYLON, MER-3
 WITH DUMMY STING, $D_3 = 0.31 D_0$
 WITH DUMMY STING, $D_3 = 0.50 D_0$



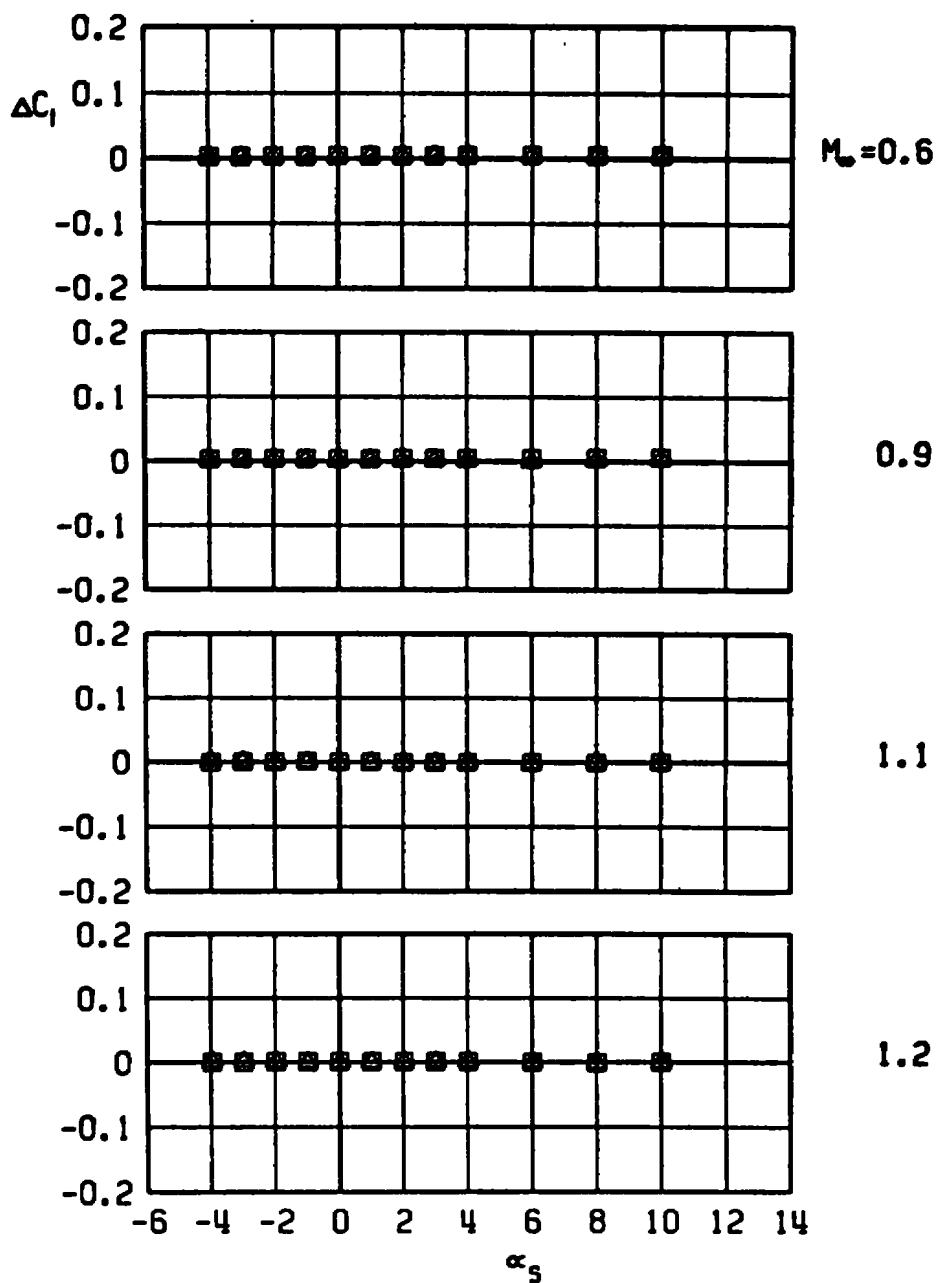
b. Side-force increment
 Figure 30. Continued.

ASP, LOB PYLON, MER-3
 □ WITH DUMMY STING, $D_3 = 0.31 D_8$
 △ WITH DUMMY STING, $D_3 = 0.50 D_8$



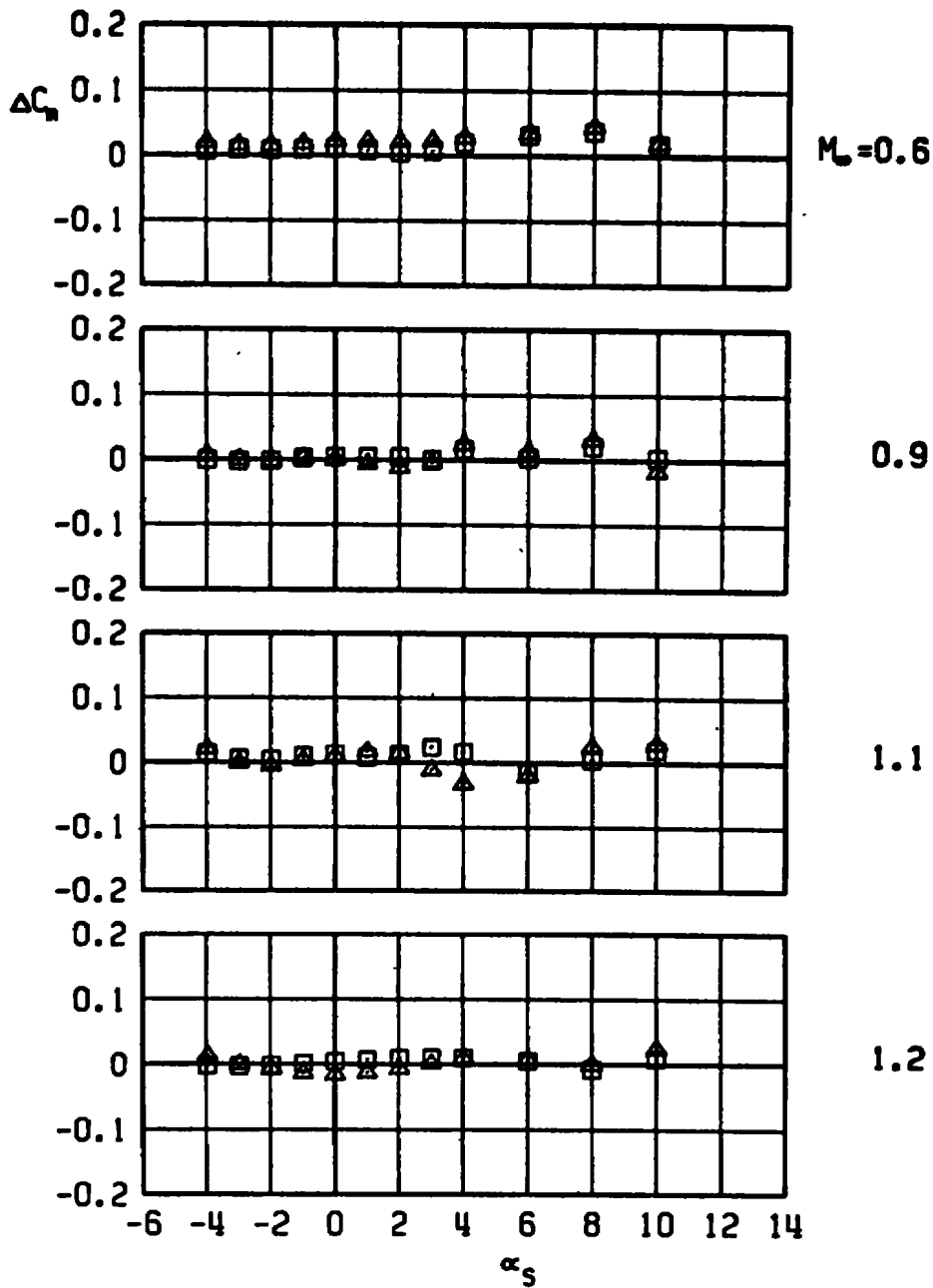
c. Axial-force increment
Figure 30. Continued.

ASP, LOB PYLON, MER-3
 WITH DUMMY STING, $D_3 = 0.31 D_0$
 WITH DUMMY STING, $D_3 = 0.50 D_0$



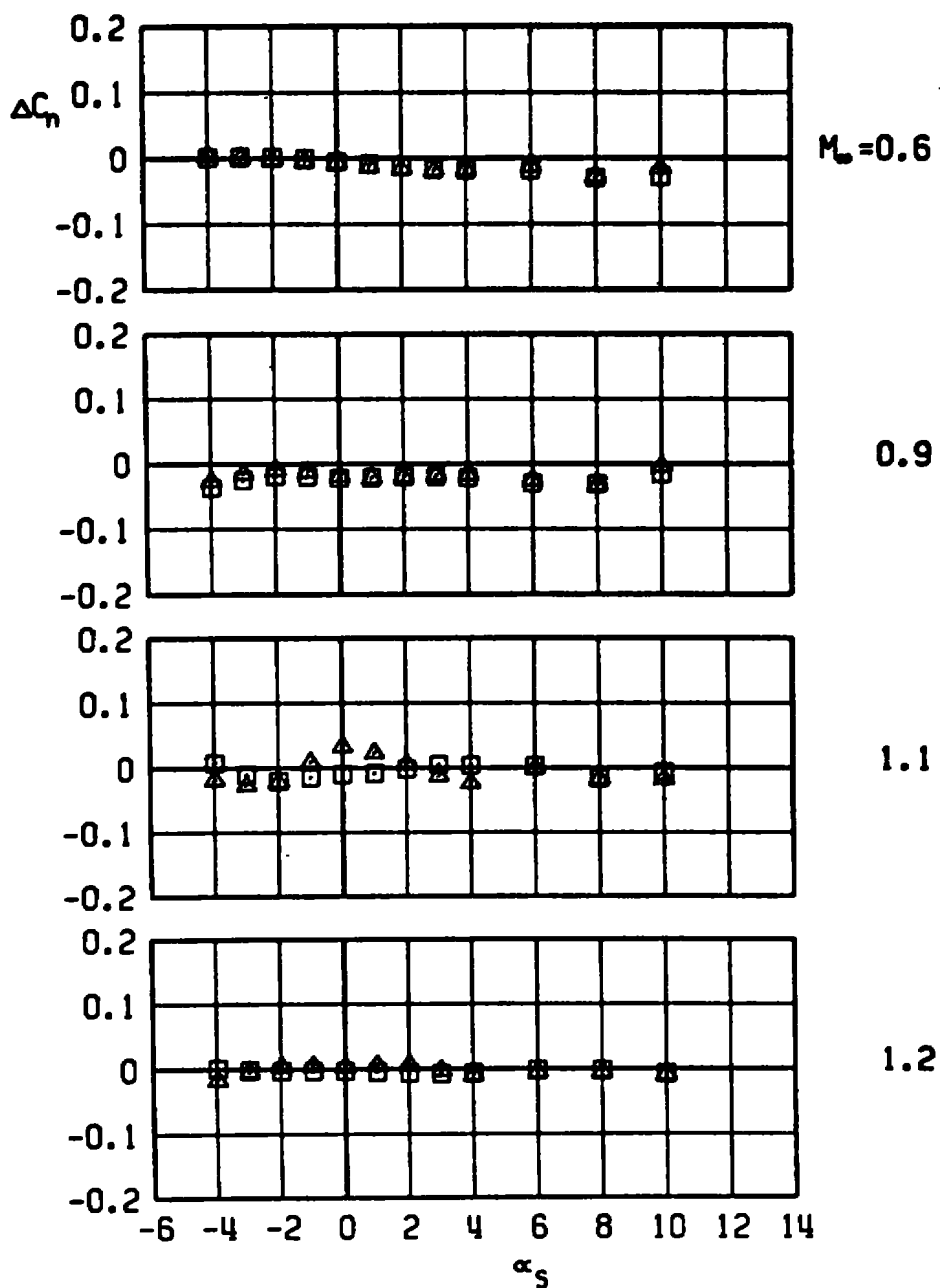
d. Rolling-moment increment
 Figure 30. Continued.

□ ASP, LOB PYLON, MER-3
 WITH DUMMY STING, $D_3 = 0.31 D_0$
 ▲ WITH DUMMY STING, $D_3 = 0.50 D_0$



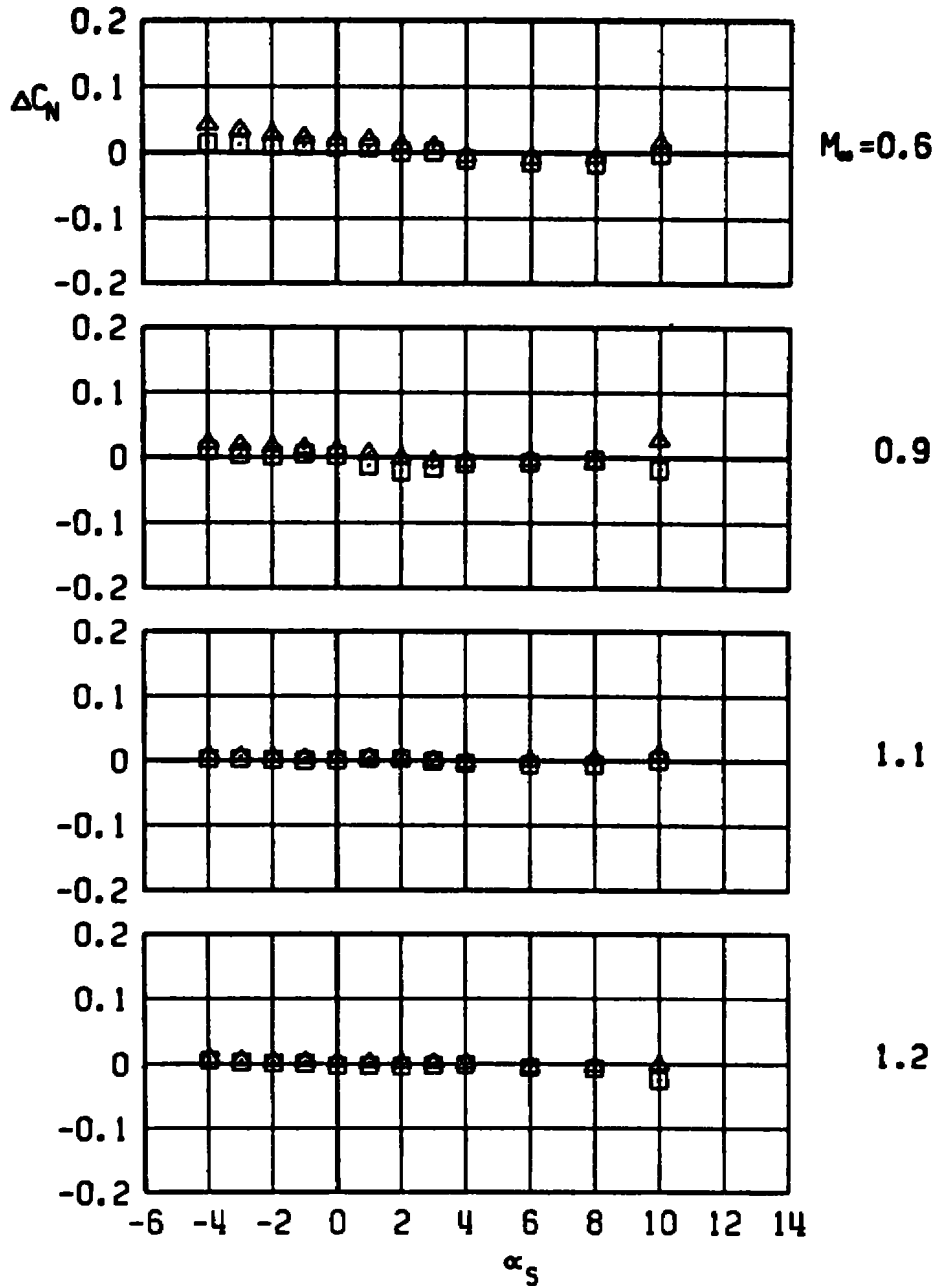
e. Pitching-moment increment
 Figure 30. Continued.

□ ASP, LOB PYLON, MER-3
 WITH DUMMY STING, $D_3 = 0.31 D_0$
 ▲ WITH DUMMY STING, $D_3 = 0.50 D_0$



f. Yawing-moment increment
 Figure 30. Concluded.

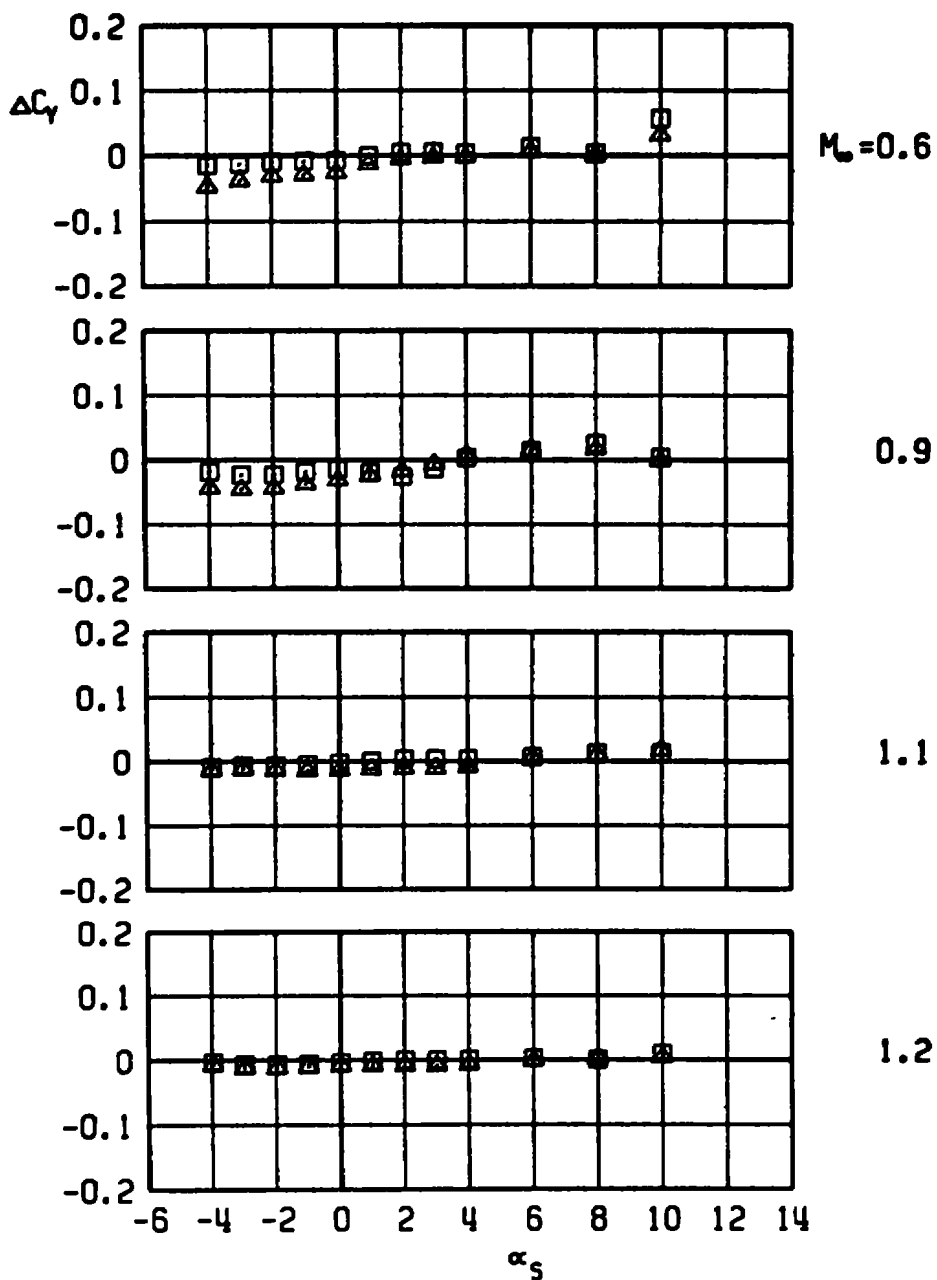
ASP, LOB PYLON, MER-4
 □ WITH DUMMY STING, $D_3 = 0.31 D_0$
 ▲ WITH DUMMY STING, $D_3 = 0.50 D_0$



a. Normal-force increment

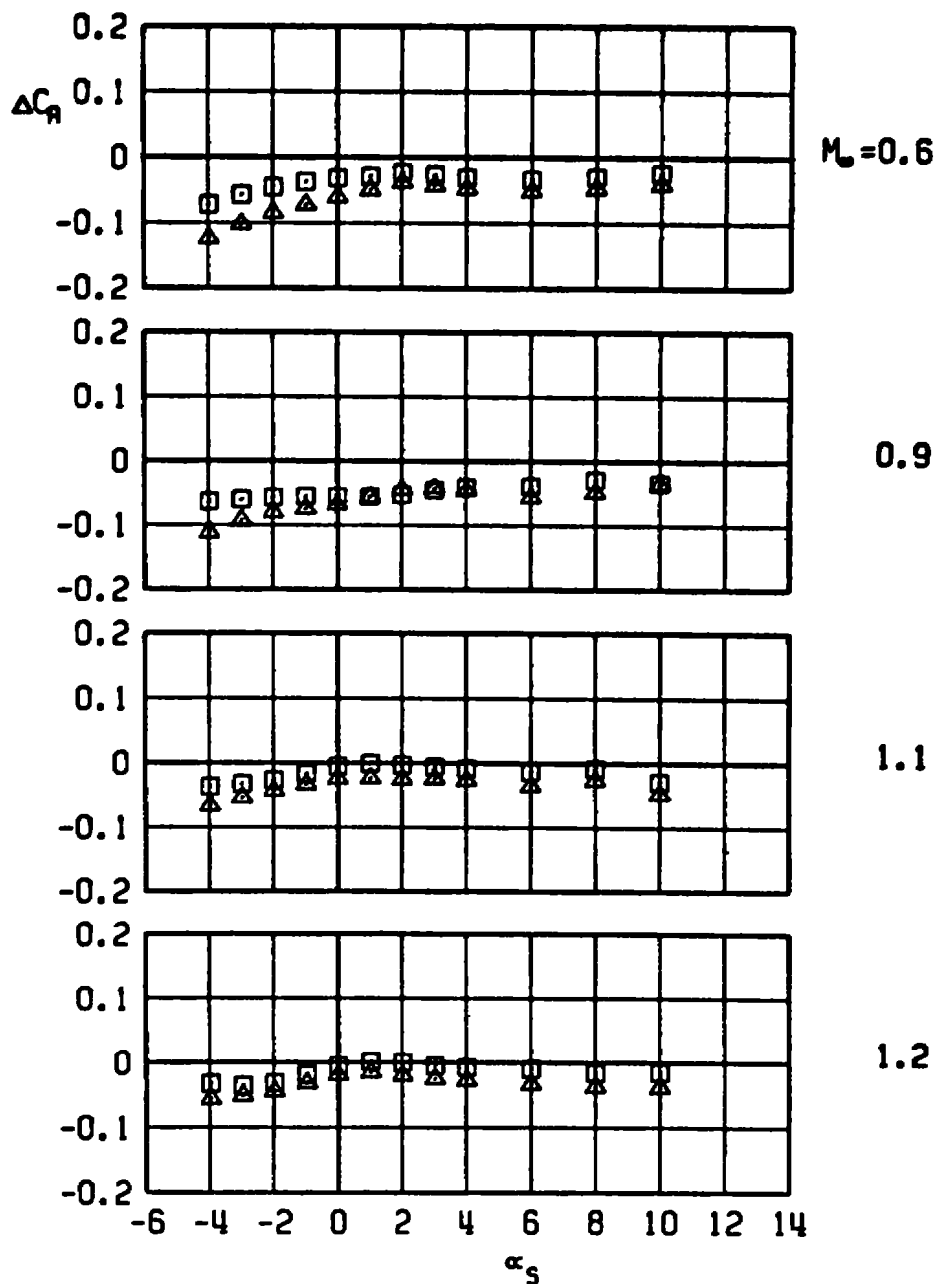
Figure 31. Sting-induced aerodynamic load increments as a function of angle of attack, unstable rack-mounted store, MER station 4, LOB pylon.

ASP, LOB PYLON, MER-4
 □ WITH DUMMY STING, $D_5 = 0.31 D_0$
 △ WITH DUMMY STING, $D_5 = 0.50 D_0$



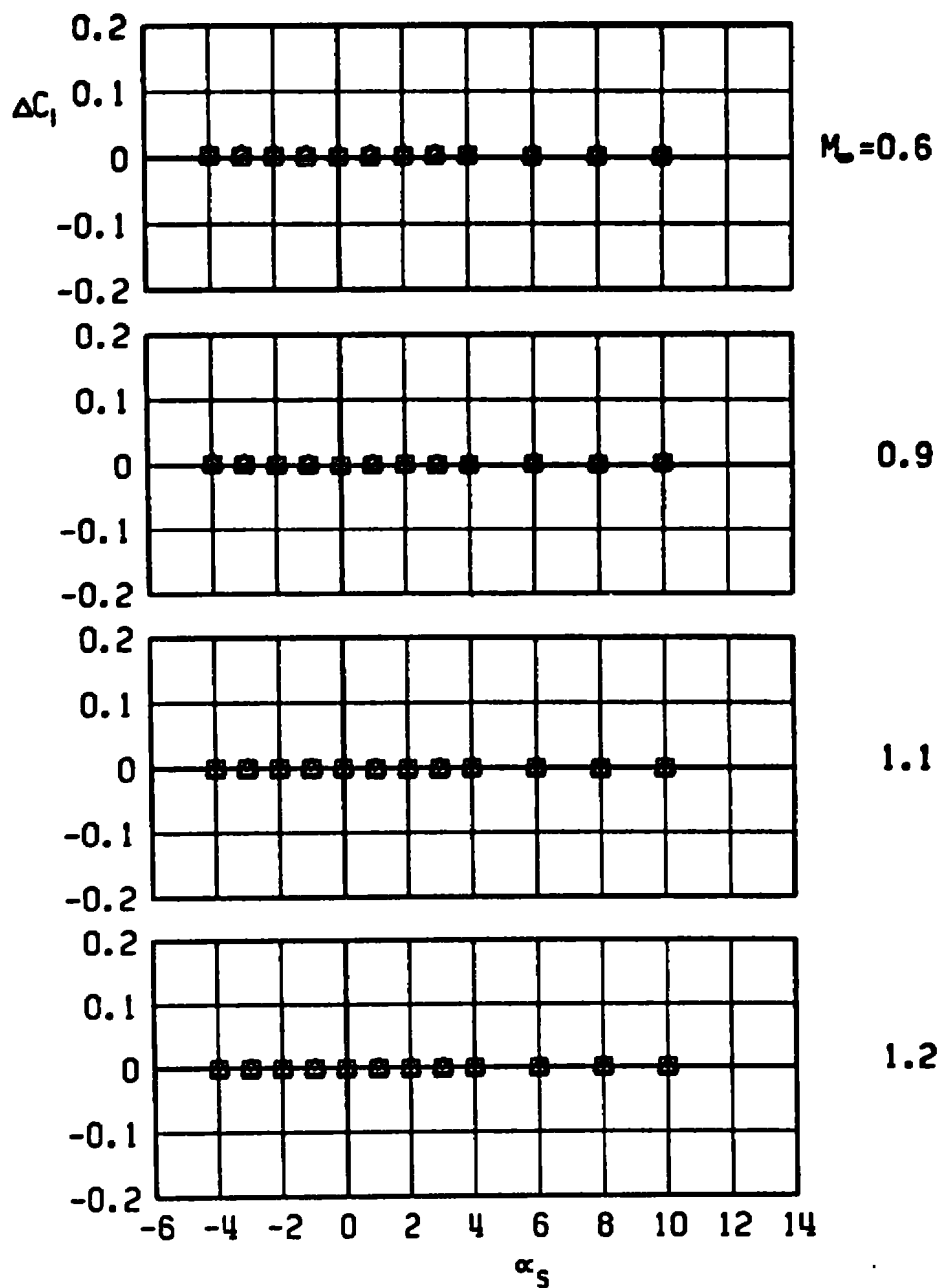
b. Side-force increment
 Figure 31. Continued.

ASP, LOB PYLON, MER-4
 WITH DUMMY STING, $D_3 = 0.31 D_0$
 WITH DUMMY STING, $D_3 = 0.50 D_0$



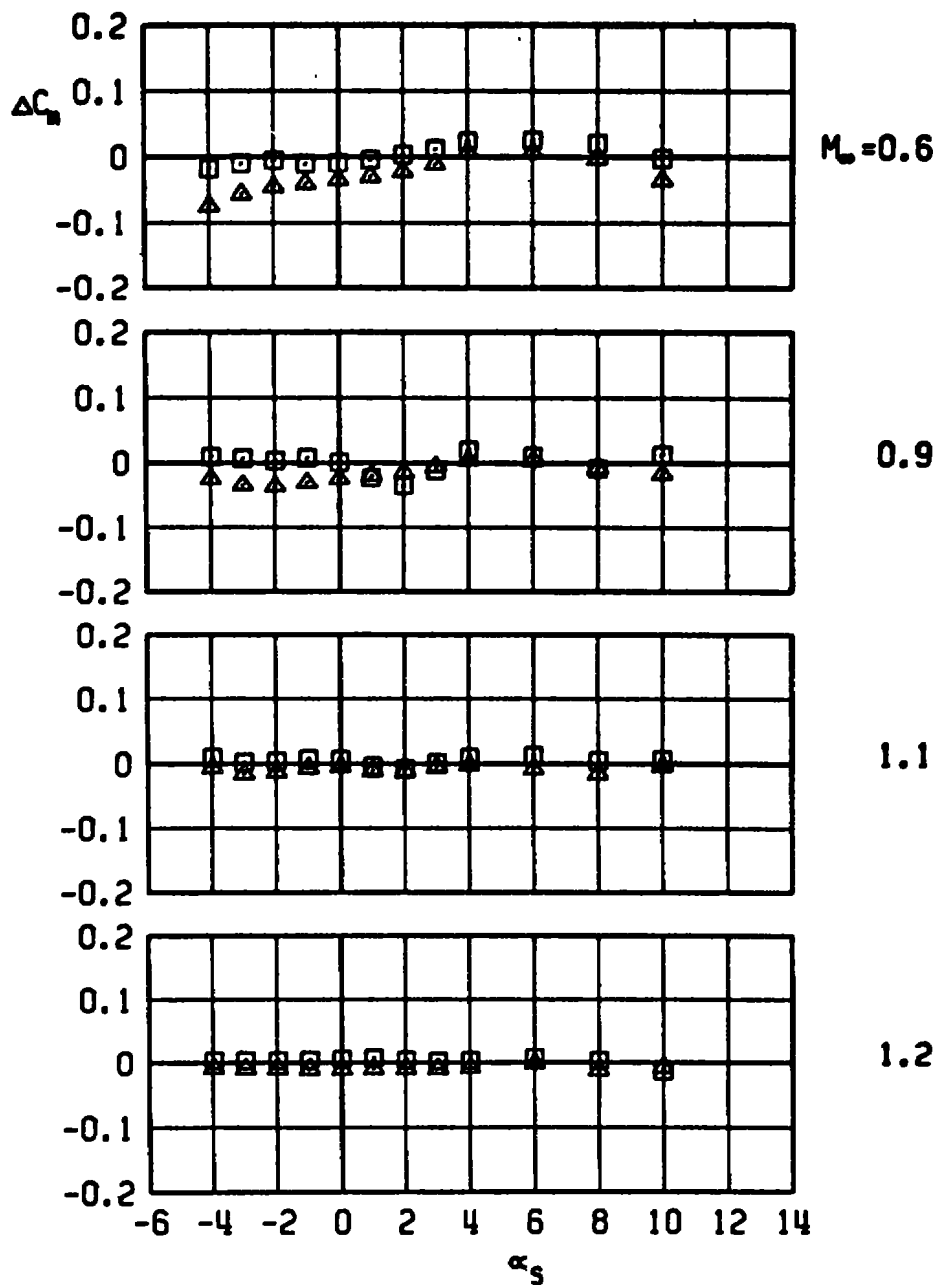
c. Axial-force increment
 Figure 31. Continued.

□ ASP, LOB PYLON, MER-4
 WITH DUMMY STING, $D_3 = 0.31 D_0$
 ▲ WITH DUMMY STING, $D_3 = 0.50 D_0$



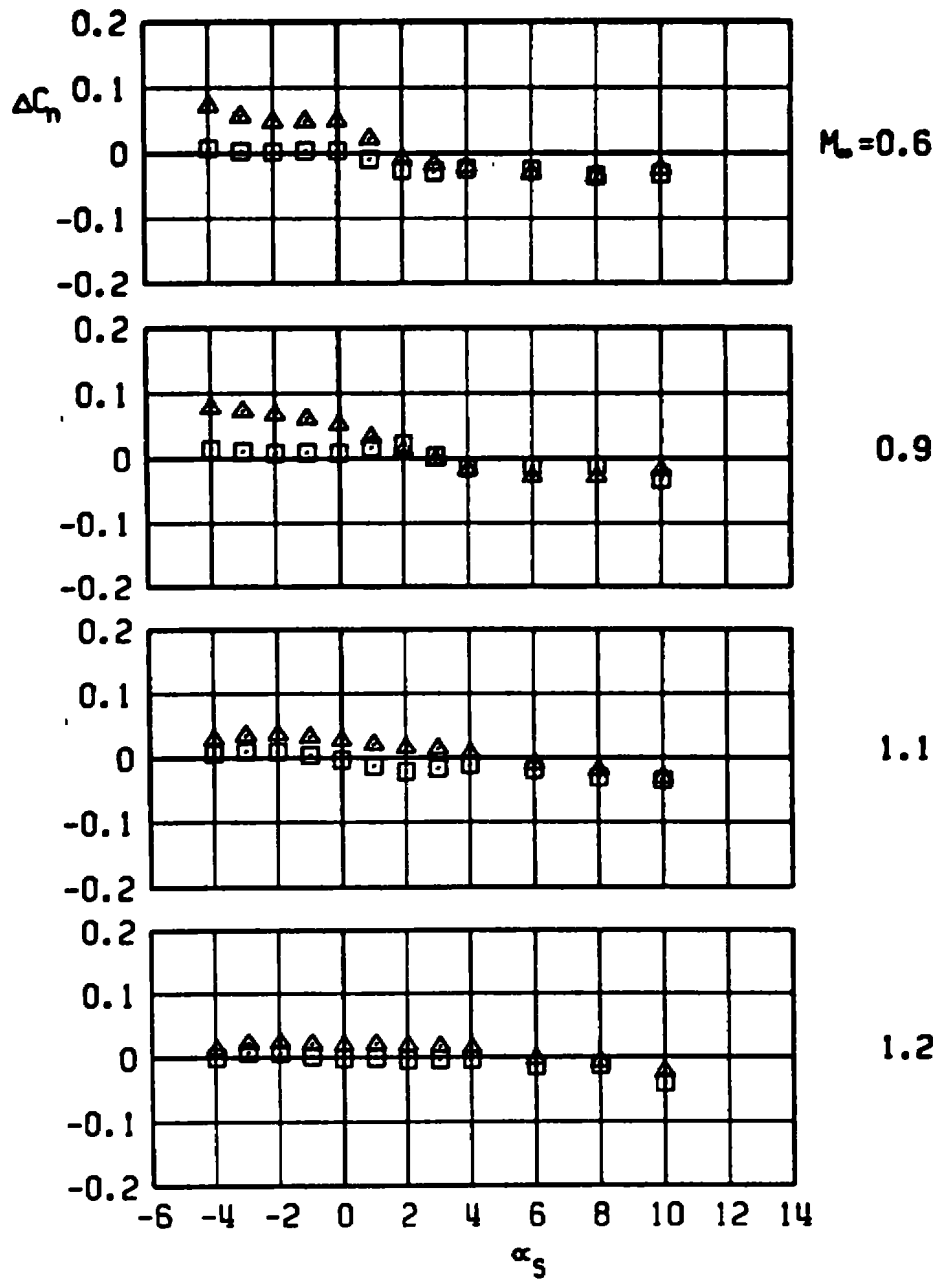
d. Rolling-moment increment
 Figure 31. Continued.

ASP, LOB PYLON, MER-4
 WITH DUMMY STING, $D_3 = 0.31 D_0$
 WITH DUMMY STING, $D_3 = 0.50 D_0$

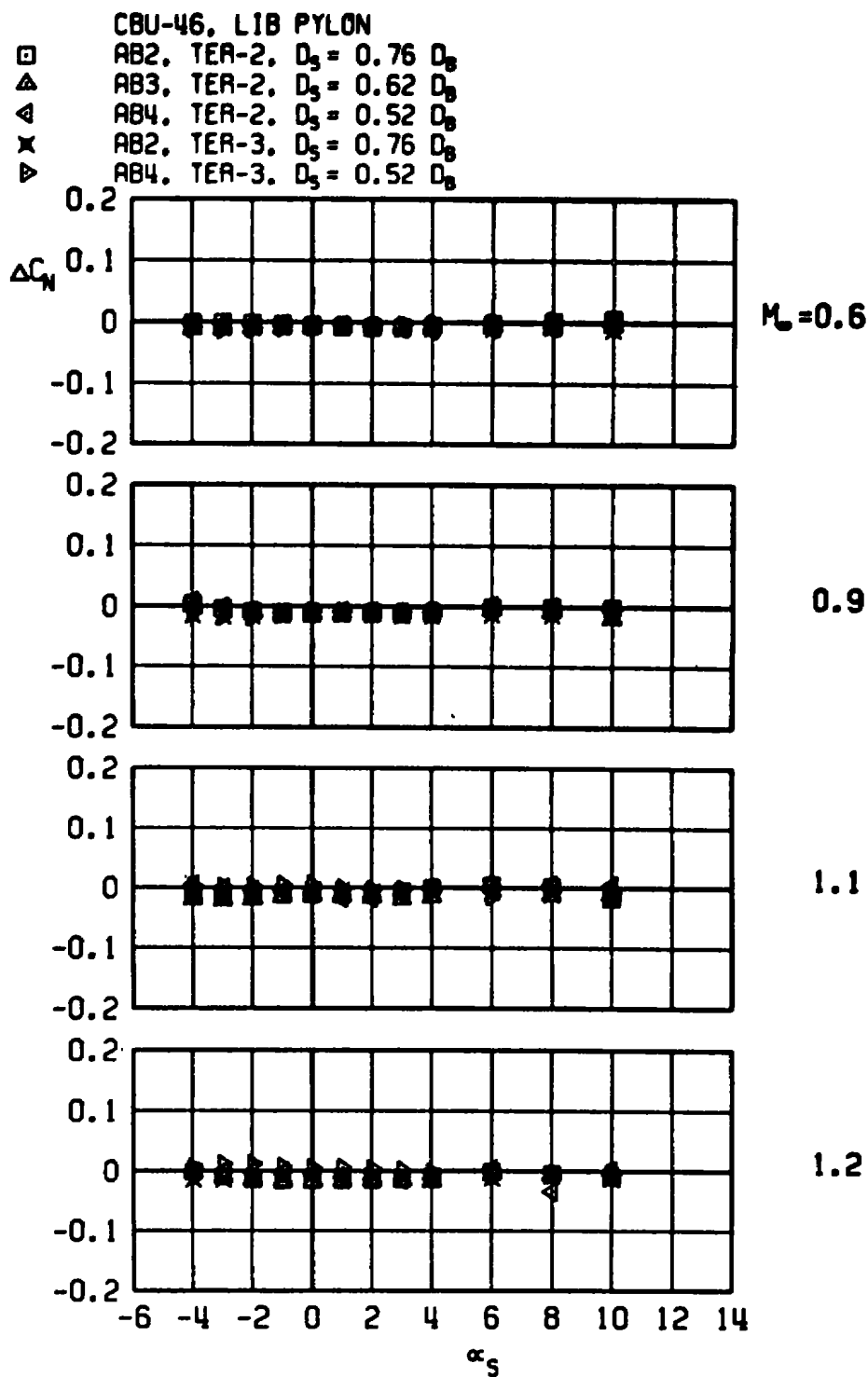


e. Pitching-moment increment
 Figure 31. Continued.

ASP, LOB PYLON, MER-4
 □ WITH DUMMY STING, $D_3 = 0.31 D_0$
 ▲ WITH DUMMY STING, $D_3 = 0.50 D_0$

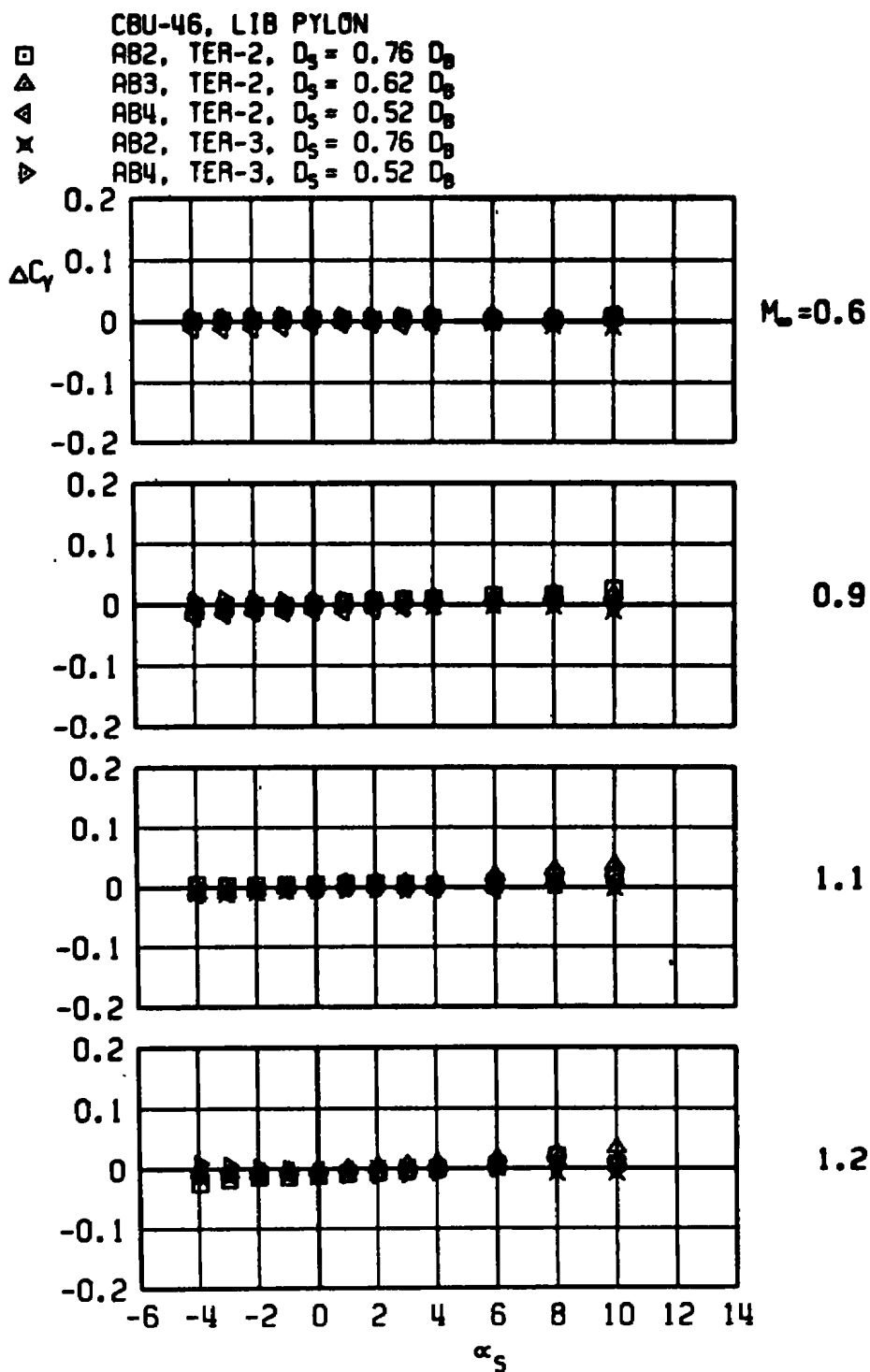


f. Yawing-moment increment
 Figure 31. Concluded.

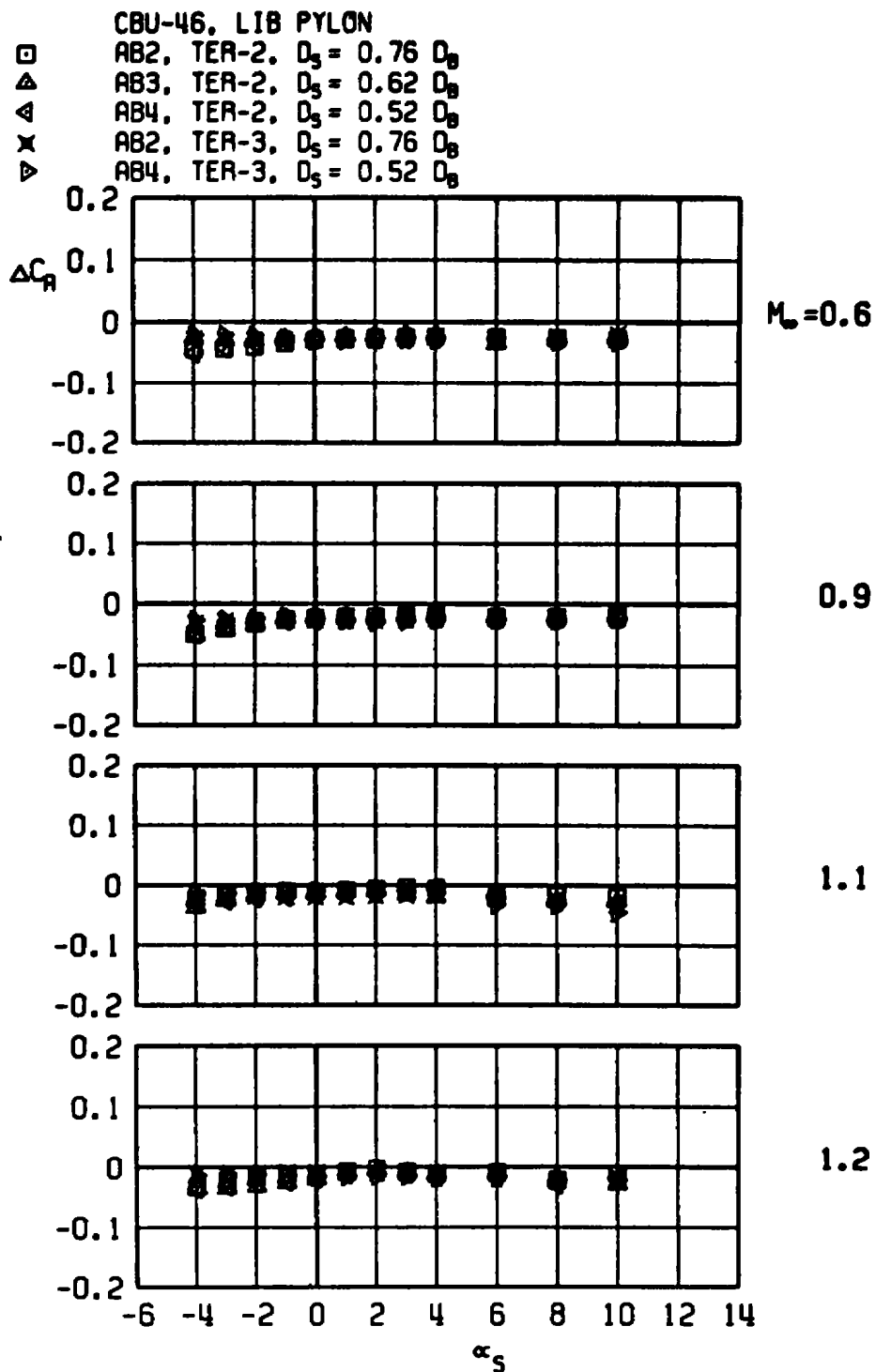


a. Normal-force increment

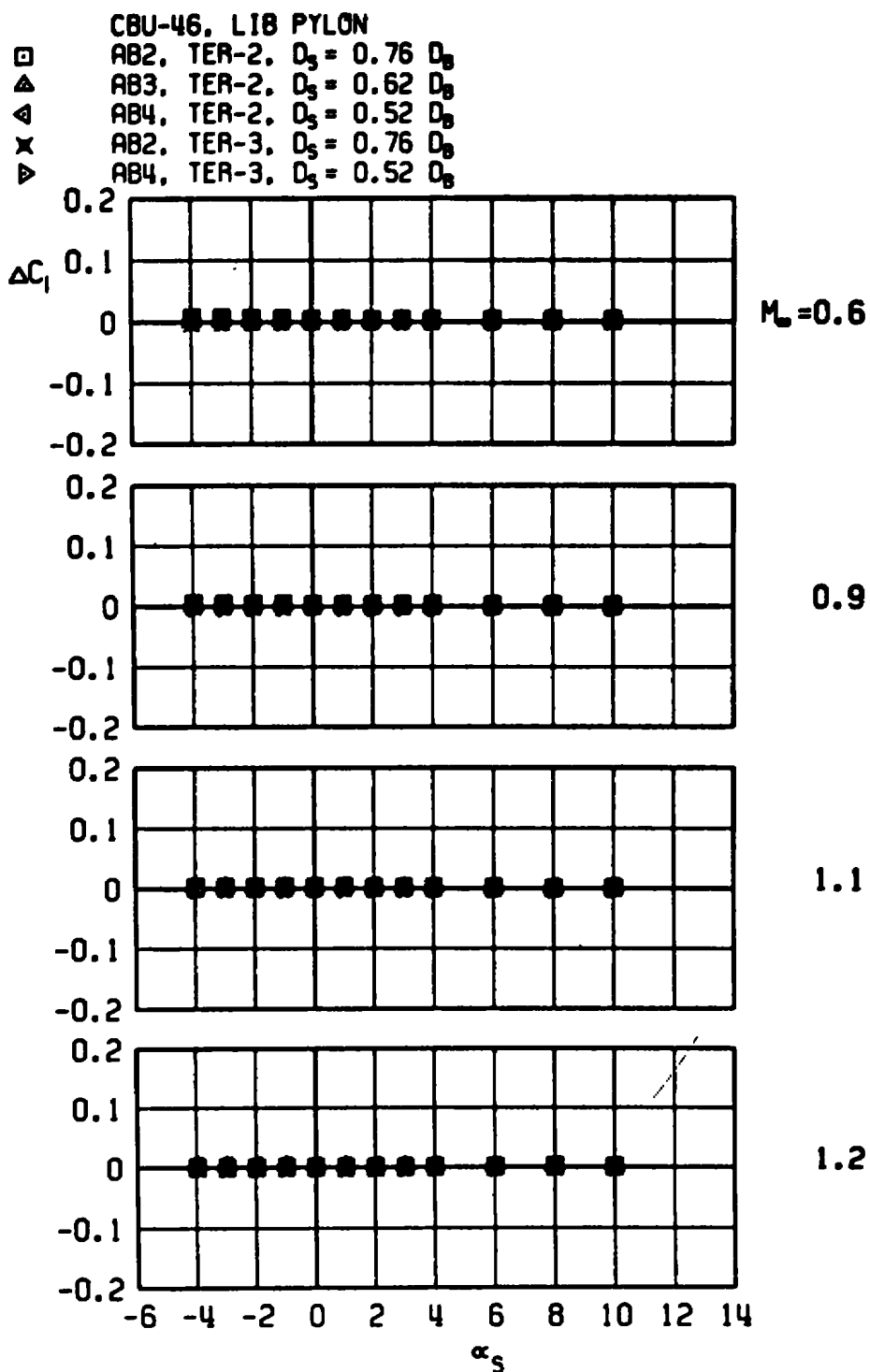
Figure 32. Sting-induced aerodynamic load increments as a function of angle of attack, unstable rack-mounted store, TER stations 2 and 3, LIB pylon.



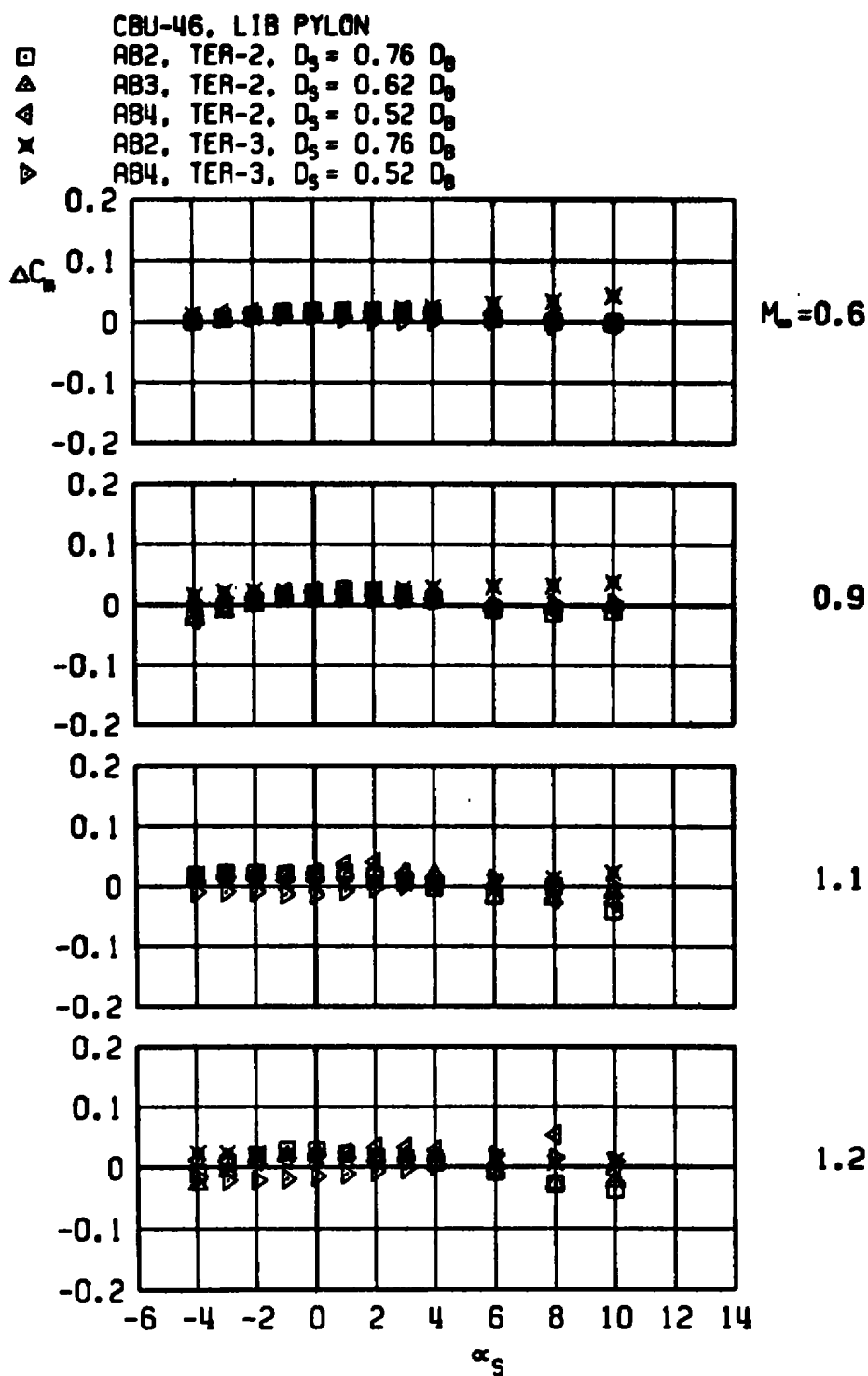
b. Side-force increment
Figure 32. Continued.



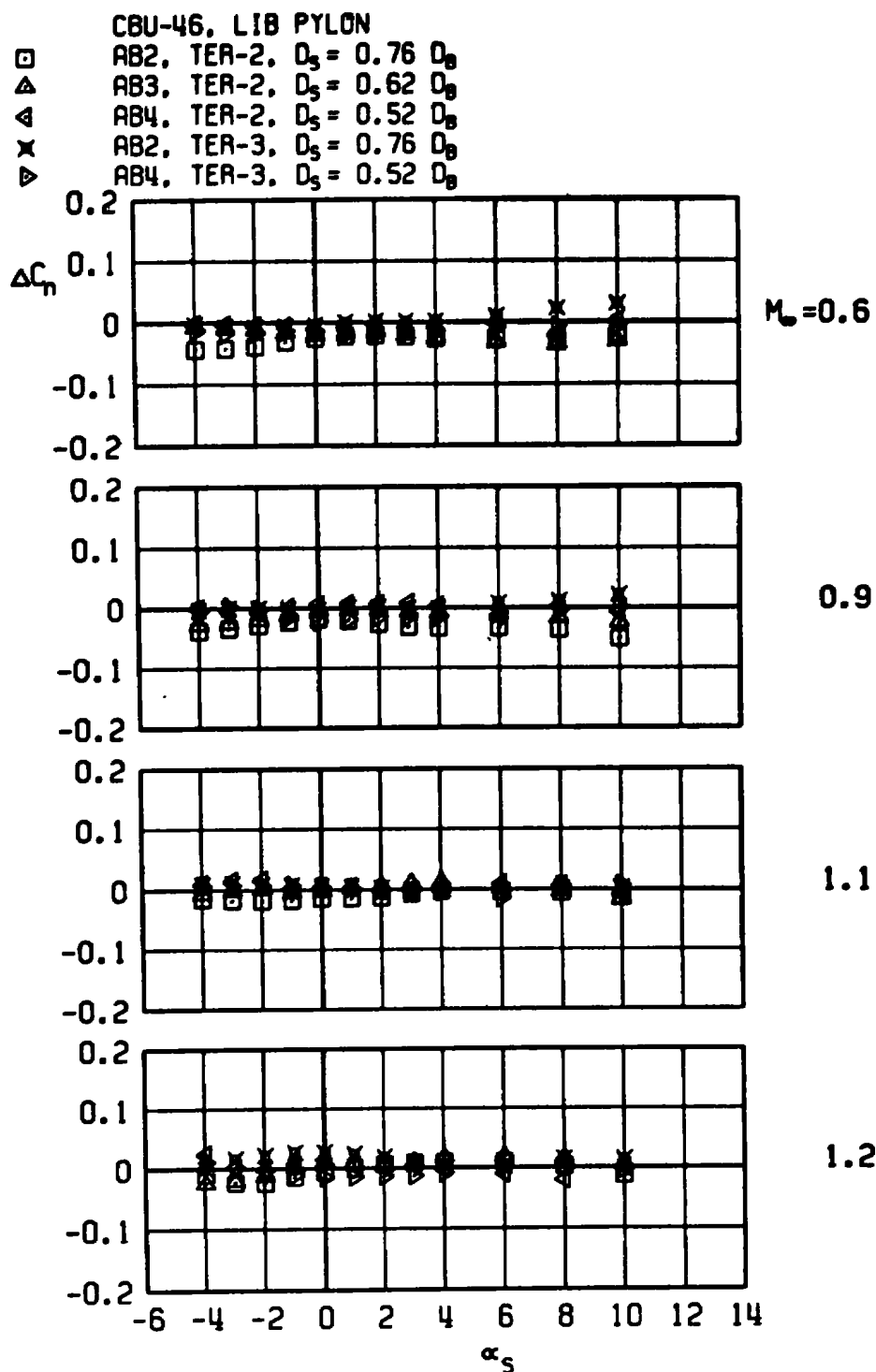
c. Axial-force increment
Figure 32. Continued.



d. Rolling-moment increment
Figure 32. Continued.

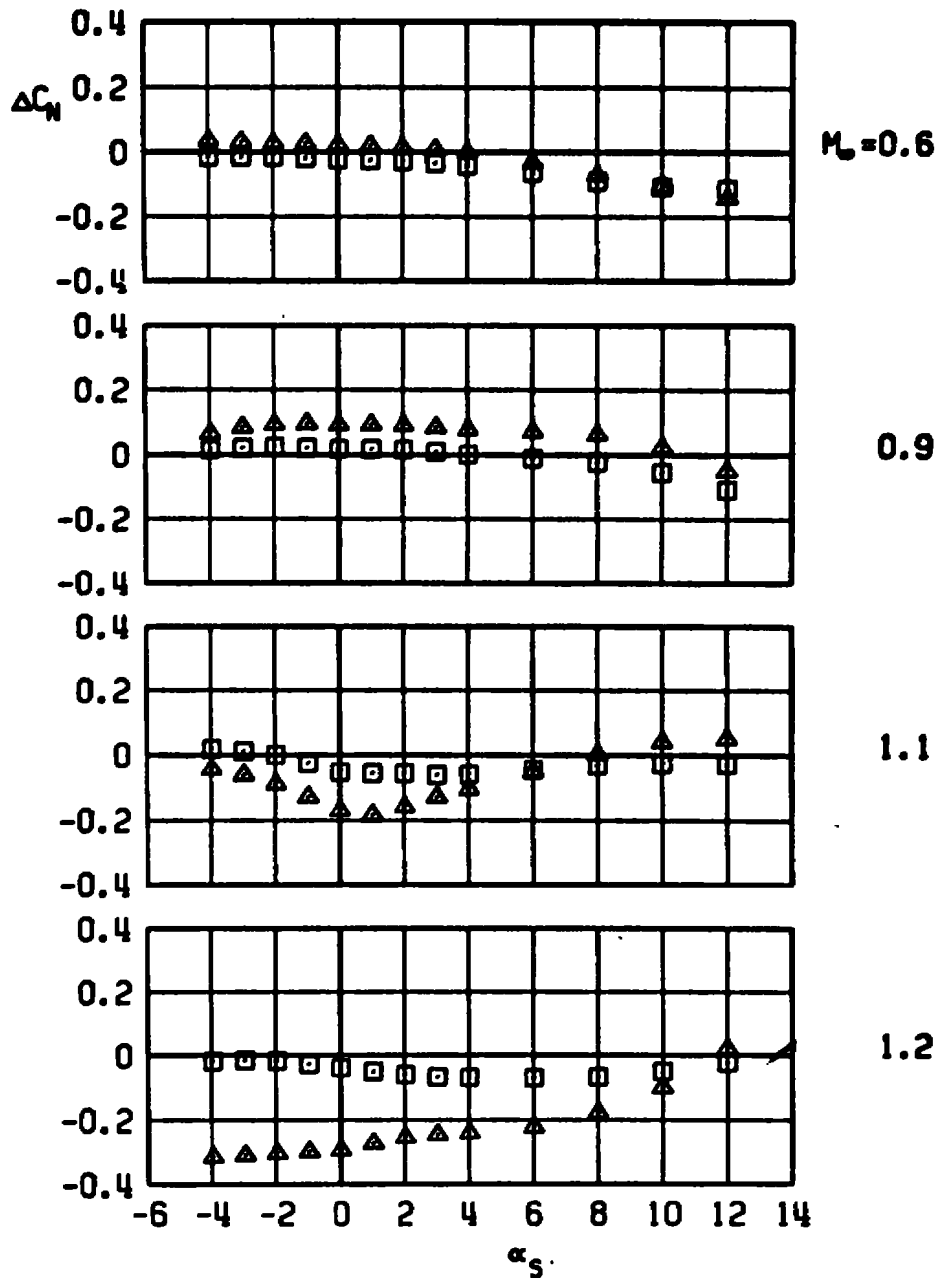


e. Pitching-moment increment
Figure 32. Continued.



f. Yawing-moment increment
Figure 32. Concluded.

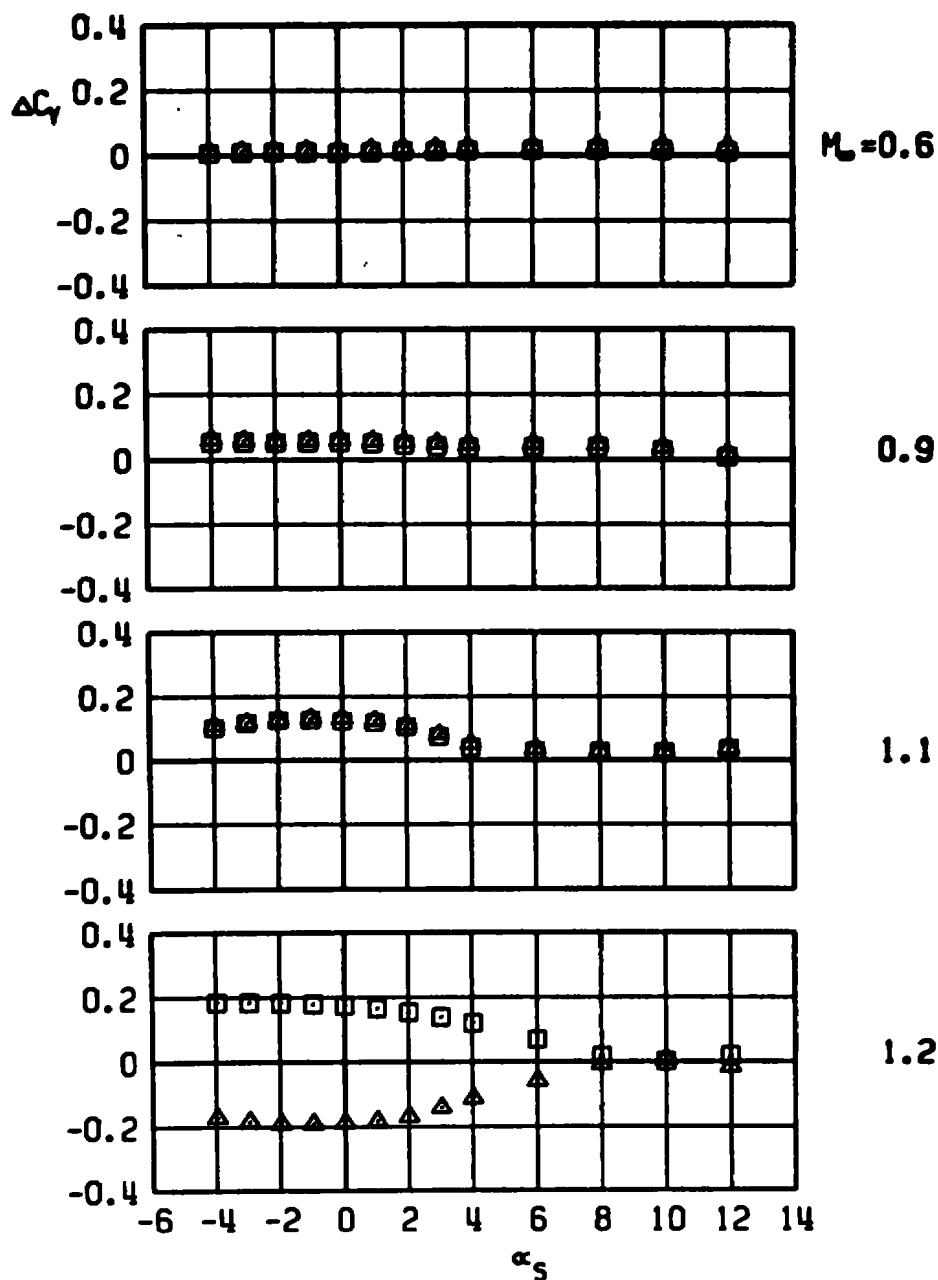
□ CBU-24, C-L PYLON, MER-1
 WITH DUMMY STING, $D_3 = 0.57 D_0$
 ▲ WITH DUMMY STING, $D_3 = 0.92 D_0$



a. Normal-force increment

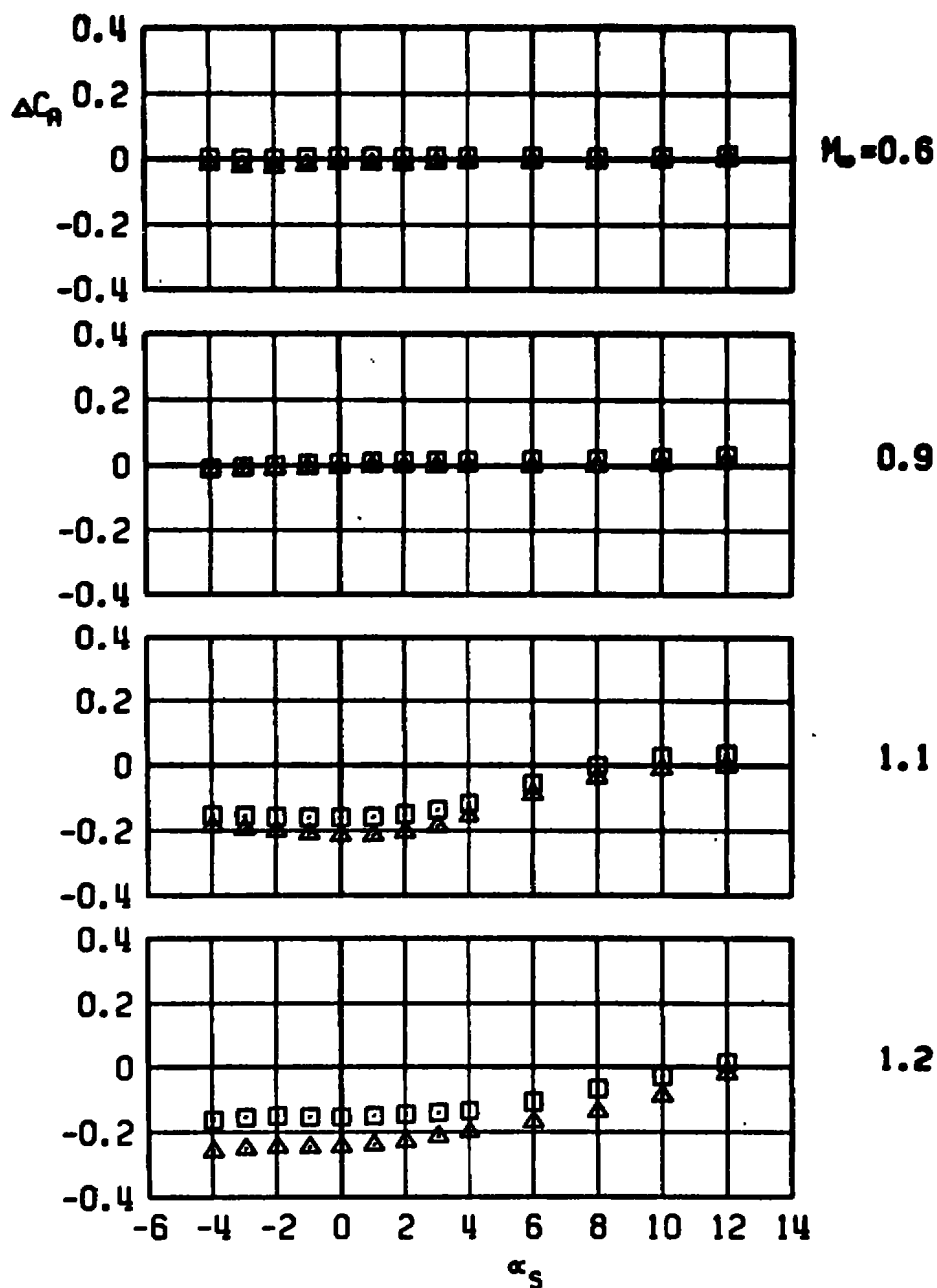
Figure 33. Sting-induced aerodynamic load increments as a function of angle of attack, stable rack-mounted store, MER station 1, C-L pylon.

CBU-24, C-L PYLON, MER-1
 WITH DUMMY STING, $D_3 = 0.57 D_0$
 WITH DUMMY STING, $D_3 = 0.92 D_0$



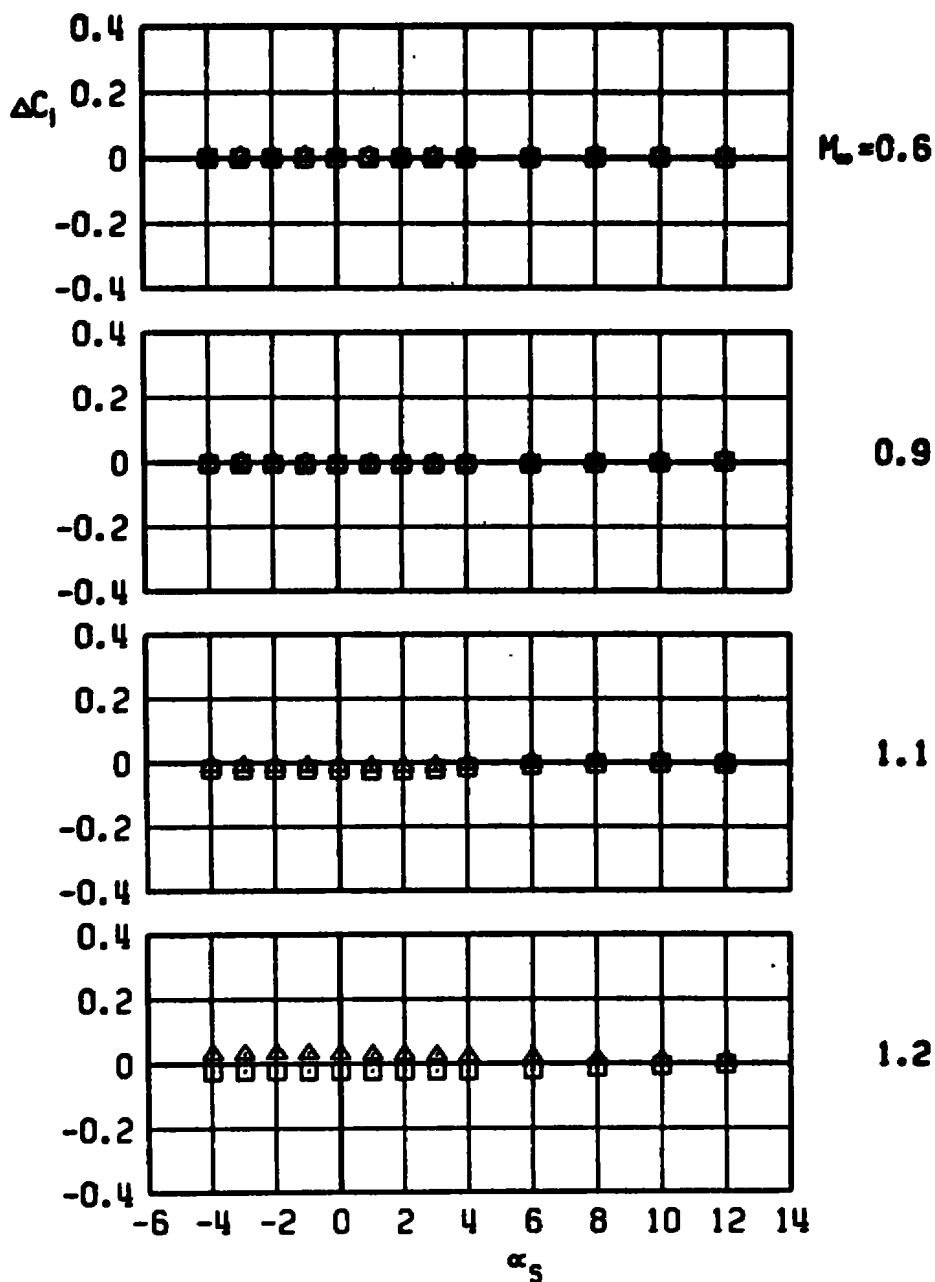
b. Side-force increment
 Figure 33. Continued.

□ CBU-24, C-L PYLON, MER-1
 WITH DUMMY STING, $D_3 = 0.57 D_0$
 ▲ WITH DUMMY STING, $D_3 = 0.92 D_0$



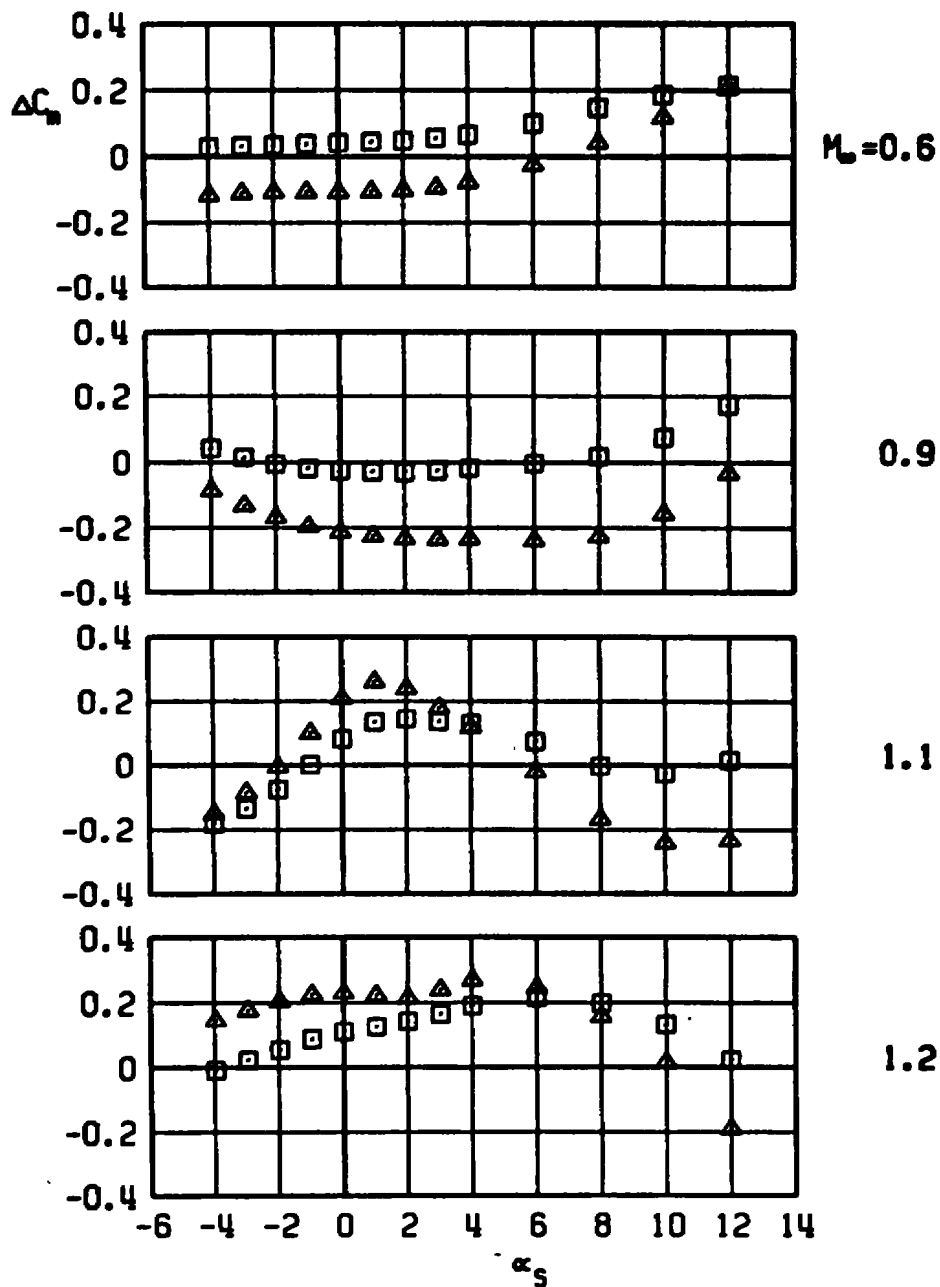
c. Axial-force increment
 Figure 33. Continued.

CBU-24, C-L PYLON, MER-1
 WITH DUMMY STING, $D_5 = 0.57 D_0$
 WITH DUMMY STING, $D_5 = 0.92 D_0$



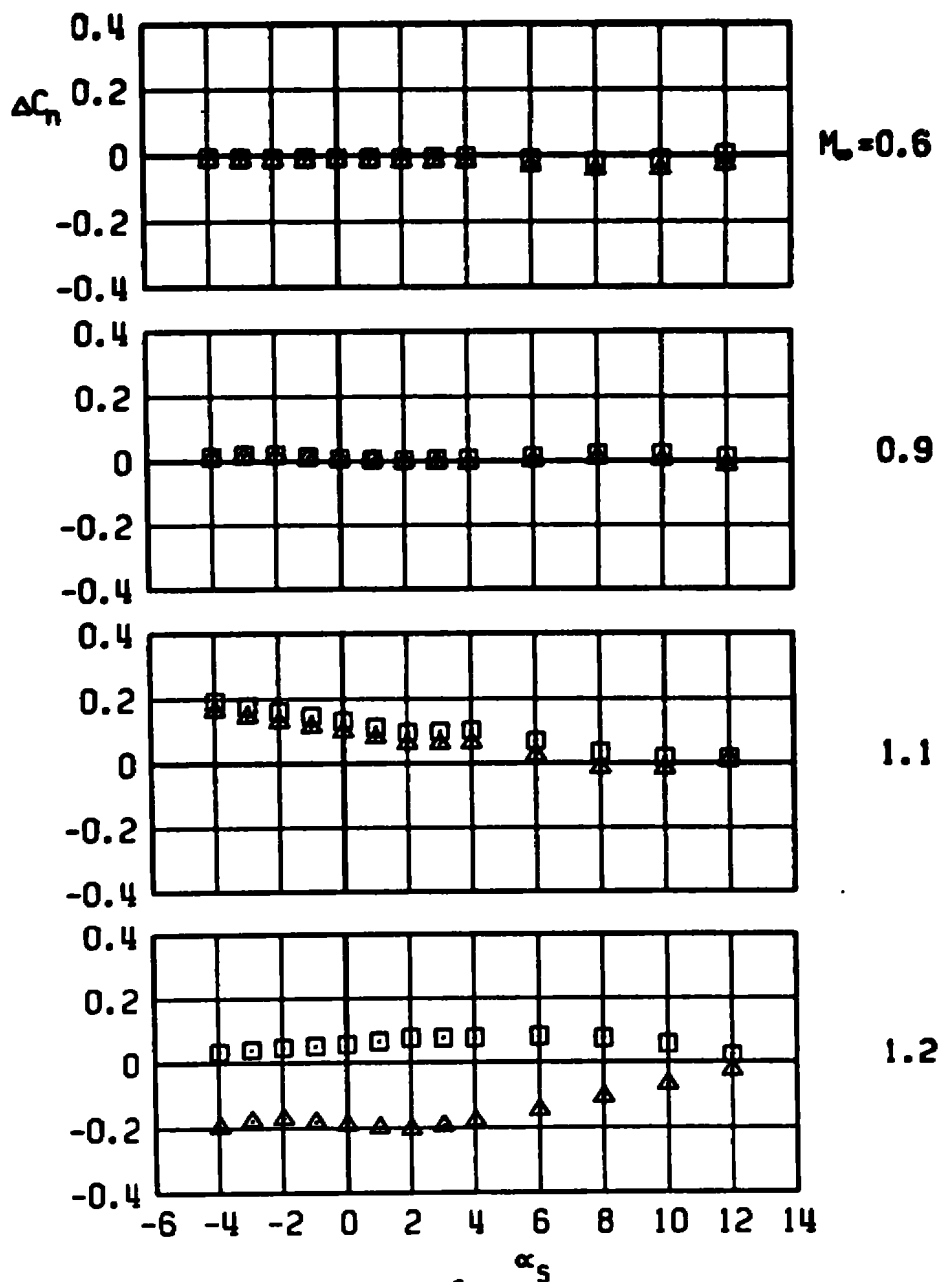
d. Rolling-moment increment
 Figure 33. Continued.

□ CBU-24, C-L PYLON, MER-1
 WITH DUMMY STING, $D_3 = 0.57 D_0$
 ▲ WITH DUMMY STING, $D_3 = 0.92 D_0$



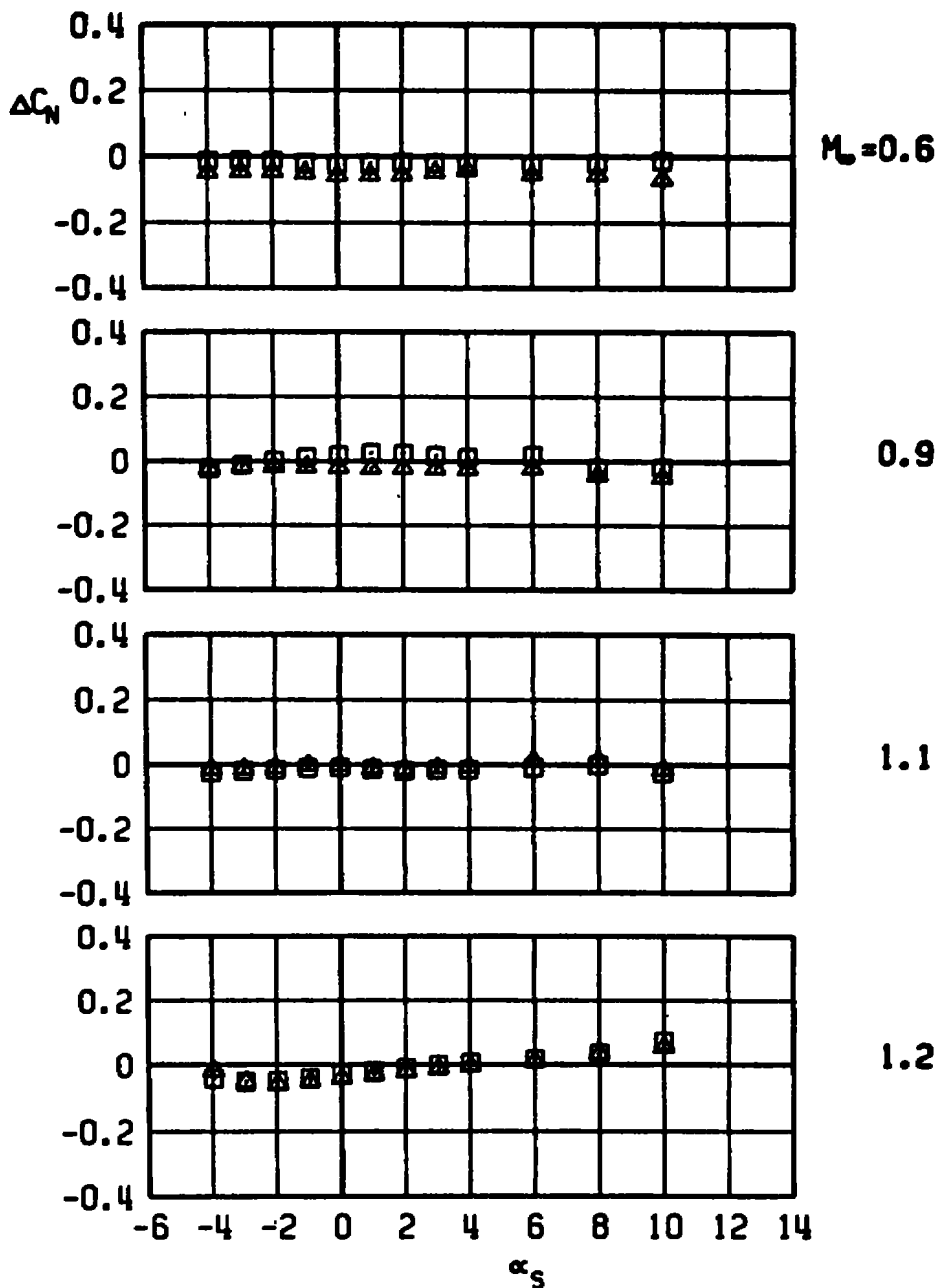
e. Pitching-moment increment
Figure 33. Continued.

CBU-24, C-L PYLON, MER-1
 WITH DUMMY STING, $D_3 = 0.57 D_0$
 WITH DUMMY STING, $D_3 = 0.92 D_0$



f. Yawing-moment increment
Figure 33. Concluded.

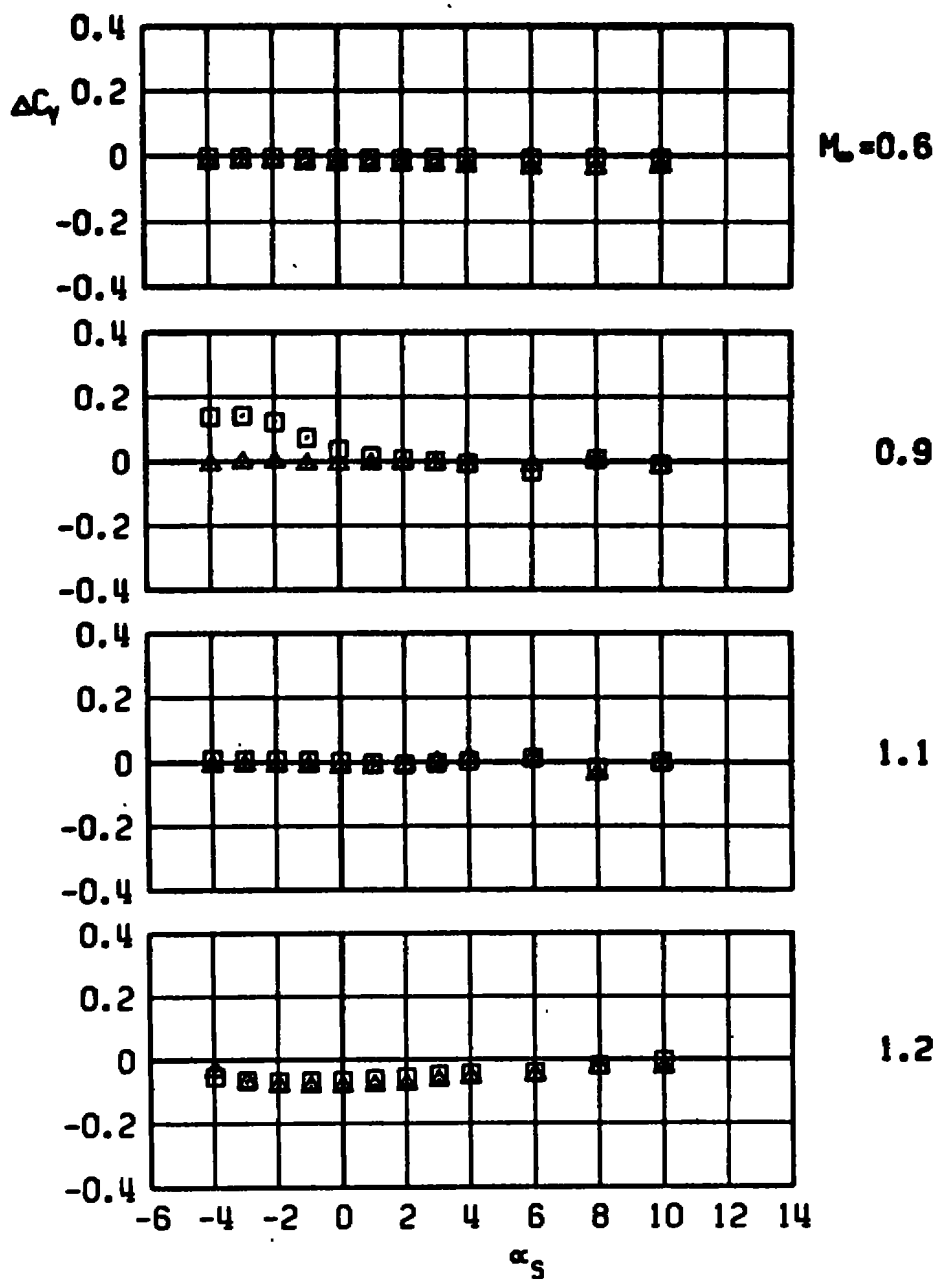
□ CBU-24, C-L PYLON, MER-2
 WITH DUMMY STING, $D_3 = 0.57 D_0$
 ▲ WITH DUMMY STING, $D_3 = 0.92 D_0$



a. Normal-force increment

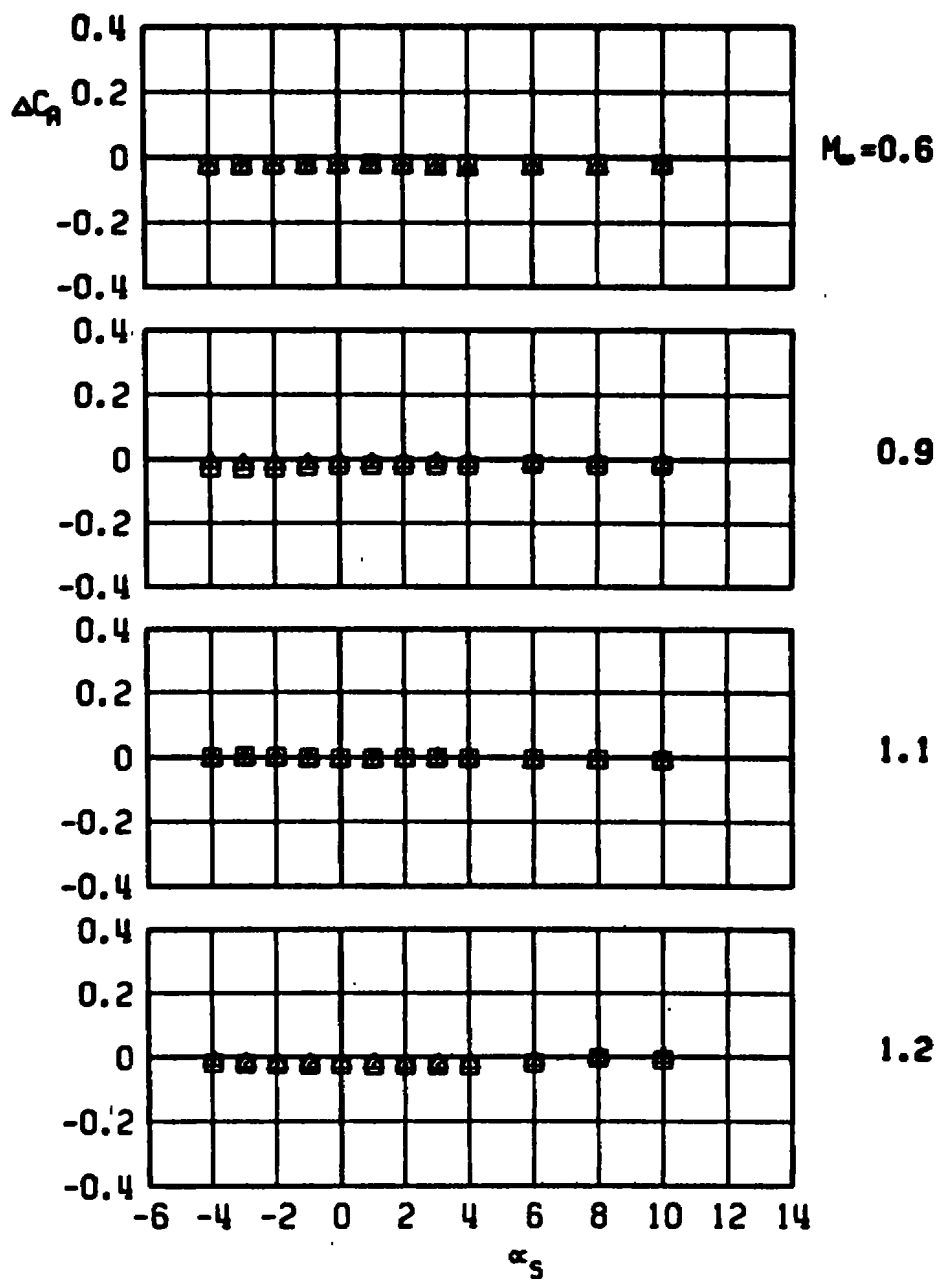
Figure 34. Sting-induced aerodynamic load increments as a function of angle of attack, stable rack-mounted store, MER station 2, C-L pylon.

□ CBU-24, C-L PYLON, MEA-2
 WITH DUMMY STING, $D_3 = 0.57 D_0$
 ▲ WITH DUMMY STING, $D_3 = 0.92 D_0$



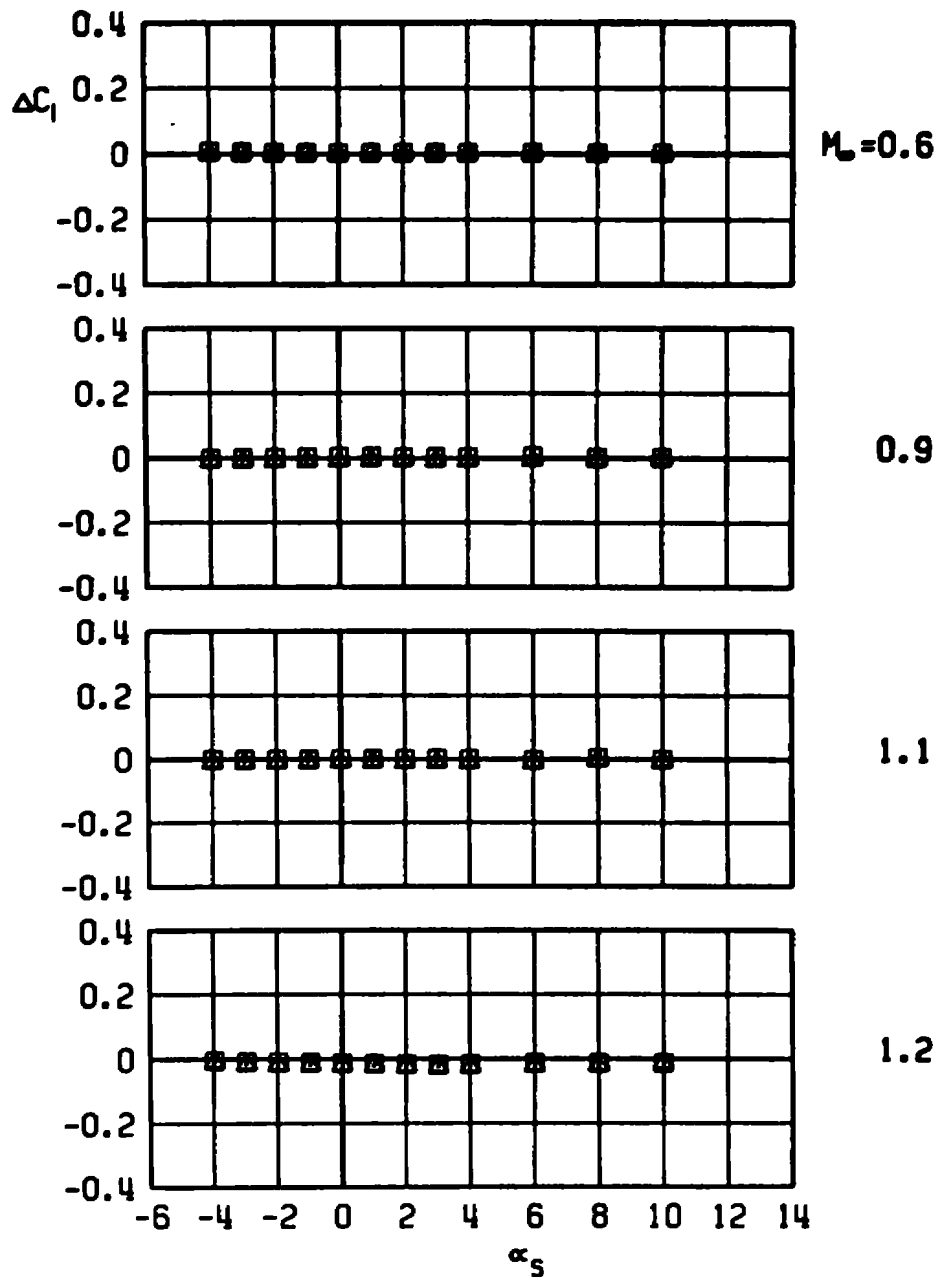
b. Side-force increment
 Figure 34. Continued.

□ CBU-24, C-L PYLON, MER-2
 WITH DUMMY STING, $D_3 = 0.57 D_9$
 ▲ WITH DUMMY STING, $D_3 = 0.92 D_9$



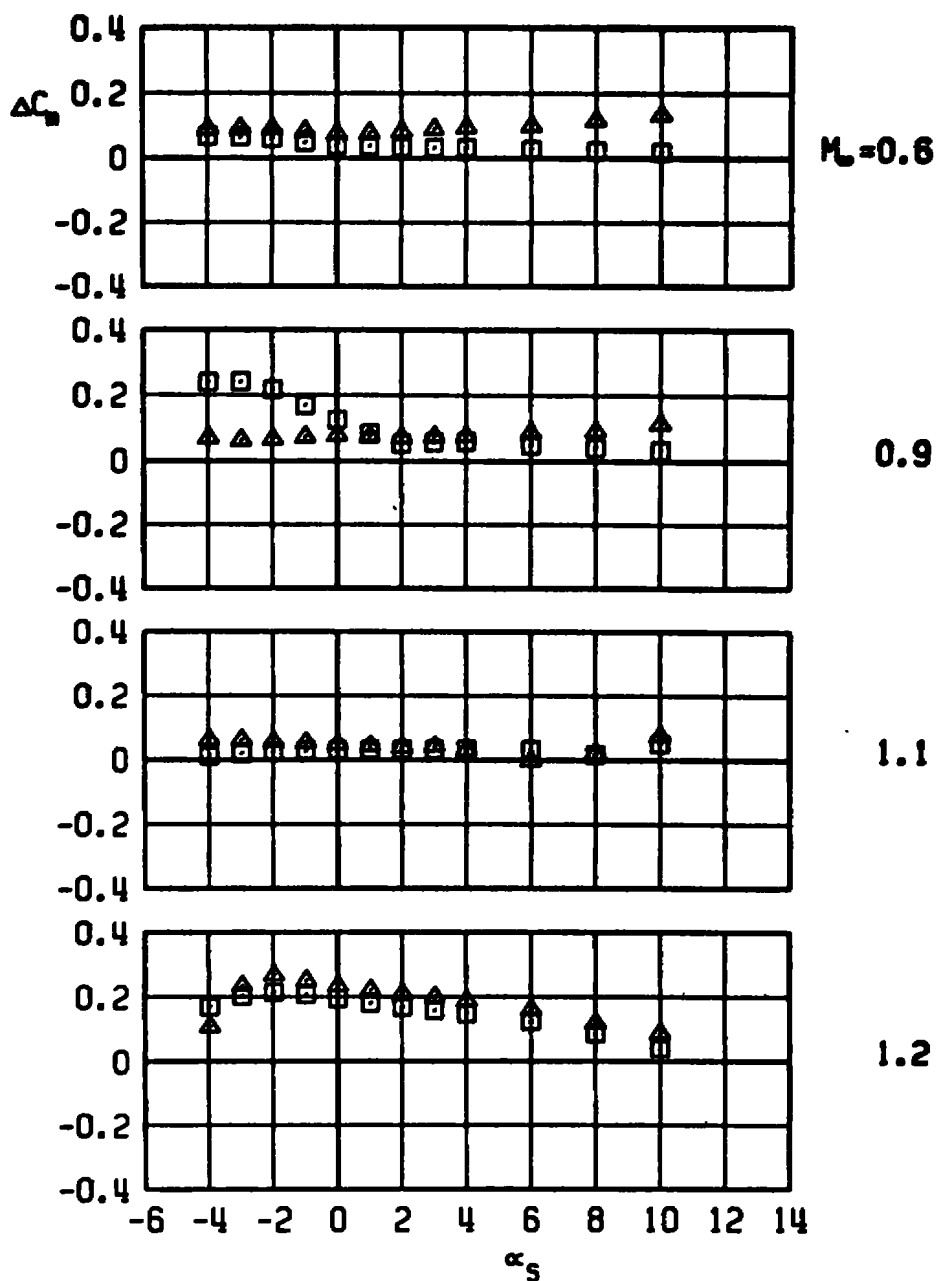
c. Axial-force increment
Figure 34. Continued.

□ CBU-24, C-L PYLON, MER-2
 WITH DUMMY STING, $D_3 = 0.57 D_0$
 △ WITH DUMMY STING, $D_3 = 0.92 D_0$



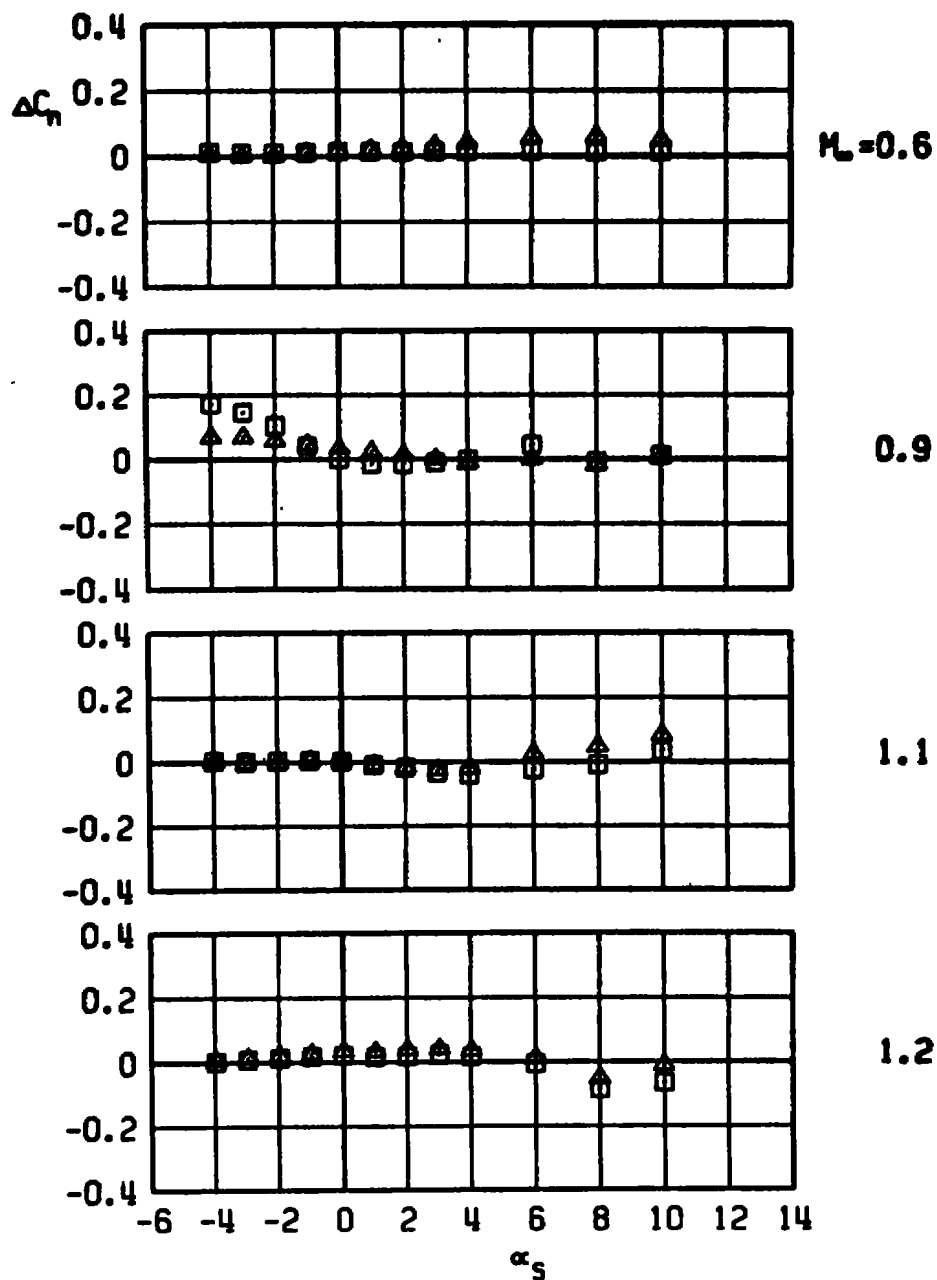
d. Rolling-moment increment
 Figure 34. Continued.

CBU-24, C-L PYLON, MER-2
 WITH DUMMY STING, $D_3 = 0.57 D_0$
 WITH DUMMY STING, $D_3 = 0.92 D_0$



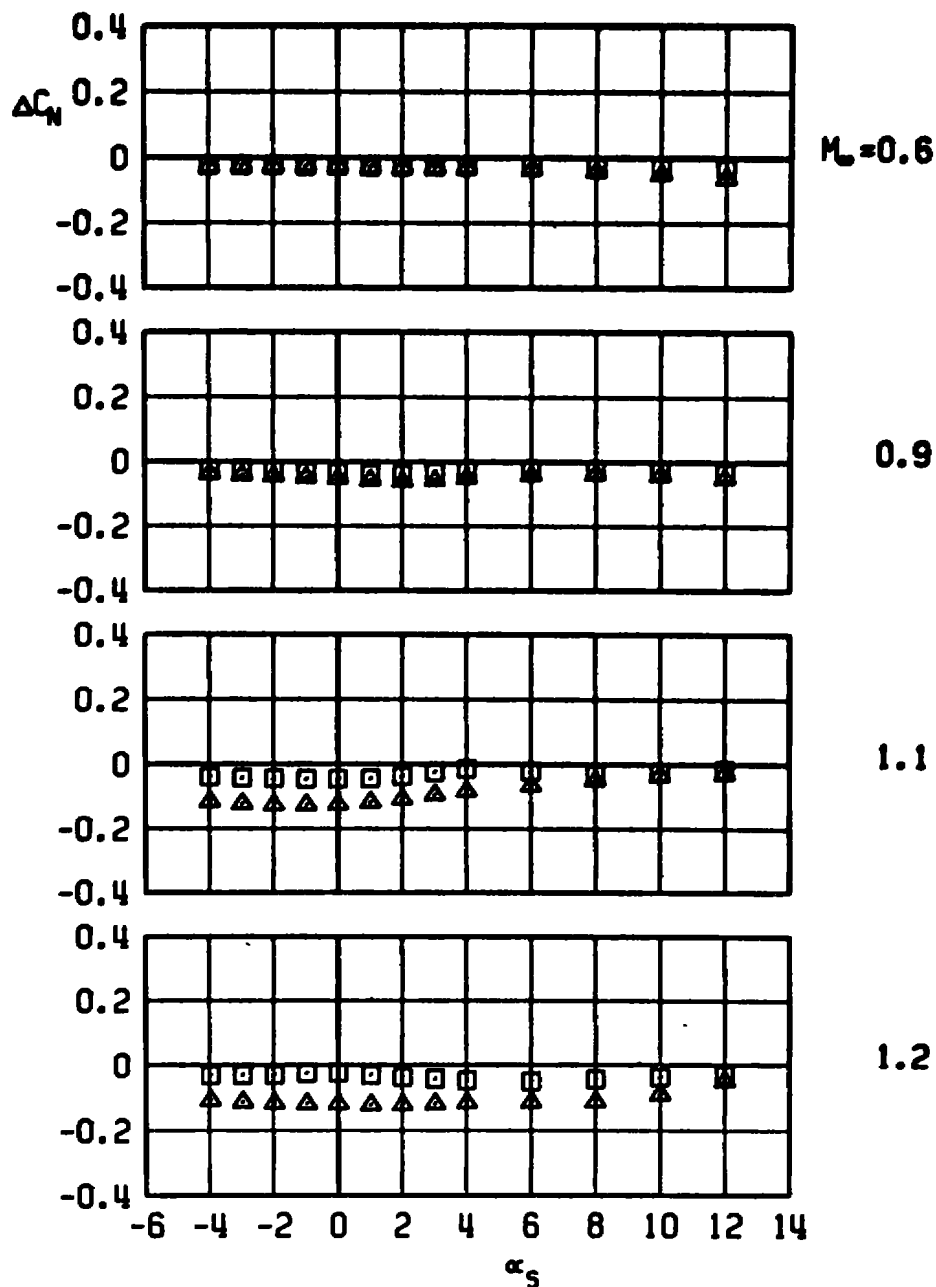
e. Pitching-moment increment
 Figure 34. Continued.

CBU-24, C-L PYLON, MER-2
 WITH DUMMY STING, $D_3 = 0.57 D_0$
 WITH DUMMY STING, $D_3 = 0.92 D_0$



f. Yawing-moment increment
 Figure 34. Concluded.

□ CBU-24, C-L PYLON, MER-3
 WITH DUMMY STING, $D_3 = 0.57 D_0$
 ▲ WITH DUMMY STING, $D_3 = 0.92 D_0$



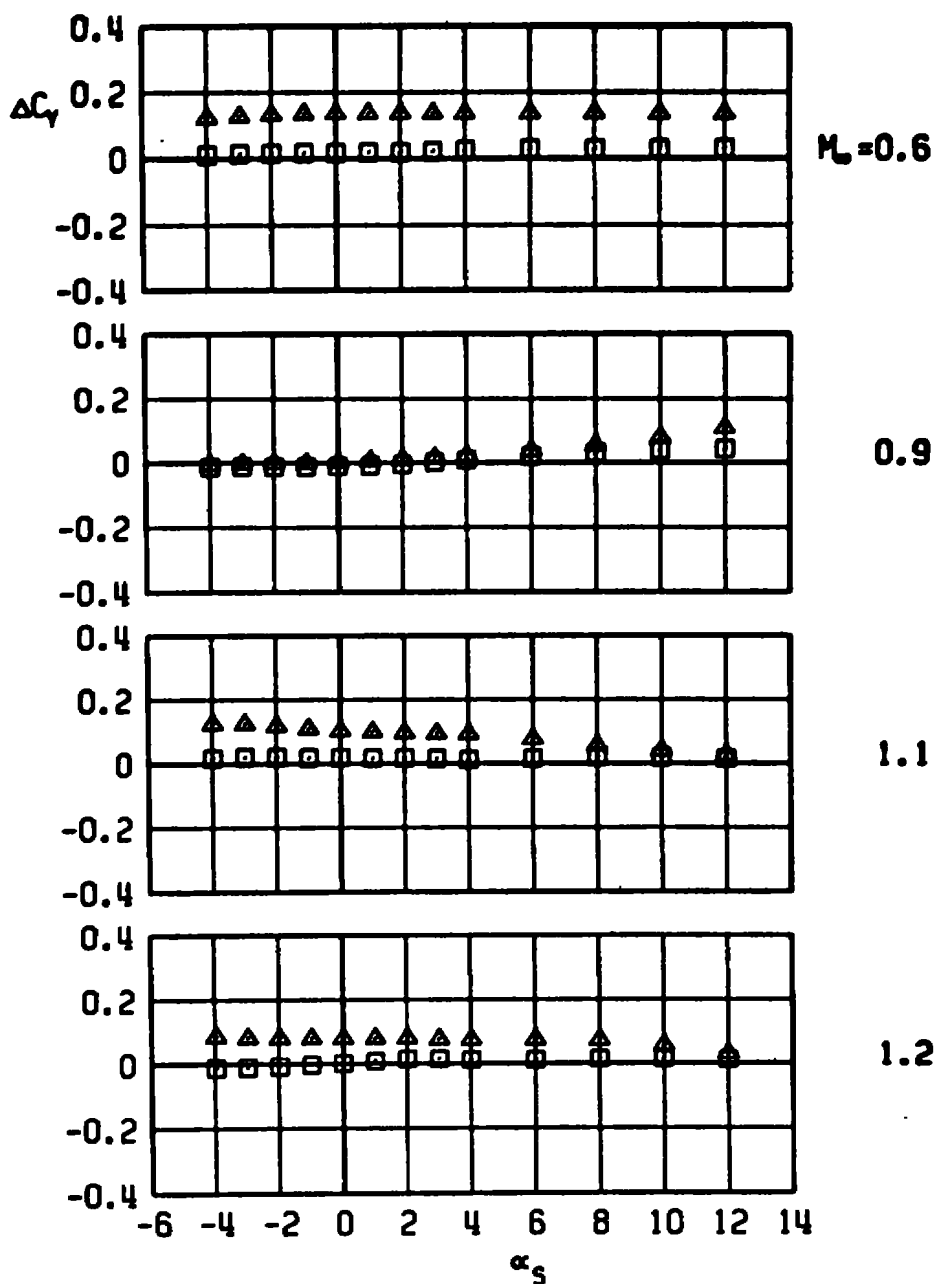
a. Normal-force increment

Figure 35. Sting-induced aerodynamic load increments as a function of angle of attack, stable rack-mounted store, MER station 3, C-L pylon.

CBU-24, C-L PYLON, MER-3

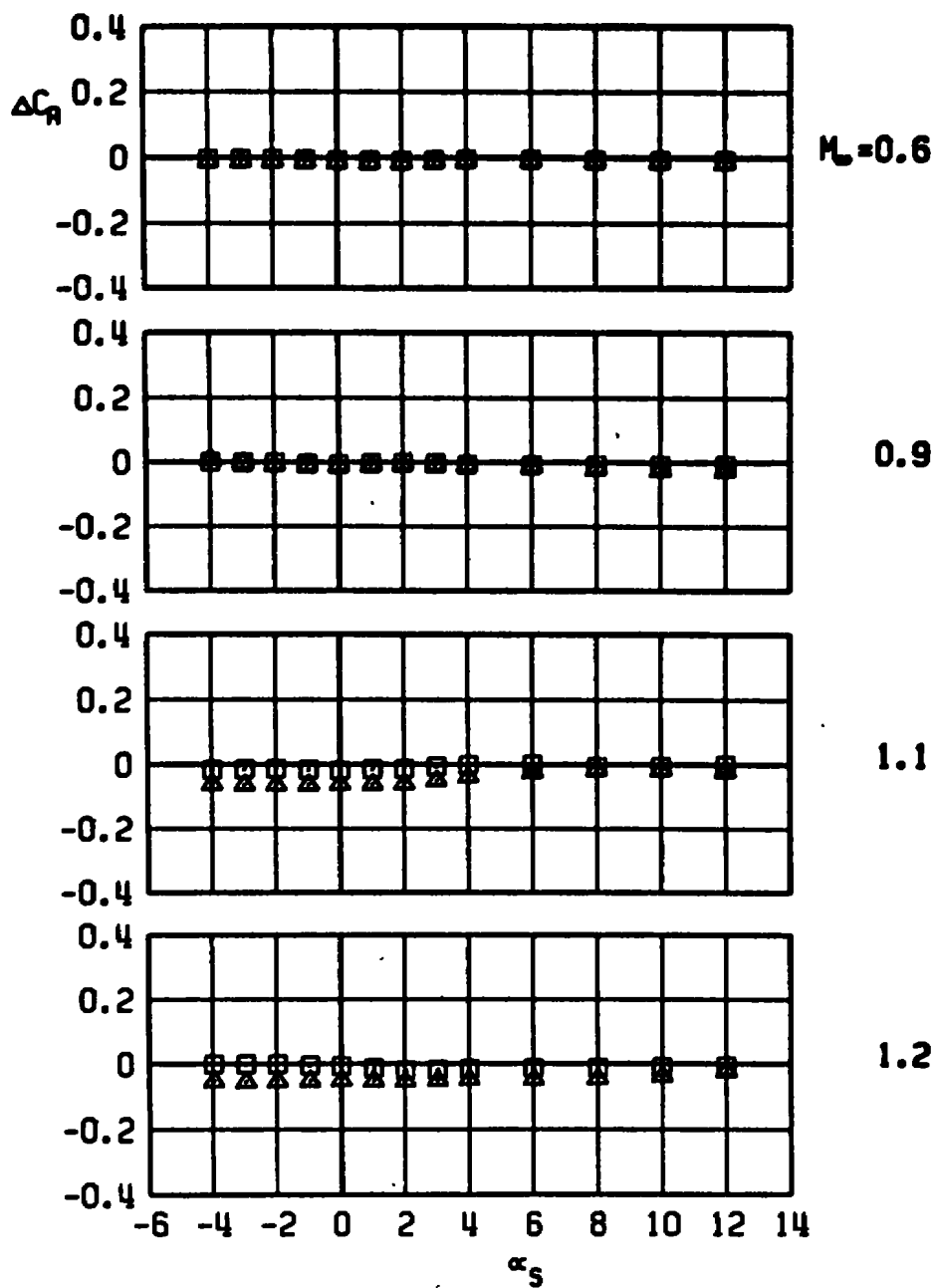
□	WITH DUMMY STING, $D_3 = 0.57 D_1$
▲	WITH DUMMY STING, $D_3 = 0.92 D_1$

Δ WITH DUMMY STING, $D_3 = 0.92 D_1$



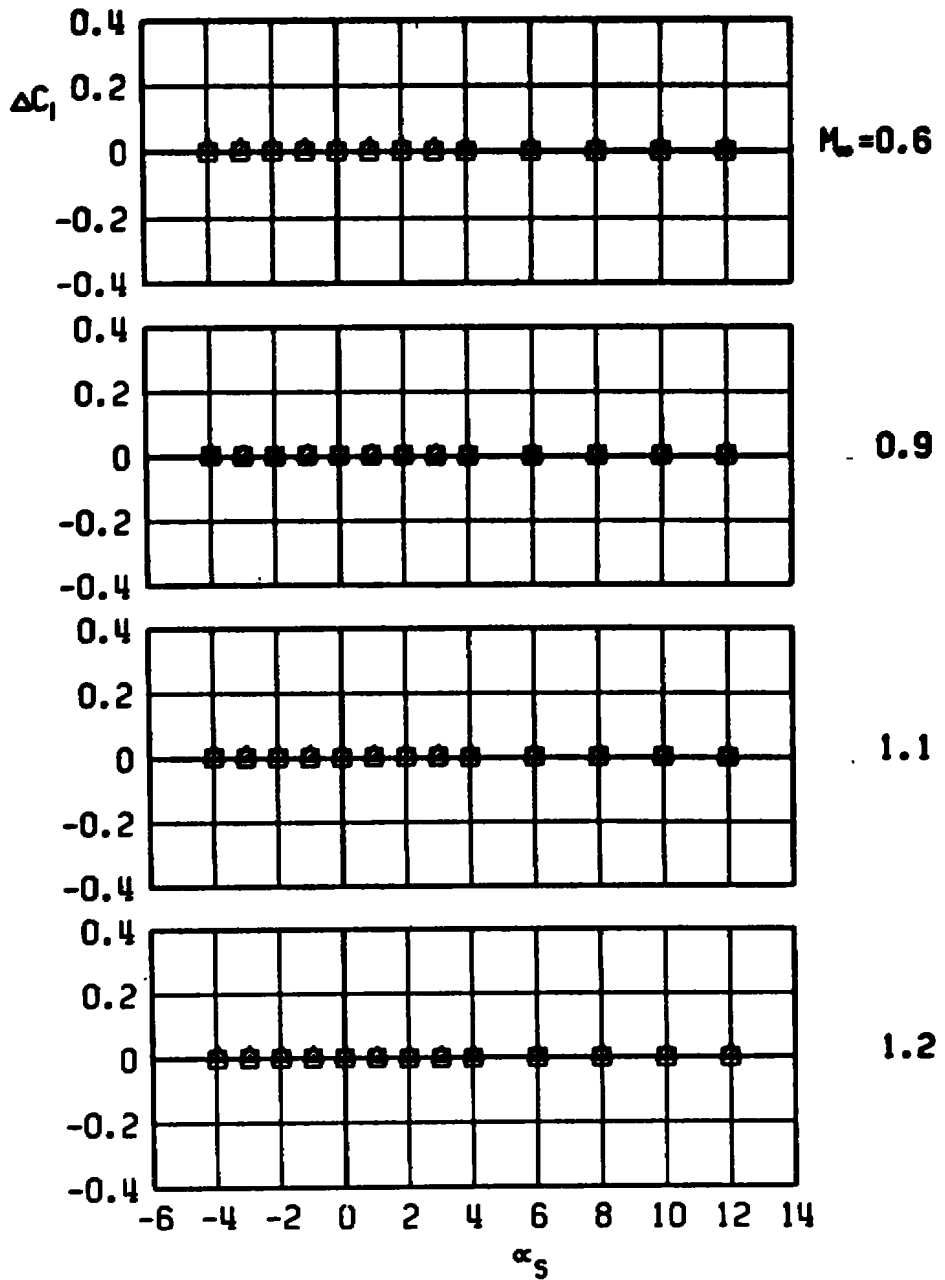
b. Side-force increment
Figure 35. Continued.

CBU-24, C-L PYLON, MER-3
 WITH DUMMY STING, $D_3 = 0.57 D_0$
 WITH DUMMY STING, $D_3 = 0.92 D_0$



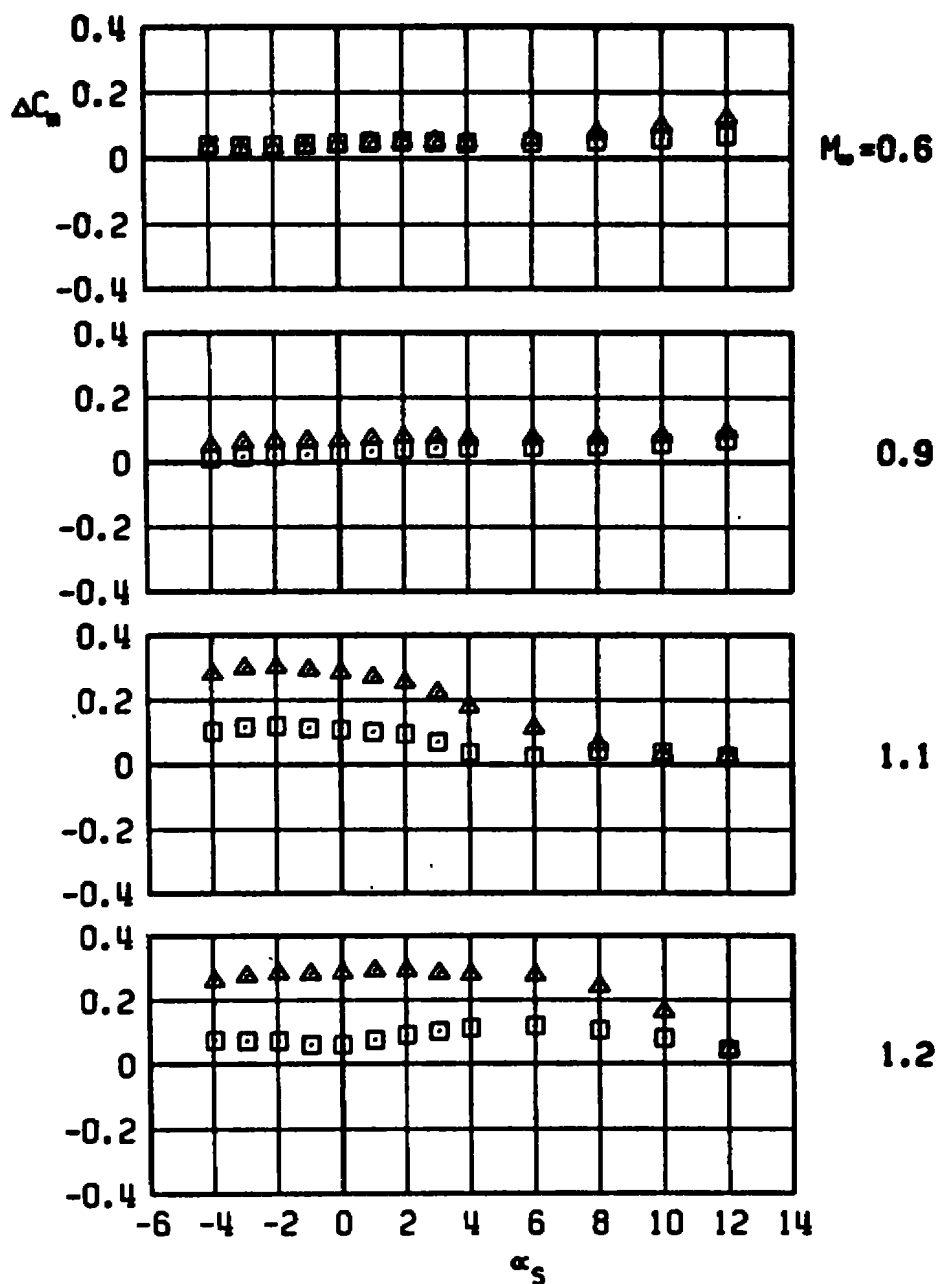
c. Axial-force increment
 Figure 35. Continued.

CBU-24, C-L PYLON, MER-3
 WITH DUMMY STING, $D_3 = 0.57 D_0$
 WITH DUMMY STING, $D_3 = 0.92 D_0$



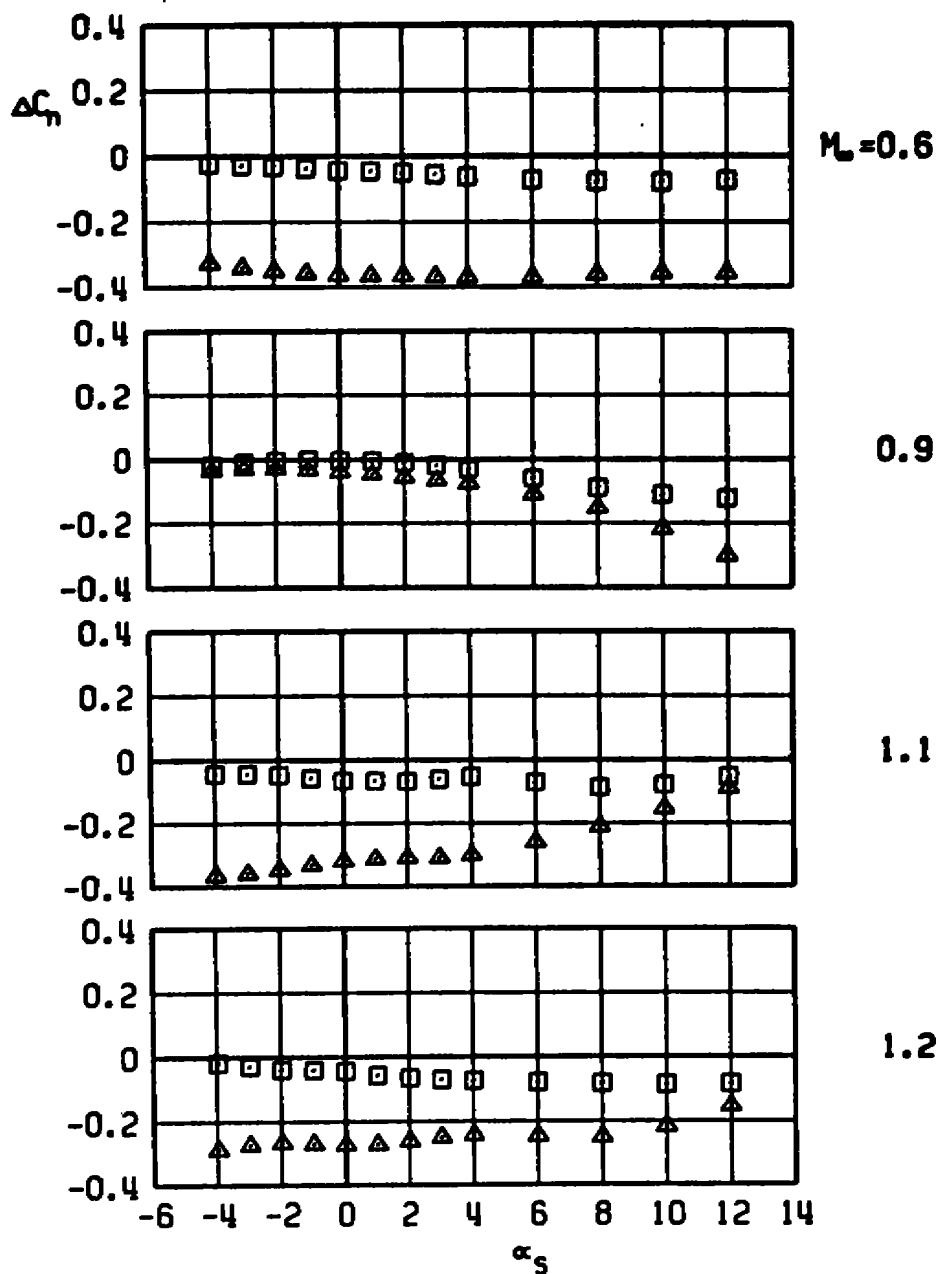
d. Rolling-moment increment
 Figure 35. Continued.

□ CBU-24, C-L PYLON, MEA-3
 WITH DUMMY STING, $D_3 = 0.57 D_0$
 ▲ WITH DUMMY STING, $D_3 = 0.92 D_0$



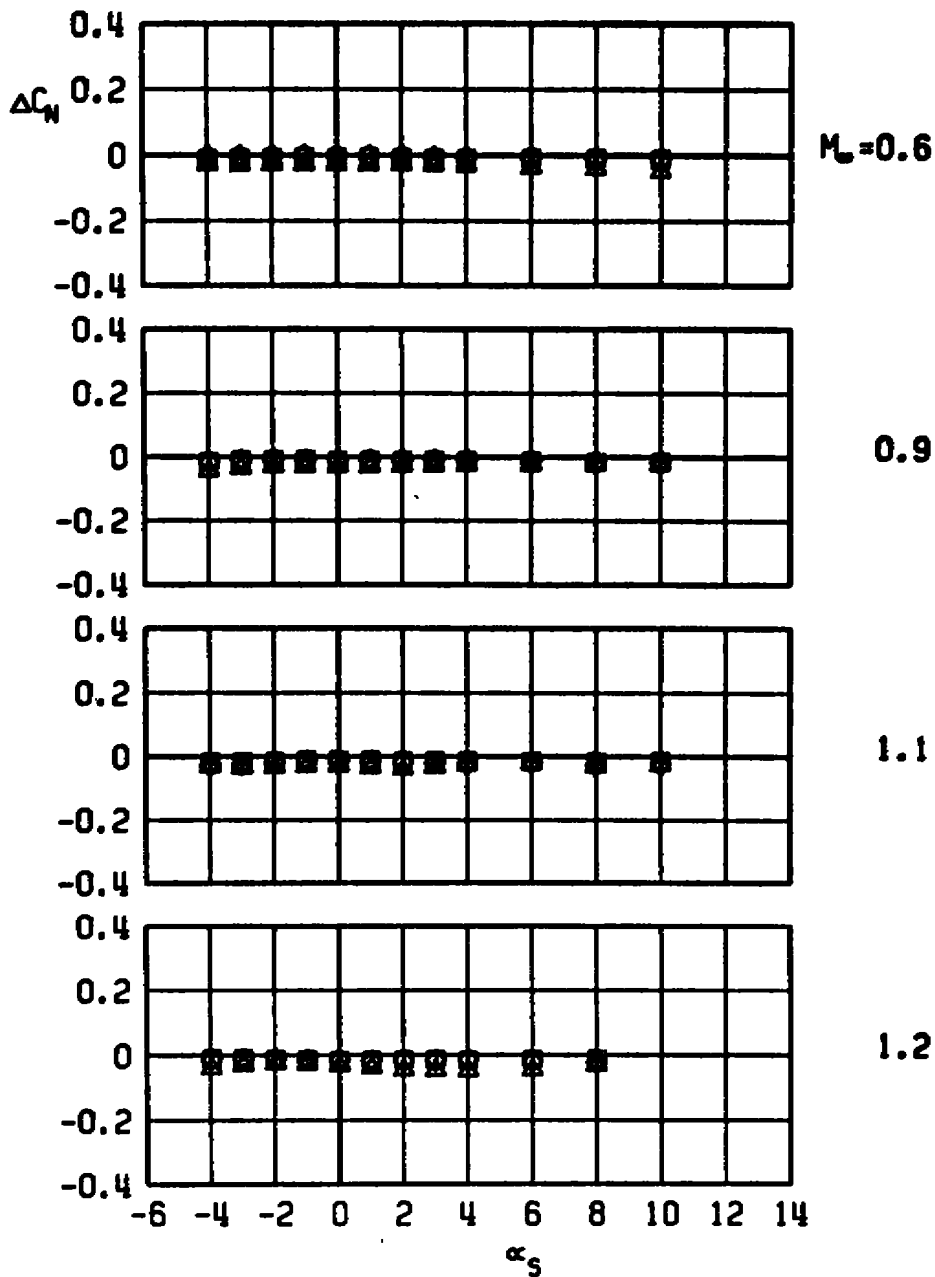
e. Pitching-moment increment
Figure 35. Continued.

CBU-24, C-L PYLON, MER-3
 □ WITH DUMMY STING, $D_3 = 0.57 D_0$
 ▲ WITH DUMMY STING, $D_3 = 0.92 D_0$



f. Yawing-moment increment
 Figure 35. Concluded.

CBU-24, C-L PYLON, MER-4
 □ WITH DUMMY STING, $D_3 = 0.57 D_9$
 ◇ WITH DUMMY STING, $D_3 = 0.74 D_9$
 ▲ WITH DUMMY STING, $D_3 = 0.92 D_9$



a. Normal-force increment

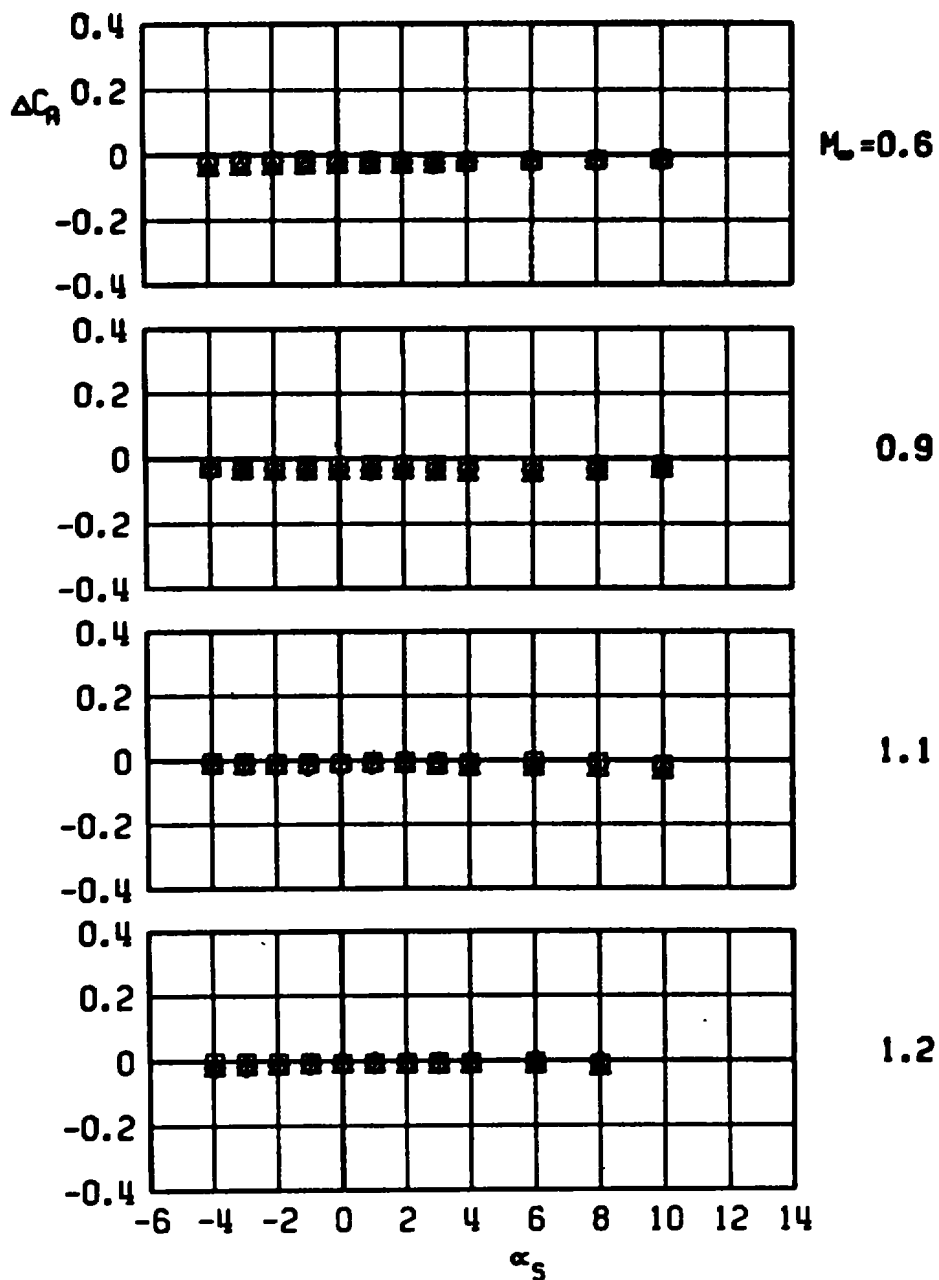
Figure 36. Sting-induced aerodynamic load increments as a function of angle of attack, stable rack-mounted store, MER station 4, C-L pylon.

CBU-24, C-L PYLON, MER-4

- | | |
|---|-------------------------------------|
| □ | WITH DUMMY STRING, $D_3 = 0.57 D_0$ |
| ◇ | WITH DUMMY STRING, $D_3 = 0.74 D_0$ |
| △ | WITH DUMMY STRING, $D_3 = 0.92 D_0$ |

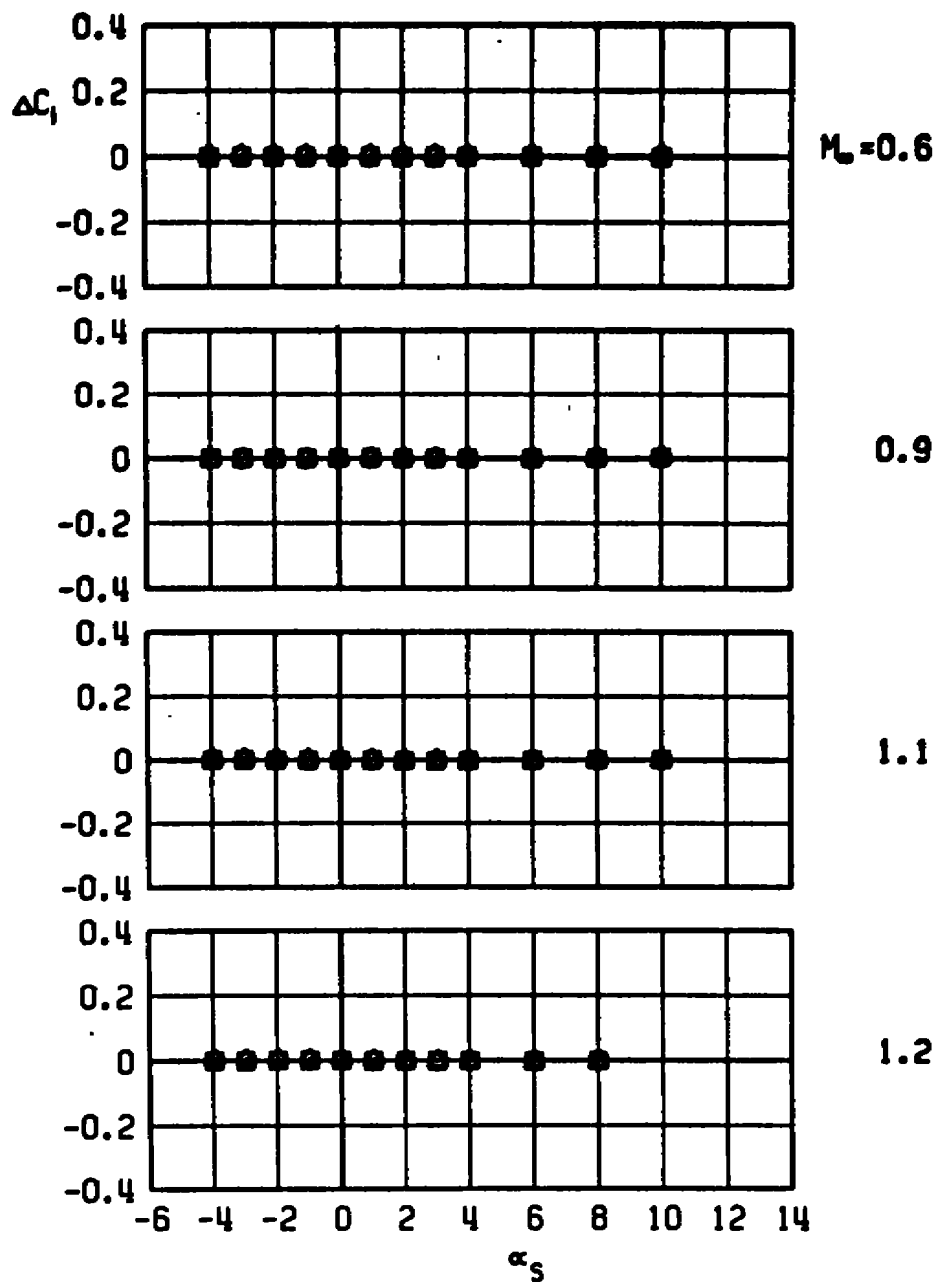
CBU-24, C-L PYLON, MER-4

- WITH DUMMY STING, $D_3 = 0.57 D_0$
 ◇ WITH DUMMY STING, $D_3 = 0.74 D_0$
 ▲ WITH DUMMY STING, $D_3 = 0.92 D_0$



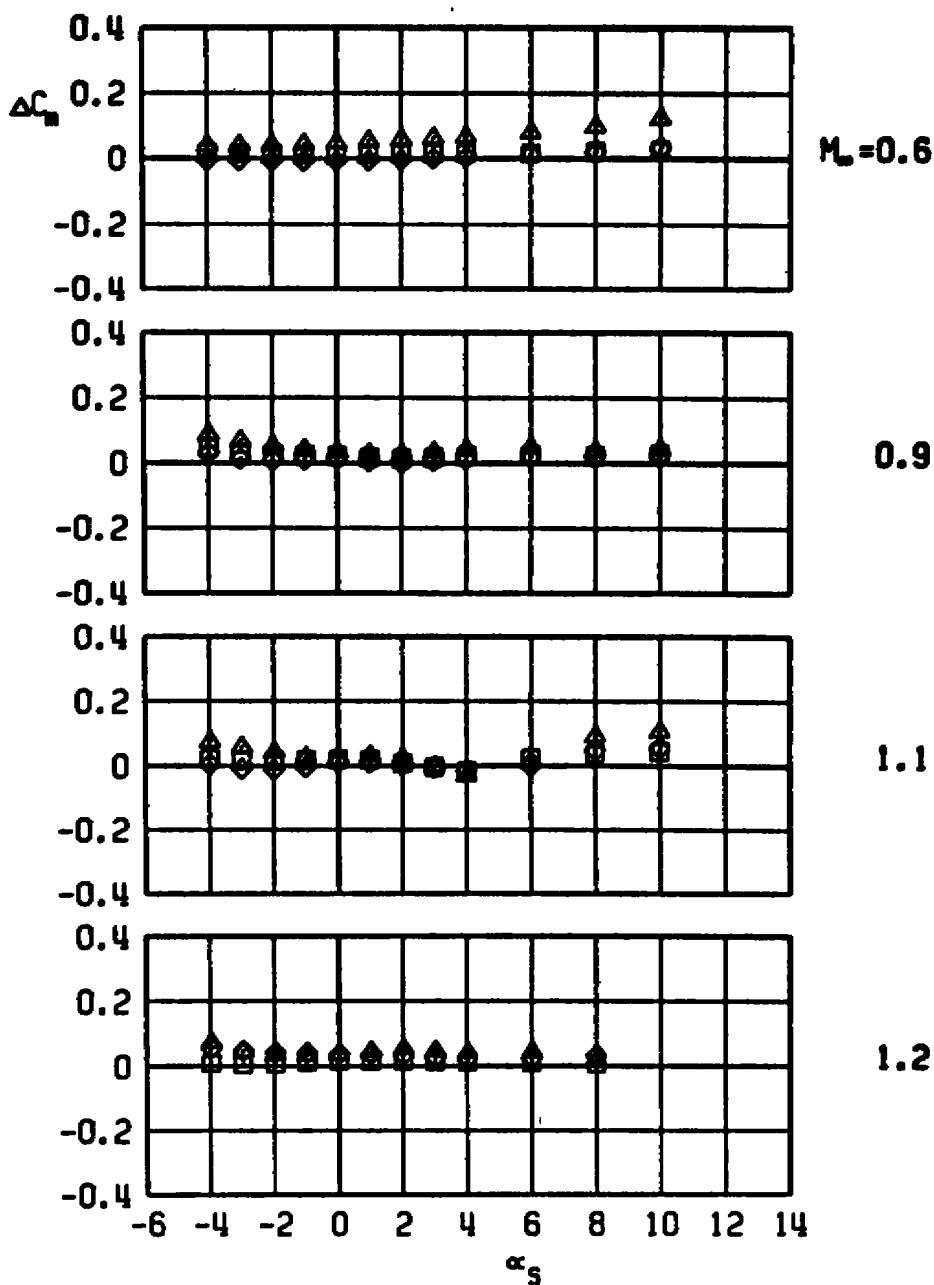
c. Axial-force increment
Figure 36. Continued.

CBU-24, C-L PYLON, MER-4
 WITH DUMMY STING, $D_3 = 0.57 D_0$
 WITH DUMMY STING, $D_3 = 0.74 D_0$
 WITH DUMMY STING, $D_3 = 0.92 D_0$



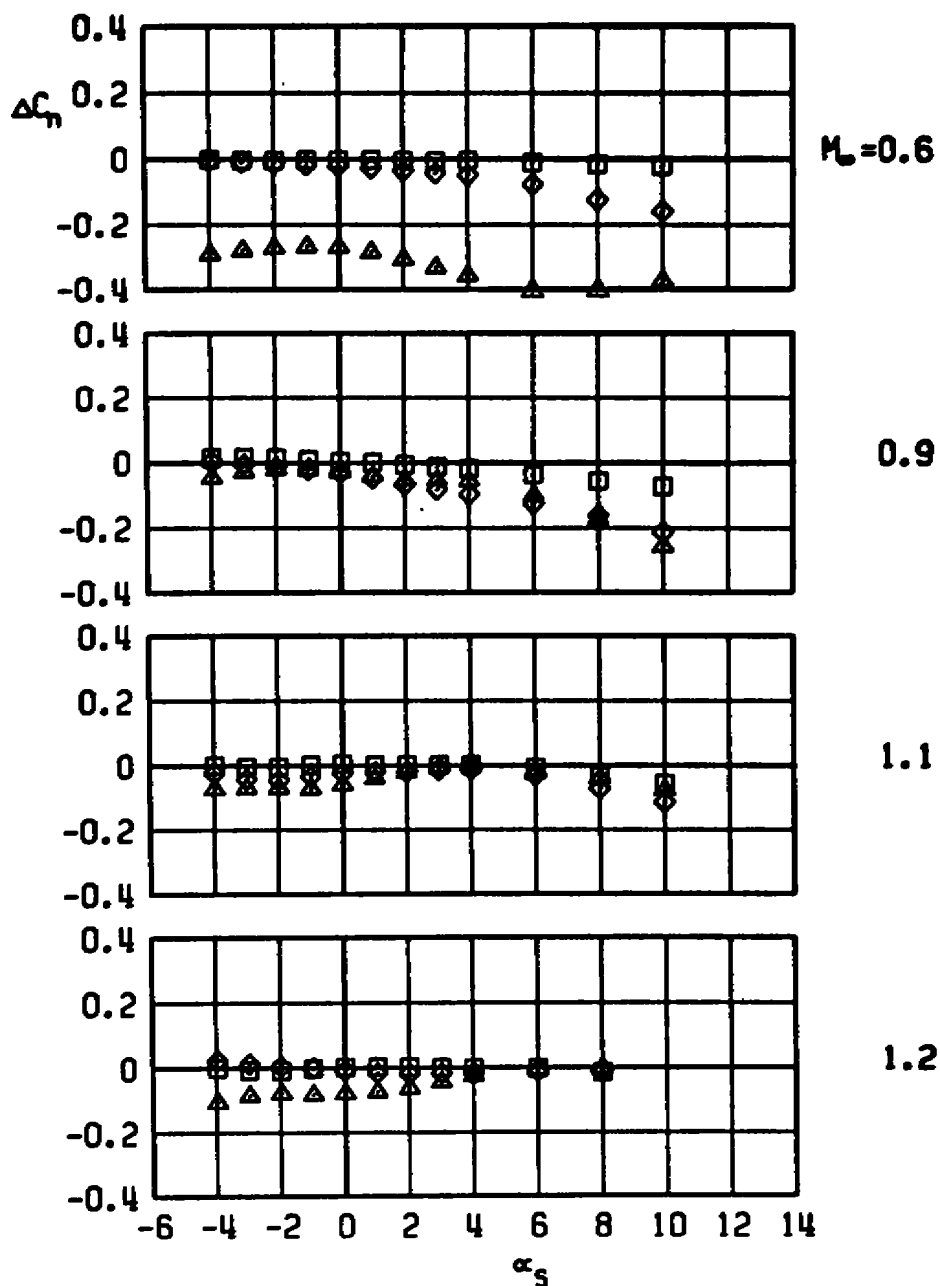
d. Rolling-moment increment
Figure 36. Continued.

CBU-24, C-L PYLON, MER-4
 □ WITH DUMMY STING, $D_3 = 0.57 D_0$
 ◇ WITH DUMMY STING, $D_3 = 0.74 D_0$
 ▲ WITH DUMMY STING, $D_3 = 0.92 D_0$



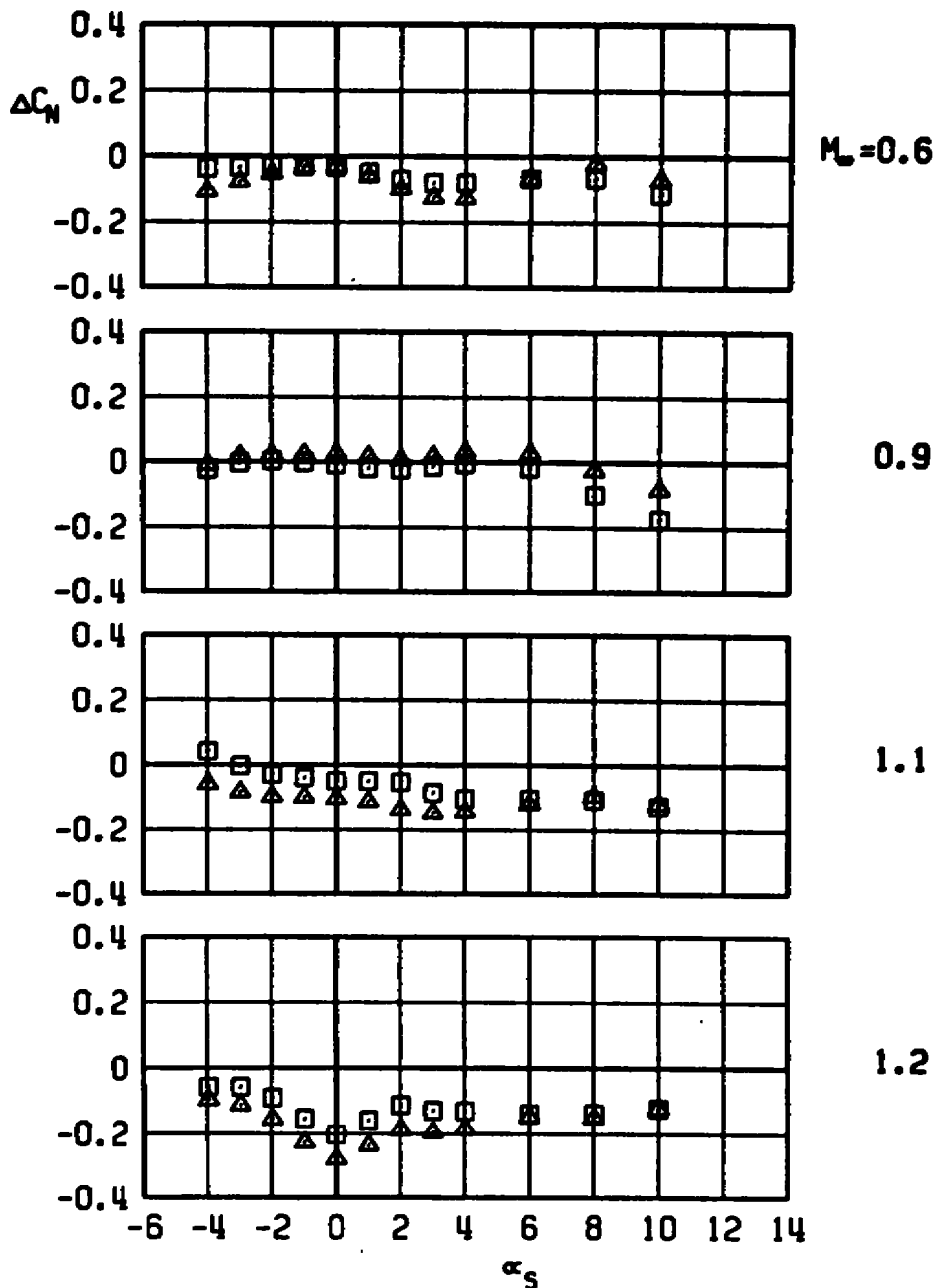
e. Pitching-moment increment
 Figure 36. Continued.

CBU-24, C-L PYLON, MER-4
 □ WITH DUMMY STING, $D_3 = 0.57 D_0$
 ◇ WITH DUMMY STING, $D_3 = 0.74 D_0$
 ▲ WITH DUMMY STING, $D_3 = 0.92 D_0$



f. Yawing-moment increment
Figure 36. Concluded.

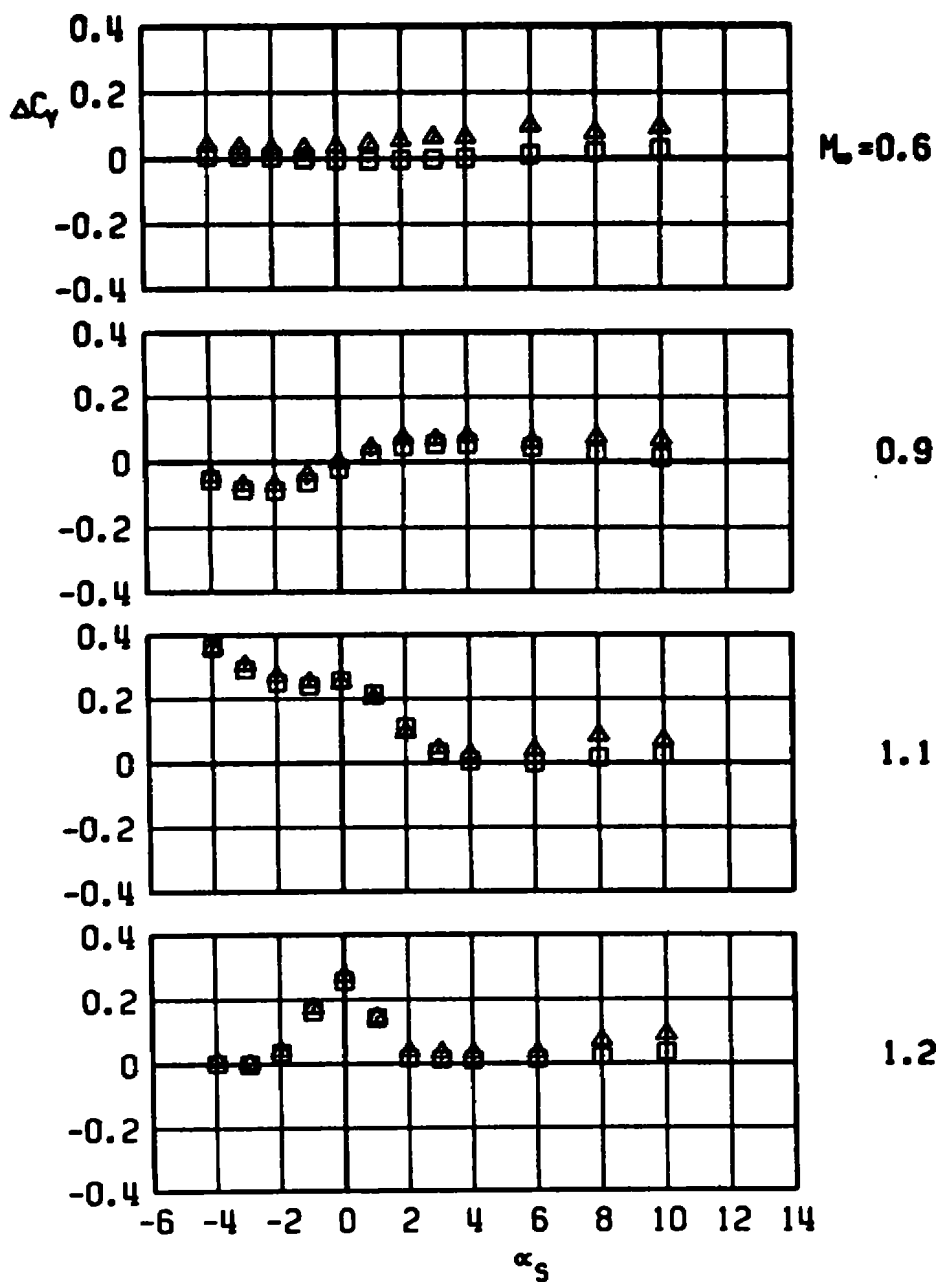
CBU-24, LOB PYLON, MER-1
 WITH DUMMY STING, $D_3 = 0.57 D_0$
 WITH DUMMY STING, $D_3 = 0.92 D_0$



a. Normal-force increment

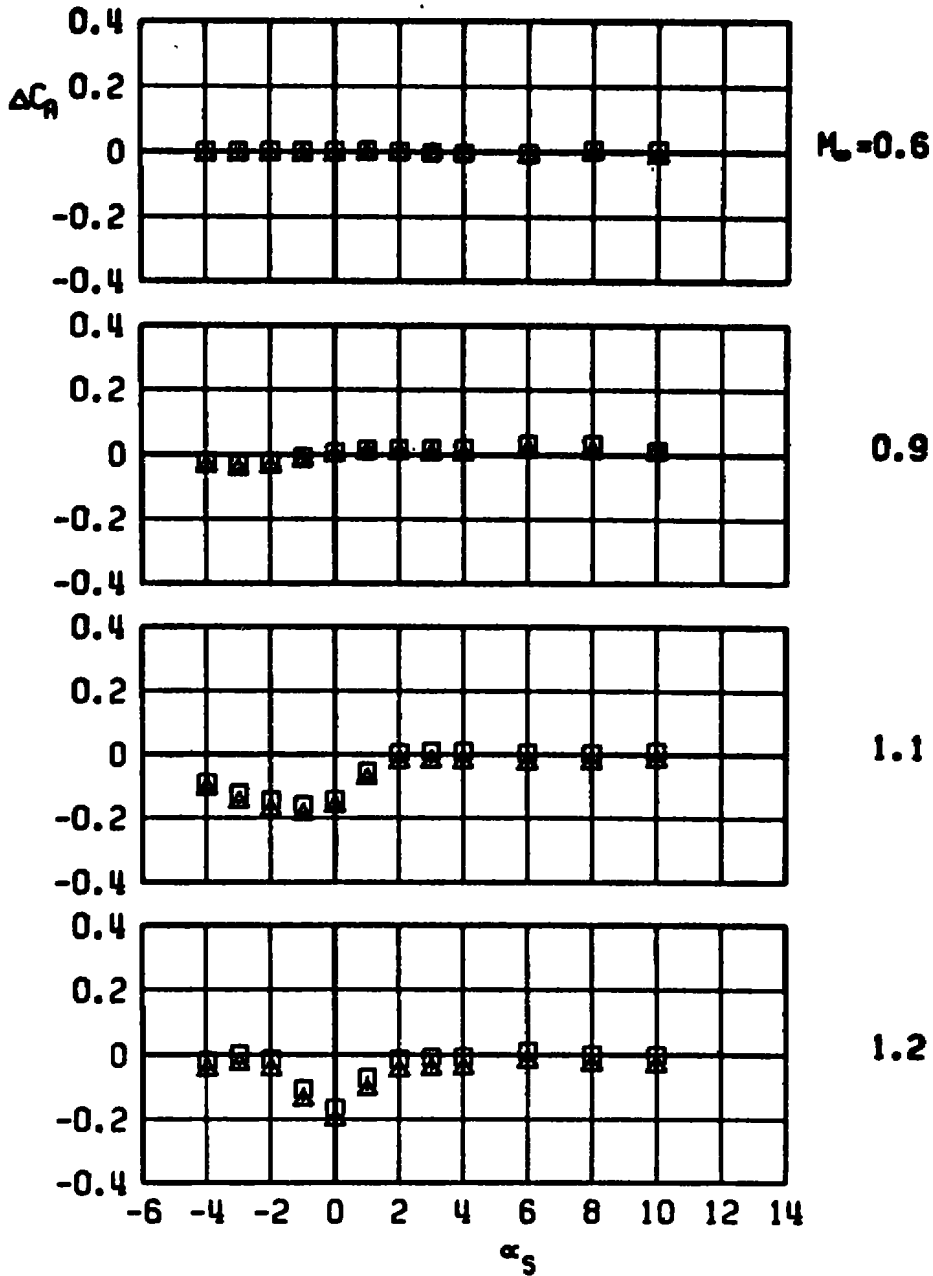
Figure 37. Sting-induced aerodynamic load increments as a function of angle of attack, stable rack-mounted store, MER station 1, LOB pylon.

CBU-24, LOB PYLON, MER-1
 WITH DUMMY STING, $D_3 = 0.57 D_0$
 WITH DUMMY STING, $D_3 = 0.92 D_0$



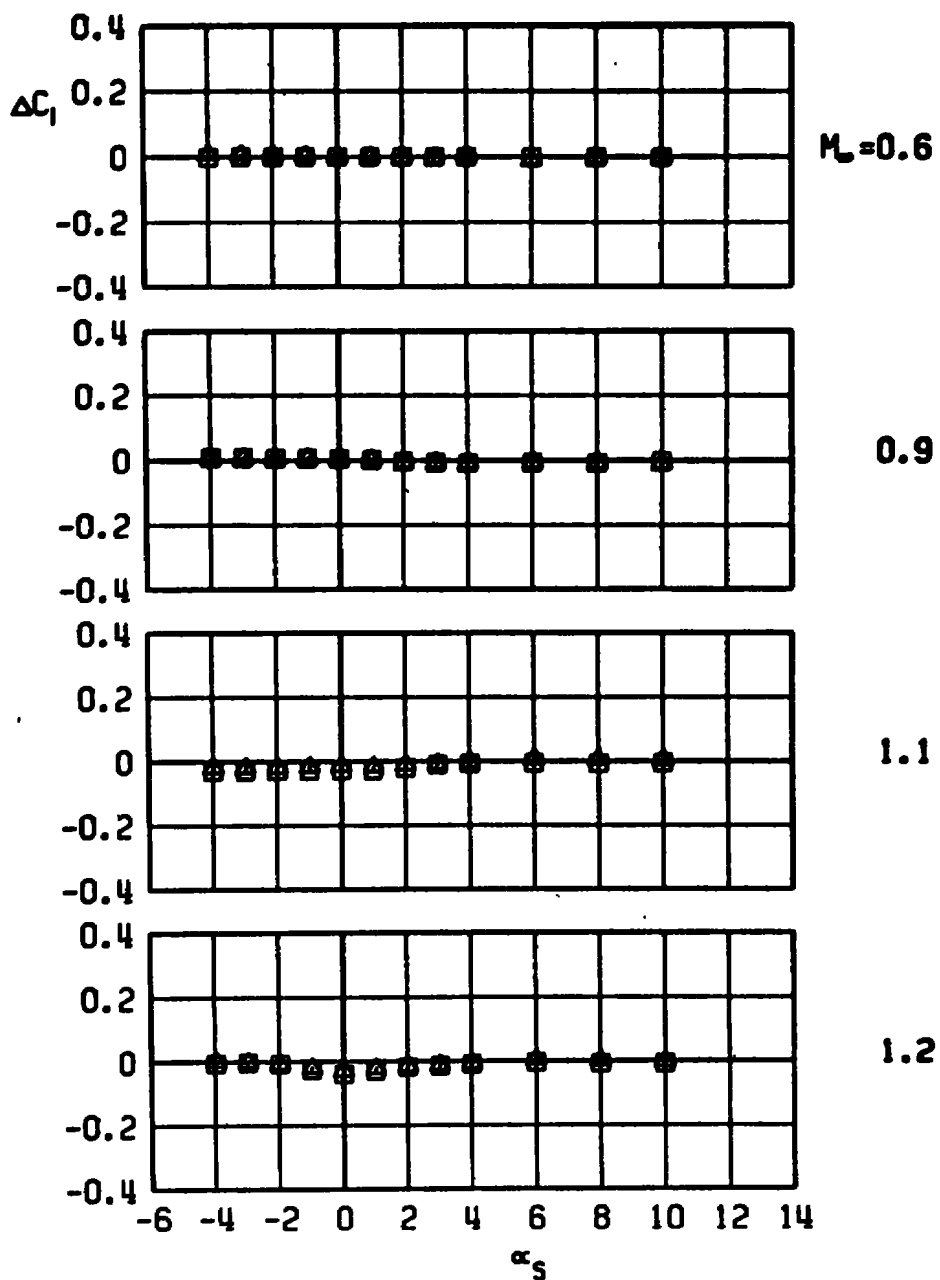
b. Side-force increment
 Figure 37. Continued.

CBU-24, LOB PYLON, MER-1
 WITH DUMMY STING, $D_3 = 0.57 D_0$
 WITH DUMMY STING, $D_3 = 0.92 D_0$



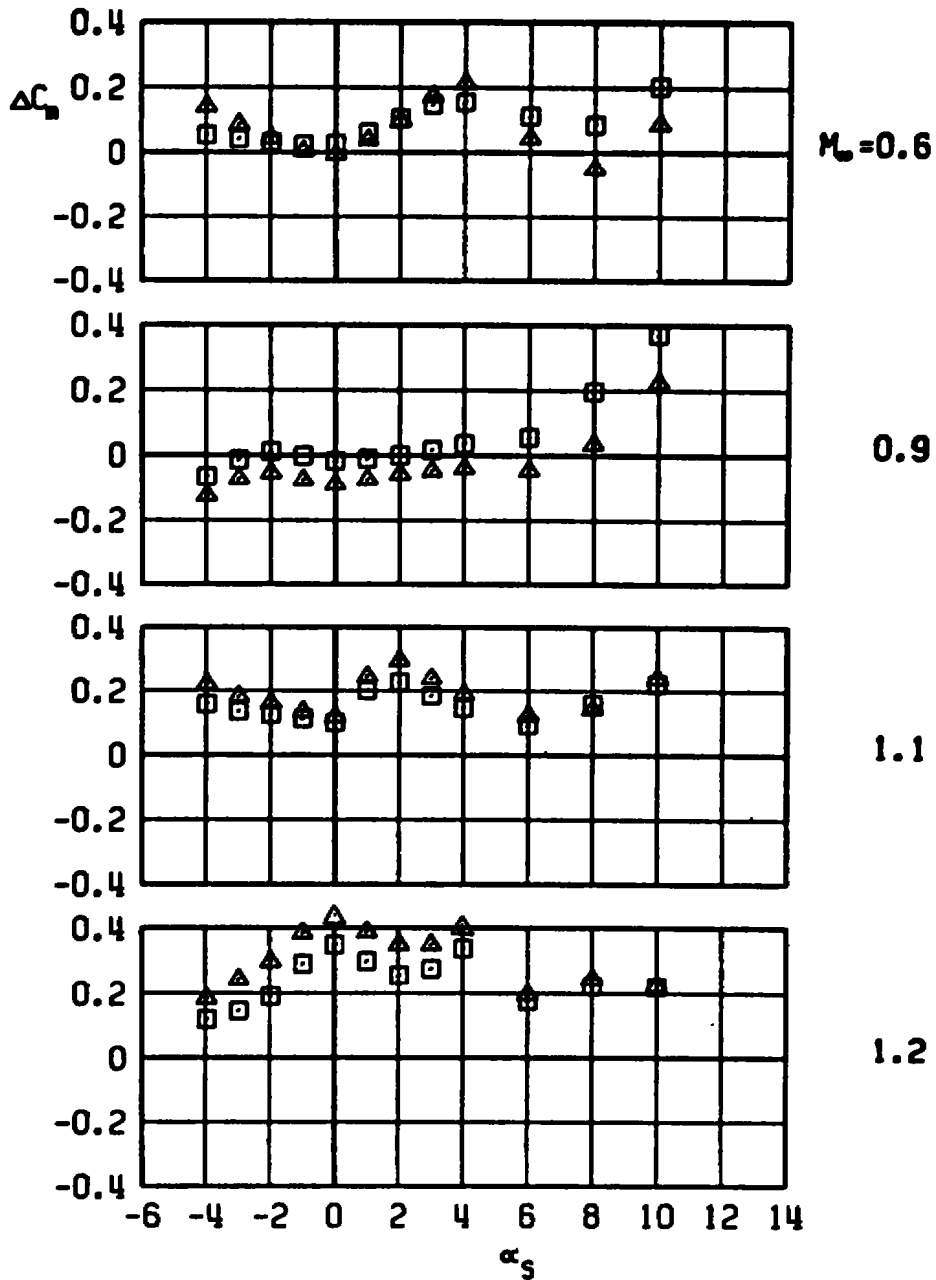
c. Axial-force increment
 Figure 37. Continued.

CBU-24, LOB PYLON, MER-1
 □ WITH DUMMY STING, $D_3 = 0.57 D_0$
 ▲ WITH DUMMY STING, $D_3 = 0.92 D_0$



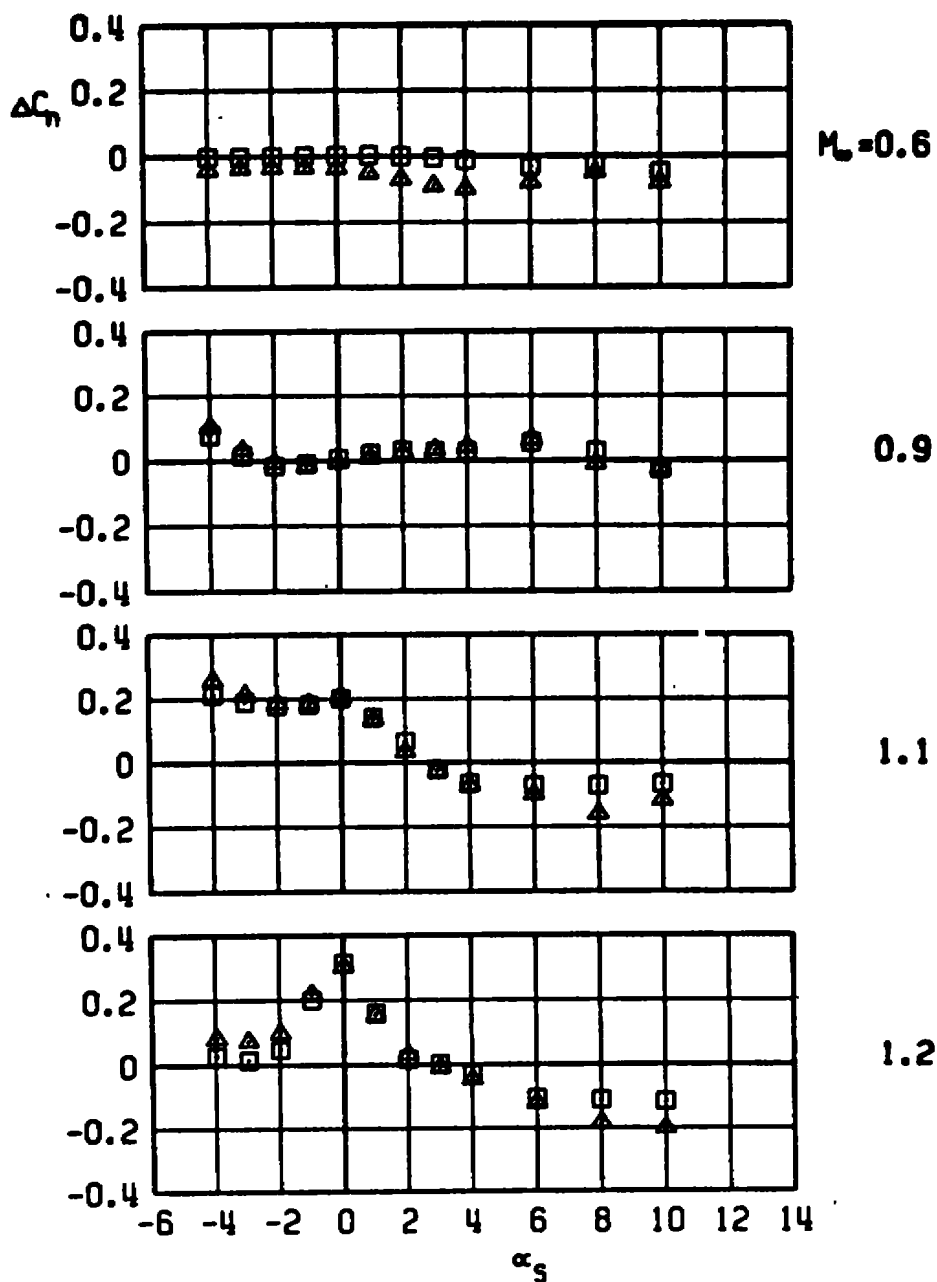
d. Rolling-moment increment
 Figure 37. Continued.

CBU-24, LOB PYLON, MER-1
 □ WITH DUMMY STING, $D_3 = 0.57 D_0$
 ▲ WITH DUMMY STING, $D_3 = 0.92 D_0$



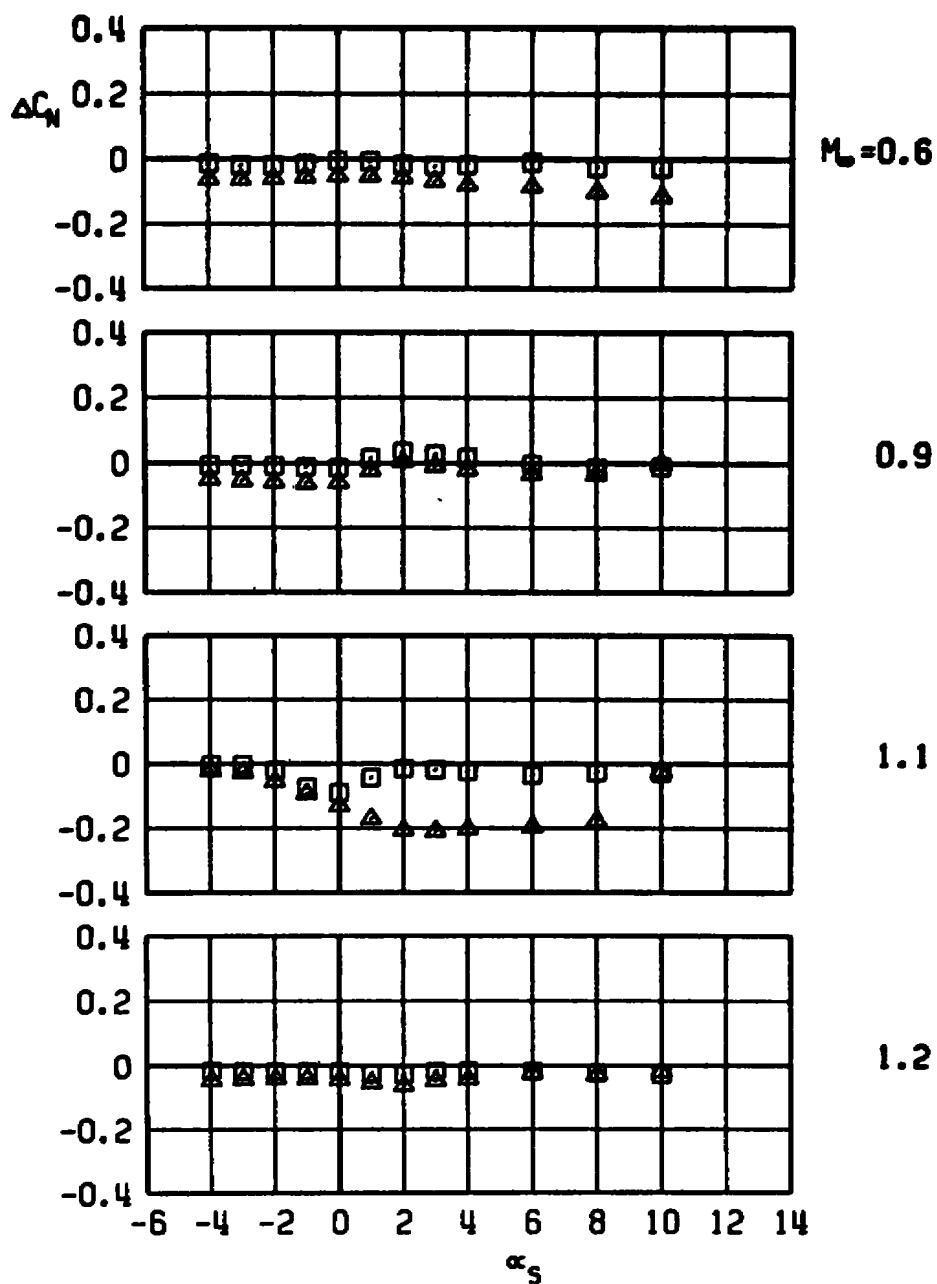
e. Pitching-moment increment
 Figure 37. Continued.

CBU-24, LOB PYLON, MER-1
 WITH DUMMY STING, $D_s = 0.57 D_0$
 WITH DUMMY STING, $D_s = 0.92 D_0$



f. Yawing-moment increment
 Figure 37. Concluded.

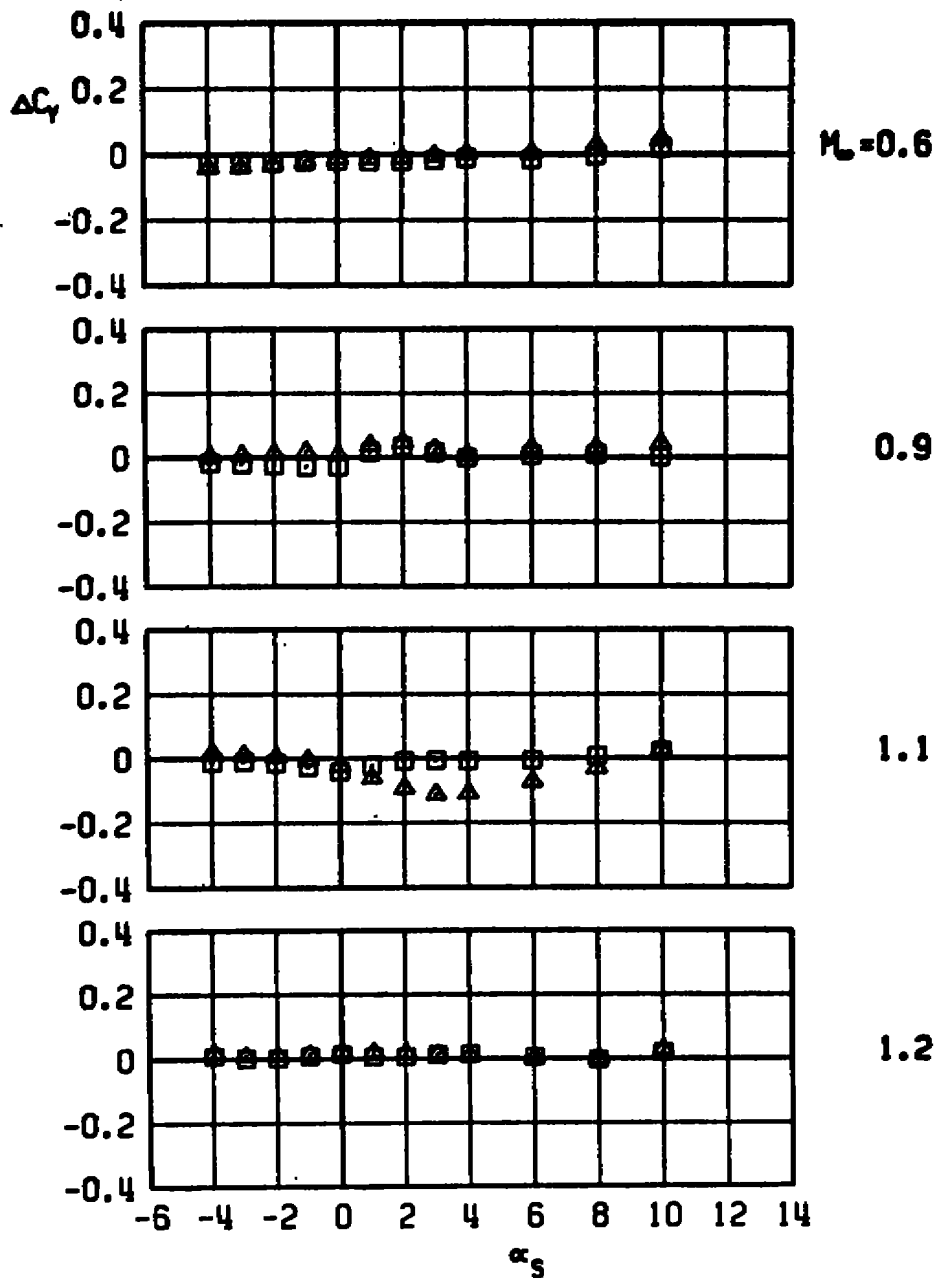
CBU-24, LOB PYLON, MER-2
 □ WITH DUMMY STING, $D_3 = 0.57 D_0$
 ▲ WITH DUMMY STING, $D_3 = 0.92 D_0$



a. Normal-force increment

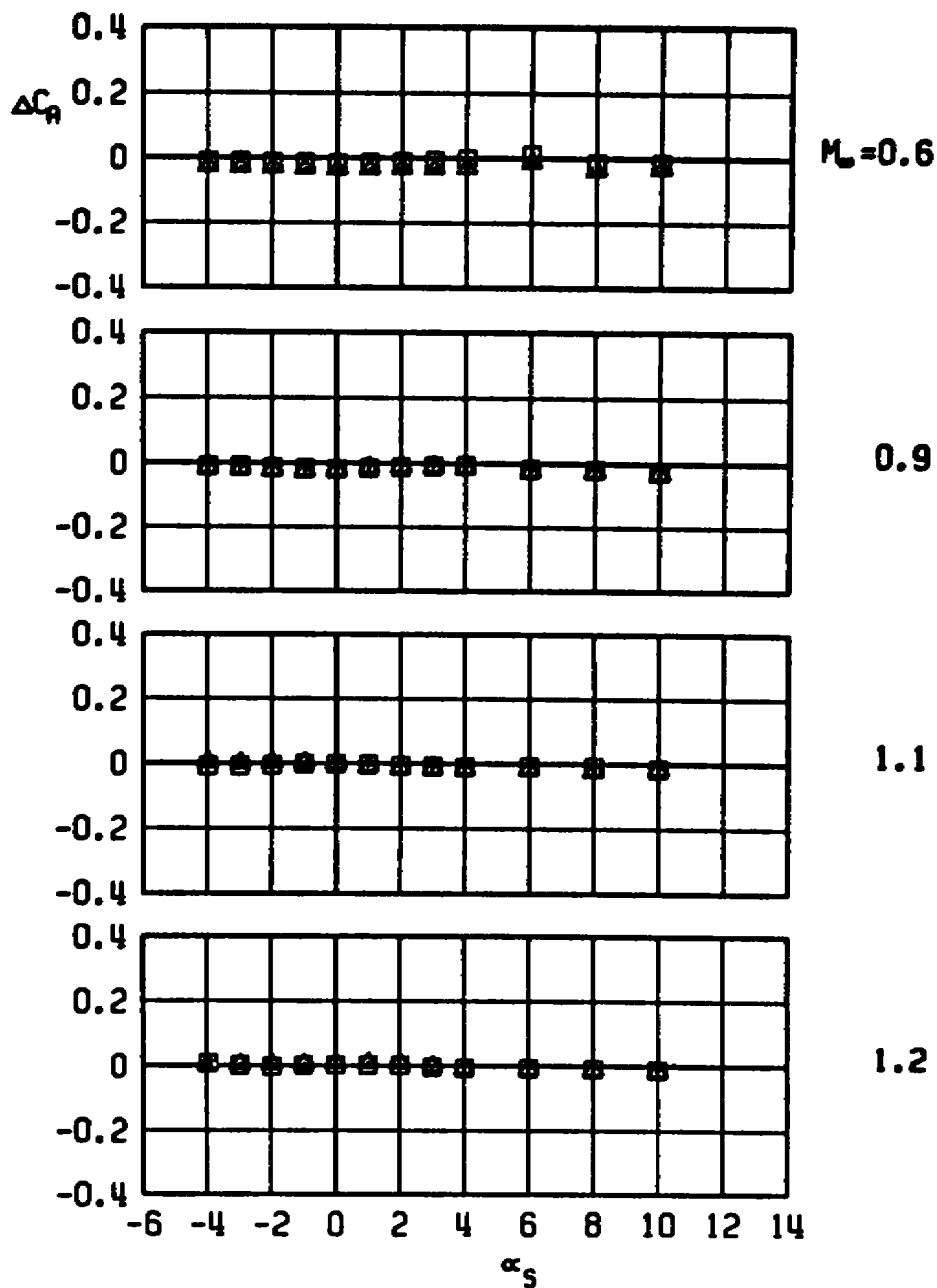
Figure 38. Sting-induced aerodynamic load increments as a function of angle of attack, stable rack-mounted store, MER station 2, LOB pylon.

CBU-24, LOS PYLON, MEA-2
 WITH DUMMY STING, $D_3 = 0.57 D_0$
 WITH DUMMY STING, $D_3 = 0.92 D_0$



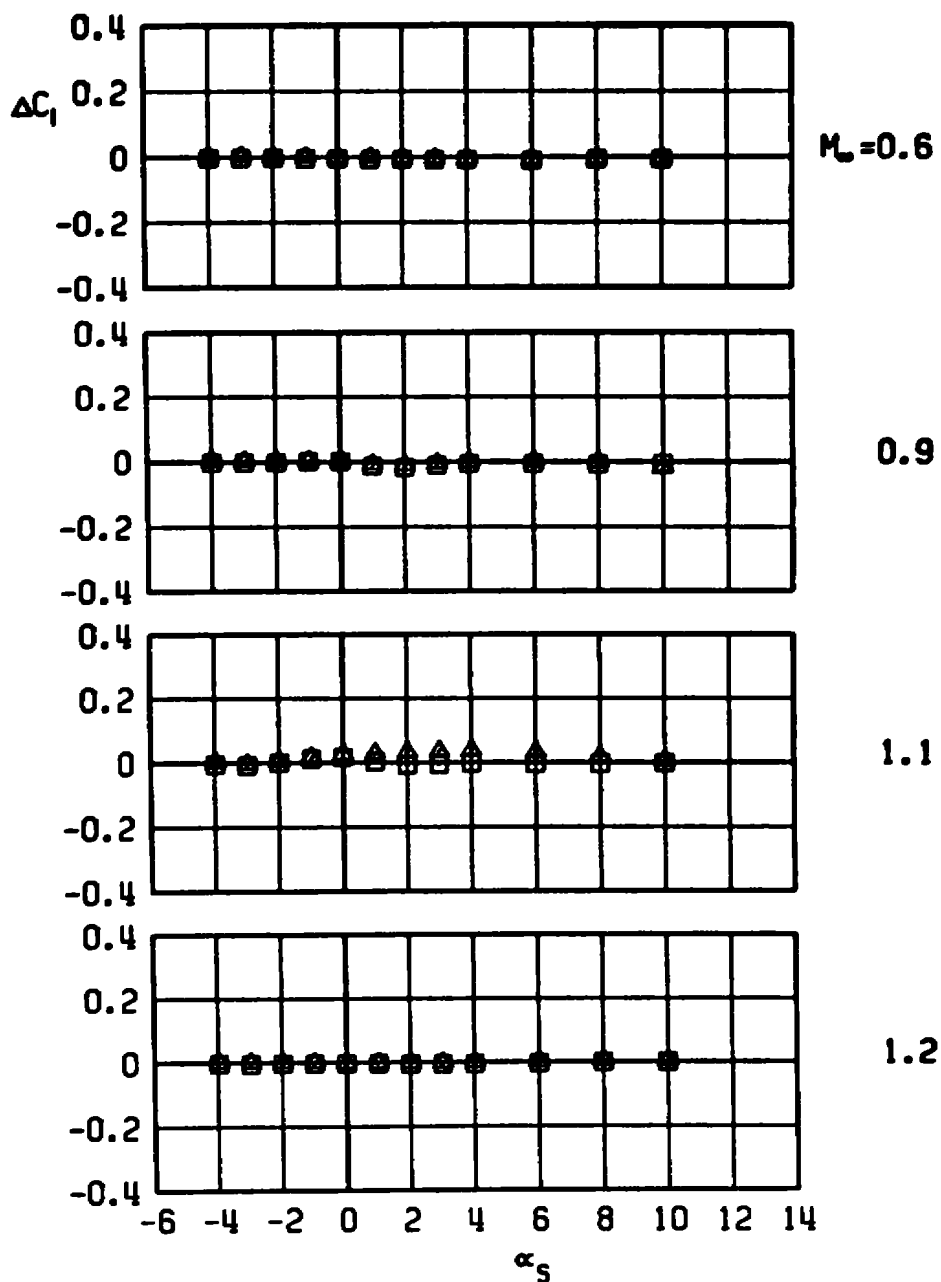
b. Side-force increment
 Figure 38. Continued.

CBU-24, LOS PYLON, MER-2
 WITH DUMMY STING, $D_3 = 0.57 D_0$
 WITH DUMMY STING, $D_3 = 0.92 D_0$



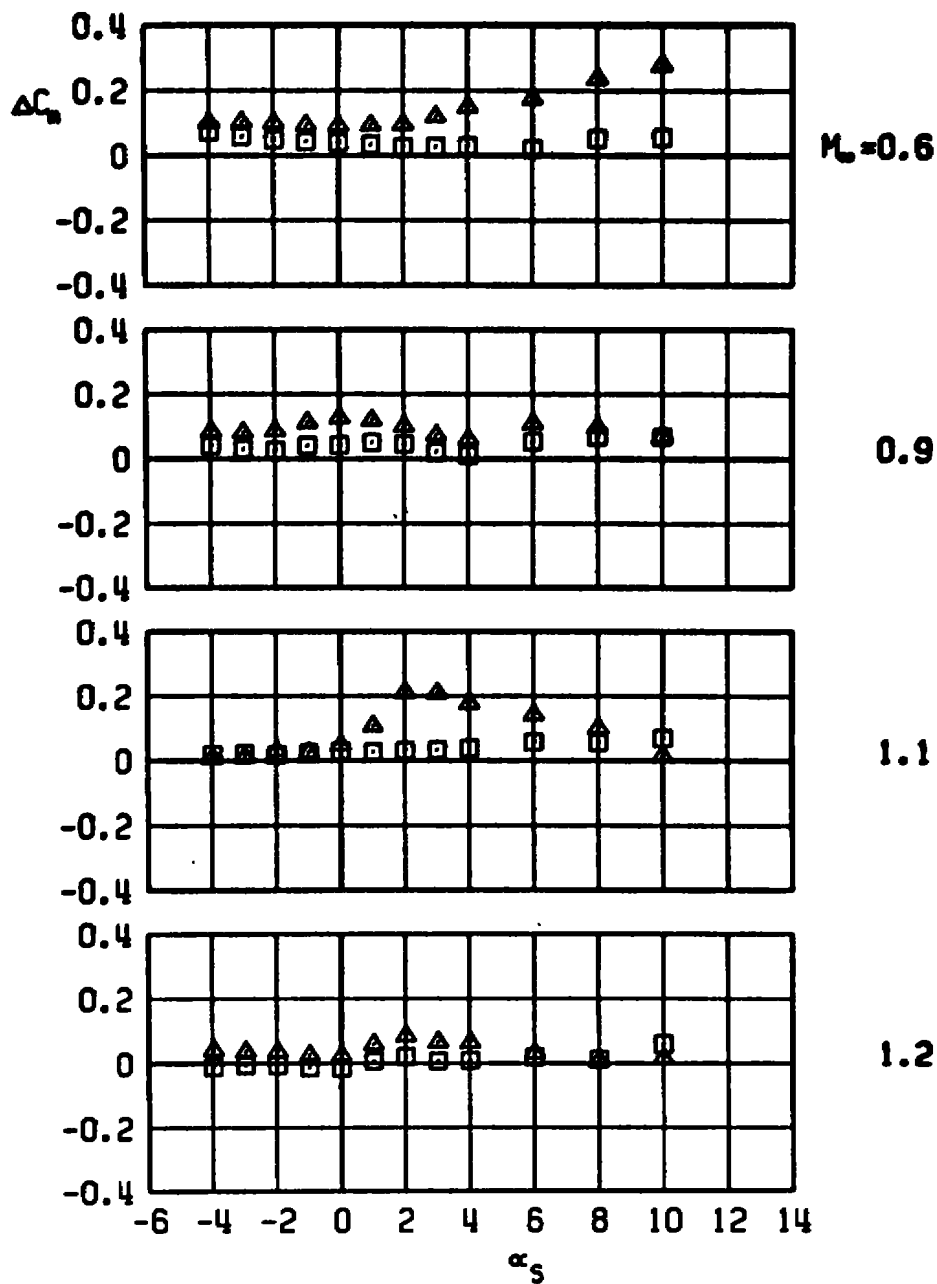
c. Axial-force increment
 Figure 38. Continued.

CBU-24, LOB PYLON, MER-2
 WITH DUMMY STING, $D_3 = 0.57 D_0$
 WITH DUMMY STING, $D_3 = 0.92 D_0$



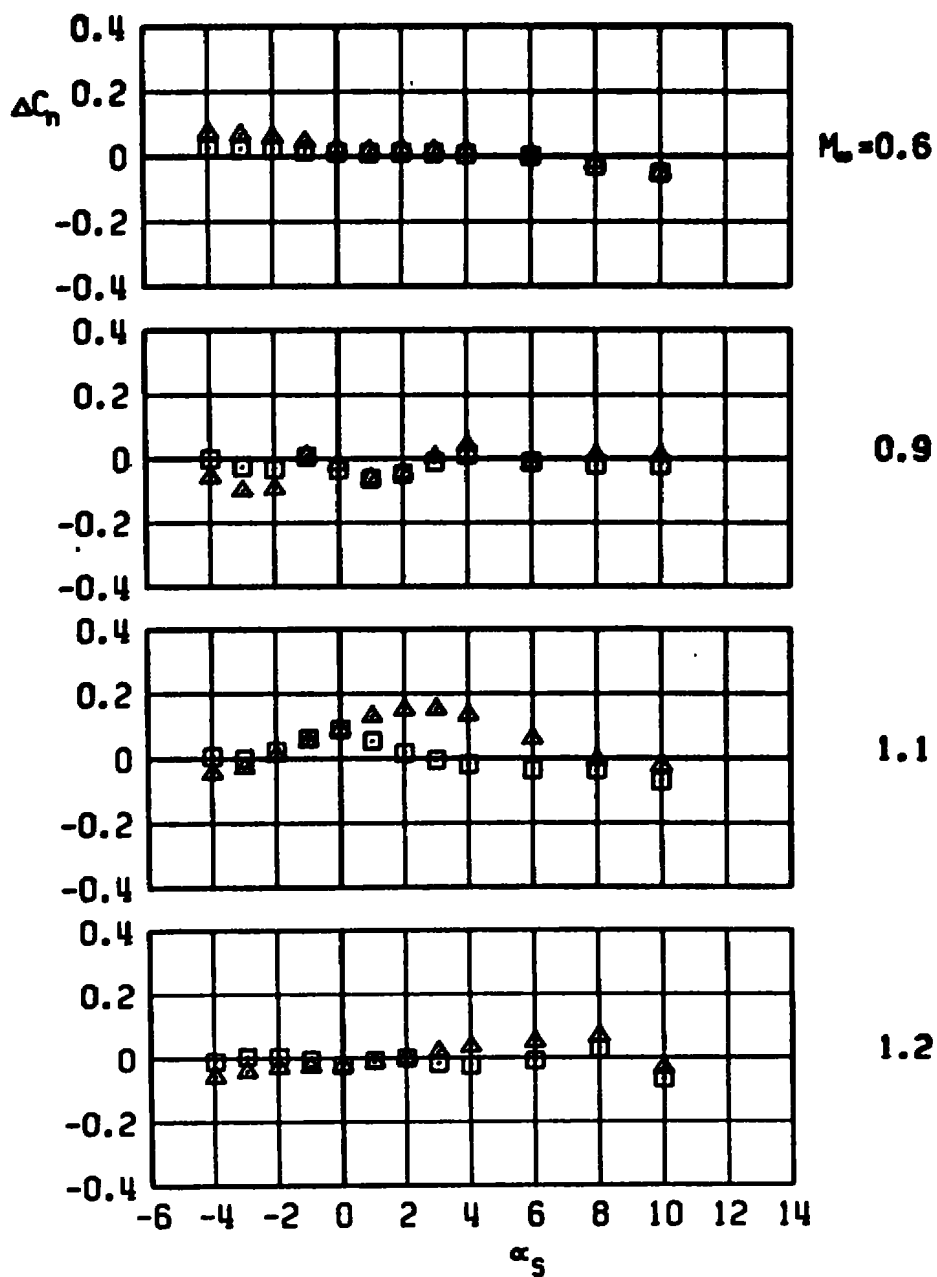
d. Rolling-moment increment
 Figure 38. Continued.

CBU-24, LOB PYLON, MER-2
 WITH DUMMY STING, $D_3 = 0.57 D_0$
 WITH DUMMY STING, $D_3 = 0.92 D_0$



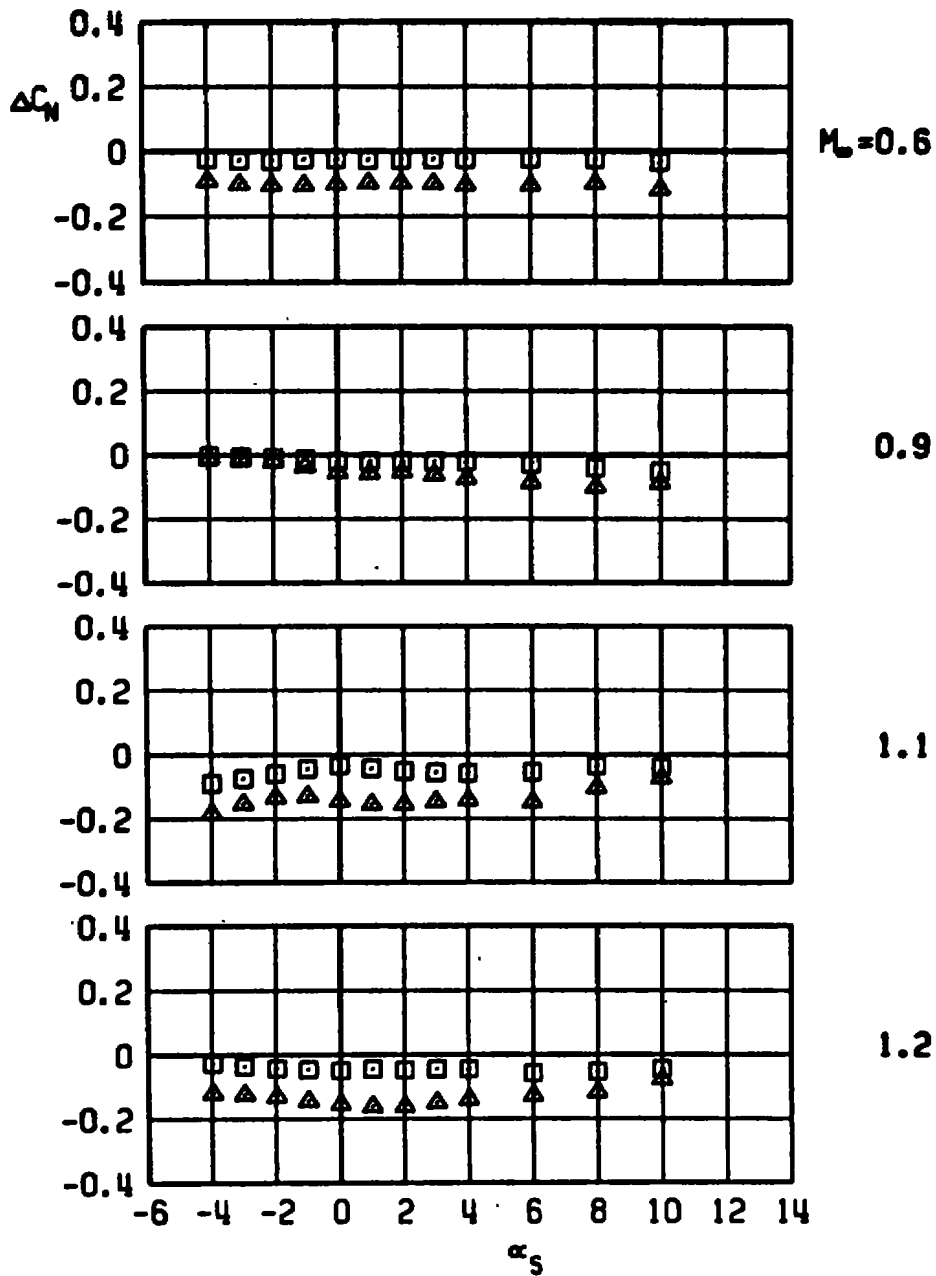
e. Pitching-moment increment
 Figure 38. Continued.

CBU-24, LOB PYLON, MER-2
 □ WITH DUMMY STING, $D_3 = 0.57 D_0$
 ▲ WITH DUMMY STING, $D_3 = 0.92 D_0$



f. Yawing-moment increment
 Figure 38. Concluded.

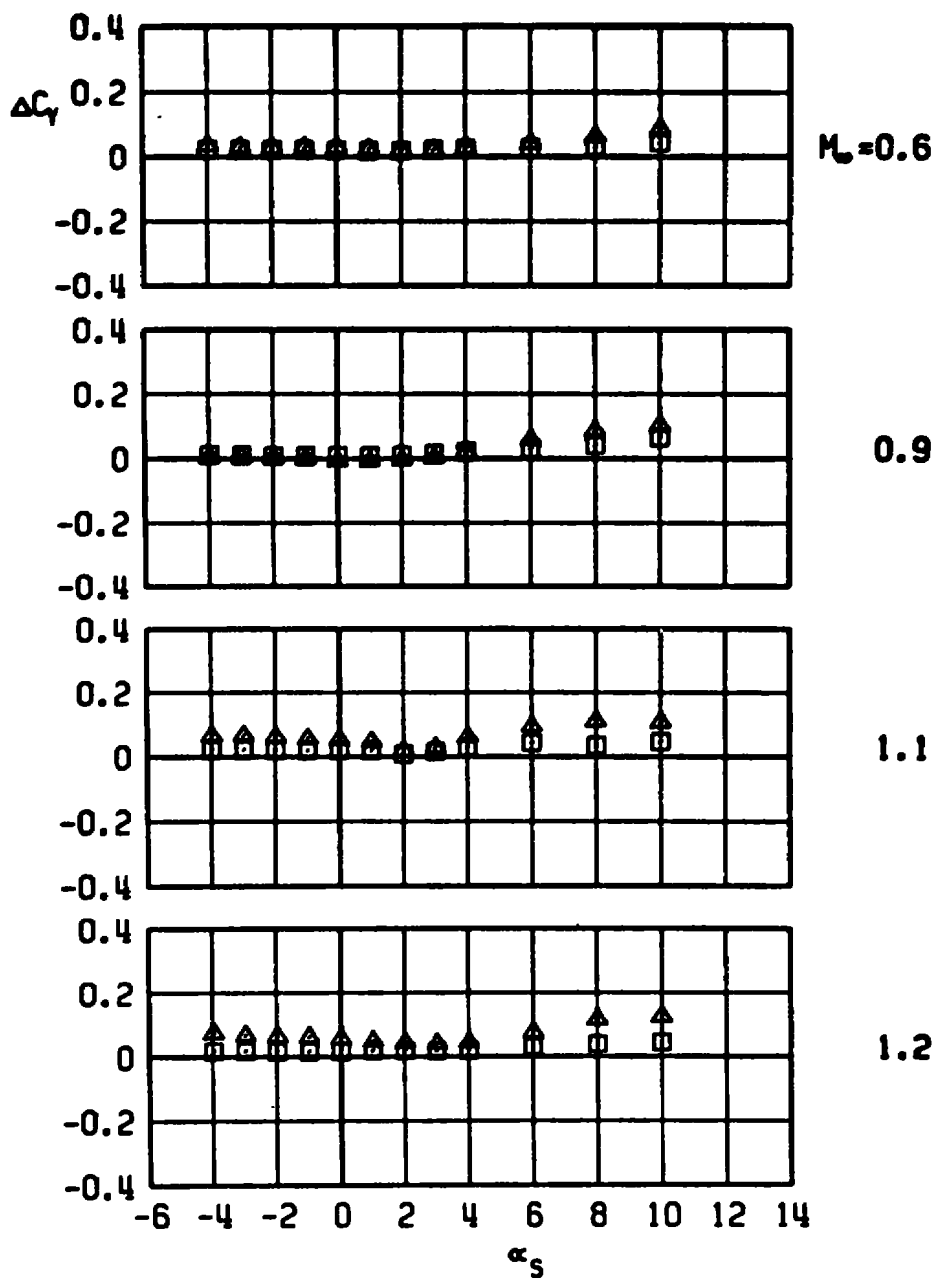
□ CBU-24, LOB PYLON, MER-3
 WITH DUMMY STING, $D_3 = 0.57 D_0$
 ▲ WITH DUMMY STING, $D_3 = 0.92 D_0$



a. Normal-force increment

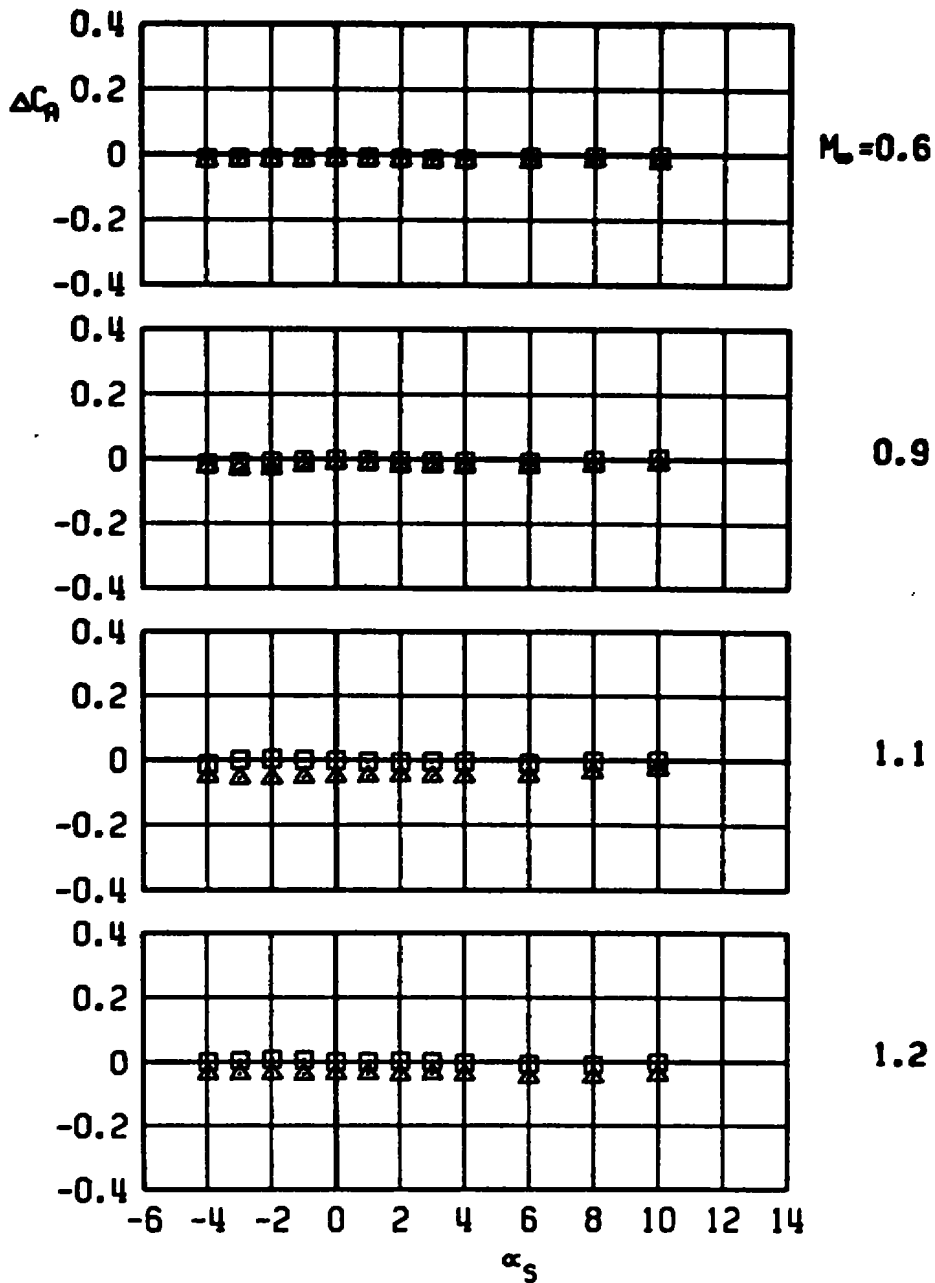
Figure 39. Sting-induced aerodynamic load increments as a function of angle of attack, stable rack-mounted store, MER station 3, LOB pylon.

CBU-24, LOB PYLON, MER-3
 WITH DUMMY STING, $D_5 = 0.57 D_0$
 WITH DUMMY STING, $D_5 = 0.92 D_0$



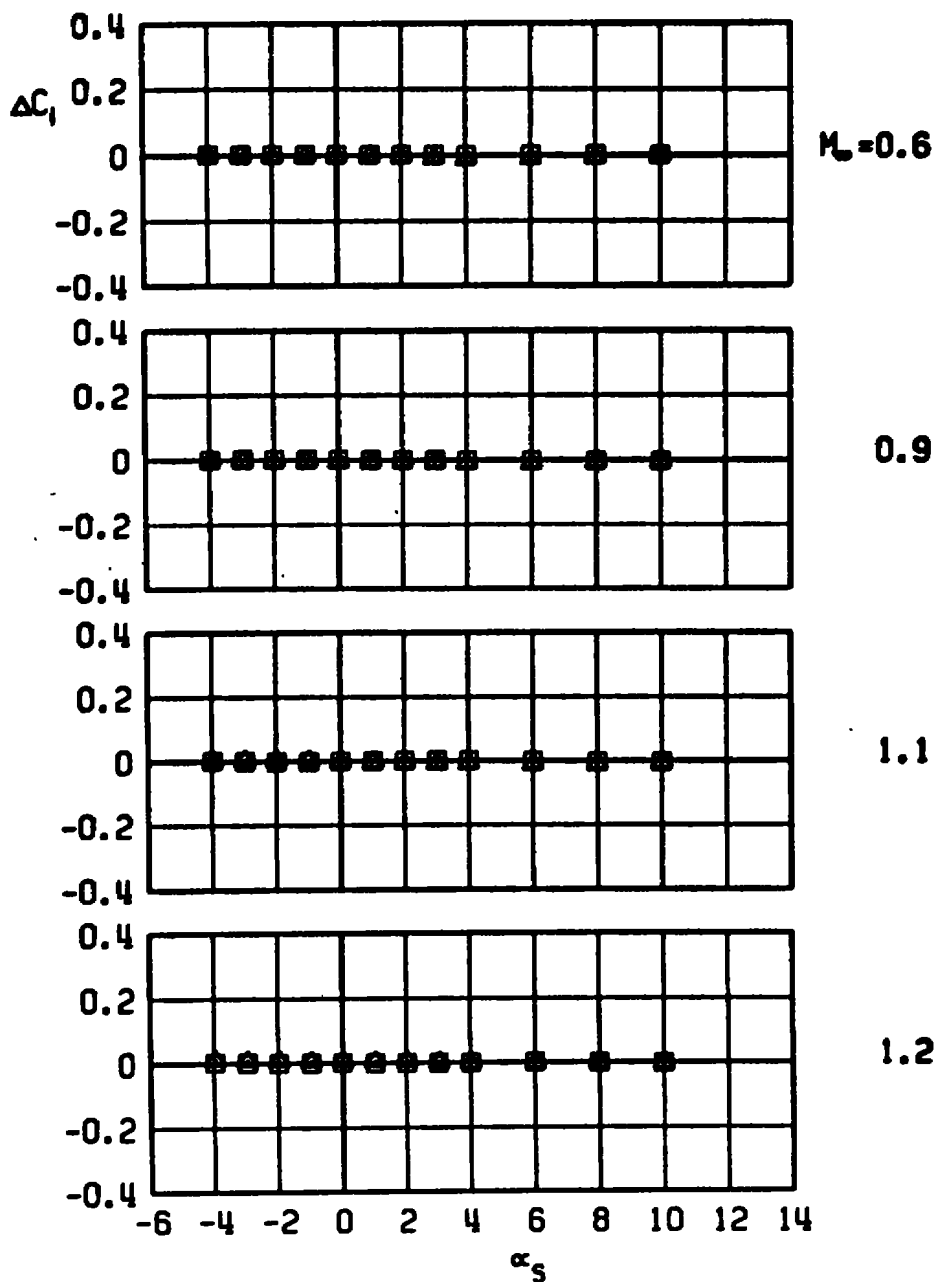
b. Side-force increment
 Figure 39. Continued.

CBU-24, LOB PYLON, MER-3
 WITH DUMMY STING, $D_3 = 0.57 D_0$
 WITH DUMMY STING, $D_3 = 0.92 D_0$



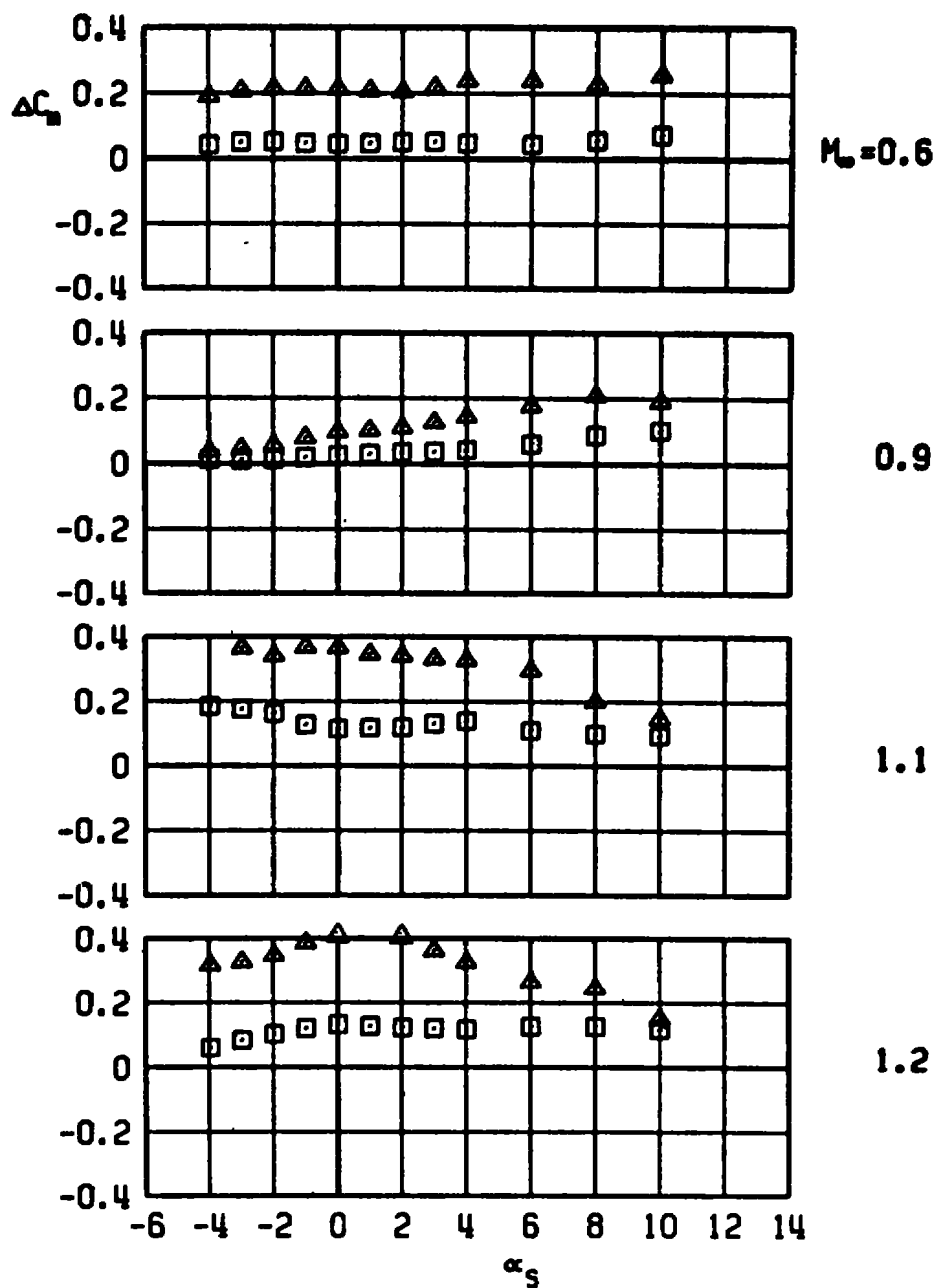
c. Axial-force increment
 Figure 39. Continued.

CBU-24, LOB PYLON, MER-3
 WITH DUMMY STING, $D_3 = 0.57 D_0$
 WITH DUMMY STING, $D_3 = 0.92 D_0$



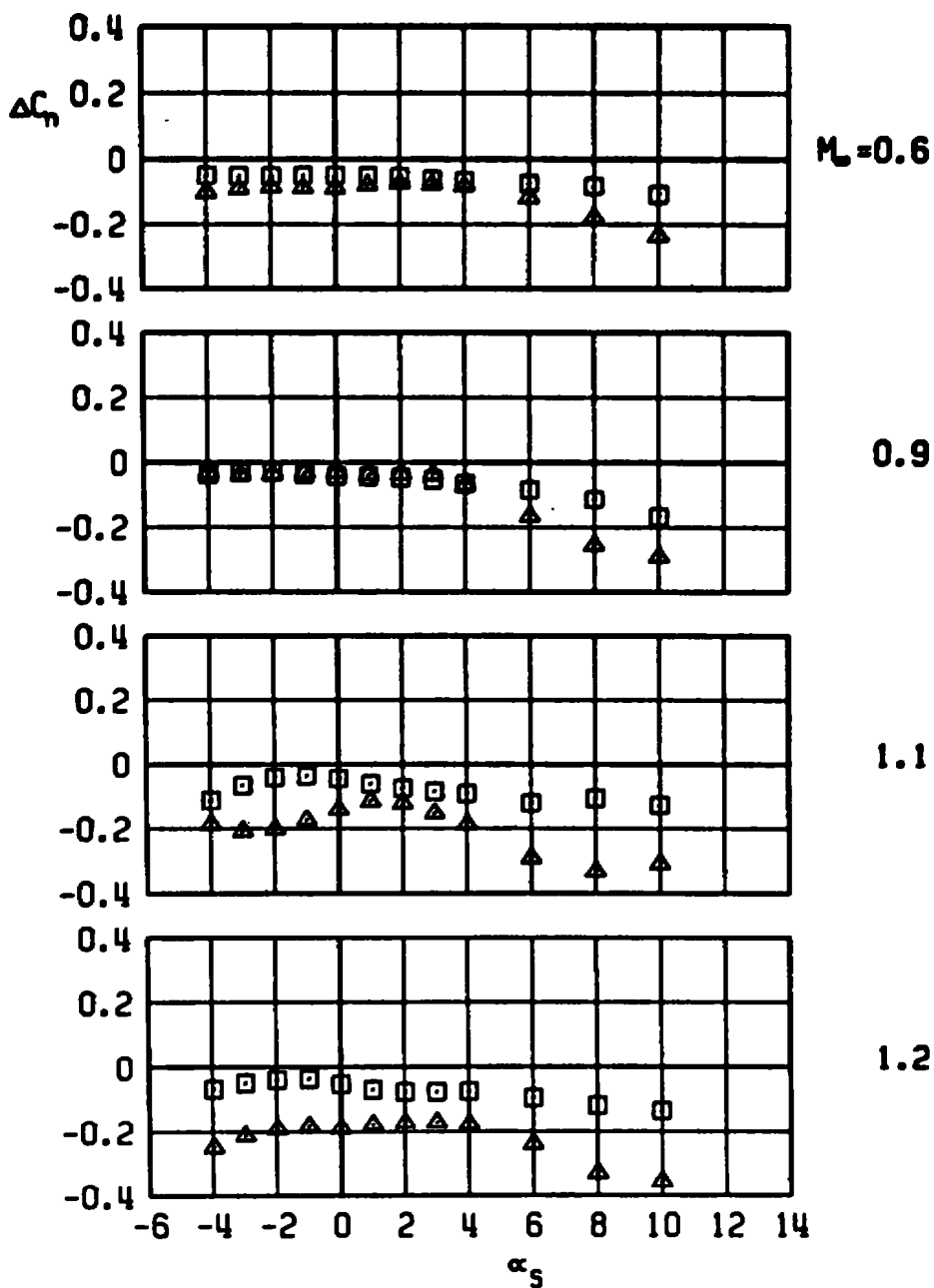
d. Rolling-moment increment
 Figure 39. Continued.

□ CBU-24, LOB PYLON, MER-3
 WITH DUMMY STING, $D_3 = 0.57 D_0$
 ▲ WITH DUMMY STING, $D_3 = 0.92 D_0$



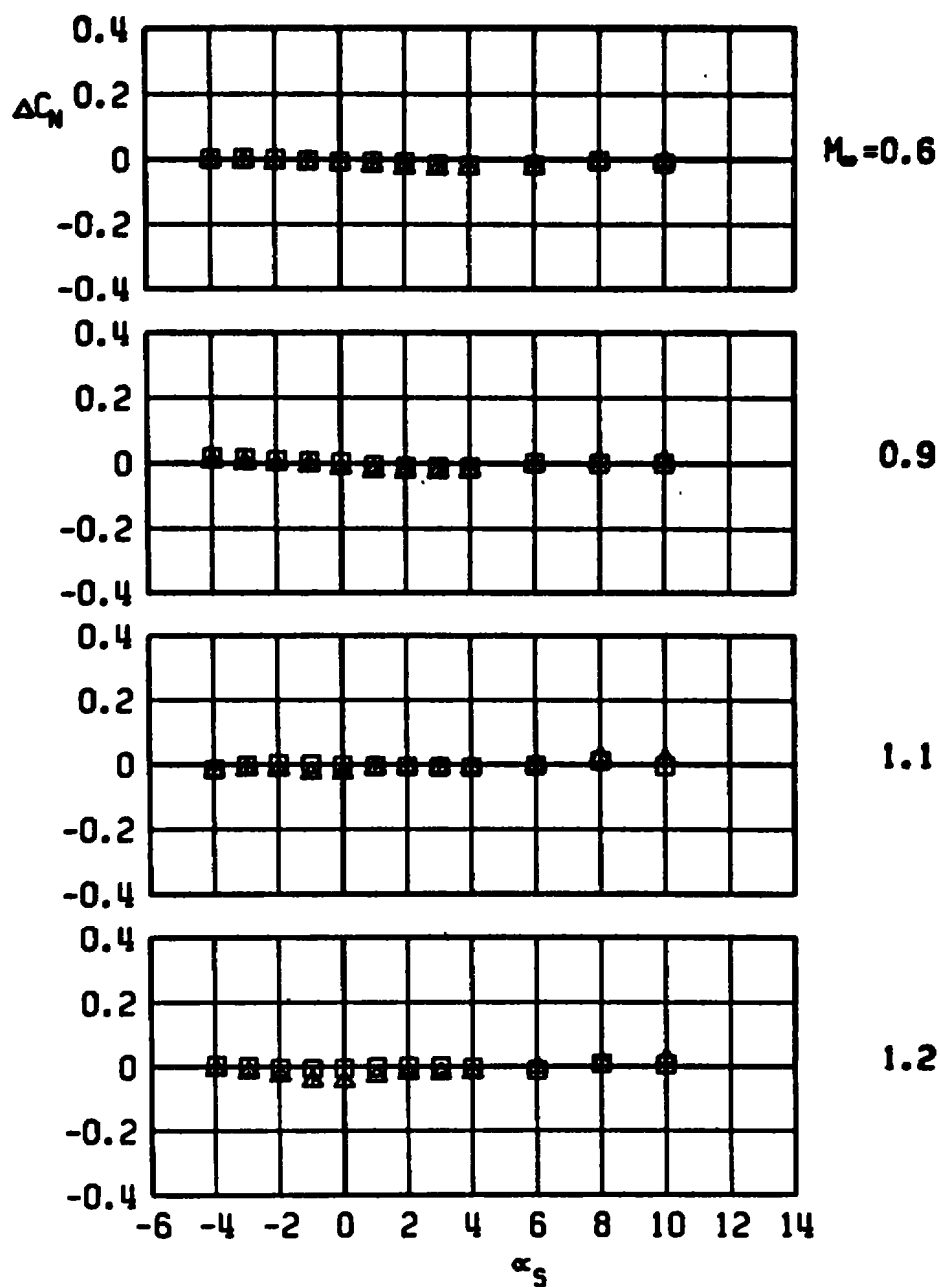
e. Pitching-moment increment
 Figure 39. Continued.

CBU-24, LOB PYLON, MER-3
 WITH DUMMY STING, $D_3 = 0.57 D_0$
 WITH DUMMY STING, $D_3 = 0.92 D_0$



f. Yawing-moment increment
 Figure 39. Concluded.

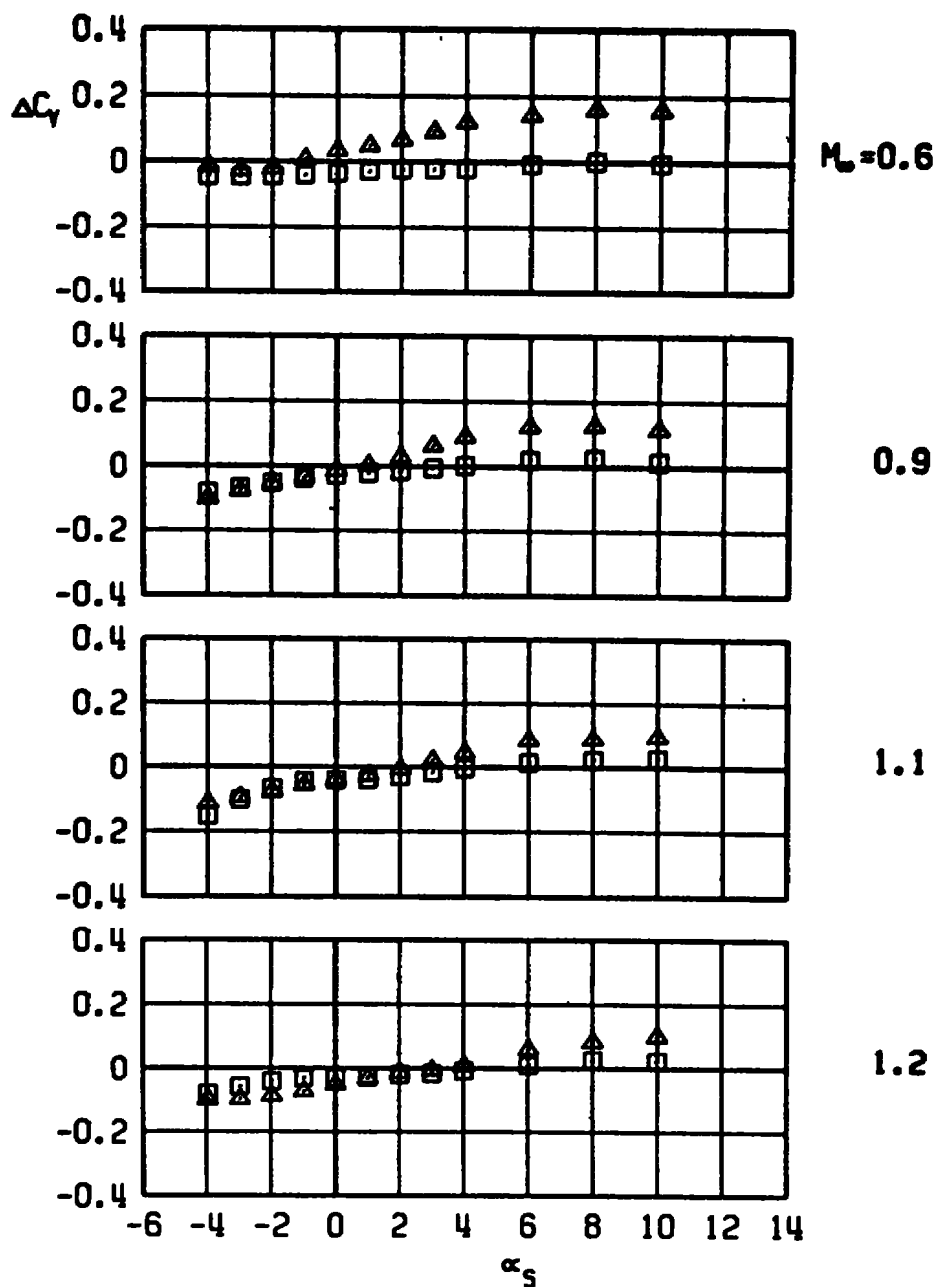
□ CBU-24, LOB PYLON, MER-4
 WITH DUMMY STING, $D_3 = 0.57 D_9$
 ▲ WITH DUMMY STING, $D_3 = 0.92 D_9$



a. Normal-force increment

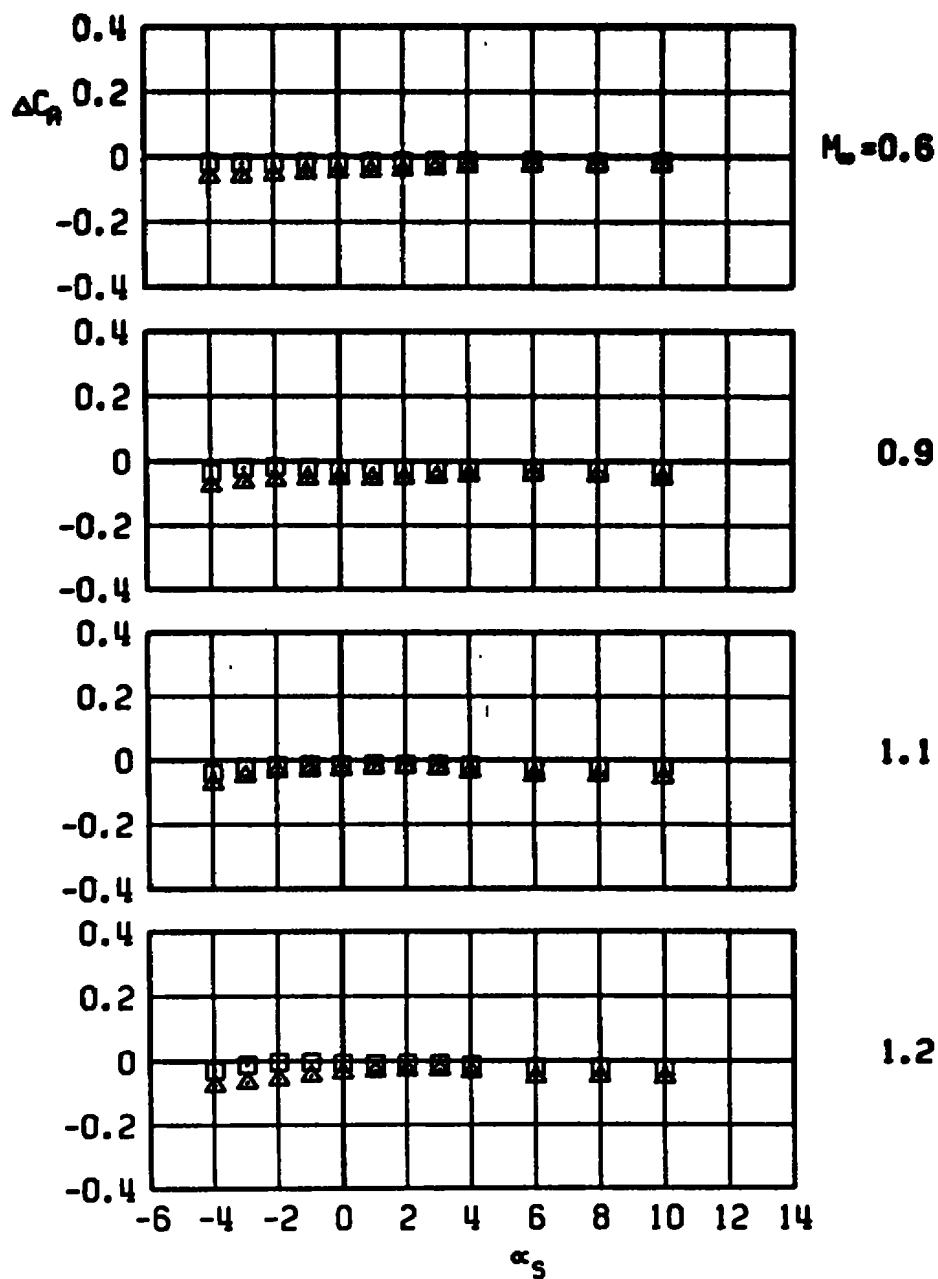
Figure 40. Sting-induced aerodynamic load increments as a function of angle of attack, stable rack-mounted store, MER station 4, LOB pylon.

CBU-24, LOB PYLON, MER-4
 WITH DUMMY STING, $D_3 = 0.57 D_0$
 WITH DUMMY STING, $D_3 = 0.92 D_0$



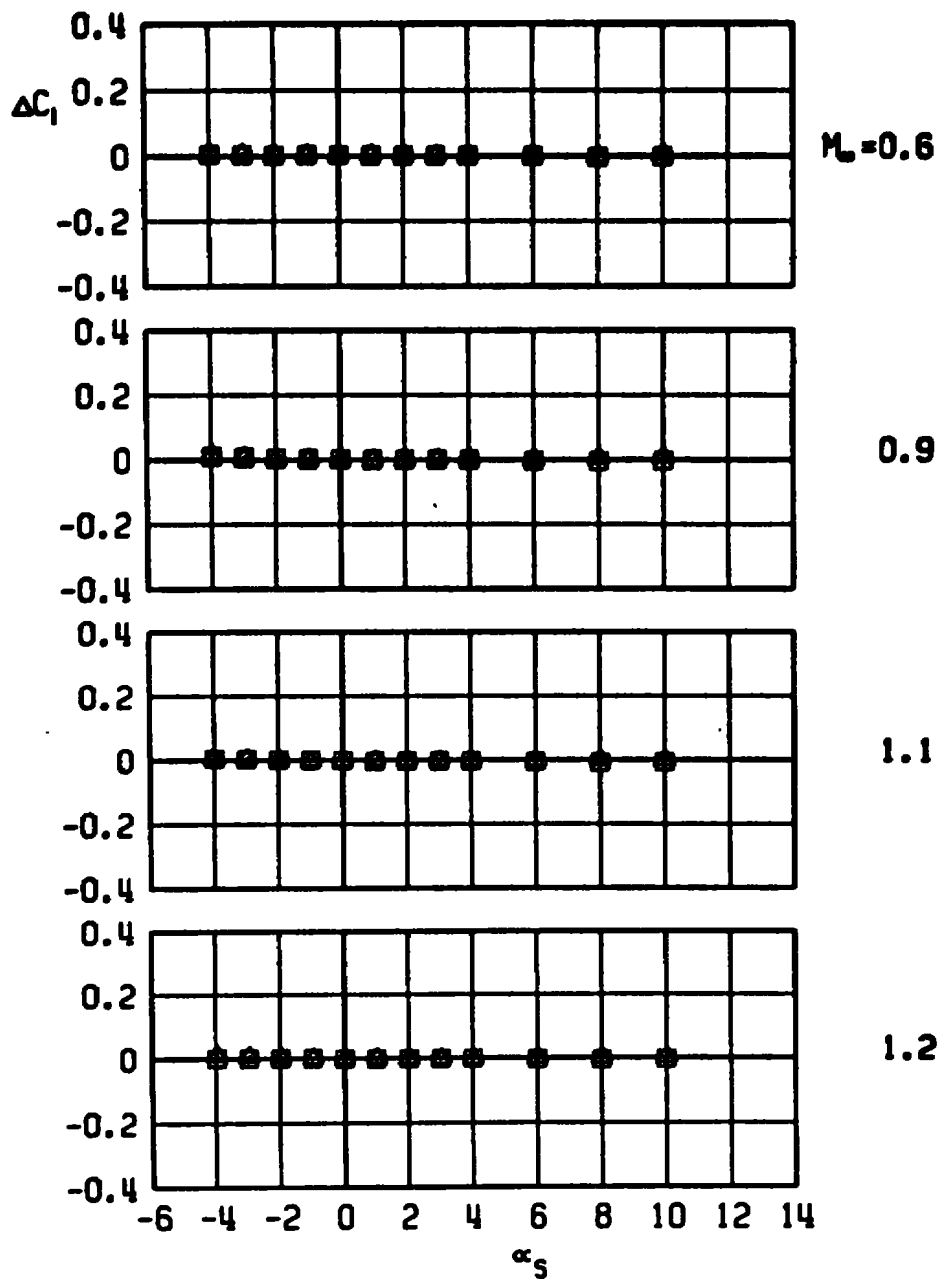
b. Side-force increment
 Figure 40. Continued.

□ CBU-24, LOB PYLON, MER-4
 WITH DUMMY STING, $D_s = 0.57 D_b$
 ▲ WITH DUMMY STING, $D_s = 0.92 D_b$



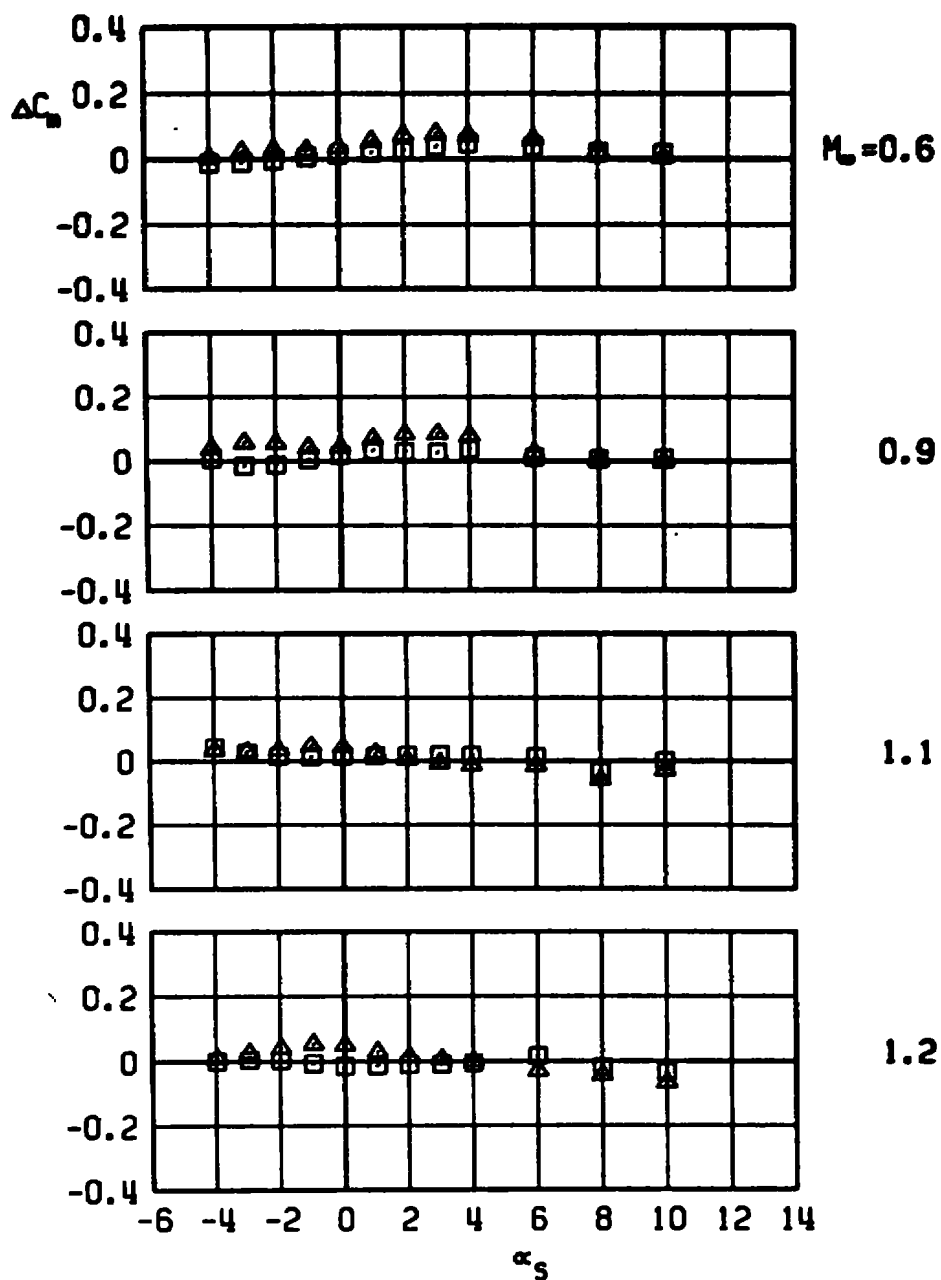
c. Axial-force increment
 Figure 40. Continued.

□ CBU-24, LOB PYLON, MER-4
 WITH DUMMY STING, $D_3 = 0.57 D_0$
 ▲ WITH DUMMY STING, $D_3 = 0.92 D_0$



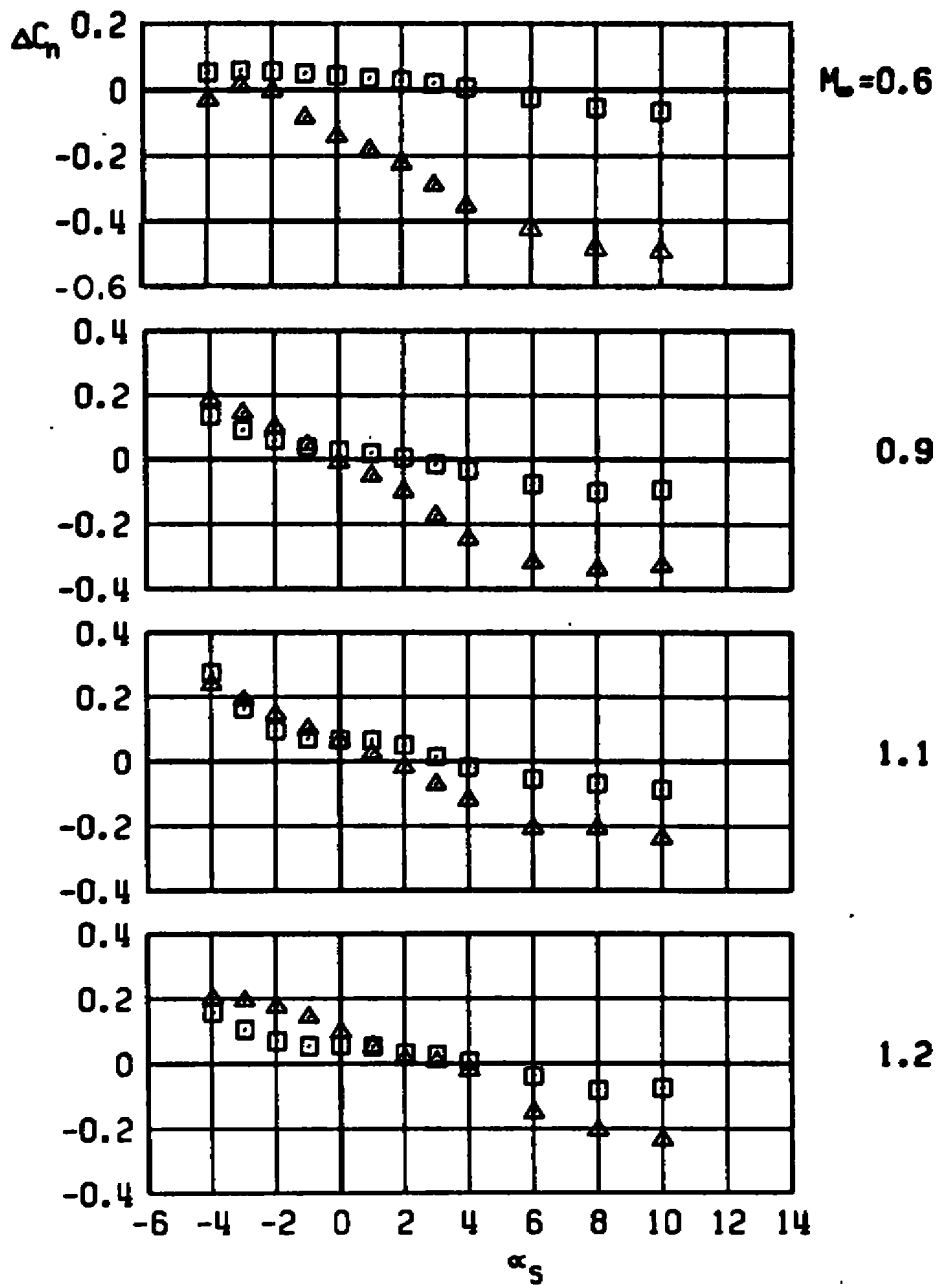
d. Rolling-moment increment
 Figure 40. Continued.

□ CBU-24, LOB PYLON, MER-4
 WITH DUMMY STING, $D_3 = 0.57 D_0$
 ▲ WITH DUMMY STING, $D_3 = 0.92 D_0$



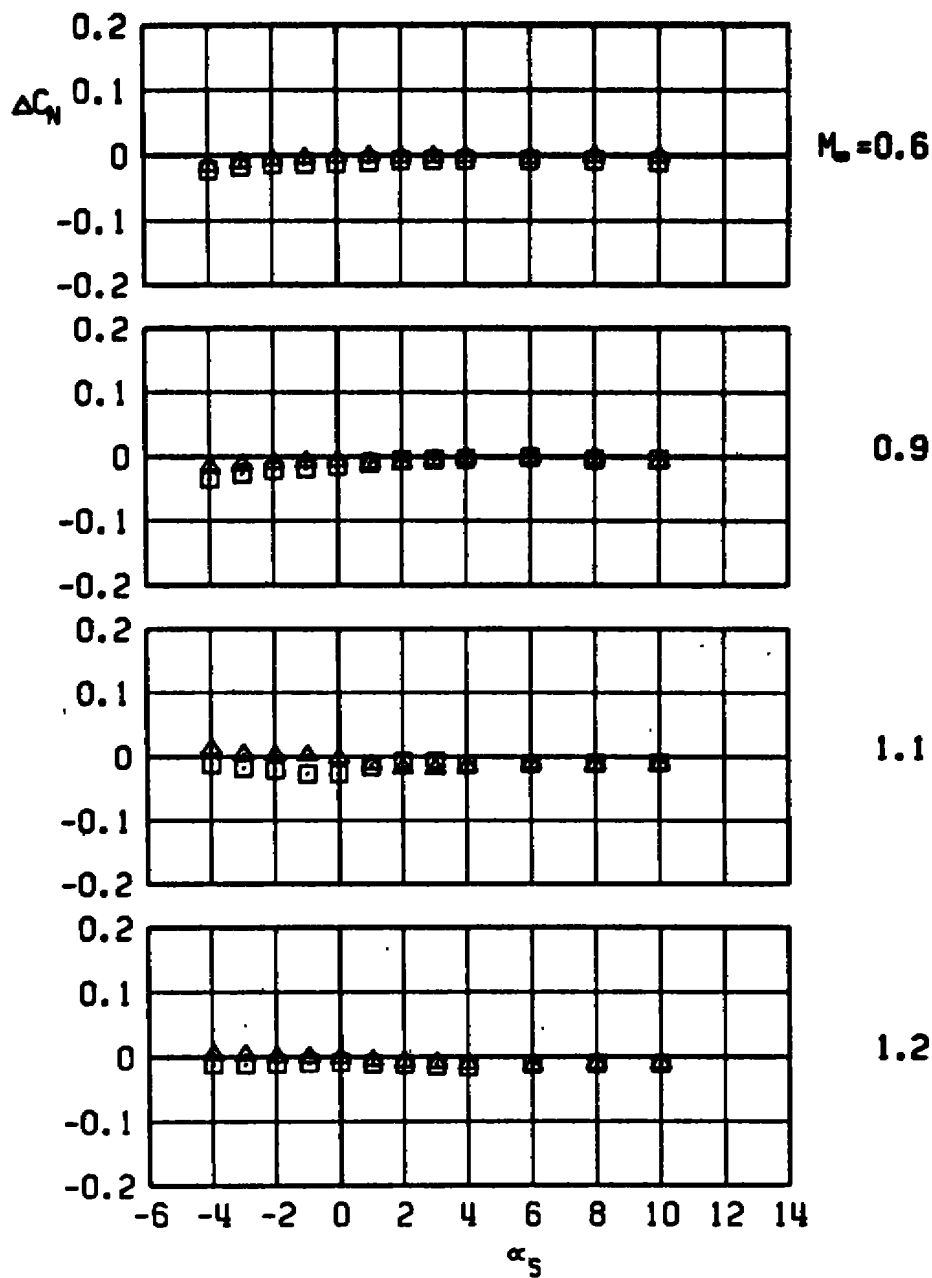
e. Pitching-moment increment
 Figure 40. Continued.

CBU-24, LOB PYLON, MER-4
 □ WITH DUMMY STING, $D_3 = 0.57 D_0$
 ▲ WITH DUMMY STING, $D_3 = 0.92 D_0$



f. Yawing-moment increment
 Figure 40. Concluded.

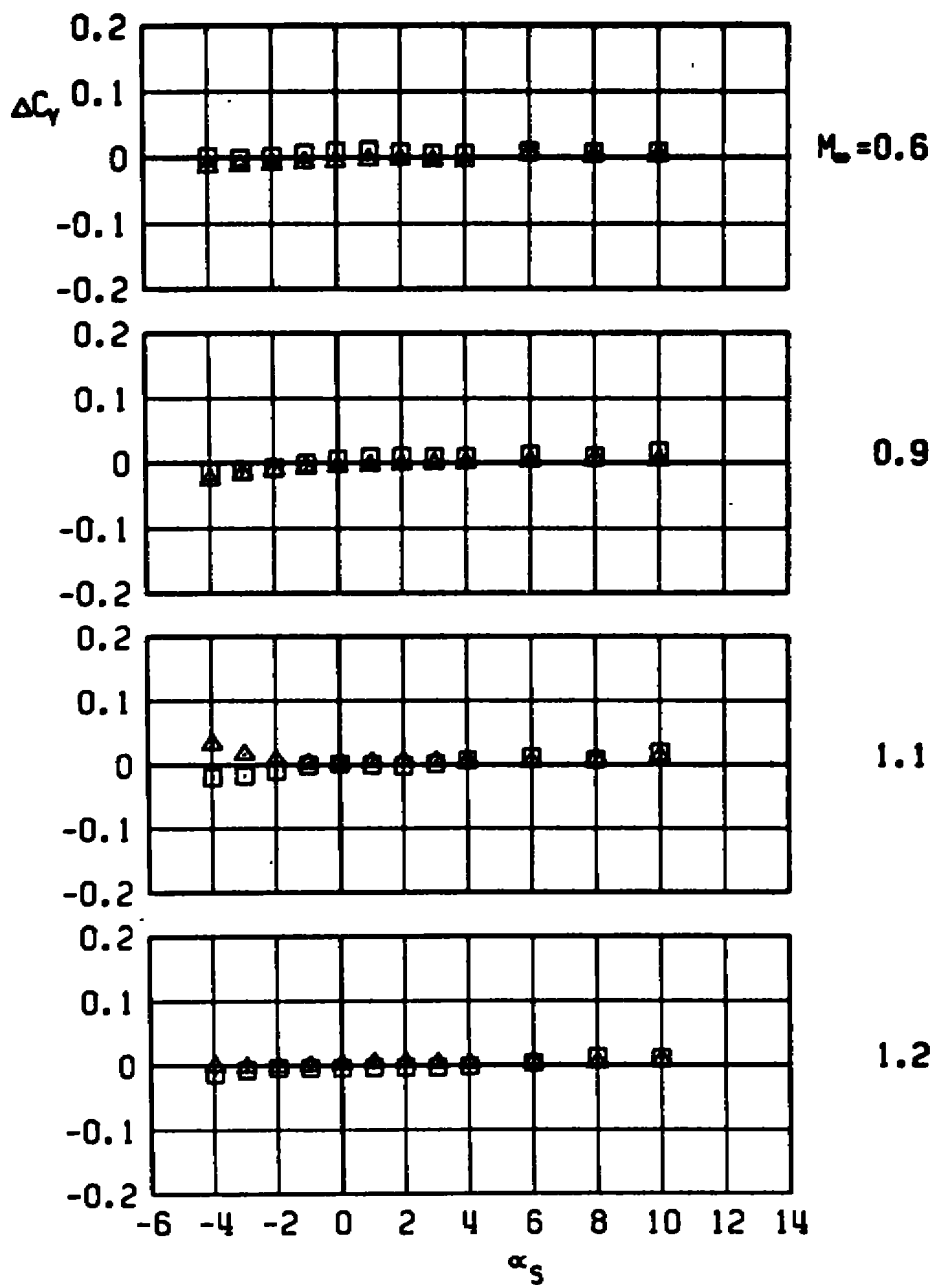
MK 83, LIB PYLON
 □ AB2, TER-3, $D_3 = 0.53 D_0$
 ▲ AB3, TER-3, $D_3 = 0.40 D_0$



a. Normal-force increment

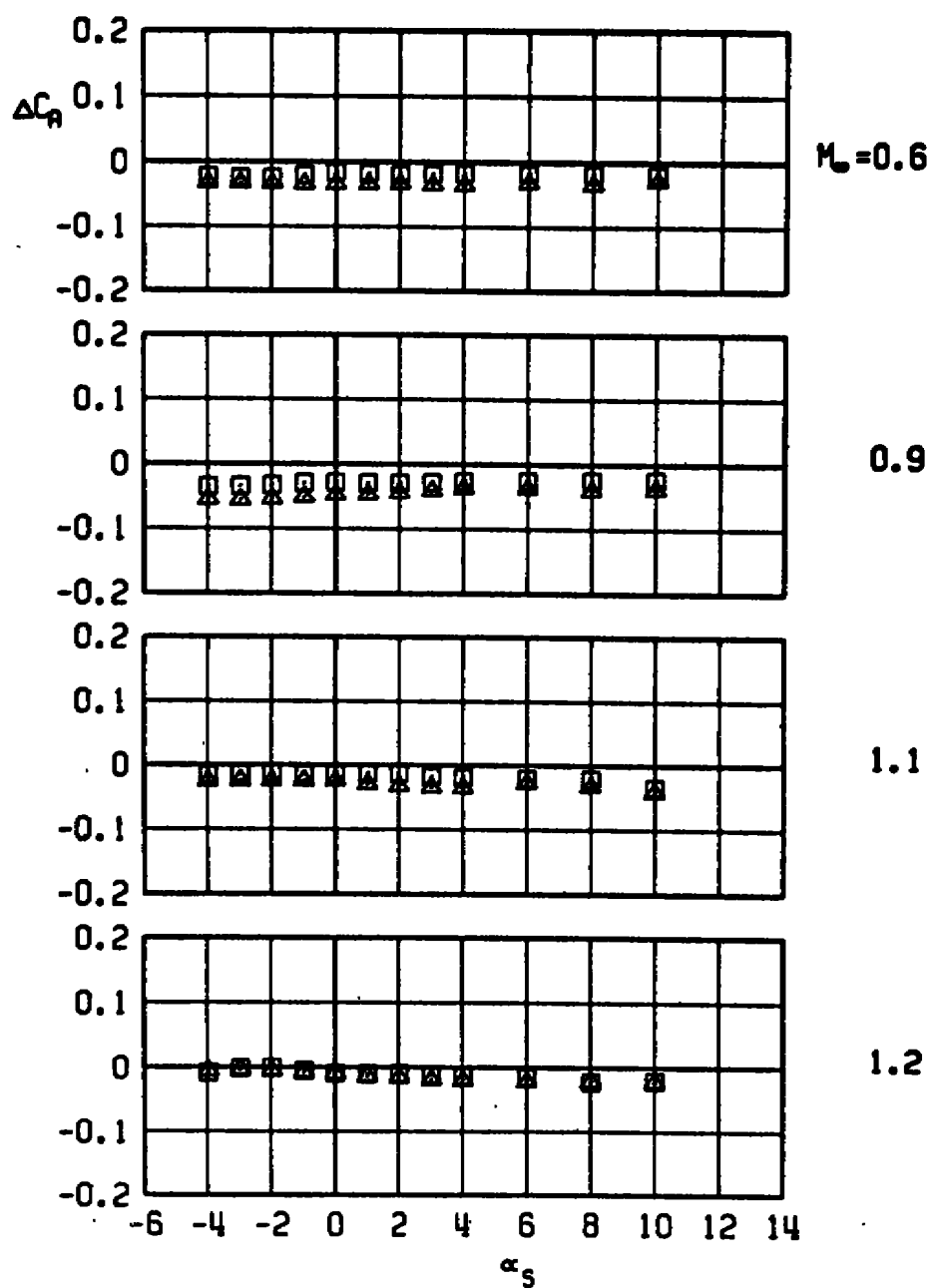
Figure 41. Sting-induced aerodynamic load increments as a function of angle of attack, stable rack-mounted store, TER station 3, LIB pylon.

MK 83, LIB PYLON
 □ AB2, TER-3, $D_3 = 0.53 D_0$
 ▲ AB3, TER-3, $D_3 = 0.40 D_0$



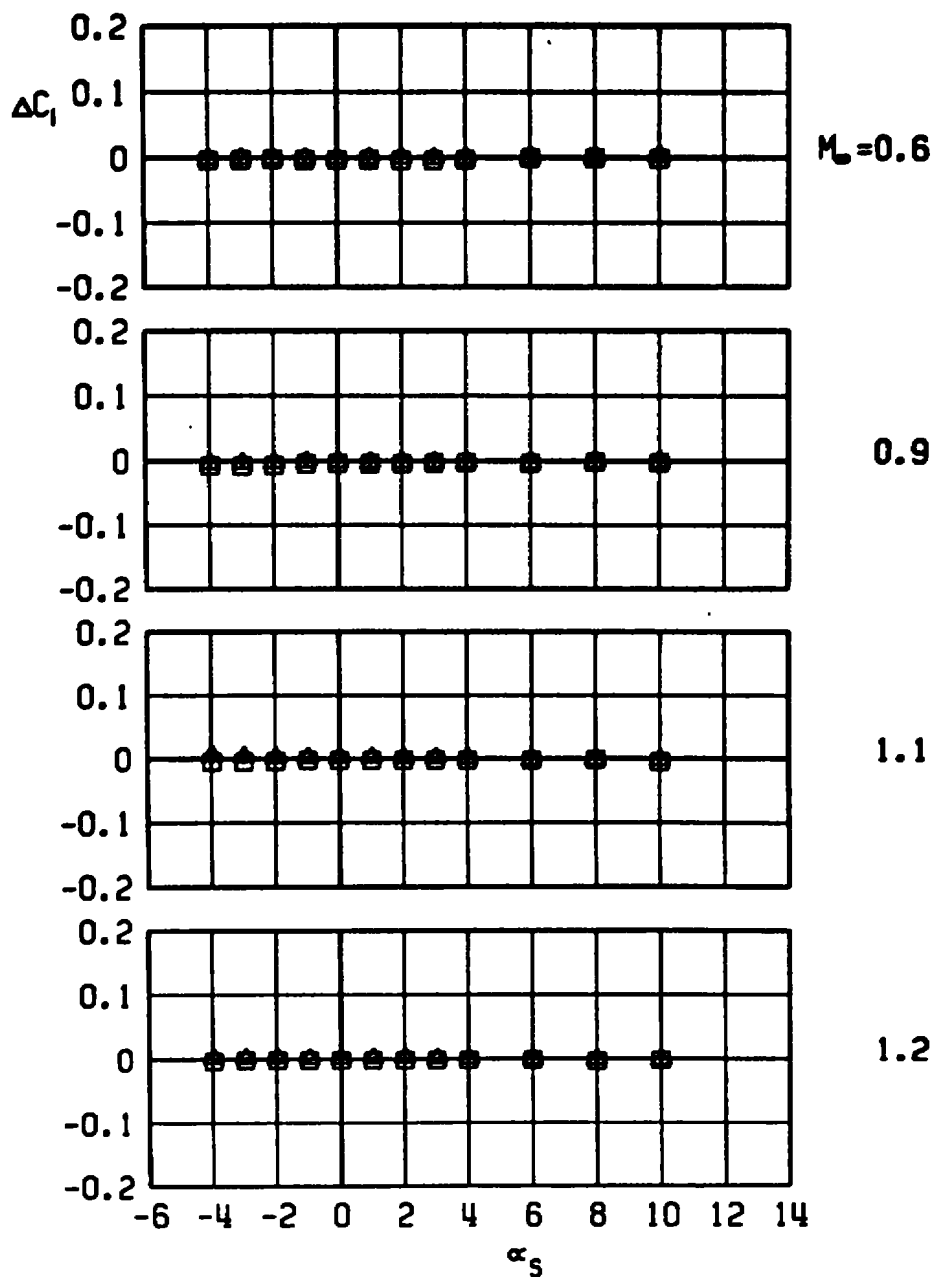
b. Side-force increment
 Figure 41. Continued.

MK 83, LIB PYLON
 □ AB2, TER-3, $D_3 = 0.53 D_9$
 △ AB3, TER-3, $D_3 = 0.40 D_9$



c. Axial-force increment
 Figure 41. Continued.

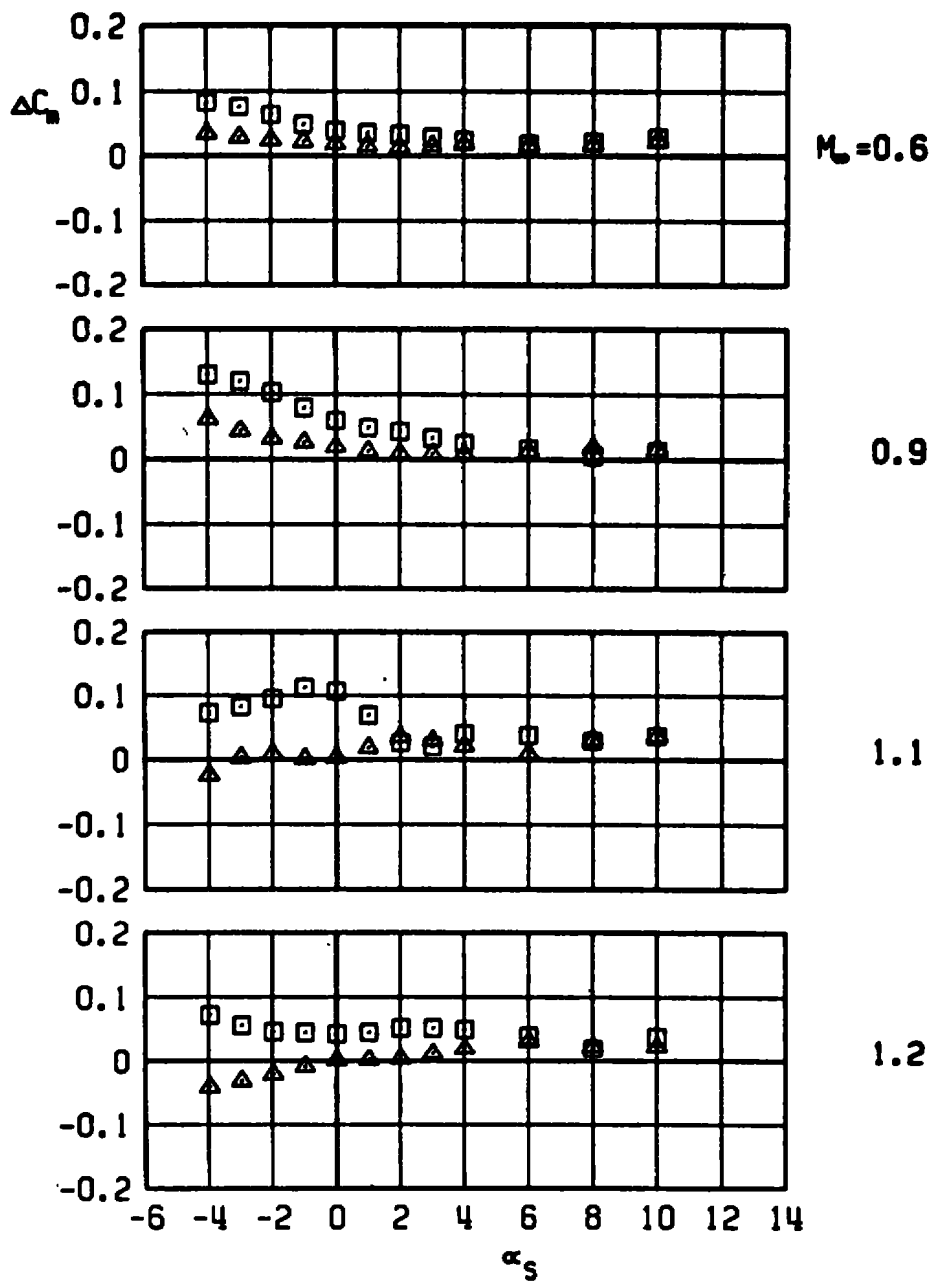
MK 83, LIB PYLON
 □ AB2, TER-3, $D_3 = 0.53 D_0$
 △ AB3, TER-3, $D_3 = 0.40 D_0$



d. Rolling-moment increment
Figure 41. Continued.

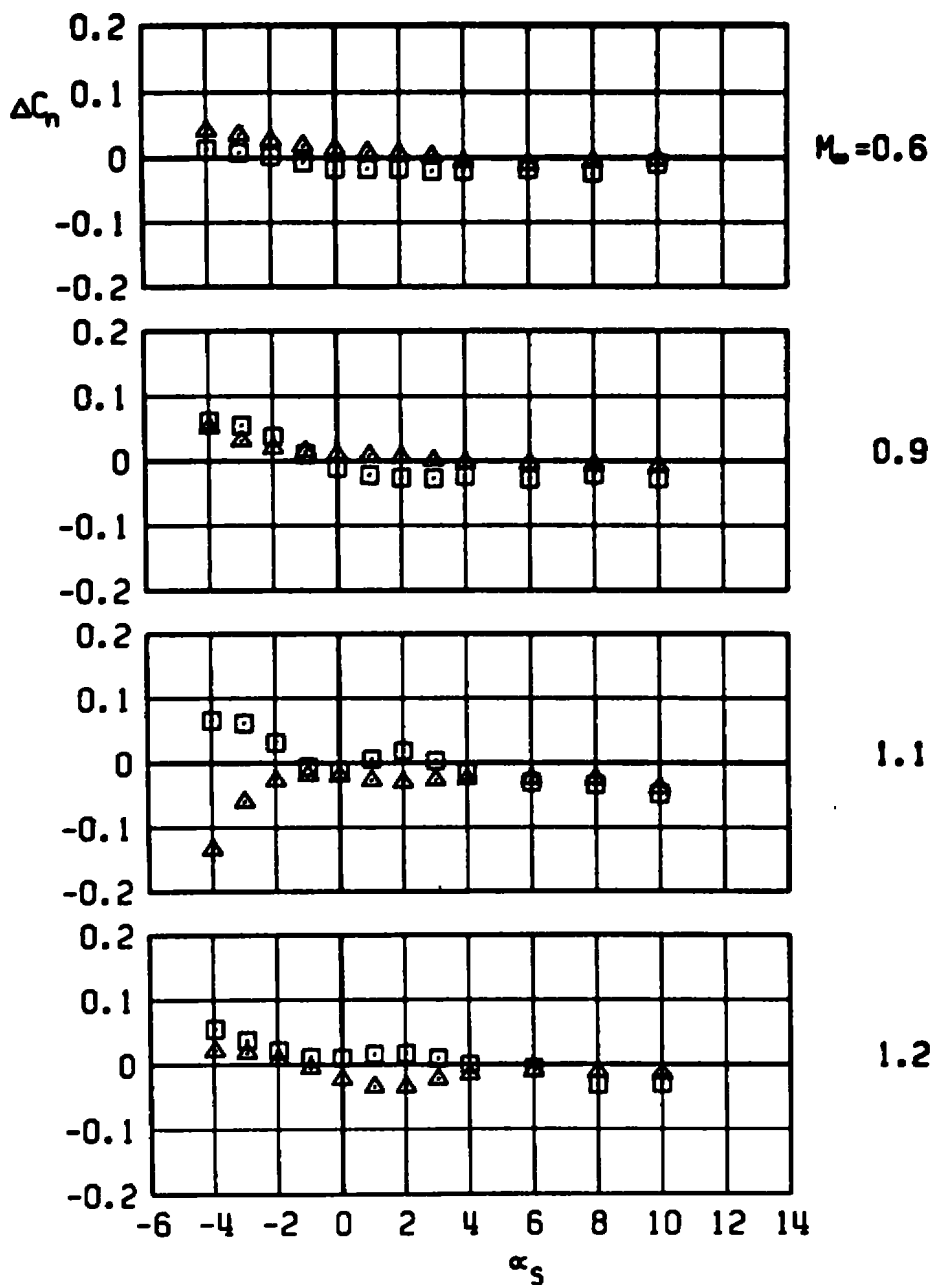
MK 83, LIB PYLON

□ AB2, TER-3, $D_3 = 0.53 D_0$
 ▲ AB3, TER-3, $D_3 = 0.40 D_0$

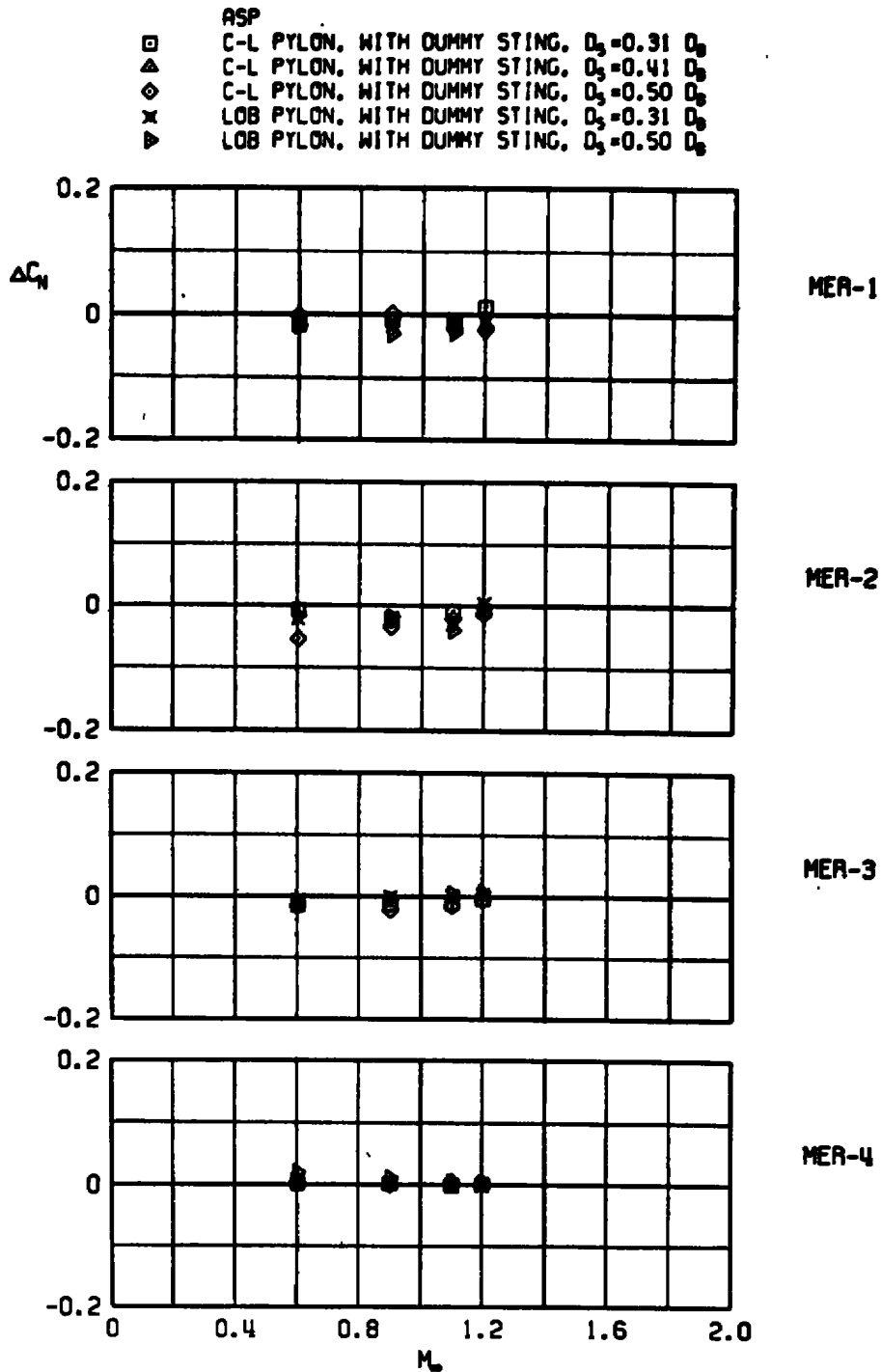


e. Pitching-moment increment
 Figure 41. Continued.

MK 83, LIB PYLON
 □ AB2, TER-3, $D_3 = 0.53 D_0$
 ▲ AB3, TER-3, $D_3 = 0.40 D_0$

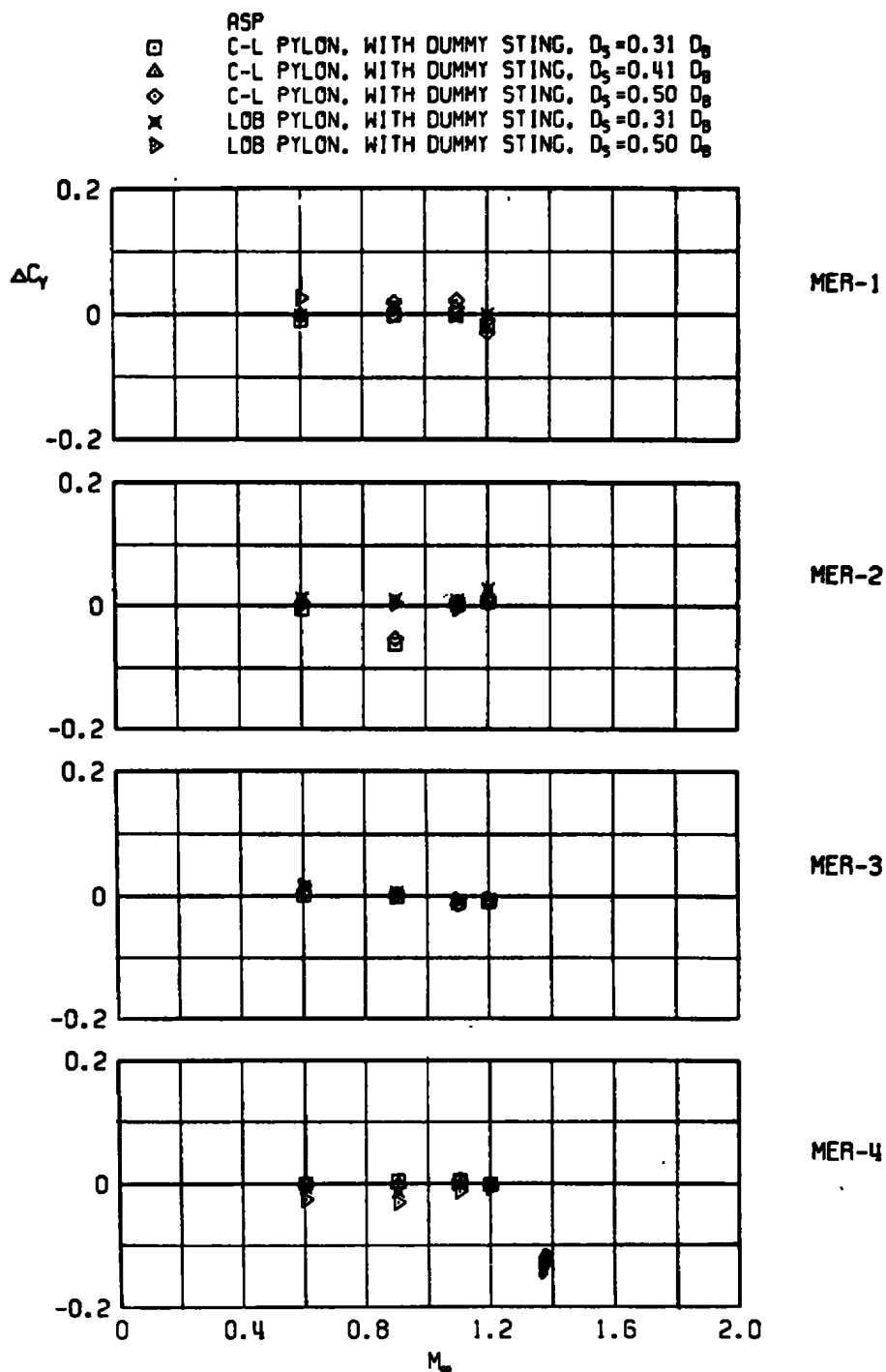


f. Yawing-moment increment
Figure 41. Concluded.

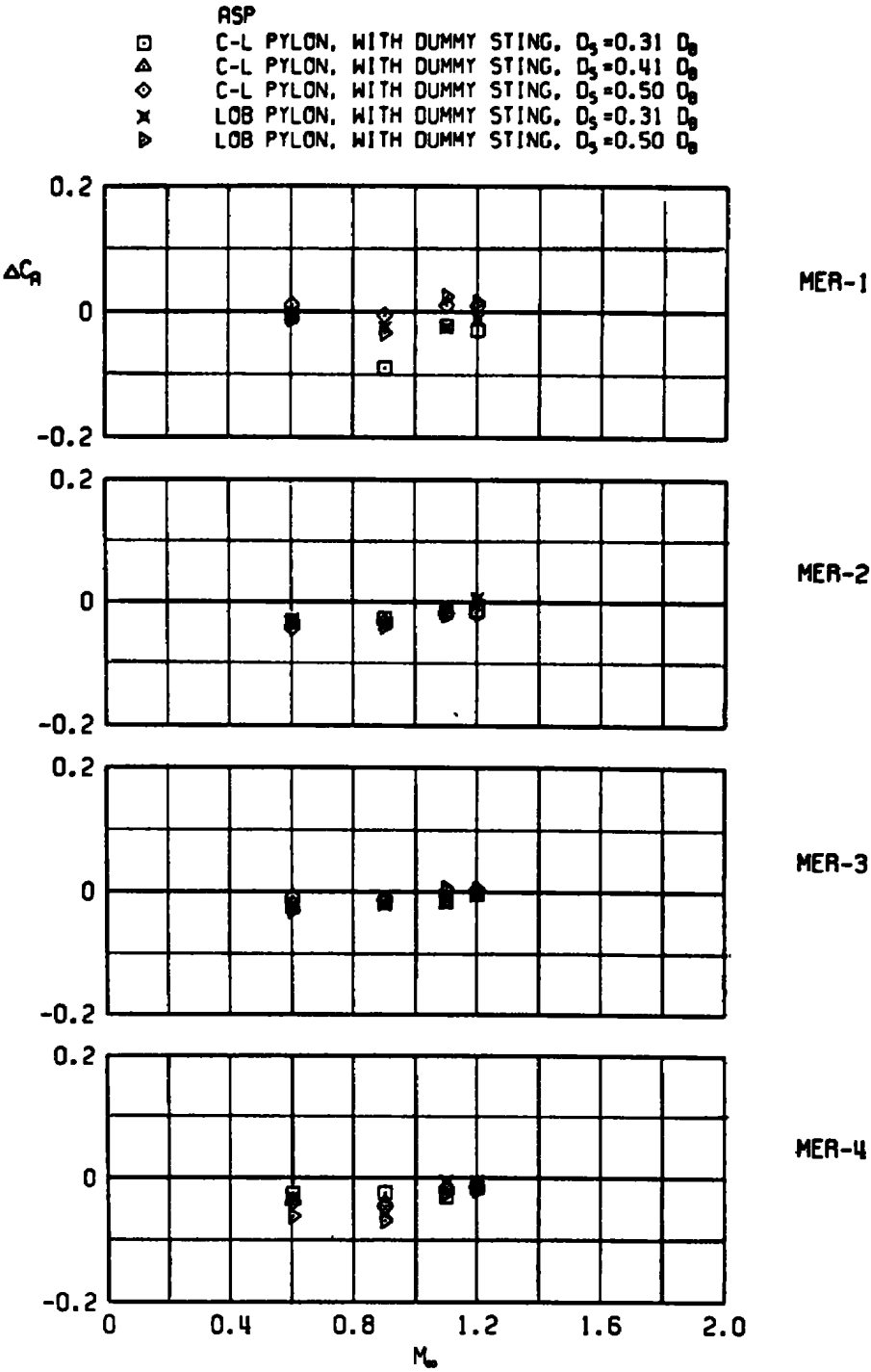


a. Normal-force increment

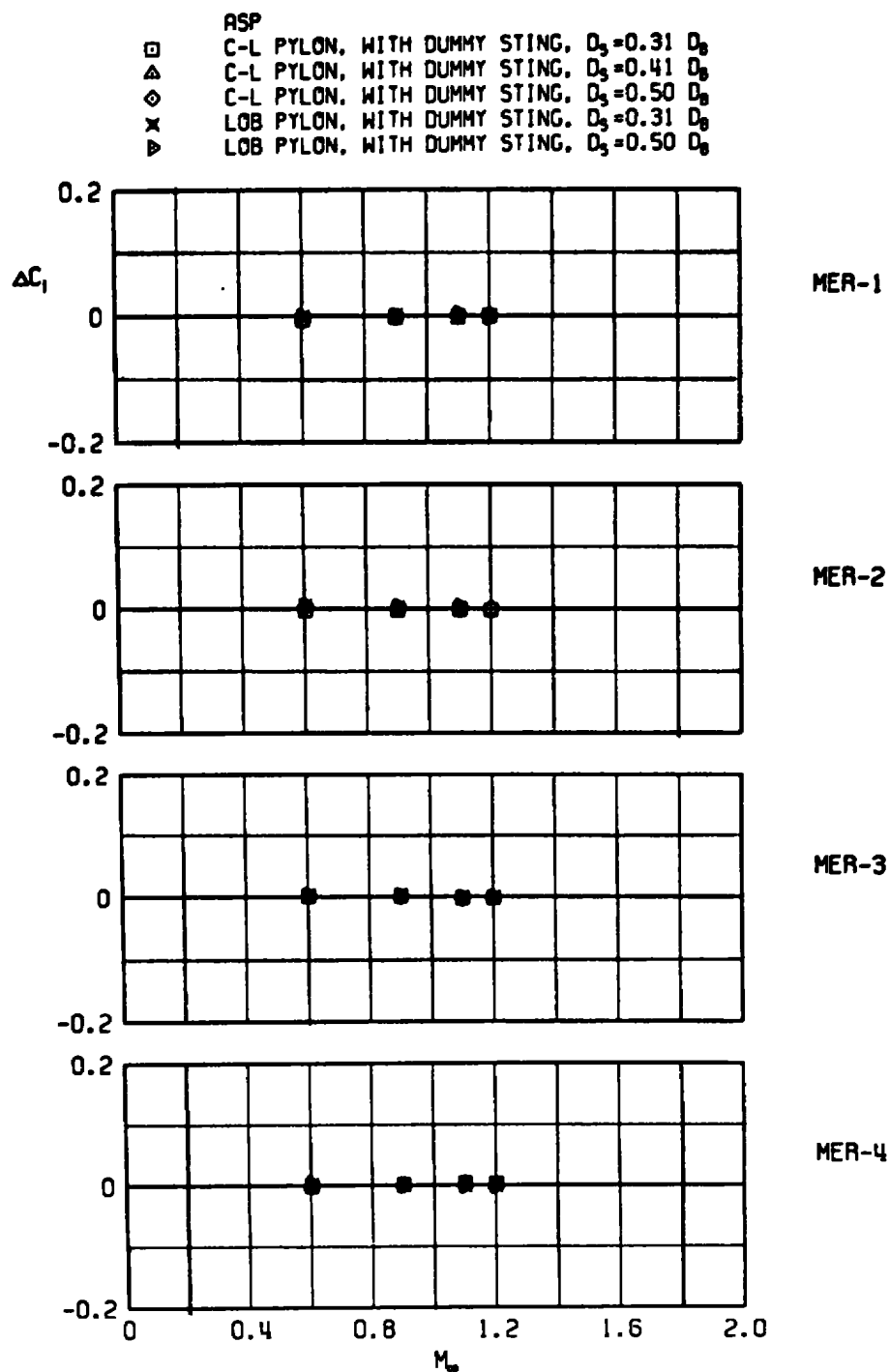
Figure 42. Sting-induced aerodynamic load increments as a function of Mach number, unstable rack-mounted store, C-L and LOB pylon.



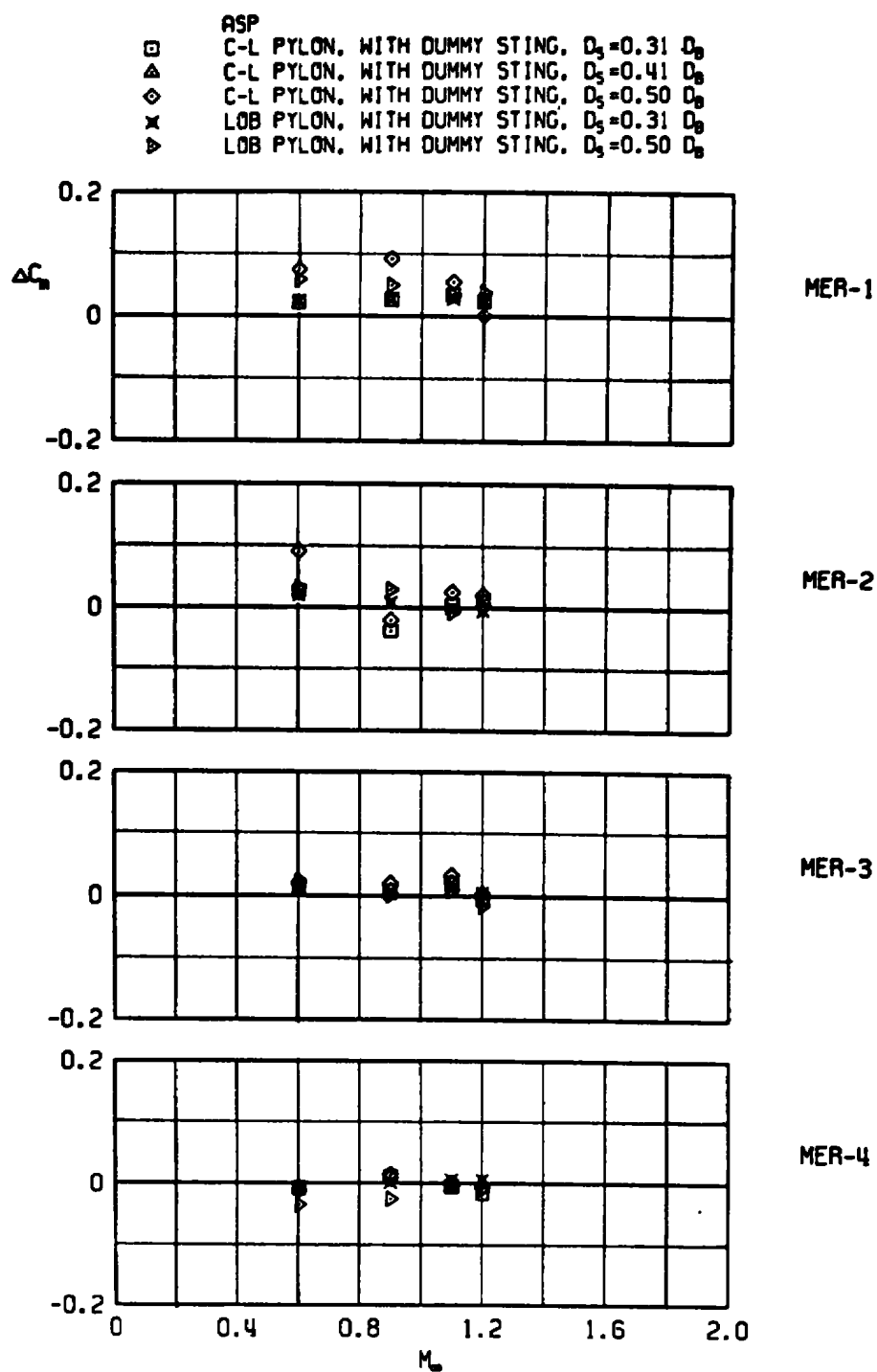
b. Side-force increment
 Figure 42. Continued.



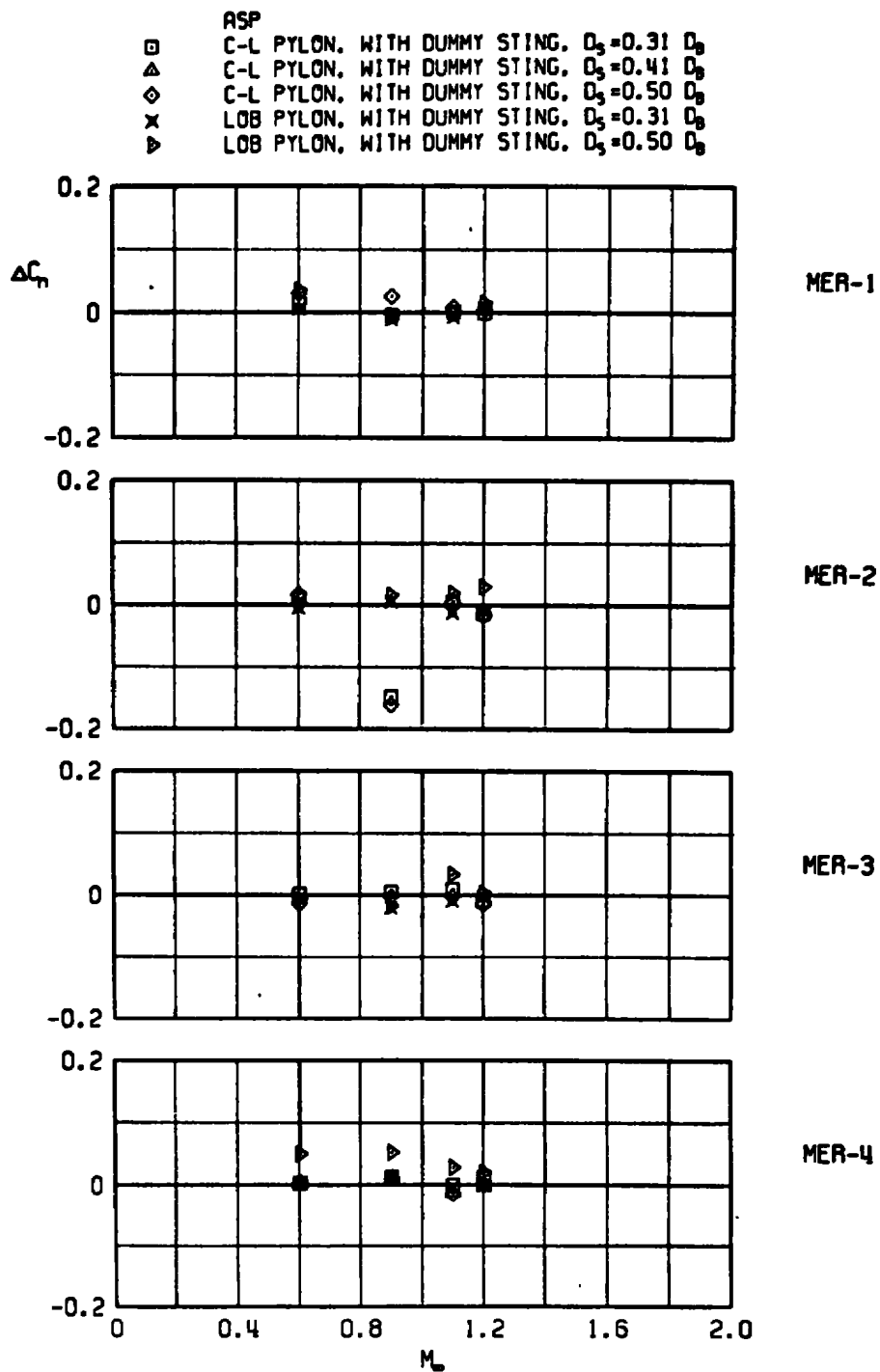
c. Axial-force increment
Figure 42. Continued.



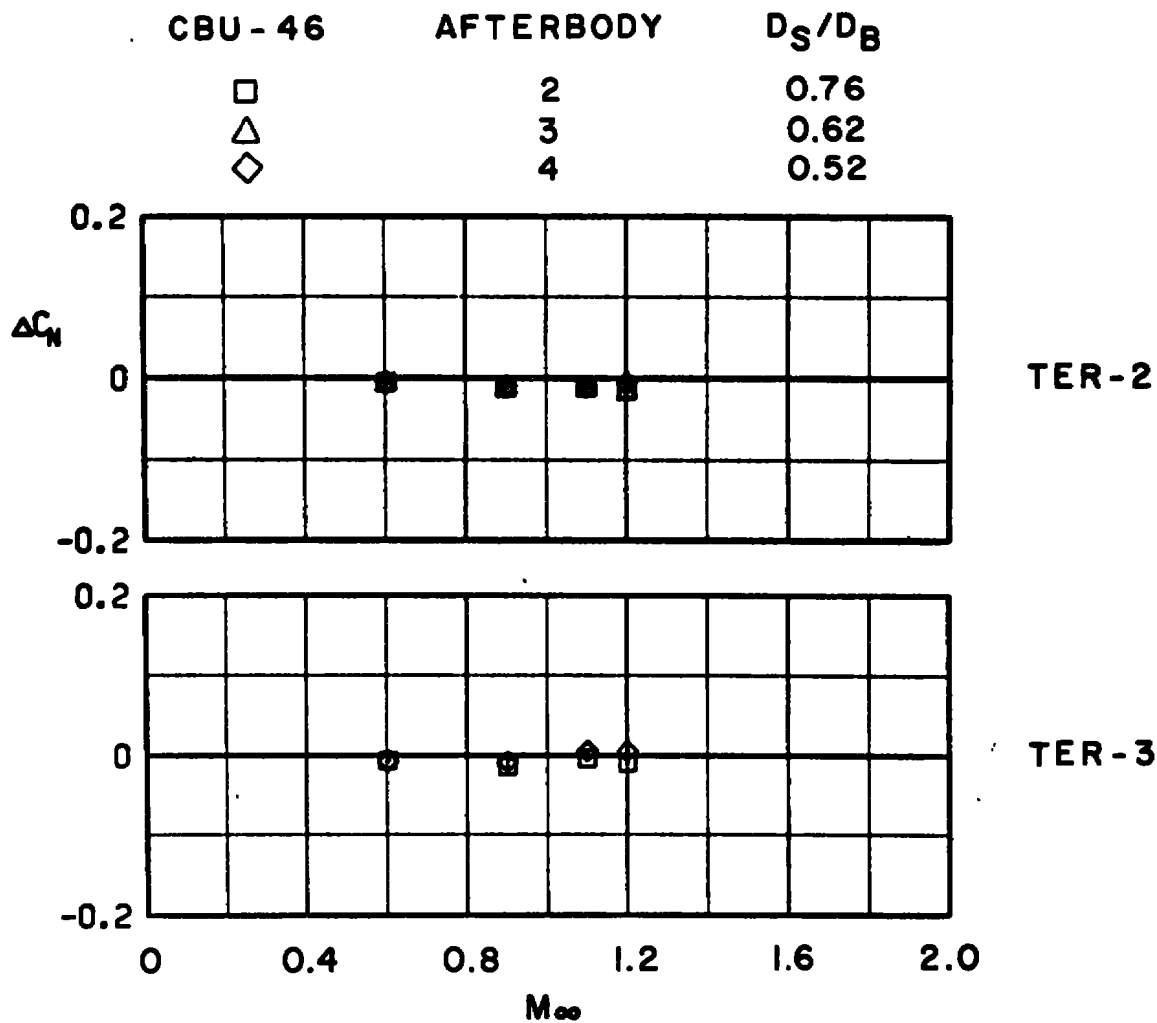
d. Rolling-moment increment
Figure 42. Continued.



e. Pitching-moment increment
 Figure 42. Continued.

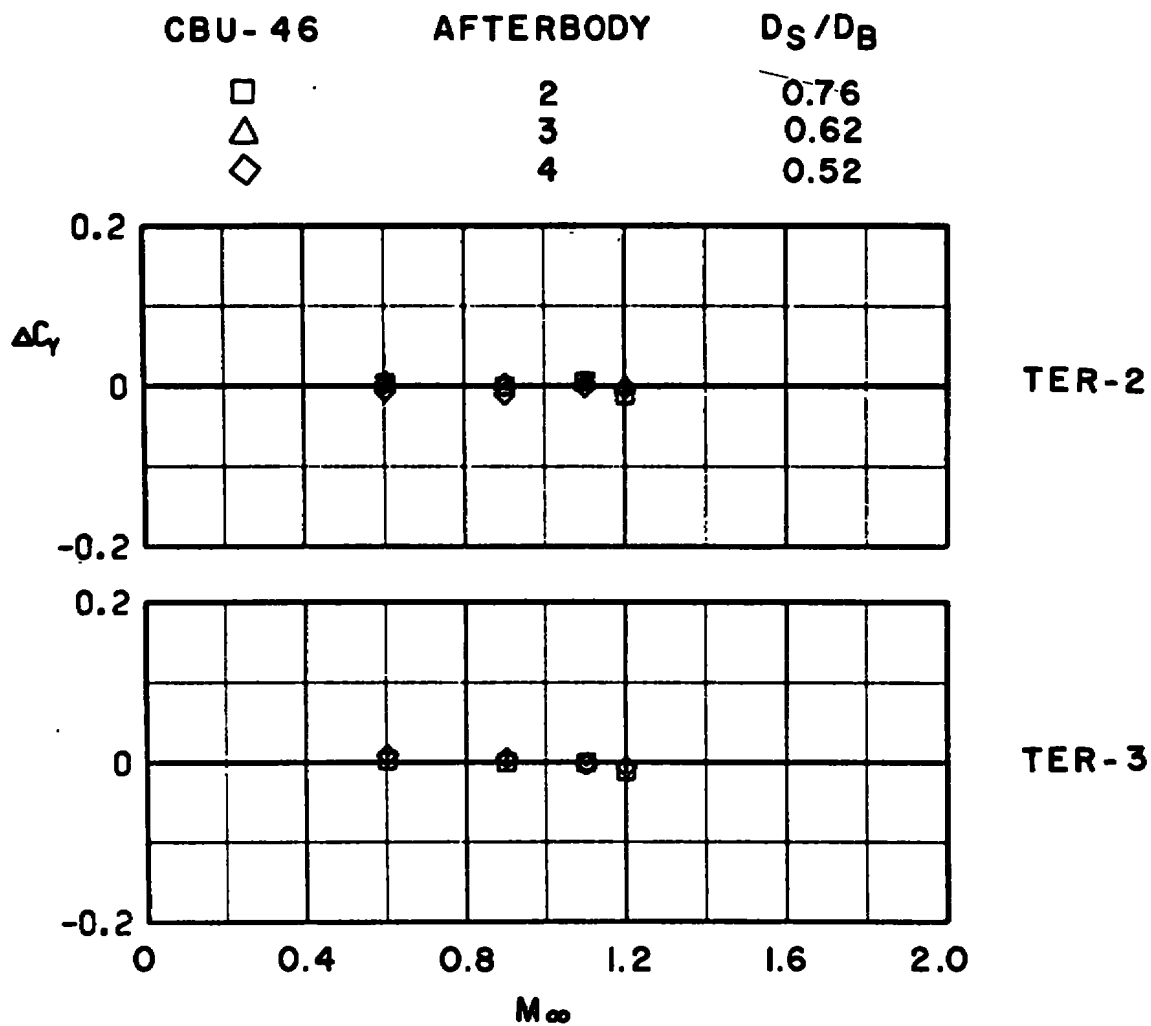


f. Yawing-moment increment
Figure 42. Concluded.

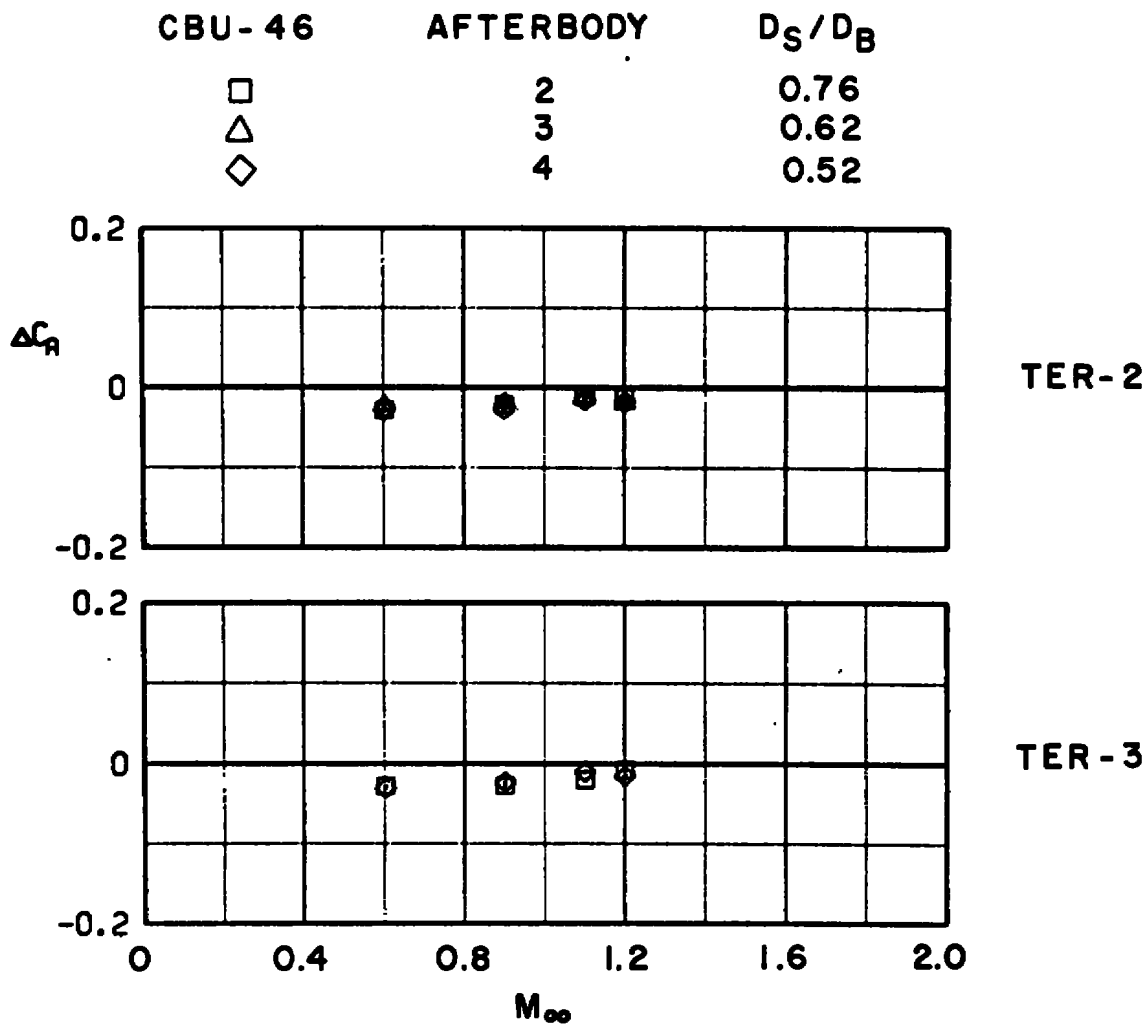


a. Normal-force increment

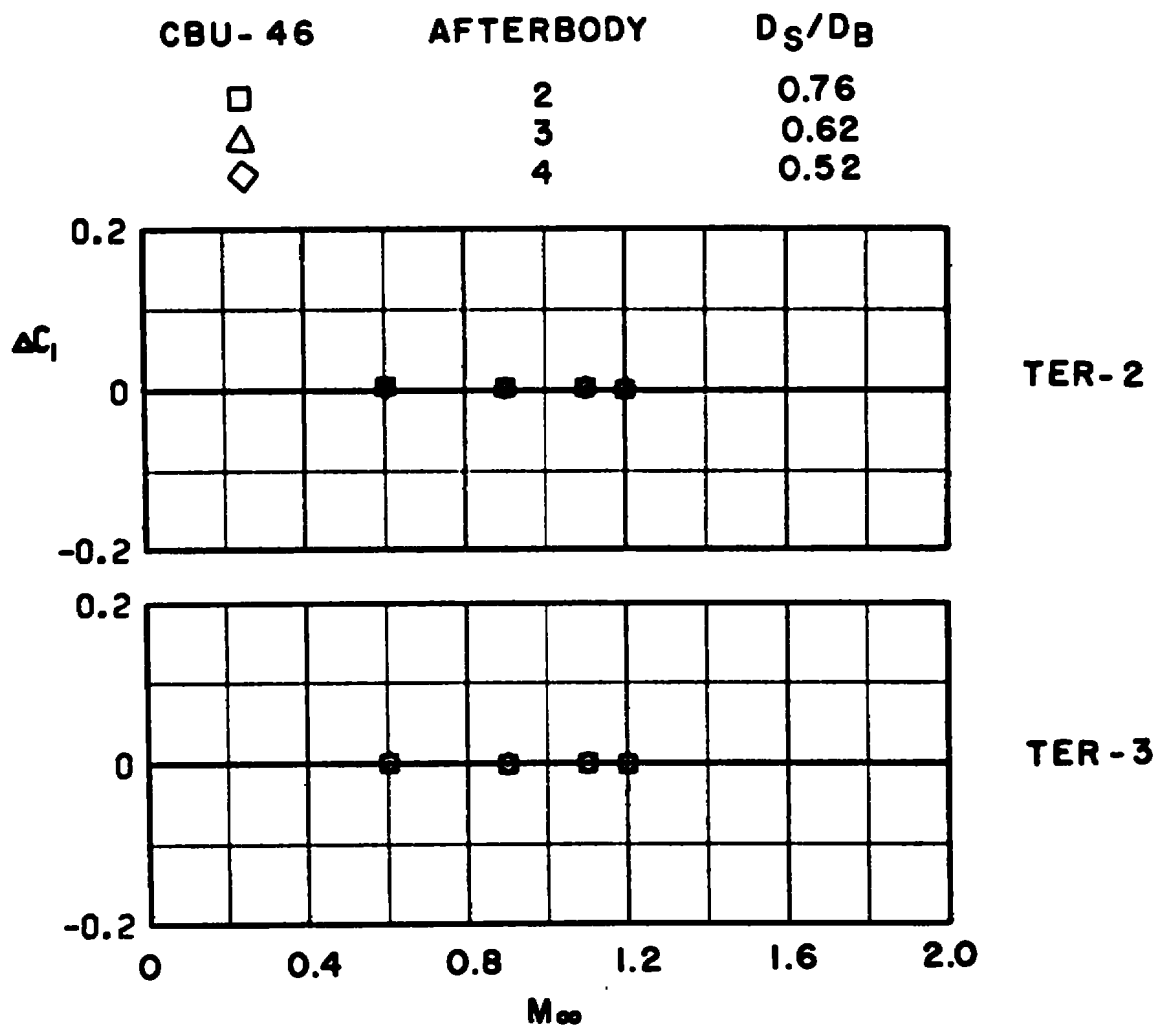
Figure 43. Sting-induced aerodynamic load increments as a function of Mach number, unstable rack-mounted store, LIB pylon.



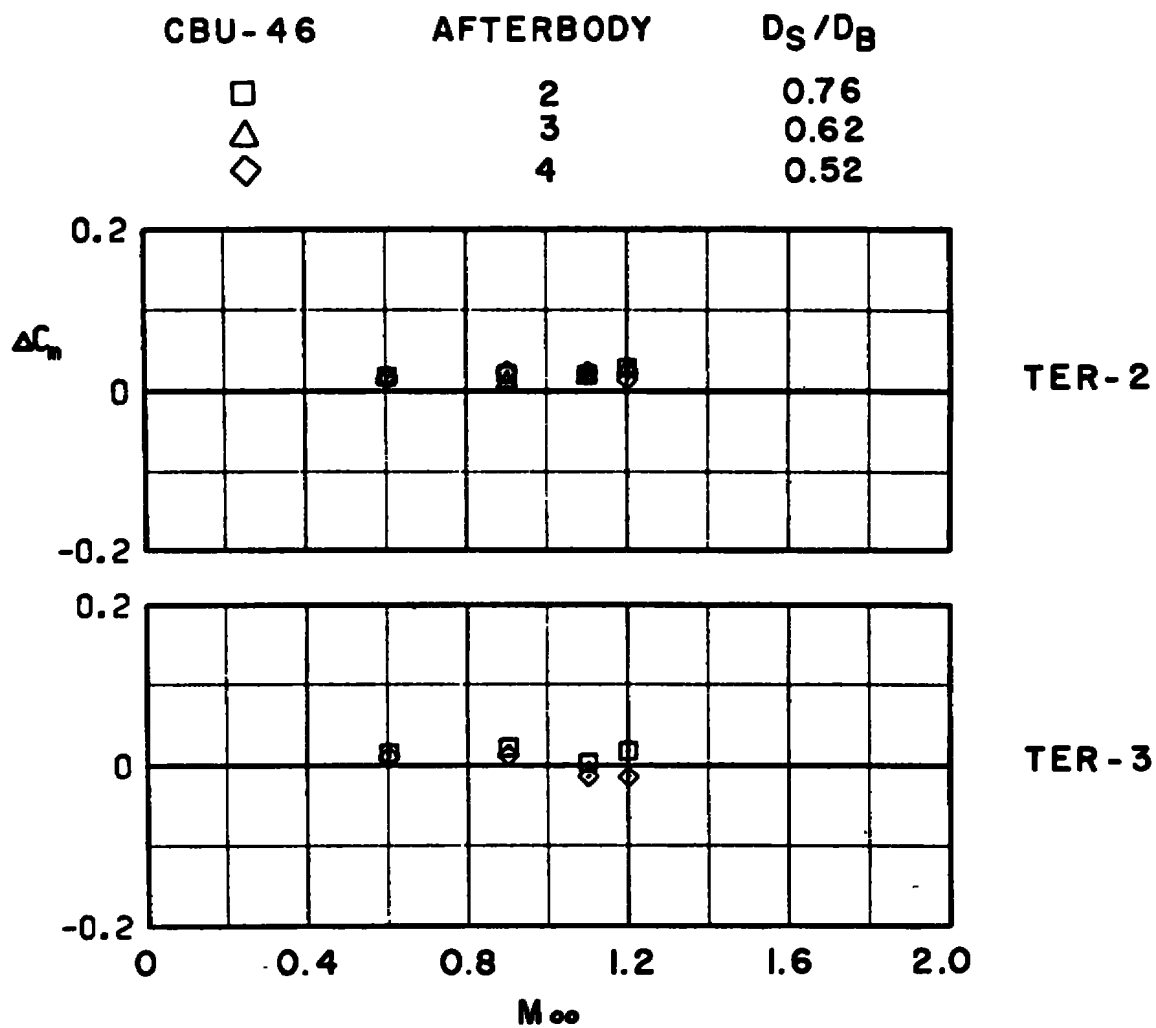
b. Side-force increment
Figure 43. Continued.



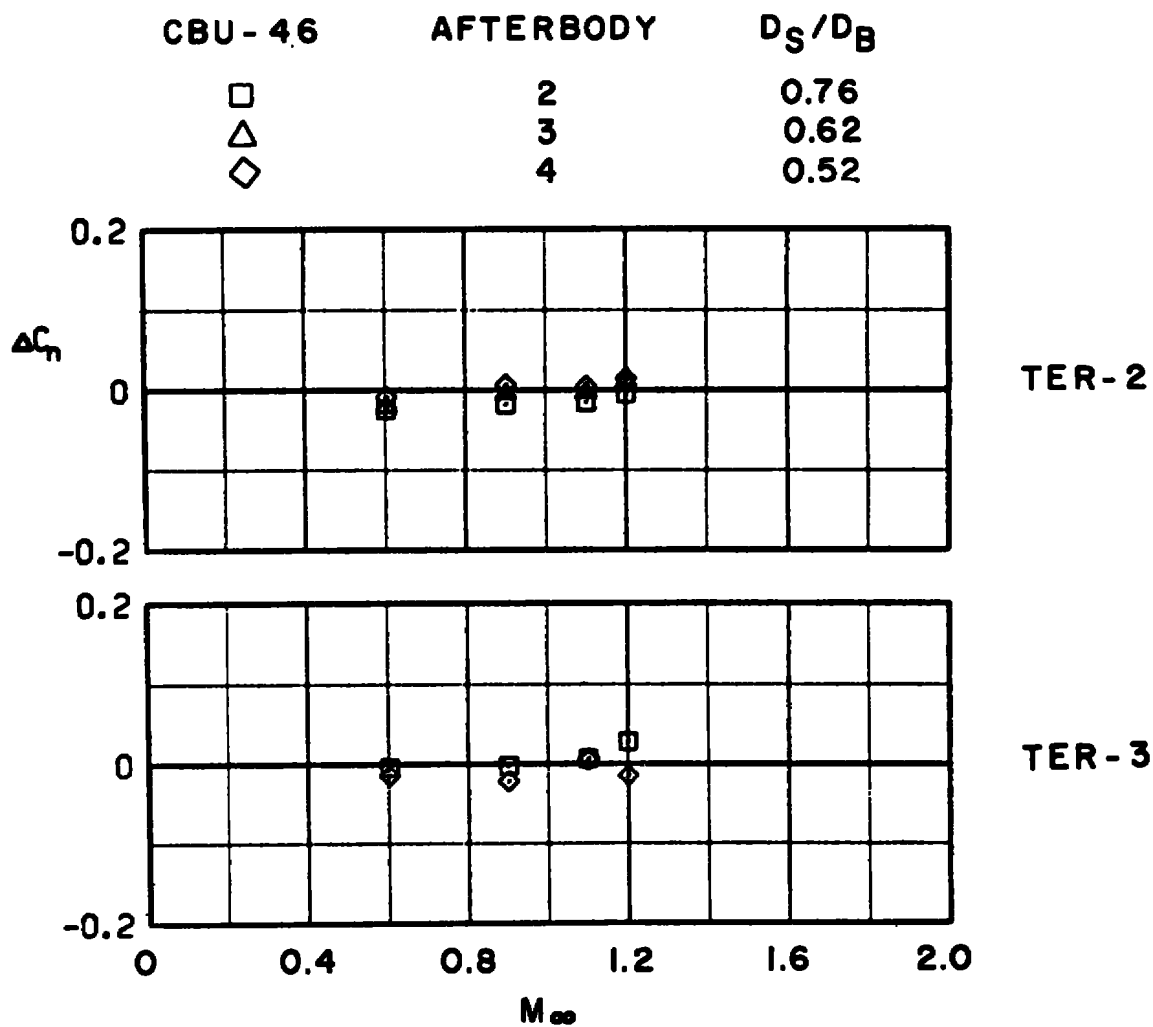
c. Axial-force increment
Figure 43. Continued.



d. Rolling-moment increment
Figure 43. Continued.



e. Pitching-moment increment
Figure 43. Continued.



f. Yawing-moment increment
Figure 43. Concluded.

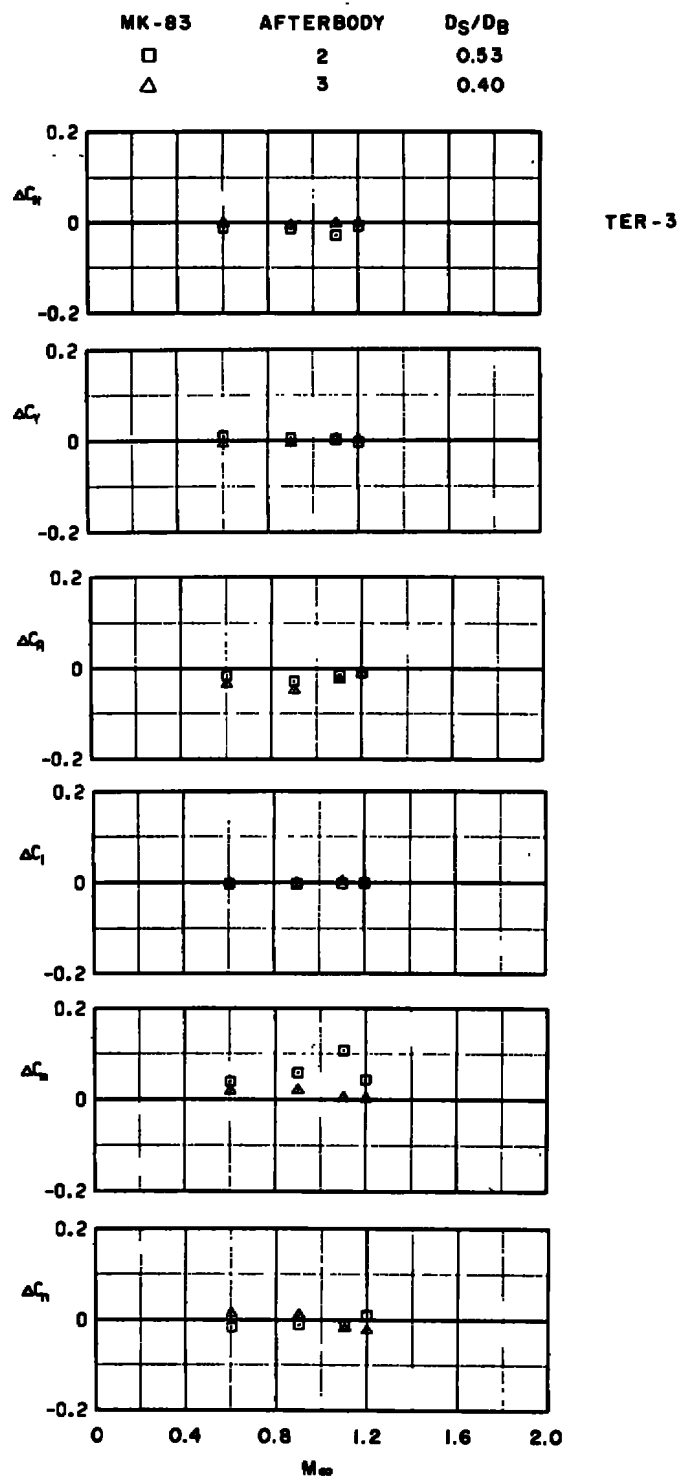
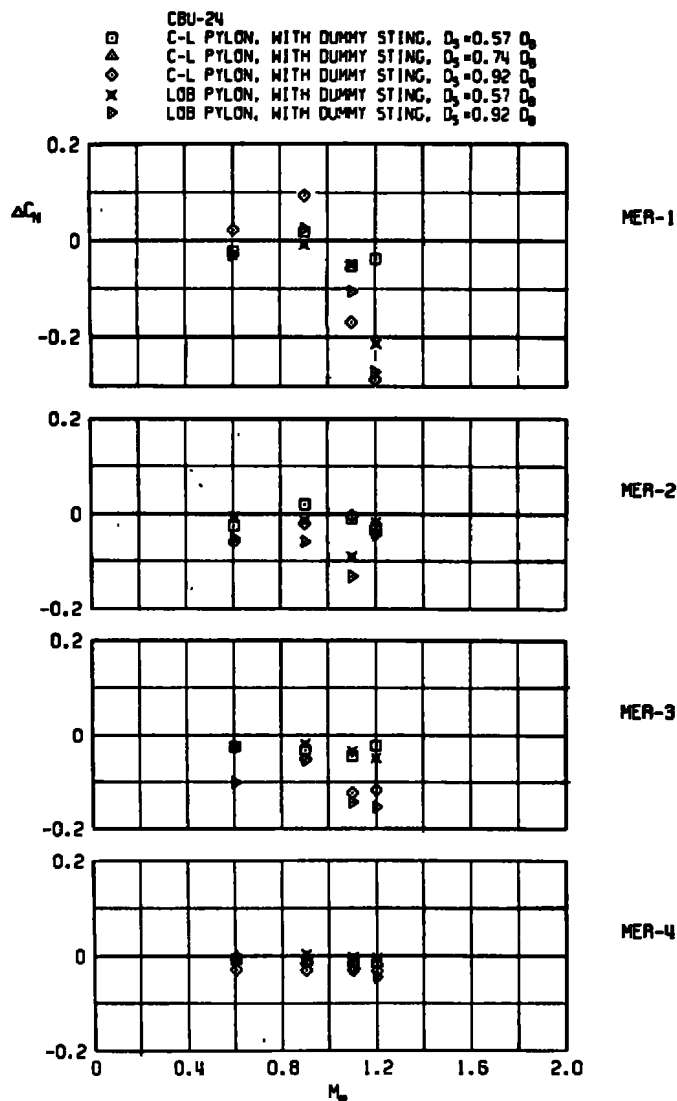
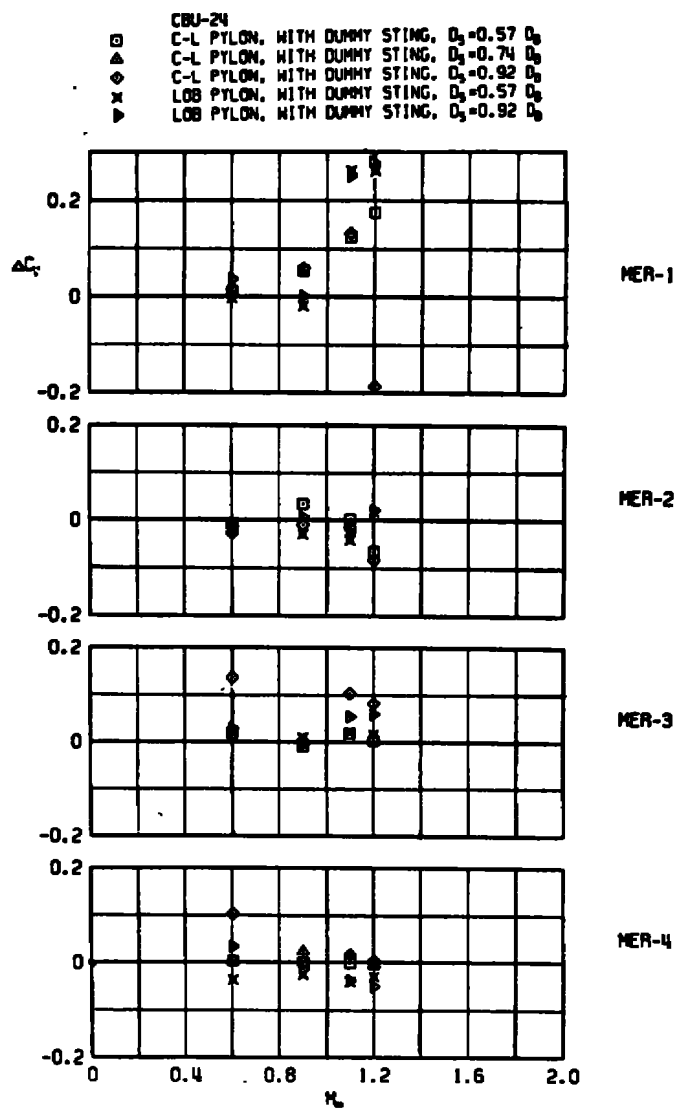


Figure 44. Sting-induced aerodynamic load increments as a function of Mach number, stable rack-mounted store, LIB pylon.

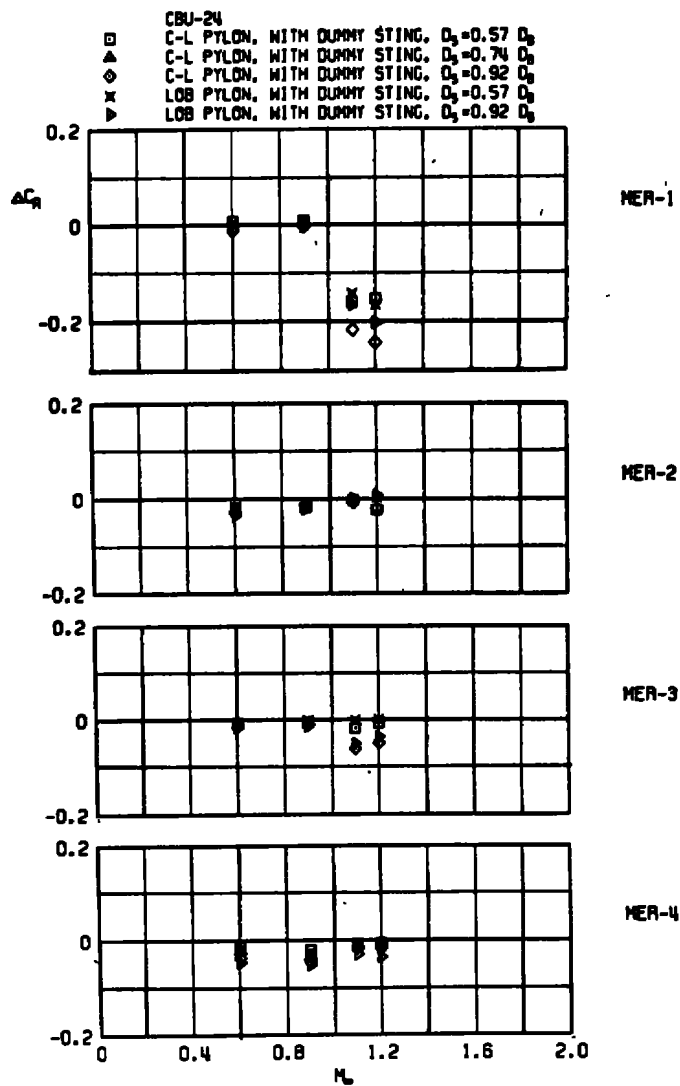


a. Normal-force increment

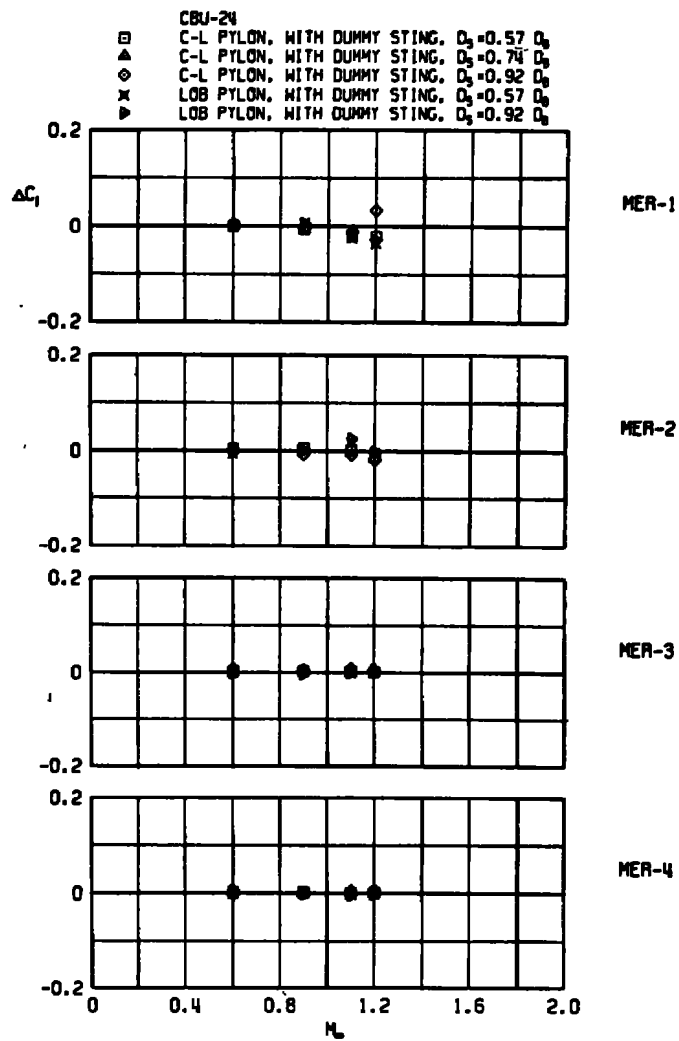
Figure 45. Sting-induced aerodynamic load increments as a function of Mach number, stable rack-mounted store, C-L and LOB pylon.



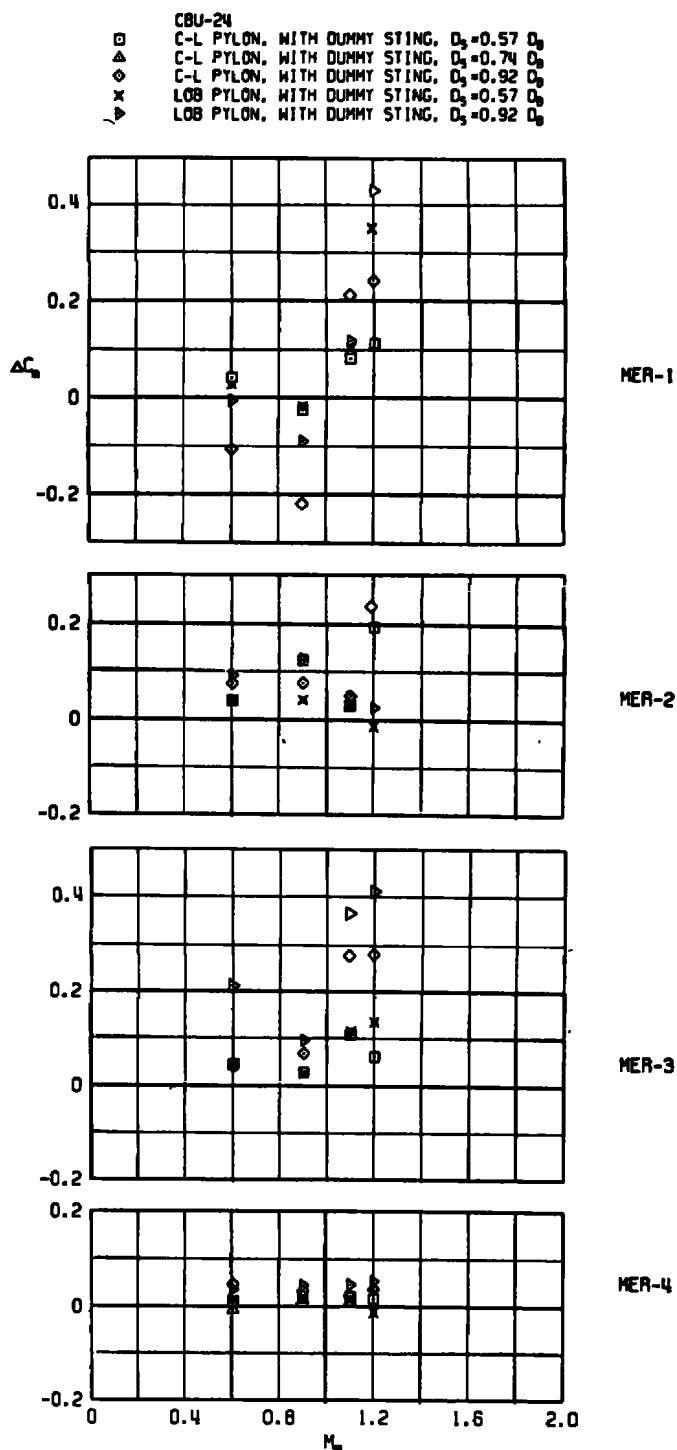
b. Side-force increment
 Figure 45. Continued.



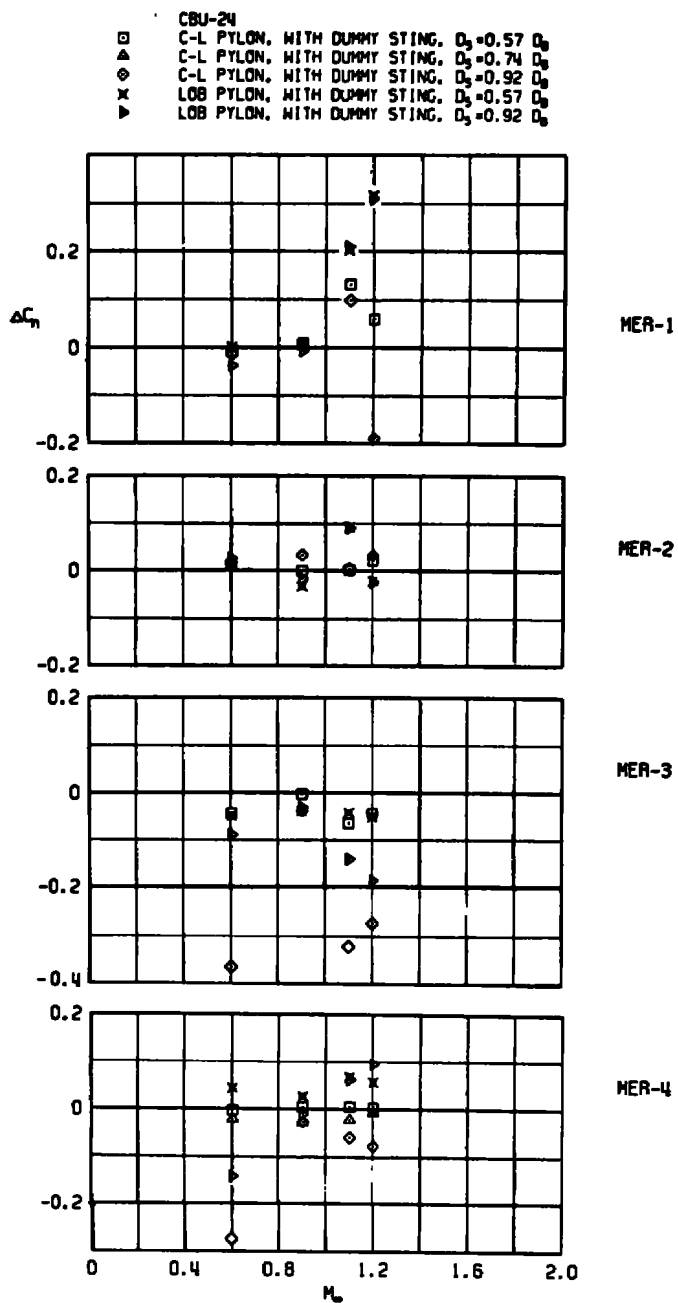
c. Axial-force increment
Figure 45. Continued.



d. Rolling-moment increment
Figure 45. Continued.

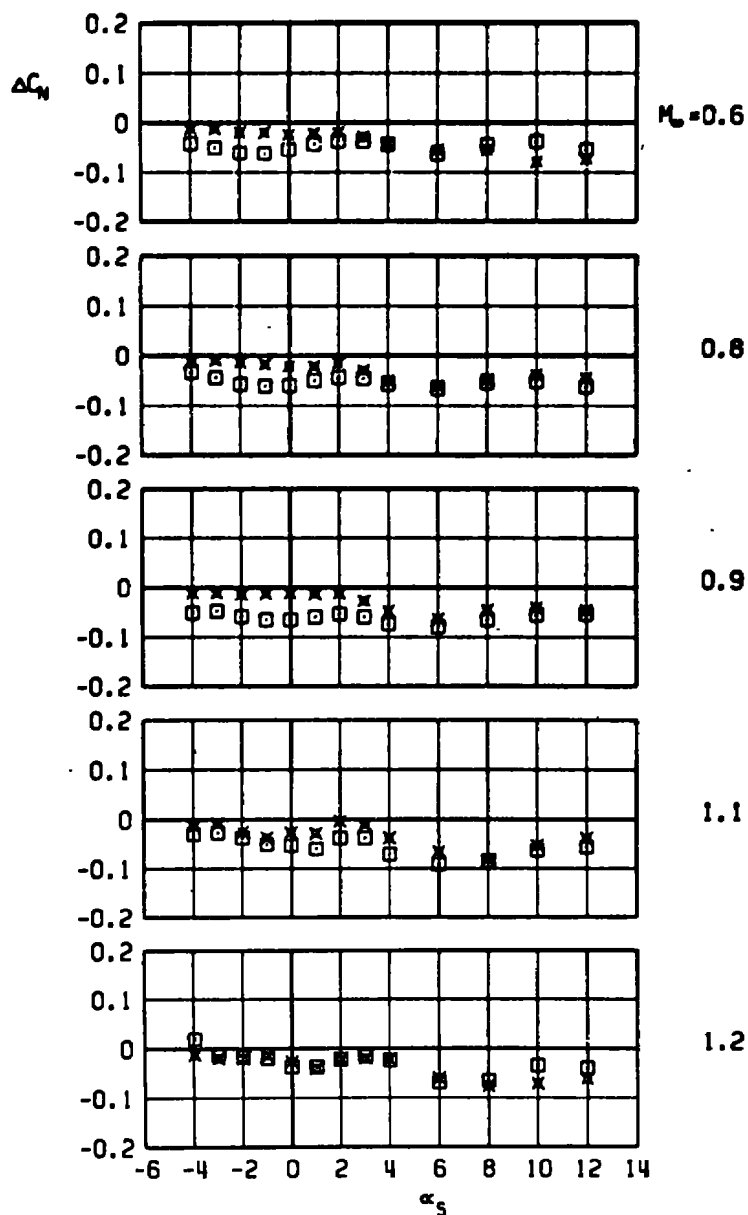


e. Pitching-moment increment
Figure 45. Continued.



f. Yawing-moment increment
 Figure 45. Concluded.

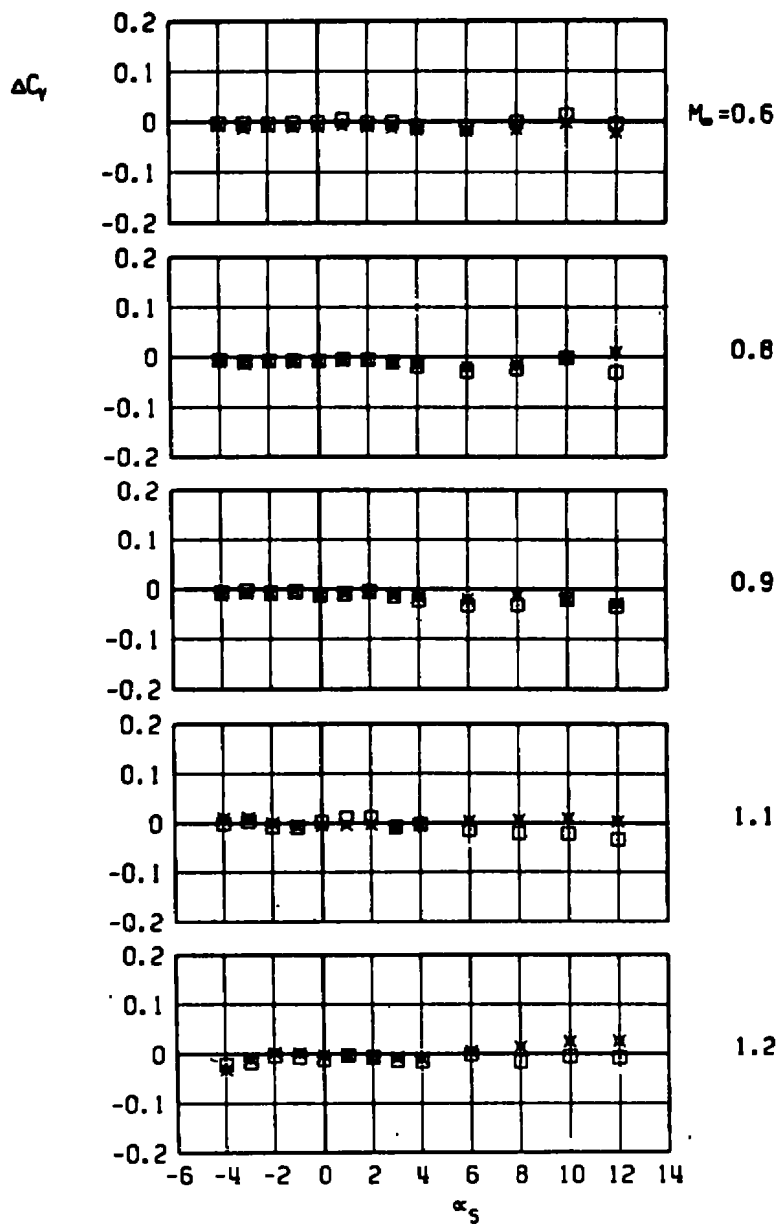
BLU-1, LIB PYLON, AB EFFECT
 □ AB 2 ONLY
 × AB 2 WITH DUMMY STING, $D_3 = 0.82 D_0$



a. Normal-force increment

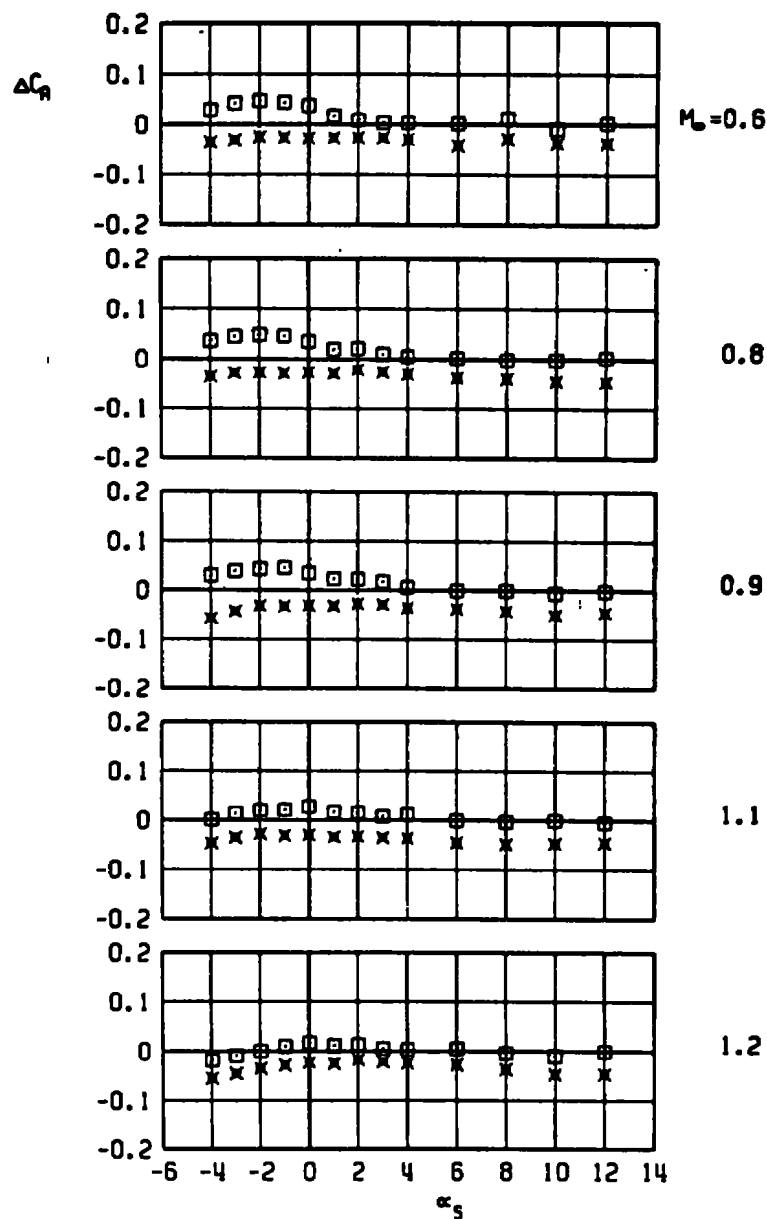
Figure 46. Aerodynamic load increments attributable to truncation of the afterbody of an unstable pylon-mounted store, BLU-1 store with AB2, LIB pylon.

BLU-1, LIB PYLON, AB EFFECT
 AB 2 ONLY
 AB 2 WITH DUMMY STING, $D_3 = 0.82 D_0$



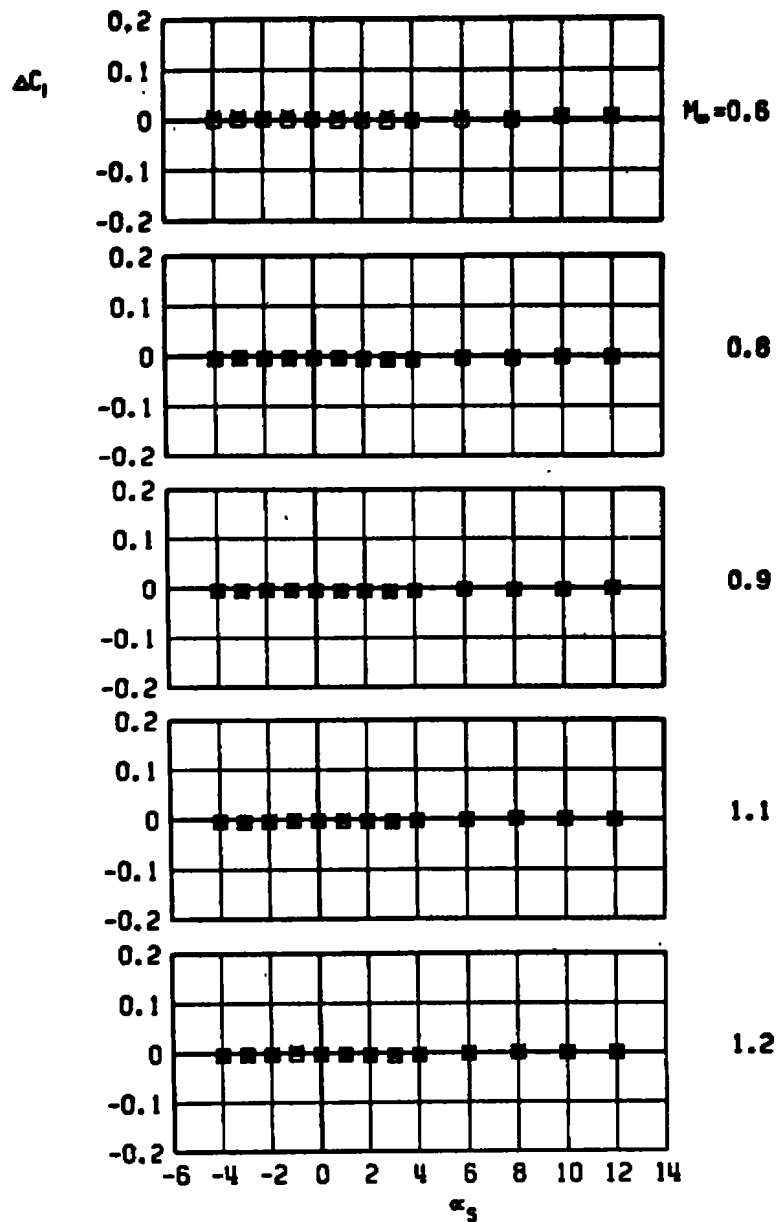
b. Side-force increment
 Figure 46. Continued.

BLU-1, L18 PYLON, AB EFFECT
 AB 2 ONLY
 AB 2 WITH DUMMY STING, $D_3 = 0.62 D_0$



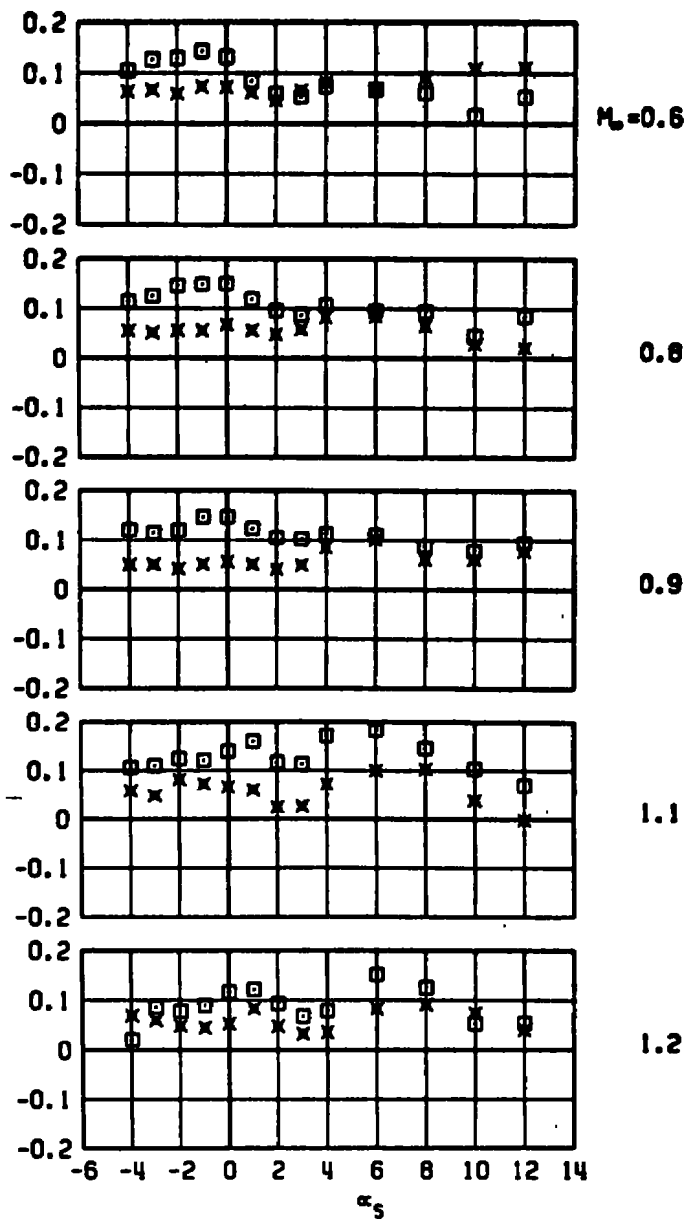
c. Axial-force increment
 Figure 46. Continued.

BLU-1, LIB PYLON, AB EFFECT
 @ AB 2 ONLY
 x AB 2 WITH DUMMY STING, $D_3 = 0.82 D_2$



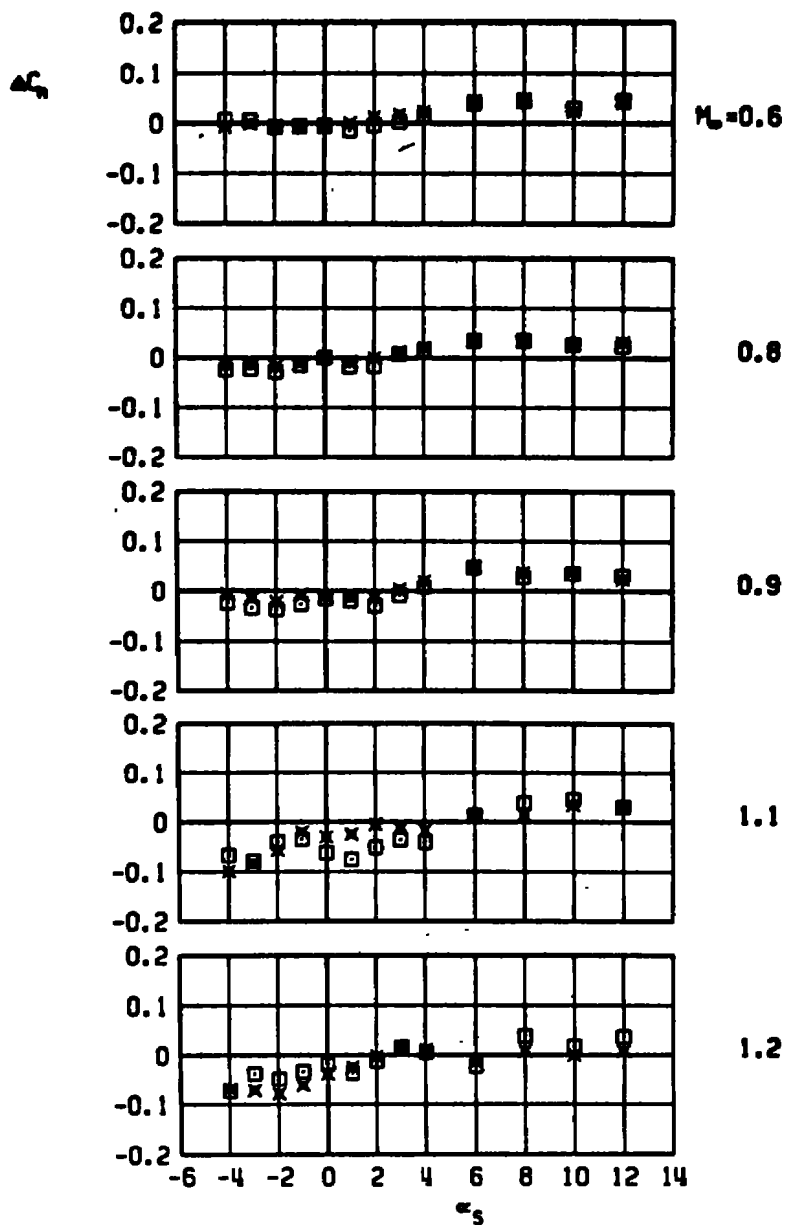
d. Rolling-moment increment
 Figure 46. Continued.

BLU-1, LIB PYLON, AB EFFECT
 □ AB 2 ONLY
 x AB 2 WITH DUMMY STING, $D_3 = 0.62 D_0$



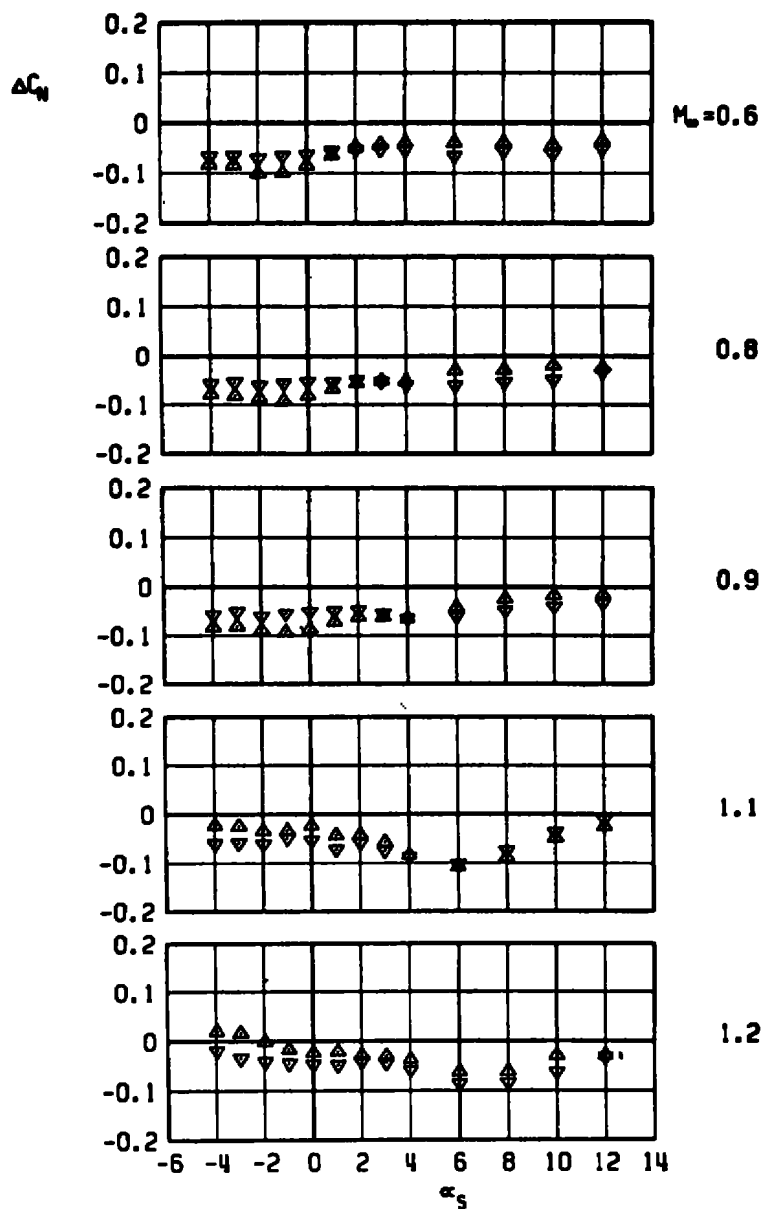
e. Pitching-moment increment
 Figure 46. Continued.

BLU-1, LIB PYLON, AB EFFECT
 AB 2 ONLY
 AB 2 WITH DUMMY STING, $Q_3 = 0.82 Q_0$



f. Yawing-moment increment
 Figure 46. Concluded.

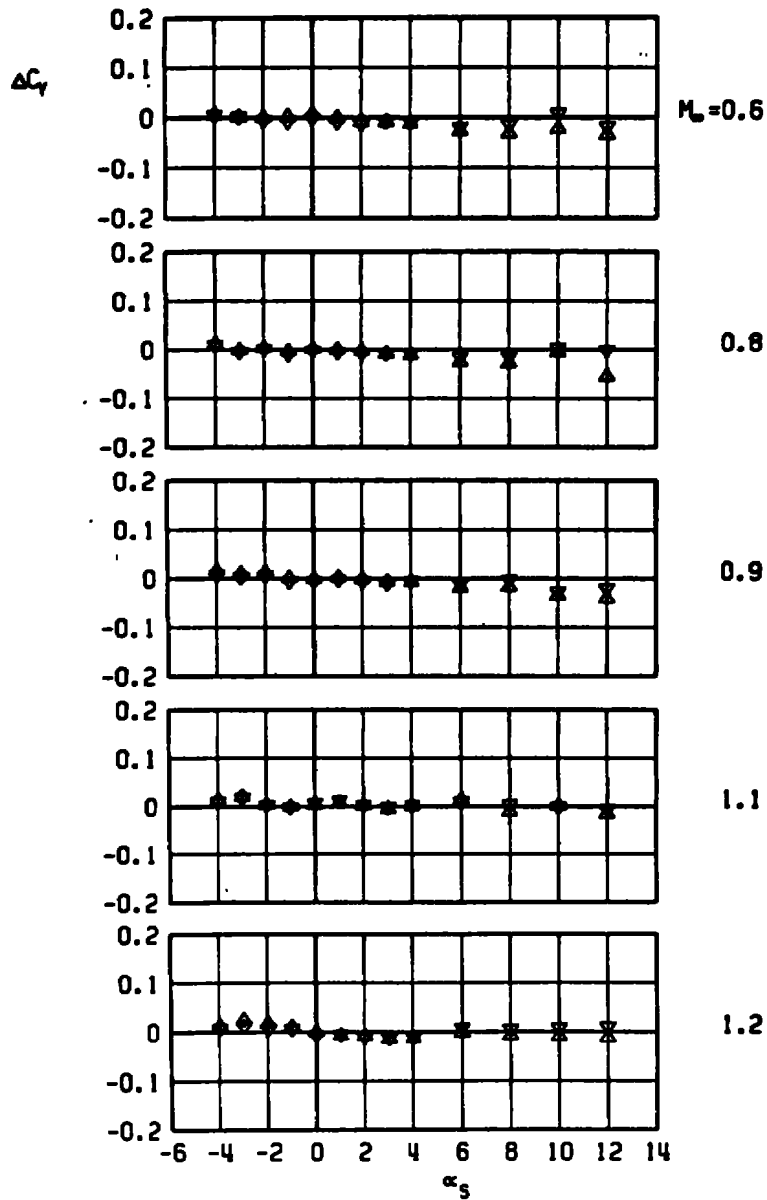
▲ BLU-1, LIB PYLON, AB EFFECT
 ▼ AB 3 ONLY
 ▽ AB 3 WITH DUMMY STING, $D_3 = 0.68 D_0$



a. Normal-force increment

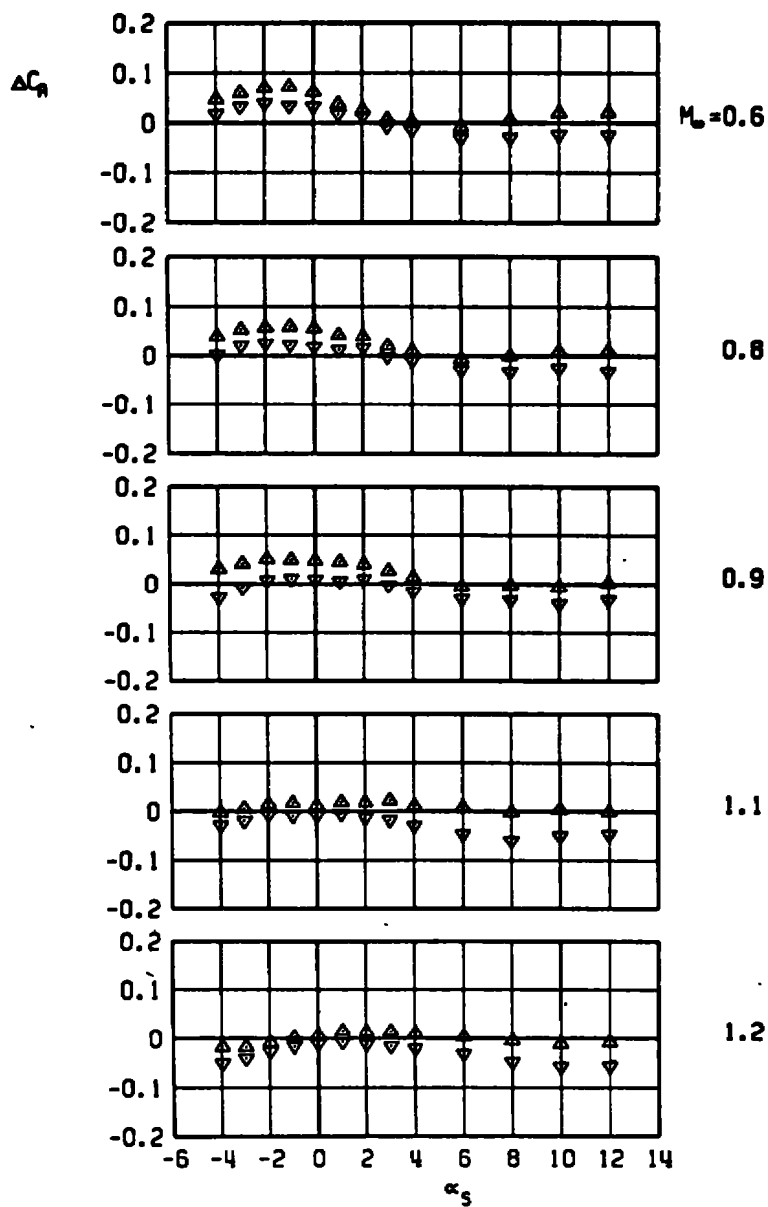
Figure 47. Aerodynamic load increments attributable to truncation of the afterbody of unstable pylon-mounted store, BLU-1 store with AB3, LIB pylon.

▲ BLU-1, LIB PYLON, AB EFFECT
 ▼ AB 3 ONLY
 ▽ AB 3 WITH DUMMY STING, $D_3 = 0.68 D_0$



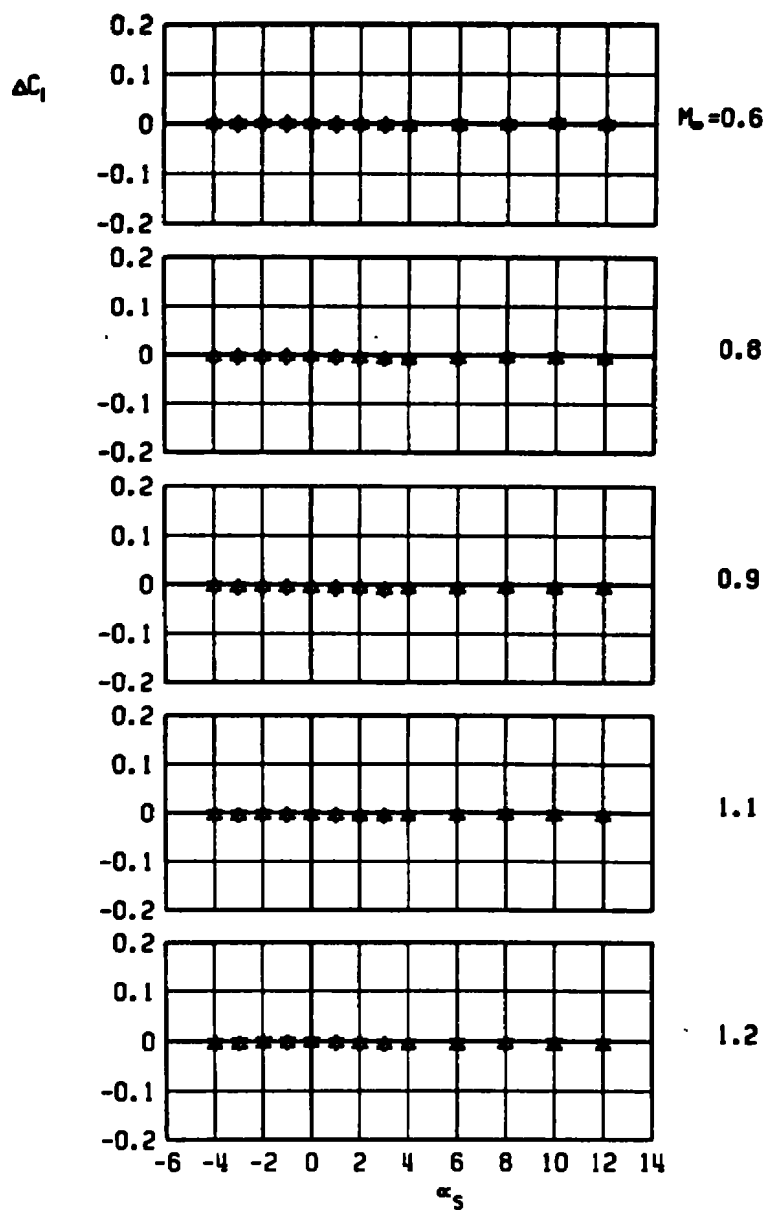
b. Side-force increment
 Figure 47. Continued.

▲ BLU-1, LIB PYLON, AB EFFECT
 AB 3 ONLY
 ▼ AB 3 WITH DUMMY STING, $D_3 = 0.68 D_0$



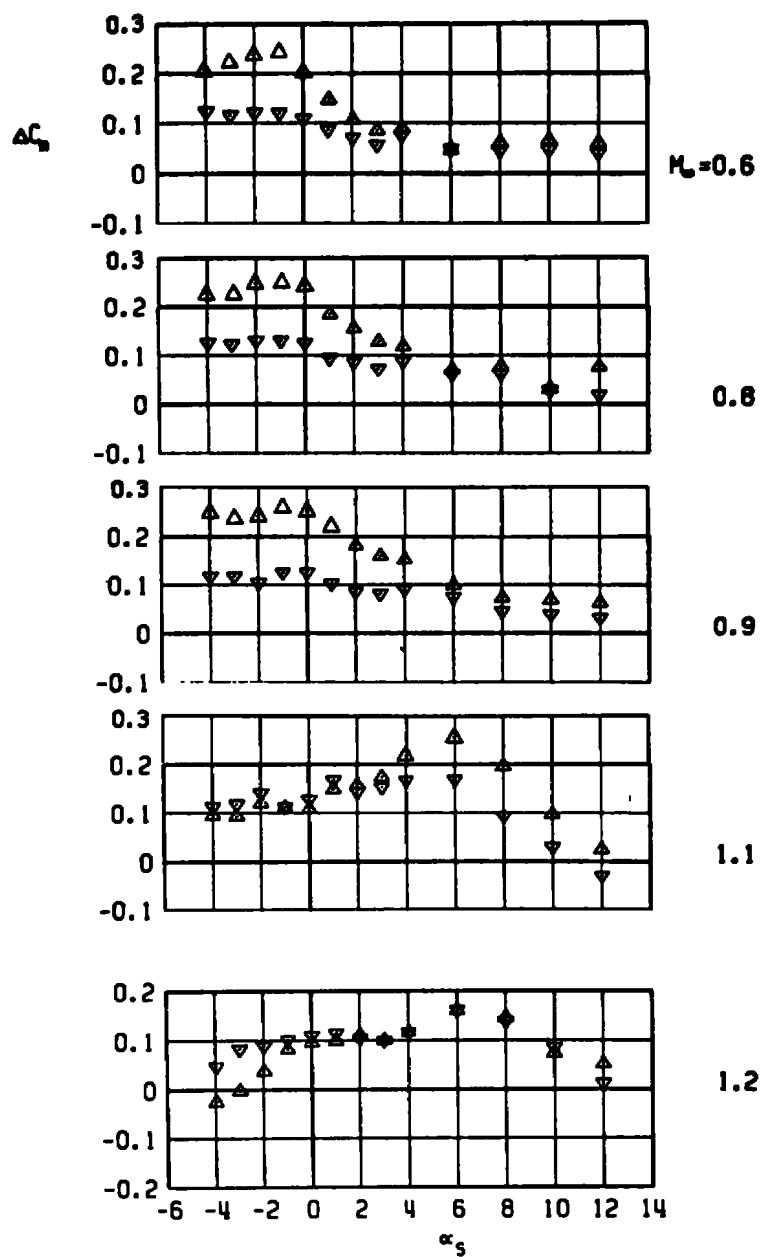
c. Axial-force increment
 Figure 47. Continued.

▲ BLU-1, LIB PYLON, AB EFFECT
 ▼ AB 3 ONLY
 AB 3 WITH DUMMY STING, $D_3 = 0.68 D_0$



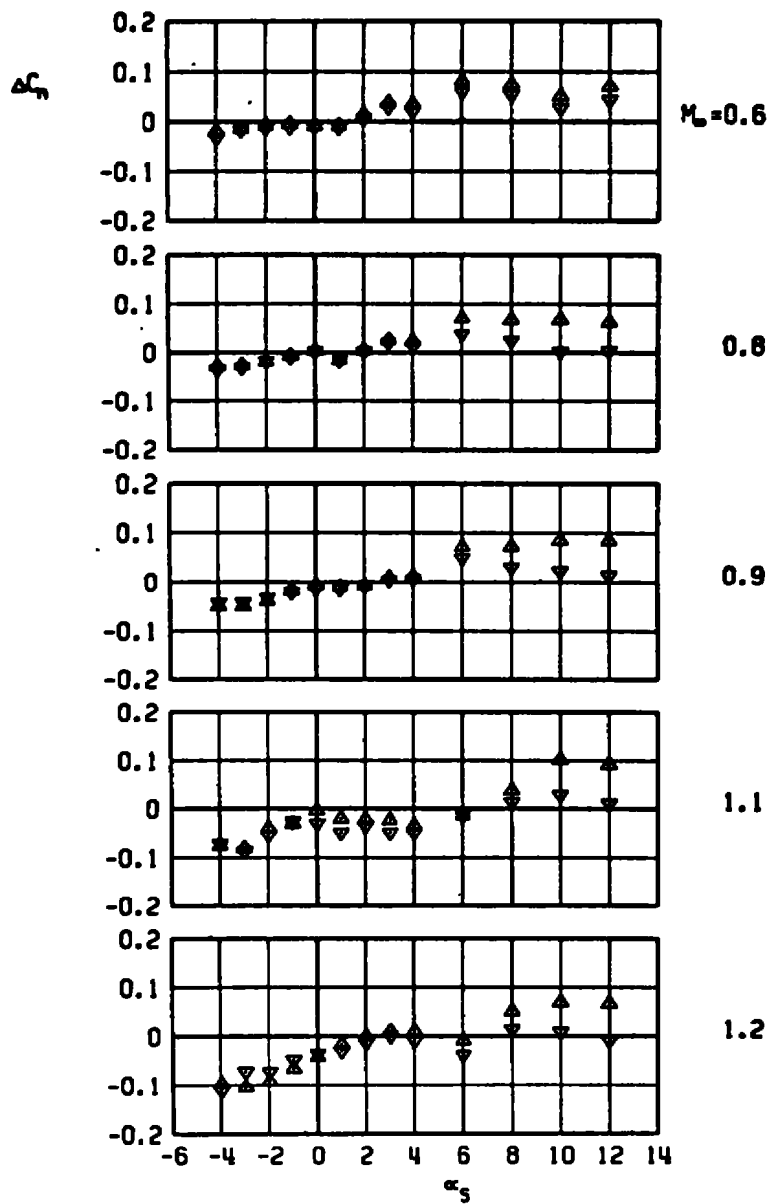
d. Rolling-moment increment
 Figure 47. Continued.

▲ BLU-1, LIB PYLON, AB EFFECT
 ▼ AB 3 ONLY
 ◆ AB 3 WITH DUMMY STING, $D_3 = 0.68 D_0$



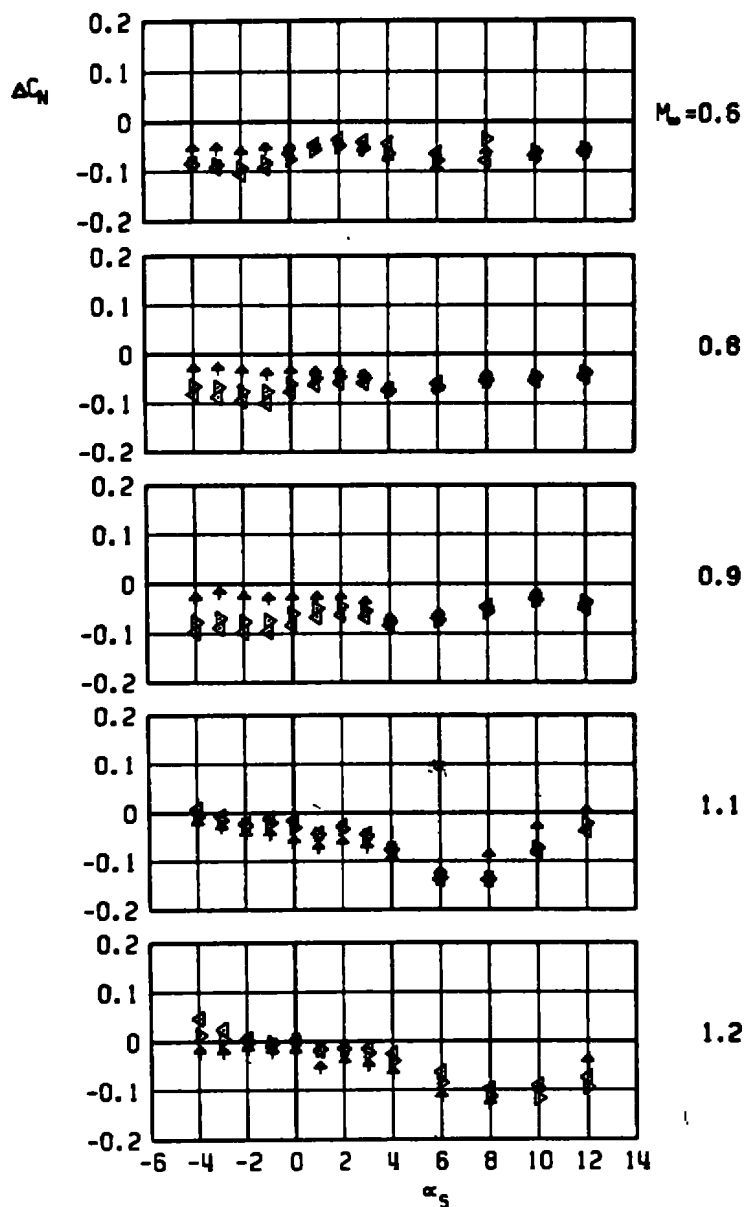
e. Pitching-moment increment
 Figure 47. Continued.

▲ BLU-1, LIB PYLON, AB EFFECT
 AB 3 ONLY
 ▼ AB 3 WITH DUMMY STING, $D_3 = 0.68 D_9$



f. Yawing-moment increment
Figure 47. Concluded.

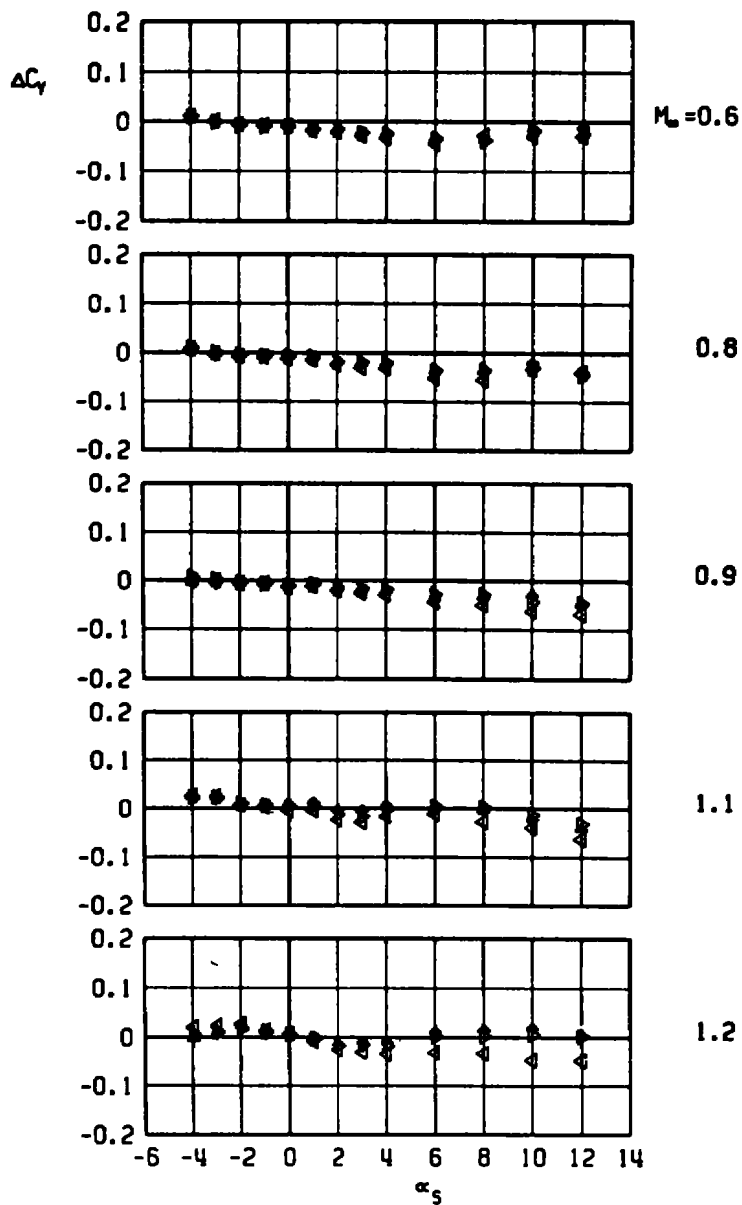
BLU-1, LIB PYLON, AB EFFECT
 AB 4 ONLY
 AB 4 WITH DUMMY STING, $D_3 = 0.58 D_0$
 AB 4 WITH DUMMY STING, $D_3 = 0.87 D_0$



a. Normal-force increment

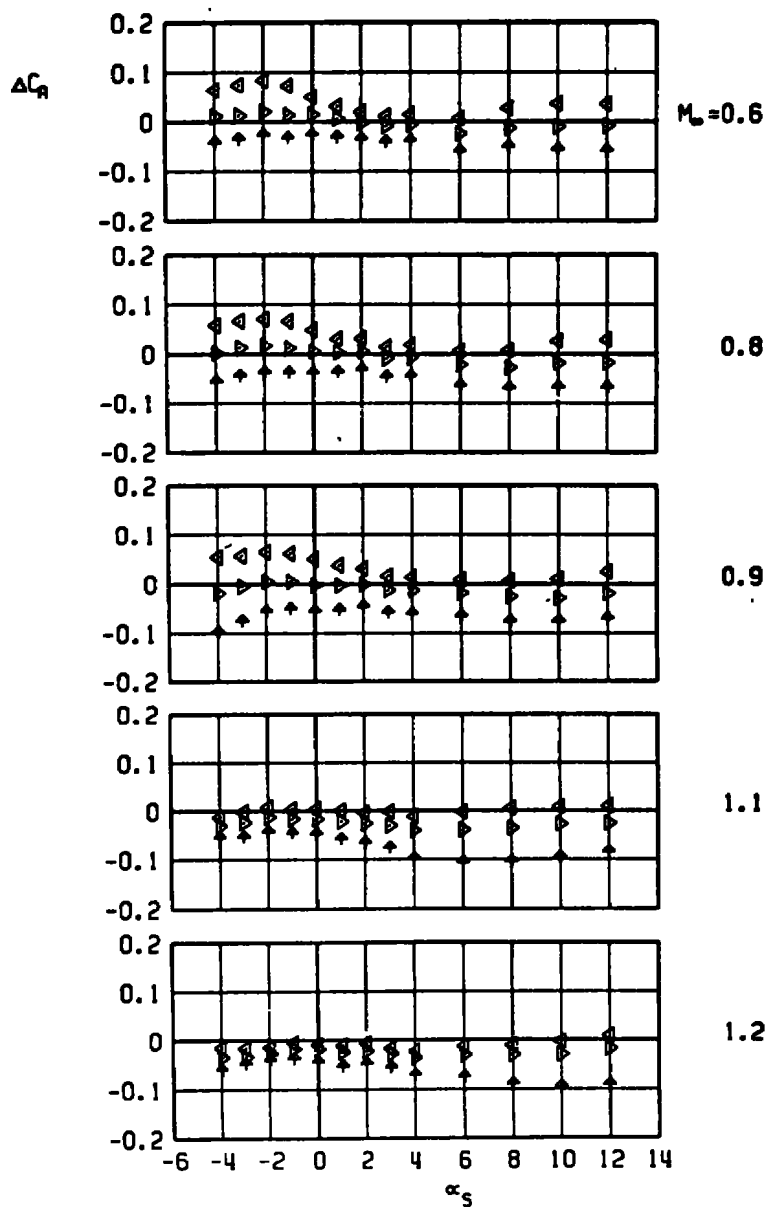
Figure 48. Aerodynamic load increments attributable to truncation of the afterbody of unstable pylon-mounted store, BLU-1 store with AB4, LIB pylon.

▲ BLU-1, LIB PYLON, AB EFFECT
 ▴ AB 4 ONLY
 ◆ AB 4 WITH DUMMY STING, $D_3 = 0.58 D_0$
 + AB 4 WITH DUMMY STING, $D_3 = 0.87 D_0$



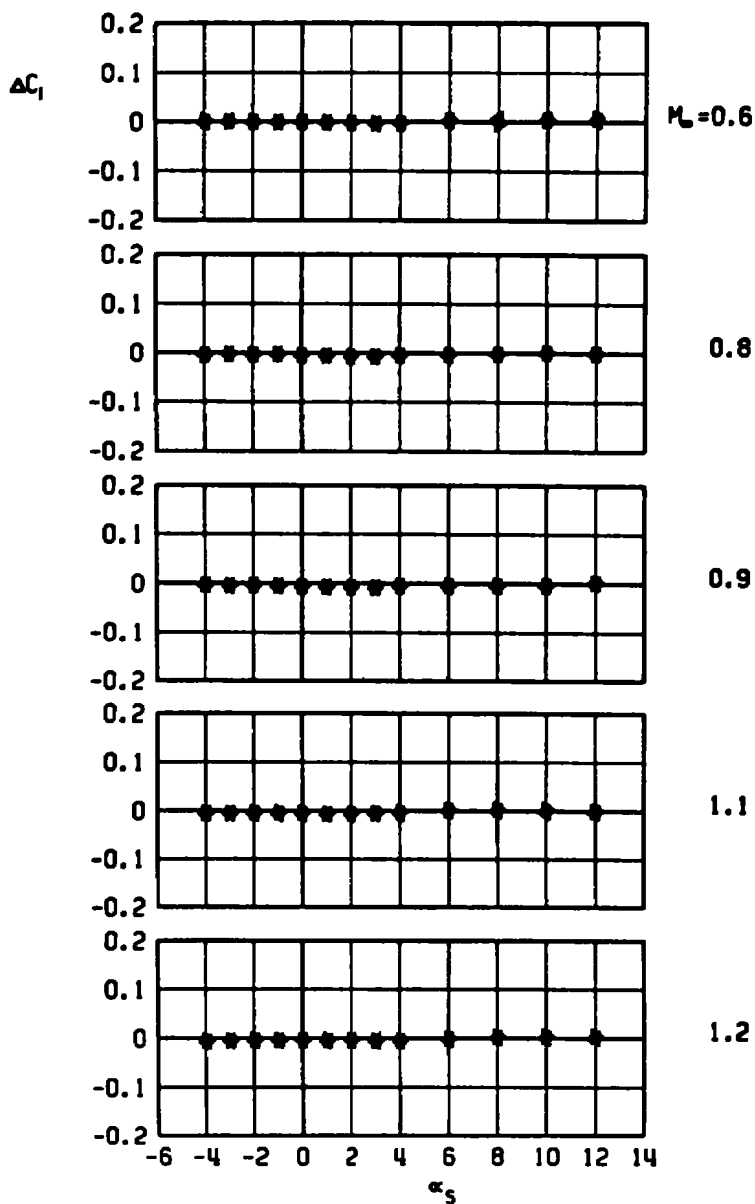
b. Side-force increment
 Figure 48. Continued.

▲ BLU-1, LIB PYLON, AB EFFECT
 ▽ AB 4 ONLY
 ◆ AB 4 WITH DUMMY STING, $D_3 = 0.58 D_0$
 ◆ AB 4 WITH DUMMY STING, $D_3 = 0.87 D_0$



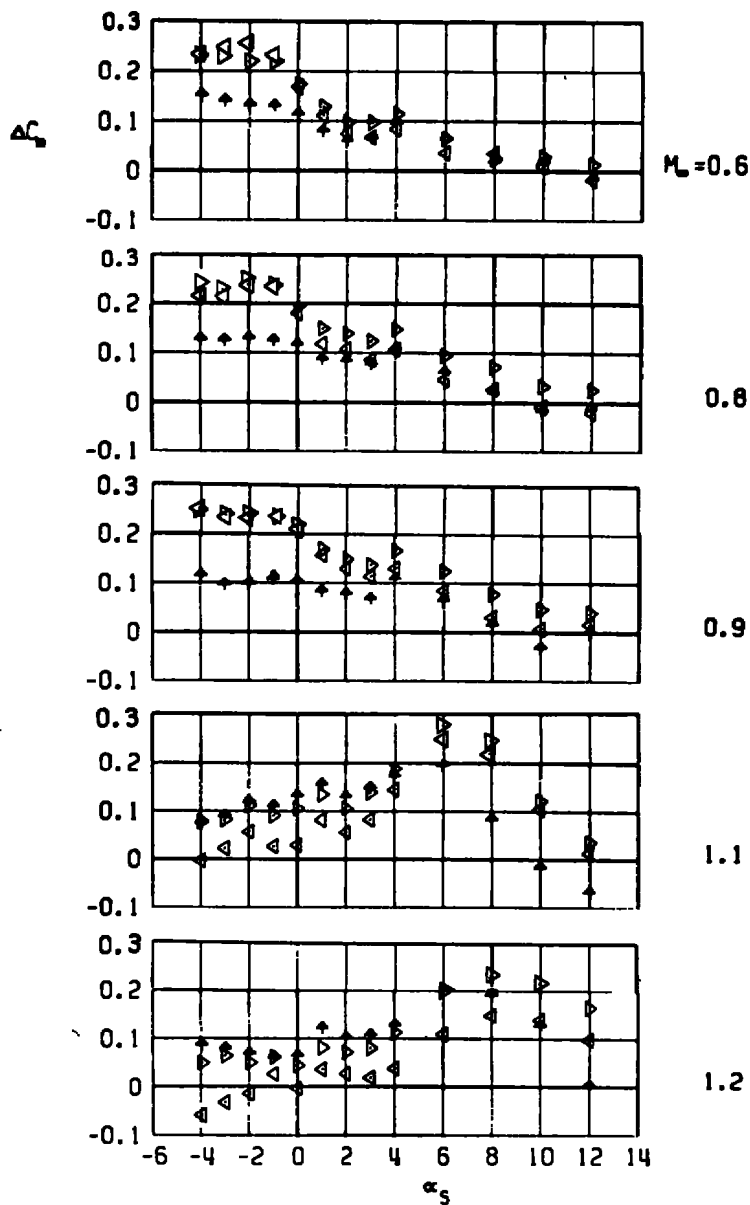
c. Axial-force increment
 Figure 48. Continued.

▲ BLU-1, LIB PYLON, AB EFFECT
 ▲ AB 4 ONLY
 ▲ AB 4 WITH DUMMY STING, $D_3 = 0.58 D_0$
 ▲ AB 4 WITH DUMMY STING, $D_3 = 0.87 D_0$



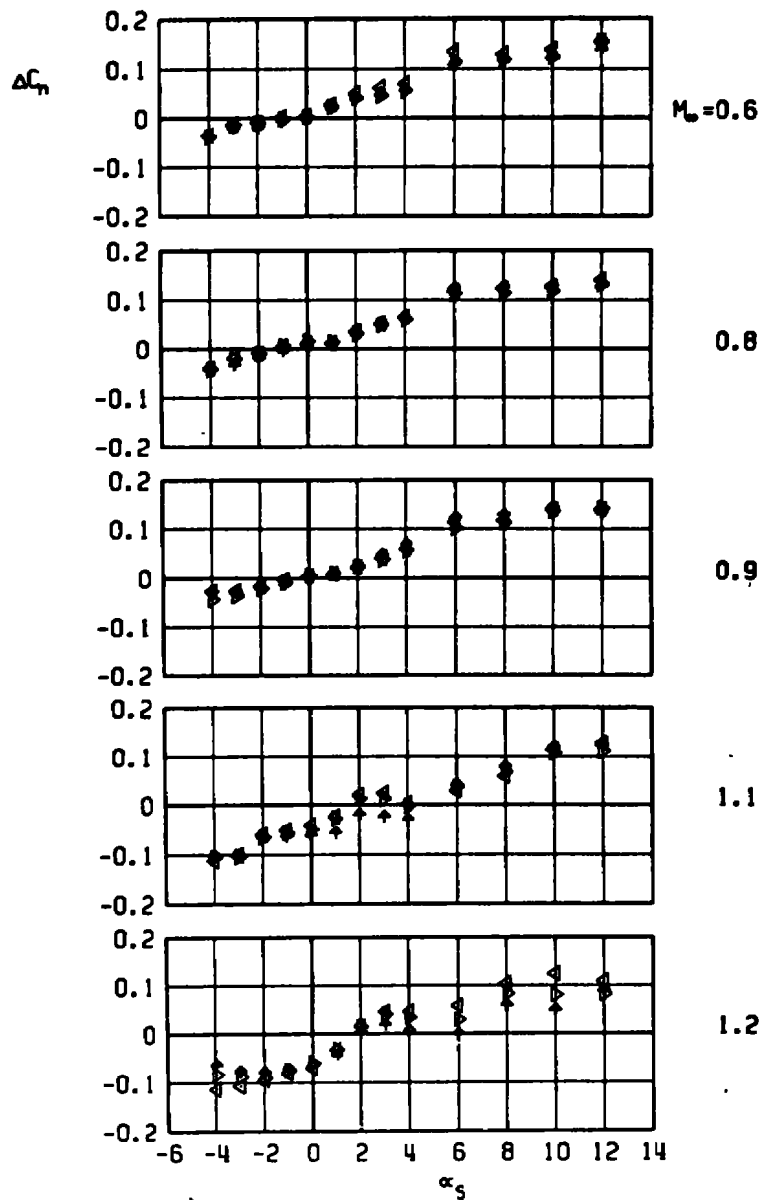
d. Rolling-moment increment
 Figure 48. Continued.

BLU-1, LIB PYLON, AB EFFECT
 AB 4 ONLY
 AB 4 WITH DUMMY STING, $D_5 = 0.58 D_0$
 AB 4 WITH DUMMY STING, $D_5 = 0.87 D_0$



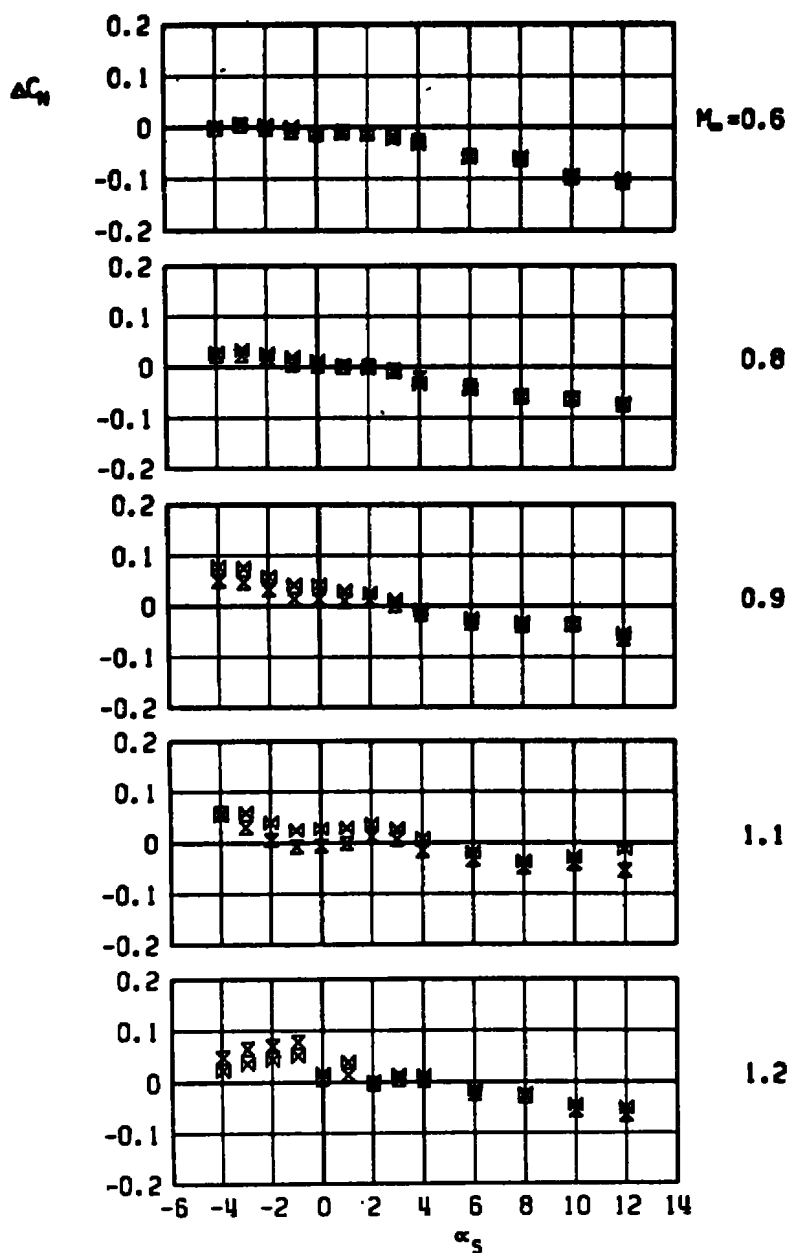
e. Pitching-moment increment
 Figure 48. Continued.

BLU-1, LIB PYLON, AB EFFECT
 AB 4 ONLY
 AB 4 WITH DUMMY STING, $D_5 = 0.58 D_0$
 AB 4 WITH DUMMY STING, $D_5 = 0.87 D_0$



f. Yawing-moment increment
 Figure 48. Concluded.

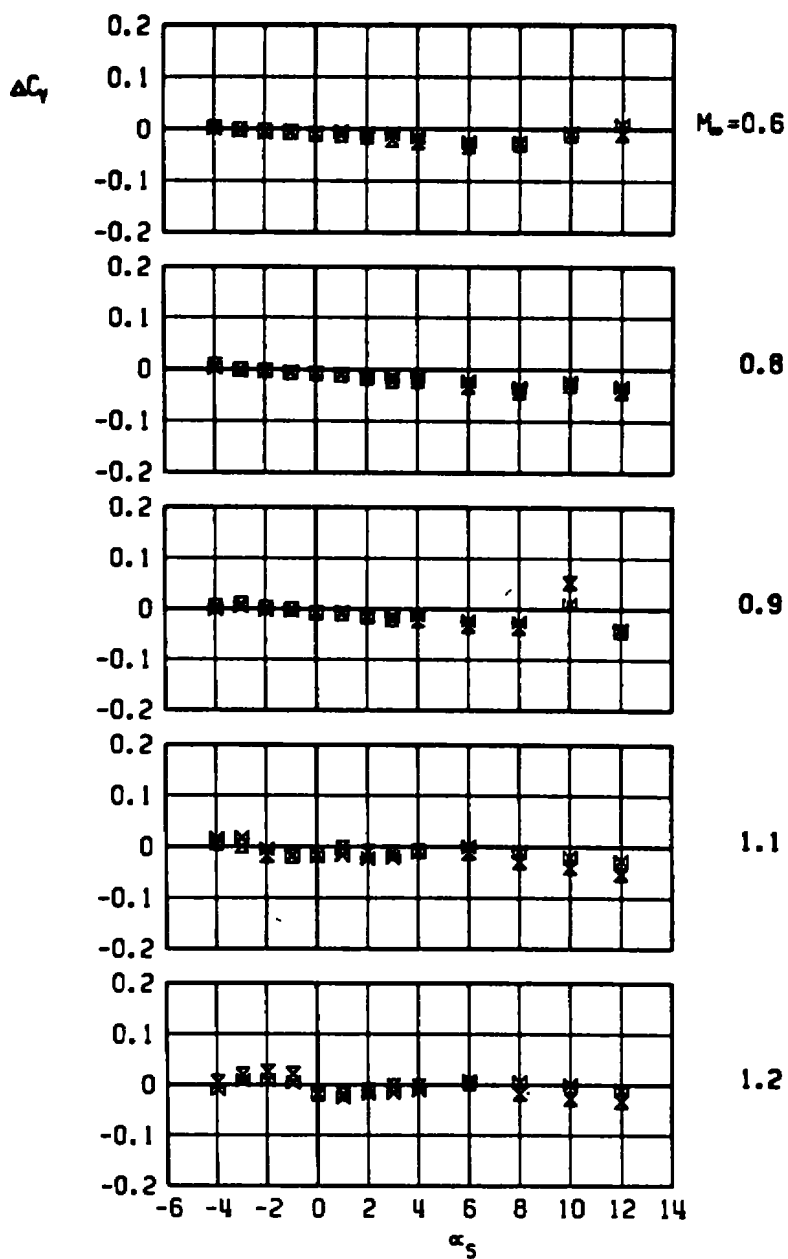
BLU-1, LIB PYLON, AB EFFECT
 Σ AB 5 ONLY
 Δ AB 5 WITH DUMMY STING, $D_3 = 0.80 D_0$



a. Normal-force increment

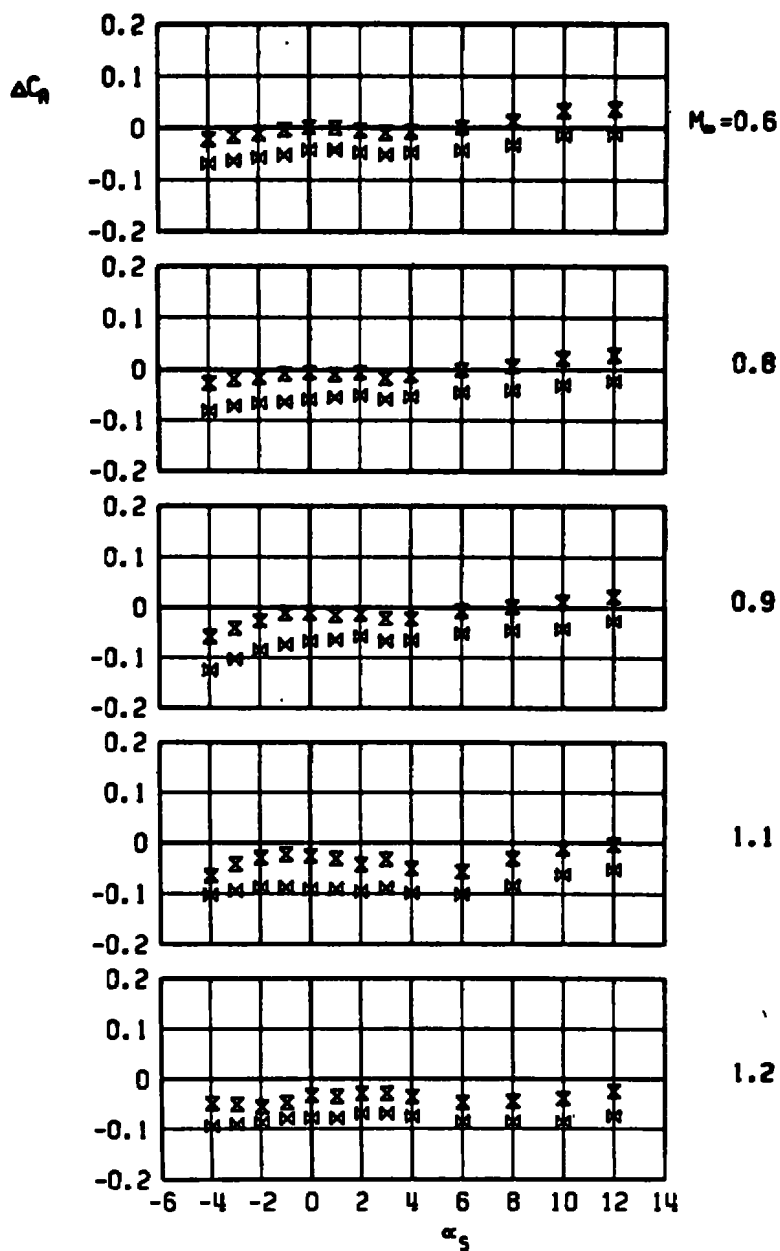
Figure 49. Aerodynamic load increments attributable to reshaping the afterbody of an unstable pylon-mounted store, BLU-1 store with AB5, LIB pylon.

BLU-1, LIB PYLON, AB EFFECT
 AB 5 ONLY
 AB 5 WITH DUMMY STING, $D_3 = 0.80 D_0$



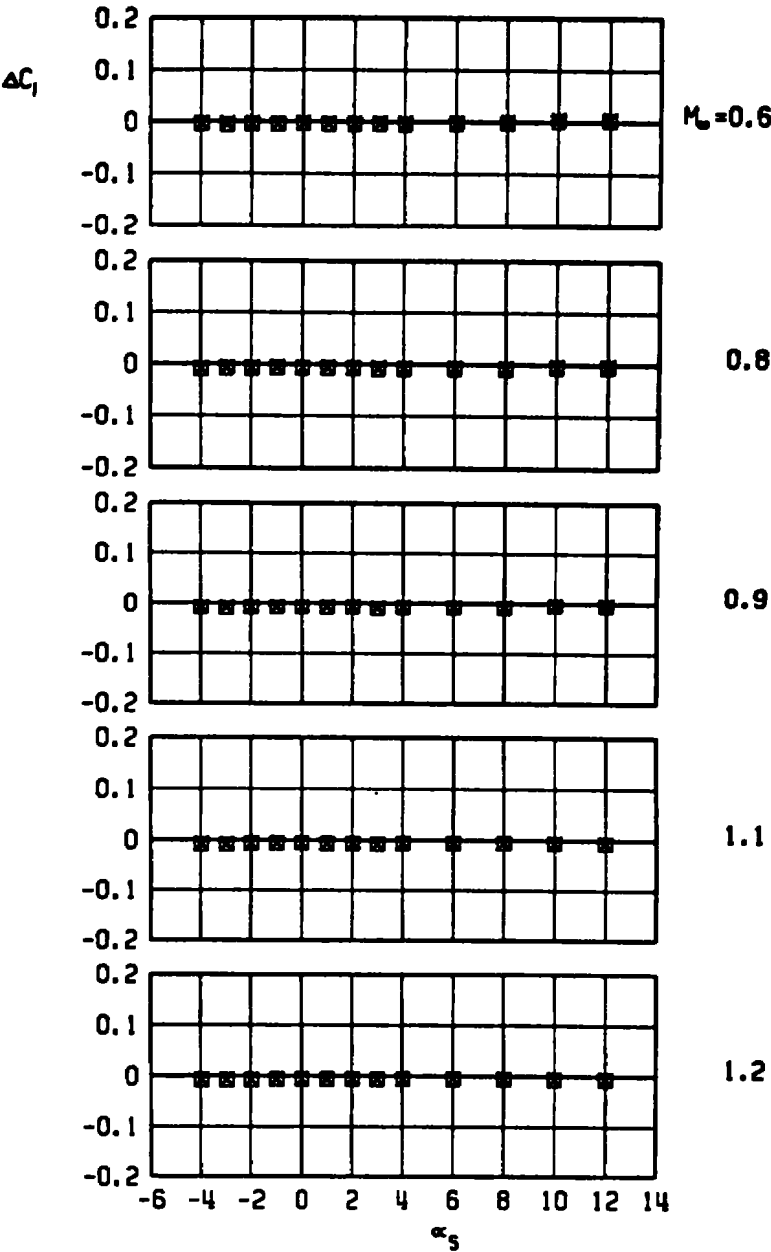
b. Side-force increment
 Figure 49. Continued.

BLU-1, LIB PYLON, AB EFFECT
 X AB 5 ONLY
 M AB 5 WITH DUMMY STING, $D_5 = 0.80 D_0$



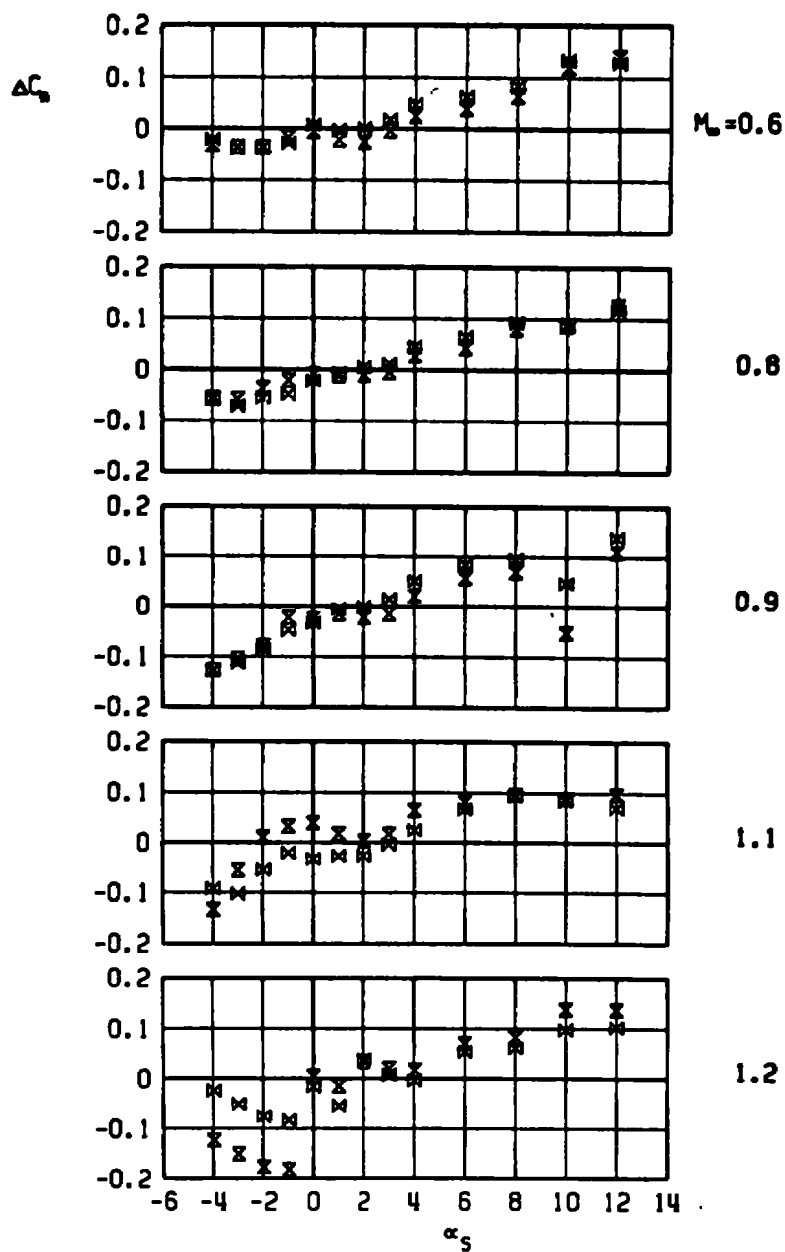
c. Axial-force increment
 Figure 49. Continued.

BLU-1, LIB PYLON, AB EFFECT
AB 5 ONLY
AB 5 WITH DUMMY STING, $D_5 = 0.80 D_9$



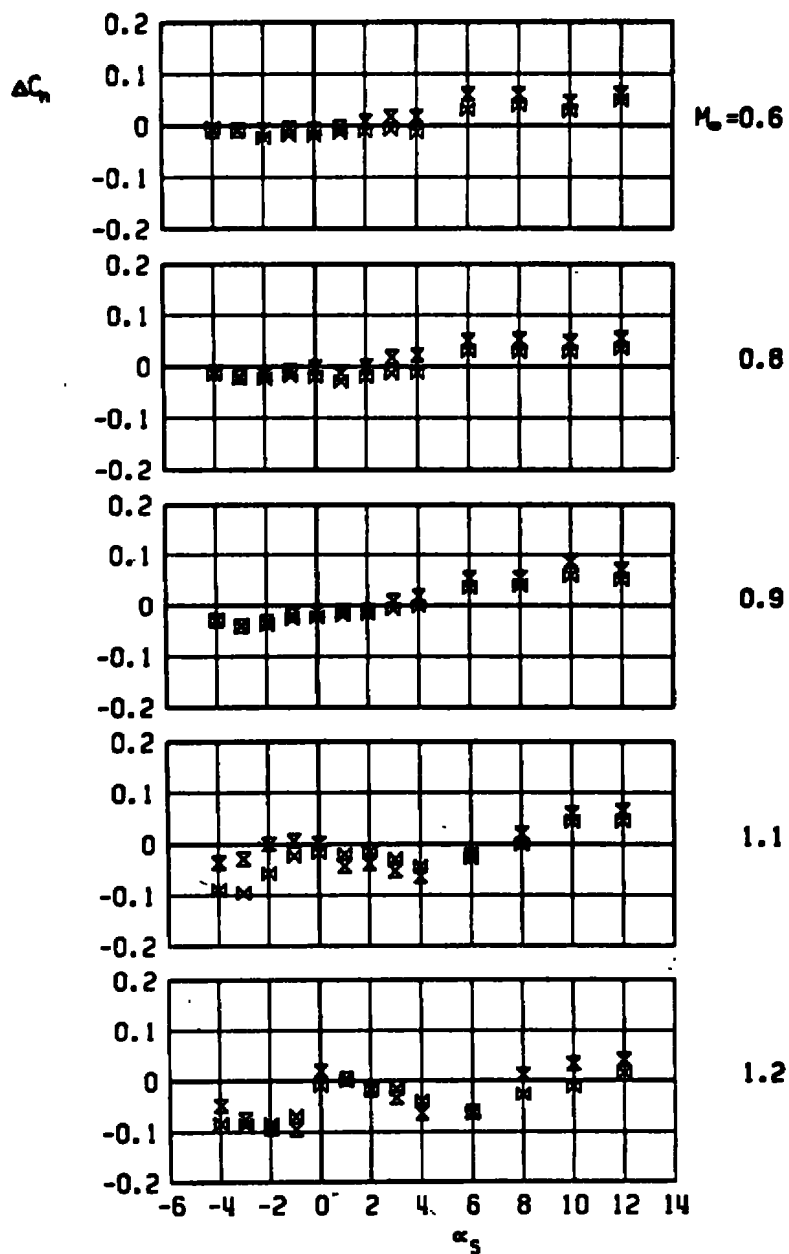
d. Rolling-moment increment
Figure 49. Continued.

BLU-1, LIB PYLON, AB EFFECT
 X AB 5 ONLY
 M AB 5 WITH DUMMY STING, $D_5 = 0.80 D_0$



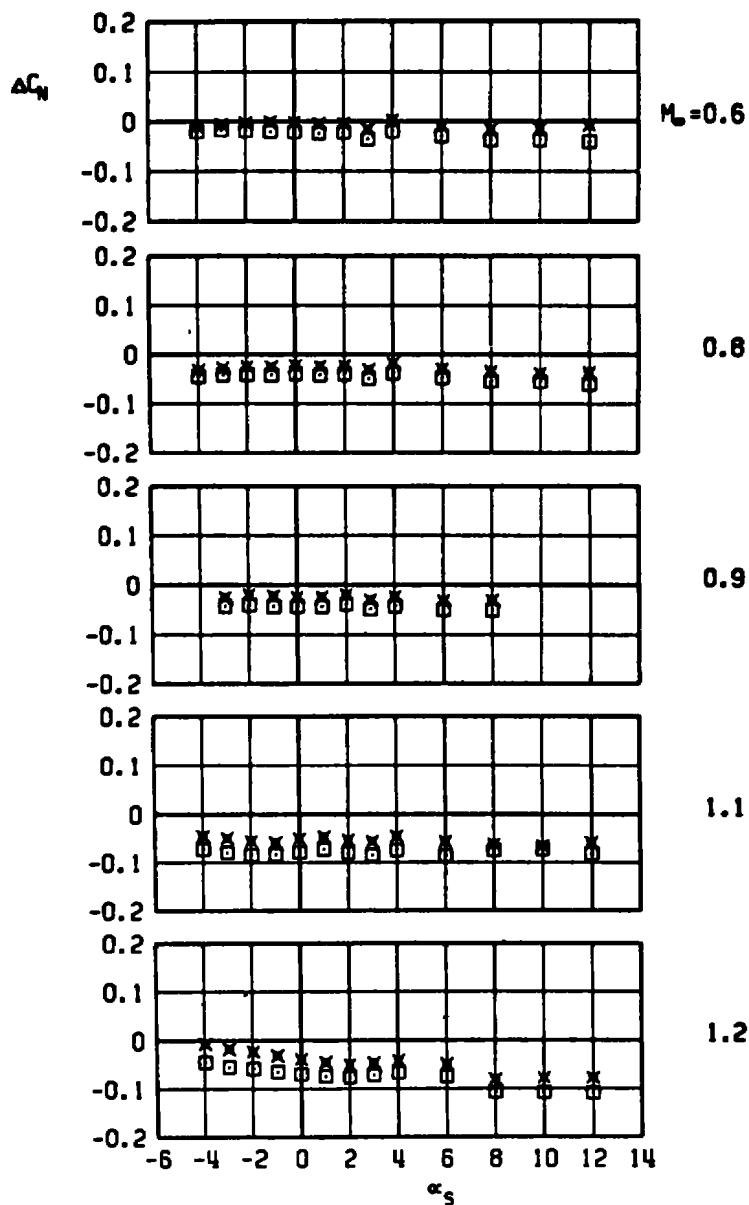
e. Pitching-moment increment
 Figure 49. Continued.

BLU-1, LIB PYLON, AB EFFECT
 AB 5 ONLY
 AB 5 WITH DUMMY STING, $D_5 = 0.80 D_0$



f. Yawing-moment increment
 Figure 49. Concluded.

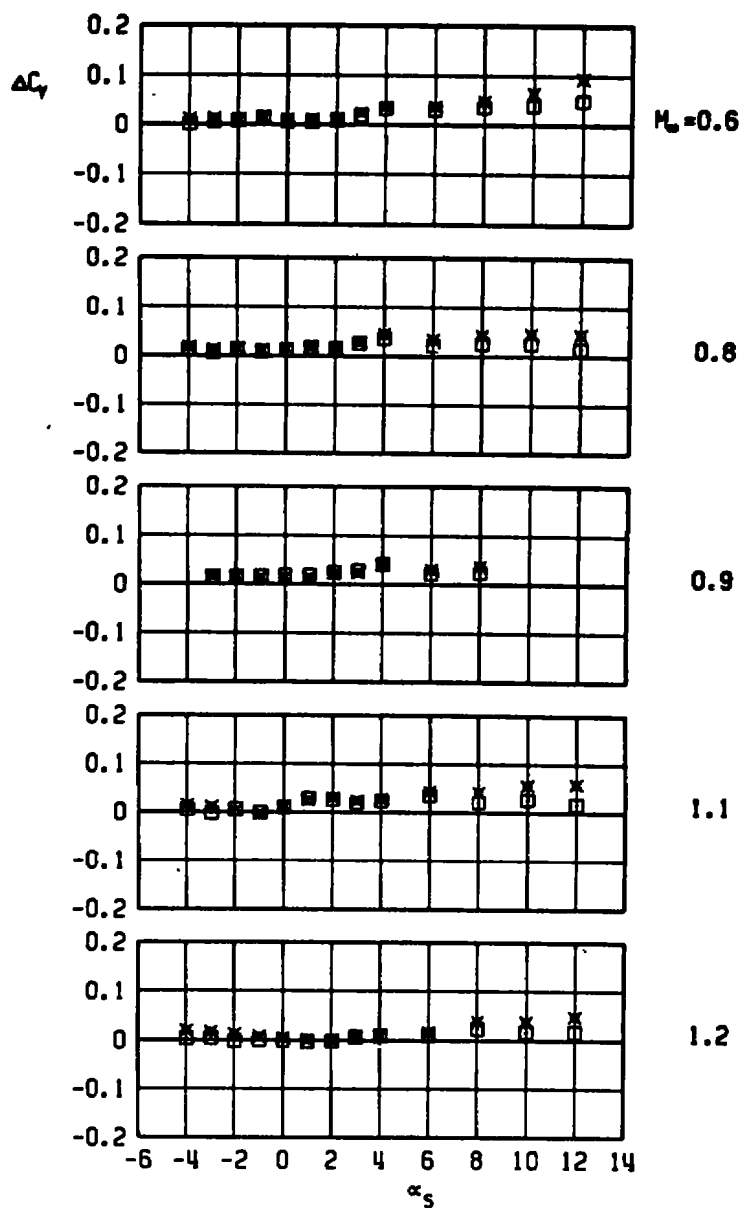
M-118, LIB PYLON, AB EFFECT
 □ AB 2 ONLY
 x AB 2 WITH DUMMY STING, $D_3 = 0.64 D_2$



a. Normal-force increment

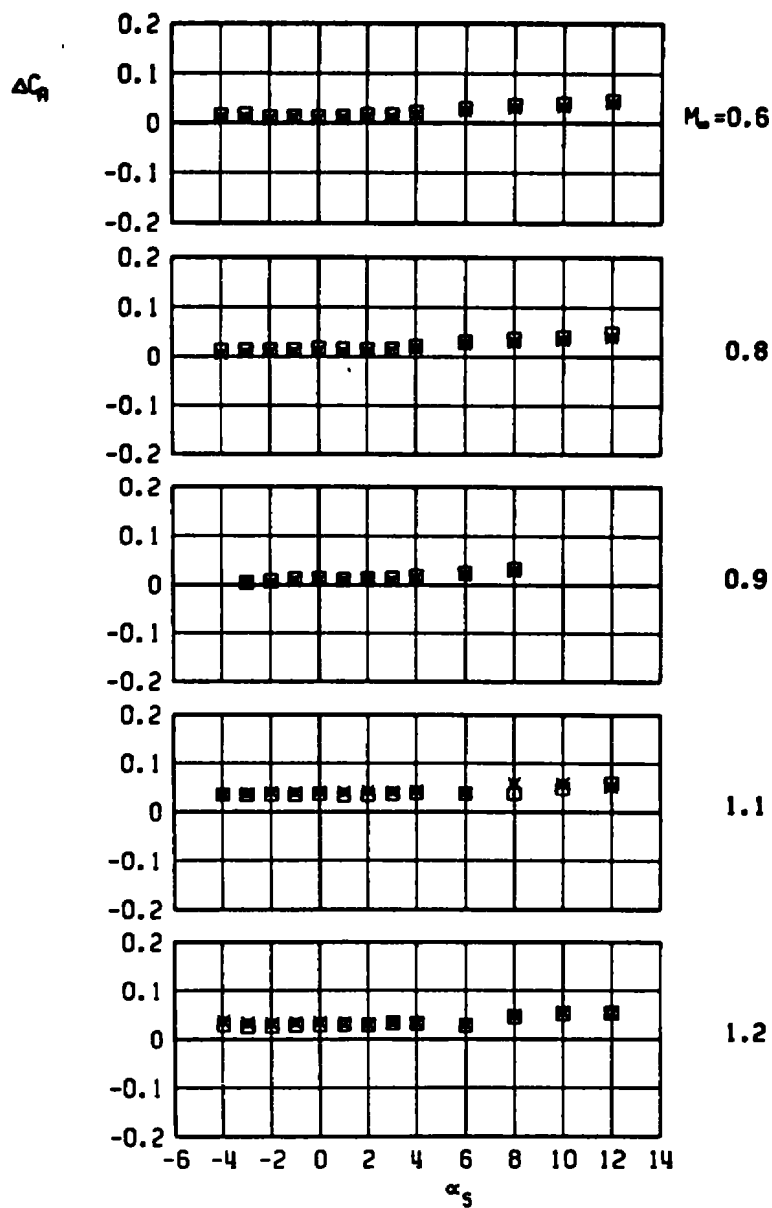
Figure 50. Aerodynamic load increments attributable to cylindrical distortion of the afterbody of a stable pylon-mounted store, M-118 store with AB2, LIB pylon.

M-118, L18 PYLON, AB EFFECT
 AB 2 ONLY
 X AB 2 WITH DUMMY STING, $D_3 = 0.64 D_9$



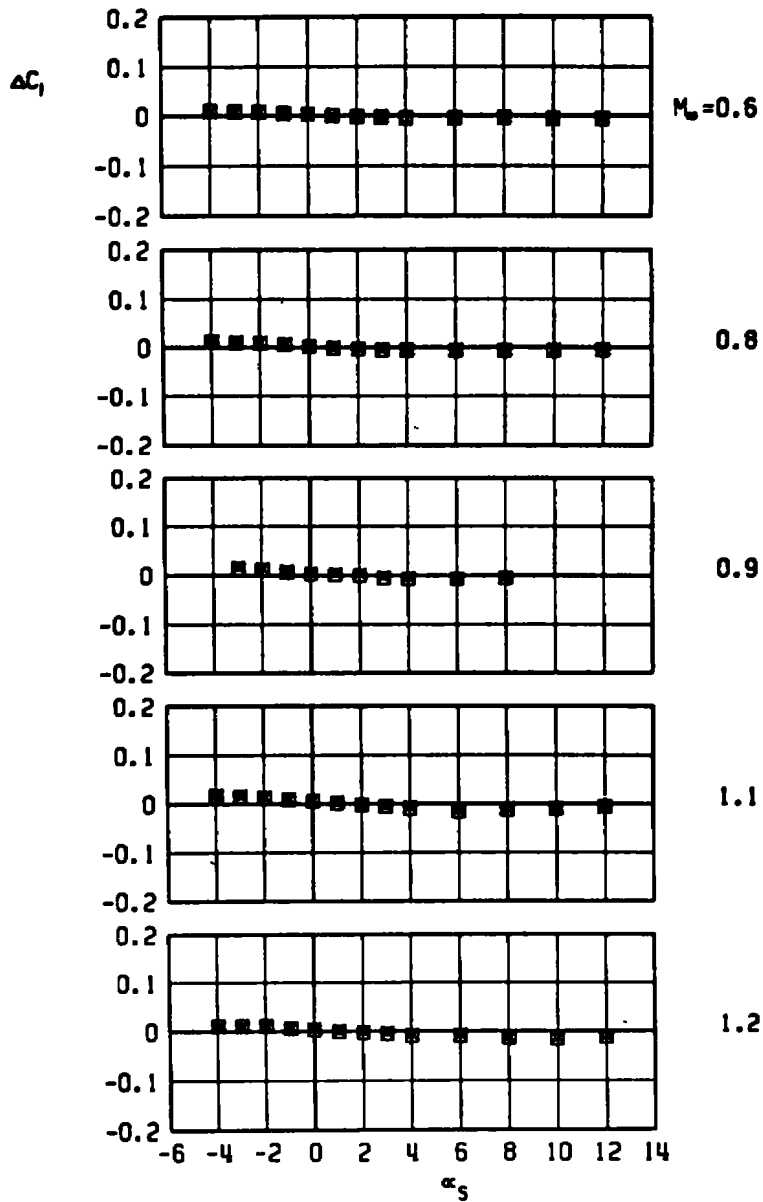
b. Side-force increment
 Figure 50. Continued.

M-118, LIB PYLON, AB EFFECT
 AB 2 ONLY
 X AB 2 WITH DUMMY STING, $D_3 = 0.64 D_0$



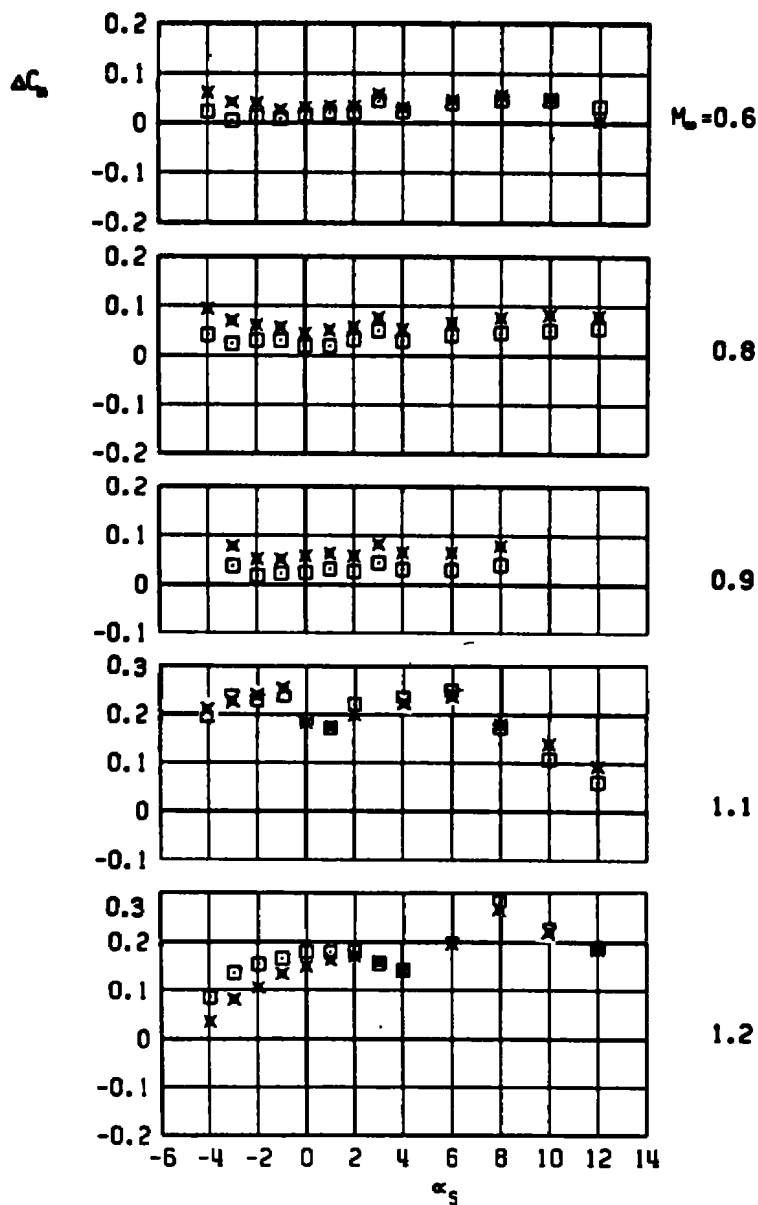
c. Axial-force increment
 Figure 50. Continued.

M-118, LIB PYLON, AB EFFECT
 □ AB 2 ONLY
 x AB 2 WITH DUMMY STING, $D_3 = 0.64 D_0$



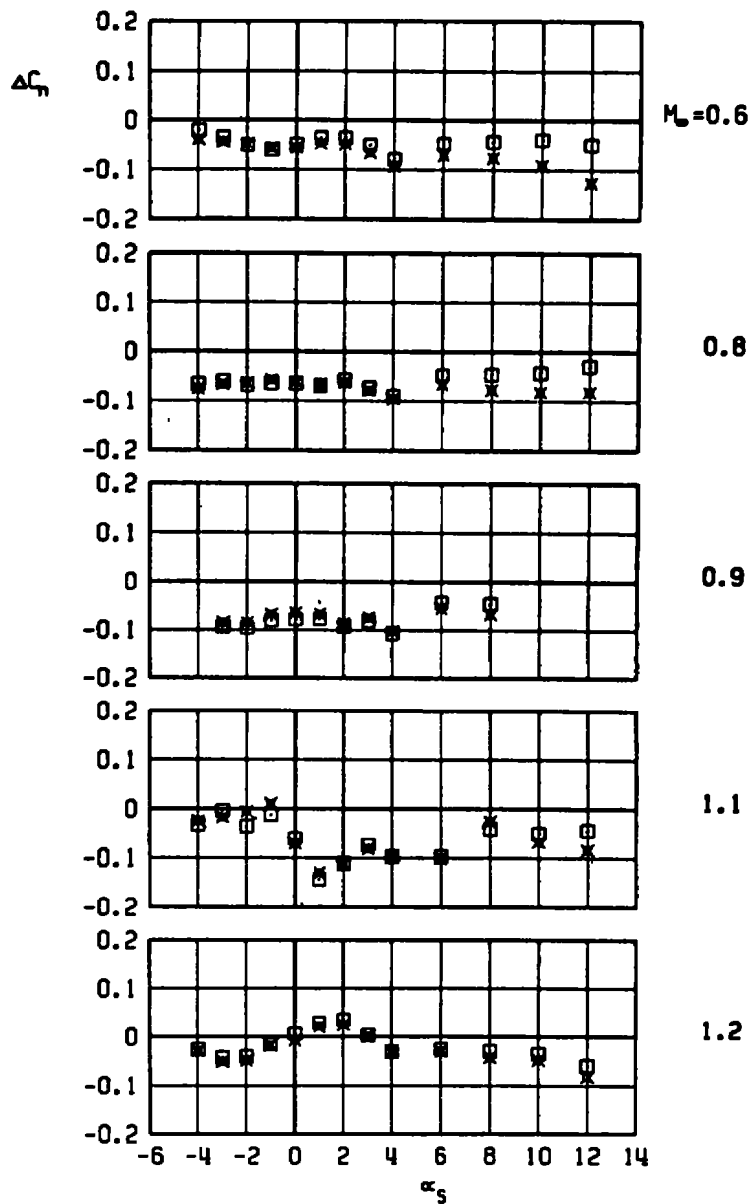
d. Rolling-moment increment
 Figure 50. Continued.

M-118, LIB PYLON, AB EFFECT
 □ AB 2 ONLY
 × AB 2 WITH DUMMY STING, $D_3 = 0.64 D_0$



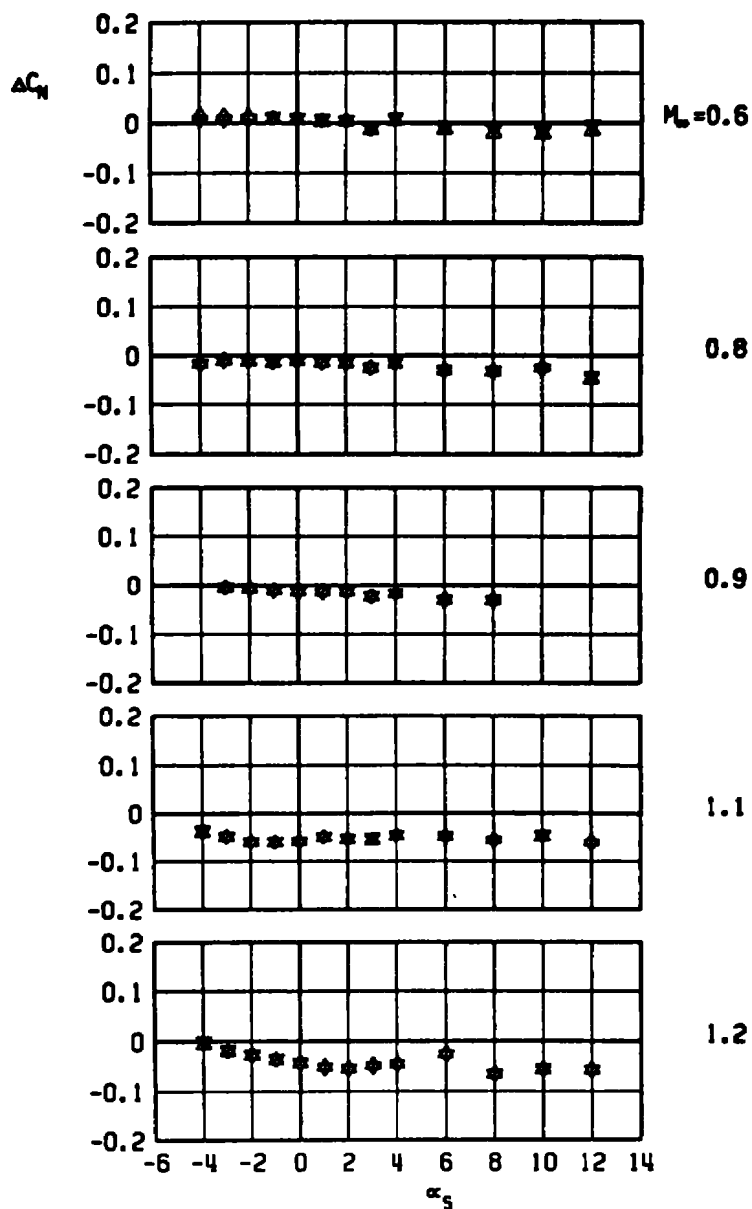
e. Pitching-moment increment
 Figure 50. Continued.

M-118, LIB PYLON, AB EFFECT
 AB 2 ONLY
 X AB 2 WITH DUMMY STING, $D_3 = 0.64 D_0$



f. Yawing-moment increment
 Figure 50. Concluded.

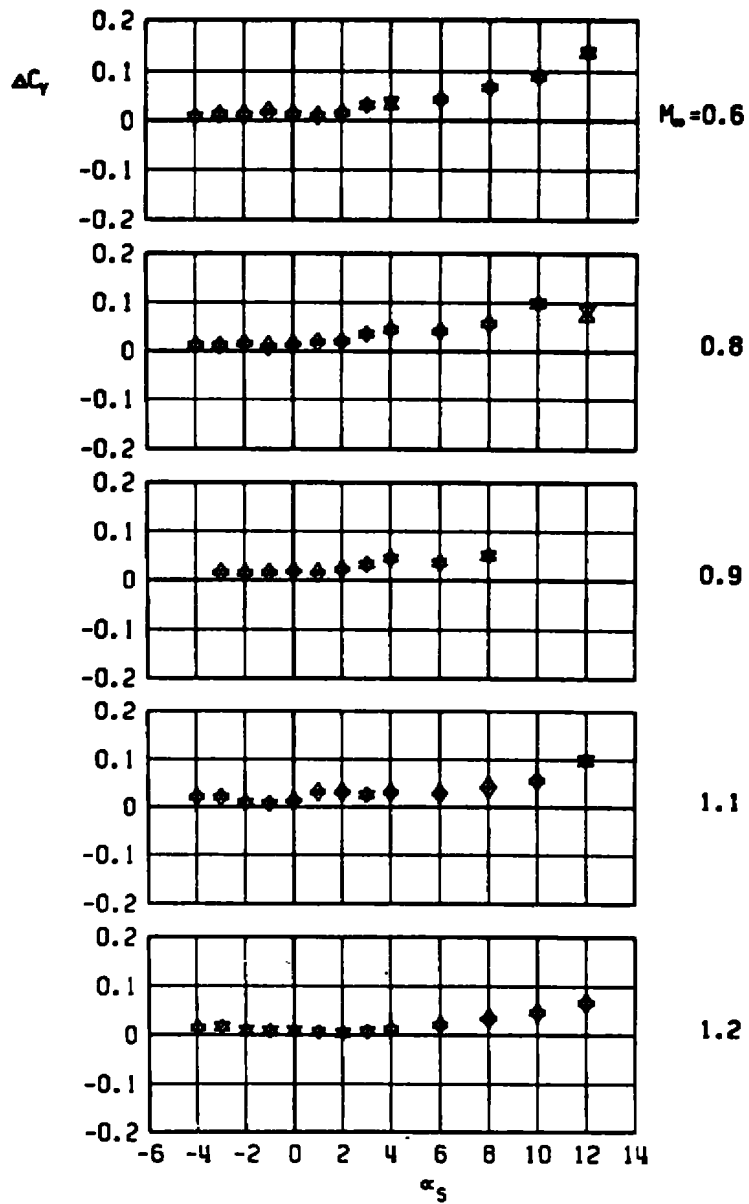
▲ M-118, LIB PYLON, AB EFFECT
 AB 3 ONLY
 ▼ AB 3 WITH DUMMY STING, $D_3 = 0.56 D_0$



a. Normal-force increment

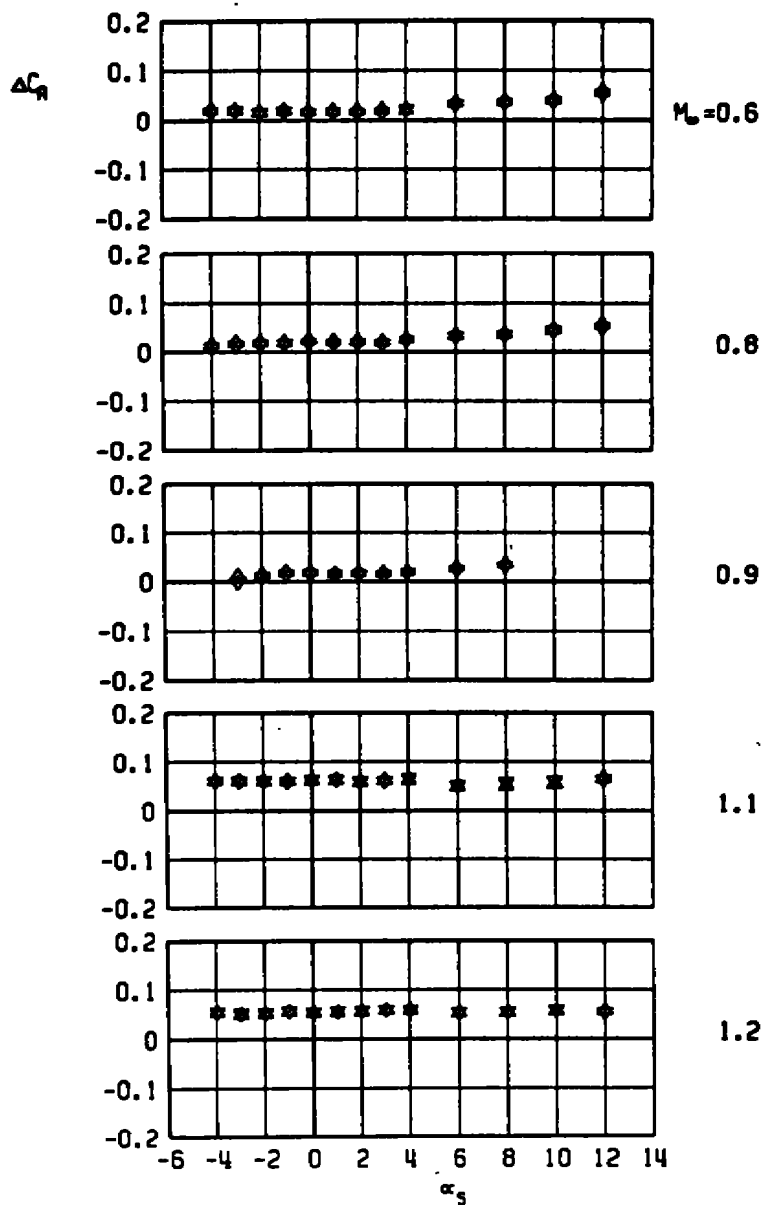
Figure 51. Aerodynamic load increments attributable to cylindrical distortion of the afterbody of a stable pylon-mounted store, M-118 store with AB3, LIB pylon.

▲ M-118, LIB PYLON, AB EFFECT
 AB 3 ONLY
 ▼ AB 3 WITH DUMMY STING, $D_3 = 0.56 D_0$



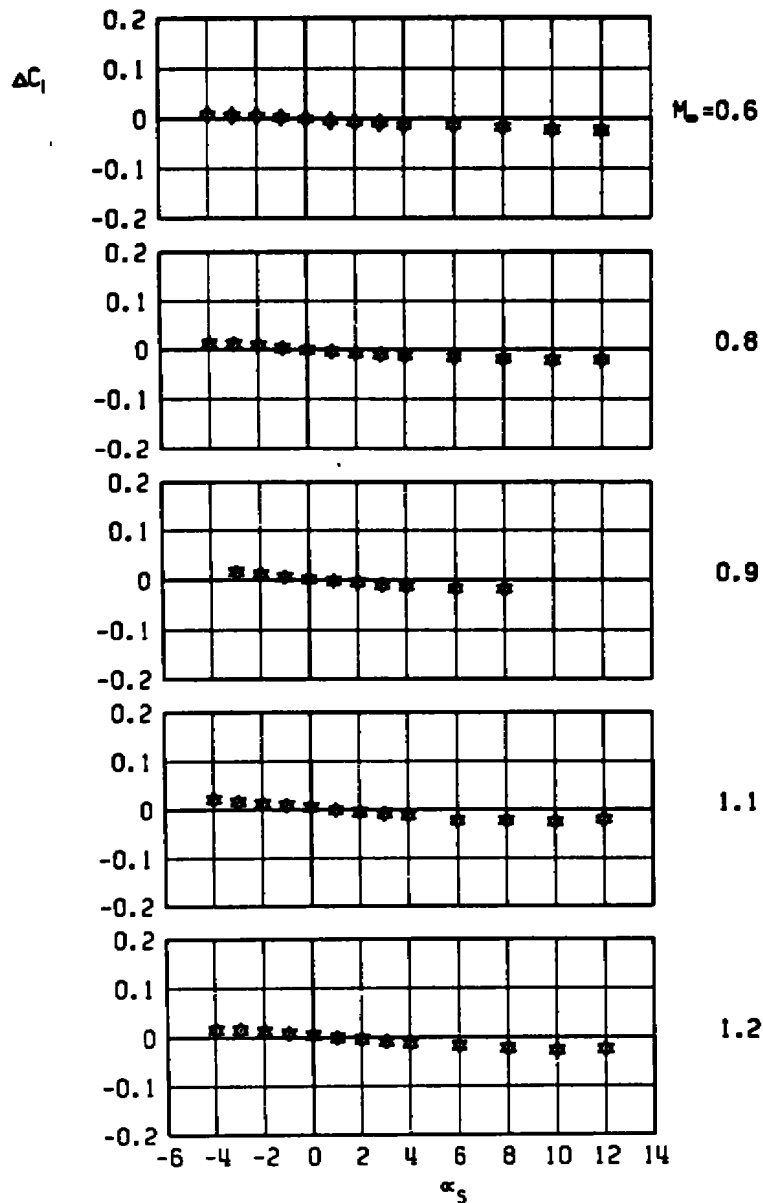
b. Side-force increment
 Figure 51. Continued.

▲ M-118, LIB PYLON, AB EFFECT
 AB 3 ONLY
 ▼ AB 3 WITH DUMMY STING, $D_3 = 0.56 D_0$



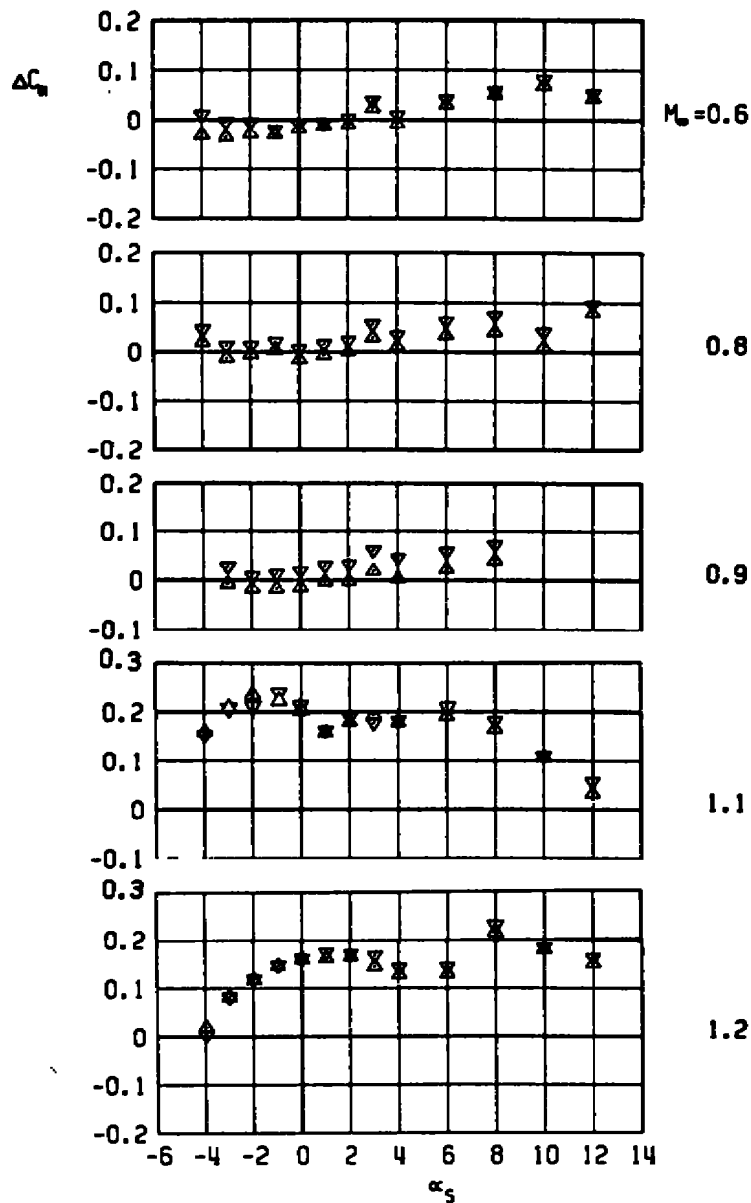
c. Axial-force increment
 Figure 51. Continued.

▲ M-118, LIB PYLON, AB EFFECT
 AB 3 ONLY
 ▼ AB 3 WITH DUMMY STING, $D_3 = 0.56 D_0$



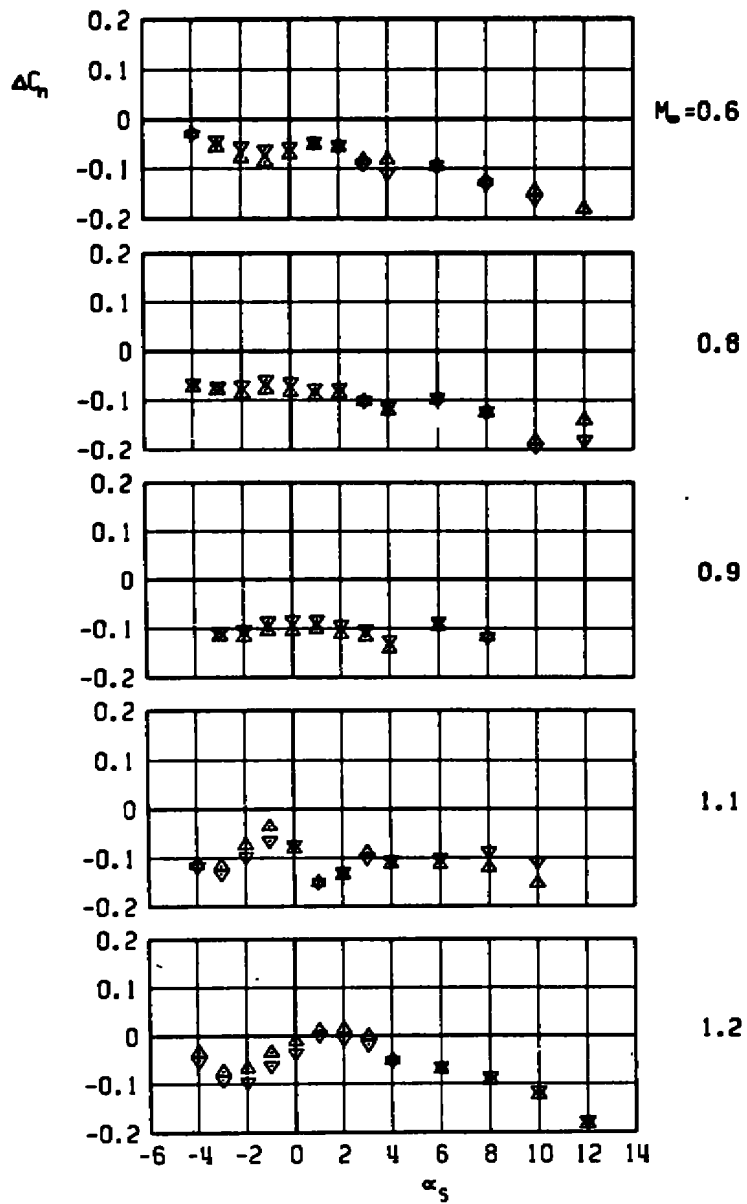
d. Rolling-moment increment
 Figure 51. Continued.

M-118, LIB PYLON, AB EFFECT
 ▲ AB 3 ONLY
 ▼ AB 3 WITH DUMMY STING, $D_5 = 0.56 D_0$



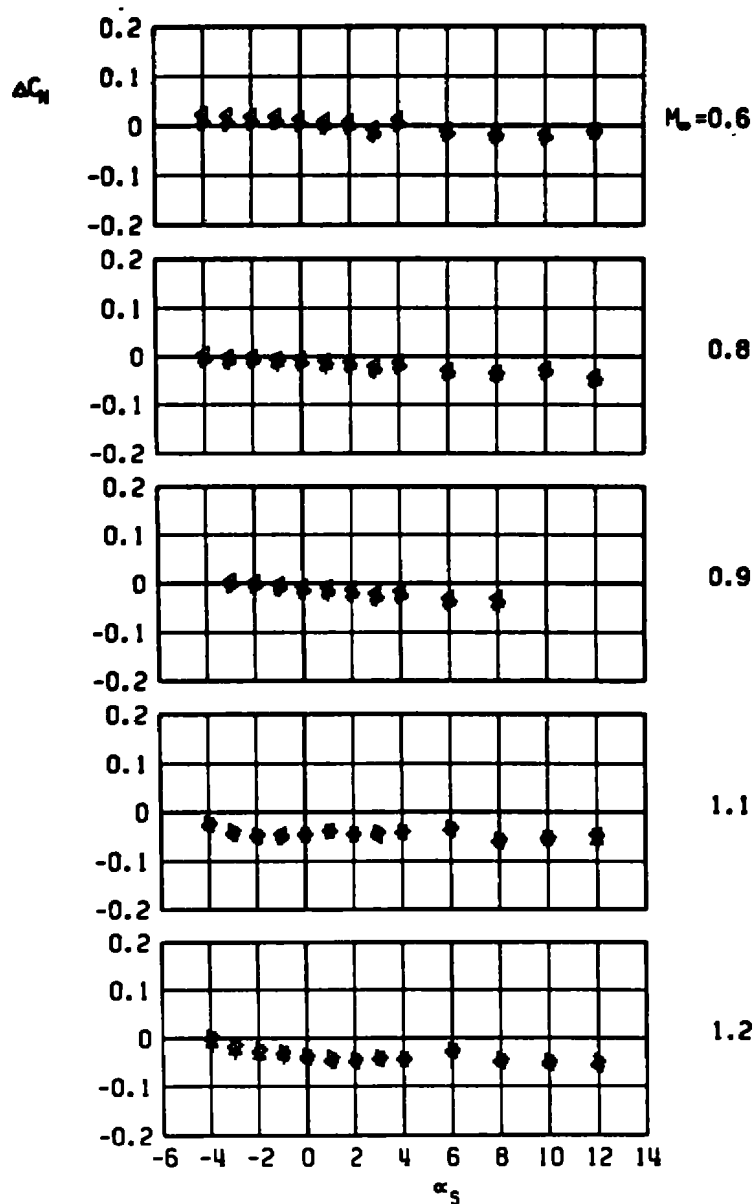
e. Pitching-moment increment
 Figure 51. Continued.

M-118, LIB PYLON, AB EFFECT
 ▲ AB 3 ONLY
 ▼ AB 3 WITH DUMMY STING, $D_3 = 0.56 D_9$



f. Yawing-moment increment
 Figure 51. Concluded.

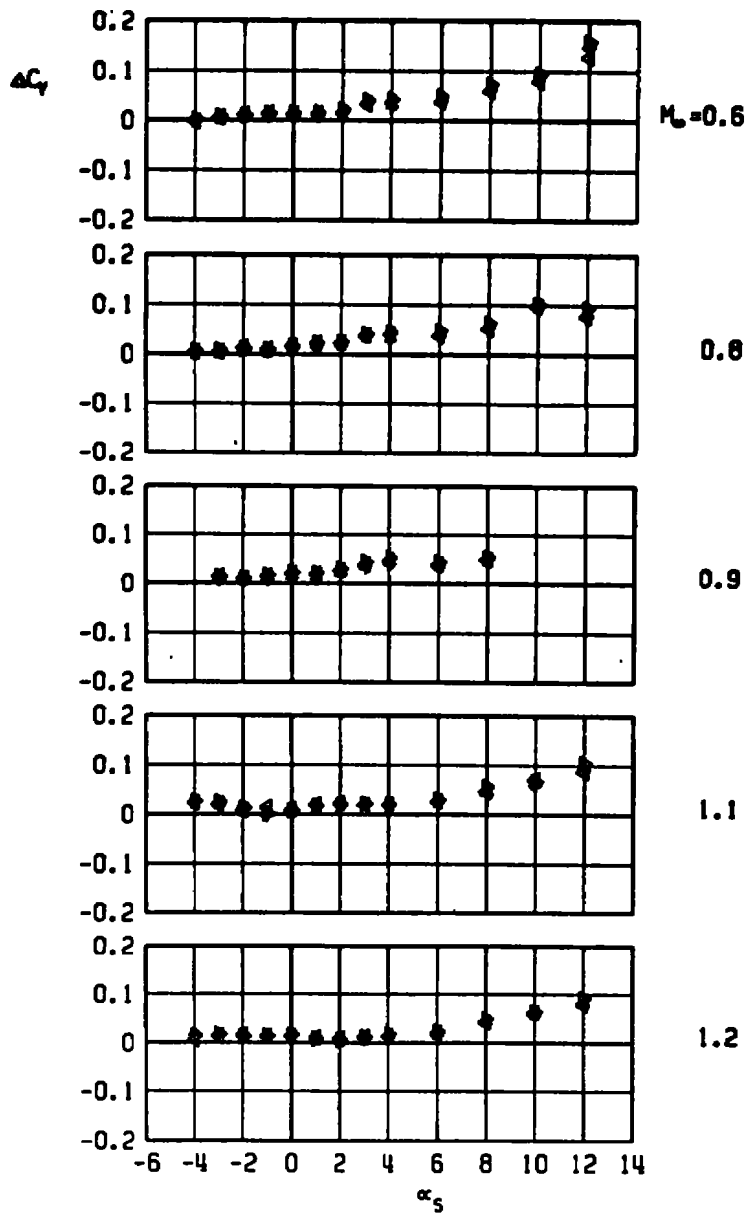
M-118, LIB PYLON, AB EFFECT
 ◀ AB 4 ONLY
 ▶ AB 4 WITH DUMMY STING, $D_3 = 0.49 D_0$
 ◆ AB 4 WITH DUMMY STING, $D_3 = 0.74 D_0$



a. Normal-force increment

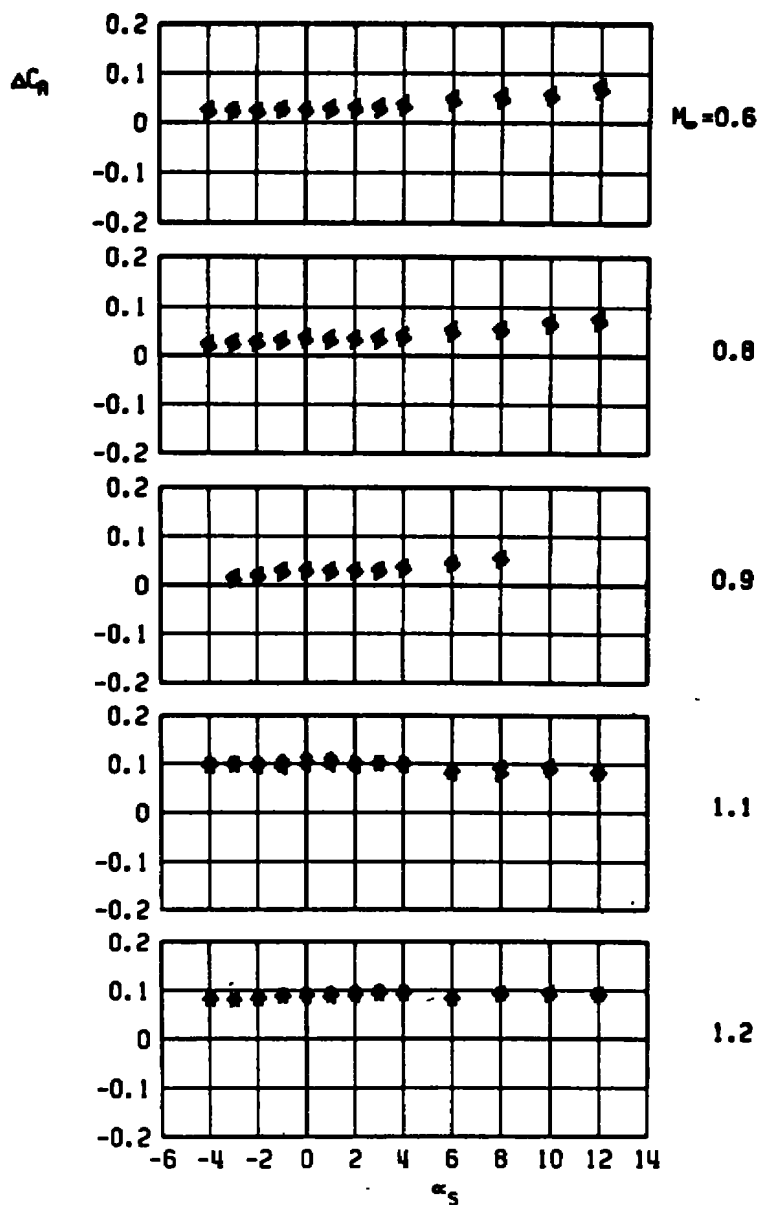
Figure 52. Aerodynamic load increments attributable to cylindrical distortion of the afterbody of a stable pylon-mounted store, M-118 store with AB4, LIB pylon.

M-118, L18 PYLON, AB EFFECT
 ▲ AB 4 ONLY
 ▴ AB 4 WITH DUMMY STING, $D_3 = 0.49 D_0$
 + AB 4 WITH DUMMY STING, $D_3 = 0.74 D_0$



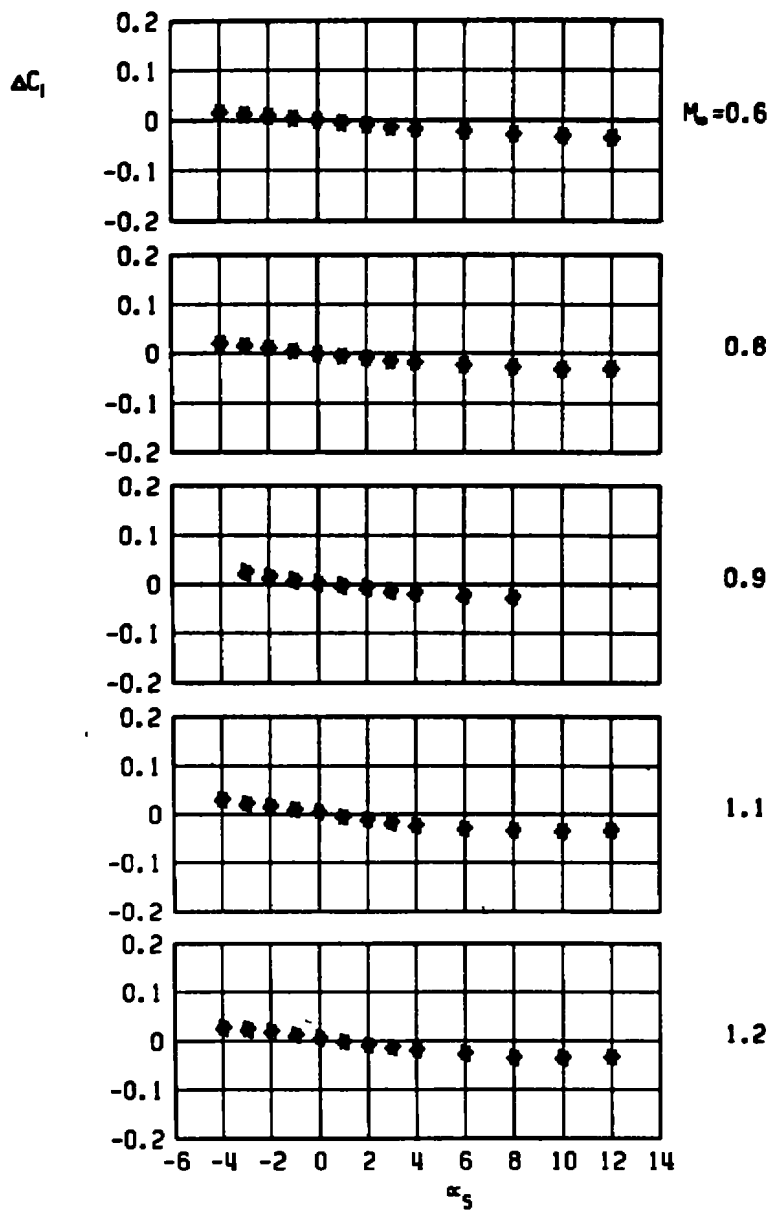
b. Side-force increment
 Figure 52. Continued.

M-118, L18 PYLON, AB EFFECT
 ▲ AB 4 ONLY
 ▴ AB 4 WITH DUMMY STING, $D_3 = 0.49 D_0$
 ◆ AB 4 WITH DUMMY STING, $D_3 = 0.74 D_0$



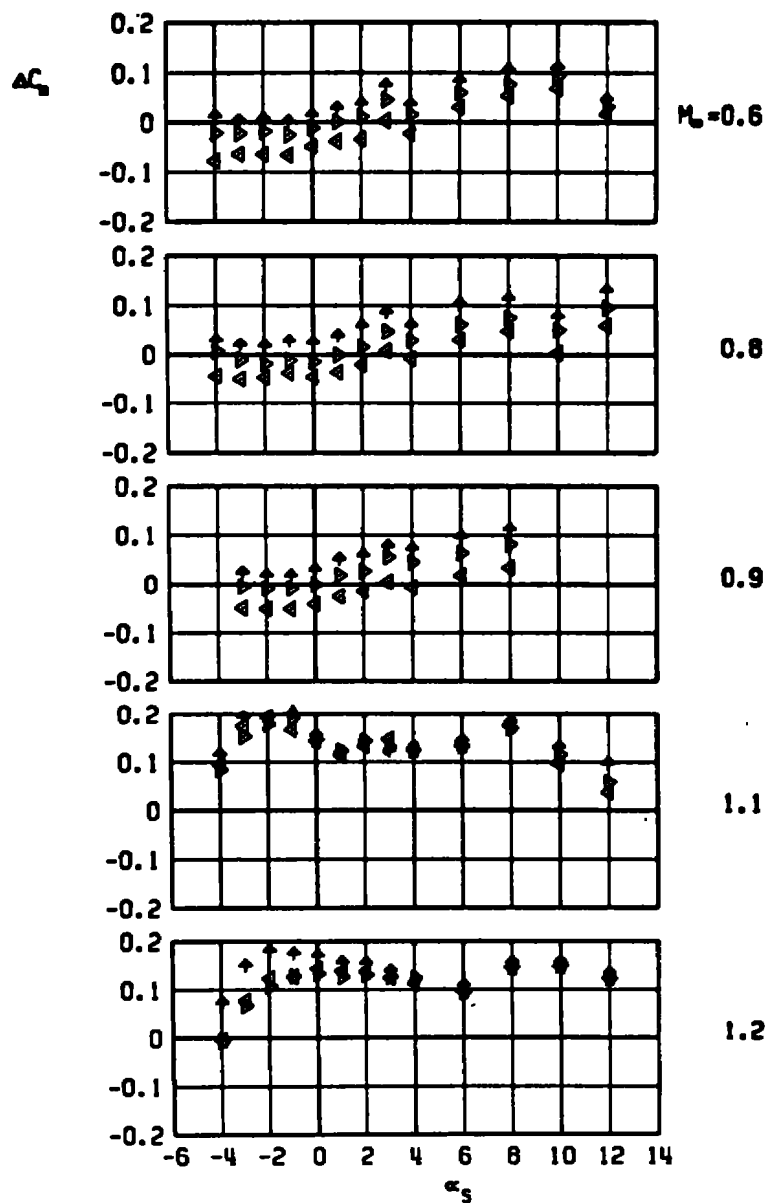
c. Axial-force increment
 Figure 52. Continued.

M-118, LIB PYLON, AB EFFECT
 AB 4 ONLY
 AB 4 WITH DUMMY STING, $D_3 = 0.49 D_0$
 AB 4 WITH DUMMY STING, $D_3 = 0.74 D_0$



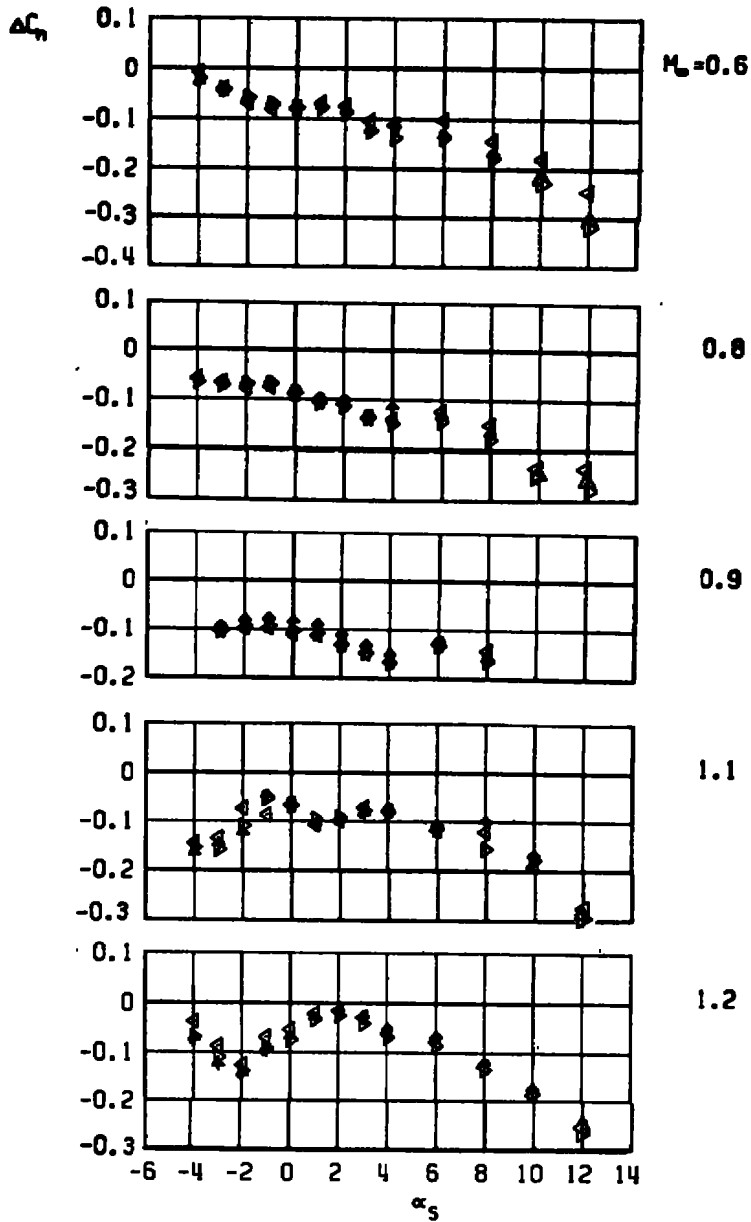
d. Rolling-moment increment
 Figure 52. Continued.

M-118, L18 PYLON, AB EFFECT
 AB 4 ONLY
 AB 4 WITH DUMMY STING, $D_3 = 0.49 D_0$
 AB 4 WITH DUMMY STING, $D_3 = 0.74 D_0$

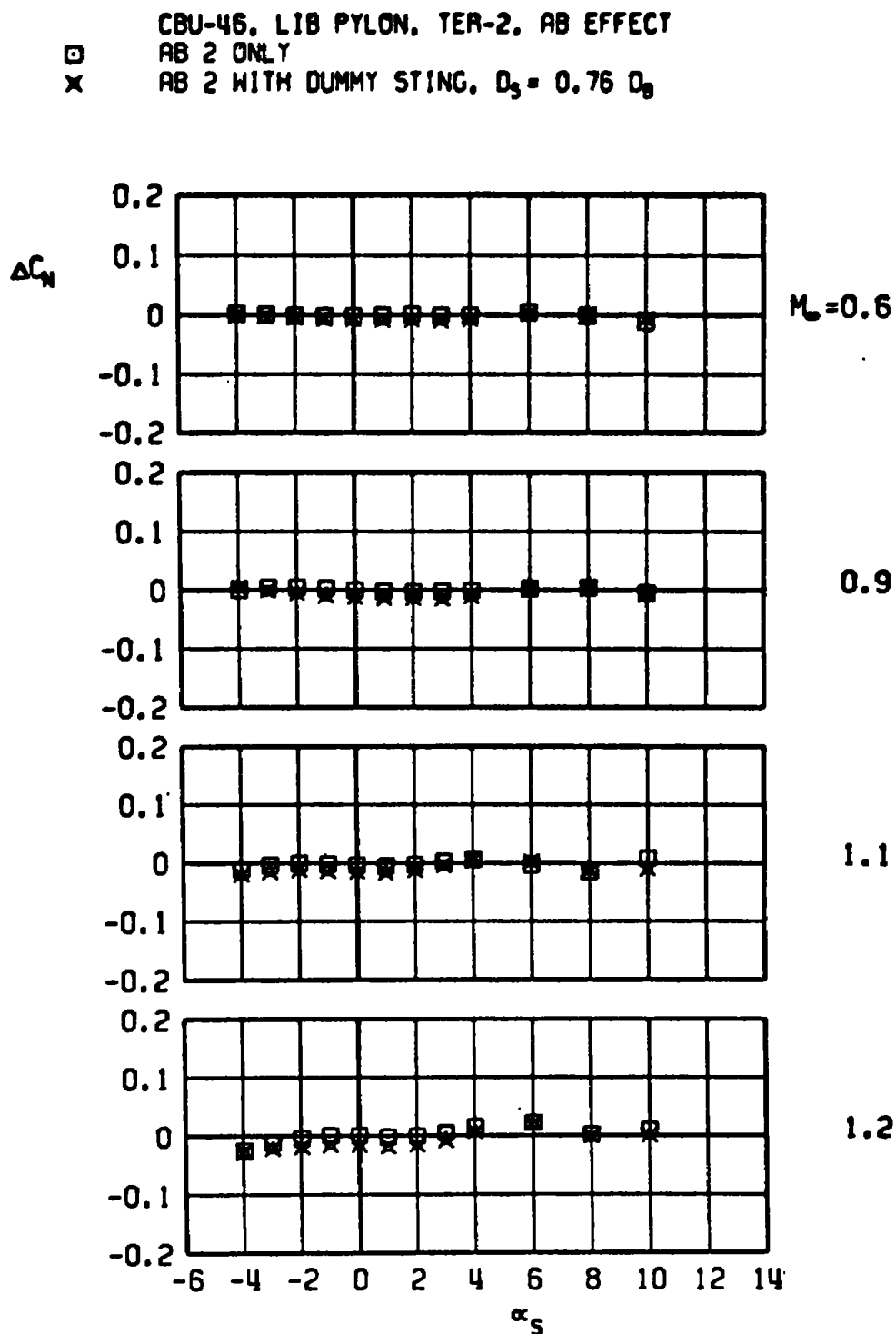


e. Pitching-moment increment
 Figure 52. Continued.

- M-118, LIB PYLON, AB EFFECT
 AB 4 ONLY
 AB 4 WITH DUMMY STING, $D_3 = 0.49 D_0$
 AB 4 WITH DUMMY STING, $D_3 = 0.74 D_0$



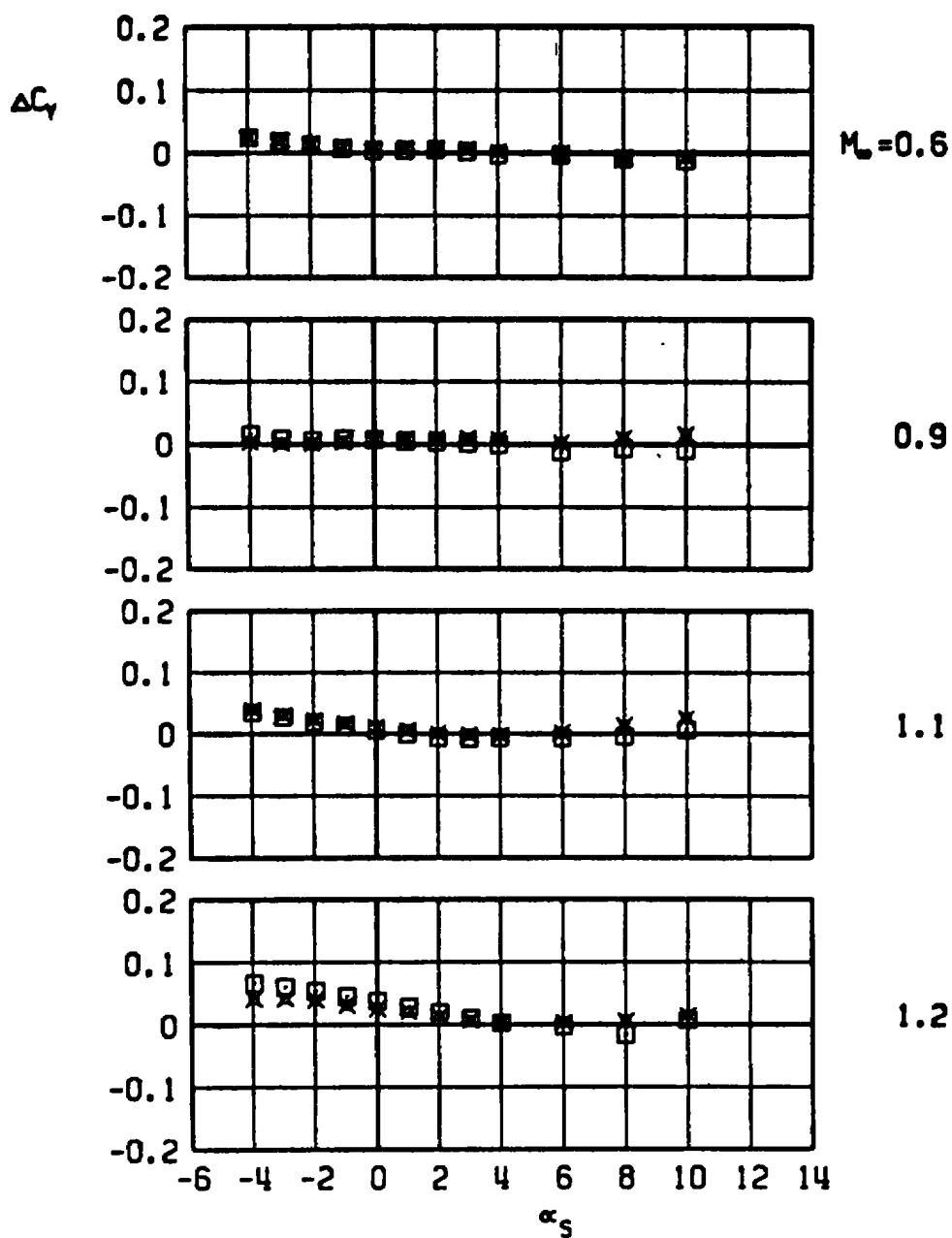
f. Yawing-moment increment
 Figure 53. Concluded.



a. Normal-force increment

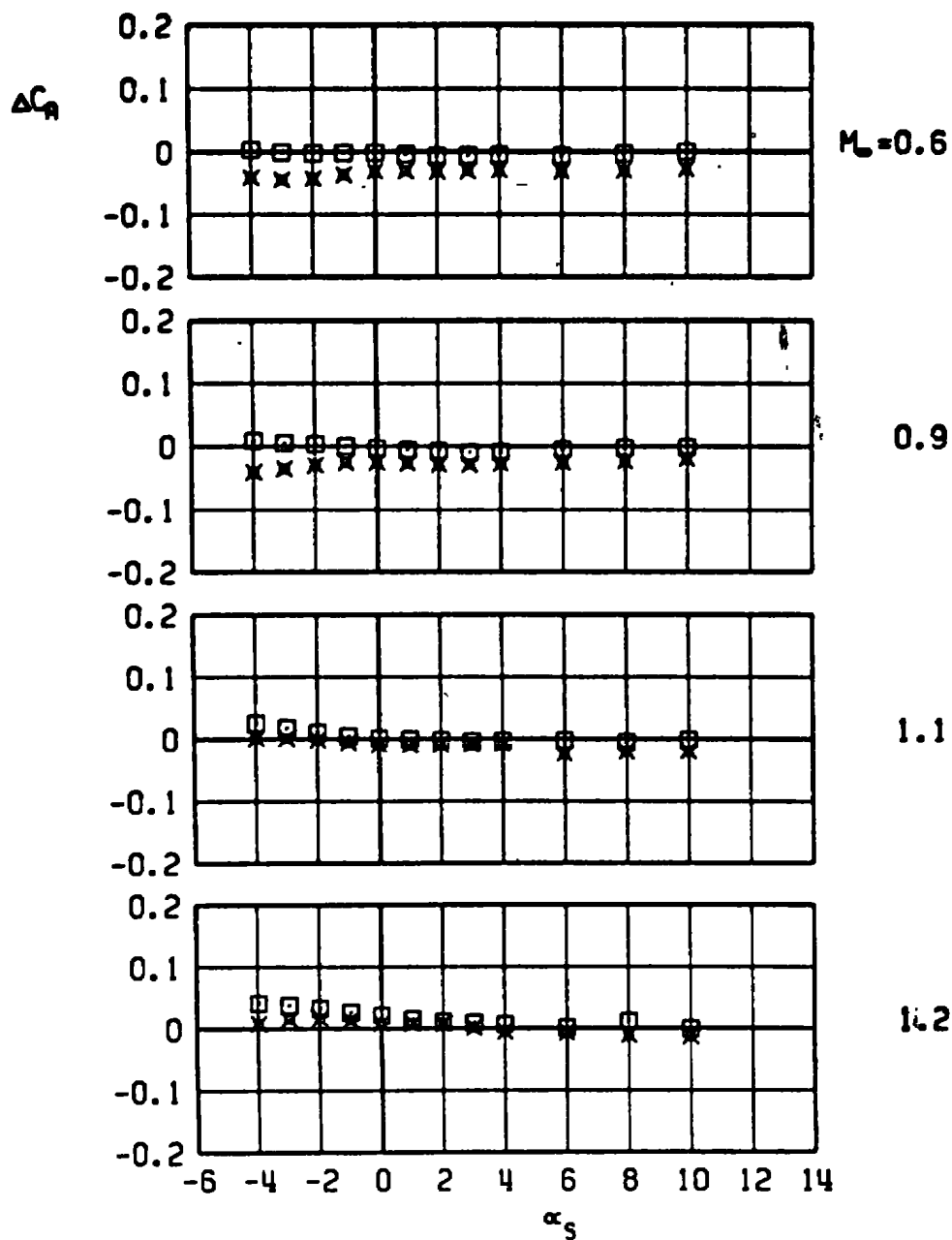
Figure 53. Aerodynamic load increments attributable to truncation of the afterbody of an unstable rack-mounted store, CBU-46 with AB2, TER station 2, LIB pylon.

CBU-46, LIB PYLON, TER-2, AB EFFECT
 AB 2 ONLY
 AB 2 WITH DUMMY STING, $D_3 = 0.76 D_0$



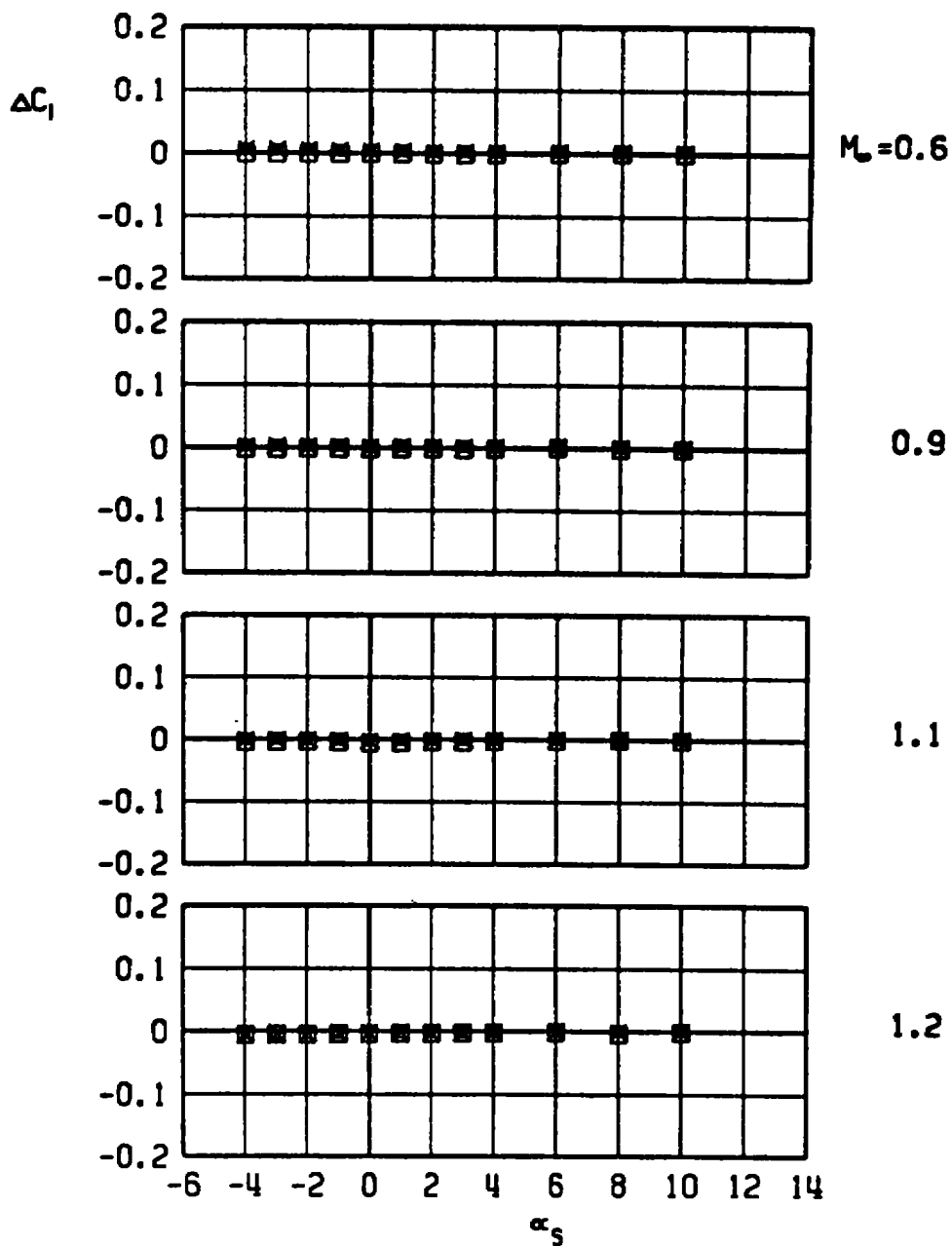
b. Side-force increment
 Figure 53. Continued.

CBU-46, LIB PYLON, TER-2, AB EFFECT
 □ AB 2 ONLY
 × AB 2 WITH DUMMY STING, $D_3 = 0.76 D_0$



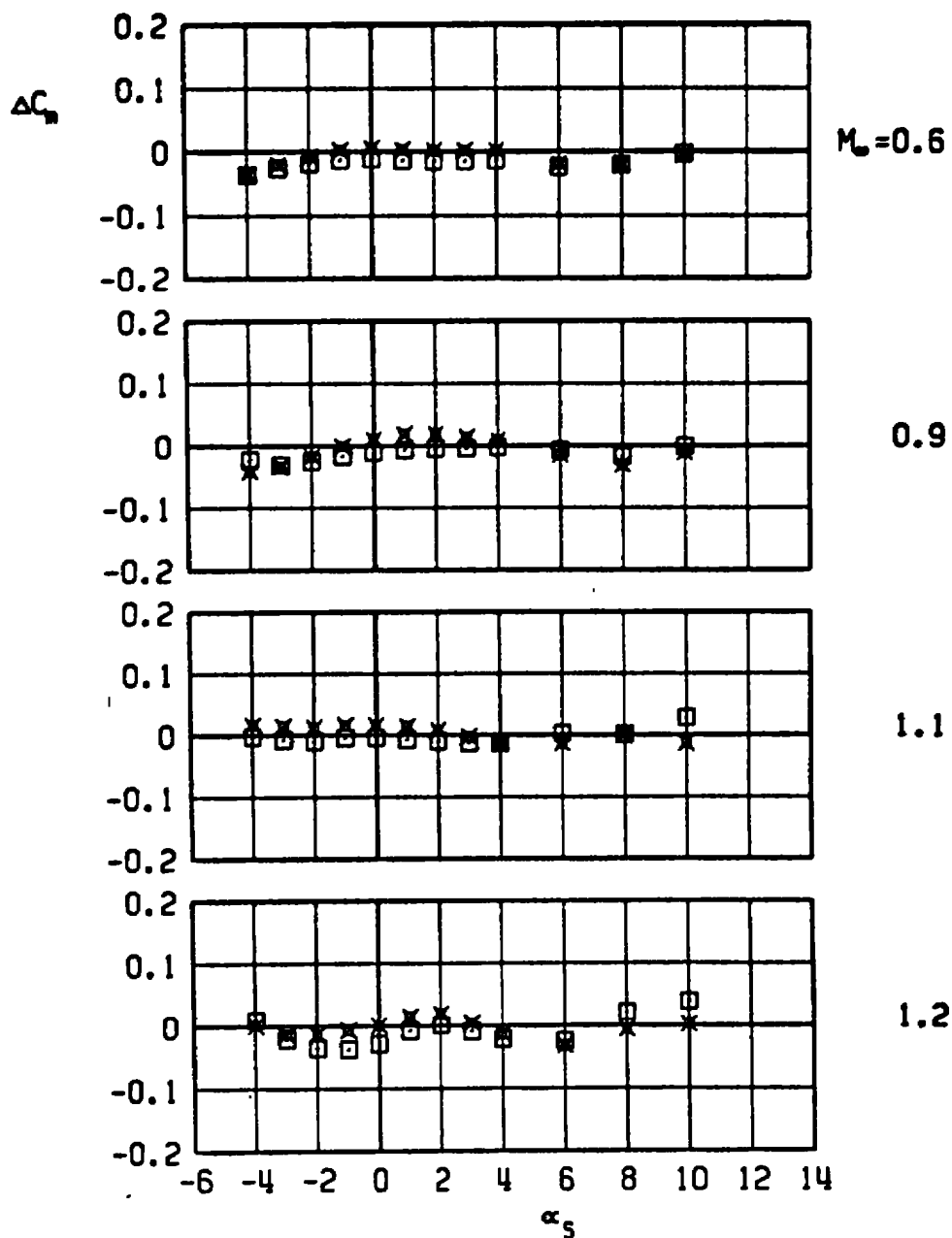
c. Axial-force increment
 Figure 53. Continued.

CBU-46, LIB PYLON, TER-2, AB EFFECT
 □ AB 2 ONLY
 × AB 2 WITH DUMMY STING, $D_3 = 0.76 D_0$



d. Rolling-moment increment
 Figure 53. Continued.

□ CBU-46, LIB PYLON, TEA-2, AB EFFECT
 AB 2 ONLY
 x AB 2 WITH DUMMY STING, $D_3 = 0.76 D_0$



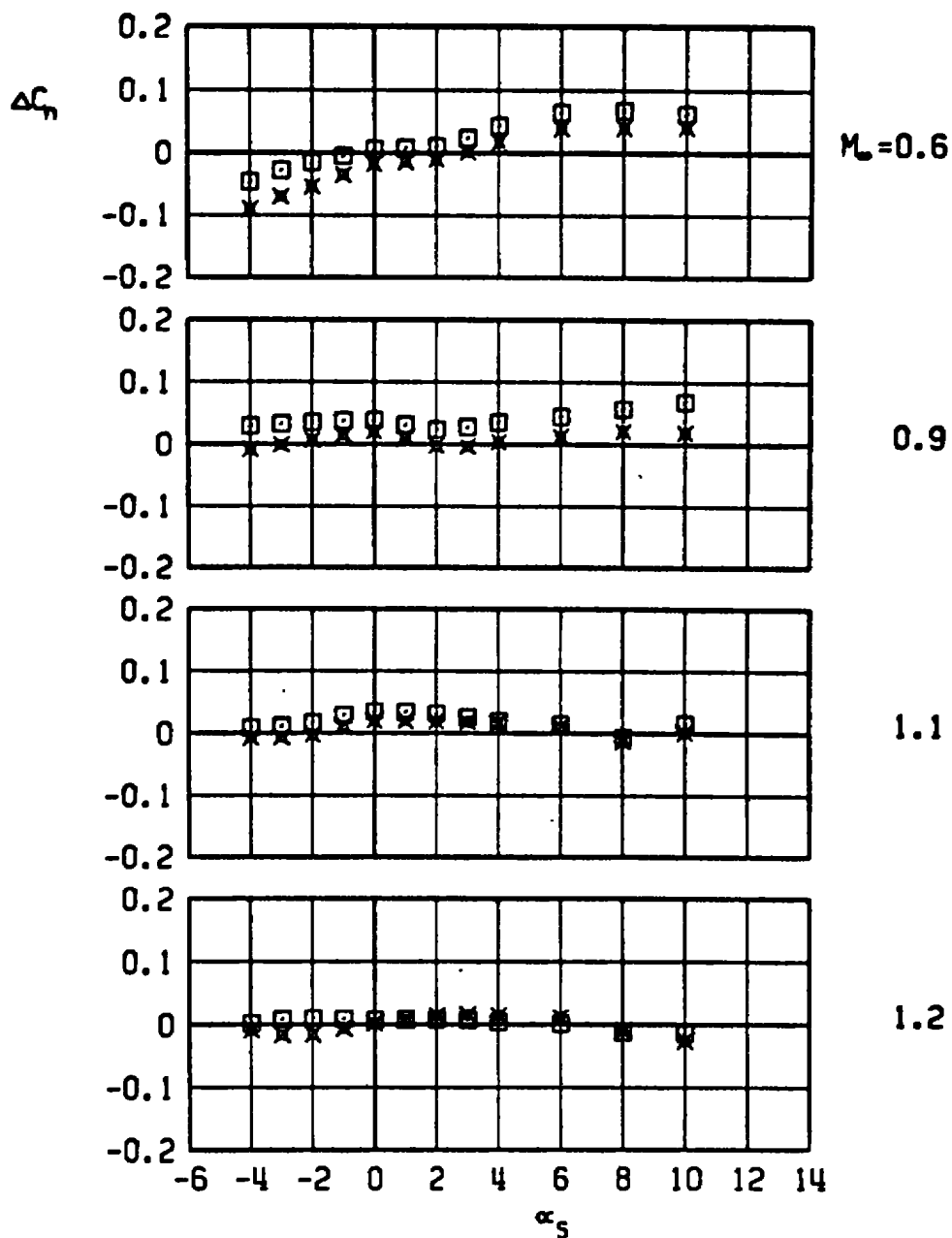
e. Pitching-moment increment
 Figure 53. Continued.

CBU-46, LIB PYLON, TER-2, AB EFFECT

□

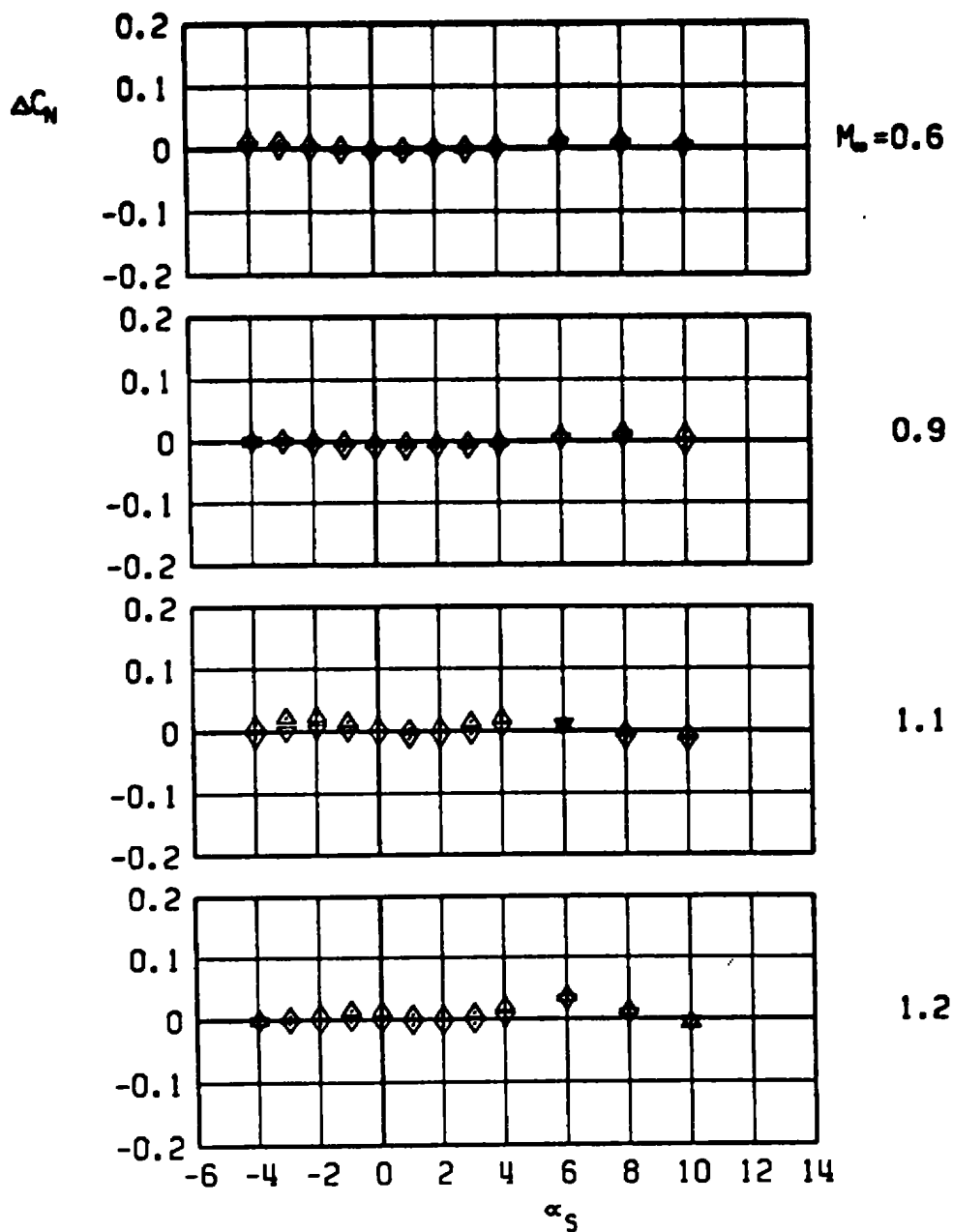
AB 2 ONLY

x

AB 2 WITH DUMMY STING, $D_3 = 0.76 D_0$ 

f. Yawing-moment increment
Figure 53. Concluded.

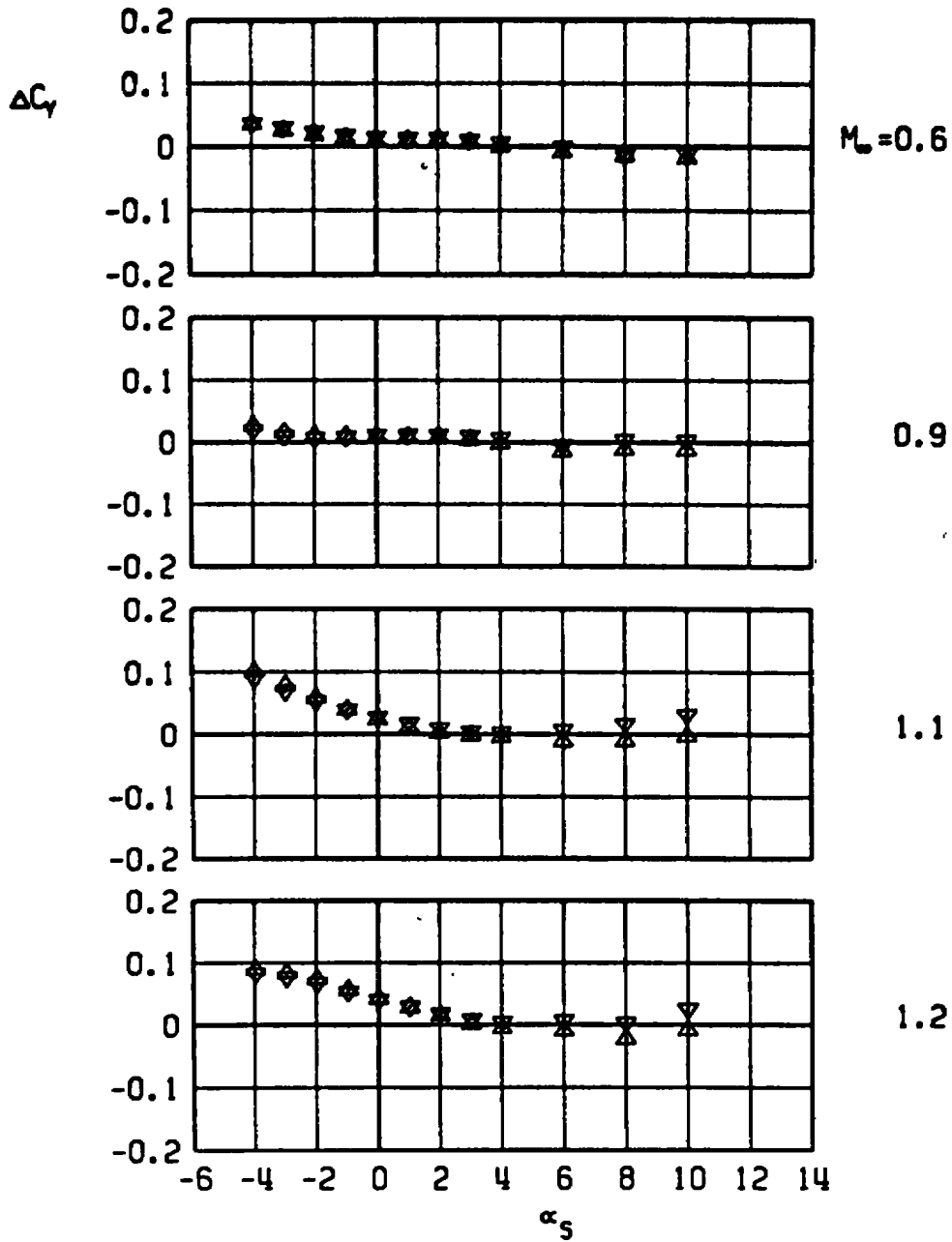
▲ CBU-46, LIB PYLON, TER-2, AB EFFECT
 AB 3 ONLY
 ▼ AB 3 WITH DUMMY STING, $D_3 = 0.62 D_0$



a. Normal-force increment

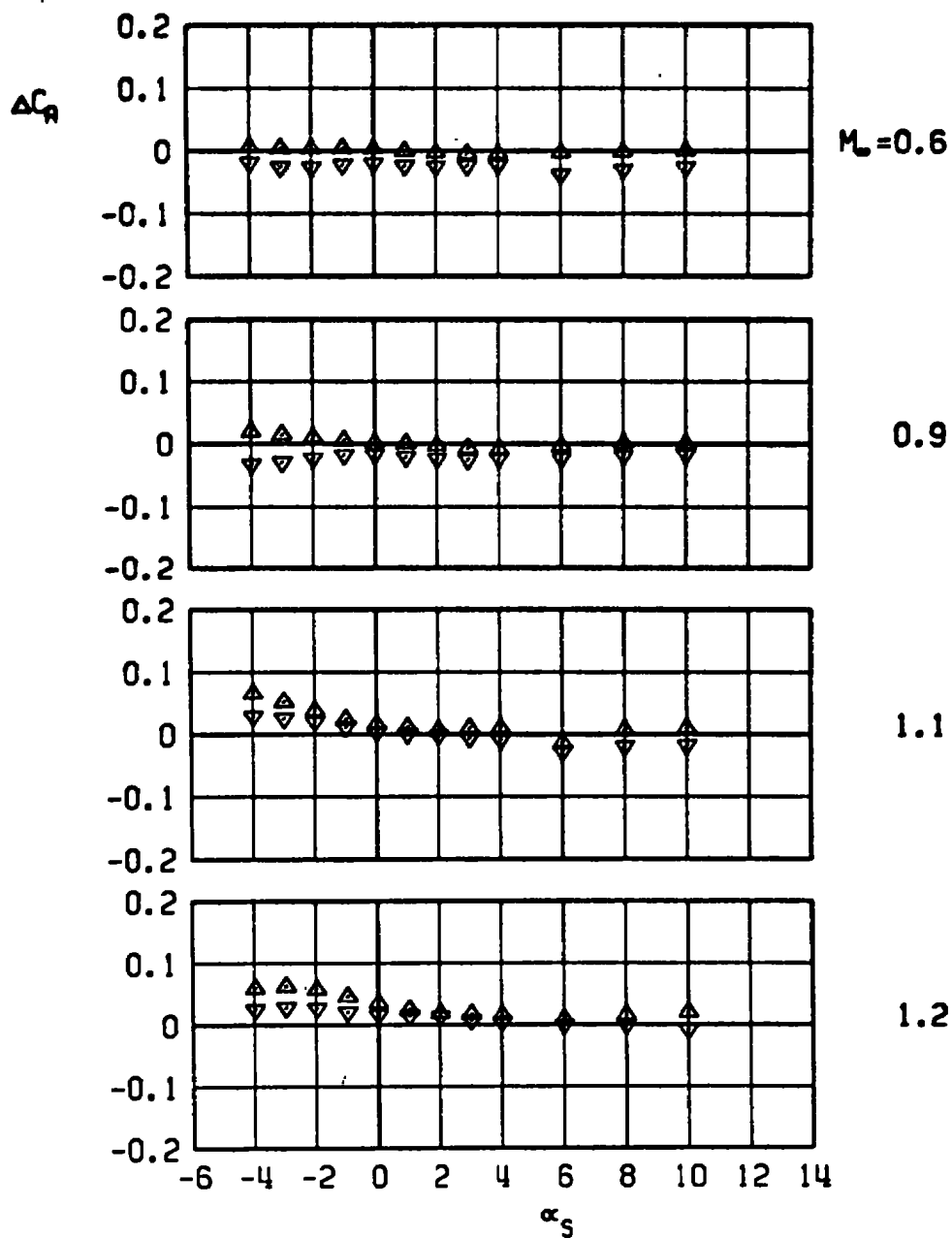
Figure 54. Aerodynamic load increments attributable to truncation of the afterbody of an unstable rack-mounted store, CBU-46 with AB3, TER station 2, LIB pylon.

▲ CBU-46, LIB PYLON, TEA-2, AB EFFECT
 AB 3 ONLY
 ▼ AB 3 WITH DUMMY STING, $D_5 = 0.62 D_6$



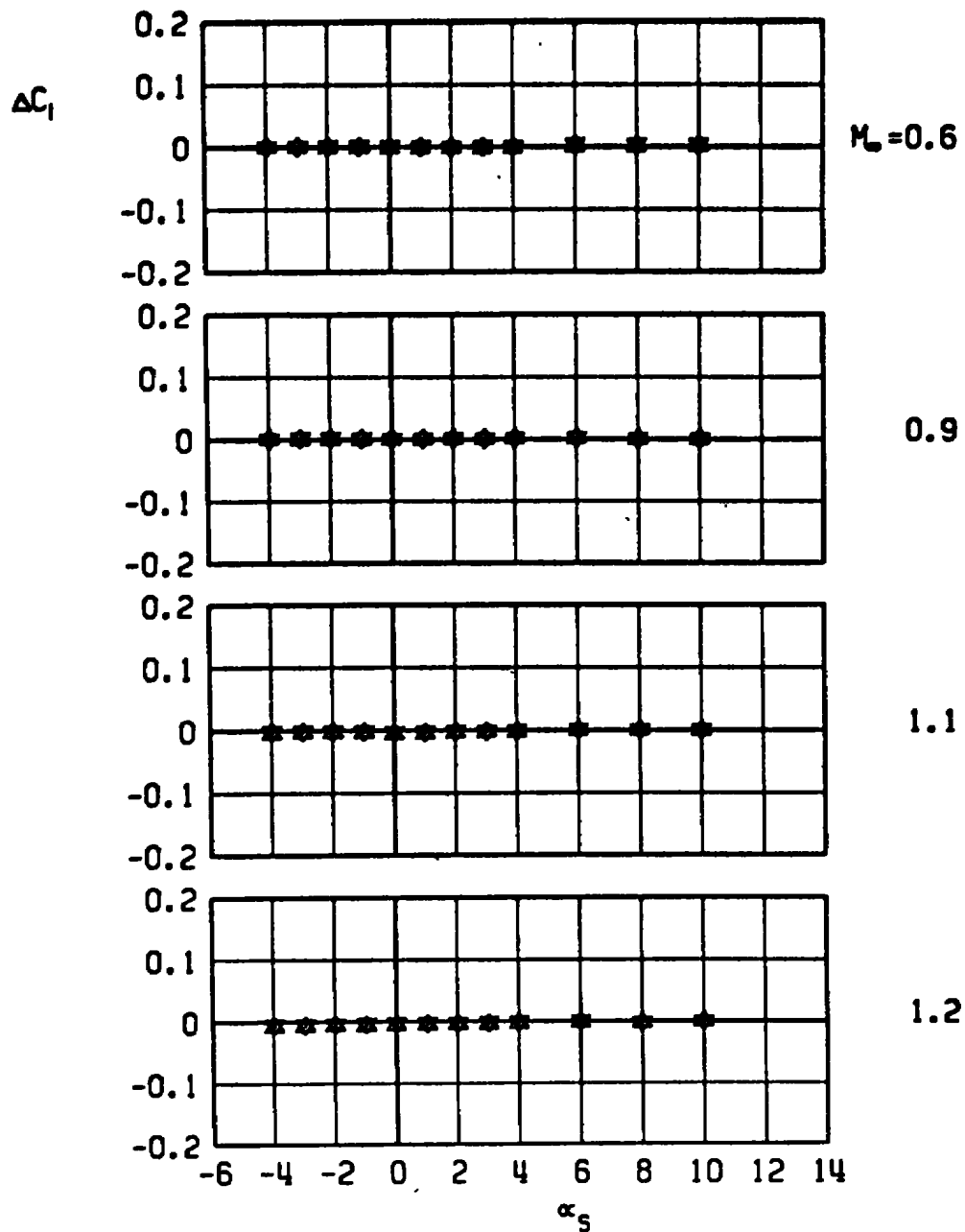
b. Side-force increment
 Figure 54. Continued.

▲ CBU-46, LIB PYLON, TER-2, AB EFFECT
 AB 3 ONLY
 ▼ AB 3 WITH DUMMY STING, $D_3 = 0.62 D_0$



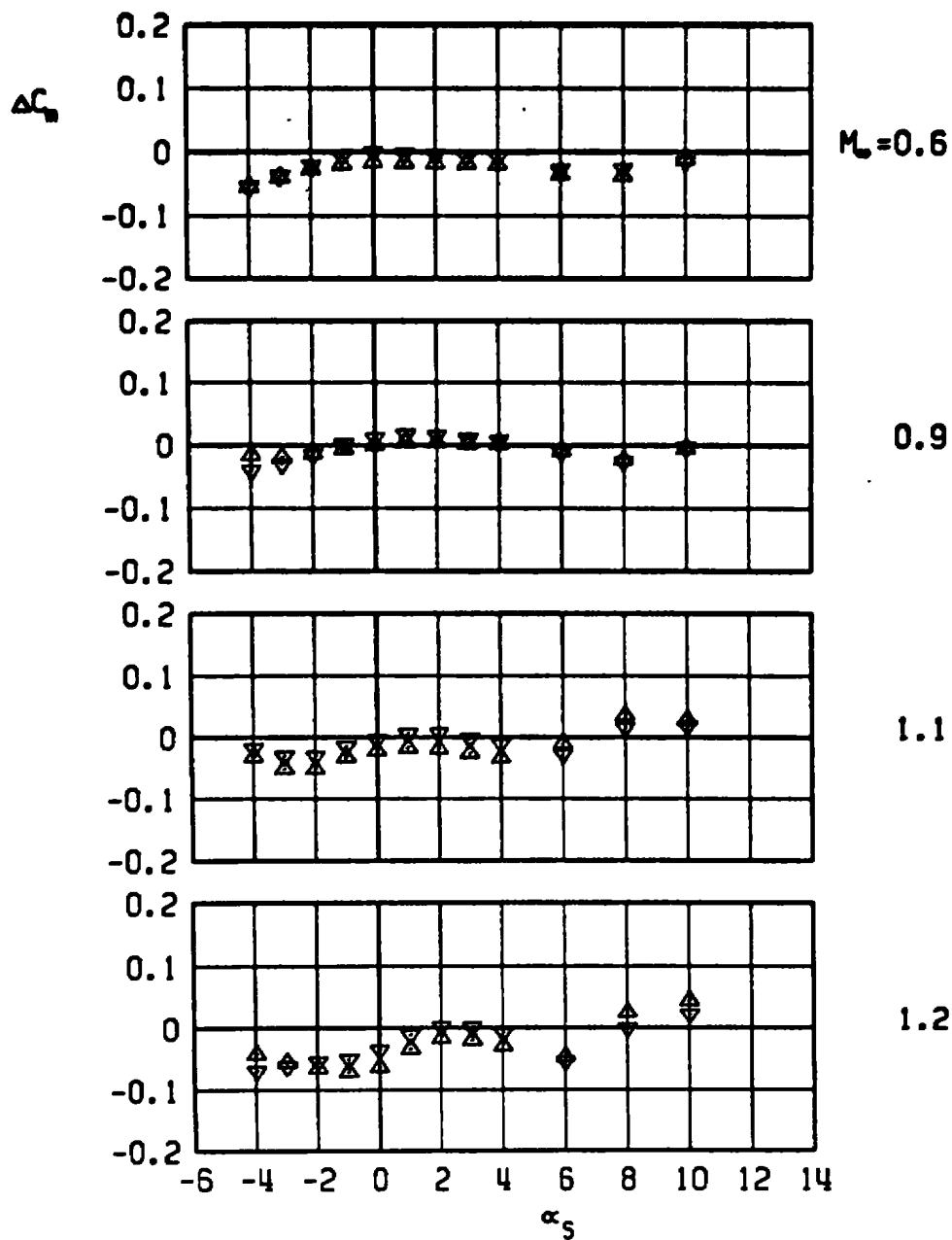
c. Axial-force increment
 Figure 54. Continued.

▲ CBU-46, LIB PYLON, TER-2, AB EFFECT
 AB 3 ONLY
 ▼ AB 3 WITH DUMMY STING, $D_3 = 0.62 D_0$



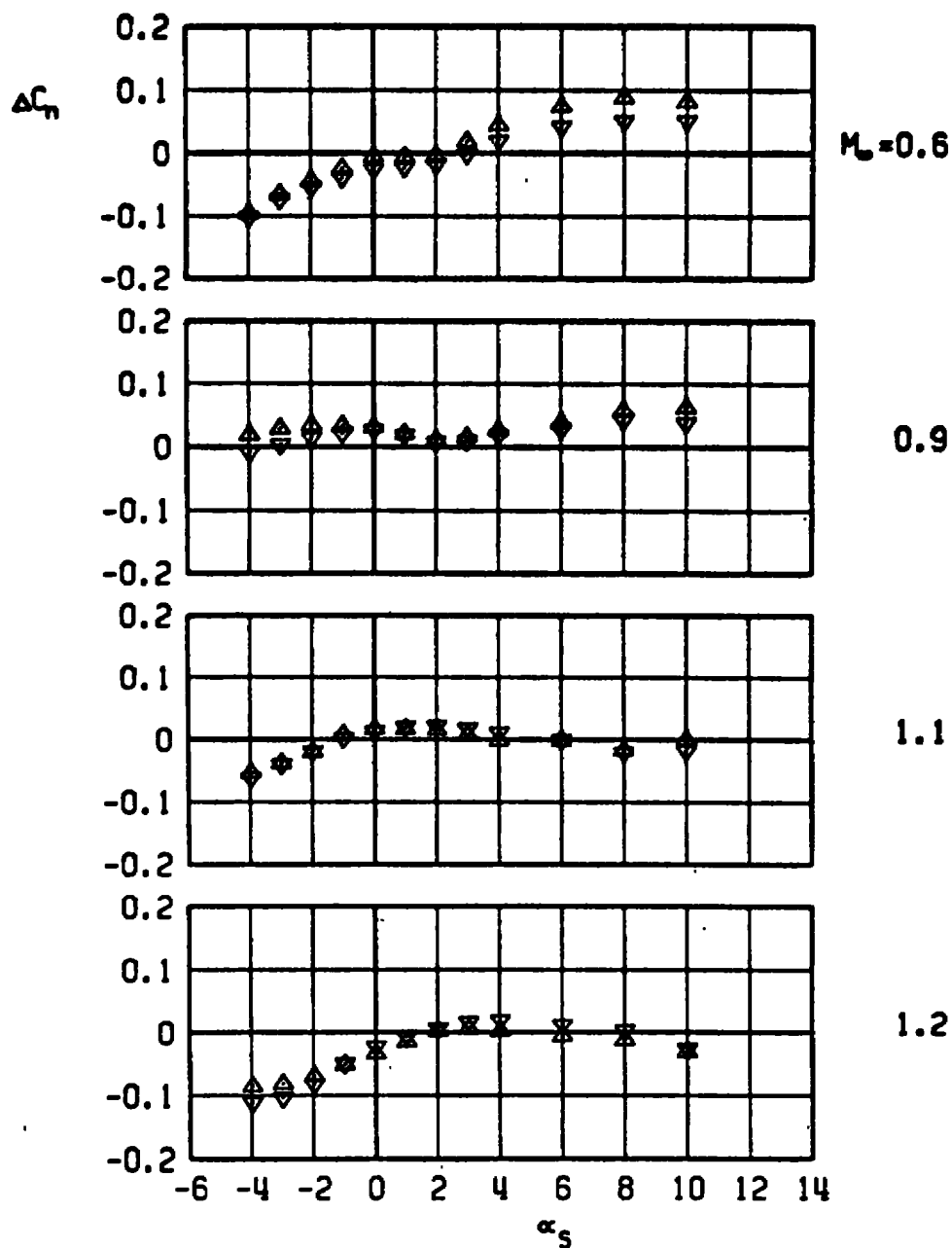
d. Rolling-moment increment
 Figure 54. Continued.

▲ CBU-46, LIB PYLON, TER-2, AB EFFECT
 AB 3 ONLY
 ▼ AB 3 WITH DUMMY STING, $D_3 = 0.62 D_9$

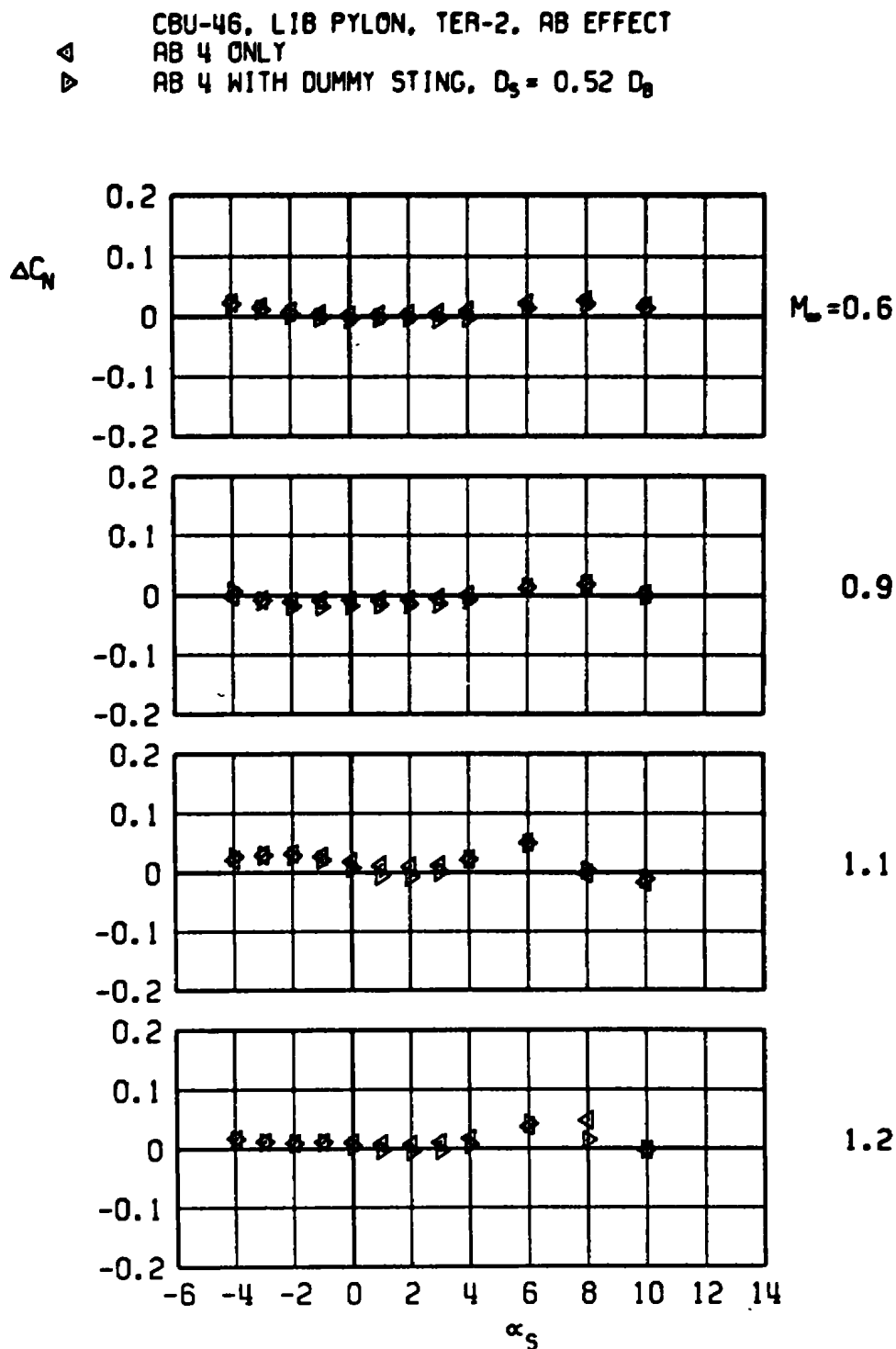


e. Pitching-moment increment
 Figure 54. Continued.

▲ CBU-46, LIB PYLON, TEA-2, AB EFFECT
 AB 3 ONLY
 ▼ AB 3 WITH DUMMY STING, $D_3 = 0.62 D_0$



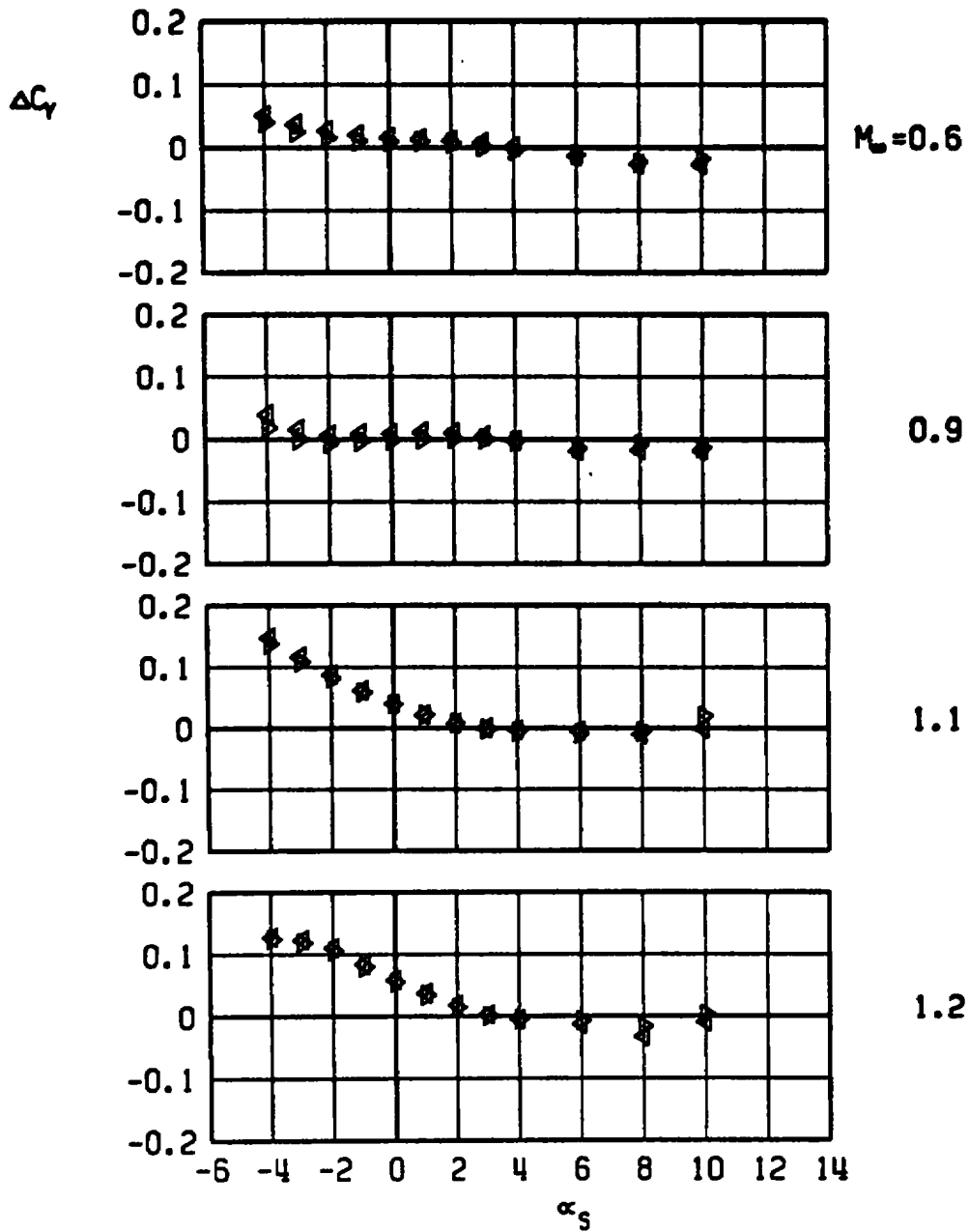
f. Yawing-moment increment
Figure 54. Concluded.



a. Normal-force increment

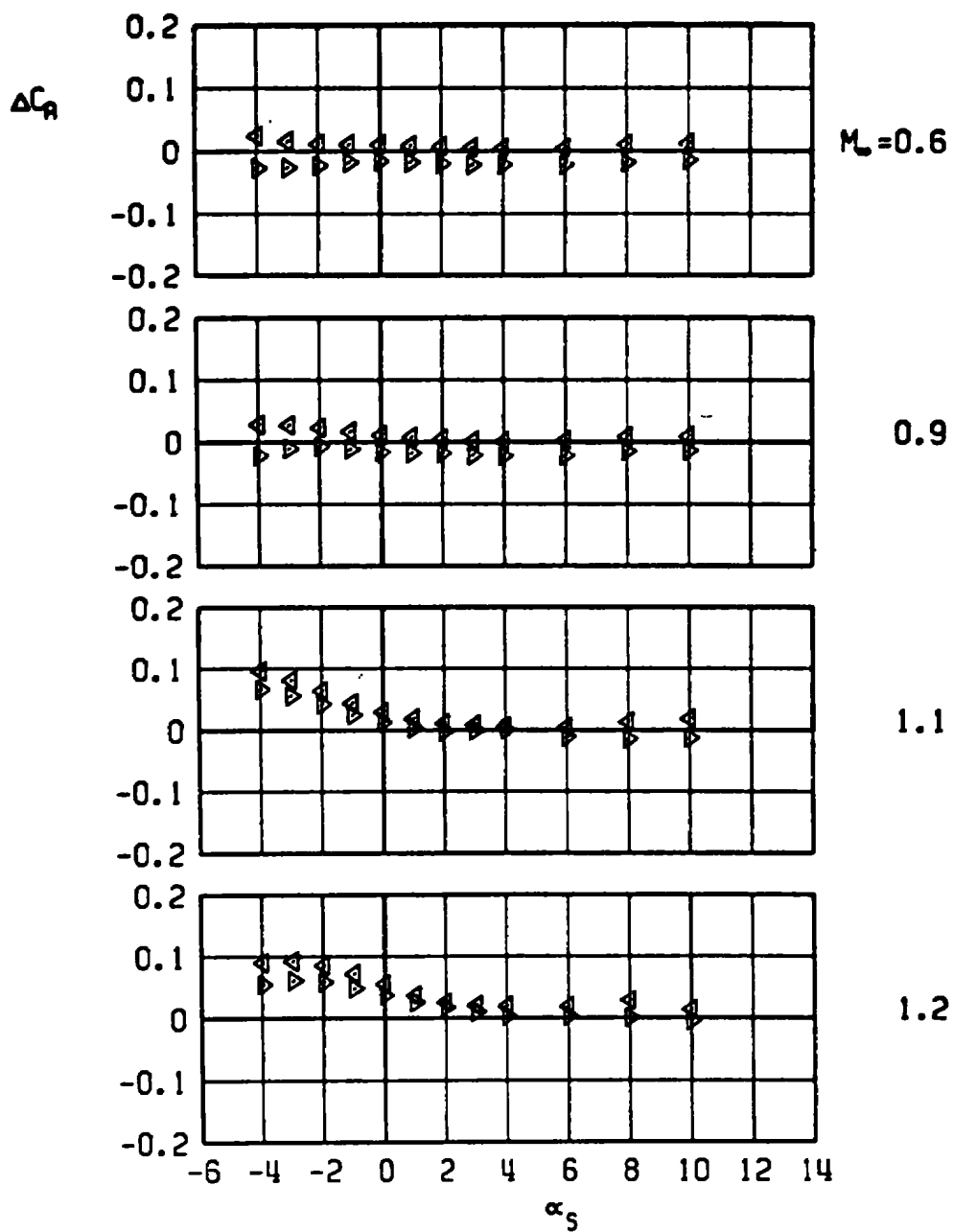
Figure 55. Aerodynamic load increments attributable to truncation of the afterbody of an unstable rack-mounted store, CBU-46 with AB4, TER station 2, LIB pylon.

▲ CBU-46, LIB PYLON, TER-2, AB EFFECT
 ▽ AB 4 ONLY
 ▽ AB 4 WITH DUMMY STING, $D_3 = 0.52 D_0$



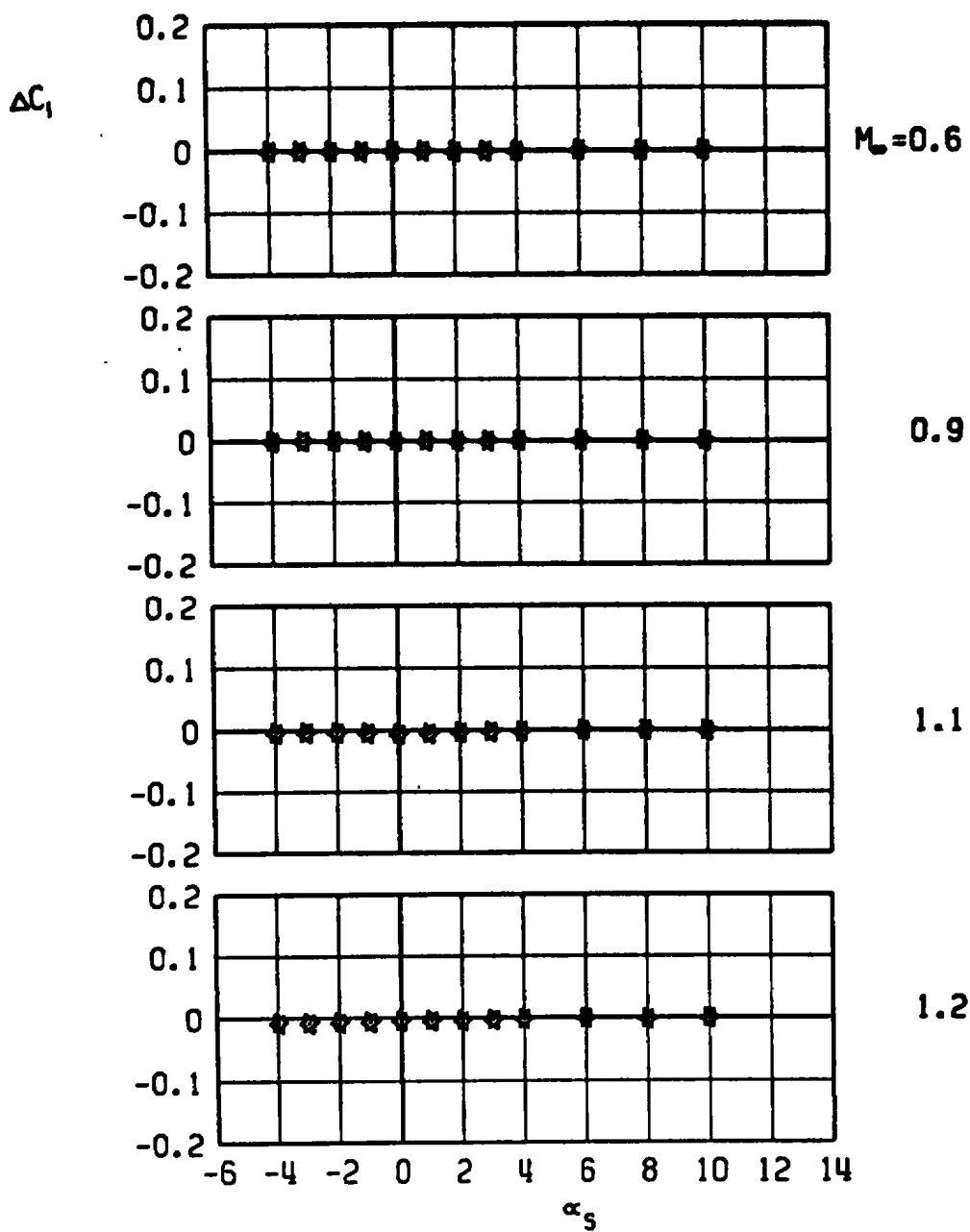
b. Side-force increment
 Figure 55. Continued.

\triangle CBU-46, LIB PYLON, TER-2, AB EFFECT
 ∇ AB 4 ONLY
 ∇ AB 4 WITH DUMMY STING, $D_3 = 0.52 D_0$



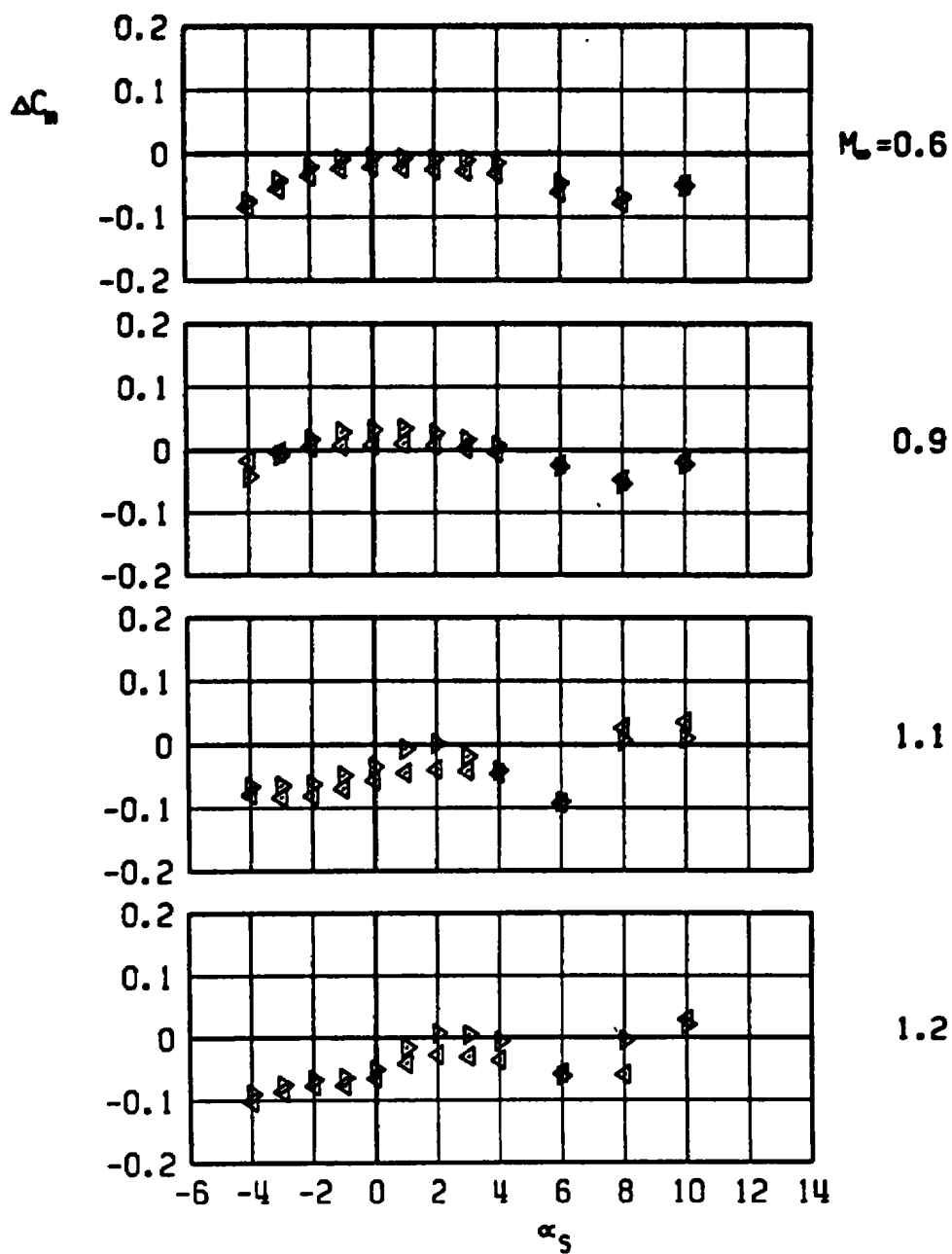
c. Axial-force increment
 Figure 55. Continued.

▲ CBU-46, LIB PYLON, TER-2, AB EFFECT
 ▽ AB 4 ONLY
 ▽ AB 4 WITH DUMMY STING, $D_3 = 0.52 D_0$



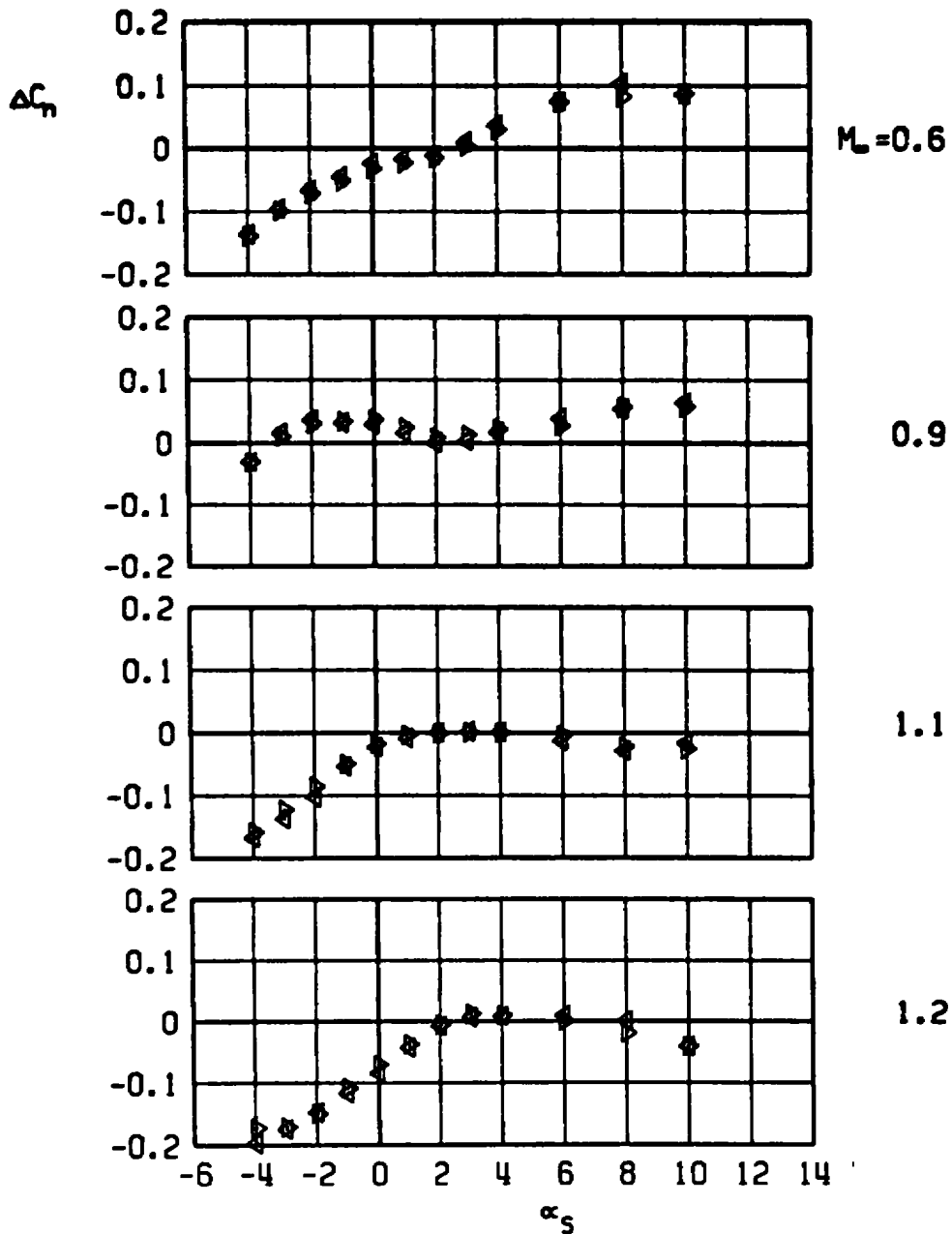
d. Rolling-moment increment
Figure 55. Continued.

\triangle CBU-46, LIB PYLON, TER-2, AB EFFECT
 ∇ AB 4 ONLY
 ∇ AB 4 WITH DUMMY STING, $D_3 = 0.52 D_0$



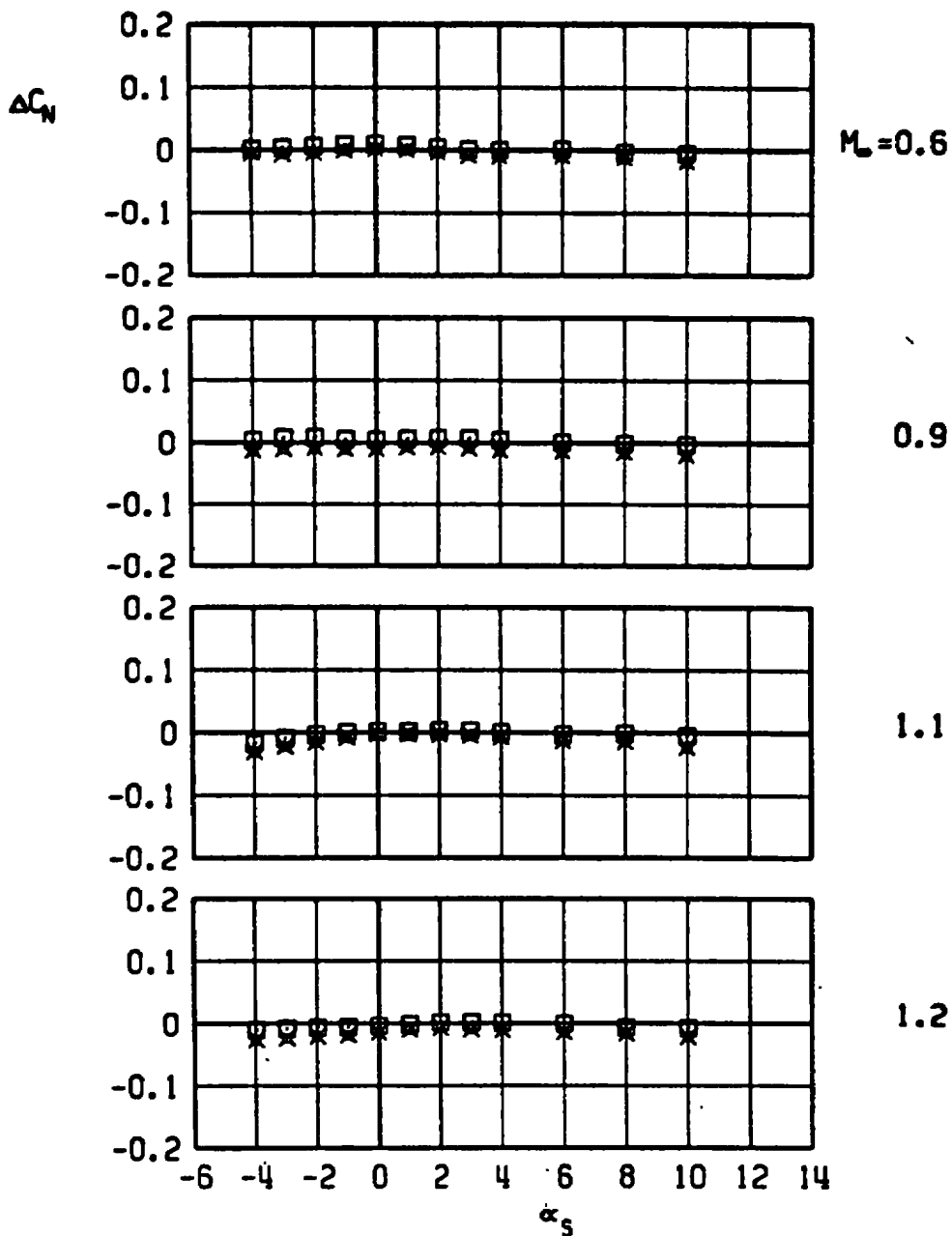
e. Pitching-moment increment
 Figure 55. Continued.

Δ CBU-46, LIB PYLON, TER-2, AB EFFECT
 ∇ AB 4 ONLY
 ∇ AB 4 WITH DUMMY STING. $D_3 = 0.52 D_0$



f. Yawing-moment increment
Figure 55. Concluded.

CBU-46, LIB PYLON, TER-3, AB EFFECT
 □ AB 2 ONLY
 x AB 2 WITH DUMMY STING, $D_3 = 0.76 D_0$



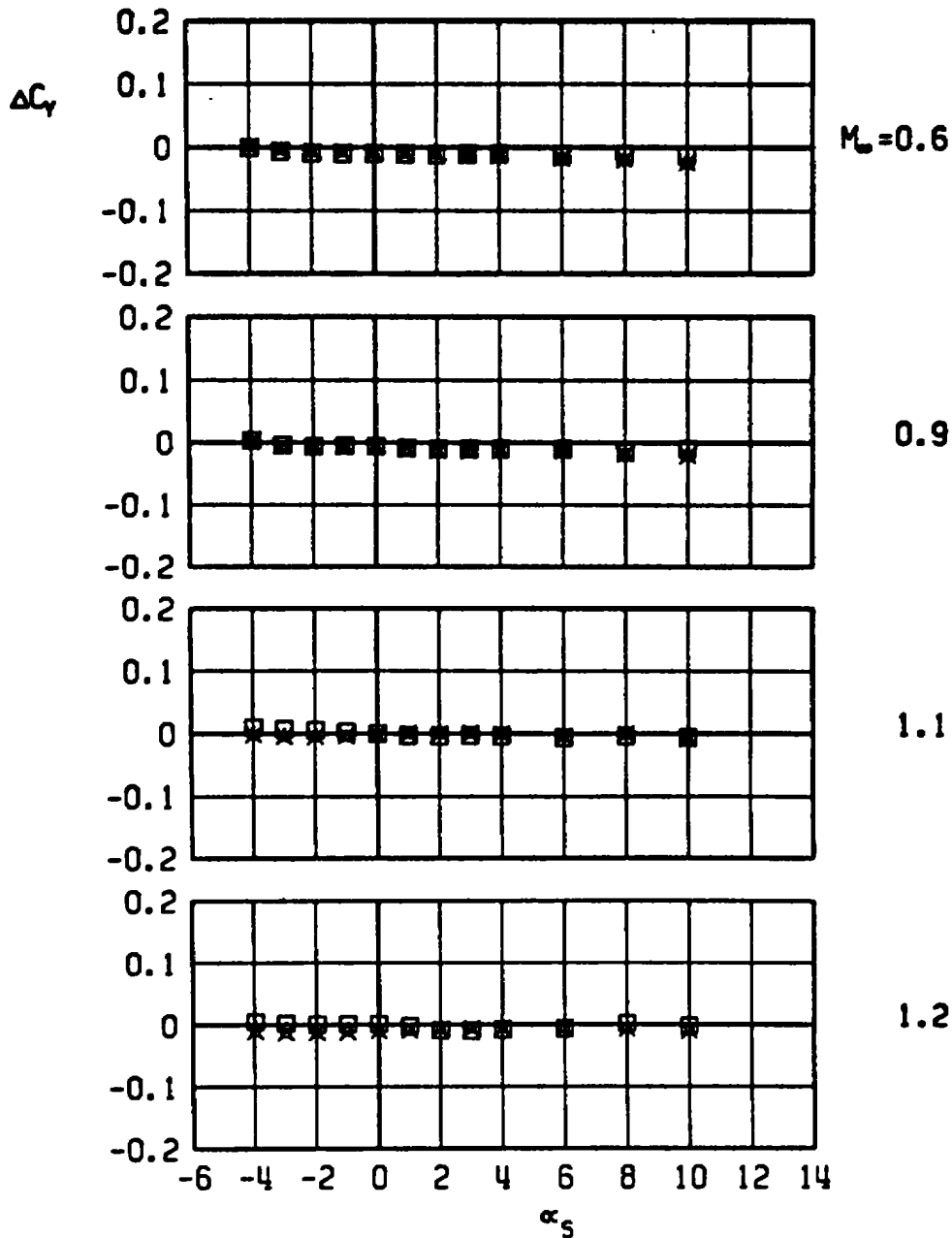
a. Normal-force increment

Figure 56. Aerodynamic load increments attributable to truncation of the afterbody of an unstable rack-mounted store, CBU-46 with AB2, TER station 3, LIB pylon.

CBU-46, LIB PYLON, TER-3, AB EFFECT

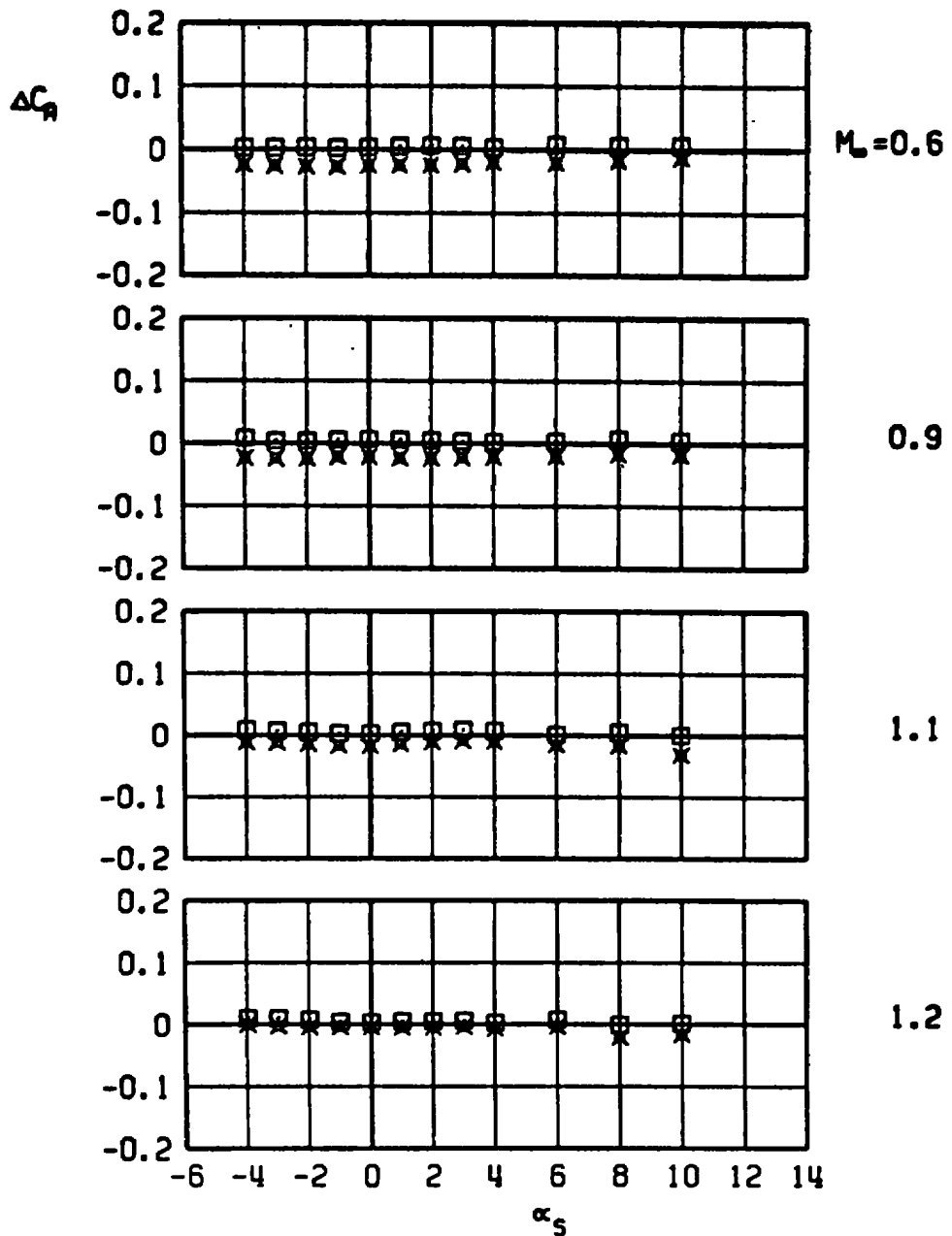
□ AB 2 ONLY

× AB 2 WITH DUMMY STING, $D_3 = 0.76 D_9$



b. Side-force increment
Figure 56. Continued.

□ CBU-46, LIB PYLON, TER-3, AB EFFECT
 AB 2 ONLY
 × AB 2 WITH DUMMY STING, $D_3 = 0.76 D_B$



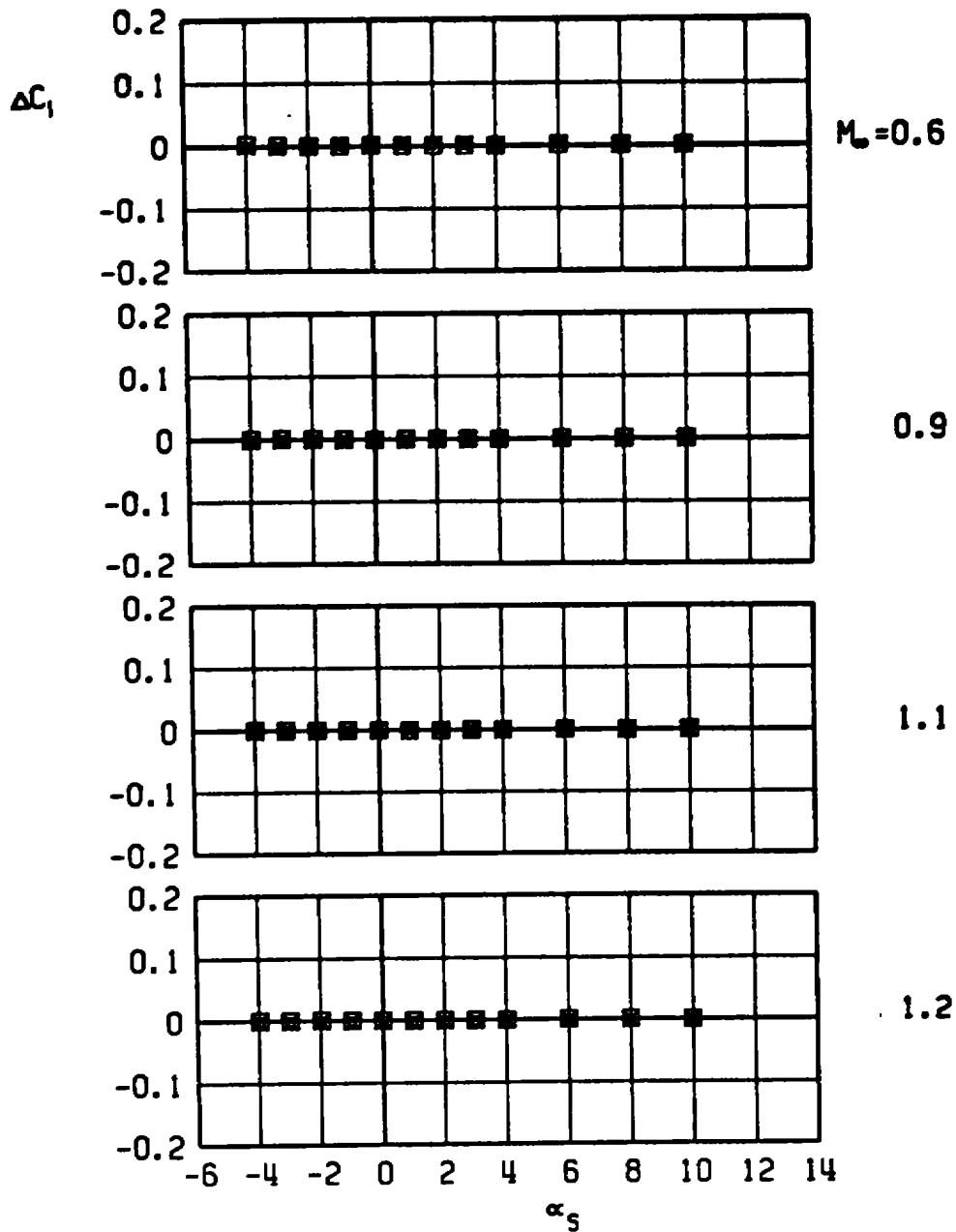
c. Axial-force increment
 Figure 56. Continued.

CBU-46, LIB PYLON, TER-3, AB EFFECT

□

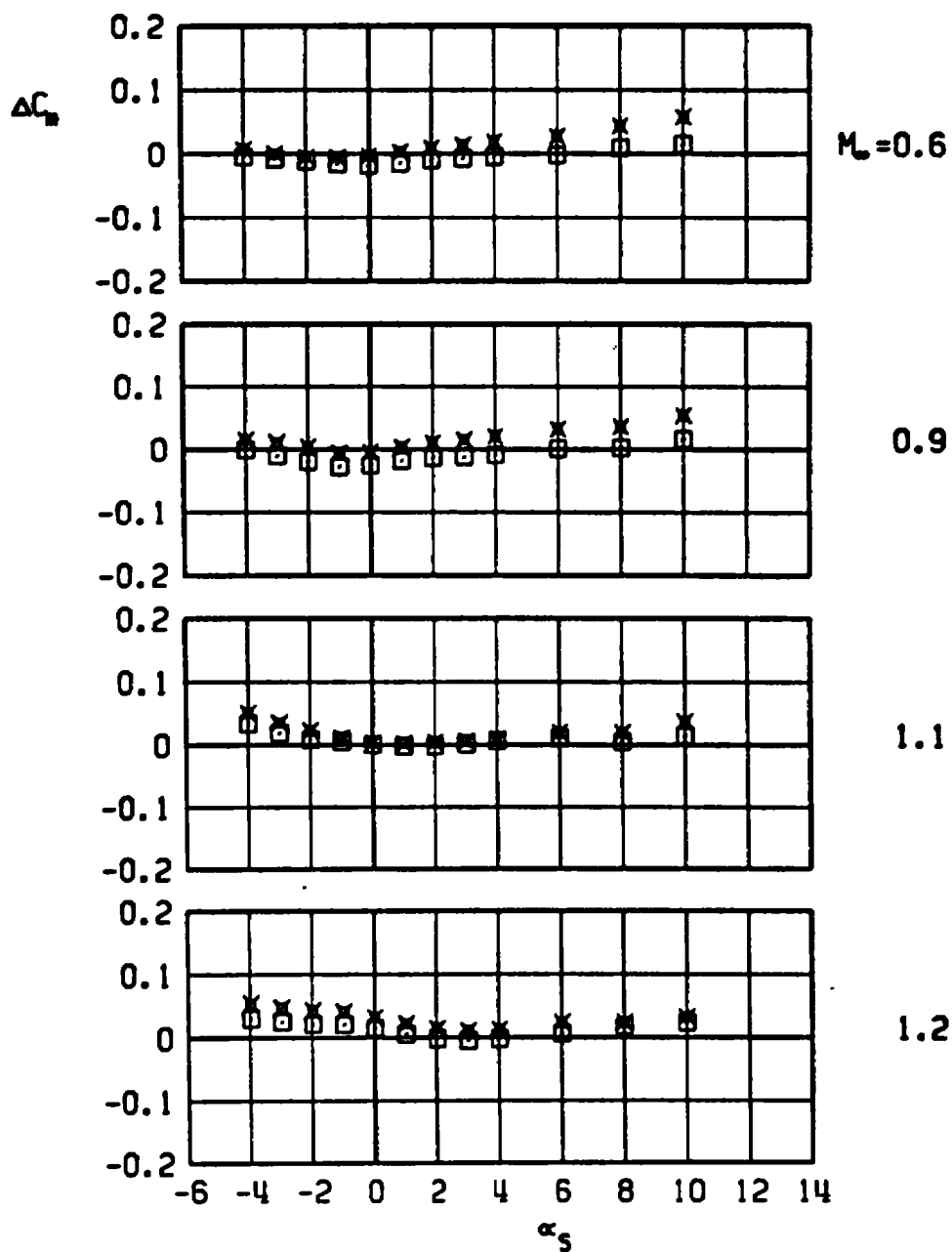
AB 2 ONLY

x

AB 2 WITH DUMMY STING, $D_3 = 0.76 D_0$ 

d. Rolling-moment increment
Figure 56. Continued.

CBU-46, LIB PYLON, TER-3, AB EFFECT
 □ AB 2 ONLY
 x AB 2 WITH DUMMY STING, $D_3 = 0.76 D_0$

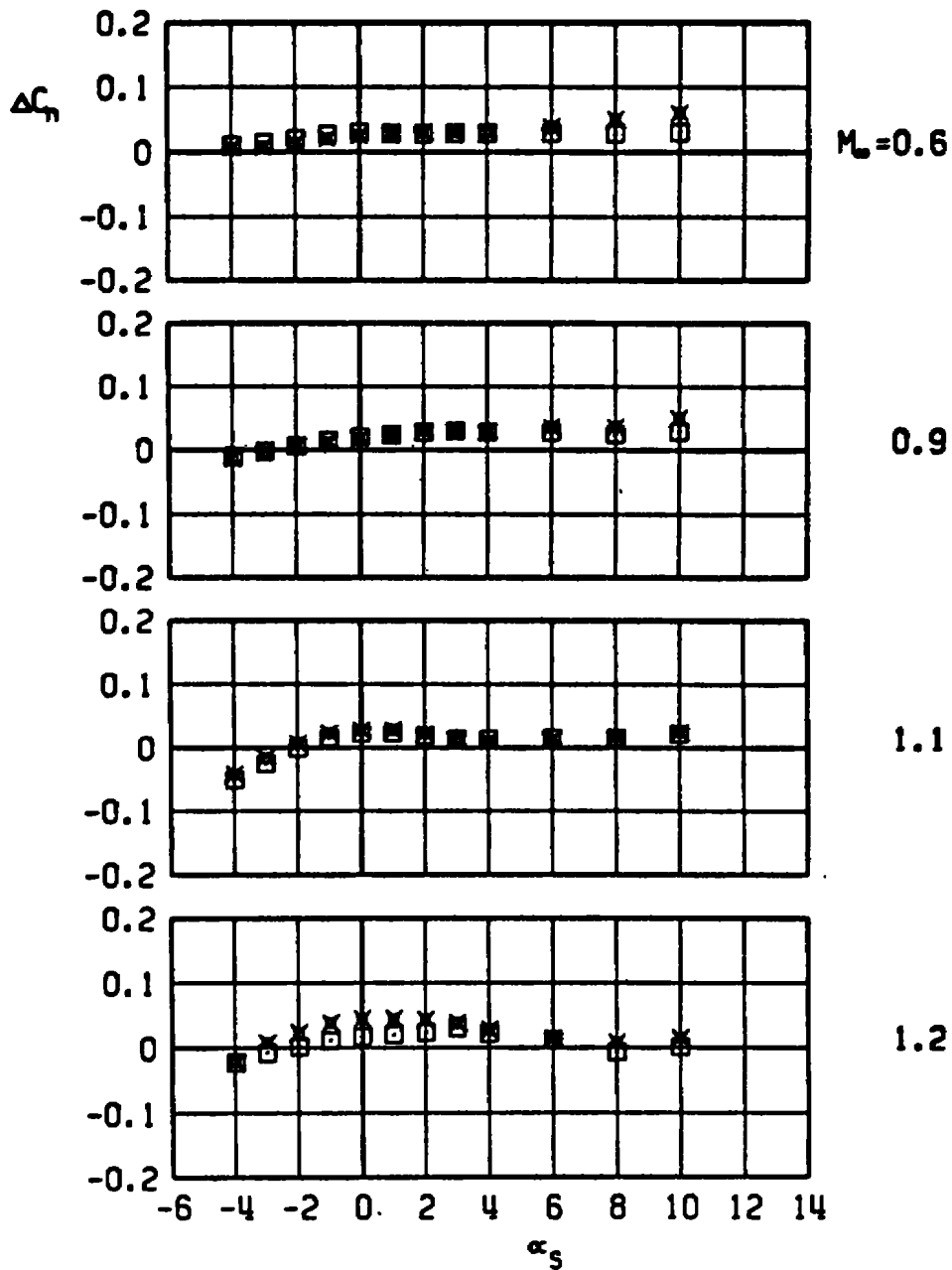


e. Pitching-moment increment
 Figure 56. Continued.

CBU-46, LIB PYLON, TER-3, AB EFFECT

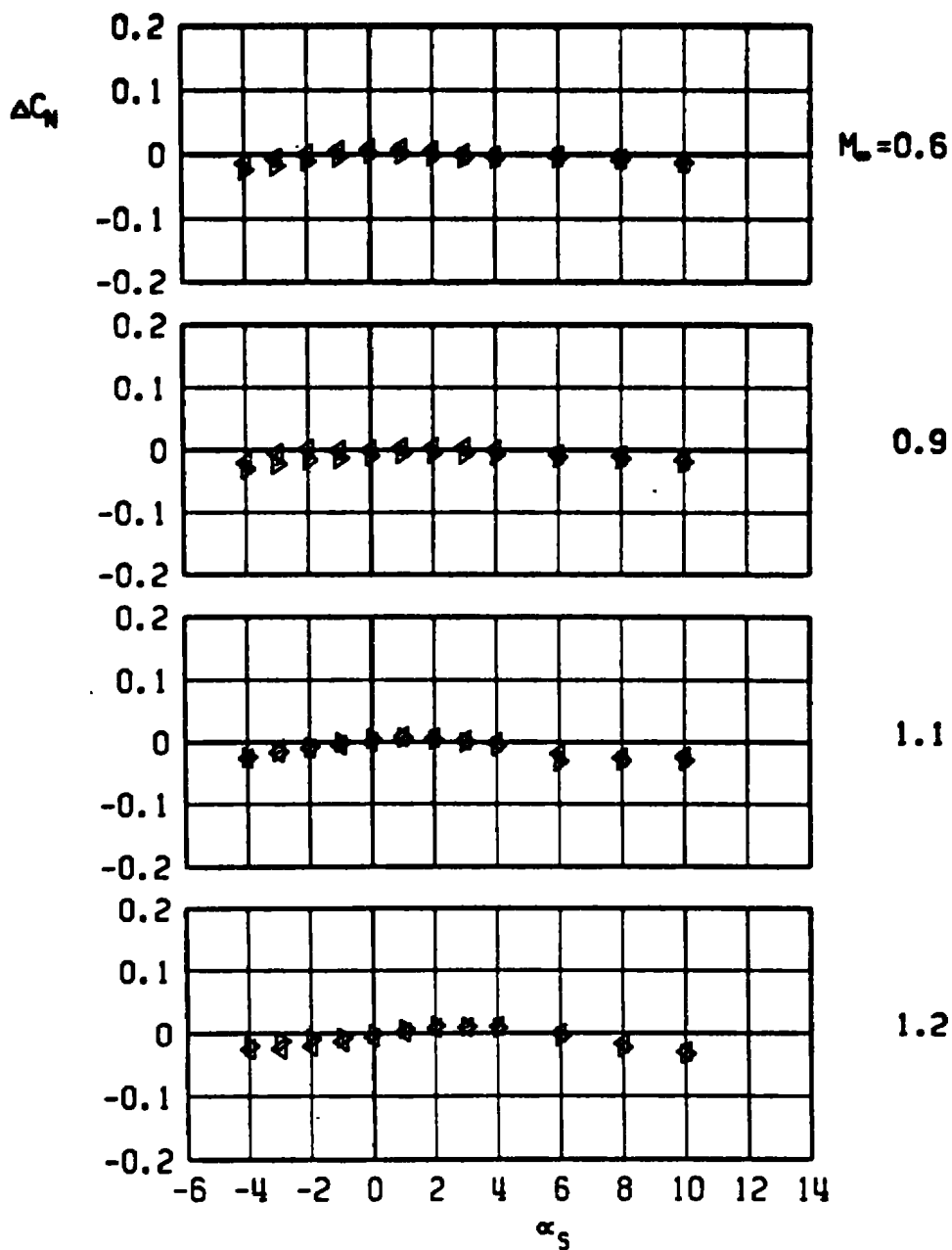
□ AB 2 ONLY

× AB 2 WITH DUMMY STING, $D_3 = 0.76 D_0$



f. Yawing-moment increment
Figure 56. Concluded.

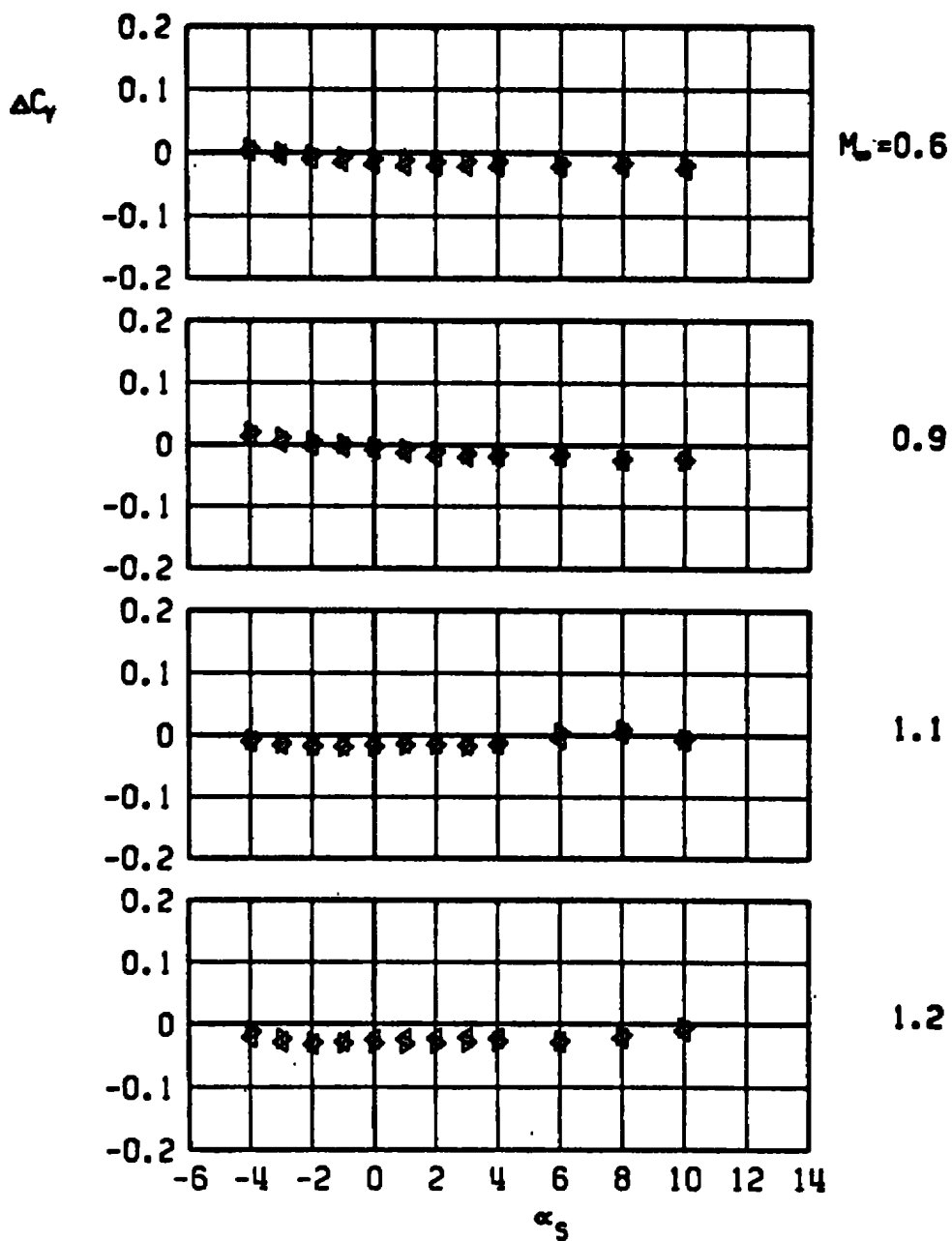
▲ CBU-46, LIB PYLON, TER-3, AB EFFECT
 ▼ AB 4 ONLY
 ▲ AB 4 WITH DUMMY STING, $D_3 = 0.52 D_0$



a. Normal-force increment

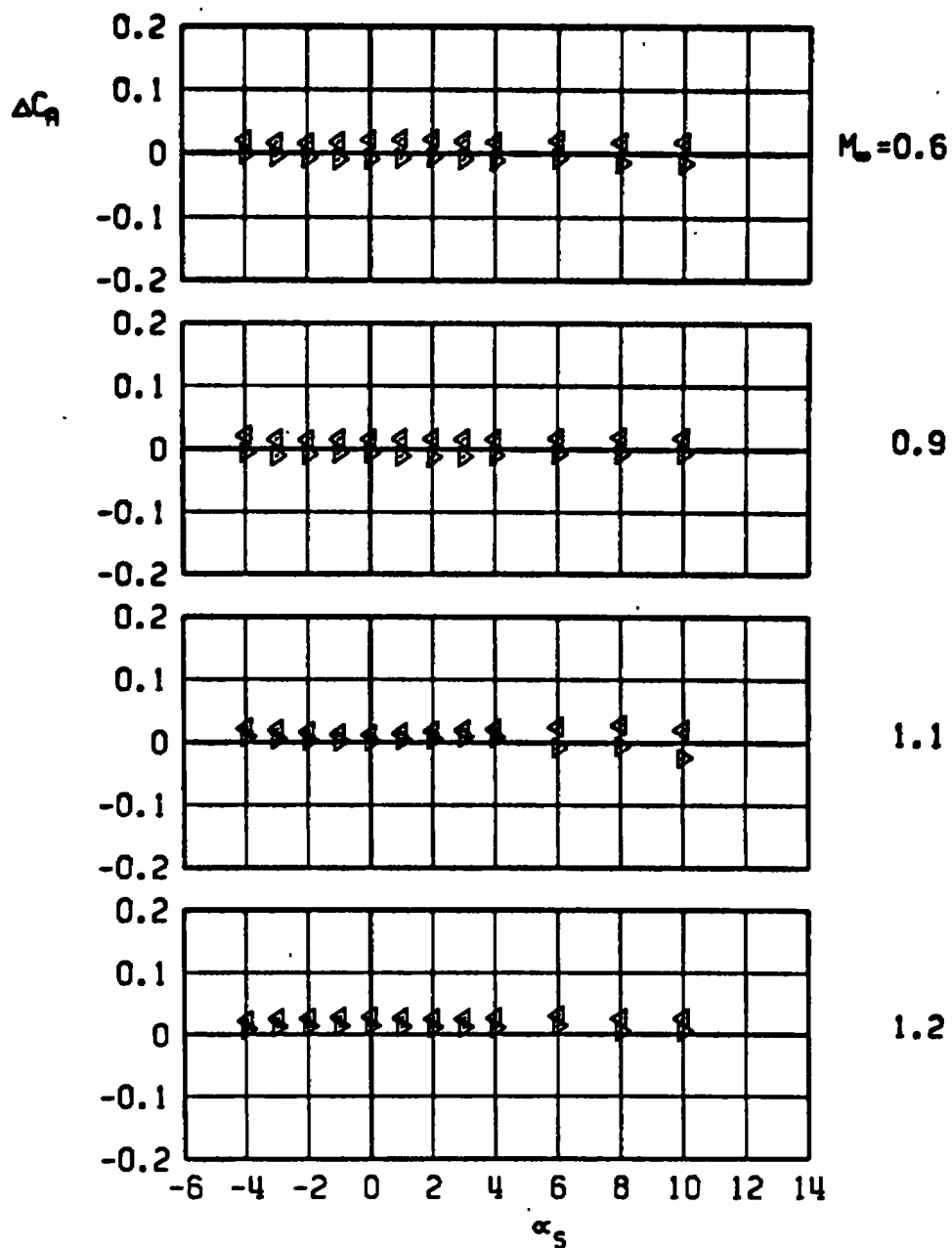
Figure 57. Aerodynamic load increments attributable to truncation of the afterbody of an unstable rack-mounted store, CBU-46 with AB4, TER station 3, LIB pylon.

▲ CBU-46, L10 PYLON, TERA-3, AB EFFECT
 AB 4 ONLY
 ▼ AB 4 WITH DUMMY STING, $D_3 = 0.52 D_0$



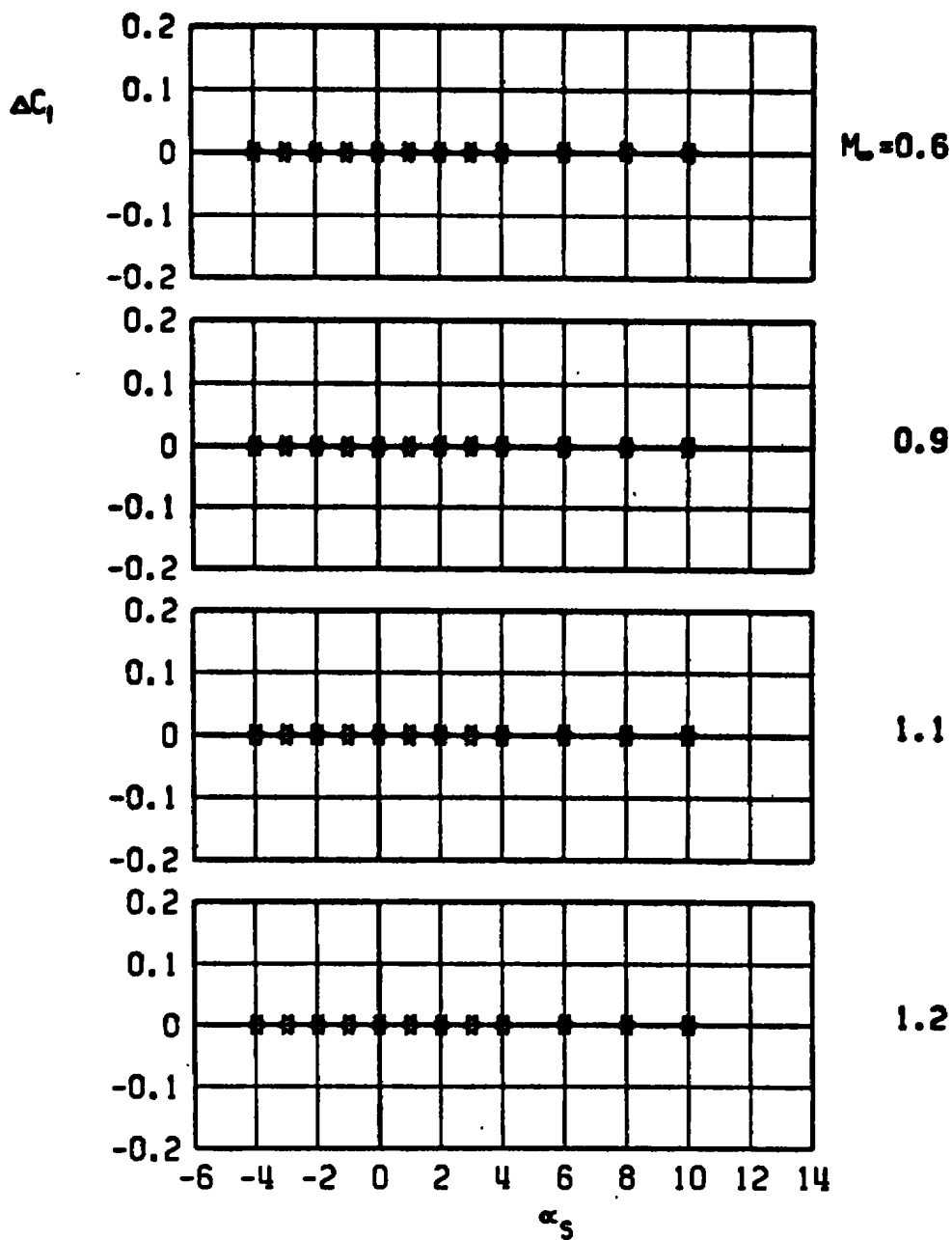
b. Side-force increment
 Figure 57. Continued.

▲ CBU-46, LIB PYLON, TERA-3, AB EFFECT
 ▼ AB 4 ONLY
 ▲ AB 4 WITH DUMMY STING, $D_3 = 0.52 D_0$



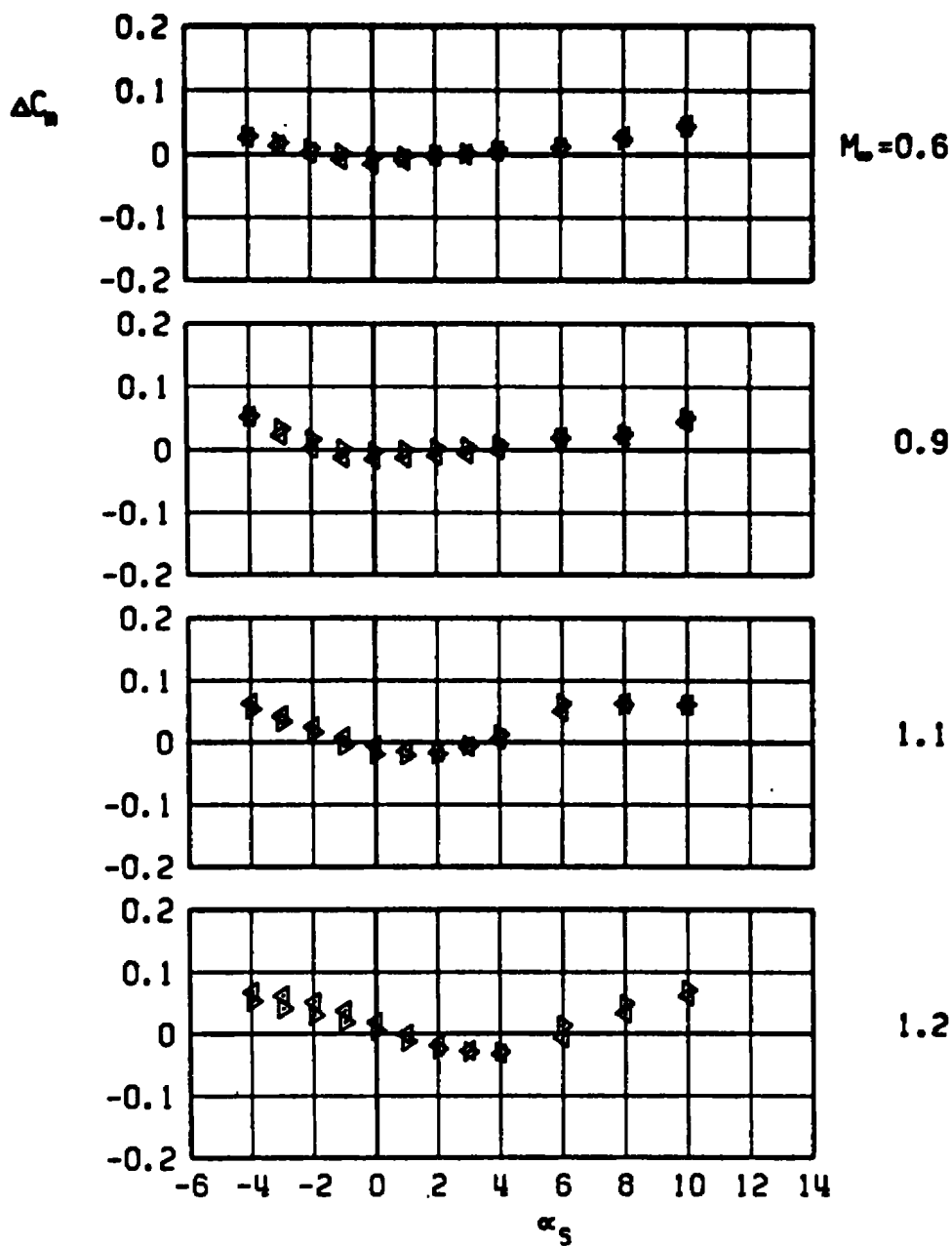
c. Axial-force increment
 Figure 57. Continued.

▲ CBU-46, LIB PYLON, TER-3, AB EFFECT
 AB 4 ONLY
 ▽ AB 4 WITH DUMMY STING, $D_3 = 0.52 D_0$



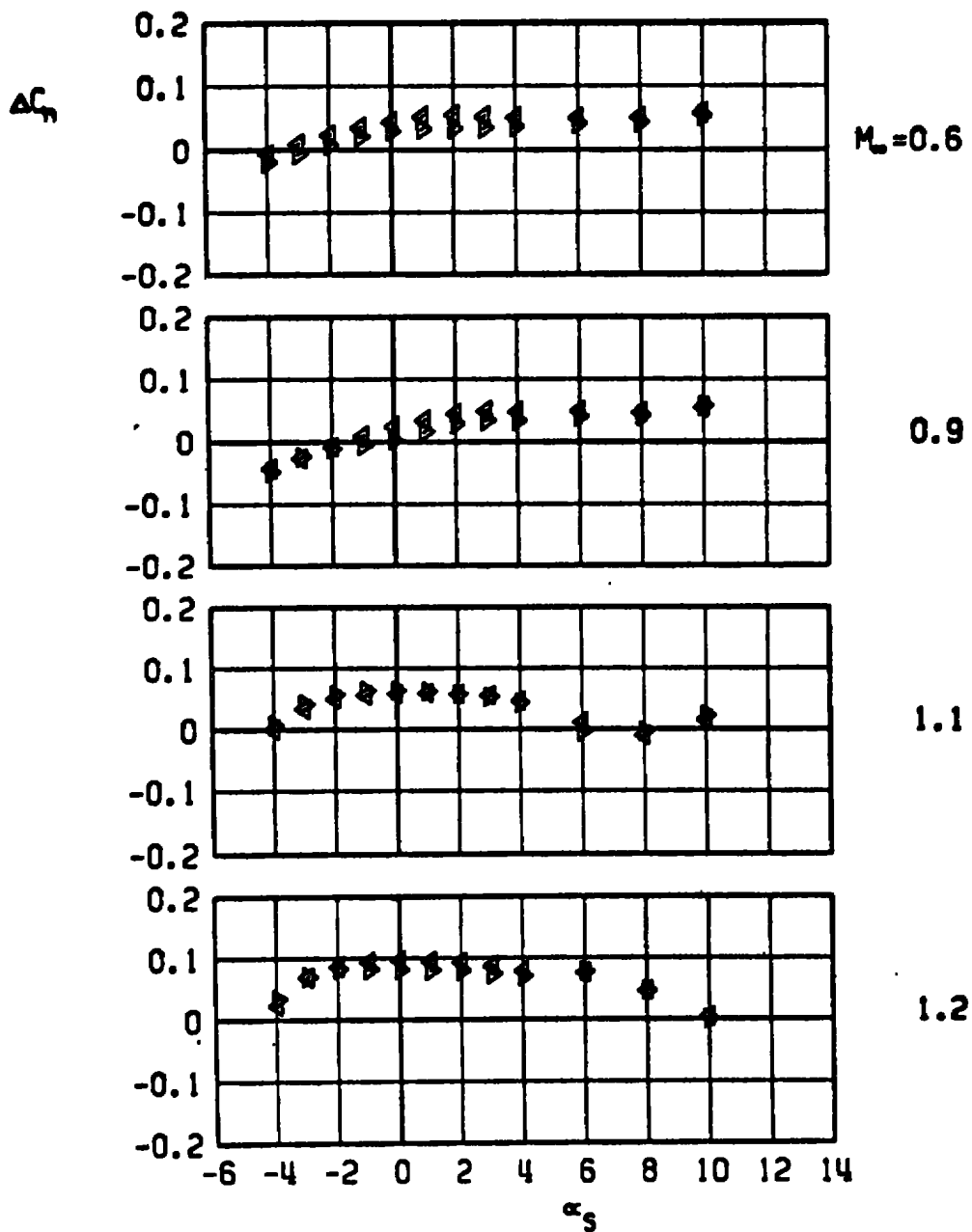
d. Rolling-moment increment
 Figure 57. Continued.

▲ CBU-46, LIB PYLON, TER-3, AB EFFECT
 AB 4 ONLY
 ▼ AB 4 WITH DUMMY STING, $D_3 = 0.52 D_9$

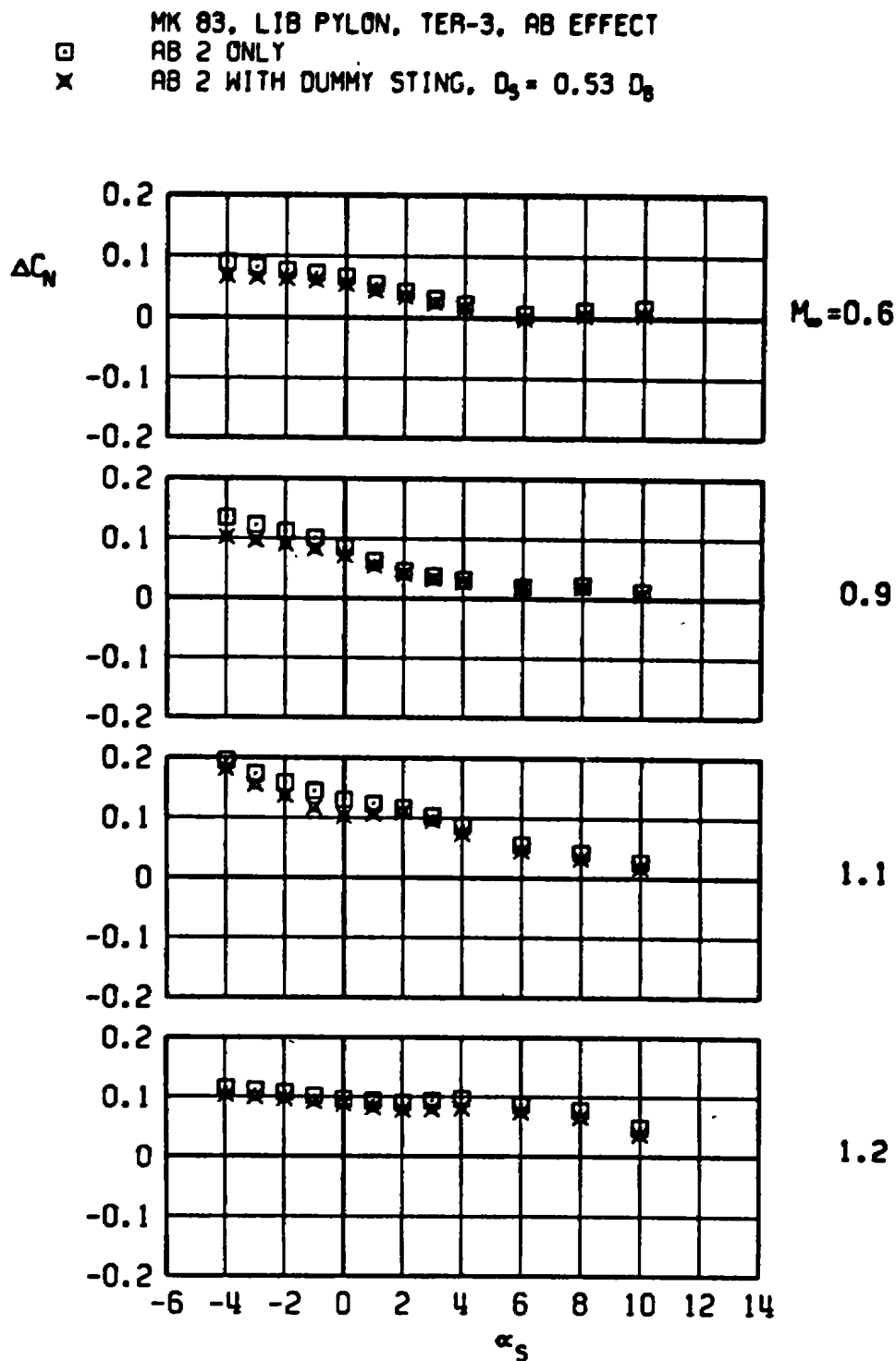


e. Pitching-moment increment
Figure 57. Continued.

▲ CBU-46, LIB PYLON, TEA-3, AB EFFECT
 ▽ AB 4 ONLY
 ▽ AB 4 WITH DUMMY STING, $D_3 = 0.52 D_0$



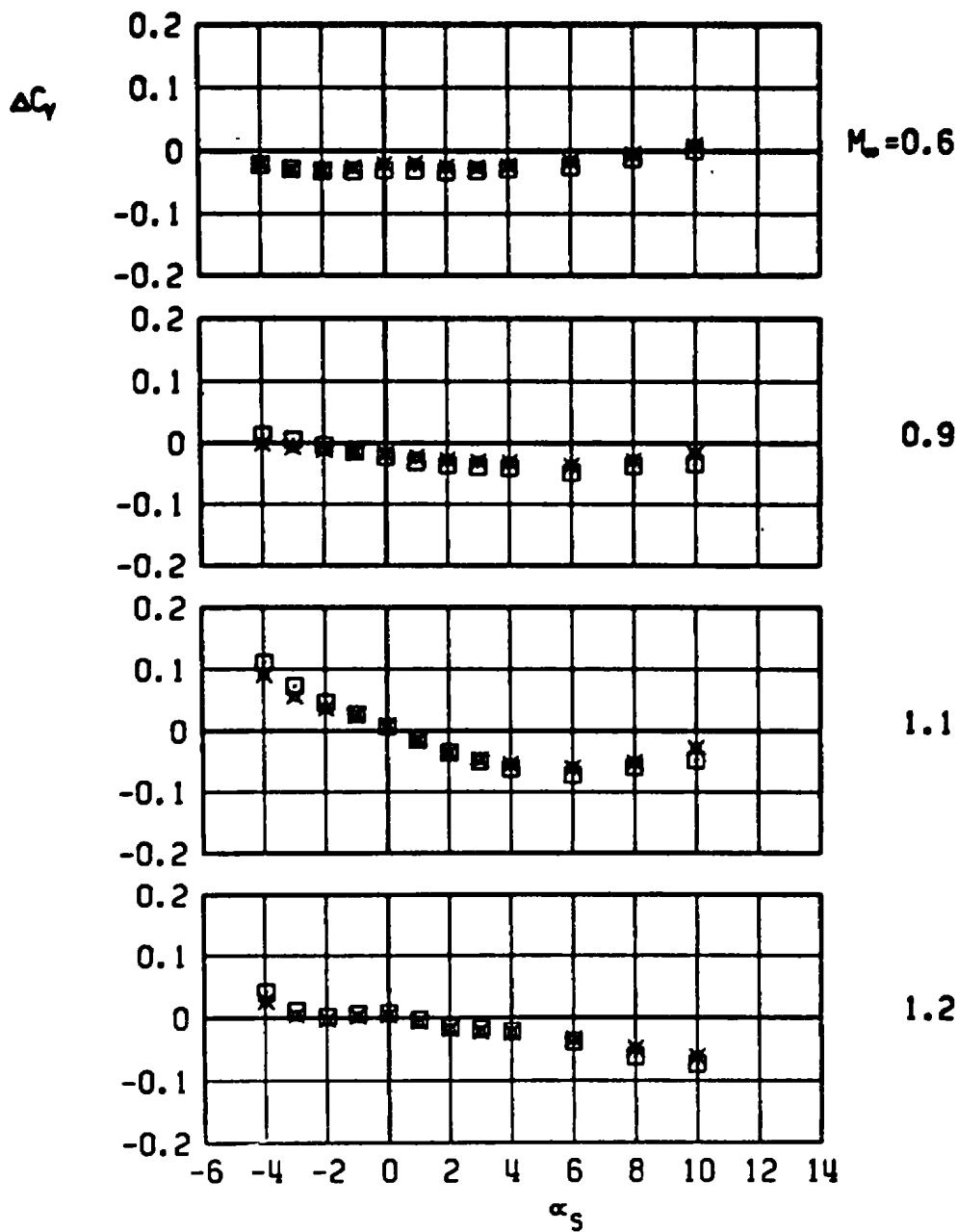
f. Yawing-moment increment
Figure 57. Concluded.



a. Normal-force increment

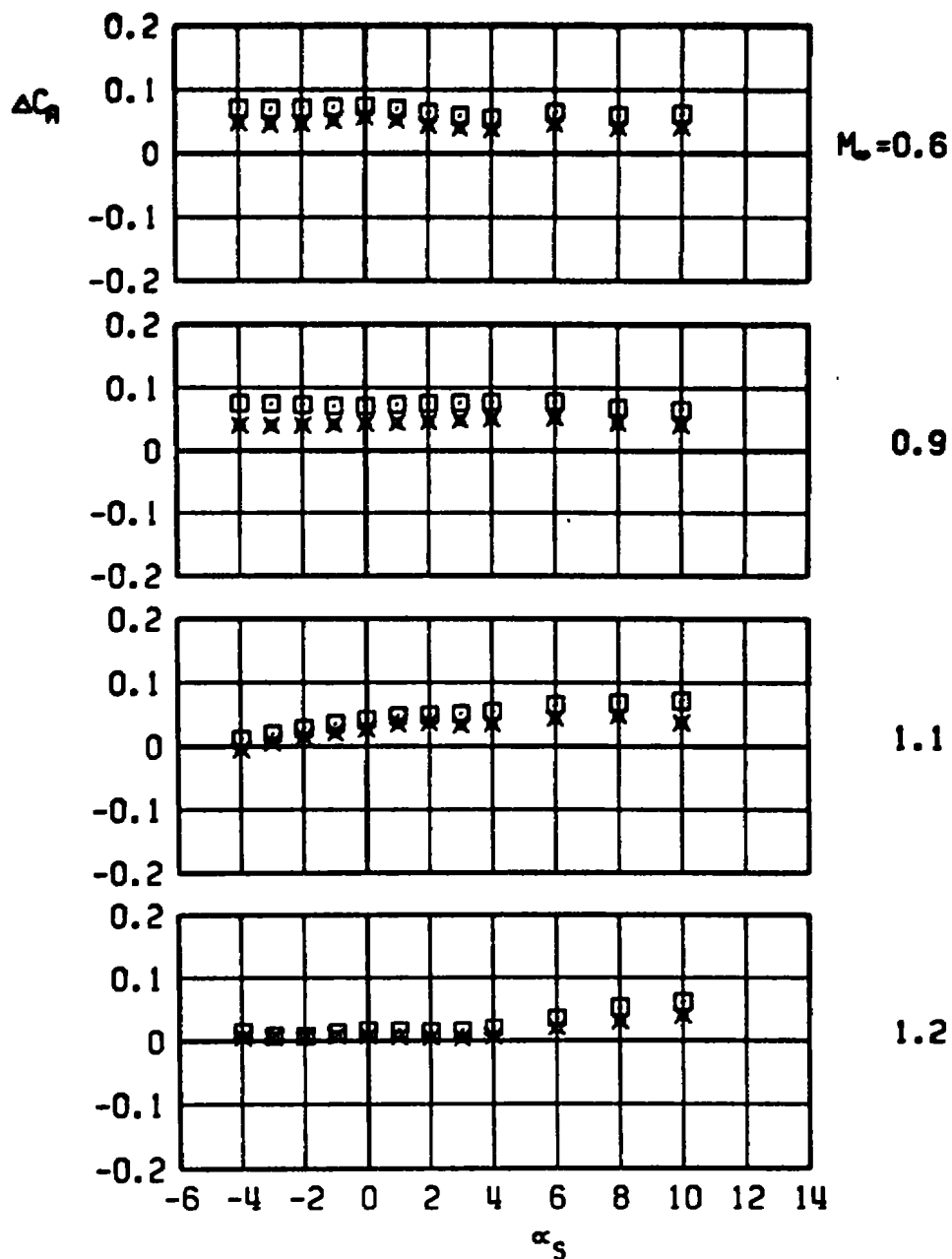
Figure 58. Aerodynamic load increments attributable to cylindrical distortion of the afterbody of a stable rack-mounted store, MK-83 with AB2, TER station 3, LIB pylon.

MK 83, LIB PYLON, TER-3, AB EFFECT
 AB 2 ONLY
 X AB 2 WITH DUMMY STING, $D_3 = 0.53 D_0$



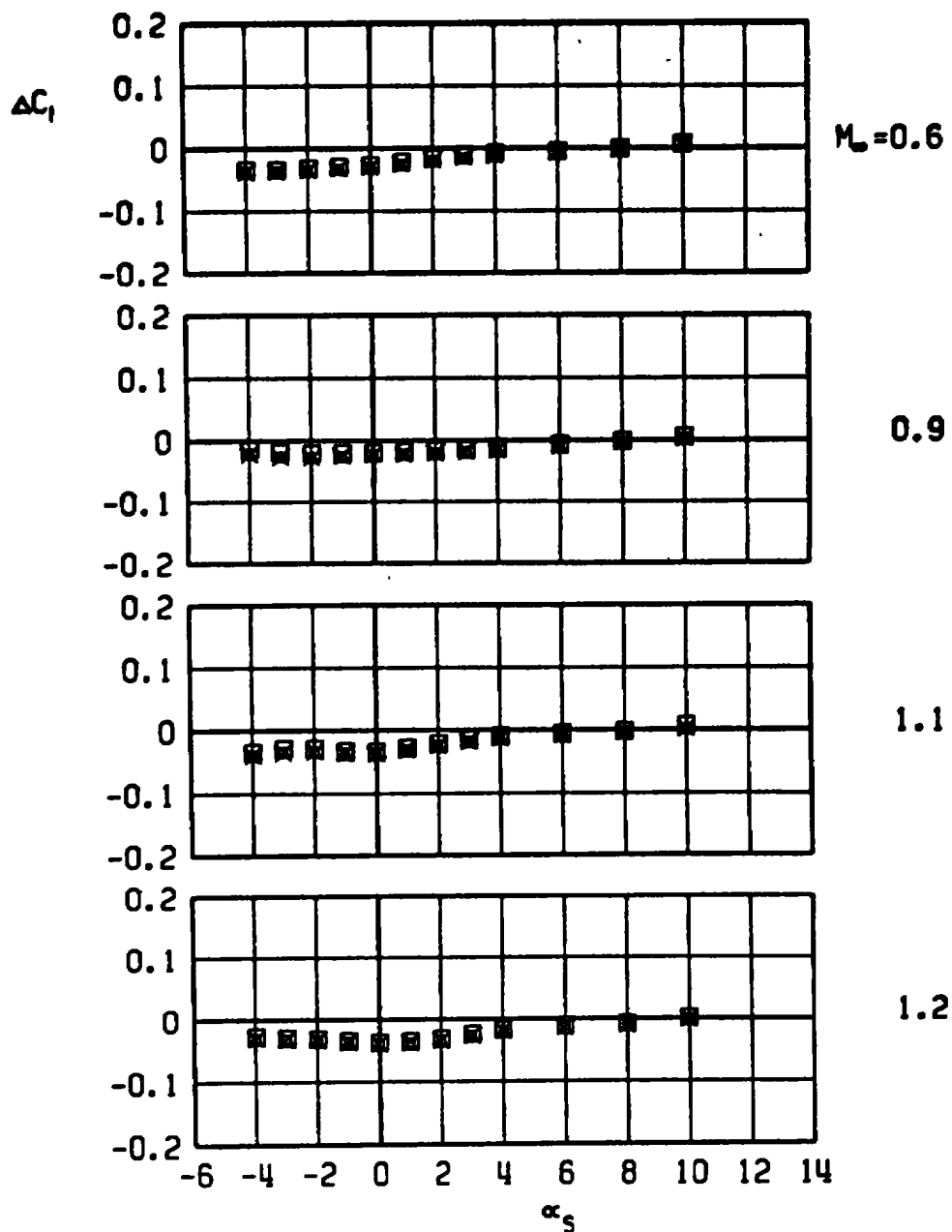
b. Side-force increment
 Figure 58. Continued.

MK 83, LIB PYLON, TER-3, AB EFFECT
 □ AB 2 ONLY
 x AB 2 WITH DUMMY STING, $D_3 = 0.53 D_0$



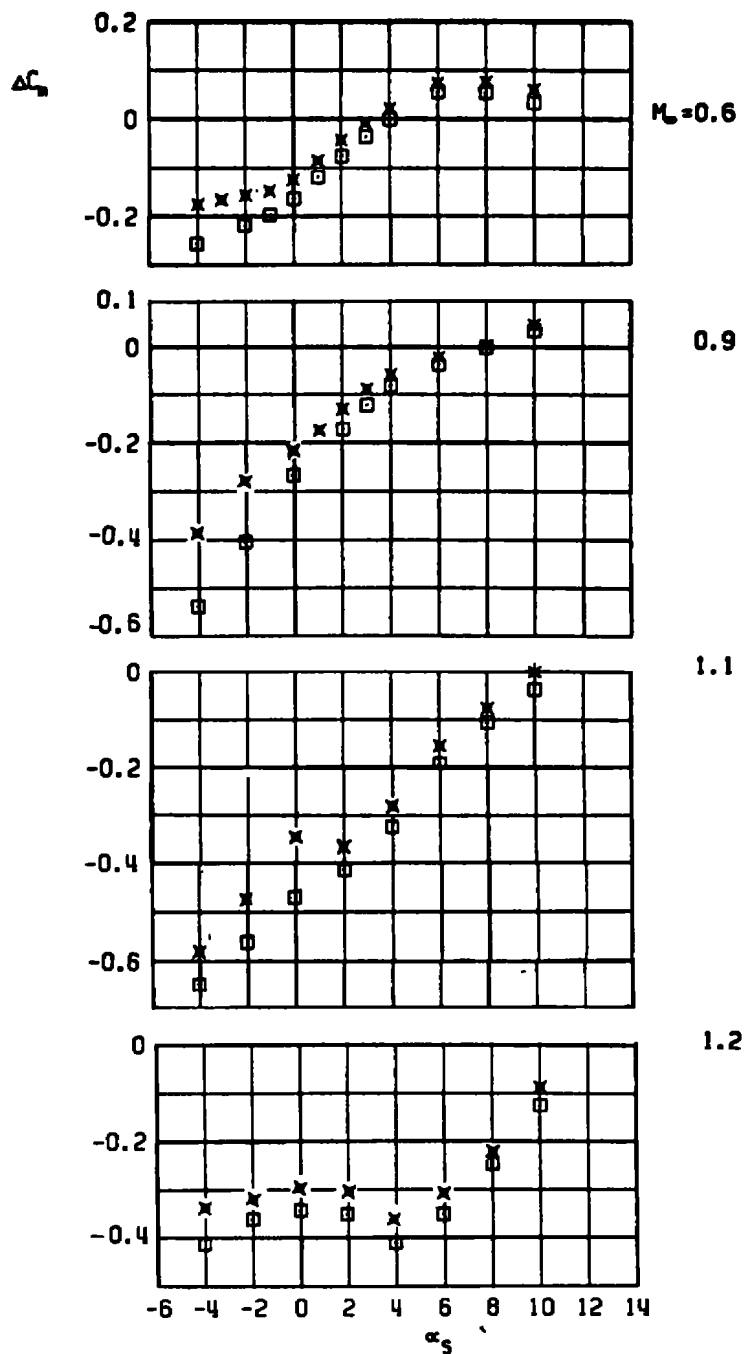
c. Axial-force increment
 Figure 58. Continued.

MK 83, LIB PYLON, TEA-3, AB EFFECT
 AB 2 ONLY
 AB 2 WITH DUMMY STING, $D_3 = 0.53 D_0$



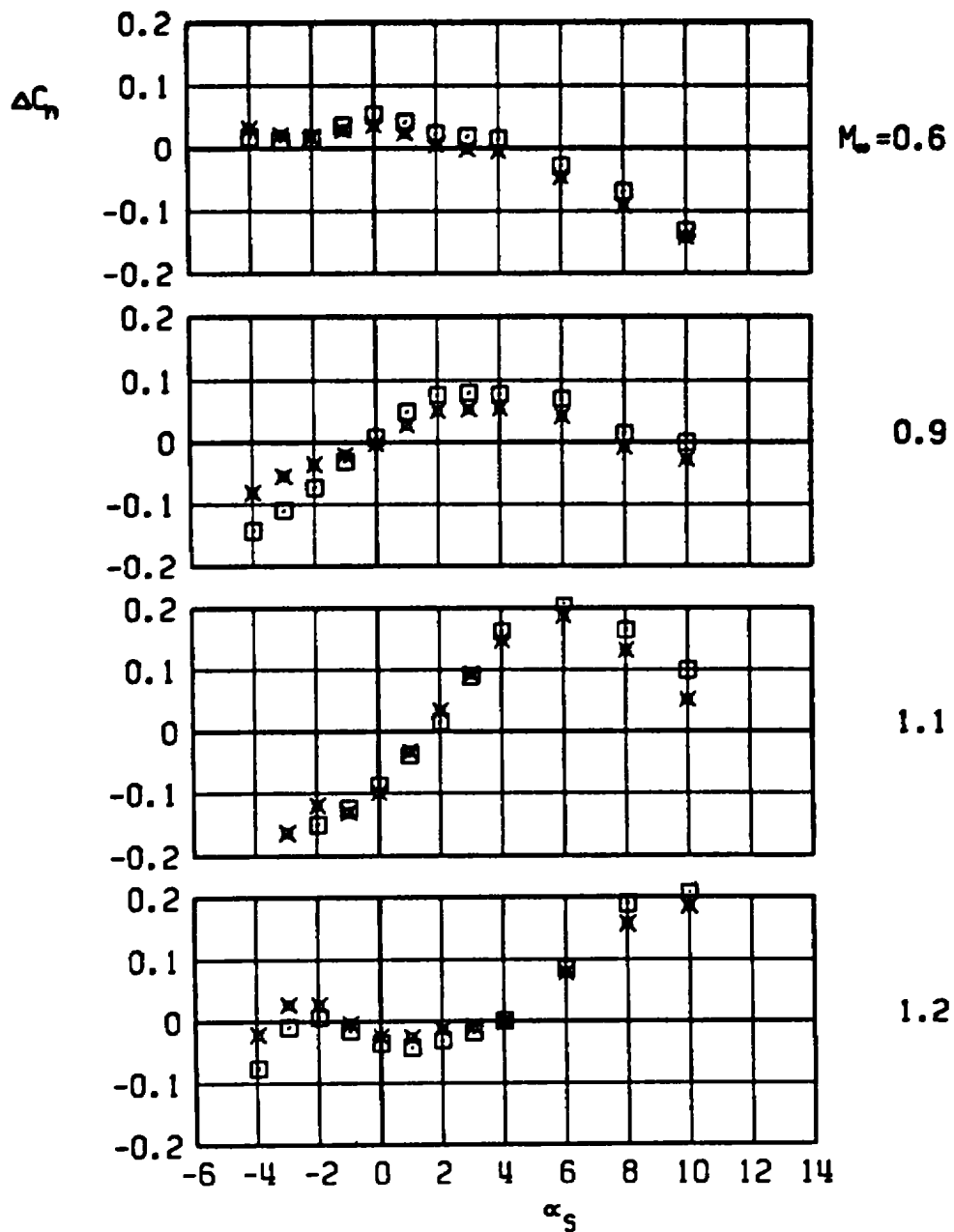
d. Rolling-moment increment
 Figure 58. Continued.

MK 83, L18 PYLON, TERA-3, AB EFFECT
 □ AB 2 ONLY
 x AB 2 WITH DUMMY STING, $D_3 = 0.53 D_0$

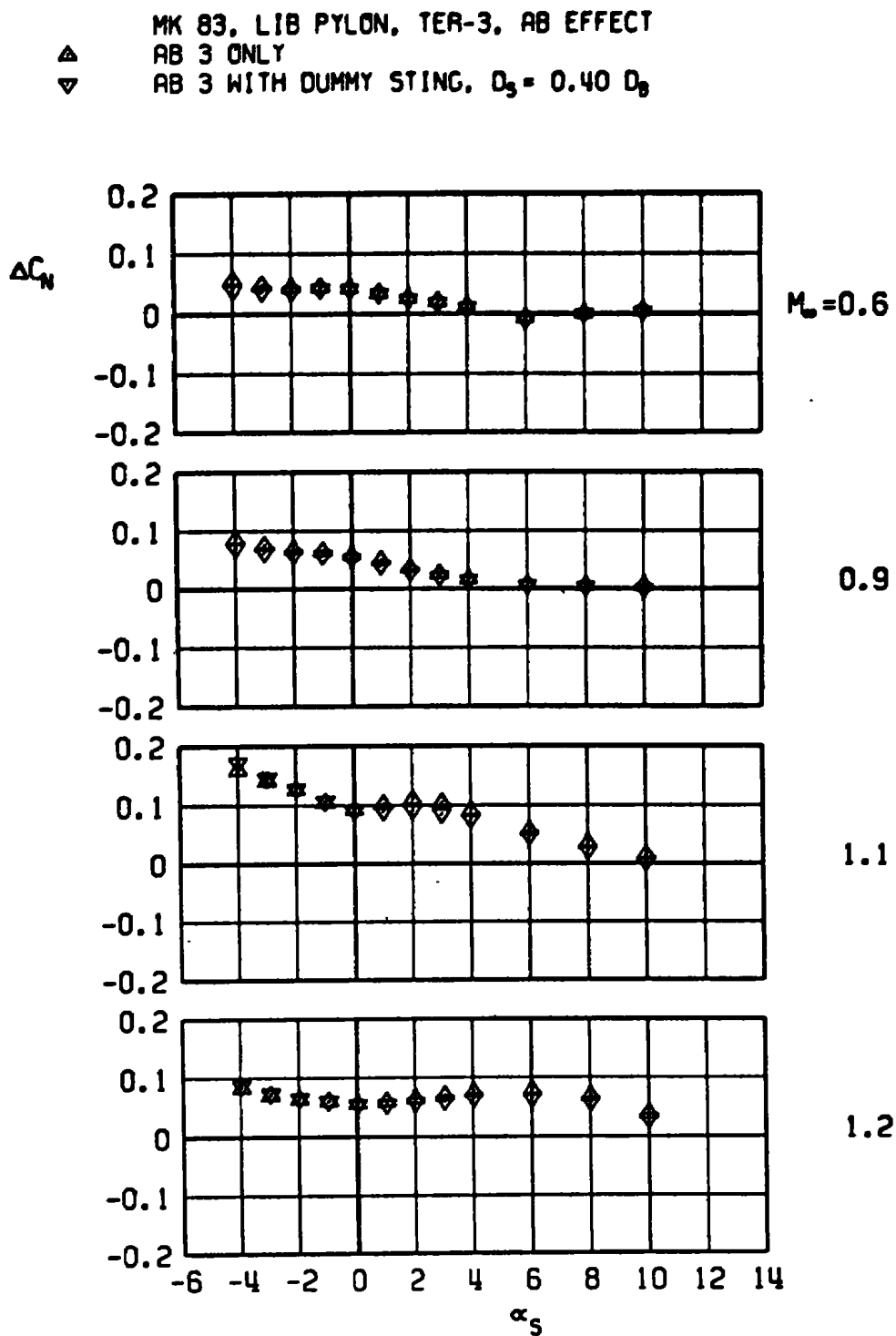


e. Pitching-moment increment
 Figure 58. Continued.

MK 83, LIB PYLON, TER-3, AB EFFECT
 □ AB 2 ONLY
 x AB 2 WITH DUMMY STING, $D_3 = 0.53 D_8$



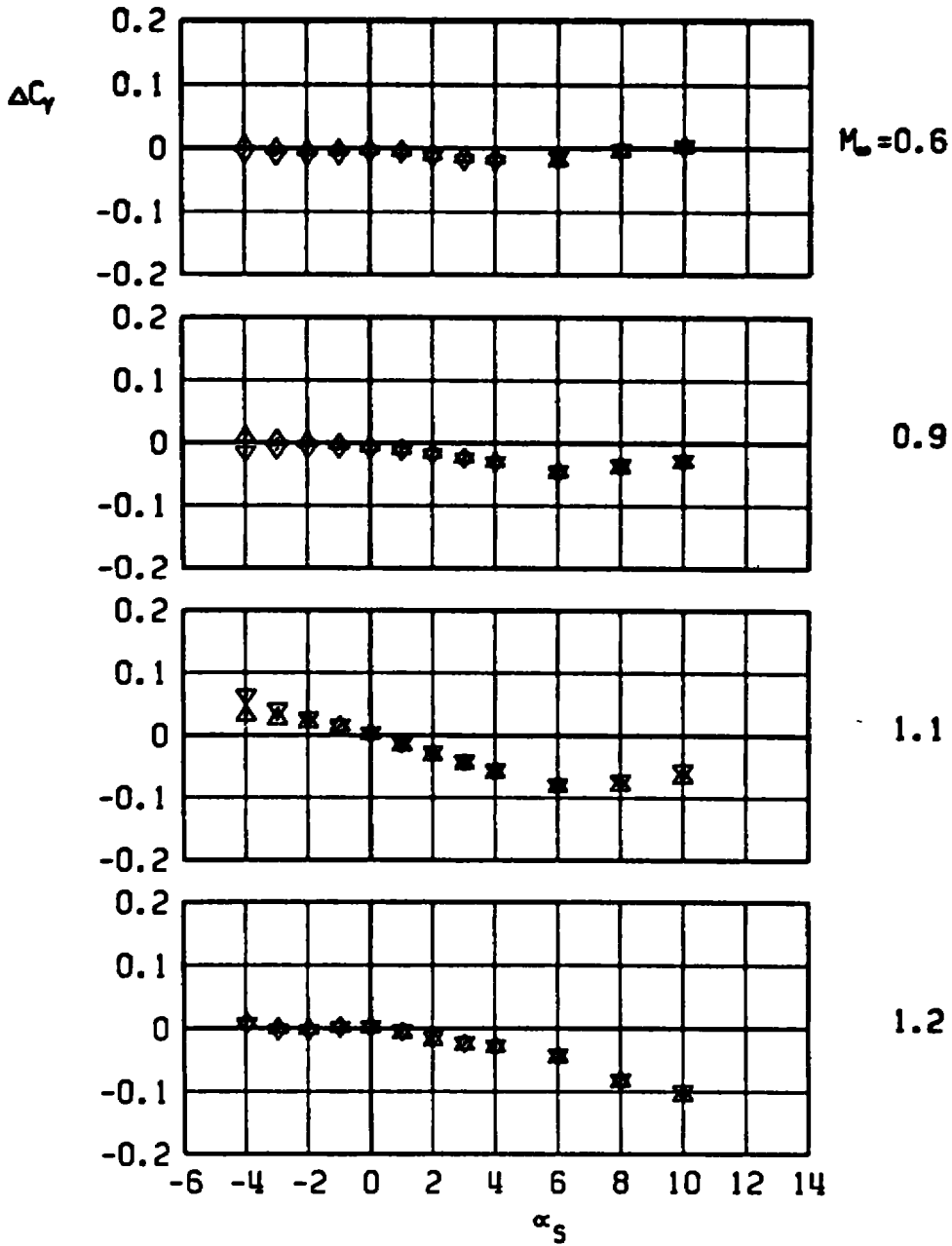
f. Yawing-moment increment
 Figure 58. Concluded.



a. Normal-force increment

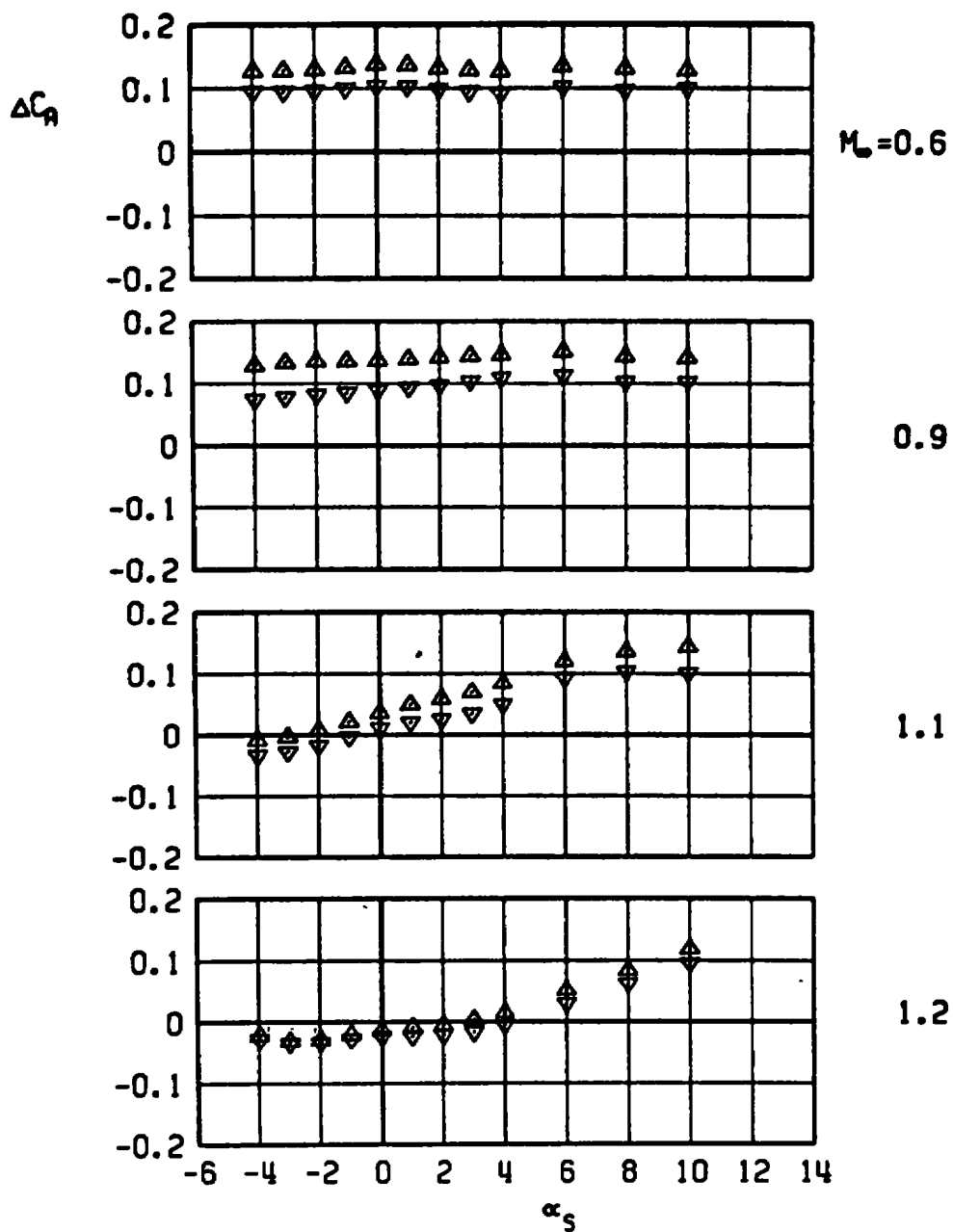
Figure 59. Aerodynamic load increments attributable to cylindrical distortion of the afterbody of a stable rack-mounted store, MK-83 with AB3, TER station 3, LIB pylon.

▲ MK 83, LIB PYLON, TER-3, AB EFFECT
 AB 3 ONLY
 ▼ AB 3 WITH DUMMY STING, $D_3 = 0.40 D_0$



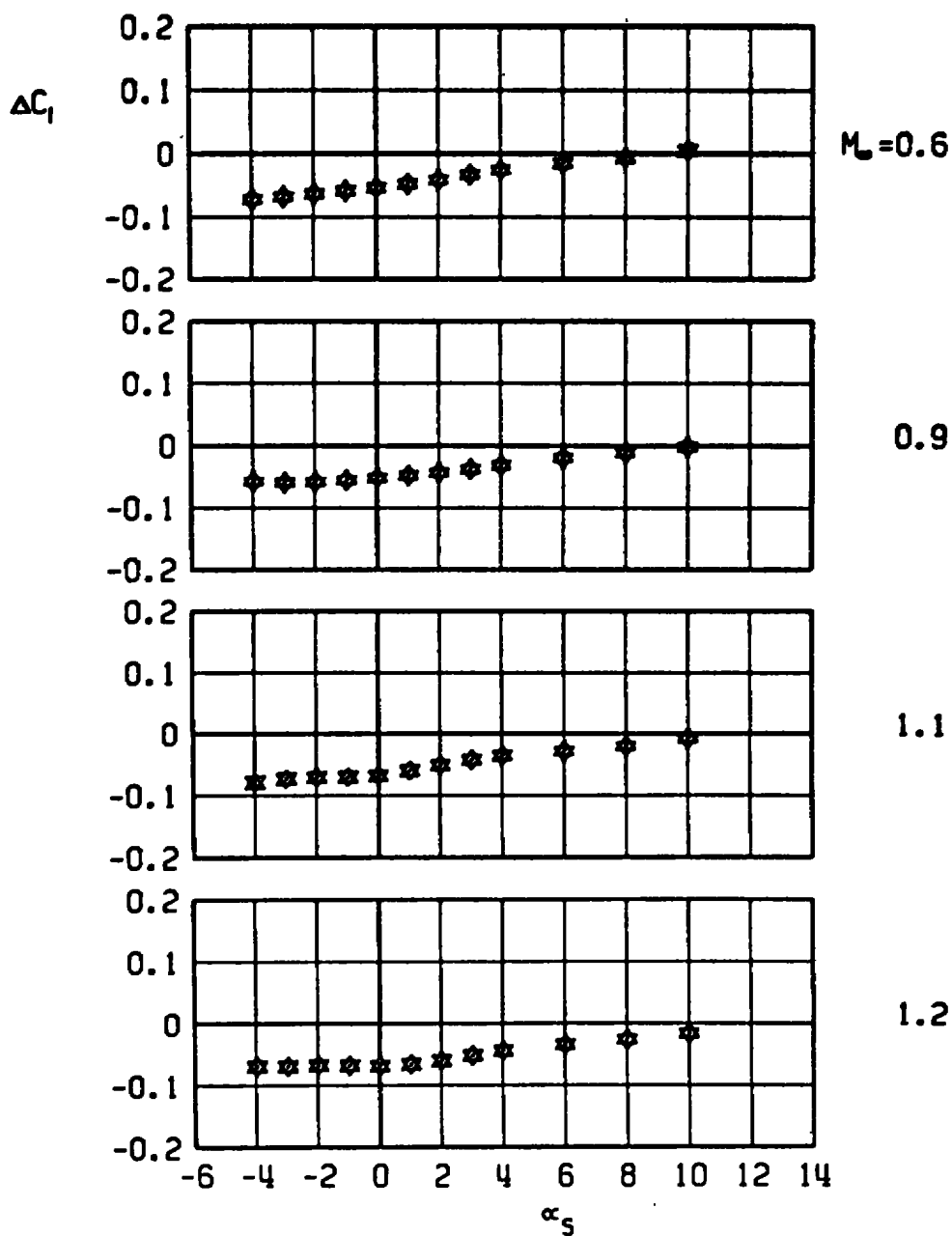
b. Side-force increment
 Figure 59. Continued.

Δ MK 83, LIB PYLON, TER-3, AB EFFECT
 ∇ AB 3 ONLY
 ∇ AB 3 WITH DUMMY STING, $D_3 = 0.40 D_0$



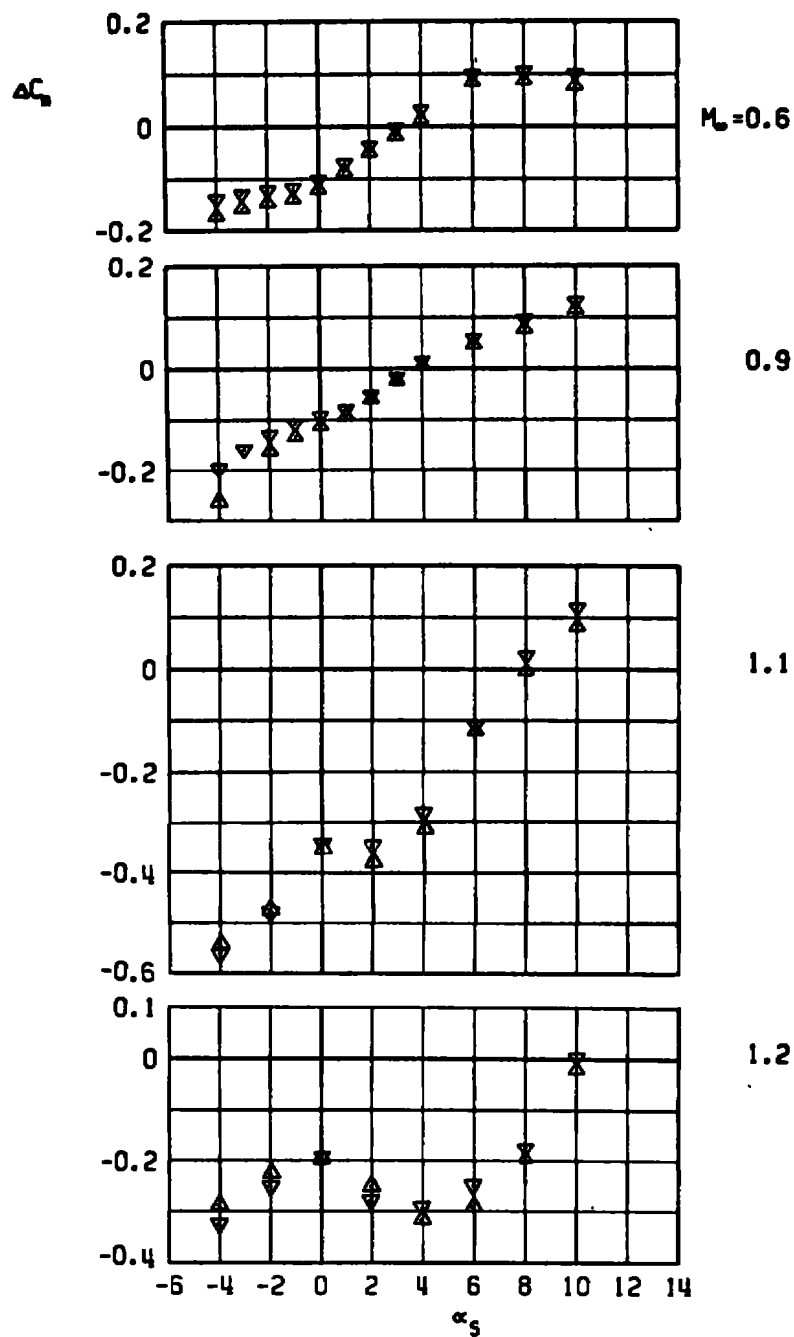
c. Axial-force increment
Figure 59. Continued.

MK 83, LIB PYLON, TERA-3, AB EFFECT
 ▲ AB 3 ONLY
 ▼ AB 3 WITH DUMMY STING, $D_3 = 0.40 D_0$



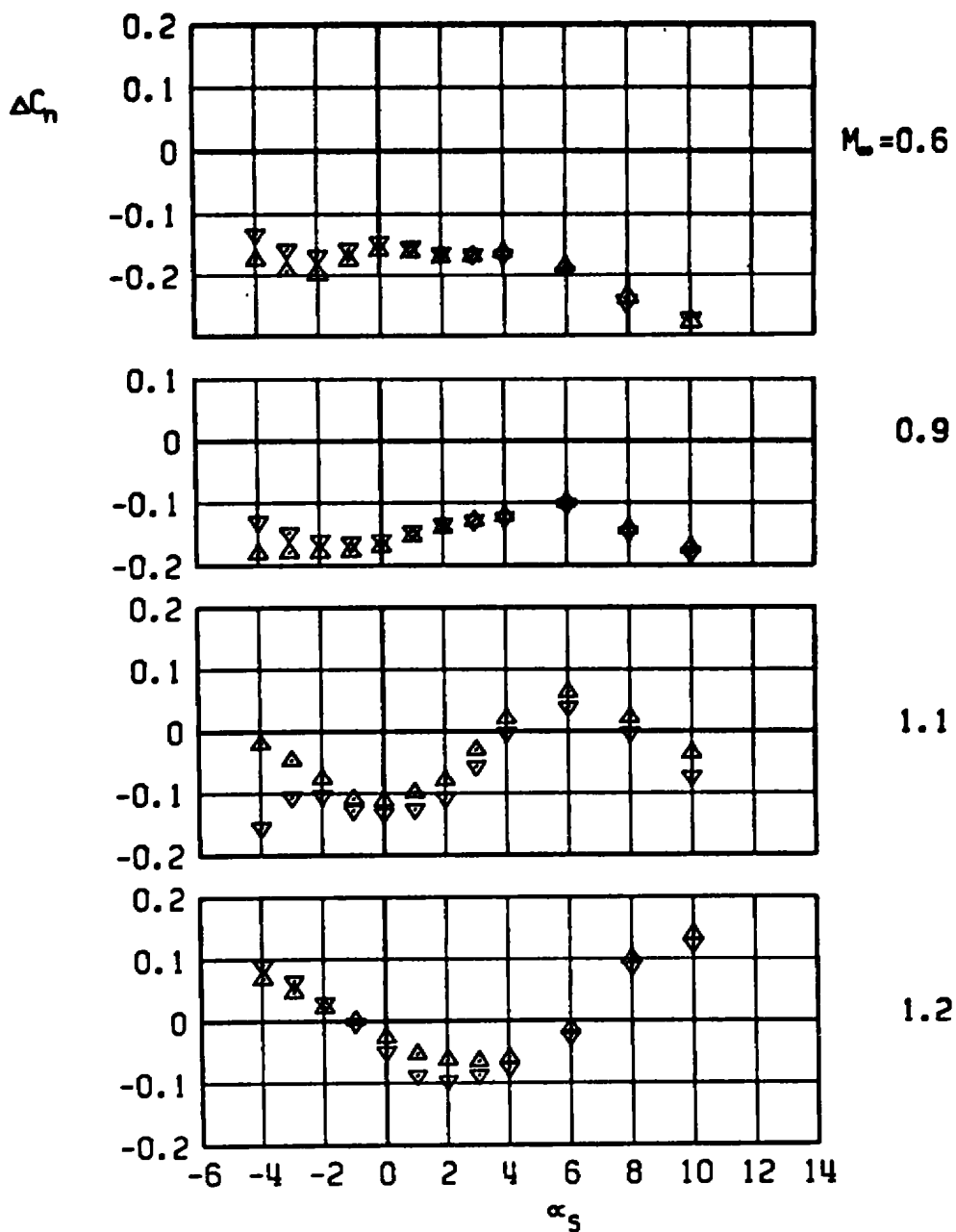
d. Rolling-moment increment
Figure 59. Continued.

▲ MK 83, L18 PYLON, TER-3, AB EFFECT
 AB 3 ONLY
 ▼ AB 3 WITH DUMMY STING, $D_3 = 0.40 D_9$



e. Pitching-moment increment
Figure 59. Continued.

▲ MK 83, LIB PYLON, TER-3, AB EFFECT
 AB 3 ONLY
 ▼ AB 3 WITH DUMMY STING, $D_3 = 0.40 D_0$



f. Yawing-moment increment
Figure 59. Concluded.

Table 1. Miscellaneous Dimensions of Store Models

Store	X_{FL} , in.	X_{CG} , in.	D , in.	AB Number	D_B , in.	D_S , in.	L_S , in.	D_S/D_B	L_S/D_B
BLACK CROW	4.546*	5.296	1.100	1	1.100	0.4	8.98	0.36	8.16
	↓	↓	↓	↓	↓	0.5	9.27	0.45	8.43
	↓	↓	↓	↓	↓	0.6	9.55	0.55	8.68
HSM	3.680*	4.430	0.900	1	0.900	0.4	8.98	0.44	9.98
	↓	↓	↓	↓	↓	0.5	9.27	0.56	10.30
	↓	↓	↓	↓	↓	0.6	9.55	0.67	10.61
BLU-1	2.875**	3.215	0.930	1	---	---	---	---	---
	↓	↓	↓	2	0.490	0.4	8.98	0.82	18.3
	↓	↓	↓	3	0.590	0.4	8.98	0.68	15.2
	↓	↓	↓	↓	↓	0.5	9.27	0.85	15.7
	↓	↓	↓	4	0.690	0.4	8.98	0.58	13.0
	↓	↓	↓	↓	↓	0.5	9.27	0.72	13.4
	↓	↓	↓	↓	↓	0.6	9.55	0.87	13.8
M-118	2.074*	2.810	1.206	5	0.502	0.4	8.98	0.80	17.9
	↓	↓	↓	1	0.319	---	---	---	---
	↓	↓	↓	2	0.627	0.4	8.98	0.64	14.3
	↓	↓	↓	3	0.710	0.4	8.98	0.56	12.6
	↓	↓	↓	↓	↓	0.5	9.27	0.70	13.1
	↓	↓	↓	4	0.810	0.4	8.98	0.49	11.1
	↓	↓	↓	↓	↓	0.5	9.27	0.62	11.4
				↓	↓	0.6	9.55	0.74	11.8

Table 1. Concluded.

Store	X_{FL} , in.	X_{cg} , in.	D , in.	AB Number	D_B , in.	D_S , in.	L_S , in.	D_S/D_B	L_S/D_B
ASP	1.990** ↓	2.335 ↓	0.800 ↓	1 ↓	0.800 ↓	0.25	4.05 ↓	0.31	5.06 ↓
						0.325		0.41	
						0.4		0.50	
CBU-24	1.700** ↓	1.933 ↓	0.800 ↓	1 ↓	0.437 ↓	0.25	4.05 ↓	0.57	9.27 ↓
						0.325		0.74	
						0.4		0.92	
CBU-46	2.615** ↓	2.990 ↓	0.780 ↓	1	0.150	---	4.05 ↓	---	12.3 ↓
				2	0.330	0.25		0.76	
				3	0.405	0.25		0.62	
				↓	↓	0.325		0.80	
				4	0.480	0.25		0.52	
				↓	↓	0.325		0.68	
MK-83	2.175** ↓	2.525 ↓	0.700 ↓	1	---	---	4.05 ↓	---	8.62 ↓
				2	0.470	0.25		0.53	
				3	0.620	0.25		0.40	
				↓	↓	0.325		0.52	
				↓	↓	0.4		0.65	

* Forward 30-in. suspension point

** Forward 14-in. suspension point

Table 2. Uncertainty Intervals in Force and Moment Coefficients for Store Models

Store	M_{∞}	$\epsilon(C_N)$	$\epsilon(C_Y)$	$\epsilon(C_A)$	$\epsilon(C_\ell)$	$\epsilon(C_m)$	$\epsilon(C_n)$
BLACK CROW	0.6	± 0.017	± 0.047	± 0.023	± 0.035	± 0.050	± 0.039
	0.8	0.014	0.038	0.018	0.028	0.039	0.031
	0.9	0.013	0.035	0.017	0.026	0.036	0.028
	1.1	0.011	0.031	0.015	0.023	0.031	0.025
	1.2	0.011	0.030	0.014	0.022	0.030	0.024
HSM	0.6	± 0.028	± 0.072	± 0.034	± 0.064	± 0.091	± 0.080
	0.8	0.022	0.057	0.027	0.052	0.072	0.063
	0.9	0.020	0.053	0.025	0.048	0.066	0.058
	1.1	0.018	0.047	0.022	0.042	0.058	0.051
	1.2	0.017	0.045	0.021	0.041	0.056	0.050
BLU-1	0.6	± 0.024	± 0.066	± 0.031	± 0.058	± 0.080	± 0.088
	0.8	0.019	0.053	0.025	0.047	0.064	0.071
	0.9	0.018	0.049	0.023	0.043	0.060	0.065
	1.1	0.016	0.043	0.020	0.038	0.053	0.058
	1.2	0.015	0.041	0.019	0.037	0.051	0.056
M-118	0.6	± 0.015	± 0.040	± 0.019	± 0.027	± 0.037	± 0.030
	0.8	0.012	0.031	0.015	0.021	0.030	0.023
	0.9	0.011	0.029	0.014	0.020	0.027	0.022
	1.1	0.009	0.026	0.012	0.017	0.024	0.019
	1.2	0.009	0.025	0.012	0.017	0.023	0.018

Table 2. Concluded

Store	M_∞	$\epsilon(C_N)$	$\epsilon(C_Y)$	$\epsilon(C_A)$	$\epsilon(C_\delta)$	$\epsilon(C_m)$	$\epsilon(C_n)$
ASP	0.6	± 0.022	± 0.017	± 0.032	± 0.016	± 0.030	± 0.025
	0.9	0.016	0.013	0.024	0.012	0.022	0.018
	1.1	0.015	0.012	0.022	0.011	0.020	0.016
	1.2	0.014	0.011	0.021	0.010	0.019	0.016
CBU-24	0.6	± 0.020	± 0.018	± 0.032	± 0.016	± 0.031	± 0.026
	0.9	0.016	0.013	0.024	0.012	0.023	0.019
	1.1	0.015	0.012	0.022	0.011	0.021	0.017
	1.2	0.014	0.011	0.021	0.010	0.020	0.016
CBU-46	0.6	± 0.023	± 0.019	± 0.034	± 0.017	± 0.032	± 0.031
	0.9	0.017	0.014	0.025	0.013	0.023	0.022
	1.1	0.015	0.012	0.022	0.011	0.021	0.019
	1.2	0.015	0.012	0.022	0.011	0.020	0.018
MK-83	0.6	± 0.026	± 0.025	± 0.025	± 0.029	± 0.041	± 0.037
	0.9	0.020	0.019	0.019	0.021	0.030	0.027
	1.1	0.018	0.017	0.017	0.019	0.027	0.025
	1.2	0.017	0.016	0.016	0.018	0.026	0.024

APPENDIX A

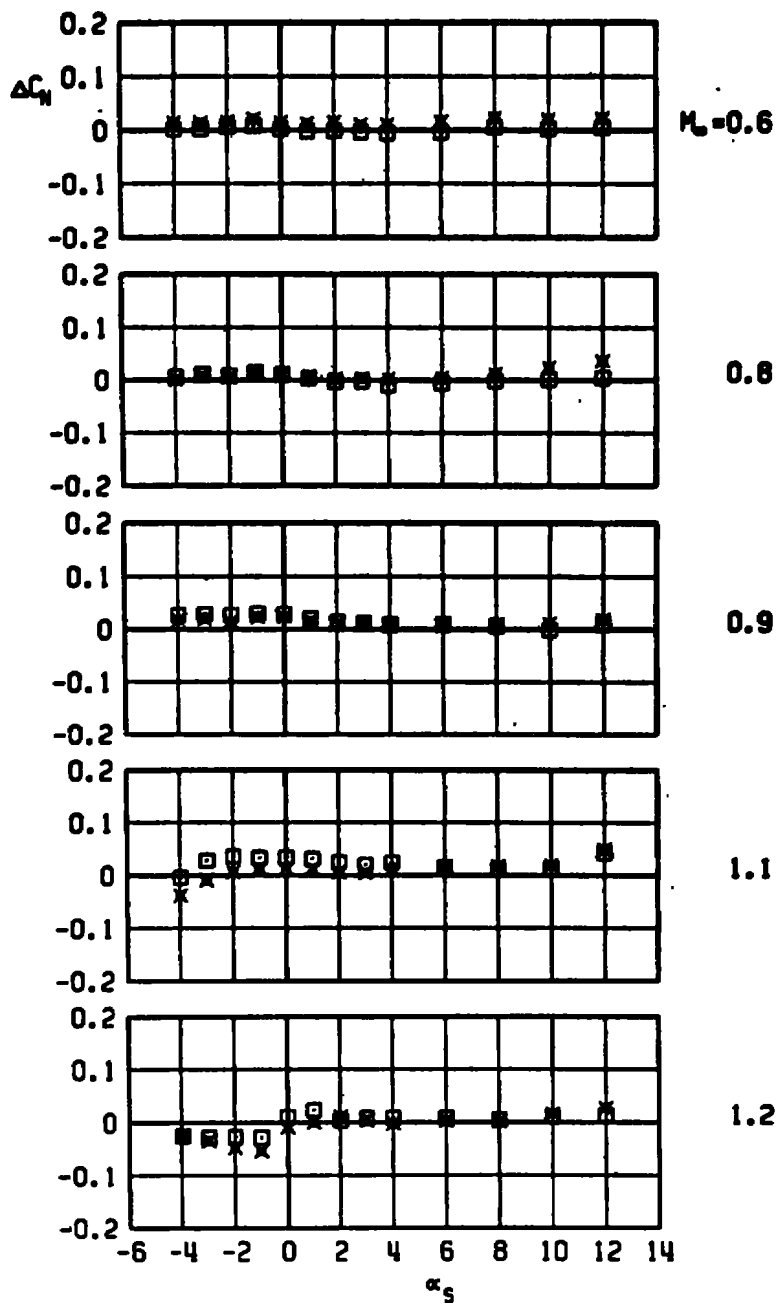
EFFECTS OF DUMMY STING MISALIGNMENT

As an adjunct to the scheduled tests, the effects of sting misalignment were briefly investigated. One configuration, the BLU-1 with afterbody 5, was installed on the left inboard pylon with intentional misalignment of the dummy sting. The sting was installed with a vertical misalignment with respect to the centerline of the store model in a compensating sense, i.e., toward the aircraft model. At the higher angles of attack during the subsequent identical repeat run of an earlier condition, the dummy sting deflected away from the aircraft model and into alignment with the store model. The resulting data are presented in Figs. A-1a through f.

Although normal force was negligibly affected at all Mach numbers, pitching moment was strongly affected, especially for Mach numbers 0.8 and above (Figs. A-1a and A-1e). A small change in normal force acting at a large distance from the moment reference center could cause such a combination of effects. It is conceivable that subsonically, a stagnation point is established at the exposed, blunt face of the deflected sting, causing an increase in pressure over the lower aft portion of the store. Furthermore, since the sting deflection is dependent on the dynamic pressure of the flow, the effects of misalignment must be a function of Mach number. (The small effect on pitching moment at $M_\infty = 0.6$ is consistent with this hypothesis.) Supersonically, it is probable that a shock forms about the protruding sting, producing, through interactions with the boundary layer, an increased pressure over the lower aft portion of the store model. Clearly, at any Mach number, an increase in pressure over the extreme downstream portion of the store model could, even though relatively small, create a disproportionately larger negative pitching moment. Lateral misalignment of the sting was not intentionally set, and side force and yawing moment correspondingly reflect only small effects (Figs. A-1b and A-1f).

BLU-1, AB5, LIB PYLON

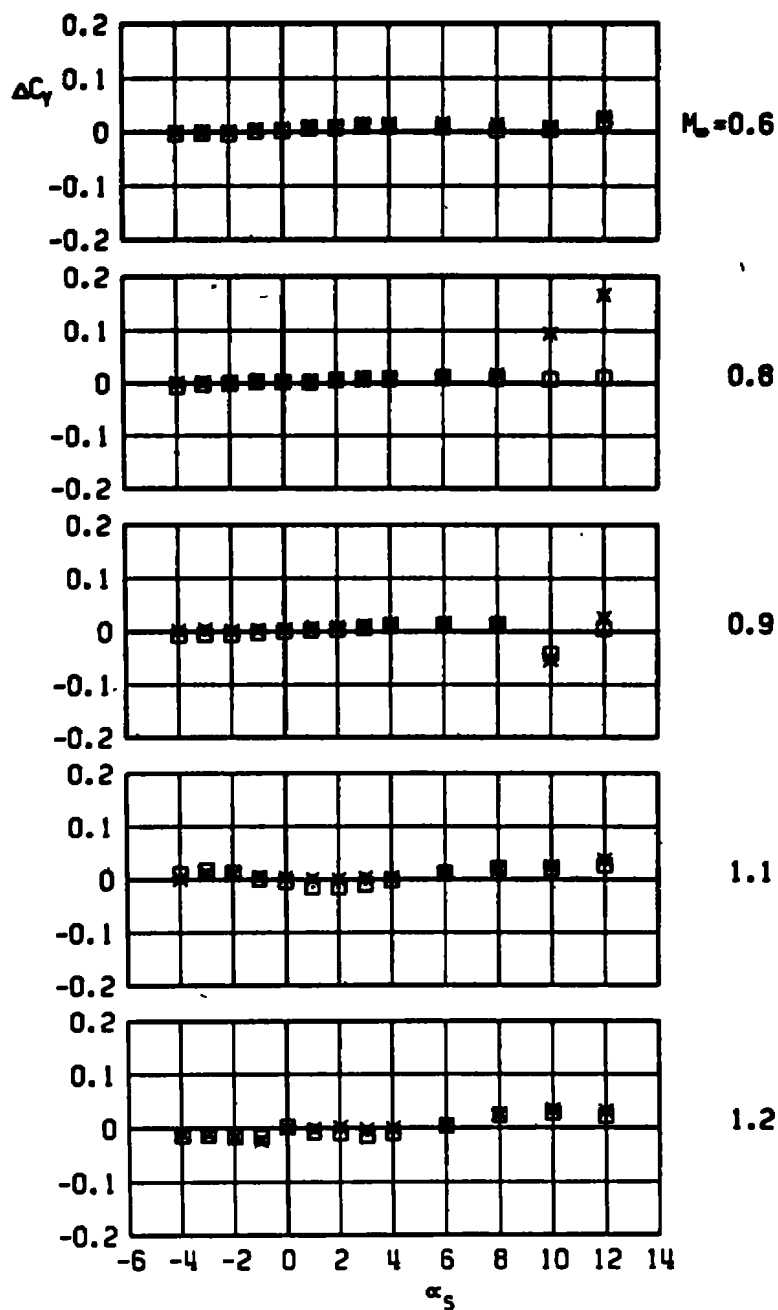
□ W/DUMMY STING, $D_3 = 0.80 D_0$, INITIALLY OFFSET
 x W/DUMMY STING, $D_3 = 0.80 D_0$, INITIALLY ALIGNED



a. Normal-force increment

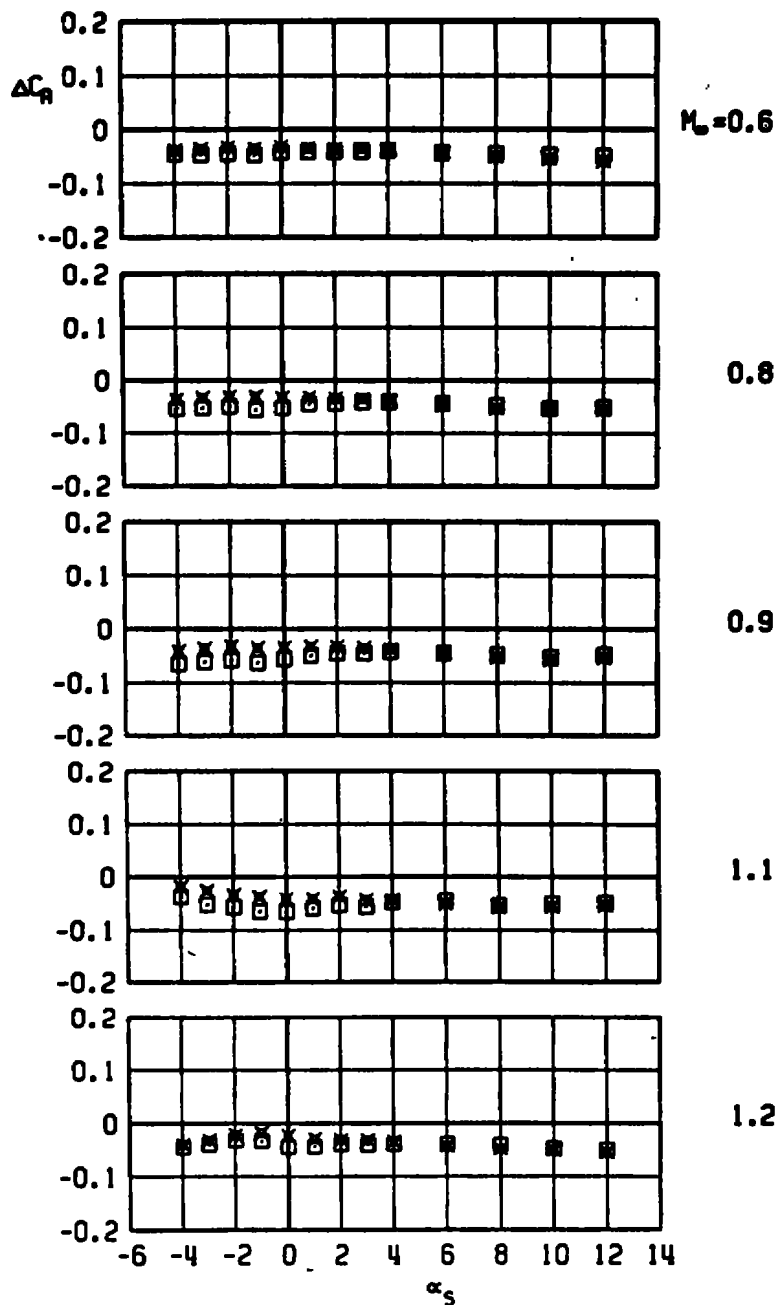
Figure A-1. This caption will be obtained later.

BLU-1, AB5, LIB PYLON
 □ W/DUMMY STING, $D_3 = 0.80 D_0$, INITIALLY OFFSET
 × W/DUMMY STING, $D_3 = 0.80 D_0$, INITIALLY ALIGNED



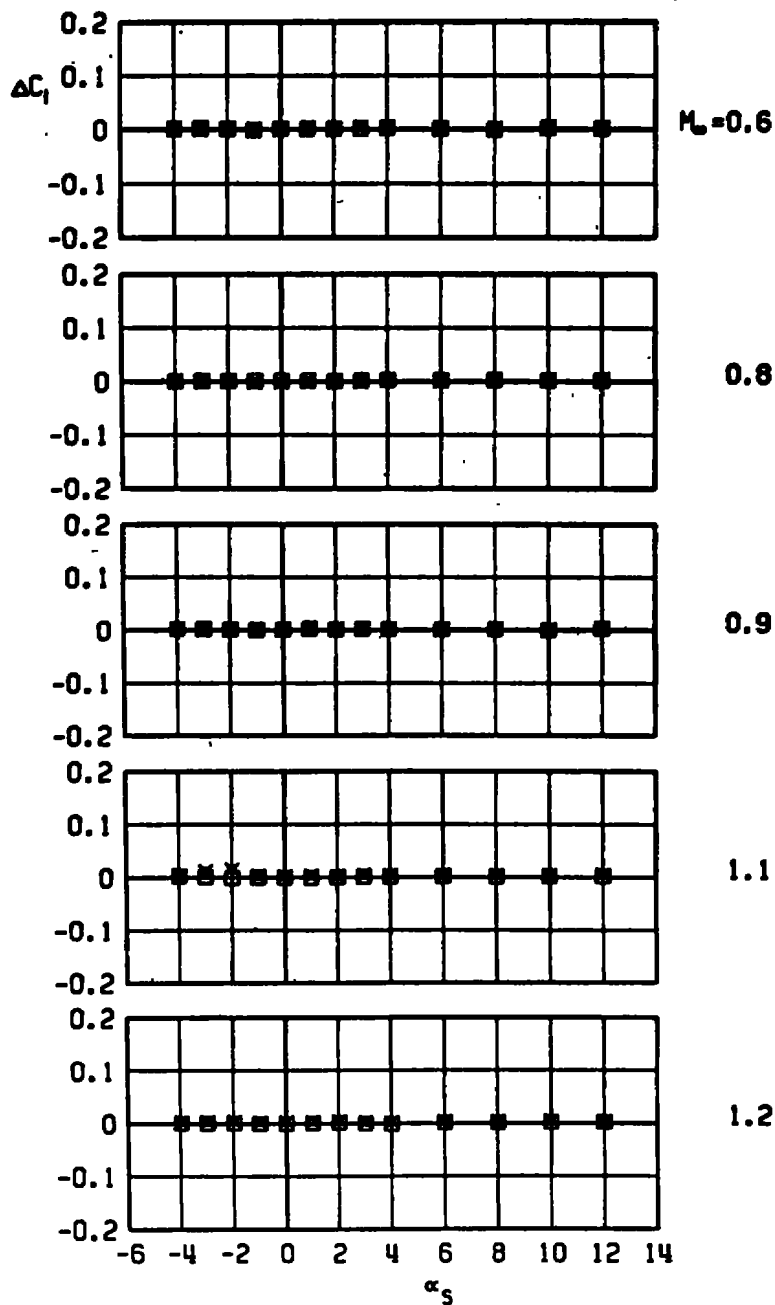
b. Side-force increment
 Figure A-1. Continued.

BLU-1, R85, L18 PYLON
 □ W/DUMMY STING, $D_3 = 0.80 D_0$, INITIALLY OFFSET
 × W/DUMMY STING, $D_3 = 0.80 D_0$, INITIALLY ALIGNED



c. Axial-force increment
 Figure A-1. Continued.

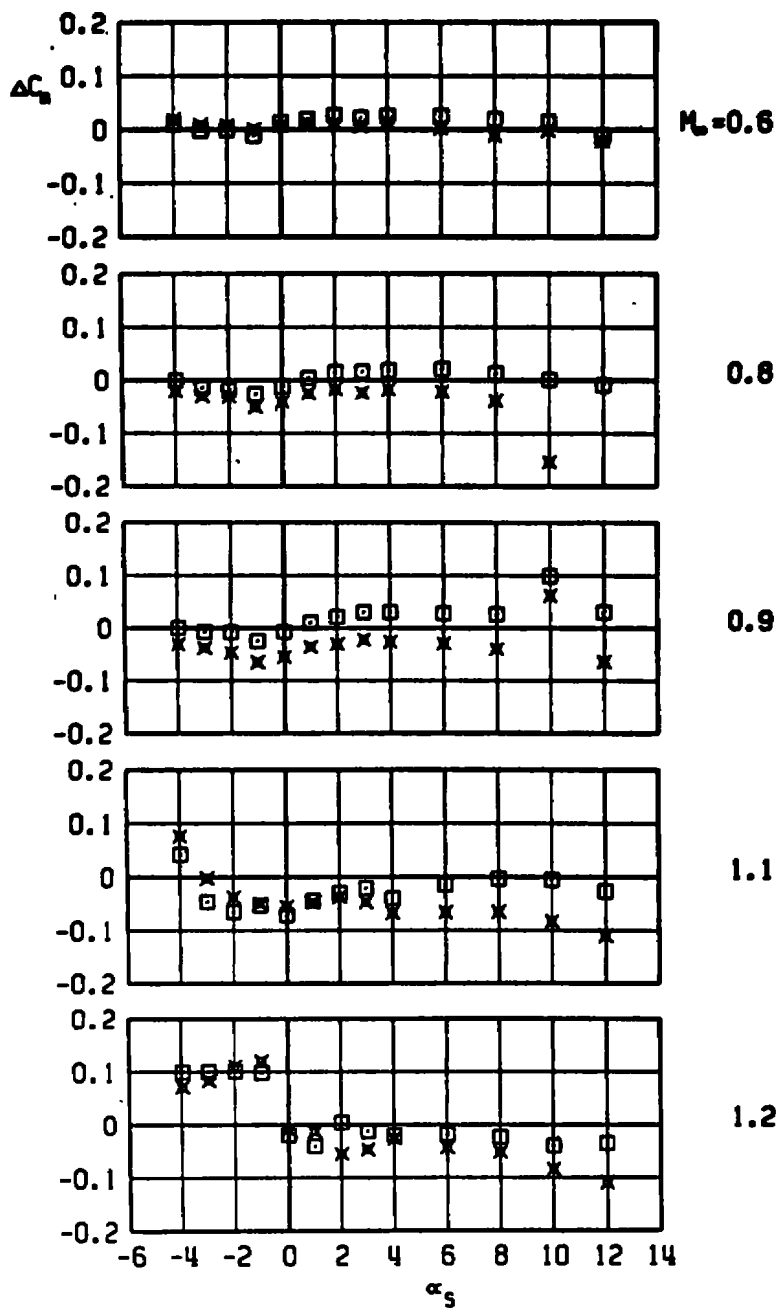
BLU-1, ABS, LIB PYLON
 □ W/DUMMY STING, $D_3 = 0.80 D_0$, INITIALLY OFFSET
 × W/DUMMY STING, $D_3 = 0.80 D_0$, INITIALLY ALIGNED



d. Rolling-moment increment
 Figure A-1. Continued.

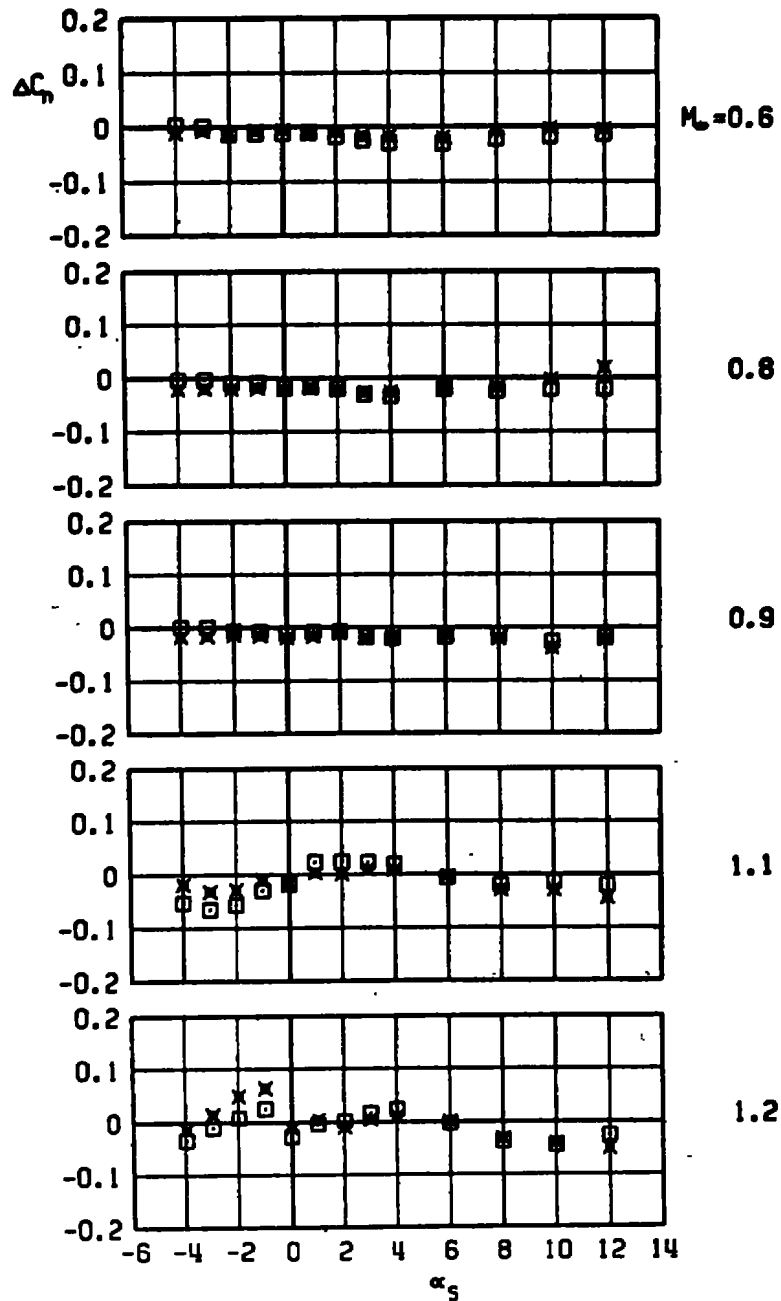
BLU-1, R85, LIB PYLON

□ W/DUMMY STING, $D_3 = 0.80$, INITIALLY OFFSET
 × W/DUMMY STING, $D_3 = 0.80$, INITIALLY ALIGNED



e. Pitching-moment increment
 Figure A-1. Continued.

BLU-1, A85, L18 PYLON
 □ W/DUMMY STING, $D_3 = 0.80 D_9$, INITIALLY OFFSET
 × W/DUMMY STING, $D_3 = 0.80 D_9$, INITIALLY ALIGNED



f. Yawing-moment increment
 Figure A-1. Concluded.

NOMENCLATURE

AB	Afterbody
BL	Aircraft buttock line, measured from the plane of symmetry, in., model scale
b	Aircraft wing span, in., model scale
C-L	Centerline
C_A	Axial-force coefficient for a store, axial force/ $q_\infty S$
C_l	Rolling-moment coefficient for a store (referenced to the axis of symmetry of the store), rolling moment/ $q_\infty SD$
C_m	Pitching-moment coefficient for a store (referenced to the center of gravity of the store), pitching moment/ $q_\infty SD$
C_N	Normal-force coefficient for a store, normal force/ $q_\infty S$
C_n	Yawing-moment coefficient for a store (referenced to the center of gravity of the store), yawing moment/ $q_\infty SD$
C_Y	Side-force coefficient for a store, side force/ $q_\infty S$
D	Maximum diameter of a store, ft, full scale
D_B	Diameter of the base of a store, in., model scale
D_s	Diameter of a sting, in.
FS	Aircraft fuselage station, in., model scale
LIB	Left inboard
LOB	Left outboard
L_s	Length of the constant-diameter portion of a sting, measured from the base of a store to the upstream extent of the variable-diameter portion of the sting, in.
M_∞	Free-stream static pressure, psfa
p_∞	Free-stream static pressure, psfa

$P_{t_{\infty}}$	Free-stream total pressure, psfa
q_{∞}	Free-stream dynamic pressure, $0.7 \rho_{\infty} M_{\infty}^2$, psf
S	Reference area of a store model, $\pi D^2/4$, ft ²
WL	Aircraft waterline, measured from the aircraft horizontal reference plane, in., model scale
X_{cg}	Location of the center of gravity of a store, measured from the nose of the store, in.
X_{FL}	Location of the forward suspension point of a store, measured from the nose of the store, in.
Y	Spanwise station, measured from the plane of symmetry of the aircraft, in., model scale
α_s	Angle of attack of a store relative to the free-stream velocity vector, deg
ΔC_x	Increment in a force or moment coefficient attributable to an effect, (coefficient with effect) - (coefficient without effect)
$\epsilon(C_x)$	Uncertainty interval of a force or moment coefficient